Research Article　　　　　　　　　　　　　　　　　　　**Open Access**

Development of a Methodology to Estimate Biomass from Tree Height Using Airborne Digital Image

J. Jenitha Ferdinent[1] and Rajchandar Padmanaban[2]

[1, 2] Department of Remote Sensing, Anna University of Technology, Chennai, Regional Centre Tirunelveli, Tamil Nadu, India

Correspondence should be addressed to J. Jenitha Ferdinent, jenithaferdinent@gmail.com and Rajchandar Padmanaban, charaj7@gmail.com

Abstract Globally biomass is becoming imperative for function such as climate change, combined heat and power generation. The biomass energy is gaining significance as a source of clean heat for domestic heating and community heating applications. Regarding climatic change and global warming, the biomass is being estimated in various ways. By including three dimensions (i.e.) height of a tree or stand height of trees in forest will greatly help in estimation biomass more accurately. Traditionally close range Photogrammetry is used to determine volume and biomass of the tree. However, this method of volume/height of a tree is not feasible in large scale applications and time consuming. Globally researchers are working to estimate this by using either airborne/space borne data. In this project, a methodology to measure tree height in case of single tree or stand height (mean tree height) of an area is developed using airborne digital camera. The height of the tree was first estimated from the airborne digital camera image data. The image taken from Airborne UltraCamD has been used. This image is 23cm X 15cm image size and 20cm resolution. Aerial Triangulation was done using Leica LPS Software. The position and altitude has taken from the GPS/IMU system. After bundle adjustments, mass points will be generated with pre-determined grid spacing. Generally airborne or space-borne data provides digital surface model (DSM) which includes surface features like trees, buildings etc., along with terrain. A filter is designed to separate surface features and terrain using height and crown width was obtained from stereo data using automated classification algorithm. The height derived from automatic method is validated with height derived from manual process i.e. photogrammetric method and measured from stereo measurements. From the obtained parameters the DBH and Biomass will be estimated; from this we can know the bio resource of the particular area.

Keywords *Aero Triangulation, Above Ground Biomass, Allometry Equation, ERDAS, Leica-LPS, Tree Height*

1. Introduction

Global climate change is widely considerable that led to the organizing of the UN Frame work on Climate Change at the 1992 UN conference on Environment and Development. The keen focusing on national greenhouse gas emission inventories, use, transform in the cover, management of forest, create sources and sinks of carbon dioxide to and from the biosphere [13]. In order to estimate the magnitude of the basis and sinks requires dependable estimates of the biomass density of the forest undergoing variation [1].

Biomass is a renewable energy resource resultant from the carbonaceous squander of different human and natural actions. It is derived from the timber industry, raw material from the forest, major element of household waste, agricultural crops and forest wood. Biomass not have the action of adding carbon dioxide in to the environment as it absorbs the similar quantity of carbon in growing as it discharge when consumed as a fuel [2]. Biomass is significant source of energy and the most imperative fuel worldwide after coal, oil and natural gas.

Scientists are trying to discover the advantages of biomass energy as an alternative energy basis as it is renewable and free from CO_2 emissions, and is richly obtainable on earth in the form of agricultural rest, metropolis garbage, livestock dung, firewood, etc. Bio-energy, in the structure of biogas, which is consequent from biomass, is predictable to become one of the key energy resources for global sustainable growth [3].

Allometry is the study about the relative size or mass of a part of an organism. In this work we are applying the tree allometry, which narrows the Allometry definition as it is the study about the tree measurements according to their species and the characters. This allometry relation is applied to find the tree menstruation such as volume, height, crown width, mass and so on. The use of allometry is widely spread in the study of forest ecology [4].

The general allometric equation for mathematics and science is

$$Y = b_0 + b_1 X \qquad \text{eq (1)}$$

The following allometry equation is used to estimate the biomass,

$$AGBM = b + a*H^2_{est} \qquad \text{eq (2)}$$

2. Study Area

In India forests cover 67.83 million hectares of area in India which symbolize 20.64% of the nation's geographical territory [14], unreliable from the arid zone forests to Himalayan temperate forests. In this the forest in Godavari river basin (between $36^o59'N$ and $96^o43'E$) which is covering of approximately $131km^2$ of area in Andhra Pradesh state; is the study area of this project is shown in Figure 1.
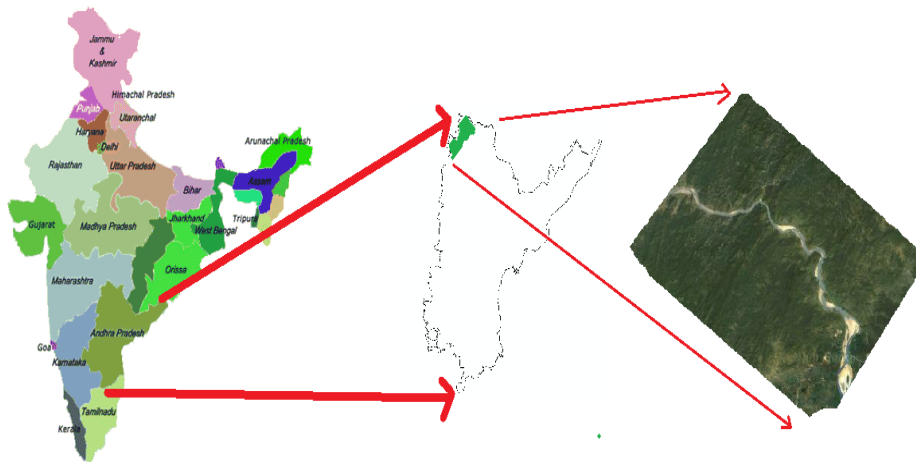
Figure 1: Study Area

Among this, study area is of 250.37km^2 with a scale of 18°35'45"N to 18°24'45"N and 80°15'00''E to 80°24'22.5000"E and it is on the bay of river Godavari. Among the total area 204.24km^2 is high dense vegetation area.

3. Methodology

The data downloaded from High Resolution Airborne Digital Image and the Geo-registrations are done. To estimation the height of the tree from the Digital Stereo Model was generated by using following technique. The stereo model was generated from the Leica LPS system then each tree were measured physically the top of the tree and the bottom of the tree; are measured manually by scrolling to the top and the bottom of the tree. From the manually collected tree top and tree bottom, the difference was calculated. Thus by the difference between the tree top and tree bottom, tree height was calculated. The following Figure 2 represents work flow of the project.

3.1. Extraction of DSM

After pre-processing of the aerial images and production of the image pyramids, result matches three kinds of features, i.e. feature points, grid points and edges, on the aerial images are finally found gradually starting from the low-density features on the images with the low resolution. Since all the matching procedures are based on the concept of multi-image matching guided from the object space, any number of images could be processed simultaneously [5]. TIN from DSM is reconstructed from the matched features on each level of the pyramid using the embarrassed Delaunay triangulation method [15], which instead is used in the consequent pyramid level for the approximations and adaptively addition of the matching parameters. Finally least squares matching methods are used to achieve more defined matches for all the features and identify some artificial matches [6]. Therefore, such design is more flexible so that the refined matching module can be an option for DSM generation. The Figure 3 shows the extracted DSM.
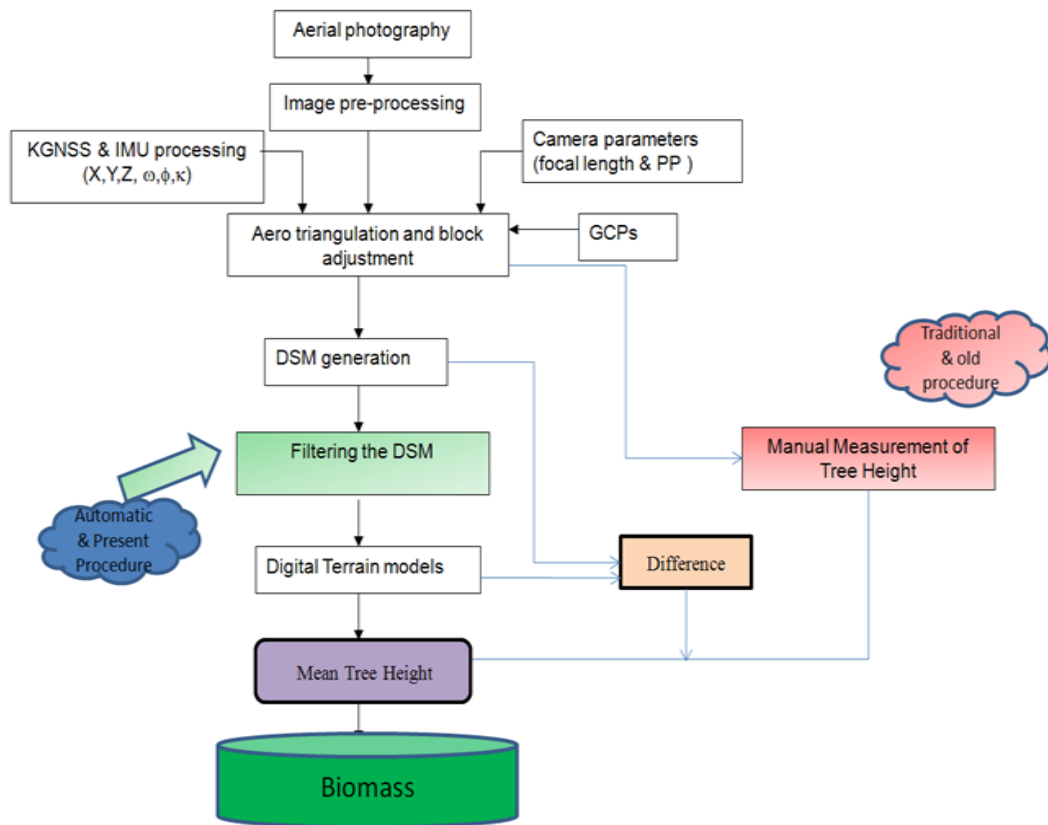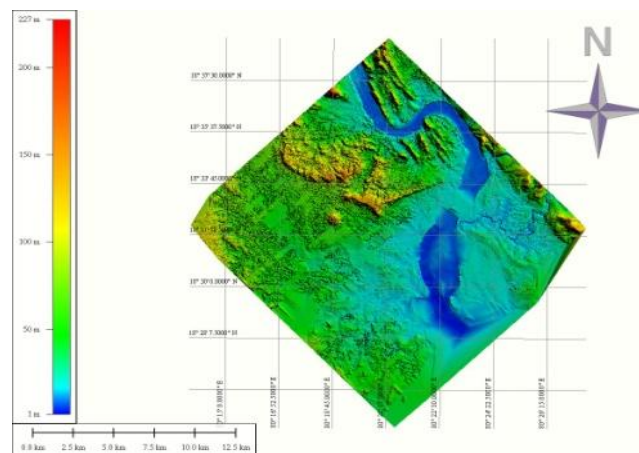
Figure 2: *Work Flow of the Project*

Figure 3: *Extraction of DSM*

3.2. Extraction of DTM

The DSM was generated by using the DEM extraction tool in ERDAS 2011 [16–18], which is in ltf format. This ltf data format was converted las format which is the point data; the following flow chart represents the process of DTM extraction in ground level. The point cloud generated was 3m X 3m [7]. The Figure 4 shows the Extraction of DTM.
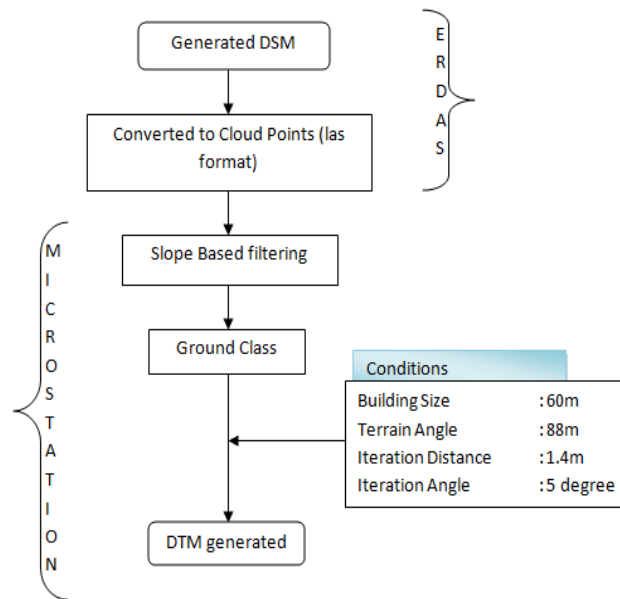
Figure 4: Extraction of DTM

3.2.1. *Filtering the Terrain* Filters are built from combinations of different elements. Therefore, to comprehend or envisage the performance and output of a filter the way in which elements are united has to be tacit. Every filter makes an assumption about the structure of Bare Earth points in a local neighborhood. This forms the concept of the filter [8].

3.2.2. *Point-to-Point* In these algorithms two points are compared at a time. The categorize purpose is based on the positions of the two points. If the output of the categorize purpose is above a certain threshold then one of the points is assumed to belong to an entity, automatically only one point can be classified at a time [9]. The Table 1 shows the Filtering class.

3.2.3. *Slope based Filtering* This algorithm used to find slope or height difference between two points. If the slope is on top of a certain threshold then the uppermost point is assumed to belong to an object. The assumption is based on the rational that the steepest slopes in a landscape fit in to objects [10]. The Figure 5 shows the slope based filtering model.
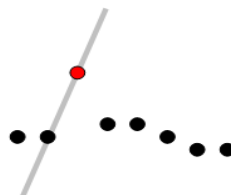

Figure 5: Slope Based Filtering

Table 1: *Filtering Class*

Item	Definition	
Landscape	The topography. A scene consisting of the earth and any other features (buildings, trees, power lines, etc.,) residing on it.	
Bare Earth	Topsoil or any thin layering (asphalt, pavement, etc.) covering it. Haugerud and Harding (2001) define Bare Earth as the continuous and smooth surface that has nothing visible below it. However, this definition is for the purpose of implementation of a filter and because of that it is restrictive.	
Object	Vegetation and other artificial features that have been crafted by human hand.	
Detached Object	Objects that rise vertically (on all sides) above the Bare Earth or other Objects.	
Attached Object	Objects that rise vertically above the Bare Earth only on some sides but not all (e.g., bridges, gangways, ramps, etc.,).	
Point-cloud	A collection of points (acquired by ALS) in a 3D Cartesian co-ordinate system.	
Filtering	Abstraction of the Bare Earth from an ALS point-cloud.	
Outlier	Point/s in a point-cloud that are not off the landscape (e.g., birds, gross errors from the ALS system, etc.).	

This filter based on morphological filter developed by Vosselman (2000, 2001). In this algorithm the data set is initially gridded, to carry a database structure, outliers are noticed and discarded. The slopes were calculated with the help of local linear regression method [11]. In the linear regression every point should compared to the lowest point in the local operator neighborhood. The height and distance dissimilarity from the near to the ground points are weighted and used as observations in the linear regression. The threshold used in formative the class of a point is based on the underlying slope in the initial DEM [12]. The following Figures 6 and 7 explain how the DEM is classified from the cloud points. The Figure 8 shows the extracted DTM.
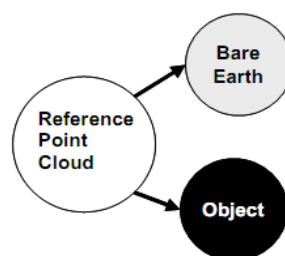
Figure 6: *Reference data for filtering*
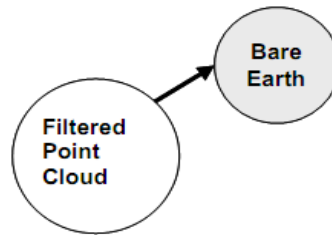
Figure 7: *Filtered data*
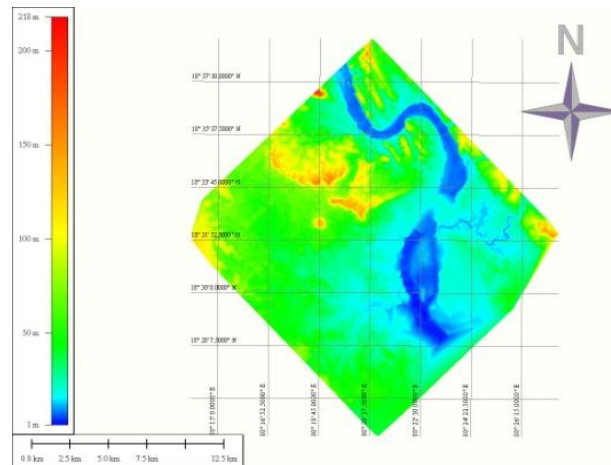
Figure 8: *Extracted DTM*

4. Results and Discussion

Automatic tree heights are taken using MICROSTATION (TERA SCAN) the DSM was generated in ERDAS and imported to MICROSTATION as point data (las format) [19].The grid points were generated in 3m X 3m. The sampled locations are overlaid in the point data and the DSM of the samples was taken. The Slope Based Filtering was applied to filter the ground value from the point data in Terra Scan tool with various conditions. They are Building Size with 60m, Terrain Angle with 88m, Iteration Angle with 6° and Iteration Distance with 1.4m.

4.1. Manually Measured Tree Heights

The tree heights are measured visually from the Stereo View generated by the ERDAS IMAGINE [20]. The values are accomplished by getting the coordinates (x, y, z) value where, x is Longitude; y is Latitude; z is Height. The following Figures 9, 10 and 11 show the comparison of the tree height values.
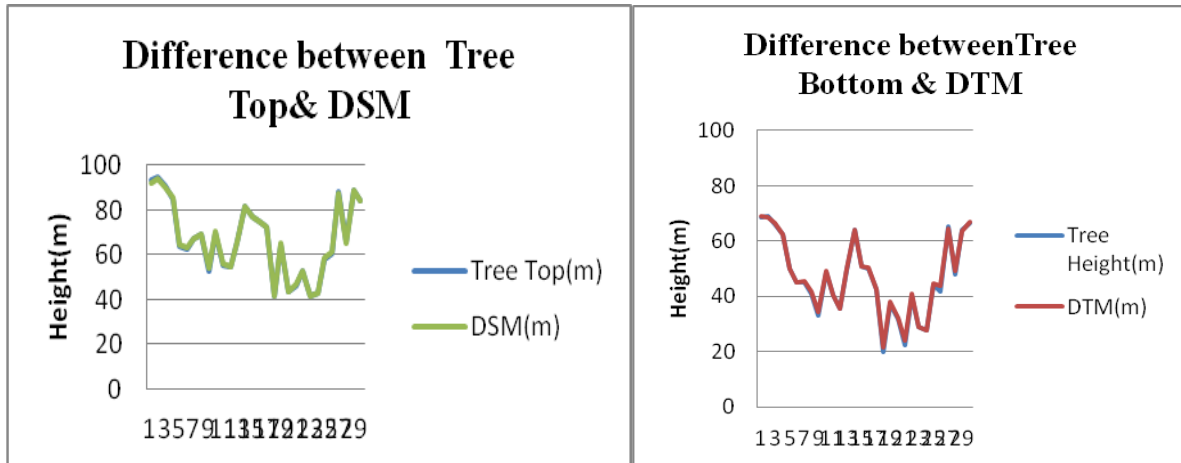
Figure 9: *Comparison of tree tops*   **Figure 10:** *Comparison of tree bottoms*
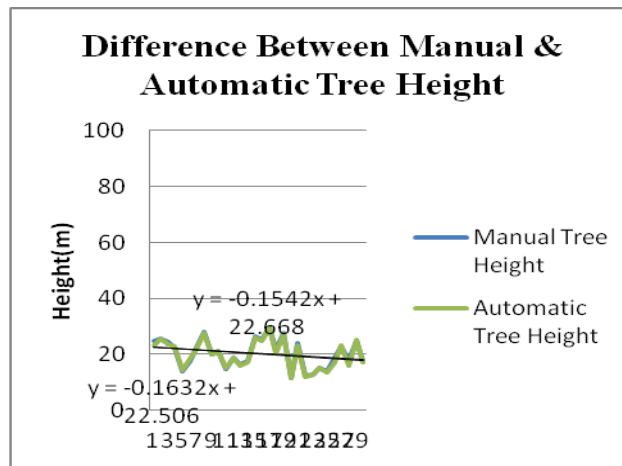
Figure 11: *Comparison of the Tree Height*

The above ground biomass was estimated by using the allometry equation as represented in equation (3) (4) and (5).

$$AGBM = b + a*H^2_{est} \qquad\qquad eq\ (3)$$

$$AGBM = 22.66 + 0.154*H^2_{est} \qquad\qquad eq\ (4)$$

Which is 85 Mg/Ha for automatically generated height.

$$AGBM = 22.50 + 0.168*H^2_{est} \qquad\qquad eq\ (5)$$

Which is 88.75 Mg/Ha for manually measured tree height. Therefore the total high denser vegetation area among the study area is 204.24km^2 and the above ground biomass of the vegetated area is 1756145.013Mg which estimated from the manually measured tree height and for the automatically measured tree height the biomass is 1812485.935Mg.

5. Conclusion

Biomass is the natural source which acts as one of the major resource of a country. Biomass also takes major part in global warming, climate changes and modeling. The bio substance can be used as an alternative for some of the resources like petrol, LPG and so on which can be replaced as Bio Fuel. In this research work the above Ground Biomass was estimated from a parameter which is height of the tree. To identify the tree height the data captured by the high resolution camera UltraD cam is used as the source. The height is estimated by developing a stereo model which the tree heights are measured manually and the heights are also estimated from the DSM by applying the slope based filtering. The difference between the DTM and DSM gives the tree height. The manually measured and automatically derived height may be, (+/-) 0.20m differences.

The derived height is applied to the Allometry Equation to estimate the above Ground Biomass. Since the allometry which is used in this study is Universal Equation that is applicable for all kind of species. But to get the actual value, the allometry differs according to the species. The built area of this research contains 75% of Mangroves and 25% other species and hence the actual value of the biomass was not able to estimate without the field survey. Even though the field survey is not taken the approximate value generated might introduce an error of about (+/-) 2 mg/m^2.

This developed methodology proves that the Biomass can be estimated for large area in short period. And it also determined that the Biomass or the tree height can be estimated without the field data, but by using the High Resolution Airborne Digital Image.

References

[1] Alongi D.M. Present State and Future of the World's Mangrove Forests. Environmental Conservation. 2002. 29 (3) 331-349.

[2] Arefi H., et al., 2005: A Morphological Reconstruction Algorithm for Separating Off-Terrain Points from Terrain Points In Laser Scanning Data. In: International Archives of Photogrammetry, Remote Sensing and Spatial Information Sciences, 36 (3/W19).

[3] Padmanaban, R.; Kumar, R. Mapping and Analysis of Marine Pollution in Tuticorin Coastal Area Using Remote Sensing and GIS. Int. J. Adv. Remote Sens. GIS **2012**, 1, 34–48.

[4] Aschbacher J., et al., 1995: Comparison of Different Sensors and Analysis Techniques for Tropical Mangrove Forest Mapping. IGARSS Proceedings, 3; 2109 – 2111.

[5] Padmanaban, R. Integrating of Urban Growth Modelling and Utility Management System using Spatio Temporal Data Mining. Int. J. Adv. Earth Sci. Eng. **2012**, 1, 13–15.

[6] Baskerville, G.L. Use of Logarithmic Regression in the Estimation of Plant Biomass. Canadian Journal of Forest Research. 1972. 2, 49-53.

[7] Monishiya, B. G.; Padmanaban, R. Mapping and change detection analysis of marine resources in Tuicorin and Vembar group of Islands using remote sensing. Int. J. Adv. For. Sci. Manag. **2012**, 1, 1–16.

[8] Carvalho J.A., et al. A Tropical Forest Clearing Experiment by Biomass Burning In the Manaus Region. Atmospheric Environment. 1995. 29 (17) 2301-2309.

[9] Carvalho J.A., et al. Biomass Fire Consumption and Carbon Release Rates of Rainforest- Clearing Experiments Conducted in Northern Mato Grosso, Brazil. Journal of Geophysical Research. 2001.

106 (D16) 17877-17887.

[10] Council of Tree and Landscape Appraisers, 1992: Guide for Plant Appraisal. 8th Ed. International Society of Arboriculture, Champaign, Illinois, 103.

[11] Visalatchi; Padmanaban, R. Land Use and Land Cover Mapping and Shore Line Changes Studies in Tuticorin Coastal Area Using Remote Sensing. Int. J. Remote Sens. **2012**, 1, 1–12.

[12] Dallman P.R., 1998: Plant Life in the World's Mediterranean Climates. California Native Plant Society. UC Press, Berkeley, CA, 245.

[13] Davis S.E., et al. Importance of Storm Events in Controlling Ecosystem Structure and Function In A Florida Gulf Coast Estuary. Journal of Coastal Research. 2004. 20 (4) 1198-1208.

[14] Padmanaban, R. Modelling the Transformation of Land use and Monitoring and Mapping of Environmental Impact with the help of Remote Sensing and GIS. Int. J. Adv. Altern. Energy, Environ. Ecol. **2012**, 1, 36–38.

[15] Fromard F. Structure, Above-Ground Biomass and Dynamics of Mangrove Ecosystems: New Data from French Guiana. Oecologia. 1998. 115; 39-53.

[16] Kremer J. Operation of the Ultracamd Together With Ccns4/Aerocontrol -First Experiences and Results. International Archives of Photogrammetry Remote Sensing and Spatial Information Sciences. 2004. 35 (Part 1) 172-177.

[17] S, S. L.; Padmanaban, R.; Thomas, V. Inventory of Liquefaction Area and Risk Assessment Region Using Remote Sensing. Int. J. Adv. Remote Sens. GIS **2013**, 2, 198–204.

[18] Leberl F., et al., 2003. The Ultracam Large Format Aerial Camera System. Proceedings of the American Society for Photogrammetry and Remote Sensing, Anchorage, Alaska.

[19] Padmanaban, R.; Sudalaimuthu, K. Marine Fishery Information System and Aquaculture Site Selection Using Remote Sensing and GIS. Int. J. Adv. Remote Sens. GIS **2012**, 1, pp 20-33.

[20] Venkatesan G; Padmanaban, R. Possibility Studies and Parameter Finding for Interlinking of Thamirabarani and Vaigai Rivers in Tamil Nadu , India. Int. J. Adv. Earth Sci. Eng. **2012**, 1, 16–26.

Research Article **Open Access**

Forest Fire Risk Zonation Using Remote Sensing and GIS Technology in Kansrao Forest Range of Rajaji National Park, Uttarakhand, India

Tahir Malik[1], Ghulam Rabbani[2] and Majid Farooq[3]

[1, 3]Jammu & Kashmir State Remote Sensing Application Centre, Srinagar, Jammu & Kashmir, India
[2]Hemwati Nandan Bahuguna Garhwal University, Uttarakhand, India

Correspondence should be addressed to Tahir Malik, tahiremails@ymail.com

Abstract Forest fire is a major cause of changes in forest structure and function. Forest fires are as old as forests themselves. Forest fires are one of the major natural risks in the Uttarakhand forests. In such areas, fires occur frequently and there is a need for supranational approaches that analyze wide scenarios of factors involved. It is impossible to control nature, but is possible to map forest fire risk zone and thereby minimize the frequency of fire. Forest and wild land fire are considered vital natural processes initiating natural exercises of vegetation succession. However uncontrolled and misuse of fire can cause tremendous adverse impacts on the environment and the human society. A risk model for fire spreading is set up for Kansrao Forest Range of Rajaji National Park where Forest and wild land fires have been taking place historically, shaping landscape structure, pattern and ultimately the species composition of ecosystems both flora and fauna. It is based upon a combination of remote sensing and GIS data. In this study, Resourcesat P6 – LISS III (spatial resolution 23.5m, 4 bands (Red) (Green) (NIR) (SWIR), Topo Sheet (SOI) no.53 J/4 on scale 1:50,000 and contour interval 20 meters, ASTER 30m and Garmin 72 GPS were used. For these analyses ArcGIS and ERDAS Imagine software was used. Land use information was obtained from the satellite images in this study. In this phase the distinction of species in the forest was determined using supervised classification. The lands that have priorities in case of fire were decided by combining the moisture of the land and slope classes that were determined by conventional approaches with the satellite images. The results of the analysis were shown by reports and graphs. The test region results should be applied all over Rajaji National Park.

Keywords LISS, Forest Fire, Risk Zonation, DEM, Disaster

1. Introduction

Wildfires are considered as a serious problem distressing many terrestrial ecosystems in the Earth system and causing economic damage for people [1] such as missing income relative to the land use, destruction and lost property, damages to agriculture, and loss of biodiversity [2, 3]. Also, it is one of the most important parts of land degradation that is caused by deforestation and desertification [4]. Information on the distribution of forest fire risk zones is essential for the effective and sound decision making process in the forest management [5]. Forest fire risk evaluation is a critical part of fire prevention, since pre-fire planning resources require objective tools to monitor when and where a fire is more prone to occur, or when will it have more negative effects [6]. Forest fire modeling involves the risk assessment and evaluation. The term "risk" is used to describe the probability that a fire might start, as affected by the nature and incidence of causative agents [7].

In India, about 2-3 % of the forest area is affected annually by fire and on an average over 34,000 ha forest areas are burnt by fire every year [8]. Remote sensing and GIS is important tool for mapping and management of forest fires. The first application of forest fire dates from 1960 when several aerial infrared scanners were tested for fire spot detection [9]. In addition to forest fire mapping, remote sensing has been effectively used in fire hazard rating system. In many fire hazard rating, critical factors were vegetation, slope, aspect and elevation. Deeming et al., 1978 [10] have used LANDSAT MSS image to obtain fuel oriented vegetation maps. Satellite remote sensing based forest fire detection methods have been developed and demonstrated by Cuomo et al., 2001 [11] and Salvador et al., 2000 [12].

In India, foresters have been debating the issue of forest fire control for a long time, but the paucity of information owing to the lack of qualitative and quantitative studies on forest fire and its effect has not resulted in any defined approach to controlling the forest fires.

Forest fire risk zones are locations where a fire is likely to start, and from where it can easily spread to other areas. A precise evaluation of forest fire problems and decision on solutions can only be satisfactory when a fire risk zone mapping is available [13]. Understanding the behaviour of forest fire, the factors that contribute to making an environment fire prone, and the factors that influence fire behavior are essential for forest fire [9]. The GIS-based model seems to be a reasonably good approach for the conditions in India, where a major part of the forested land is being encroached upon by the population [14, 15].

In the present study, an attempt is made to prepare a forest fire risk zone map by integrating a satellite image, topographical and other ancillary data from a geographic information system(GIS) for Kansrao Range which is the most forest fire sensitive area in Rajaji National Park. This study is also an attempt to exploit the capabilities of remote sensing and GIS techniques and to suggest an appropriate methodology for forest fire risk zone mapping. Such maps will help forest department officials prevent or minimize fire risk activities within the forest and take proper action when fire breaks out [16].

2. Study Area

Kansrao forest range is located in Rajaji National Park, the park extends from 29° 52` to $30^o$ 15` north latitude to 78° 57` to $78^o$ 23` east longitude in north India and covers an area about 820.42 km^2.The study area is situated between 78° 02` to $78^o$ 18` east longitude to 30° 15` to $30^o$ 05` north latitude. The study area covers an area about 79.33 km^2. The area is located in the Garhwal Shivaliks behind Haridwar across the Rishikesh-Haridwar road in India. The area has an uneven topography, with elevation ranging from 360 m to 860 m. The area is covered with thick green forest, mainly Sal, Teak, and other varieties of deciduous trees, along with grass and shrubs. Kansrao can be reached from

Cheering Crossing via Jabbarwala check post that lies 7 Kms further ahead. If this road is not motor able then Jabbarwala check post can be reached alternatively from Doiwala (3 kms from lachiwala railway bridge crossing on the highway).
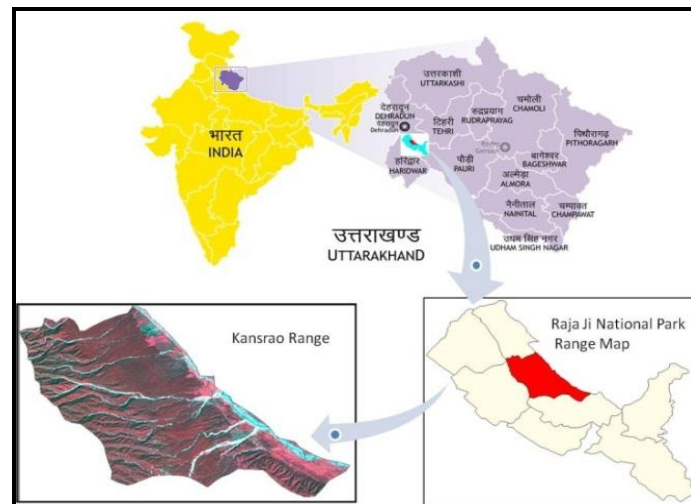
Figure 1: *Location of Study Area*

3. Material and Methods

3.1. Data

The data used is Resourcesat P6 – LISS III of December 2009 (spatial resolution 23.5m), Topo Sheet (SOI) No.53 J/4 on scale 1:50,000 with contour interval 20 meters, ASTER 30m and Garmin 72 GPS for defining and identifying the burned area and for estimating the vegetation loss. The data prepared for this study area were the following: forest type map, vegetation map, elevation, slope, aspect, standard topographic map and climate data (average wind, rainfall data, and temperature).

3.2. Methods

With the help of survey of India (SOI) website toposheet required for the study area has been identified. LISS III data was used for image analysis work. ASTER data was used to generate Digital Elevation Model (DEM) for the study area. The topographical factors like, altitude, slope and aspect layers were derived from DEM. The satellite images were corrected for the influence of atmosphere and topographic relief. These data were geo-coded with the help of rectified toposheets according to Geographic (lat. /long.) projection system with Everest ellipsoid and India–Bangladesh datum was used using ERDAS Imagine software. Boundary of Kansrao forest range was digitized from toposheet in vector form with the help of ERDAS 9.1 using vector tool, an area of interest boundary generated using the vector file helped in to get the subset image of Kansro forest range from satellite data.

Complete road network was digitized from toposheet and buffer was created for distance of 200m, 400m, 500m and 600m from the center of the road.

The flowchart for the methodology is shown in Figure 2.
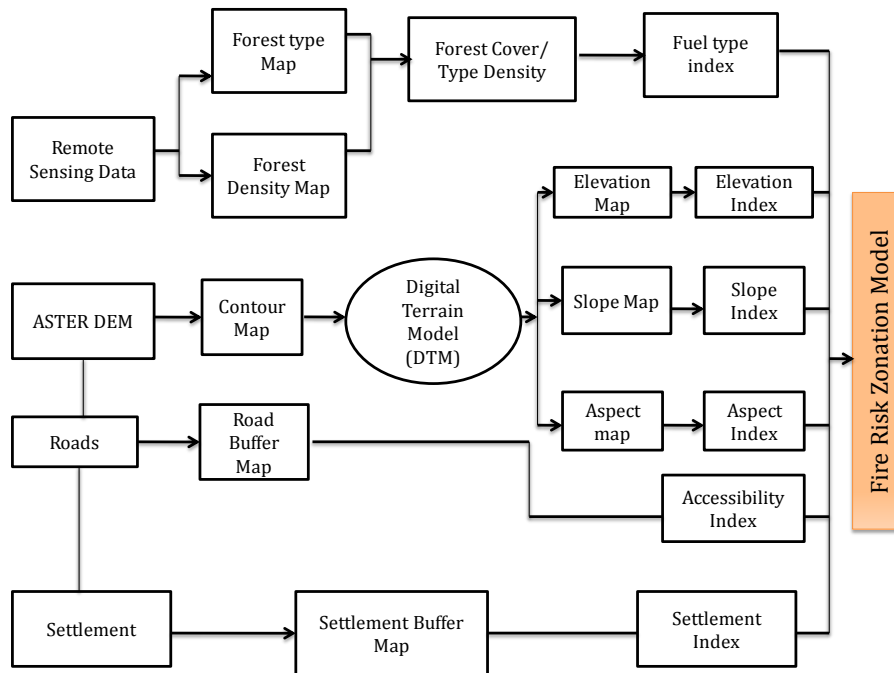
Figure 2: Methodology Flowchart

Settlement areas were digitized in point vector form, as the settlement was outside the Kansrao forest range the settlement buffer were created for 1000m, 2000m and 3000 m distance. The FCC of LISS III December 2009 image was used in the study. FCC was rectified with toposheet using first order nearest neighbor rules. A total of 20 ground points were used to register the image with the rectification error of less than 1 pixel, with the help of ERDAS.

3.3. Generation of Thematic Layers

For inputting spatial data in GIS, it is necessary that the resource information is in the form of map; hence the mapping of the thematic layers is one of the primary requirements. Remote sensing, coupled with limited ground checks, is the most ideal way for generating resource maps.

A. *Generation of Forest Type and Density Type Layers* In this study density mapping employed the use of LISS III data, which was free from cloud cover. Unsupervised classification approach was used for forest density mapping using ERDAS. The study area was classified into 50 spectral classes using unsupervised image classification approach. Eventually the forest cover of study area was stratified into four major types on the basis of density viz; VDF (very dense forest), MDF (moderately dense forest), OF (open forest) NF (non forest), as per the fundamental criteria of FSI for forest cover mapping (FCM).

Supervised approach was used for forest type classification in which 20 training sets were taken from Google earth as ground control points. Based on the field visit the study area was classified into Moist Sal forest, Deciduous forest, Plantation and Degraded forest.

B. *Generation of Slope, Aspect and Elevation from DEM (Digital Elevation Model)* A subset of the ASTER 30 m DEM of study area was clipped with the help of boundary vector layer. Elevation, Aspect and Slope were generated from ASTER 30m DEM with the help of ERDAS EMAGINE 9.1 using topographic analysis tool.

3.4 Generating Index Value Maps

In the present study the map layers generated above viz. forest density (Figure 3), vegetation type map (Figure 4), fuel type map (Figure 5), slope map (Figure 6), aspect map (Figure 7), elevation map (Figure 8), road map (Figure 9) and settlement map (Figure 10) and were reclassified for assigning weightage Weights were given to each factor according to their influence on fire behavior by having experience and the opinion of the experts in the field (Tables 1 to 6).

Table 1: Elevation Index Map and Weights

Elevation in Meters	Weights
300-500	1
500-900	2

Table 2: Slope Classes and Weights

Slope % (degrees)	Weights
0-3	1
3-15	2
15-45	3
Above 45 %	4

Table 3: Aspect Classes and Weights

Aspect	Weights
North	1
East	2
West	3
South	4

Table 4: Road Buffer Distance and Weights

Roads Buffers (m)	Weights
200 m	4
400 m	3
500 m	2
600 m	1

Table 5: Settlement Buffer Distance and Weights

Settlement Buffer (m)	Weights
1000 m	1
2000 m	2
3000 m	3

Table 6: *Fuel Type Index*

Type	Density	Weights
Deciduous forest	High	4
	Medium	4
	Low	3
Degraded forest	High	3
	Medium	2
	low	1
Plantation	High	2
	Medium	2
	Low	1
Moist Sal forest	High	2
	Medium	1
	Low	1

4. Fire Risk Zonation Index/Fire Risk Modeling

In this study spatial modeling has been done to obtain the combined effect of fuel type index, elevation index, slope index, aspect index, road index and settlement index. Different weights have been assigned as per the importance of the particular variables in relation to the area under study. Highest weight of nine have been given to the fuel type index, because, fuel contributes to the maximum extent due to inflammability factor. The second highest weights has been given to slope and aspect, because, sun facing aspects receive direct sun rays and make the fuel drier and highly inflammable; higher slopes contribute to convectional preheating and easy ignition and spreading of fire. Besides on steep slopes, the dry biomass is more close to fire flames causing the fire to spread more speedily. Spatial analysis using a function in model maker tool of ERDAS was carried out which revealed that on a 36% slope, the rate of fire spread is twice as compared to fire on a slope of 18%.

$$FRZI = \frac{(FUI * 9) + (SLI * 8) + (ASI * 7) + (RDI * 6) + (STI * 5) + (ELI * 4)}{10}$$

The following equation was used in the map calculation:

Where FRZI = Fire Risk Zonation Index

FUI = Fuel Type Index
SLI = Slope Index
ASI = Aspect Index
RDI = Road Index
STI = Settlement Index
ELI = Elevation Index

As different weights were tried for different variables and the weights given in the equations were used to generate fire risk zonation map. The fire risk index values in this map (FRZI) were ranging from 14 to 135. Based on the statistics of different weight classes, the map was reclassified into five classes as very low, low, moderate, high and very high to generate fire risk area map.

Figure 3: *Forest Density Map*
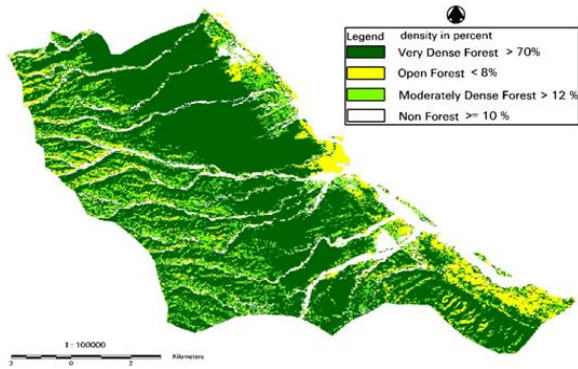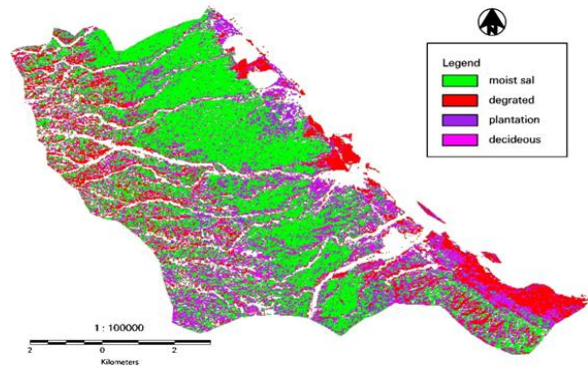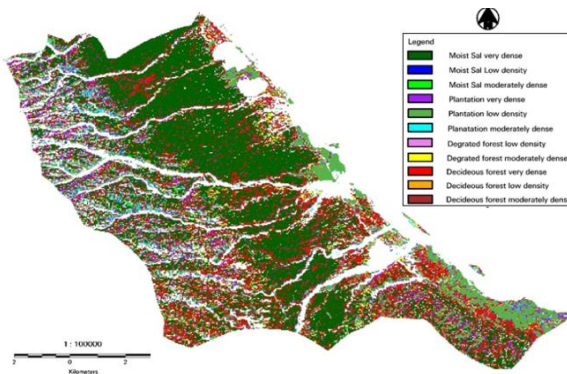

Figure 4: *Vegetation Type Map*

Figure 5: *Fuel Type Map*
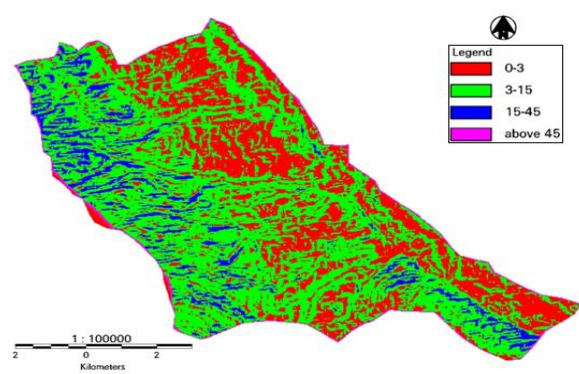
Figure 6: *Slope Map*
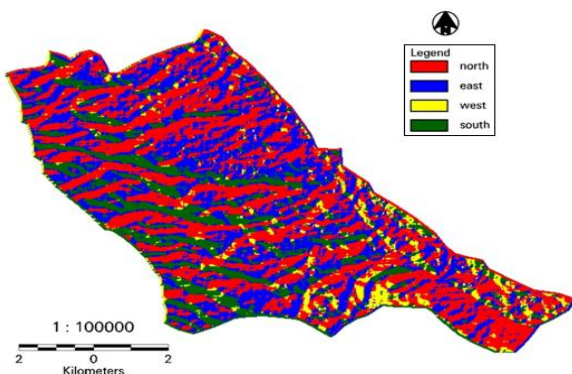
Figure 7: *Aspect Map*
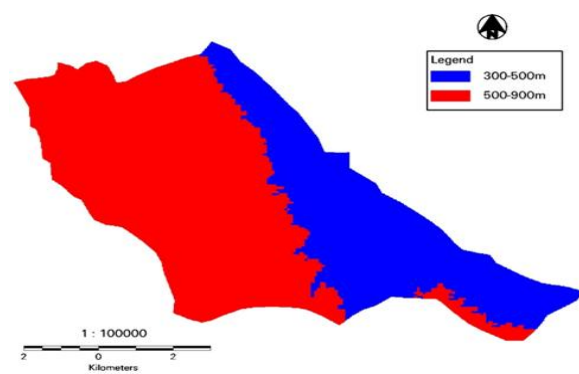
Figure 2: *Elevation Map*
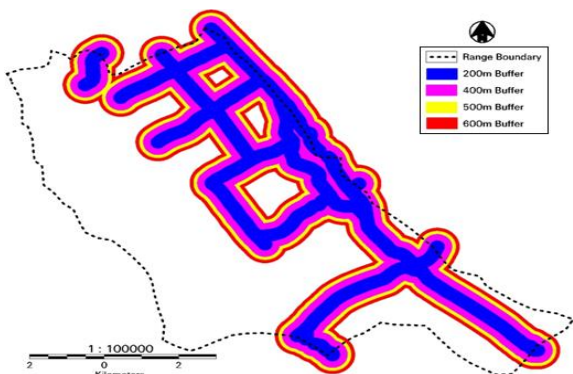
Figure 9: *Road Buffers*
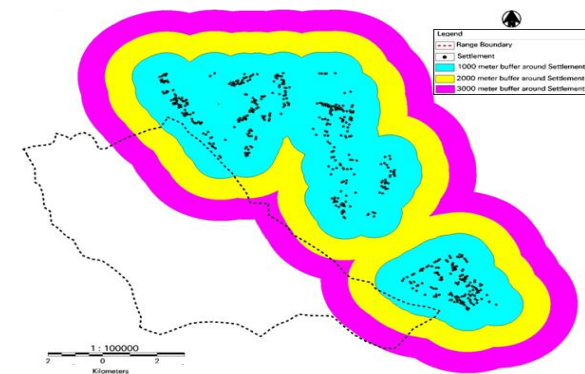
Figure 2: *Settlement Buffers*

5. Results and Discussion

Settlement, accessibility and forest types had played an important role in fire risk zonation modeling. The other variables elevation and slope have comparatively less impacting estimation of fire risk zonation. The area under different fire risk zones is summarized in Table 7.
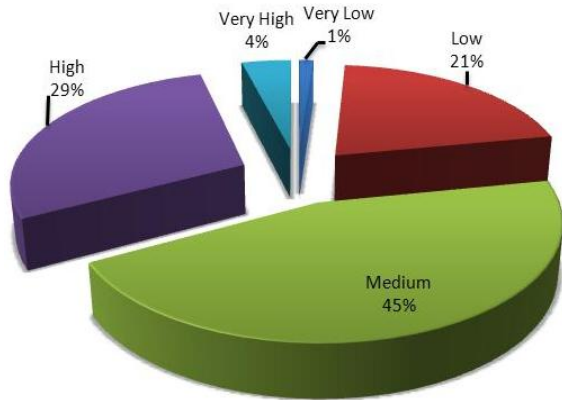
Table 7: *Table Showing Fire Risk Percentage*

Fire Risk	Percentage	Area in km^2
Very high	4%	3.0
High	29%	21.93
Moderate	45%	34.45
Low	21%	15.84
Very low	1%	0.88

Figure 11: *Showing Fire Risk Percentage*

5.1. Fire Risk Zonation Map

A further study of risk zonation map (Figure 12) with forest type map showed that deciduous and degraded forest types having high fuel content were falling on very high and high risk areas where as moist sal and plantation were falling on low and very low fire risk areas. Very high and high fire risk areas were mostly lying in southern and western aspect having warmer and dry conditions, whereas northern and eastern slopes were falling on low and very low fire risk areas. This may be attributed to the fact that southern and western aspects receive high amount of sun insulation for the major part of the day and accordingly are warmer than other aspects. Fire could thus certainly be averted by taking precautionary measures. Hence, despite the fact that no fire prone areas can be demarcated where fire occurs due to natural or intentional human causes, it is advantageous to have a fire risk map to avert possible disasters caused by fire due to human activities. It should prove to be helpful to the Forest Department, as this type of fire risk zone map would enable the department to set up an appropriate fire-fighting infrastructure for the areas more prone to fire damage. Such a map would help in planning the main roads, subsidiary roads, inspection paths, etc. and may lead to a reliable communication and transport system to efficiently fight small and large forest fires.

Figure 12: *Forest Fire Risk Zonation Map*

5.2. Validation of Forest Fire Risk Model

The final forest fire risk model was validated with past fire incidences data that was collected from field visits and fire points were taken from Forest Survey of India website. The results of the study showed that out of 27 fire incidences 20 incidences had occurred in very high and high risk areas.

6. Conclusion

Fire risk modeling using multi criteria analysis and integrating different layers resulted in developing fire risk assessment of study area. Fire risk index map can be used to prioritize for taking forest fire prevention initiatives at management level. Forest type, density maps and other parameters can be helpful in installation of suitable watch towers for prevention of fire.

Layers generation for slope altitude and forest density can be used for calculating response time for the disaster. Digital elevation model can be effectively used for studying terrain characteristics and for generating a view shed.

The precision in the modeling could be increased by adding more number of variables in the analysis. However, the selection of variables should be based on knowledge base of the area. The areas shown under very high, high and moderate 'fire risk' zones are those areas where fire can be unintentionally caused by human activities, and where fire could thus certainly be averted by taking precautionary measures. Hence, despite the fact that no fire prone areas can be demarcated where fire occurs due to natural or intentional human causes, it is advantageous to have a fire risk map to avert possible disasters caused by fire due to human activities. It should prove to be helpful to the Forest Department, as this type of fire risk zone map would enable the department to set up an appropriate fire-fighting infrastructure for the areas more prone to fire damage. Such a map would help in planning the main roads, subsidiary roads, inspection paths, etc. and may lead to a reliable communication and transport system to efficiently fight small and large forest fires.

Acknowledgment

References

[1] Butry D.T., et al. *What is the Price of Catastrophic Wildfire*? Journal of Forestry. 2001. 99; 9-17.

[2] Burke T.E., et al. *An Internet–Based Forest Fire Information System*. Unasylva. 1997. 48 (2) 32-38.

[3] Pettenella D., et al., 2009: *Proposal for a Harmonized Methodology to Assess Socio-Economic Damages from Forest Fires in Europe*. Final Reports of Studies on Forest Fires Done Under Forest Focus Regulation. Economic Damages Study. Joint Research Centre (JRC) and the Directorate General for Environment (DG ENV) of the European Commission (EC).

[4] Hernandez-Leal P.A., et al. *Fire Risk Assessment Using Satellite Data.* Advances in Space Research. 2006. 37; 741-746.

[5] Hussin Y.A., et al. 2008: *The Applications of Remote Sensing and GIS in Modeling Forest Fire Hazard in Mongolia*. The International Archives of the Photogrammetry, Remote Sensing and Spatial Information Sciences, ISPRS Archives -Volume XXXVII, Part B5, Beijing, China, 289–294.

[6] Chuvieco E., et al. *Development of a Framework for Fire Risk Assessment Using Remote Sensing and Geographic Information System Technologies*. Ecological Modelling. 2010. 221 (1) 46-58.

[7] Keane R.E., et al. *A Method for Mapping Fire Hazard and Risk across Multiple Scales and Its Application in Fire Management.* Ecological Modelling, 2010. 221; 2-18.

[8] Kunwar P., et al. *Spatial Distribution of Area Affected by Forest Fire in Uttaranchal using Remote Sensing and GIS Techniques*. Journal of Indian Society of Remote Sensing, 2003. 31 (3).

[9] Chuvieco E., et al. *Application of Remote Sensing and Geographic Information Systems to Forest Fire Hazard Mapping.* Remote Sensing of Environment. 1989. 29; 147-159.

[10] Deeming J. E., et al, 1978: *The National Fire Danger Rating System*. Gen. Tech. Rep. INT-39. Department of Agriculture, Forest Service, Ogden, 63.

[11] Cuomo V., et al. *Evaluation Of A New Satellite Based Method For Forest Fire Detection*. International Journal of Remote Sensing. 2001. 22 (9) 1799-1826.

[12] Alvador S., et al. *Asemi-Automatic Methodology to Detect Fire Scars in Shrubs and Evergreen Forest with Landsat MSS Time Series.* International Journal of Remote Sensing. 2000. 21; 655-67.

[13] Jaiswal R.K., et al. *Forest Fire Risk Zone Mapping From Satellite Imagery and GIS*. International Journal of Applied Earth Observation and Geoinformation. 2002. 4; 1-10.

[14] Jain A., et al. *Forest Fire Risk Modeling using Remote Sensing and Geographic Information System.* Current Science. 1996. 70 (10) 928.

[15] Roy N., et al. Forest Fire Risk Zonation using Geo-spatial Modeling in Part of Rajaji National Park, India. Asian Journal of Geoinformatics. 2004. 5 (2).

[16] Chuvieco E., et al. *Mapping the Spatial Distribution of Forest Fire Danger Using GIS*. International Journal of Geographical Information Systems, 1996. 10 (3) 333-345.

Cloud Publications

Research Article	Open Access

Morphometric Analysis of Tandava River Basin, Andhra Pradesh, India

G. Ashenafi Tolessa, P. Jagadeeswara Rao and N. Victor Babu

Department of Geo-Engineering, College of Engineering (A), Andhra University, Visakhapatnam, Andhra Pradesh, India

Correspondence should be addressed to G. Ashenafi Tolessa, glovashu@gmail.com

Abstract The seasonal abrupt flood event in the Tandava River Basin was the major loss for socio-economic infrastructure. The main objective of this study is to characterize the Morphometric parameters of Tandava River Basin (TRB) which depicted on toposheets 65; K/5, K/6, K/7, K/10 and K/11 with scale 1:50,000 were used for Morphometrical analysis. In this study, morphometric parameters were delineated through onscreen digitization on topographic map in ArcGIS-9.3. The TRB is covering about 1283 Km^2 consists of hills, valleys and plains. The longest flow path was calculated and found to be 83.360 Km. The study reveals that; such information derived from GIS would be very useful in practicing water management activity and designing of water harvesting project with minimum cost, efforts and time in reducing rates of natural degradation in the basin.

Keywords *Morphometry, Tandava River Basin, Drainage Characteristic, Sub-Basins*

1. Introduction

Morphometric study has got its foundation from stream flow analysis. Morisawa [1], who observed that stream flow, can be expressed as a general function of geomorphology of a sub-basin. The assertion still stand valid following Jain and Sinha [2], Okoko and Olujimi [3] and Ifabiyi [4] who reported that the geomorphic characteristics of a drainage basins play a key-role in controlling the basins hydrology. Morphometric analysis is a bit very advantageous for the study of minor (intermittent) river like Tandava River Basin and hence this study is intended to present the characteristic of Tandava River Basin (TRB) by following scientific formula and procedures.

2. Study Area

The area of study is bounded in between latitudes $17^0 20$'N to $17^0 50$`N and longitudes $82^0 20$`E to $82^0 40$' E. It forms part of Survey of India Toposheets 65 K/5, K/6, K/7, K/10 and K/11 and covers an area of 1283 Km^2. Major part of the area is in Visakhapatnam district but adjacent part of East Godavari district is also included to see the total morphometry of the drainage basin (Figure1).
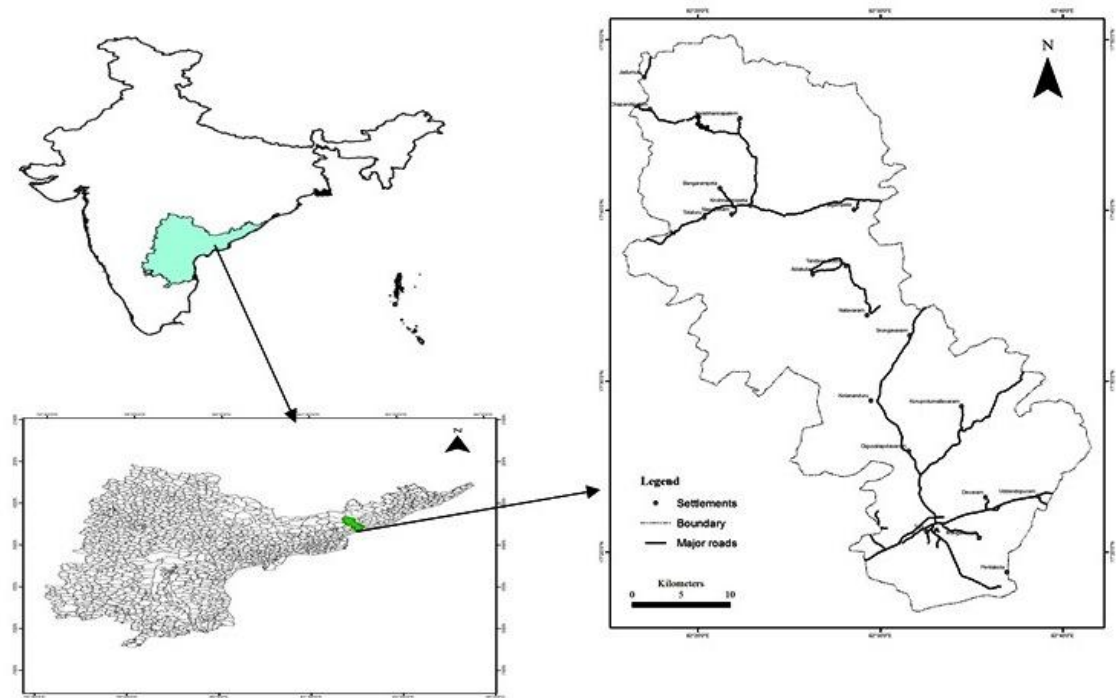
Figure 1: Location Map of the Study Area
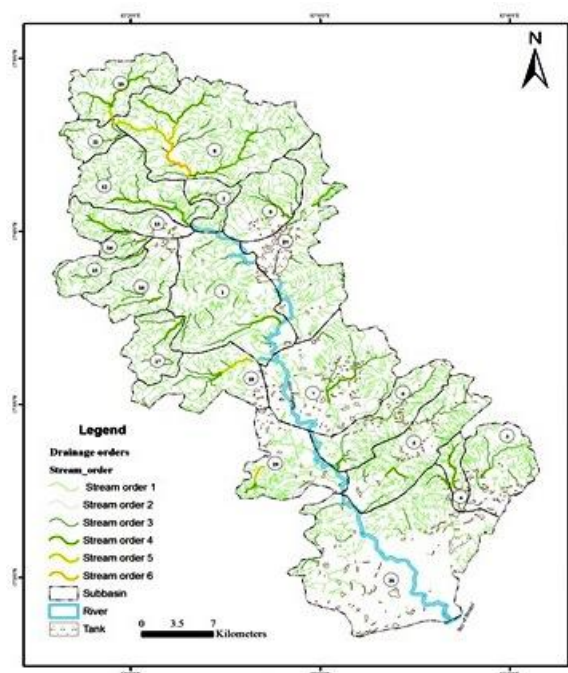
Figure 2: Drainage Network of Tandava River Basin

3. Methodology

This work is based on map analysis carried out onscreen digitization. Toposheet number 65; K/5, K/6, K/7, K/10 and K/11 with the scale of 1:500,000. (Survey of India) were mosaic to subset the study region. The subset image is geometrically corrected through the process of rectification. Strahler's, Horton's and Schumm's methods have been employed to assess the fluvial characteristics of the

study region [5, 6]. The maps were georeferenced and digitized in ArcGIS-9.3 and Erdas Imagine-9.1 software's and attributes were assigned to create the digital database (Figure 3). The map showing drainage pattern in the study area (Figure 2) was draped over ASTER 30m resolution and SRTM 90m resolution DEM data for further clarification. Morphometric analysis was carried out at sub-basin level in the GIS System (ArcGIS - 9.3). Based on the drainage order, the drainage channels were classified into different orders [6]. In GIS, drainage channel segments were ordered numerically as order number 1 from a stream's headwaters to a point downstream. The stream segment that results from the joining of two first order streams was assigned order 2.
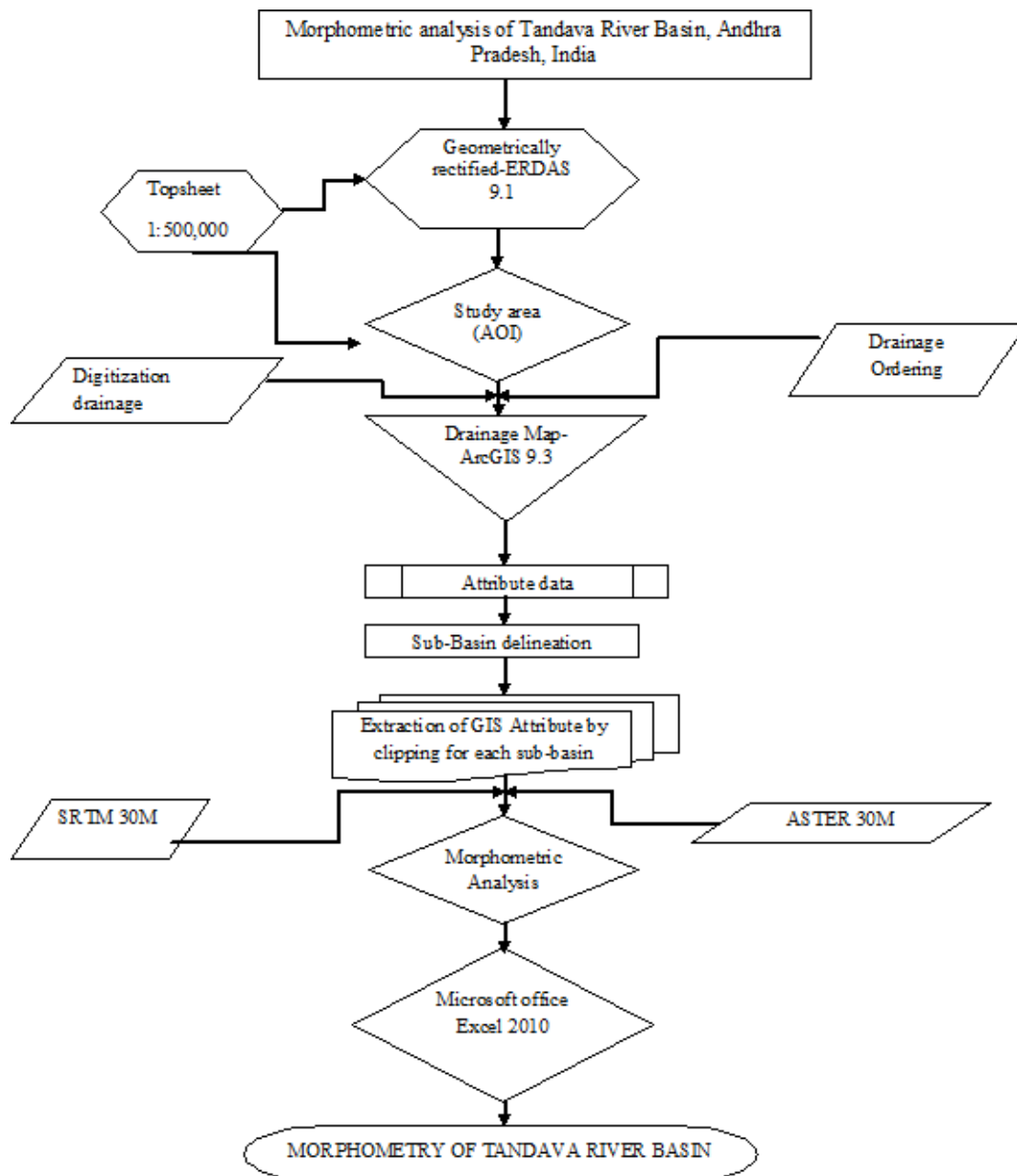
Figure 3: Flow Chart of Methodology

4. Results and Discussion

Various morphometric result of TRB is calculated in ArcGIS-9.3 and is summarized in tables. The basin area is divided into 21 sub-basins of fourth order streams. Orders above the fourth were disregarded because the relatively small sample of these streams is less reliably representative than those of the lower order [7] (Table 1).

Table 1: Area and Perimeter of Sub-Basin of TRB

Sub-Basin	Area	Perimeter
1	113	49
2	17	25
3	51	31
4	14	20
5	74	47
6	54	41
7	61	39
8	111	44
9	140	56
10	74	43
11	46	35
12	17	20
13	60	43
14	30	30
15	10	13
16	23	24
17	43	32
18	31	27
19	53	41
20	55	39
21	206	74

4.1. Linear Aspect

Drainage basin analyses begin by designation of stream orders. The channel segment of the drainage basin has been ranked according to Strahler stream ordering system using ArcGIS-9.3 The study area is a 6th order drainage basin [6] (Figure 2). The total number of 3882 streams identified of which 2851 are 1st order which is 73.44%, 828 are 2nd order which amounts 21.32%, 176 are 3rd order which is 4.53% and 27 in 4th order which is 0.69% (Table 2) .

Table 2: Number of Streams in Each Order in Each Sub-Basin

Sub-Basin No.	Number of Streams in Each Order				
	N_1	N_2	N_3	N_4	ΣN
1	277	67	25	1	370
2	55	15	5	1	76
3	100	23	6	1	130
4	38	13	4	1	56
5	243	51	12	1	307
6	146	179	12	1	338
7	171	47	9	1	228
8	383	89	22	3	497
9	97	25	5	1	128
10	109	23	6	2	140
11	42	9	4	2	57
12	164	41	11	1	217
13	65	18	5	1	89
14	31	7	3	1	42
15	68	23	6	1	98
16	103	23	6	1	133
17	79	17	4	1	101
18	97	29	9	2	137
19	126	30	6	2	164
20	266	56	9	1	332
21	191	43	7	1	242
Total Streams	2851	828	176	27	3882

In the study, streams of relatively smaller lengths are characteristics of areas with larger slopes such as sub-basin 2, 4, 10, 11, 14, 15 and 18 shows large slope and finer texture. The relationship between stream order Vs log of number of stream and log of total length was examined (Figures 4a & 4b), it seems to be in geometric progression and agree with Horton's law of stream length. The study shows the total length of stream decreases with increasing order of stream. The stream lengths of different order of streams of TRB are given in Table 3.
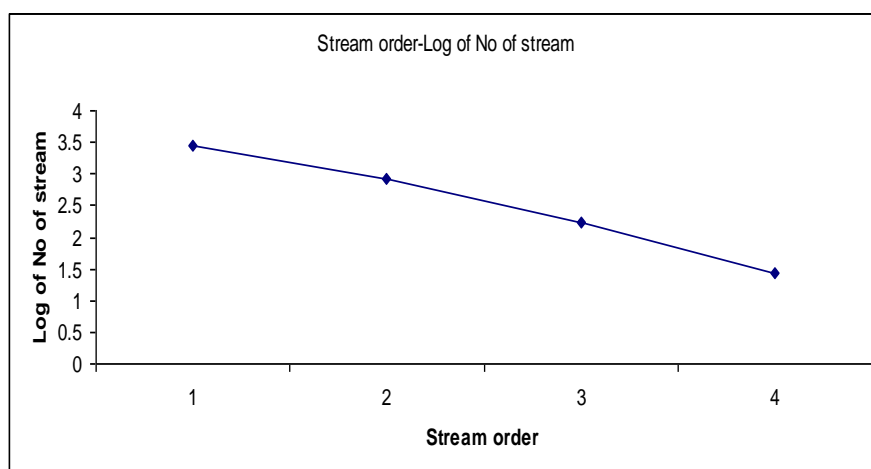
Figure 4: a) Stream Order V_S Log of No. of Streams

Table 3: *Area (Km^2), Number of Streams Length in Each Order, and Mean Stream Length and Cumulative Stream Length in 21 Sub-Basins of TRB*

Sub-basin	Area	Basin length	L_1	L_M	L_2	L_M	L_3	L_M	L_4	L_M	Cumulative stream length
1	113	58.694	159.80	0.58	43.96	0.66	15.48	0.56	3.53	3.53	61.92
2	17	10.820	29.60	0.54	7.70	0.51	2.46	0.53	1.38	1.38	14.09
3	51	24.302	60.95	0.61	20.15	0.88	15.06	1.00	1.05	1.05	27.21
4	14	8.309	21.38	0.56	4.53	0.35	3.10	1.26	4.86	4.86	12.55
5	74	46.553	130.33	0.54	37.41	0.73	16.06	1.00	2.41	2.41	50.56
6	54	36.097	90.83	0.62	31.32	0.17	20.38	1.00	1.85	1.85	38.32
7	61	41.962	103.75	0.61	37.05	0.79	13.12	0.61	5.37	5.37	45.04
8	111	83.360	209.84	0.55	69.28	0.78	21.67	0.61	18.83	6.28	31.29
9	140	25.760	63.57	0.66	26.08	1.04	12.16	1.18	3.12	3.12	29.57
10	74	27.682	68.52	0.63	24.06	1.05	7.63	0.74	7.77	3.89	17.97
11	46	11.559	20.56	0.49	8.94	0.99	11.83	0.72	0.21	0.11	8.04
12	17	38.620	93.10	0.57	35.80	0.87	3.64	0.23	9.70	9.70	42.23
13	60	17.158	45.25	0.70	15.52	0.86	27.48	8.49	4.62	4.62	23.68
14	30	7.055	18.48	0.60	5.49	0.78	3.24	0.89	0.62	0.62	10.23
15	10	14.741	35.10	0.52	15.22	0.66	4.60	0.60	1.02	1.02	17.53
16	23	23.617	54.31	0.53	26.88	1.17	15.87	1.34	1.45	1.45	26.87
17	43	18.120	43.29	0.55	14.13	0.83	8.26	0.68	2.89	2.89	20.90
18	31	25.564	59.57	0.61	27.10	0.93	12.29	0.94	2.46	1.23	15.88
19	53	28.065	78.01	0.62	29.65	0.99	10.38	3.34	1.50	0.75	24.23
20	55	52.424	144.28	0.54	48.73	0.87	20.19	1.30	1.21	1.21	56.94
21	206	44.881	121.52	0.64	47.73	1.11	7.38	1.00	2.89	2.89	52.24
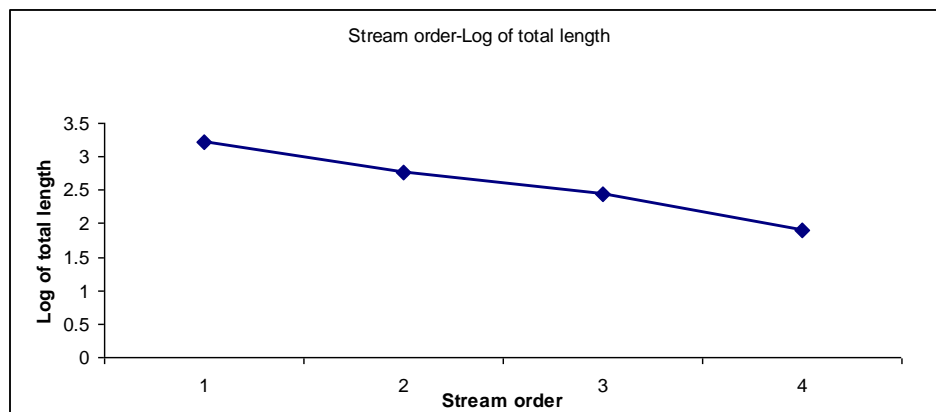
Figure 4: *b) Stream Order V$_S$ log of Total Length*

4.2. Areal Aspects

4.2.1. Drainage Density (D$_d$)

The drainage density of the study area is 0.702 Km/ Km^2. This value indicates that for every square kilometer of the basin, there is 0.702 kilometer of stream channel. In other word, 0.702 is the mean length of stream channel for each unit area. According to Deju values of drainage density under 0.5 are poor density; those with values of 0.5 to 1.5 are medium density basins while basins with values above 1.5 are excellent density basins [8]. From this classification, TRB falls into the group of medium density basins. It is suggested that the poor drainage density in sub-basin 8, 9, 10, 11, 13, 14, 17, 19 and 21 indicates highly permeable subsoil and thick vegetative cover [9]. The type of rock also affects the drainage density.

4.2.2. Stream Frequency (F_u)

Stream frequency is the ratio of number of streams in a drainage basin to the area of the drainage basin [4]. The TRB area has a stream frequency of 85.267 streams per Km. The value of stream frequency for the basin exhibit positive correlation with the drainage density value of the area indicating the increase in stream population with respect to increase in drainage density.

Table 4: Stream Frequency, Drainage Density, Types of Drainage, Constant Channel Maintenance

Sub-basin No.	Area	Stream Frequency	Drainage Density	Types of Drainage	Constant of Channel Maintenance
1	113	3.274	0.548	M	1.825
2	17	4.471	0.829	M	1.207
3	51	2.549	0.534	M	1.874
4	14	4.000	0.897	M	1.115
5	74	4.149	0.683	M	1.464
6	54	6.259	0.710	M	1.409
7	61	3.738	0.738	M	1.354
8	111	4.477	0.282	P	3.548
9	140	0.914	0.211	P	4.735
10	74	1.892	0.243	P	4.119
11	46	1.239	0.175	P	5.722
12	17	12.765	2.484	E	0.403
13	60	1.483	0.395	P	2.534
14	30	1.400	0.341	P	2.932
15	10	9.800	1.753	E	0.570
16	23	5.783	1.168	M	0.856
17	43	2.349	0.486	P	2.057
18	31	4.419	0.512	M	1.953
19	53	3.094	0.457	P	2.187
20	55	6.036	1.035	M	0.966
21	206	1.175	0.254	P	3.943

4.2.3. Drainage Texture (T)

According to Smith the drainage texture may be defined as the relative spacing of drainage lines. The drainage density and drainage frequency have been collectively defined as drainage texture. Based on the values of T it is classified as [10]:
0 – 4 – Coarse
4 – 10 – Intermediate
10- 15 – Fine
>15 – Ultra Fine (bad land topography)

A. *Texture Ratio* The first order streams being the maximum in number, they are considered to be equivalent number to crenulations in the present investigation. The texture ratio directly or indirectly reflects the drainage density. It has been generally marked that the texture ratio increases with the increase in the area of the intrabasins. The texture and texture ratio are calculated for the 21 sub-basins using definition and the values are given in Table 5. The value varies from low of 0.193 for Sub-basin No. 9 to high 31.71 for sub-basin No. 12. For TRB the mean drainage texture ratio is 3.765 indicating the massive and resistant rocks cause coarse texture. Coarse drainage density is likely to

appear in areas of permeable rocks and low rainfall intensity. A drainage basin in humid regions often shows medium drainage density. The value of Weighted means texture ratio (T_m) for TRB is 0.174. Thus, the weighted mean topographic texture (0.18) of TRB is a coarse texture.

***Table 5:** Texture, Texture Ratio, Weighted Mean Texture*

Sub-Basin No.	Texture	Texture Ratio (T_m)	Weighted Mean (T_m)
1	1.794	5.653	0.498
2	3.705	2.200	0.029
3	1.360	3.226	0.128
4	3.586	1.900	0.021
5	2.834	5.170	0.298
6	4.441	3.561	0.150
7	2.760	4.385	0.208
8	1.262	8.705	0.753
9	0.193	1.732	0.189
10	0.459	2.535	0.146
11	0.217	1.200	0.043
12	31.709	8.200	0.109
13	0.585	1.512	0.071
14	0.477	1.033	0.024
15	17.181	5.231	0.041
16	6.755	4.292	0.077
17	1.142	2.469	0.083
18	2.263	3.593	0.087
19	1.415	3.073	0.127
20	6.250	6.821	0.292
21	0.298	2.581	0.414

4.2.4. Bifurcation Ratio (R_b)

Horton [5] had defined the bifurcation ratio as the ratio of the number of streams of an order to the number of those in the next higher order. According to Strahler [6], the values of bifurcation ratio characteristically range between 3.0 and 5.0 for drainage basin in which the geological structures do not disturb the drainage pattern. The bifurcation ratio varies with the variations in drainage basin geometry and lithology and displays geometric similarity. The bifurcation ratio is estimated to be 5.17; on the average, there are 3 times as many channel segments of any given order as of the next higher order. It varies between 2.97 and 10.60, which indicates the control of the lithology and geologic structures giving rise to the distorted trellis drainage pattern and the geological disturbances such as faults and folds are encountered frequently in the sub-basin 1, 5, 6, 7, 8, 11, 12, 20 and 21 and hence, the mean bifurcation ratio of all 21 sub-basin lies between 2.97 and 10.60 (Table 6).

Miller [11], Strahler [6], opined that lithological variations do not cause differences in bifurcation ratio. Because of chance of irregularities, bifurcation ratio between successive orders differ within the same basin even if a general observance of a geometric series exists [12], thus, the bifurcation ratio of the first, second and third orders differ from each order in each of the sub-basin. In the present study, the higher values of Rb indicates strong structural control on the drainage pattern, while the lower values indicative of sub-basin that are not affect by structural disturbances.

Table 6: Bifurcation Ratio in Individual Sub-Basins of TRB

| Sub-Basin No. | Bifurcation Ratio | | | |
	Rb_1	Rb_2	Rb_3	Mean Rb
1	4.13	2.68	25	10.60
2	3.67	3.00	5	3.89
3	4.35	3.83	6	4.73
4	2.92	3.25	4	3.39
5	4.76	4.25	12	7.00
6	0.82	14.92	12	9.24
7	3.64	5.22	9	5.95
8	4.30	4.05	7.33	5.23
9	3.88	5.00	5	4.63
10	4.74	3.83	3	3.86
11	4.67	2.25	2	2.97
12	4.00	3.73	11	6.24
13	3.61	3.60	5	4.07
14	4.43	2.33	3	3.25
15	2.96	3.83	6	4.26
16	4.48	3.83	6	4.77
17	4.65	4.25	4	4.30
18	3.34	3.22	4.5	3.69
19	4.20	5.00	3	4.07
20	4.75	6.22	9	6.66
21	4.44	6.14	7	5.86

4.2.5. Elongation Ratio

Smaller the fraction more elongated is the shape of the basin, and larger the fraction the more circular is the shape of the basin. It is generally marked that the elongation ratio remains high where rock strata is hard and slope remains steep. The elongation ratio value of the study area is 0.172; the basin in the study area assumes a rotundity and low degree of integration characteristics.

4.2.6. Circulatory Ratio (R_c)

The study reveals that the circularity ratio value (0.505) of the basin does not corroborates the Miller's range which indicated that the basin is weakly elongated in shape, high discharge of runoff and highly impermeability of the subsoil condition but rather the basin of the study area is rotundity and low degree of integration characteristics.

4.2.7. Form Factor (R_f)

The ratio of the basin area to the square of basin length is called the form factor. The form factor of the TRB is 0.12 Km^{-1}. It is used as a quantitative expression of the shape of basin form which is stretched elliptical. The form factor for all sub-basin varies from 0.01 – 0.6 (Table 7). This observation shows that the sub-basins are more or less circular. The elongated Sub-basin with low value of R_f indicates that the basin will have a flatter peak flow for longer duration. Flood flows of such circular basins are difficult to manage than from the elongated. Among the TRB's Sub basins; Sub-basin 14 with the form factor 0.6 seems to be highly elongated when compared to other Sub-basins of the drainage basins. Analysis of form factor (R_f) reveals that sub-basins having low R_f have less side flow

for shorter duration and high main flow for longer duration. The sub-basin with high R_f have side flow for longer duration and low main flow for shorter duration causing high peak flows in a shorter duration.

Table 7: Dimensionless Ratio (Elongation, Circularity and Form Factor)

Sub-Basin No.	Area(A_u)	Perimeter	Mean Stream Length	Elongation	Circularity	Form Factor
1	113	49	58.69	0.102	0.591	0.03
2	17	25	10.82	0.215	0.342	0.15
3	51	31	24.30	0.166	0.667	0.09
4	14	20	8.31	0.254	0.440	0.20
5	74	47	46.55	0.104	0.421	0.03
6	54	41	36.10	0.115	0.403	0.04
7	61	39	41.96	0.105	0.504	0.03
8	111	44	83.36	0.071	0.720	0.02
9	140	56	25.76	0.259	0.561	0.21
10	74	43	27.68	0.175	0.503	0.10
11	46	35	11.56	0.331	0.472	0.34
12	17	20	38.62	0.060	0.534	0.01
13	60	43	17.16	0.255	0.408	0.20
14	30	30	7.06	0.438	0.419	0.60
15	10	13	14.74	0.121	0.743	0.05
16	23	24	23.62	0.115	0.502	0.04
17	43	32	18.12	0.204	0.527	0.13
18	31	27	25.56	0.123	0.534	0.05
19	53	41	28.07	0.146	0.396	0.07
20	55	39	52.42	0.080	0.454	0.02
21	206	74	44.88	0.180	0.472	0.10

5. Conclusion

The study come across the conclusion is that the Morphometric study for river basin especially for those which exposed seasonal fluctuation has a boost impact for water development, water sustainability and water resource management. The result presented and the conclusion derived in this paper will suggested and recommended to develop better water usage mechanisms for better application of the river basin.

References

[1] Morisawa M.E. *Measurement of Drainage Basin Outline Form*. Journal of Geol., 1957. 66; 86-88.

[2] Jain V., et al. *Evaluation of Geomorphic Control on Flood Hazard Through Geomorphic Instantaneous Unit Hydrograph.* Current Science .2003. 85 (11) 26-32.

[3] Okoko E.E., 2003: *The Role of Geomorphic Features in Urban Flooding: The Case of Ala River in Akure, Nigeria.* Int. Journal of Environmental Issues, 1 (1) 192-201.

[4] Ifabiyi I.P. *A Reduced Rank Model of Drainage Basin Response to Runoff in Upper Kaduna Catchment of Northern Nigeria*. Geostudies Forum. 2004. 2 (1) 109-117.

[5] Horton R.E. *Erosional Development of Streams and Their Drainage Basins: Hydro Physical Approach to Quantitative Morphology.* Geol. Soc. Am. Bull. 1945. 56: 275-370.

[6] Strahler A.H, 1964: *Quantitative Geomorphology of Drainage Basins and Channel Networks*. Handbook of Applied Hydrology, McGraw Hill Book Company, New York, 4-39/4-76.

[7] Strahler A.N. *Hypsometric (Area – Altitude) Analysis of Erosional Topography.* Geol. Soc. Amer. Bull., 1952. 63; 117-142.

[8] Deju A. Raul, 1971: *Regional Hydrology Fundamentals*. Gordon & Breach Publishing Group, Newark, New Jersey, United States 204.

[9] Nag S.K. *Morphometric Analysis Using Remote Sensing Techniques in the Chaka Sub basin Purulia District, West Bengal.* J. Indian Soc. Remote Sensing. 1998. 26; 6976.

[10] Smith K.G. *Standards for Grading Texture of Erosional Topography*. Am J Sci. 1950. 248; 655668.

[11] Miller V.C., 1953: *A Quantitative Geomorphic Study of Drainage Basin Characteristics in the Clinch Mountain Area*, Virginia and Tennessee. NR Technical Report 3, Office Naval Research Project.

[12] Schumm S.A. *The Evolution of Drainage Systems and Slopes in Badlands at Perth Amboy, New Jersey*, Geol. Soc. Amer. Bull., 1956. 67: 597-646.

Research Article   **Open Access**

Assessment of Spatial Distribution of Rural Crime Mapping in India: A GIS Perspective

Thangavelu A.[1], Sathyaraj S.R.[2], and Balasubramanian S.[3]

[1]Department of Environmental Science, Central University of Kerala, Kasaragod, Kerala, India
[2]DRDO-BU CLS, Bharathiar University, Coimbatore, Tamil Nadu, India
[3]Department of Environmental Science, JSS University, Mysore, Karnataka, India

Correspondence should be addressed to Thangavelu A., thangavelgis@gmail.com

Article Link: http://technical.cloud-journals.com/index.php/IJARSG/article/view/Tech-62

Abstract This paper identifies the distribution of the crimes to challenge facing the police departments that pursue to implement computerized crime mapping systems. The paper highlights the importance of police departments identifying the thematic mapping creating for the rural crime areas. The Geographical Information system (GIS) also using for the how to we create for the crime maps and which mode we are giving the solution for the society or environment. GIS can be used as a tool to identify factors contributing to crime, and thus allow police to proactively respond to the situations before they become problematic. Generally, GIS includes data transfer, geocoding, data integration, system customization, and confidentiality issues are discussed in detail. Finally, we have illustrated the temporal crime incidences also implementing for the GIS analysis. This article will explore the use and possibilities of GIS by Indian Police in describing and analyzing crime action.
Keywords *Crime Data, Distribution, GIS, Spatial Analysis, Temporal Incidence, Thematic Mapping*

1. Introduction

Crime mapping is the use of geographic information to identify and analyze crime and police data. In 1990s, "crime mapping" referred to geographic analysis, even those that involved pushpins, colored dots, and paper maps. Now, however, "crime mapping" usually means the specific use of computerized GIS. Criminal investigative analysis is smaller in use which determines the aspect of crime analysis that includes activities such as geographic profile [1, 2, 3] and specific case support for crime investigations. The history of crime mapping enhanced from the supportive result [4, 5].

Computerized crime maps have recently begun to emerge as a significant tool only in crime and justice that assists police departments in strategic planning, operations and crime analysis. They may display information about the relationships between geographic areas, crime and a number of risk factors. As crime and delinquency are known to be localized processes, criminological maps have proved useful in assisting police operations and in supporting crime prevention initiatives [4]. Maps

also assist in the assessment of the regional distribution of crime. Computerized crime mapping is rapidly a developing technology that assists police departments in strategic planning. The method of investigation is to quickly view and compare patterns of the crime events. Crime has abundant references relating crime patterns to specific geographic features for example, some crimes such as robbery, snatching and pocket picking, may be particularly enhanced by the existence of commercial areas, parking places and industrial complexes [1, 6].

Criminal geographic targeting is based on study of Brantingham and Brantingham (1981) model for crime site selection and recurrence of such activities [7]. Geographic analysis of crime is strongly supported [8, 9] and the practical applications of this analysis have been demonstrated [10, 11, 12, 13]. Some areas are more prone to criminal activities than the others [14, 15] and majority of crimes are not random events, nor are they randomly distributed in terms of where they occur [16]. Spatial variability is a result of the spatially non-random distribution of people who will be motivated to be responsible for a crime and the spatially non-random distribution of causative factors that increase the chances that a person or property will be victimized [17].

Automated crime mapping applications [18, 19] shows the potential results for visual representations of the crime patterns through the spatial maps by the computer. The crime setting or place, the "where and when" of the criminal act, (Brantingham and Brantingham, 1981) describe the fourth dimension of crime, which is the primary concern of environmental criminology.

Criminological theory has two control factors for analysis,

(i) Individual
(ii) Communities

The two major questions for this theory are

(i) Why this person and not that one committed a crime?
(ii) Why is there more increased of crime in society now than before?

Brantingham and Brantingham (1994) [20] successively proved how house breaks induced crimes having the multiple effects in the neighborhoods at which they are located, raising the robbery and theft levels in the surrounding area. Crime analysis may help in the determination of multiple effects of crime and to improve the efficiency of police activity [5, 21]. The incidence of crime is affected by the presence and effectiveness of the police [22, 23, 24, 25].

Crime distribution can be identified on the maps like choropleth maps which use color pattern, shading to indicate the magnitude of a numeric variable. Isopleth map lines are the geographic distribution of a value category. Isopleth or contour maps are used to create continuous areas that connect the points which are having the same value. The contour lines are superimposed on a layer that displays the geographic boundaries. A cartogram is a variant of the choropleth map in which the two dimensional boundaries of geographic units are distorted so that the surface area of each geographic unit is proportional to the amount of the value being measured.

Crime density was used [26, 27] for investigating the associates of crime through statistical models. Furthermore, it is also possible to employ GIS to calculate density of crime in a more accurate way under certain circumstances.

2. Objective

The present study is to produce crime distribution maps based on the following dimensions of the criminal instances in Coimbatore rural police jurisdiction.

    i. Allocation of police stations
    ii. Boundary of police stations
    iii. Crime rate and density in a specific area
    iv. Trend of crime in a given time frame
    v. Top five prominent crime types
    vi. To prepare the thematic map of crime distribution incidences
    vii. To measure the crime data in statistical analysis crime rate
    viii. To summarize the temporal incidences in the particular areas in Coimbatore rural police jurisdiction.

3. Study Area

Coimbatore is popularly famous as 'The Manchester of South India'. Coimbatore district of Tamilnadu has geographic area of 105.60 Square Kilometer. Coimbatore rural division is situated between 10° 68" and 11°16" Northern latitude and 76.68° and 77.15° Southern longitude in the extreme west of Tamil Nadu near Kerala. The study area for this expression is India, in the State of Tamilnadu; Coimbatore coordinates rural zones which have been identified by the Development of Police as an area with the high number of crime hits. Coimbatore rural police jurisdiction area has been divided into two sub-division namely Perur.and Periyanaickenpalayam. Totally, fourteen police jurisdictions namely Sirumugai, Mettupalayam, Pillur, Karamadai, Periyanaickenpalayam, Thudiyalur, Vadavalli, Thondamuthur, Alandurai, Karunya, Perur, Madukarai, Podanur and Kinathukadavu.

4. Data Preparation and Methodology

The Crime incidence data is collected from the Superintendent of Police Office (SPO) and the Population data from Census of India for the preparation of the spatial crime map for the present two subdivisions and fourteen police stations in the Coimbatore rural jurisdictions with the help of software ArcGIS 9.1. The methodology includes the use of the digitized map of the rural jurisdictions in Coimbatore. The attribute data table of this area consisted of SPO name, jurisdiction to which it belongs, crime incidence data, the population size of the area under the SPO, the number of police stations and the number of subdivisions in each constituency.

The population density of each SPO area was calculated based on population/ area in sq. kms. This value was used as a factor to prepare crime map of the population level for crime incidence in Coimbatore rural division. Maps are prepared thematically to identify the crime areas based on the data available for the population and natural breaks. The population based on the were identified three classes namely highly populated, moderately populated and lowly populated.

5. Crime Incidences in Rural Police Jurisdiction

5.1. Thematic Map of Crime incidences in Rural Police Jurisdiction

Thematic mapping is the process of representing the geographical database on the attribute data available and the value, size, color, represents the data on the map. Thematic maps can be used to highlight individual features or illustrate a series of features. Thematic mapping involves data classification methods, which is known as the most common method for map manipulation. Generally, five data classification methods are available: equal interval, frequency levels, mean and standard

deviation, natural breaks and a user defined. Equal interval uses a constant class interval in classification. Equal frequency, also called quantile, divides the total number of data values by the number of class and ensures that each class contain the equal proportion of area. Mean and standard deviation sets the class breaks at the units of standard deviation above or below the mean. The method of natural breaks uses a computing algorithm to minimize differences between data values in the same class and to maximize differences between classes. For the present study, natural break classification methods were chosen to prepare maps.

5.2. Distribution of Crime Incidences

As mentioned earlier, the study area boundary is digitized and used for creating the distribution of mean crime incidences in Coimbatore city. There are fourteen police stations Sirumugai, Mettupalayam, Pillurdam, Karamadai, Periyanaickenpakayam, Thudiyalur, Vadavalli, Perur, Thondamuthur, Alandurai, Karunya, Madukarai, Podanur and Kinathukadavu. The jurisdictions having low moderate geographical area are Thondamuthur, Vadavalli, and Podanur present in the rural police division limits and under the superintendent of police.

The mean criminal incidences (2003-2006) of Coimbatore rural police division were used for the preparation of thematic maps. For this present study, natural break classification was used to classify the criminal incidence data for thematic mapping.

It was observed that out of the fourteen jurisdictions in Coimbatore rural police jurisdiction, one jurisdiction was classified as high incidence jurisdiction (Thudiyalur), five jurisdictions were classified as moderate jurisdictions Mettupalayam, Karamadai, Periyanaickenpakayam, Vadavalli and Podanur as area two jurisdictions were identified as moderate (Sirumugai and Perur) in the low incidence area, and the remaining six jurisdictions were identified (Pillurdam, Thondamuthur, Alandurai, Madukarai, Karunya and Kinathukadavu) as very low incidence areas.

The total area of the Coimbatore rural police boundary covers about 142.35 Sq.kms. The high incidence area covers nearly 16.97 Sq.kms and the calculated percentage of that area covered is 11.92% .The moderate incidence area occupies 57.64 Sq.kms and the percentage is 40.48%. The low incidence area covers 17.41 Sq.kms (12.22%) and the remaining very low incidence area covers 51.36 Sq.kms (36.08%). However, the increasing number of incidences depends on the density of the population rather than the area occupied. Therefore, a density based thematic map was prepared.

5.3. Temporal Crime Incidences

The collected crime incident for four years are calculated from the basic records and represented in the temporal observation Table 1. The rate of crime incidents for the reported cases is decreased with effect of this thematic preparation of the crime areas. But the trend was not uniform for crime records. It is increasingly and decreasingly reported from the SPO action to the instruction.

For the year 2003-2006, auto vehicle crime thematic map was prepared and presented as Map 1 by using Natural breaks classification. The thematic map was classified into very low, low, moderate and high incidence areas. The very low incidence jurisdictions are Pillur, Thondamuthur, Karunya, Thondamuthur and Kinathukadavu. The low incidences were observed in Perur and Madukarai. The moderate incidence was observed in Sirumugai, Karamadai, Periyanaickenpakayam, Vadavalli and Podanur and the remaining high incidence was observed in Mettupalayam and Thudiyalur of the Coimbatore rural jurisdiction.

The thematic map of 2003-2006 for grave crime is represented as Map 2. It shows a more or less similar pattern to that of the auto crime map. In addition to these maps, the house breaking day (HB

day) thematic map shows the increasing tendency of crime incidences in the areas than the previous type. Similarly, the moderate incidence areas were also found to decrease to low crime from six to five police stations. There is not much variation on the mean crime incidences. The pattern of criminal distribution was found to differ while studying the thematic map presented in House breaking night crime Map 4, i.e., the high incidence areas are found in the central part of the Coimbatore rural division that is Thudiyalur, Mettupalayam and Podanur.

The Map 5 of Murder for gain (MF gain) Mettupalayam, Periyanaickenpakayam, Thudiyalur and Podanur, shows moderate incidences and the remaining areas show high, low and very low incidences. The temporal Map 6 of Murder crime shows more or less the same pattern as pocket picking. The high incidence area was Thudiyalur and the remaining areas showed very low, low and moderate incidences as shown in Map 7. Unfortunately, a criminal incidence data of Robbery showed very low incidence in Sirumugai and other no incidence area are presented in Map 8. (Map 1, Map 2, Map 3, Map 4).

However, in snatching crime, very low incidence areas increased to nine as represented in Map 9. High incidence areas decreased to one in Snatching. The low incidence area decreased whereas the moderate and high incidences decreased among the jurisdictions. The summary of the temporal changes of crime incidences in different jurisdictions of Coimbatore rural police jurisdiction was prepared and presented in the temporal observation. From the temporal observed that there is no jurisdiction in crime spread among and between the jurisdictions except in Thudiyalur jurisdiction.

The remaining jurisdictions shows the following pattern of distribution,

(i)   Very low and Low incidences are interchanged in some jurisdictions spatially and temporally.
(ii)   Low incidence areas changed to Moderate incidence areas
(iii) High incidences areas are distorted to moderate incidence area and
(iv)   Very low incidence areas are altered to low incidence area.

From the above observations, it is concluded that the criminal broadcast in Coimbatore rural division is mixed, which is influenced by the local environment. Control measures of the respective jurisdictions or stations are rather than a uniform outbreak as the observations carried out in other crime countries as in Iceland, Sweden, and other. Therefore, the conceptual study is required for effective measures to control criminal incidences at regional level in Coimbatore rural jurisdiction. (Map 5, Map 6, Map 7, Map 8, Map 9).

5.4. Thematic Map Prepared Using Geographical Area

From the results of Map 10, it is observed that two jurisdiction which has a large geographical area are Thudiyalur and Mettupalayam. The jurisdictions having moderate geographical areas are Sirumugai, Periyanaickenpakayam, Madukarai and Kinathukadavu. The jurisdictions having low geographical areas are Pillur dam, Karamadai and Podanur. The five jurisdictions recorded to have a very low geographical area are Vadavalli, Thondamuthur, Perur, Alandurai and Karunya below 142.35 Sq.kms.

The population distribution of the study area was collected for each Police station and represented as Map 11. From this map, it is found that Coimbatore jurisdiction has the highest recorded population in Karamadai. Thudiyalur jurisdiction has moderate area. The other jurisdictions Sirumugai, Mettupalayam, Periyanaickenpakayam Alandurai, Podanur, Madukarai and Kinathukadavu have low distributed population. The remaining five jurisdictions have low and very low distributed population.

Based on the population density of the SPO area, a characteristic was introduced in the following equation to establish a relationship between population and crime incidence. The crime rate at that particular area was calculated based on the following equation and as

$$\text{Crime rate} = \frac{\text{Number of crime in the area}}{\text{Population of the area}} \times 100000$$

For each jurisdiction area, a thematic map of crime distribution Coimbatore was prepared. Natural breaks classification method was used to classify the area into high, moderate, low and very low incidence zones. The population density of each jurisdiction was calculated based on the population by total geographical area of the jurisdictions and represented as Map 12. The highest population density in Coimbatore jurisdiction was recorded of the rural area Vadavalli. (Map 10, Map11)

Moderate density of population was recorded at Mettupalayam, Periyanaickenpakayam, Thudiyalur and Podanur. Low density of population was recorded at Sirumugai, Karamadai and Perur. The remaining jurisdictions were very low populated. The average percentage of the crime cases was calculated for four years by using the obtained values. The crime density based on population was calculated and used as a crime factor for preparing the population density on a crime map for Coimbatore rural police jurisdiction (Map 12) (Table 1).

6. Conclusion

The resultant map clearly indicates the major crime prone areas in Coimbatore rural police jurisdiction. The crime incidence map clearly visualized the regions where efforts are to be maintained for crime control. These areas require necessary funds and suitable measures. Effective suggestions, put forward are

i.   In-depth study of these areas has been taken by integrating the population wise data, heavy forces of crime controlled in the surrounding areas.

ii. Crime mapping techniques are not widespread in police forces and Home affairs office and remains to be explored to be fullest extent. It provides major availabilities at the local level for greater utilization of GIS for crime analysis.

iii. Crime analysts and problem-solvers also use computer maps to identify emerging patterns of crime activity for the using of Police department.

iv. Many police officials want to have available effective representations of crime location patterns. For analytical and decision making purposes, useful representations of hot spots and other location information are needed. Simulations are becoming more important as visualization techniques become more sophisticated.

v.   We propose that different police agencies need different types of crime mapping systems. Moreover, even within a police agency, different police functions will most likely demand different types of applications.

vi. However, this research is necessary to evaluate the above mentioned techniques for executing the map with a particular interval because accurate population data is critical for the assessment of human population density on crime rate and attribution of risk to crime incidences.

vii. Therefore, we suggest that police departments need to identify the primary end-user from the outset, and then prioritize the customization of crime mapping systems accordingly.

viii. The new technology that features mapping representations would be helpful to police, especially in the study of crime patterns in large buildings and underground structures. In general, geographic presentation is an area with vast potential for developing new types of maps and charts that can aid police authorities.

ix. Finally, the map also serves as a guide for crime affairs/surveyors/officers in identifying the proper study for environment international trials and also as assistance for the population who would be benefitted from the new interventions.

From the field work investigation, interviews and data obtained from the primary and secondary sources one could find that the high crime rate as well as different kinds of crime occur more frequently in the poorer sections of the society like that in slum prone areas, areas lacking street lights and other adequate facilities for daily living and areas having low literacy rates.
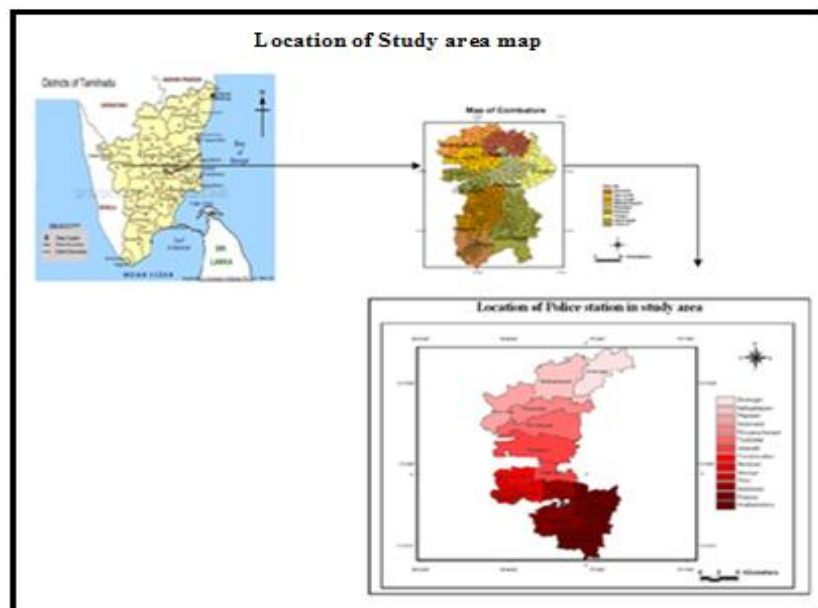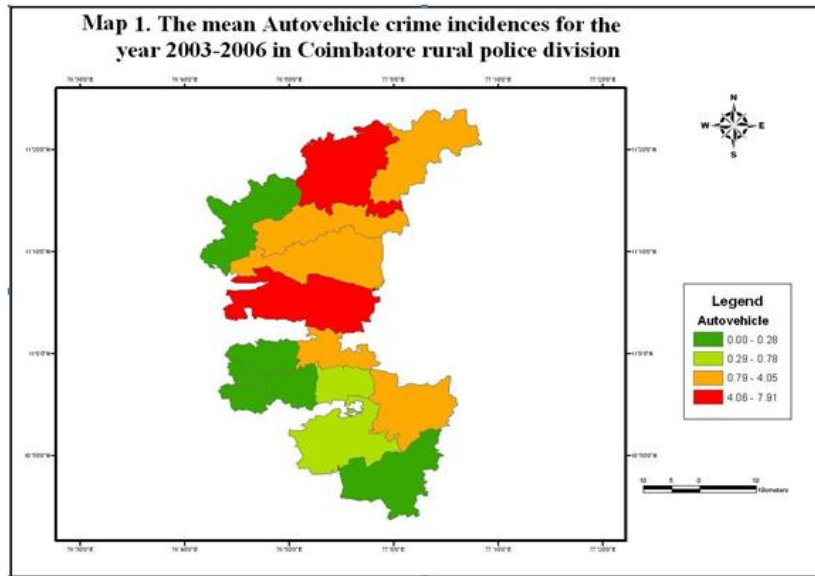
Figures

Figure 1: Location of Study Area

Figure 2: *The Mean Auto Vehicle Crime Incidences for the Year 2003-2006 in Coimbatore Rural Police Division*
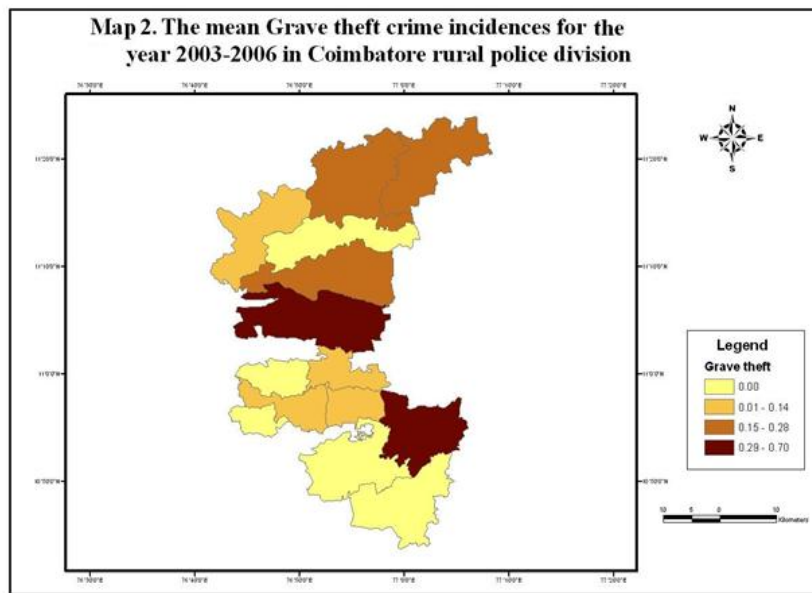

Figure 3: *The Mean Grave Theft Crime Incidences for the Year 2003-2006 in Coimbatore Rural Police Division*

Figure 4: *The Mean HB Day Crime Incidences for the Year 2003-2006 in Coimbatore Rural Police Division*

Figure 5: *The Mean HB Night Crime Incidences for the Year 2003-2006 in Coimbatore Rural Police Division*
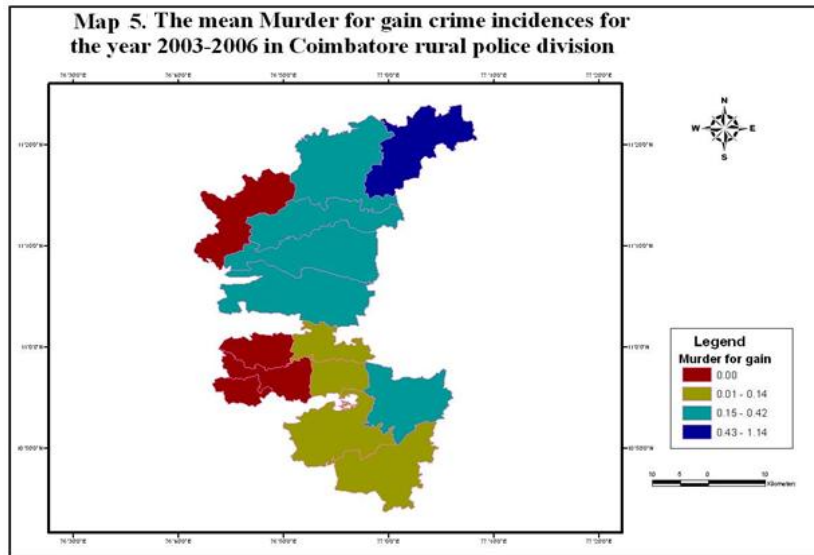
Figure 6: *The Mean Murder for Gain Crime Incidences for the Year 2003-2006 in Coimbatore Rural Police Division*
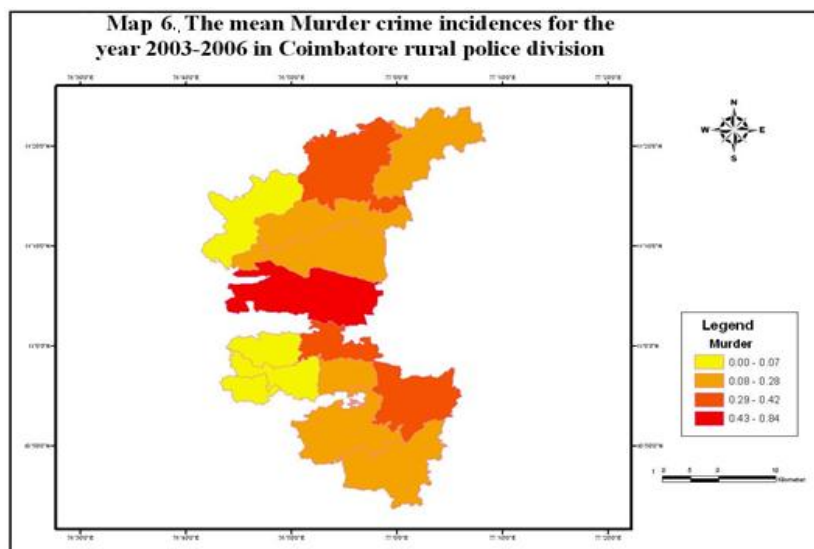
Figure 7: *The Mean Murder Crime Incidences for the Year 2003-2006 in Coimbatore Rural Police Division*
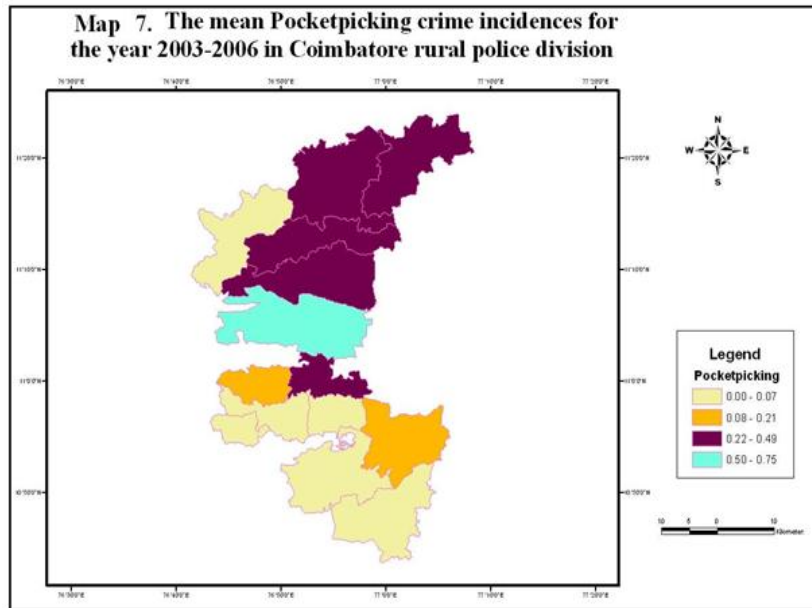
Figure 8: *The Mean Pocket Picking Crime Incidences for the Year 2003-2006 in Coimbatore Rural Police Division*
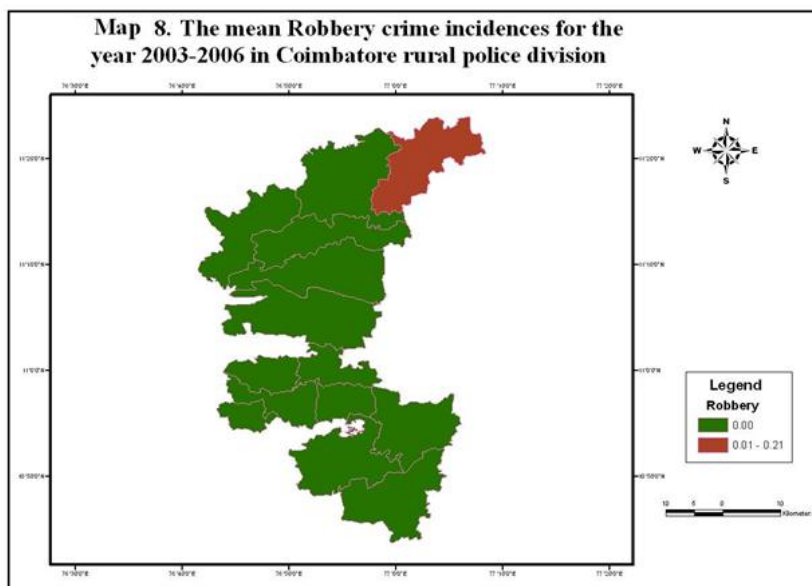
Figure 9: *The Mean Robbery Crime Incidences for the Year 2003-2006 in Coimbatore Rural Police Division*
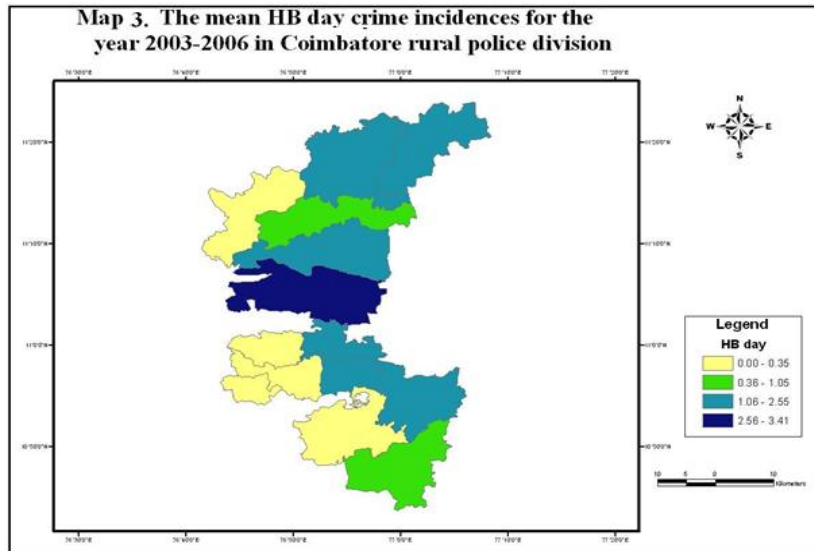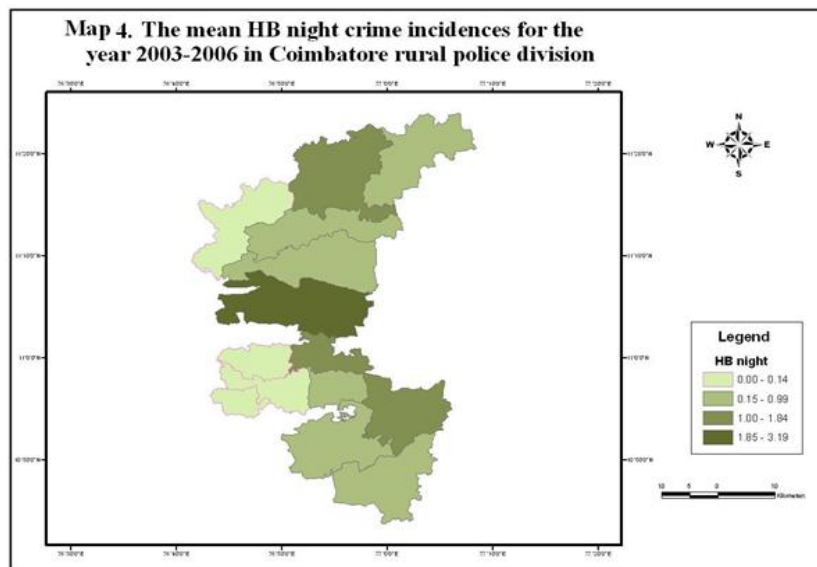
Figure 10: *The Mean Snatching Crime Incidences for the Year 2003-2006 in Coimbatore Rural Police Division*

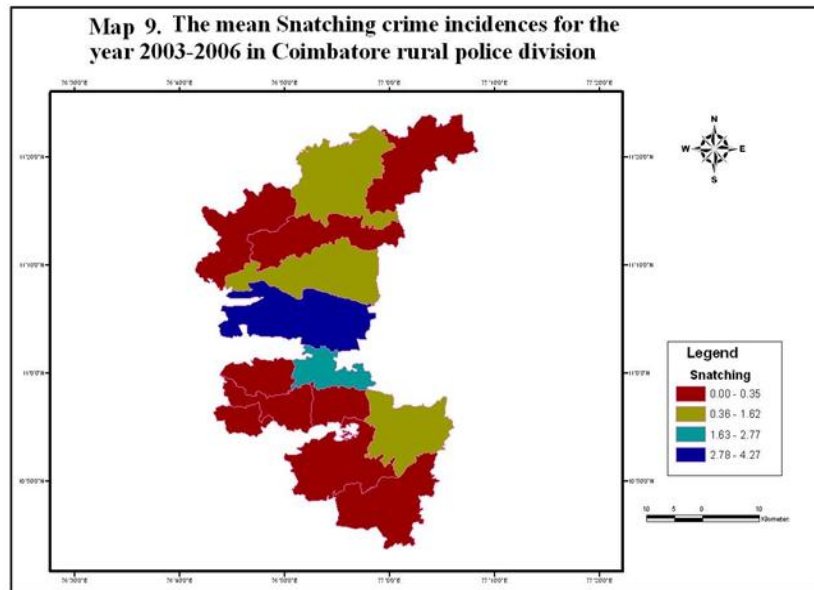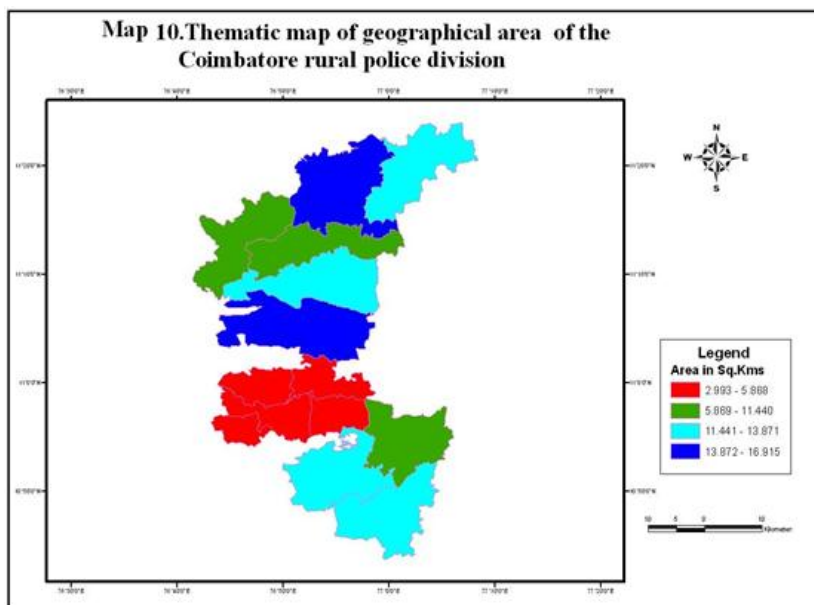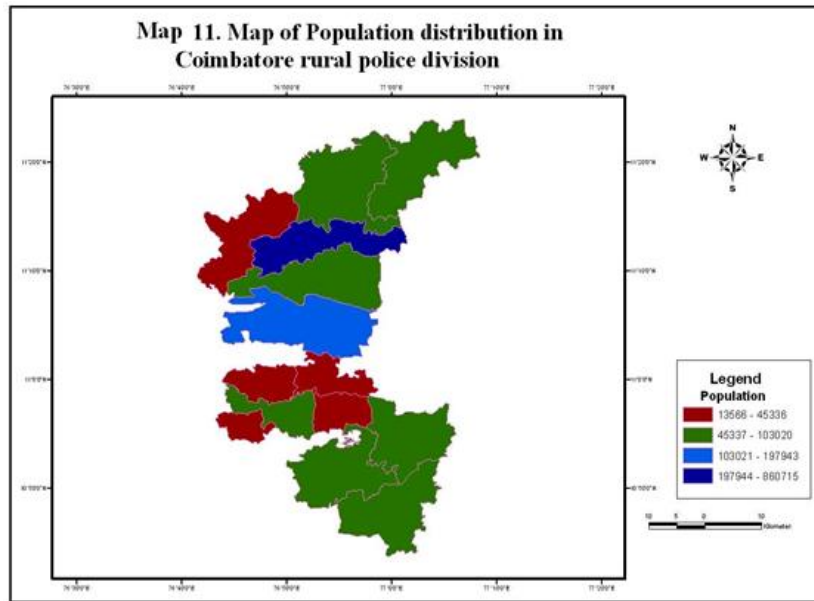***Figure 11:*** *Thematic Map of Geographical Area of the Coimbatore Rural Police Division*

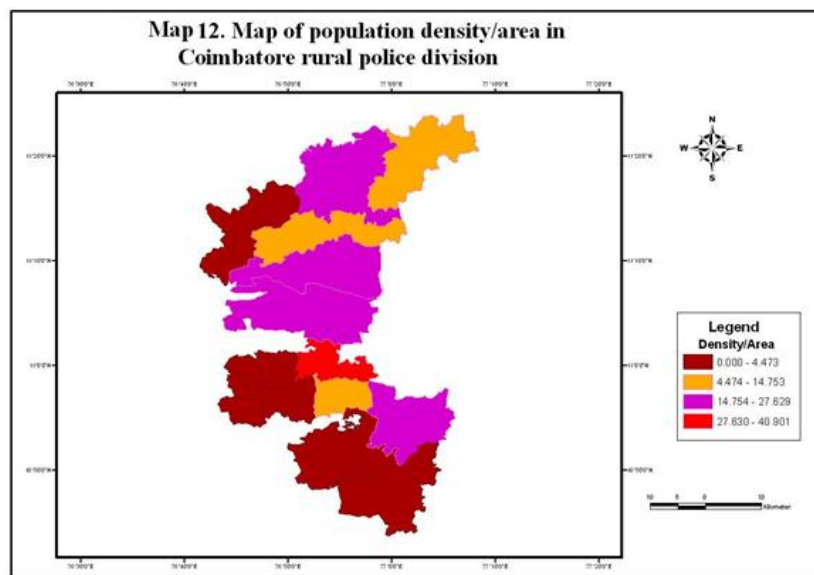*Figure 12: Map of Population Distribution in Coimbatore Rural Police Division*

Figure 13: Map of Population Density/Area in Coimbatore Rural Police Division

Table

Table 1: *Temporal Observation / Changes of Recorded Crime Incidences in the Police Jurisdictions of Coimbatore Rural of India (2003-2006)*

Police Jurisdiction	Auto	Grave	HB Day	HB Night	MF Gain	Murder	Pocket Picking	Robbery	Snatching
Sirumugai	**	***	***	**	***	**	**	***	*
Mettupalayam	***	***	***	***	****	***	****	***	**
Pillur dam	*	**	*	*	*	*	*	*	*
Karamadai	**	*	**	**	***	**	***	***	*
PN palayam	**	***	***	**	****	**	***	***	**
Thudiyalur	****	****	****	****	****	***	****	***	****
Vadavalli	**	**	***	***	***	****	**	****	***
Thondamuthur	*	*	*	*	*	*	*	**	*
Alandurai	**	**	*	*	*	*	*	*	*
Karunya	*	*	*	*	*	*	*	*	*
Perur	*	**	***	**	**	**	*	**	*
Madukarai	*	*	**	*	****	**	*	*	*
Podanur	**	****	****	***	***	***	***	**	**
Kinathukadavu	*	*	*	**	***	**	**	*	*

Very low	6	5	5	5	4	4	6	5	9
Low	6	4	2	5	1	6	3	3	3
Moderate	1	3	5	3	5	3	3	5	1
High	1	2	2	1	4	1	2	1	1

Key

* Very low incidences
** Low incidences
*** Moderate incidences
**** High incidences

References

[1] Canter D., et al. *Predicting Serial Killers' Home Base Using A Decision Support System*. Quantitative Criminology. 2000. 16 (4) 457-478.

[2] Rossmo D. K. 2000: *Geographic Profiling*. Boca Raton, CRC Press, FL.

[3] Santtila P., et al. *Testing the Utility of a Geographical Profiling Approach in Three Rape Series of A Single Offender: A Case Study*. Forensic Science International. 2003. 131; 42-52.

[4] Weisburd D., et al. 1997: *Introduction: Crime Mapping and Crime Prevention*. Crime Mapping and Crime Prevention. Vol. 8. Criminal Justice Press, New York, 1-23.

[5] Harries K., 1999: *Mapping Crime: Principles and Practice*. US Department of Justice, Washington DC.

[6] Hill B. 2003: *Operationalizing GIS to Investigate Serial Robberies in Phoenix, Arizona.* GIS In Law Enforcement: Implementation Issues and Case Studies. Taylor & Francis Inc., New York, 146-158.

[7] Felson M., 1986: *Linking Criminal Choices, Routine Activities, Informal Control, and Criminal Outcomes.* The Reasoning Criminal: Rational Choice Perspectives on Offending. Springer-Verlag. New York.

[8] Buck G.A., 1973: *Police Crime Analysis Unit Handbook.* Law Enforcement Assistance Administration, U.S. Department of Justice, Washington, DC.

[9] Chang S.K., 1979: *Crime Analysis System Support: Descriptive Report of Manual and Automated Crime Analysis Functions.* International Association of Chiefs of Police, Gaithersburg, MD.

[10] Harries K.D. 1974: *The Geography of Crime and Justice.* McGraw-Hill, New York.

[11] Pyle G.F., et al*., 1974: *The Spatial Dynamics of Crime.* Department of Geography, University Of Chicago, Chicago, 221.

[12] Brantingham P.J., et al. 1981: *Environmental Criminology.* Beverly Hills, Sage, CA.

[13] LeBeau J.L. *The Journey to Rape: Geographic Distance and the Rapist's Method of Approaching the Victim.* Journal of Police Science and Administration. 1981. 15; 129-136.

[14] Roncek D., et al. *Bars, Blocks and Crimes Revisited: Linking the Theory of Routine Activities to the Empiricism of Hot Spots.* Criminology. 1991. 29 (4) 725-751.

[15] Coombs M. *Crime Risk In Urban and Rural Neighbourhoods: An Experimental Analysis Of Insurance Data.* Environment and Planning B: Planning and Design. 1994. 21; 489-504.

[16] Rossmo D.K., 1995: *Place, Space, and Police Investigations: Hunting Serial Violent Criminals.* Crime and Place, Crime Prevention Studies. Vol. 4. Criminal Justice Press, NY.

[17] Hakim S., 1981: Introduction: In Crime Spillover, Beverly Hills, Sage Publishers, CA.

[18] Pauly G.A., et al., 1967: *Computer Mapping-A New Technique in Crime Analysis.* Law Enforcement Science and Technology. Vol. 1. Thompson Book Company, New York.

[19] Carnaghi J., 1970: *Automatic Pinning.* Law Enforcement Science and Technology. Vol. III. Illinois Institute of Technology Research, Chicago.

[20] Brantingham P.L., 1994: *Location Quotients and Crime Hot Spots in the City.* In Proceedings of Workshop on Crime Analysis through Computer Mapping, Illinois Criminal Justice Information Authority and Loyola University, Chicago.

[21] Goldsmith V., et al., 2000: *Analyzing Crime Patterns: Frontiers of Practice.* Thousand Oaks, Sage Publications, CA.

[22] Ehrlich Isaac. *Crime, Punishment, and the Market for Offenses.* Journal of Economic Perspectives. 1996. 10 (1) 43-67.

[23] Levitt S. *Using Electoral Cycles in Police Hiring to Estimate the Effect of Police on Crime.* American Economic Review. 1997. 87; 270-90.

[24] Levitt S. *Why Do Increased Arrest Rates Appear to Reduce Crime: Deterrence, Incapacitation, or Measurement Error?* Economic Inquiry. 1998. 36; 353- 72.

[25] Canter P.R., 1997: *Geographic Information Systems and Crime Analysis in Baltimore County, Maryland.* Crimed Prevention Studies. Willow Tree Press, NY.

[26] Nicolau R., 1994: Social Representations and Crime Distribution Patterns in Urban Settings, EGIS Foundation.
http://libraries.maine.edu/Spatial/gisweb/spatdb/egis/eg94159.html.

[27] Harries K. *Property Crimes and Violence in the United States: An Analysis of the Influence of Population Density.* International Journal of Criminal Justice Sciences. 2006. 1 (2) 24-34.

Case Study **Open Access**

Geo-Environmental Analysis Using Multitemporal Satellite Data and GIS Techniques- A Case Study for Bhavani River Basin, Tamil Nadu, India

S. Muthusamy[1], R.R. Krishnamurthy[1], M. Jayaprakash[1] and P. Mohana Perumal[2]

[1]Department of Applied Geology, University of Madras, Chennai, Tamil Nadu, India
[2]Centre for Remote Sensing, Sathayabama University, Chennai, Tamil Nadu, India

Correspondence should be addressed to S. Muthusamy, muthusamy.geo@gmail.com

Abstract The northern and north-eastern (Eastern Ghats), the southern and south-eastern sides of the basin are dominated by rugged discontinuous hills, with altitudes ranging from 300 to 1,000 meters. Based on the quantitative analysis on LULC, it was observed that a rapid growth in built-up land between 1973 and 2003 while the periods between 1993 and 2003 witnessed a reduction in this class. It is expected that the expansion of built-up area will follow the same trend from the year 2003 onwards. Considerable changes in agricultural pattern in this study area though there is not much changes in water resources may be an indication that the influence of climate change induced effects are expected to be vital factor in Bhavani River Basin. Considerable changes in agricultural pattern in this study area though there is not much changes in water resources may be an indication that the influence of climate change induced effects are expected to be vital factor in Bhavani River Basin. However this should be further validated by the analysis of socio-economic, hydro-meteorological and other field data pertaining to the study area.
Keywords *Landuse Landcover, Change Detection, Remote Sensing, Environmental Changes, Bhavavni Basin*

1. Introduction

Landcover information is needed to monitor the impact and effectiveness of management actions associated with sustainable development policies (Sedano *et al.* 2005). Countries within the tropics are developing rapidly, producing land cover changes of ecological and climatic significance, such as colonization of marginal lands, deforestation, dry lands degradation, landscape fragmentation and rapid urbanization (Lambin 1999). Inevitably these processes place great pressure on natural resources, perhaps most noticeably on forests (Foody 2003).

In recent years, satellite remote sensing techniques have produced multi-sensor satellite data at very high spatial, spectral and temporal resolutions (Liang 2004). This data coupled with improved computer processing and storage capabilities (Bossler 2002) have proved to be of immense value for preparing up to date and accurate land use/cover maps in less time, lower cost and with better accuracy (Foody 2003; Cingolani *et al.* 2004; Jansen and Di Gregorio 2004; Tottrup 2004). In cases of inaccessible regions this technique is perhaps the only method of obtaining the required data in a cost and time-effective manner (Sedano *et al.* 2005). Geographic Information Systems (GIS) which excel in storage, manipulation and analysis of spatial and socioeconomic data (Burrough and Mc Donnell 1998), provide a wider application when combined with remote sensing techniques which have been effective in land use/cover mapping of tropical environments (Baban and Wan-Yusof 2001; Colombo *et al.* 2004).

1.1. Land Use and Land Cover Classification Systems

Each classification is made to suit the needs of the user. In order to address the issues associated with classification like class definitions, multiple land uses on a single land parcel, minimum representable area and to standardize the LULC information that could be generated using remote sensing data. Anderson (1976) and NRSA (2009) developed some criteria for classification systems.

- The minimum level of interpretation accuracy in the identification of land use and land cover categories from remote sensor data should be at least 85 percent.
- The accuracy of interpretation for the several categories should be about equal.
- Repeatable or repetitive results should be obtainable from one interpreter to another and from one time of sensing to another.
- The classification system should be applicable over extensive areas.
- The categorization should permit vegetation and other types of land cover to be used as surrogates for activity.
- The classification system should be suitable for use with remote sensor data obtained at different times of the year.
- Effective use of subcategories that can be obtained from ground surveys or from the use of larger scale or enhanced remote sensor data should be possible.
- Comparison with future land use data should be possible.
- Multiple uses of land should be recognized when possible.
- Image analysts determine the measurement of spectral reparability by determining quantitatively the relation between class signatures. Signatures are refined by improved ground truth and accuracy assessment analysis. By utilizing the developed signatures in multi-spectral classification and thematic mapping, the analyst generates new data for analysis (ERDAS, 1999).
- Contemporary global change consists of two broad types: systemic and cumulative. Systemic change operates directly on the biochemical flows that sustain the biosphere and, depending on its magnitude, can lead to global change, just as fossil fuel consumption increases the concentration of atmospheric carbon dioxide. Systemic change is largely associated with, but not limited to, the Industrial Age and thus has grown especially important over the more recent past. Cumulative change has been the most common type of human-induced environmental change since antiquity. Cumulative changes are geographically limited, but if repeated sufficiently, become global in magnitude. Changes in landscape, cropland, grasslands, wetlands, or human settlements are examples of cumulative change. Some cumulative changes reached continental and even global proportions long before the 20th century, including deforestation and modification of grasslands (Turner and Butzer, 1992).

2. Study Area

The study area falls in the Latitude 11º30'00"N, Longitude 76º30'00"E (Figure 1). Survey of India Toposheets (58A11, 58A12, 58A14, 58E15, 58A16, 58E2, 58E6, 58E7, 58E10, 58E11) and the satellite imagery of Landsat MSS: 1973 Landsat ETM+: 1993, Landsat ETM+: 2003, SRTM-DEM-90M are used. The choice of data sources is considered comprehensively the spatial resolution, spectral resolution, time resolution, price and other factors. In this study, LANDSAT TM / ETM+ data and DEM data in 90m of resolution are used. TM / ETM data has 30 m in spatial resolution, 7-band of the spectral resolution, Spectral Range 0.450 - 2.35 µm and 16 days for time resolution. ERDAS IMAGINE 8.7 and ArcGIS 9.2 are used to process analyse the above mentioned remote sensing data.

Bhavani Basin is the fourth largest (6,500 km^2) sub-basin in the Cauvery Basin (81,000 km^2). The western part (Western Ghats) is hilly terrain with an altitude ranging from 300 to 2,400 meters. The northern and north-eastern (Eastern Ghats), the southern and south-eastern sides of the basin are dominated by rugged discontinuous hills, with altitudes ranging from 300 to 1,000 meters.

Bhavani Valley, a flat terrain covering around 20% of the basin area, starts from the foothills of Western Ghats and stretches eastward all the way to the confluence of the Bhavani River with the Cauvery river (NWDA 1993). The northern part of the upper Bhavani Basin is drained by the Moyar River and the southern part by the Bhavani River. Below the Lower Bhavani Project (LBP) reservoir the Bhavani River continues eastward traversing the Bhavani Valley. In the upper Bhavani Basin the major part of the yearly precipitation falls from June to September, during the south-west monsoon.

In the lower Bhavani Basin most of the rain falls during the less reliable north-east monsoon, from October to December. Yearly average precipitation in the upper Bhavani is estimated at 1,600 mm per year and the value of 700 mm per year is an approximation for the lower Bhavani. The total average yearly areal precipitation is about 6,500 Mm3 above the LBP reservoir (4,100 km^2) and approximately 1,700 Mm^3 below (2,400 km^2). Potential yearly evapotranspiration (ET) in the central upper Bhavani Basin is about 800 mm and around 1,600 mm in the lower Bhavani Basin (based on soil map information from the Indian Department of Agriculture).

The population in the basin has increased about 200% during the last 50 years to about 2.5 million. More than 50% of the workforces in the Nilgiris district are occupied with livestock, forestry, fishing, hunting, plantations or orchards, and 14% are working in the agriculture sector as cultivators or agricultural labourers. In the Erode district, almost 55% work in agriculture and about 45% in the non-agriculture sector (Census of India 1991a, b). In the parts of the Bhavani Basin that fall within the Erode and Coimbatore districts there are irrigated lands with canals and groundwater, and rain-fed crop lands, often with supplemental groundwater irrigation. Cultivated crops are Sugarcane, paddy, groundnut, pulses, fodder sorghum, sugar cane, coconut, sesame, turmeric and banana.
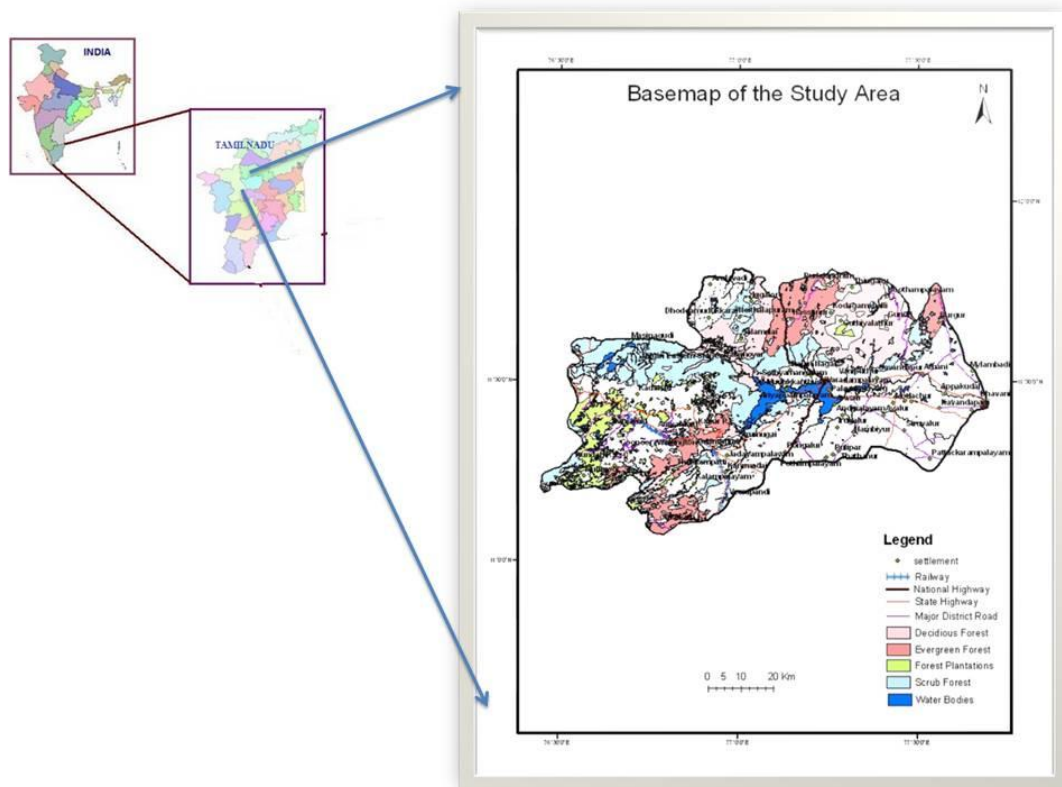
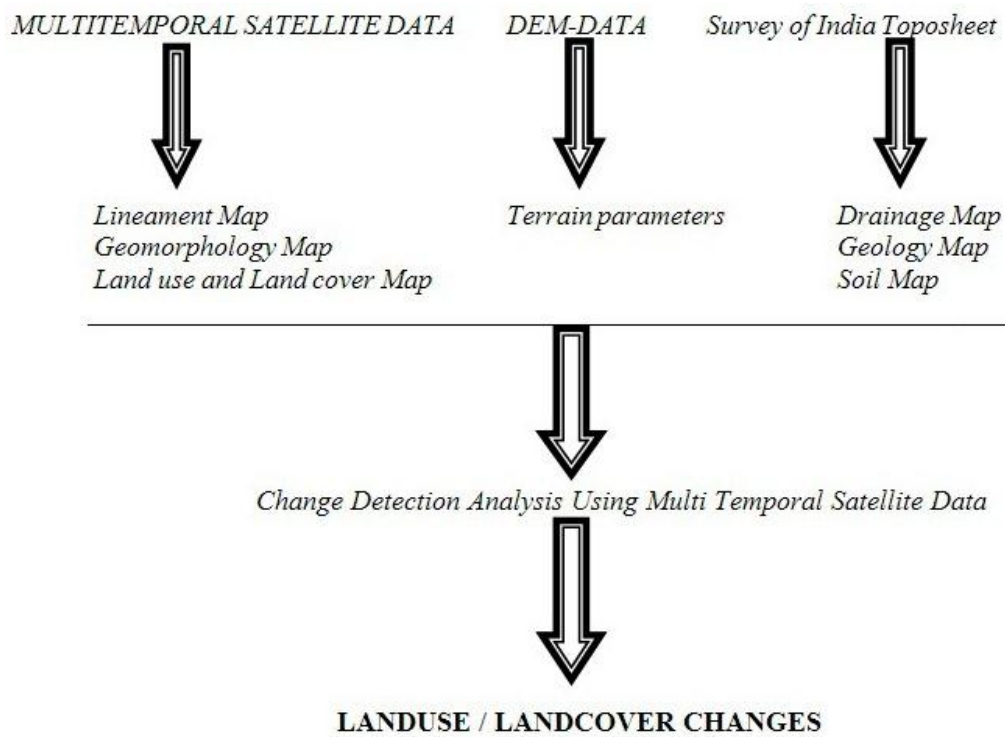*Figure 1:* Map Showing the Study Area

3. Methodology

Figure 2: Shows the Methodology Flow Chart

The interactions of geomorphology, geology, hydrology, topography, soil, drainage and even anthropogenic disturbances can result in a complex of Geo-environmental types where deciduousness and moisture are highly variable and dynamic. Hence, in this study the combination of remote sensing and GIS techniques have been used to prepare relevant thematic maps and more particularly to study the land use and land cover changes in the study area. Following the Anderson (1976) classification, present area of imagery from the individual years, a post classification, approach of subtracting the classification maps, 1973, 1993 and 2003, was applied. This is perhaps the most common approach to change detection and has been successfully used by (Yang and Lo *et al.* 2002) to detect land changes in the Atlanta, Georgia area. Since this study involves the preparation to thematic maps, creation of digital elevation model and organization and integration of spatial information using a GIS the above methodology (Figure 2) has been adopted for this study.

4. Results and Discussion

4.1. Thematic Maps of the Study Area

A) Geology of the Study Area

The vast expanse of granulite -gneiss terrain of central and northwest Tamil Nadu encloses discrete, isolated sequences of high grade schists and basic rocks which occupy a supracrustal status in the lithostratigraphic column. These are referred to as 'Sathyamangalam' in Tamil Nadu. The rocks of Sathyamangalam Group generally occur as dismembered bands and lenses within the Peninsular Gneissic Complex (Bhavani Group) in an east- west trending linear belt in central Tamil Nadu occupying parts of Coimbatore, Erode, Salem, Namakkal and Tiruchirapalli Districts (GSI, 2006). Bhavani Group is a mixture of gneisses of different composition and texture such as highly fissile mica gneiss, quartzo-feldspathic gneiss, augen gneiss, hornblende gneiss, hornblende-biotite gneiss, biotite gneiss, granitoid gneiss and pink migmatite. Part of this gneiss is considered to be para as well as ortho-gneiss and part their migmatitic equivalents shows in the study area (Figure 3).

B) Geomorphylogy and Soil Types

The Bhavani Basin forms part of the uplands of the state. Physiographically the basin can be divided into hilly area, the upland area and plains area. The prominent geomorphic units identified in the district through interpretation of Satellite imagery are 1) Structural hills, 2) Inselberg, 3) Ridges, 4) Valley fill, 5) Pediments, 6) Shallow Pediments, (GGWB, 2006). The hilly area is represented by the Western Ghats in the northwestern part, the Biligiri Rangan hills in the north, Bodamalai Betta hills in the northwestern parts and Konbattarayan hills in the north central part. The Kongunadu uplands lie south of Bhavani River and the Lower Bhavani canal passes through these uplands. Scattered hillocks and knolls of moderate elevations occur within these uplands. The plains area is characterised by an undulating topography with a general gradient due east and southeast. The plains are limited to the east and southwestern border of the study area (Figure 3).

The soils of study area can be broadly classified into 6 major soils types viz., Red calcareous soil, Red non calcareous soil, Black soil, Alluvial and Colluvial soils, Brown soil and Forest soil. Major part of the study area covered by red calcareous soils. They are mostly sandy to loamy and characterised by the hard and compact layer of lime of the study area (Figure 3).

C) Drainage

A Drainge map of the area was prepared from survey of india toposheet and SRTM data. Digital elevation map of Drainage produced and presented in the (Figure 3). This Digital Elevation Model

(DEM) clearly presents the elevator hillocks and mountains in the study area and its shows the drainage pattern of water bodies.
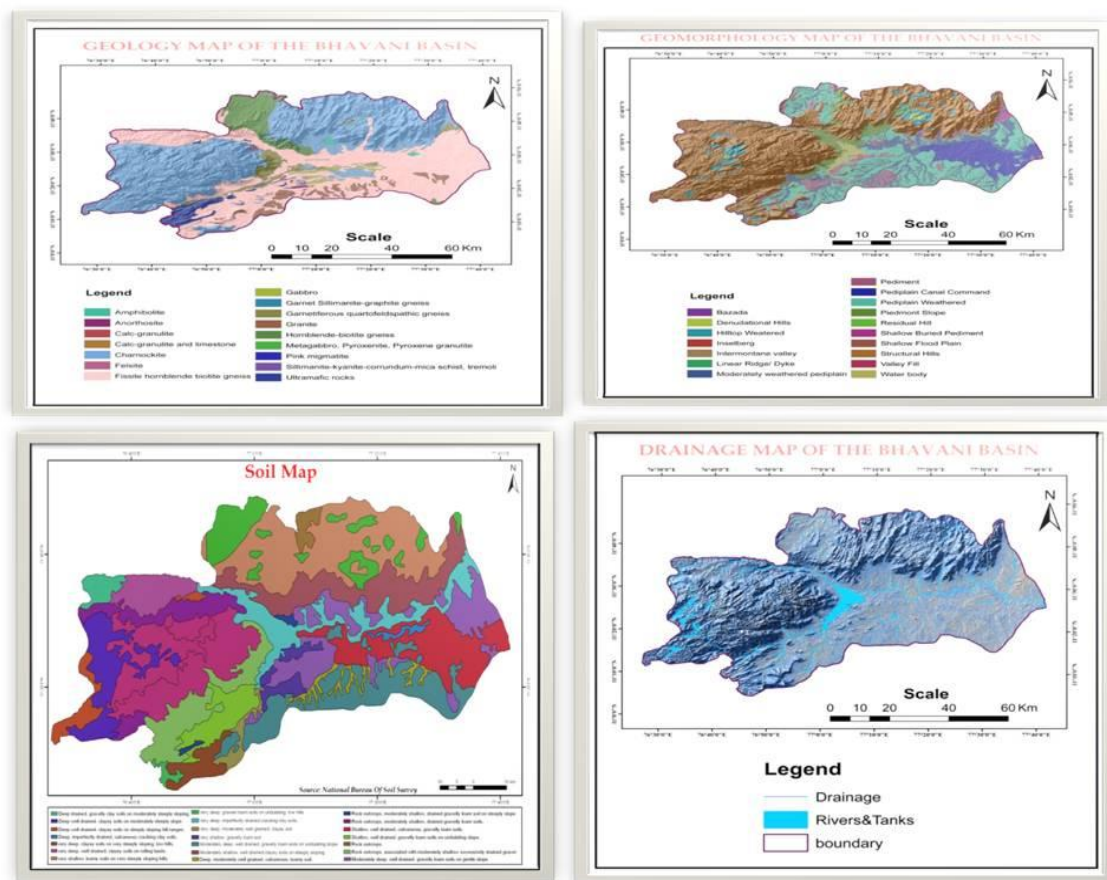
Figure 3: *Map Showing The Thematic Maps*
(Geology, Geomorphology, Soil, Drainage) of the Study Area

4.2. Ground Truth Validation

The LULC maps prepared using Multidate remote sensing data of this study are validated in the field by choosing random sampling method showing in the (Figure 4). All the important categories are verified and the total accuracy of this classification is estimated as 98 percent.

4.A. SUGARCANE CULTIVATED LAND AS SEEN IN THE STUDY
AREA

4.B. CROP LAND AS SEEN IN THE STUDY AREA

4.C. FALLOW LAND AS SEEN IN THE STUDY AREA

4.D. FOREST LAND AS SEEN IN THE STUDY AREA

4.E. BHAVANI SAGAR RESERVOIR AS SEEN IN THE STUDY
AREA

4.F. UNCONTROLLED MINING IN THE STUDY AREA
(NEARBY BHAVANI SAGAR DAM)

Figure 4: *Showing the Ground Truth Validation of the Study Area*

Figure 5: *Chart Showing the LULC Changes in the Years of 1973, 1993 and 2003*

Table 1: *Calculated Values of Land Use/Land Cover Changes in Bhavani River Basin*

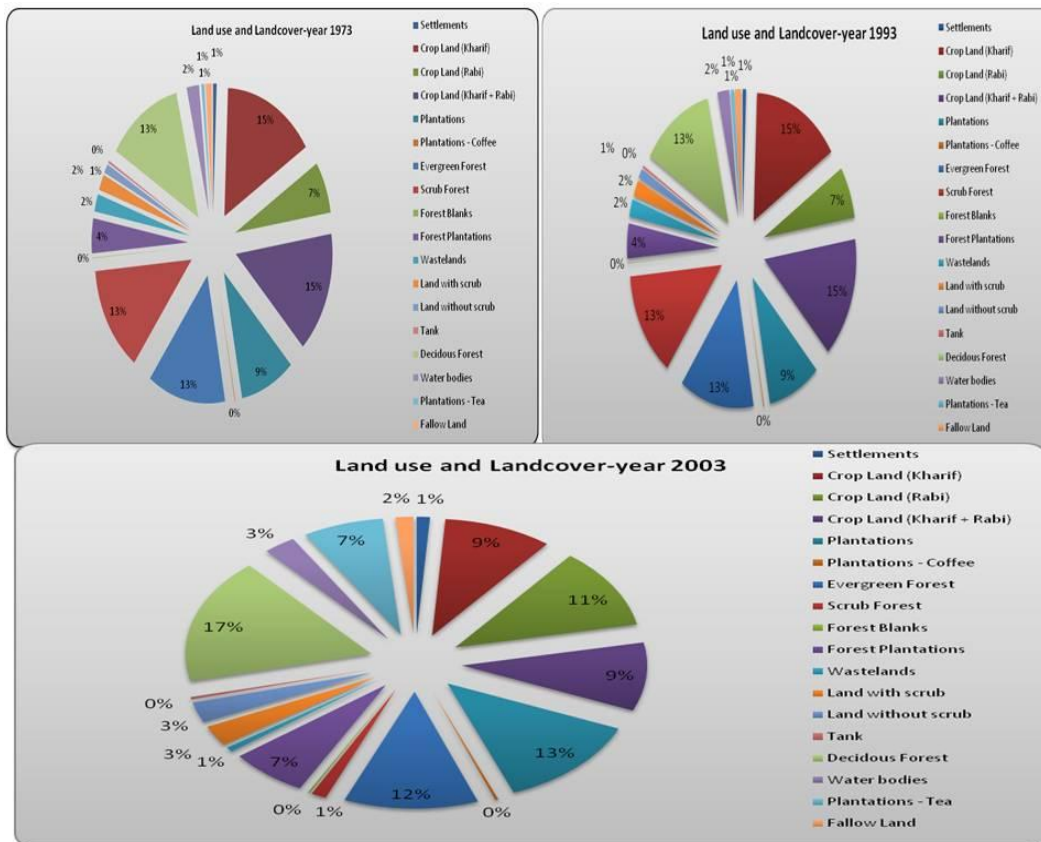| S. No.	Land Use/ Landcover	1973	1993	2003	Percentage of Changes
1	Settlements	45.20	53.20	63.05	0.81
2	Crop Land (Kharif)	886.72	626.45	620.53	-30.09
3	Crop Land (Rabi)	507.53	503.53	526.45	5.15
4	Crop Land (Kharif + Rabi)	1186.72	858.27	985.60	-30.13
5	Plantations	708.04	714.04	713.80	0.26
6	Plantations - Coffee	4.30	5.30	11.30	0.27
7	Evergreen Forest	1010.30	993.30	949.91	-16.42
8	Scrub Forest	1038.62	1024.62	971.36	-43.97
9	Forest Blanks	5.38	8.38	10.38	0.23
10	Forest Plantations	340.74	410.74	545.69	1.77
11	Wastelands	170.58	249.58	35.83	-6.14
12	Land with scrub	155.55	452.55	158.12	0.12
13	Land without scrub	90.23	99.23	81.46	3.09
14	Tank	24.05	34.05	18.28	-0.26
15	Decidous Forest	975.34	963.34	962.87	-0.57
16	Water bodies	160.27	155.27	156.08	-0.19
17	Plantations - Tea	40.31	46.31	389.70	15.92
18	Fallow Land	83.54	95.54	86.55	0.14
19	Total area	7433.42	7433.42	7433.42	
All the values are in KM^2					

From the above Table 1 & Figure 5 Chart derived, it can be seen that there has been a major decrease in the crop land and forest area. The percentage of scrub forest has drastically declined to around 44%. Next to scrub forest is Crop land (Kharif + Rabi), which has gone down by 30.09%. Equally the cropland (Kharif + Rabi), the percentage of crop land (Kharif) has decreased by 30.09 %. Around 16% of decrease in Evergreen forest, while wasteland has been decreased by 6%. Also there is very little decrease noted in the water bodies and Decidious forest area. While most of the wasteland area has been lost, there is notable increase in Crop land (Rabi) and Land without Scrub. Also, around 1% increase is noted in settlements and less than 1% was noted in Plantations. The percentage of both Plantations and Coffee plantation has increased to same extent at around 0.3 %. All above, Tea plantation has increased drastically by around 16%.In the present Study, Survey of India (SOI) toposheet of 1973 and the satellite imagery of Landsat MSS: 1973 Landsat ETM+: 1993, Landsat ETM+: 2003 of different years from 1973, 1993, 2003 were compared qualitatively and quantatively. This study has given the land use changes during these years. Different Environmental land use categories were identified viz. Settlements, Evergreen Forest, Forest Plantations, Decidious Forest, Forest Blanks, Plantations, Crop Land (Rabi), Crop Land (Kharif + Rabi), Crop Land (Kharif) Wastelands, Land with scrub, Fallow Land, Scrub Forest, Land without scrub, Tanks, Water bodies. The results of landuse/landcover assessment based on visual interpretation for different years of satellite data (From 1973, 1993, 2003) and its area are showing in Table 1. The variations in the land use pattern (Figures 5.1 & 5.2) are clearly shown and the changes in area can be seen. More pixels of Crop Land (Kharif), Evergreen Forest, Scrub Forest, Crop Land (Kharif + Rabi) are seen in 1973 LULC map than 2003 map (Figures 5.1 & 5.2). But the sudden decrease in the subsequent years in 1973 to 2003. Constant increase in Plantations- Tea, Land without scrub, Crop Land (Rabi). Agricultural and fallow lands are changing based different agricultural practices and monsoonal effect.

The overall Landuse/Landcover according to the 1973 data has been calculated as 7737Km^2 and sparsely irrigated as 50%. Out of total area, around 26% of the area is covered with forest; in the

remaining, 24% of the area is covered by other geomorphologic features. Similarly, for the year 1993, land cover changes reveal that forest land covered 26% of the area; sparsely irrigated surface covered 20% in the (Figure 5.1). For the year 2003, the irrigated and forest land are reduced approximately 5% and its shows settlements are gradually increased from 1973 to 2003 in the (Figure 5.2).
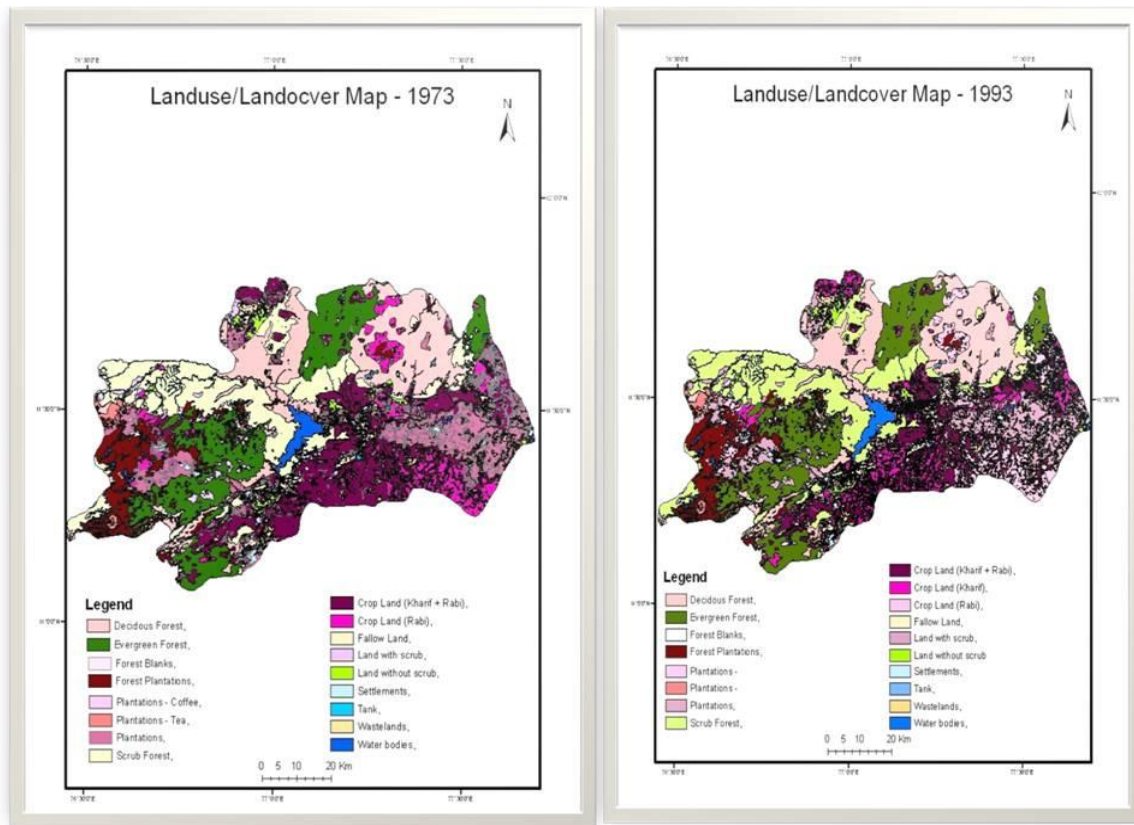

Figure 5.1: *Showing the Landuse/Landcover Map of the Study Area for the Year of 1973 & 1993*
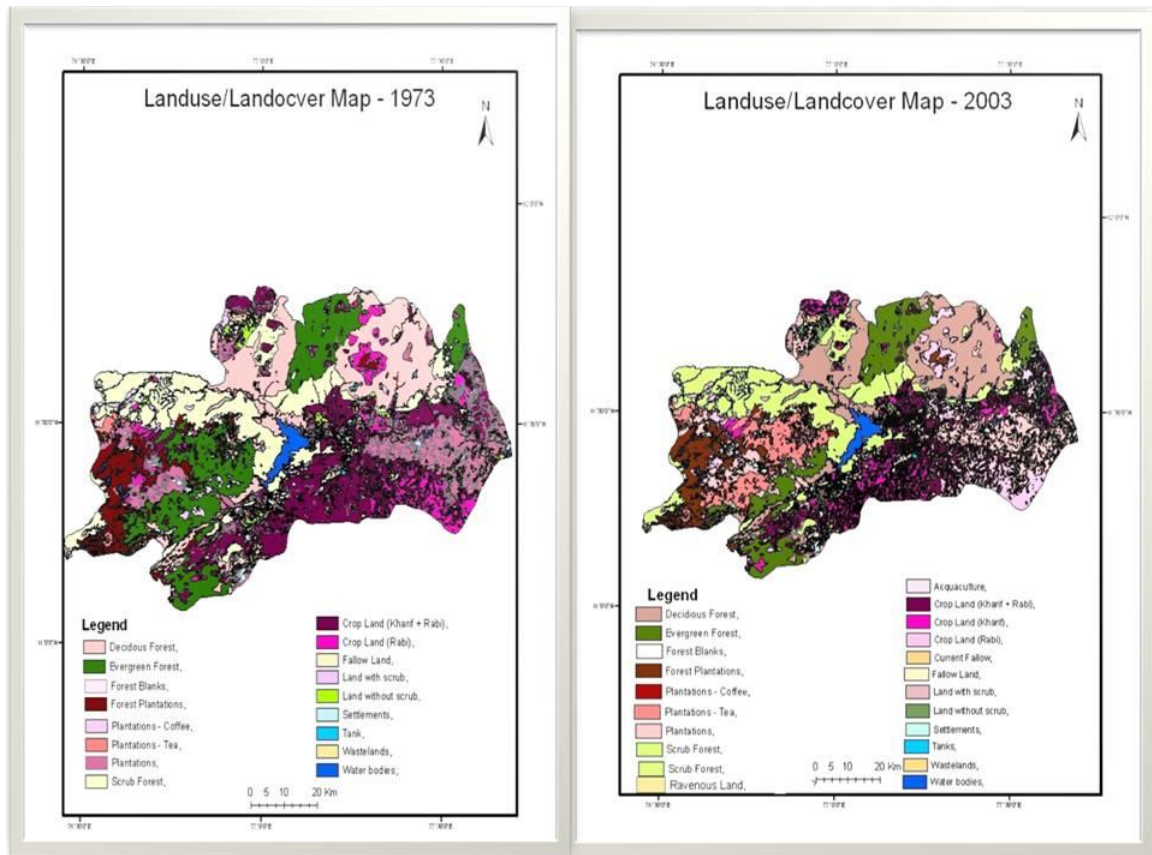
Figure 5.2: *Showing the Landuse/Landcover Map of the Study Area for the Year of 1973 & 2003*

5. Conclusion

Considerable all the important land use and land cover categories both the scrub forest and cropland areas are undergone major changes during 1973-2003. LULC changes describes results confirm that both the scrub forest and cropland area might have converted mainly for forest plantations especially in tea plantation. Several important land use and land cover categories such as settlements, agriculture, plantations, forest blanks and fallow lands have not undergone many changes during the last three years. Considerable part of waste land areas are reduced during the last three years. This may be an indication that the study area has the impact of proper land use planning adopted by the local government through various rural development authorities. The reduction in cropland equally kharif shows that there is a considerable shift in cropping practices in the study area. This might have attributed by the availability and changes in socio economic conditions.

Recommendations

Since the study area comprised of Hilly area, Flood plain area, undulating terrain with scrub forest cover there should an integrated management approach is required for effective management of this River Basin as detailed below:

a) The proper integrated hill area management plan (IHAM) should be adopted to enhance the density of the forest.
b) Due to rapid conversion of agriculture area, the study area needs to adopt proper land management practices.

c) The water storage potential of Bhavani Sagar reservoir should be regularly monitored through proper watershed management practices.

d) There are uncontrolled mining activities, observed during field visits especially near by the Bhavani sagar reservoir dam and this should be regulated by the authorities.

References

Anderson et al., 1976*: A Land Use and Land Cover Classification System for Use with Remote Sensor Data.* Geological Survey Professional Paper No. 964*,* U.S. Government Printing Office, Washington, D.C., 28.

Baban S.M.J., et al. *Mapping Land Use/Land Cover Distribution in Mountainous Tropical Environments Using Remote Sensing and GIS*. International Journal of Remote Sensing. 2001. 22 (10) 1909-1918.

Bossler J., 2002: *Manual of Geospatial Science and Technology*. New York: Taylor & Francis.

Burrough P., et al. 1998: *Principles of Geographic Information Systems.* New York: Oxford University Press.

Cingolani A. *Mapping Vegetation in a Heterogeneous Mountain Rangeland Using Landsat Data: An Alternative to Define and Classify Land-Cover Units.* Remote Sensing of the Environment. 2004. 92: 84-97.

Colombo S., et al. *Variographic Analysis of Tropical Forest Cover from Multi-Scale Remotely Sensed Imagery.* ISPRS Journal of Photogrammetry and Remote Sensing. 2004. 58; 330-341.

Congalton R.G. *Accuracy Assessment: A Critical Component of Land Cover Mapping.* Gap Analysis. American Society for Photogrammetry and Remote Sensing. 1996. 119-131.

ERDAS, 1999. Earth Resources Data Analysis System. Field Guide. ERDAS Inc. Atlanta, Georgia, 628.

Foody G.M. *Remote Sensing of Tropical Forest Environments: Towards the Monitoring of Environmental Resources for Sustainable Development*. International Journal of Remote Sensing. 2003. 20; 4035-4046.

Foody G.M. *On the Compensation for Chance Agreement in Image Classification and Accuracy Assessment.* Photogrammetric Engineering and Remote Sensing, 1992. 58 (10) 1459-1460.

Geological Survey of India, 2006: Miscellaneous Publication No.30, Geology and Mineral Resources of the States of India.

Jansen L. *Obtaining Land-Use Information from a Remotely Sensed Land Cover Map: Results from a Case Study in Lebanon*. International Journal of Applied Earth Observation and Geoinformation. 2004. 5; 141-157.

Lambin E.F. *Monitoring Forest Degradation in Tropical Regions by Remote Sensing: Some Methodological Issues.* Global Ecology and Biogeography*.* 1999. 8; 191-198.

Liang S. 2004. *Quantitative Remote Sensing of Land Surfaces*. Remote Sensing and Image Interpretation. 5th Ed. John Wiley & Sons, New Jersey.

NRSA, 2009: Remote Sensing Application in Land Use Land Cover Classification System. National Remote Sensing Agency.

R.M. Manickavasagam et.al. *Tectonometamorphic Evolution of Moyar, Bhavani and Palghat-Cauvery Shear Zones of Southern Granulite Terrane, India*. Gondwana Research. 2001. 4 (4) 697.

Riebsame et al. *Integrated Modeling of Land use and Cover Change*. Bioscience. 1994. 44; 350.

Riebsame W.E., et al. 1994. *Modeling Land-use and Cover as Part of Global Environmental Change*. Climate Change. 1994. 28; 45.

Robinove C.J., 1981: The Logic of Multispectral Classification and Mapping of Robinove, C.J. 1986. Principles of Logic and the Use of Digital Geographic Information Systems. U.S. Geological Survey Professional Paper No. 977. U.S. Gov. Printing Office, Washington, D.C., 19.

Rosenfield G., et al. *A Coefficient of Agreement as a Measure of Thematic Classification Accuracy*. Photogrammetric Engineering & Remote Sensing. 1986. 52 (2) 223-227.

Scialabba N., 1998: Integrated Coastal Area Management and Agriculture, Forestry and Fisheries. FAO Guidelines. Environment and Natural Resources Service, Food and Agriculture Organization, Rome.

Sedano F. *Land Cover Assessment with MODIS Imagery in Southern African Miombo Ecosystems.* Remote Sensing of Environment. 2005. 98 (4) 429-441.

Tottrup C. *Improving Tropical Forest Mapping Using Multi-Date Landsat TM Data And Pre-Classification Image Smoothing.* International Journal of Remote Sensing*. 2004*. 25 (4) 717-730.

Turner B.L., et al. The Columbian Encounter and Land-Use Change. Environment. 1992. 34 (8) 16-44.

Yang X., et al. *Using a Time Series of Satellite Imagery to Detect Land Use and Land Cover Changes in the Atlanta, Georgia Metropolitan Area*. International J. of Remote Sensing. 2002. 23 (19) 1775-1798.

Cloud Publications

Review Article   **Open Access**

Inventory of Liquefaction Area and Risk Assessment Region Using Remote Sensing

Shankar Lingam S.[1], Rajchandar Padmanaban[2] and Vinson Thomas[3]

[1]Regional Centre of Anna University of Technology, Tirunelveli, Tamil Nadu, India
[2]Institute for Geoinformatics, University of Muenster, Muenster, Germany
[3]Anna University of Technology, Chennai, Tamil Nadu, India

Correspondence should be addressed to Rajchandar Padmanaban, charaj7@gmail.com

Abstract This proposed paper is focused on the identification of liquefaction areas for the communal protection and suggesting the suitable build up region to improve the inventory of areas .The water-logged sediments get loose up from the strong vibration of the earthquake causing liquefaction, so identifying the more vulnerable areas which become the source for the earthquake-related secondary effects, such as landslides, mud flow, ground subsidence and effects on human infrastructure should be considered gravely. The conventional methods used in analysis of liquefaction factor may be time consuming and really expensive, but the wide range of modern satellite imagery can easily be adopted for communal to access the bare earth and features, in the same advance used in this project for spotting the liquefaction areas which may cause various disaster/Land transform in future. Geographic Information Systems (GIS) and Remote Sensing methods along with the associated geo-databases can be assisted by local and national authorities to be better prepared and organized in providing infrastructure to the public. The assessment of satellite imageries, digital topographic data and Geo-data contribute to the attainment of the exact geologic and geomorphologic situation influencing the local site circumstances in an area and estimate all the probable damages that could happen. The main goal of this research is delineating the region which mainly corresponds to high liquefaction potential through the various Images processing technique and GIS analysis, using satellite imagery such as Landsat 7 ETM+ sensor and advanced space borne Thermal Emission and Reflection Radiometer (ASTER), collectively with different indices calculation, ground water table, digital elevation model, geomorphology and geological studies.
Keywords *Remote Sensing, Liquefaction Factor, Indices Computation, Multi Criteria Evaluation, Digital Image Processing, Geographic Information System Analysis*

1. Introduction

As we all know, the eternal fact about our Mother Earth is that the predominant movement of the tectonic plates. To be mentioned, this kind of activity is a nonstop aspect which actually does result in the displacement or the transferring of the continents in a very slow manner. But when this is in process, there are several factors like overlapping of the plates, clinging, drifting, elasticity etc., by their movements, that may happen that make it become clumsier which could as well result in some natural calamities such as earthquake, tsunami, volcanization etc., and when these occur, there are some other related secondary effects, such as landslides, mud flow, Ground subsidence and effects on human infrastructure that probably become the violent and worse environmental impacts. One among those secondary effects is the Liquefaction.

Liquefaction happens when the water-logged sediments get loose up from the strong vibration of the earthquake and such other hazards. The problem of liquefaction of soil during seismic event is one of the mentionable criteria in the field of Geotechnical Earthquake Engineering. Liquefaction of soil generally occurs in loose cohesion less saturated soil when pore water pressure increases suddenly due to induced ground motion and shear strength of soil decreases to zero and leading the structure situated above to undergo a large settlement, or failure. The failures take place due to liquefaction induced soil movement spread over few square km area continuously. The 8 types of failure commonly associated with soil liquefaction include sand boils, flow failures of slopes, lateral spreads, ground oscillation, loss of bearing capacity, buoyant rise of buried structures, ground settlements and failure of retaining walls.

And hence, this is a great problem where spatial variation involves and to represent this spatial variation, remote sensing technology and Geographic Information System (GIS) are very useful in analysing and decision making for the area being subjected to liquefaction. The resulting integrated paradigm of liquefaction analysis permits on focusing during the design phase on optimising the various elements of the design by incorporating the spatial component of the geotechnical data explicitly in the analysis.

2. Data and Description

A remote sensing image provides the wider range of synoptic segment of features about earth surface widely used in recognizing various parameters which can be useful for various analysis and interpretation. The elite capabilities of satellite based sensors in providing a wide-ranging spectrum of information accessible through the electromagnetic spectrum in recurring and synoptic coverage over in accessible and larger areas in recurrent intervals made the Remote Sensing technology an effectual tool, this advanced technology can be useful for inventory of liquefaction area and accessing risky region. Here in this paper, two types of satellite data are taken into account so as to analyse the liquefaction susceptible area and they are Landsat ETM+ data and ASTER data.

2.1. Aster Data

The Advanced Space borne Thermal Emission and Reflection Radiometer (ASTER) is an imaging instrument onboard Terra, the flagship satellite of NASA's Earth Observing System (EOS) launched in December 1999. ASTER data is used to create detailed maps of land surface temperature, reflectance, and elevation. Its main goal is improving a scientific understanding of the Earth as an integrated system, its response to change, and to better predict variability and trends in climate, weather, and natural hazards. The Table 1 shows the characteristic of ASTER data.

Table 1: *Technical Characteristics of ASTER Data*

Subsystem	Band Number	Spectral Range(μm)	Radiometric Resolution	Absolute Accuracy (σ)	Spatial Resolution	Signal Quantization
VNIR	1	0.52-0.60	NE Δρ ≤ 0.5%	≤ 4%	15m	8 bits
	2	0.63-0.69				
	3N	0.78-0.86				
	3B	0.78-0.86				
SWIR	4	1.600-1.700	NE Δρ≤ 0.5%	≤ 4%	30m	8 bits
	5	2.145-2.185	NE Δρ ≤ 1.3%			
	6	2.185-2.225	NE Δρ ≤ 1.3%			
	7	2.235-2.285	NE Δρ ≤ 1.3%			
	8	2.295-2.365	NE Δρ ≤ 1.0%			
	9	2.360-2.430	NE Δρ ≤ 1.3%			
TIR	10	8.125-8.475	NE ΔT ≤ 0.3 k	≤ 3K(200-240K)	90m	12 bits
	11	8.475-8.825		≤ 2K(240-270K)		
	12	8.925-9.275		≤ 1K(270-340K)		
	13	10.25-10.95		≤ 2K(340-370K)		
	14	10.95-11.65				

2.2. Landsat Enhanced Thematic Mapper plus Data

Landsat Thematic Mapper (TM) is a multispectral scanning radiometer that was carried onboard Landsat 4 and 5. The TM sensors have been providing nearly continuous coverage since July 1982 till now. The Landsat Enhanced Thematic Mapper (ETM) was introduced with Landsat 7. ETM data cover the visible, near-infrared, shortwave, and thermal infrared spectral bands of the electromagnetic spectrum.

The Landsat Project is a joint initiative of the U.S. Geological Survey (USGS) and the National Aeronautics and Space Administration (NASA) [1,2]. Landsat's Global Survey Mission is embarked to establish and execute a data acquisition strategy that ensures repetitive acquisition of observations over the Earth's land mass. The Enhanced Thematic Mapper Plus (ETM+) instrument is a fixed "whisk-broom", eight-band, multispectral scanning radiometer capable of providing high-resolution imaging information of the Earth's surface. It detects spectrally-filtered radiation in VNIR, SWIR, LWIR and panchromatic bands from the sun-lit Earth in a 183 km wide swath when orbiting at an altitude of 705 km.

3. Methodology

In concern to the method of approach suggested in this paper, there are 3 main steps viz. Image processing, GIS analysis and interpretation and map generation that are to be handled broadly in order to delineate the task absolutely and optimistically. The imagery data for the analysis are obtained from two major sensors viz. Landsat ETM+ and ASTER and are processed with ERDAS 11.0.4/ENVI 5 image processing software for the effective progress .The well processed image is then calibrated and corrected using Radiometric/Geometric calibration.

3.1. Radiometric Correction

The process of radiometric correction involves 3 steps, initially the DN (digital number) values recorded by the sensor are converted to spectral radiance (at the sensor) after processing DN values [3], the converted spectral radiance is further converted to apparent reflectance (at the sensor) and finally removal of atmospheric effects due to absorption and scattering is done (atmospheric correction) and providing the reflectance of pixels at the Earth's surface.

3.2. Geometric Correction

The Geometric calibration process involves different levels of correction to the remotely sensed imagery viz. Registration, Rectification, Geocoding and Ortho-rectification. The alignment of one image to another of the same area is done with the process of registration [4]. In rectification, the alignment of image to a map is done so that the image turns out to be planimetric, just like the map. Rectification can also be termed as geo-referencing. Geocoding is a special case of rectification that adds in scaling to a uniform standard pixel GIS. The use of standard pixel sizes and coordinates authorizes convenient layering of images from sensors and maps into GIS. Ortho-rectification is the correction of the image, pixel by pixel for topographic distortion done making the image to be in a strict orthographic projection.

3.3. DEM Generation

DEM generation described below requires the application of PHOTOMOD 4.4 software. Digital Elevation Model abbreviated as DEM is essential to handle wide tasks notably generating contour lines and ortho images, erosion control, agricultural developments, flood planning, 3D-views, visibility checks and other such norms. The initial move in the satellite data processing is focused on the stereo orientation which could be achieved by creating a catalogue of the Ground Control Points (GCP's) identified using photo interpretation. TIE points are added on both images to perform the Block adjustment, so as to improve the positioning, fix the deformations and reduce the shift between the images [5]. The resultant is the precise positioning of the stereo pair with regards to the GCP's.

DEM is obtained using TIN (Triangular Irregular Network). The pickets are created over an 8 meter grid using the adaptive method that calculates 3D coordinates for points being the most correlated with each grid node of the TIN nodes coordinate. The final TIN is triangulated from grid nodes with the modified Delaunay algorithm. Different methodologies including photo interpretation, insertion of break lines are to be integrated with the purpose of enhancing the model. The table containing the GPS measurements is formatted as input file to Photomod to facilitate as TIN break lines [6]. Pickets, from which the TIN is generated, are exported from the Photomod and imported into the GIS project (ESRI ArcMap 9.3).

The outcome of the analysis of height distribution of the points to find the anomalies is verified manually using photo interpretation. After the pickets are controlled and modified, they are again imported into Photomod to generate an optimized TIN. The DEM is then generated from the TIN. The high spatial resolution of the satellite image would enhance the quality of the DEM. With the intension of maintaining a uniform representation of the territory, a smoothing technique is applied. The final result is compared with the GPS measurements gathered, proving the effectiveness of the methodology and validating the high degree of accuracy of the DEM.

3.4. Indices Calculation

An image processing apparatus includes a processing amount index calculation unit configured to analyze content of image data that is independent of print resolution and to calculate a processing amount index indicating a processing amount necessary in converting the image data into a bitmapped image, a storing unit configured to store the calculated processing amount index as additional information associated with the image data, and a sending unit configured to send the image data and the additional information [7]. Here 5 indices are identified to delineate the liquefaction factor as Simple ratio, NDVI, TNDVI, SAVI and MNDWI.
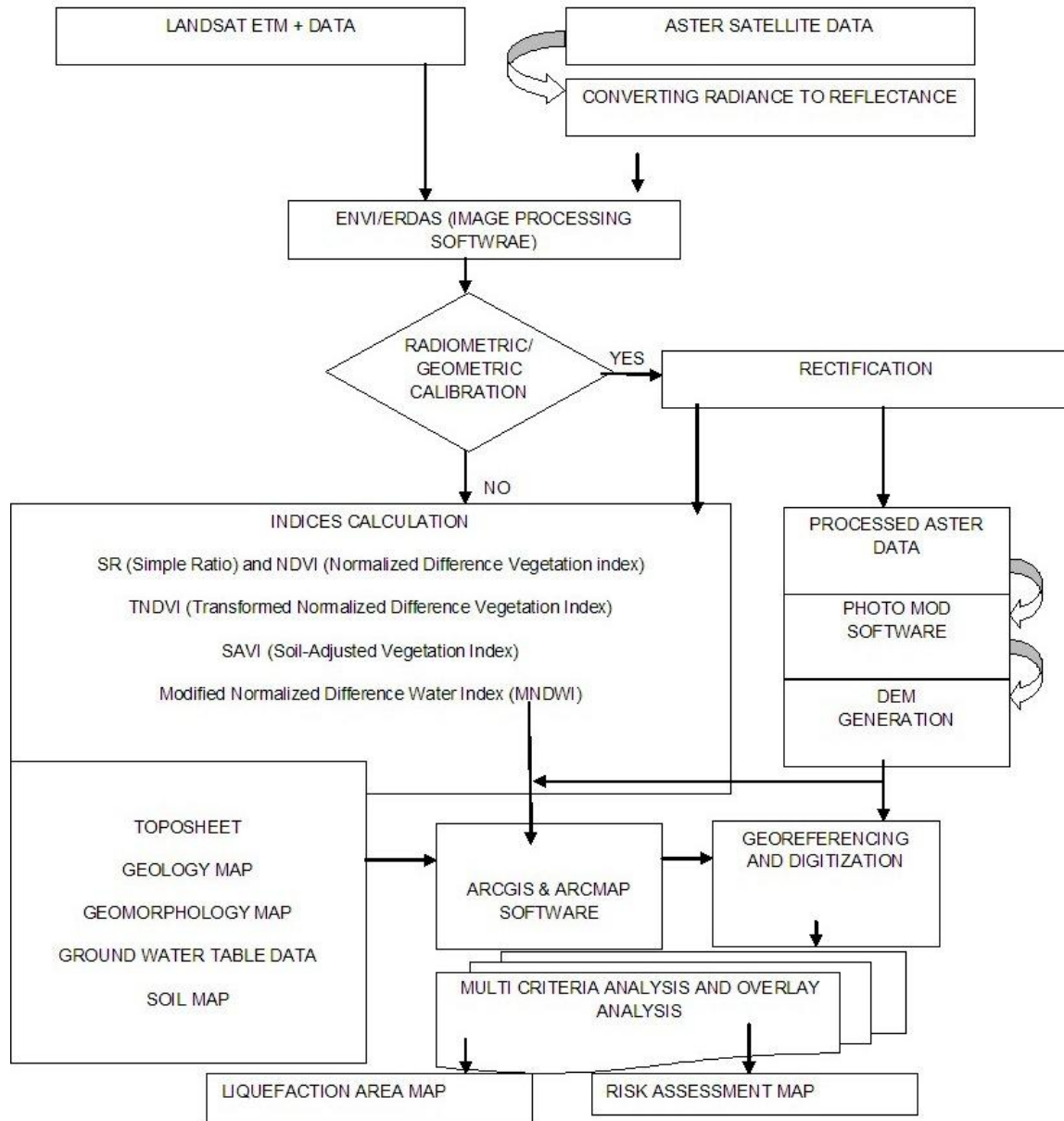
Figure 1: Work Flow of Inventory of Liquefaction Area and Risk Assessment Region

3.4.1. SR (Simple Ratio)

It is the ratio of the highest reflectance; absorption bands of chlorophyll makes it both easy to understand and effective over a wide range of conditions. As with the NDVI, it can saturate in dense vegetation when LAI becomes very high. Its value ranges from 0 to more than 30 [8]. SR is defined by the following equation no 1:

$$SR = \rho_{NIR} / \rho_{RED} \text{ --------- Eqn 1}$$

3.4.2. NDVI (Normalized Difference Vegetation Index)

It is the most frequently used vegetation index and the combination of its normalized difference formulation and use of the highest absorption and reflectance regions of chlorophyll make it robust over a wide range of conditions. Its value ranges from -1 to +1 [9,10]. The equation 2 shows the NDVI calculation.

NDVI = $\rho_{NIR} - \rho_{RED} / \rho_{NIR} + \rho_{RED}$ ---------- Eqn 2

3.4.3. TNDVI (Transformed Normalized Difference Vegetation Index)

TNDVI stands for Transformed Normalized Difference Vegetation Index. This index has a more complex ratio form for calculating the vegetation but still only uses Band 3 and Band 4. The equation 3 shows the TNDVI calculation [11].

[(Band 4 - Band 3) / (Band 4 + Band 3) +.5] ^ (1/2) --------- Eqn 3

(Or the square root of ([Infrared - Red] / [Infrared + Red] + .5)

3.4.4. SAVI (Soil-Adjusted Vegetation Index)

SAVI is a hybrid between a ratio index (NDVI) and a perpendicular index (PVI) [12]. Its equation is

SAVI = ((NIR-Red) / (NIR + Red+ L)) * (1+L) ---------- Eqn 4

L is a correction factor and its value is dependent on the vegetation cover. For total vegetation cover it receives a value of zero, effectively turning SAVI into NDVI. For very low vegetation cover, it receives the value of 1.

3.4.5. MNDWI (Modified Normalized Difference Water Index)

NDWI was unable to completely separate built-up features from water features. NDWI showed positive values in built-up features which were similar to water because the NIR reflectance was lower than the green reflectance [13]. To compensate the drawbacks of NDWI, overcome by Modified NDWI.

3.5. Multicriteria Analysis

GIS is capable of analysing several criteria utilizing spatial and attribute data. With a view to the Multicriteria evaluation, which is nothing but the process of evaluating the spatial features weighing them by allocating values to each pixel owing to their actual properties with the guidance of weighted Overlay Analysis, The weightage to every pixel is determined and it is performed in raster maps to create parametric thematic maps. For the task of delineating the liquefied zones, weighing the 4 statistical zones is done registering their values from 1 to 4 say, 1 for non-liquefaction susceptible zone, 2 for low-liquefaction susceptible zone, 3 showing moderate liquefaction susceptible zone and the final 4 indicating high-liquefaction susceptible zone. These different strengthened zonal parameters are thus created and attributed to compile the Liquefaction Area Map.

3.6. Overlay Analysis

Overlaying hereby probably determines the merging of differently featured imagery maps of the same or part of the same area, immersing them into a single compact monotonic data getting the idea of their spatial relationship. Weighing average is finally performed to every individual layer of parameters identifying the hot spots or high liquefaction area, so as to generate the Risk Assessment Map.

4. Conclusion

The above proposed criterion will surely be time and cost efficient and one among the successful ways of approach that tends to bear the stress of the researchers and geotechnical engineers so as to assess the environmental impacts and geotechnical hazards. This will probably pave the way for

further improvement in emerging the strategic ideas and techniques in these kinds of inventory works. Thus the compilation and generation of the Map with the delineation of the liquefaction susceptible zones over the study area which is the prime motto of this review can be done in an absolute manner with the above prescribed methodology utilizing the remote sensing and Geographical Information System (GIS) technologies and overall accurate and well-organized output can be obtained without any degree of failure to the attempt pursued. This henceforth makes an enthusiastic belief subjected to the expected output and may help and support the communal developers and the government in further planning of the towns and cities and designing of their infrastructure in an effective and brawny way.

References

1. Ferdinent, J.; Padmanaban, R. Development of a Methodology to Estimate Biomass from Tree Height Using Airborne Digital Image. *Int. J. Adv. Remote Sens. GIS* **2013**, *2*, 49–58.

2. Padmanaban, R. Location Privacy in Location Based Services: Unsolved Problem and Challenge. *Int. J. Adv. Remote Sens. GIS* **2013**, *2*, 398–404.

3. Visalatchi; Padmanaban, R. Land Use and Land Cover Mapping and Shore Line Changes Studies in Tuticorin Coastal Area Using Remote Sensing. *Int. J. Remote Sens.* **2012**, *1*, 1–12.

4. Monishiya, B. G.; Padmanaban, R. Mapping and change detection analysis of marine resources in Tuicorin and Vembar group of Islands using remote sensing. *Int. J. Adv. For. Sci. Manag.* **2012**, *1*, 1–16.

5. Ferdinent, J.; Padmanaban, R. Development of a Methodology to Estimate Biomass from Tree Height Using Airborne Digital Image. *Int. J. Adv. Remote Sens. GIS* **2013**, *2*, 49–58.

6. Padmanaban, R. Integrating of Urban Growth Modelling and Utility Management System using Spatio Temporal Data Mining. *Int. J. Adv. Earth Sci. Eng.* **2012**, *1*, 13–15.

7. Padmanaban, R.; Kumar, R. Mapping and Analysis of Marine Pollution in Tuticorin Coastal Area Using Remote Sensing and GIS. *Int. J. Adv. Remote Sens. GIS* **2012**, *1*, 34–48.

8. Venkatesan G; Padmanaban, R. Possibility Studies and Parameter Finding for Interlinking of Thamirabarani and Vaigai Rivers in Tamil Nadu , India. *Int. J. Adv. Earth Sci. Eng.* **2012**, *1*, 16–26.

9. Padmanaban, R. Modelling the Transformation of Land use and Monitoring and Mapping of Environmental Impact with the help of Remote Sensing and GIS. *Int. J. Adv. Altern. Energy, Environ. Ecol.* **2012**, *1*, 36–38.

10. Padmanaban, R.; Sudalaimuthu, K. Marine Fishery Information System and Aquaculture Site Selection Using Remote Sensing and GIS. *Int. J. Adv. Remote Sens. GIS* **2012**, *1*, pp 20-33.

11. Green, E. P.; Mumby, P. J.; Edwards, A. J.; Clark, C. D.; Ellis, A. C. Estimating leaf area index of mangroves from satellite data. *Aquat. Bot.* **1997**, *58*, 11–19.

12. Cabral, P.; Zamyatin, A. Three Land Change Models for Urban Dynamics Analysis in Sintra-Cascais Area. *Image Rochester NY* **2006**, *2–3*.

13. Kovacs, J. M.; Wang, J.; Flores-Verdugo, F. Mapping mangrove leaf area index at the species level using IKONOS and LAI-2000 sensors for the Agua Brava Lagoon, Mexican Pacific. *Estuar. Coast. Shelf Sci.* **2005**, *62*, 377–384.

Research Article   **Open Access**

Geospatial Techniques Based Assessment of Groundwater Recharge Site Suitability

Nemika Kumari and Akhouri Pramod Krishna

Department of Remote Sensing, Birla Institute of Technology (BIT) Mesra, Ranchi, Jharkhand, India

Correspondence should be addressed to Akhouri Pramod Krishna, apkrishna@eastwestcommunity.org

Abstract Ranchi city in Jharkhand state of India has been facing the problem of ground water availability in recent times believed largely due to rapid urbanization coupled with the presence of hard rock strata. For assessing the groundwater recharge suitability zones through geospatial techniques, this study was undertaken in the Kanke administrative block area within and around the Ranchi city. Artificial recharge is expected to become increasingly necessary in future as the growing population requires more water and thus, more storage is required to conserve water for use in the times of shortage. Geospatial techniques employing remote sensing (RS) and geographical information system (GIS) are increasingly being used in the field of hydrology and water resources development. One of the greatest advantages of using remote sensing data for hydrological investigations and monitoring is its ability to generate information in spatial and temporal domain, which proved very crucial for successful analysis, prediction and validation. For assessing potential groundwater recharge locations, the relevant hydrological characteristics were determined through suitable thematic details. In addition, groundwater data of the recent years were analyzed to understand the current trend of depletion. Analysis and integration of thematic layers as per certain decision rules resulted in the map indicating potential areas for artificial ground water recharge with different degrees of suitability.

Keywords *Geospatial Techniques, GIS, Ground Water, Hydrogeology, Recharge, Remote Sensing*

1. Introduction

With rapid urbanization and increasing population in the urban areas, demand for water is bound to grow and may result in the likely depletion of ground water reservoirs. Therefore, restoration of the depleting ground water reservoirs (aquifers) to their original state should be important. This can be done by recharging the aquifers artificially. Sub-surface reservoirs are very attractive and technically feasible alternatives for storing surplus monsoon run off. Such reservoirs can store substantial quantity of water within suitable geological formations for storing water that comes from sources located on the land surface. Basic purpose of artificial recharge of ground water is to restore supplies from aquifers depleted due to excessive ground water development. Modern techniques like remote

sensing and GIS are increasingly becoming important day by day in all real world problems of geo-spatial nature. Field of hydrology and water resources development is also the area having extensive scope of deriving benefits from these tools of geoinformatics [1-4]. Remote sensing provides multispectral, multi-temporal and multi-sensor data of the earth's surface. One of the greatest advantages of using remote sensing data for hydrological investigations and monitoring is its ability to generate information in spatial and temporal domain, which is very crucial for successful analysis, prediction and validation [5-6]. GIS technology is becoming an important tool as a platform to efficiently manage large and complex information organized around its core [7]. It also provides suitable alternatives for efficient management of the large and complex databases.

Artificial recharge involves augmenting the natural movement of surface water into underground formations [8]. Recharge can be either direct or indirect. In direct recharge, water is introduced into an aquifer via injection wells. The injected water is treated to ensure that it does not clog the area around the injection well. Indirect recharge involves spreading surface water on land so that the water infiltrates through the vadose zone, the unsaturated layer above the water table, down to the aquifer. Methods for spreading water include over-irrigation, creating basins, using construction methods, or making artificial changes to natural conditions such as modifying a stream channel. Artificial recharge techniques normally contribute to enhance the sustainable yield in areas where over-development has depleted the aquifer, and conserving the excess surface water for future requirements. Therefore, this study aimed at information generation for facilitating recharge zone site selections using integrated geospatial techniques. This was coupled with the consideration of hydrogeological factors for potential recharge site assessment and generating spatial information on suitability of potential recharge locations.

1.1. Study Area

This study has been carried out in Kanke block (Figure 1.1) with its parts falling within the Ranchi municipal area. Kanke is a census town having an average elevation of 611 metres in Ranchi district in the Indian state of Jharkhand. Ranchi is capital city of Jharkhand, a new state formed on 15 November 2000 by carved out from the erstwhile state of Bihar. Subarnarekha is the main river of this area, which flows from west to east direction and takes a turn towards south east direction near Hatia. Harmu River, Pandra River, Potpoto River and Jumar River are the tributaries of the river Subarnarekha. All the tributaries of the river Subarnarekha flow in west to east direction.

The area consists mainly of three types of geomorphologic units - plateau weathered moderate, plateau weathered shallow and plateau dissected. Inselberg, residual hillocks are found and the Ranchi hill, Tagore hill and Bariatu hill are the three major hillocks. Topography of the area is relict type, controlled by the hard and resistant rocks which form a part of the Chhotanagpur plateau. Middle portion of the region have very prominent physiographical features marked by the hills and hillocks. Ranchi has a humid subtropical climate with average maximum temperature ranging from 31.60^0C to 38.10^0C during the months of April to June while the average minimum temperature ranges from 18.40^0C to 24.30^0C. Average annual rainfall has been recorded between 1300 to 1400 mm over a reference period of the years 2004 to 2008. Ground water data of three wells in Kanke block located at Chauri Basti, Jahaj Kothi and Kanke for the years 2007 to 2010 suggests that monthly fluctuation in depth at these sites has almost similar trend (Table 1.1). Depth to ground water tends to increase from the April month and reaches its maximum value in June. This is made more explicit in the Figure 1.2 with depth to ground water plotted for the Kanke well location.

1.2. Geological and Hydrogeological Characteristics

This area comprises of Chhotanagpur gneissic complex composed mainly of meta-sedimentary rocks intercalated with granitic rocks. Rocks of the Chhotanagpur pleateau around Ranchi consist mostly of granite and granite-gneisses, with bands of feldspathic schist and quartzite. Different rock types occurring in the area are: schistose rocks, granitic rocks, laterites and older alluvium. Schistose rocks occur as enclaves of the granitic rock and older units of these rocks are profusely intruded by quartzo-feldspathic veins. Meta-sedimentary rocks were originally argillaceous, arenaceous and calcareous in nature. The intrusive basic rocks are reported from the adjoining areas. The various units of granitic rocks are aplites, pegmatite, augen-gneiss, porphyroblast-gneiss and quartz veins etc.

In general, the regional strikes of the meta-sedimentary and granitic rocks are E-W with northerly dip. The meta-sedimentary have suffered intense regional metamorphism of amphibolite facies. The foliation strike and dip of granitic rocks tally with those of meta-sediments. There are subordinate igneous intrusions like pegmatite and quartz veins. Post-pleistocene weathering has resulted in lateretization which occurs as capping. Laterites are commonly associated with meta-sedimentary and granitic rocks. Two types of aquifers such as weathered zone aquifer and fractured zone aquifers are found around Ranchi area. Thickness of weathered aquifer varies between 5.50 m to 29.50 m below ground level (bgl). In weathered zone, ground water occurs near surface under the water table or phreatic aquifers in unconfined condition and in the fractured zone, ground water occurs in semi confined to confined condition.

3. Materials and Methods

In this study, a multi thematic overlay analysis of various relevant mapped features was carried out. A soil erosion potential map was prepared by overlaying various themes of land use/land cover, geomorphology, slope and drainage prepared by interpretation from the IRS LISS III satellite data based on the visual image interpretation keys. Thematic layers of soil and geology were prepared based on the data available from National Bureau of Soil Survey and Land Use Planning (NBSS & LUP) and Geological Survey of India (GSI) respectively. Information related to artificial recharge site selection usually include: source of recharge water, availability of a geological formation suitable for artificial recharge, thickness and permeability of material overlying the geological formation considered suitable for recharge, proximity of the potential recharge site to the cone of depression of an appropriate well and water level differences between the aquifer and the recharge site. In this study, an attempt has been made to include factors such as lineaments, hydrogeomorphic and hydrogeological features, land use and drainage density to assess artificial recharge site. The thematic maps were assigned weightages and by giving their respective percentage influence to obtain a suitable relative scores. All the relevant themes were digitized using ArcGIS software package. Overlay analysis of different thematic layers was carried out as per the decision rules to assess areas and sites suitable for artificial recharge. Data for the resource/thematic mapping were derived from the remote sensing images viz. satellite imagery of IRSIC LISS-III of February, 2009 with a spatial resolution of 23.5 m, along with Survey of India topographical sheets, geological map and the soil map of the area.

Digital image processing of satellite data was carried out using ERDAS Imagine software. This helped in generating information about the latest land use-land cover pattern of the area and its temporal changes. Present status of land use/land cover of Kanke block area was evaluated and thematic maps on rock-soil contact, folded structures, lineaments and soil types were generated in conjunction with secondary information. In satellite false color composite (FCC) image, the barren and vegetative rock exposures normally show light tone and medium to coarse texture, high peaked hills and features with relief, whereas the soil-covered zones exhibit medium to darker tone, fine texture and moderate drainage patterns. Fluvial geomorphic landforms were interpreted from digitally processed

satellite data. Three types of fluvial land forms identified in the study area were piedmont zone, colluvial fills and flood plains. All these land forms should have high amounts of unconsolidated sediments, and hence, must have a higher rate of infiltration, thus favorable areas for artificial recharge.

Lineament density and hydrological soil groups based on infiltration rate, texture, depth, drainage condition and water infiltration capacity were also identified. Digital Elevation Model (DEM) using ASTER satellite data (http://www.glcf.umd.edu/data/aster/) of the area was generated with ArcGIS software. This was used to generate contours and thereby slope analysis of the area. Relevant morphometric parameters for the basin area were calculated based on various standard techniques and methods. This study used the model for estimating surface runoff as developed by the United States Soil Conservation Service (SCS). SCS has developed a widely used runoff curve number procedure for estimating the runoff, in which the effect of land use and land cover, various soil cover and antecedent moisture condition are considered. If more than one land use or soil cover occurs, then the composite curve number method is adopted [9]. After calculating the curve number, the potential maximum soil retention (S) was calculated using the following formula:

$$S = \frac{25400}{CN} - 254$$

Table 2.1 shows the run-off thus calculated for different soil hydrological groups of the study area. Followed by the potential maximum soil retention estimation, the initial abstractions are calculated. Initial abstractions pertain to water losses, e.g. plant interceptions, infiltration and surface storage which occur prior to runoff and are then subtracted for the total runoff [10]. For artificial recharge, catching the run-off to infiltrate, ground water recharge structures serve the purpose of enhancing the ground water potential of the area under consideration [11]. These structures are generally constructed on active aquifer and on scrub or barren land. Slope of the area should not be more than 5% and soil should be highly permeable. Presence of lineaments in the study area is considered favorable to construct these structures within the influence zone of lineaments.

Data integration and prioritization were performed through thematic map integration and statistical analysis in ArcGIS environment. Thematic layers, namely geology (Figure 3.1), geomorphology (Figure 3.2), soil type (Figure 3.3), lineament and drainage were created. The base vector files were created so that further analysis could be done based on these layers. After preparing these base layers, drainage layer was converted to drainage density layer and lineament layer was converted to lineament density layer (Figures 3.4-3.5). Land use/land cover map of the area was generated through supervised method of maximum likelihood classification (MLC) of the satellite digital data i.e. IRS LISSIII of the year 2009 (Figure 3.6). Different land use/cover classes were assigned suitable weights. ASTER DEM of the study area was subset and reclassified into 5 different elevation classes. Weights were assigned to the reclassified DEM based on topographic suitability for water recharging. Other layers were also reclassified and weights were assigned as per their suitability for ground water recharge (Tables 3a-e). Geology was classified into 7 weight classes which included structure viz. fault/joint, geomorphology was classified into 8 weight classes, soil types into 4 weight classes, drainage density was reclassified in to 6 weight classes and lineament density was reclassified in to 5 weight classes. All these assigned weights were normalized by dividing the individual weights upon cumulative weight for the individual layers.

These normalized weights were multiplied with the assigned weights for the different thematic layers already generated, and these calculated weights were considered the total weight. Further to this, all the vector layers were converted to raster layers based on the assigned total weights. In this process, every thematic map representing certain areas as favorable zones for artificial ground water recharge was generated. For demarcation of precise site suitability, all the layers were added based on the

total weights assigned to different classes of thematic layers. After adding all the layers, site suitability map was generated with reclassification into different categories (Figure 3.7). This included three classes namely, priority one (highly suitable), priority two (moderately suitable), and not suitable (least priority area).

4. Conclusion

Thematic mapping was undertaken for the study area with its inherent characteristics using geospatial techniques. Groundwater data for some wells over certain recent period were analyzed to understand the trend of ground water depletion. It showed that the water table had a decreasing trend seasonally. Catchment characteristics indicated that the sub-watersheds covering the study area had dendritic to sub dendritic drainage pattern with moderately dense drainage texture. High bifurcation ratios indicated a strong structural control on the drainage and were indicative of strong head ward erosion taking place. Overlay analysis of different thematic layers resulted in the final map showing the suitable zones for ground water recharge. South-eastern and north-eastern parts of the study area were inferred better suited for the ground water recharge purposes. Methods of artificial recharge for the identified recharge locations can be decided using the results of different studies like runoff estimation, sub surface materials, etc. as the inputs. Runoff quantity can decide the size of the recharge structure. Land use classification studies of the area can be used in assessing the current status of the land use pattern and further planning the future development in view of the increasing pressures of urbanization. Catchment characteristics studies along with runoff estimation studies may find application in detailed hydrological studies of the area in future. Results of such studies can be significant for the development and maintenance of surface water bodies in the study area.
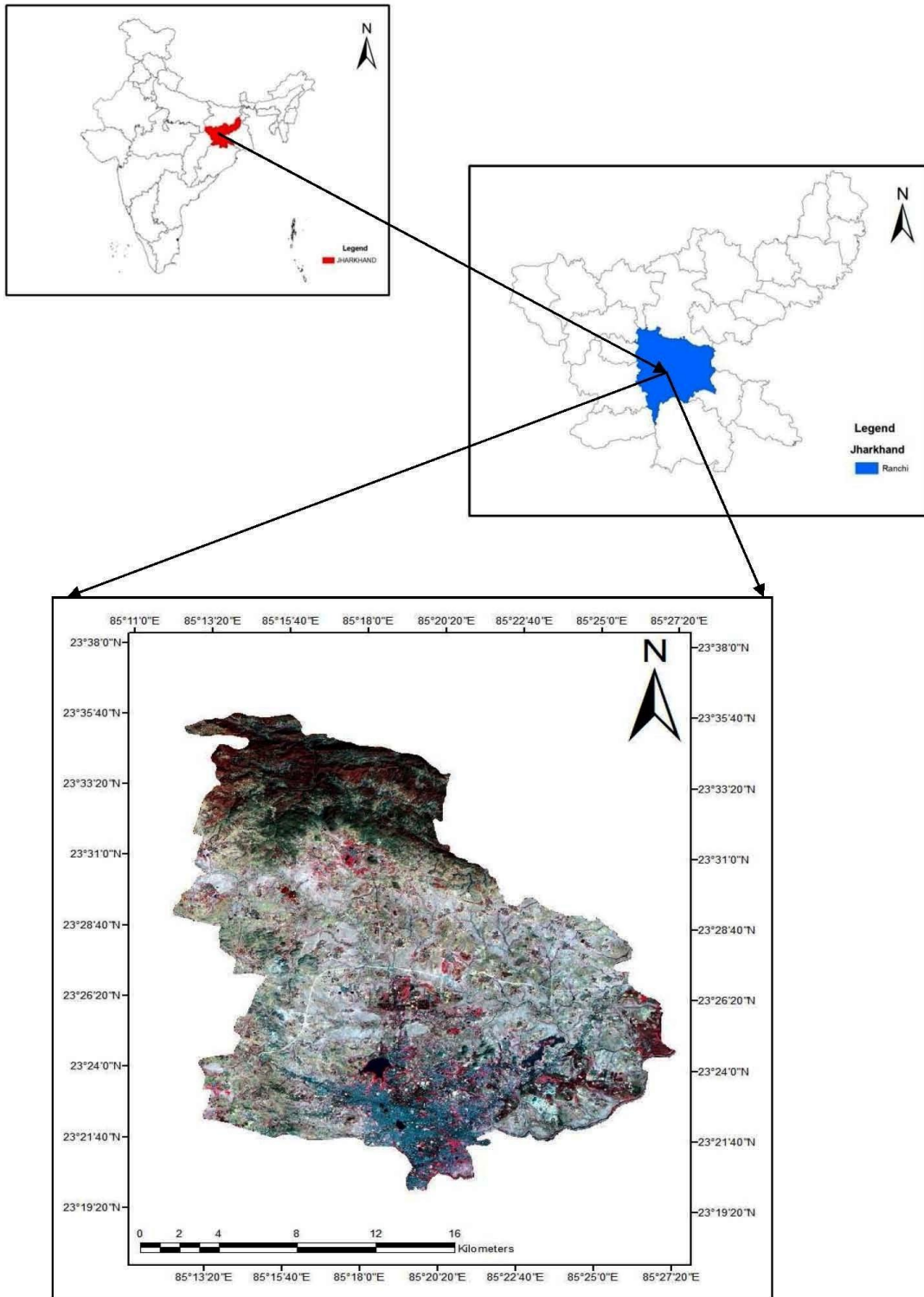
Acknowledgments

Figures

Figure 1.1: *Location Map of the Study Area*

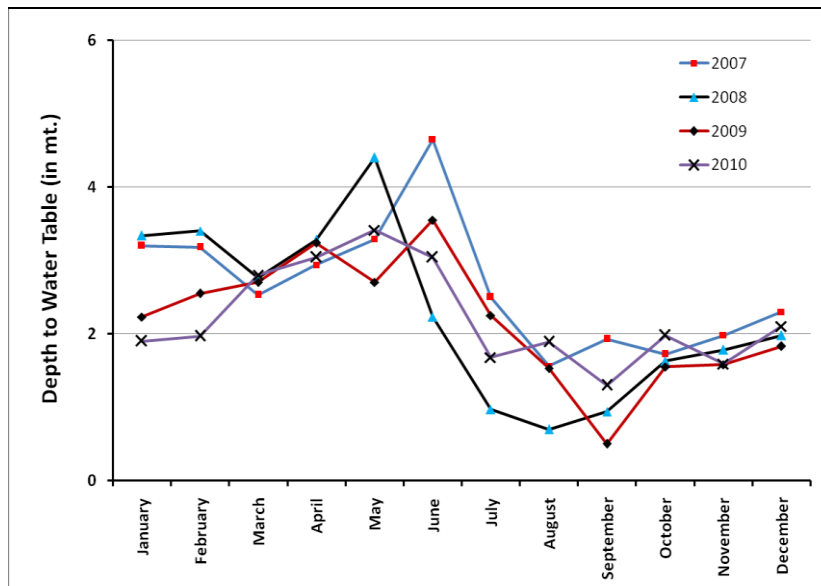***Figure 1.2:*** *Monthly Variations in the Ground Water Table Over the Years 2007 To 2010 Based On the Kanke Well Location*
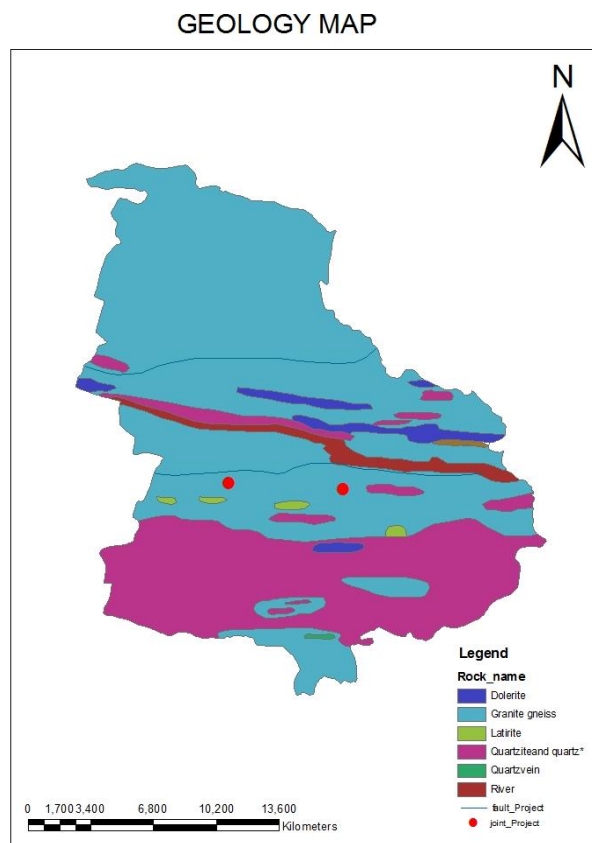
GEOLOGY MAP

Figure 3.1: *Geology of the Study Area (after GSI)*
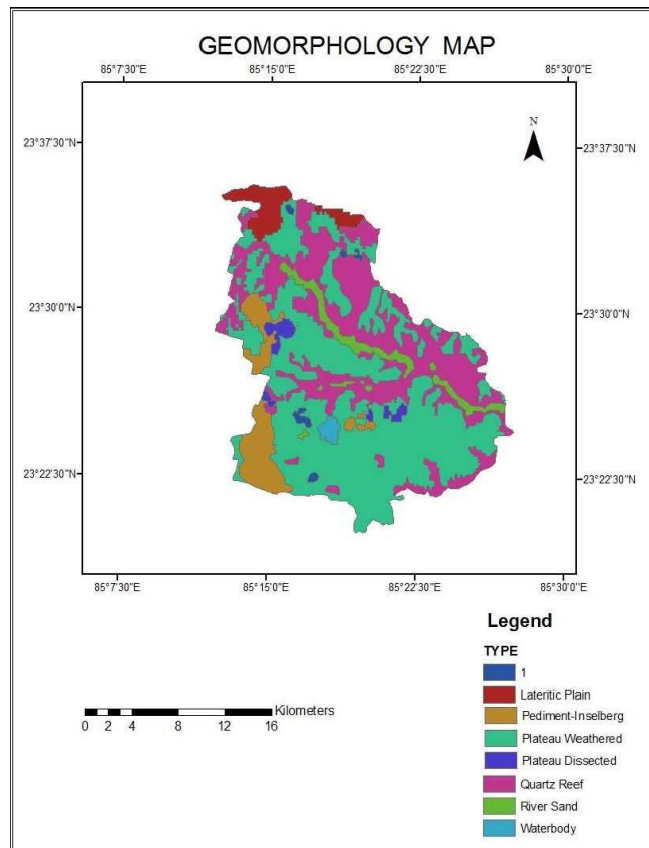
Figure 3.2: Geomorphology of the Study Area

Figure 3.3: Soil Types of the Study Area (After NBSS & LUP)

Figure 3.4: Lineament and Density Map of the Study Area

Figure 3.5: Drainage and Drainage Density Map of the Study Area

Figure 3.6: Land Use/Land Cover Map of the Study Area Generated Using IRS LISSIII Satellite Data of the Year 2009

Figure 3.7: Site Suitability Map Generated For Groundwater Recharge Zones of the Study Area

Tables

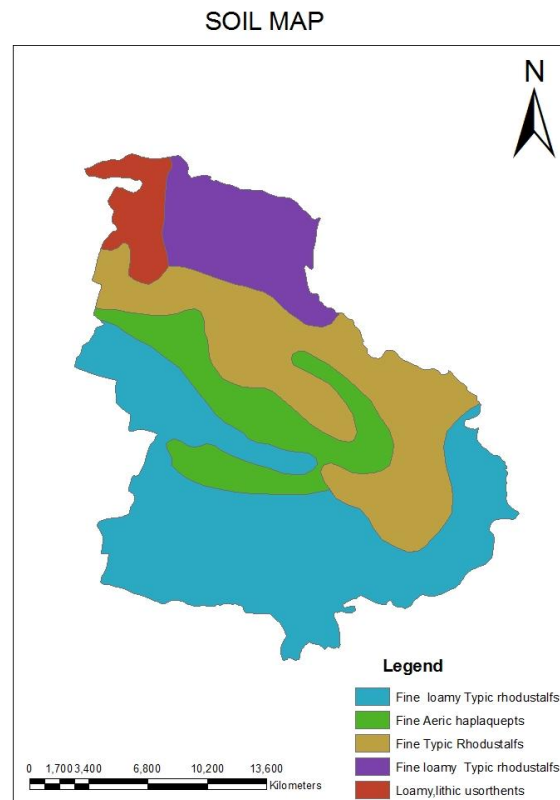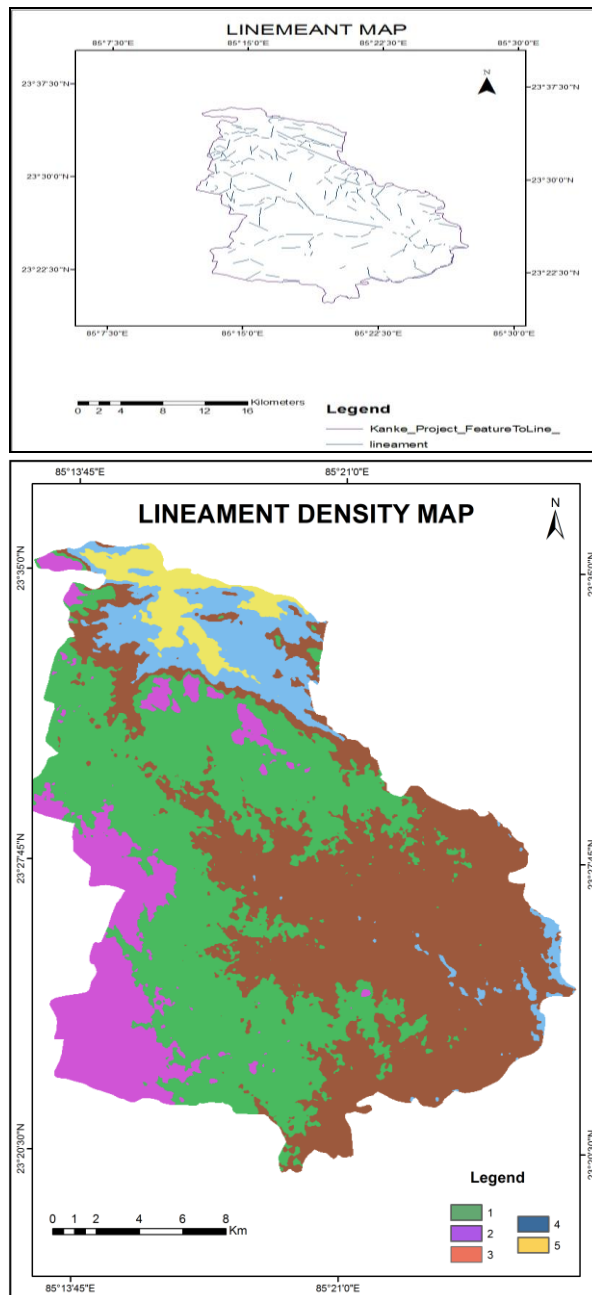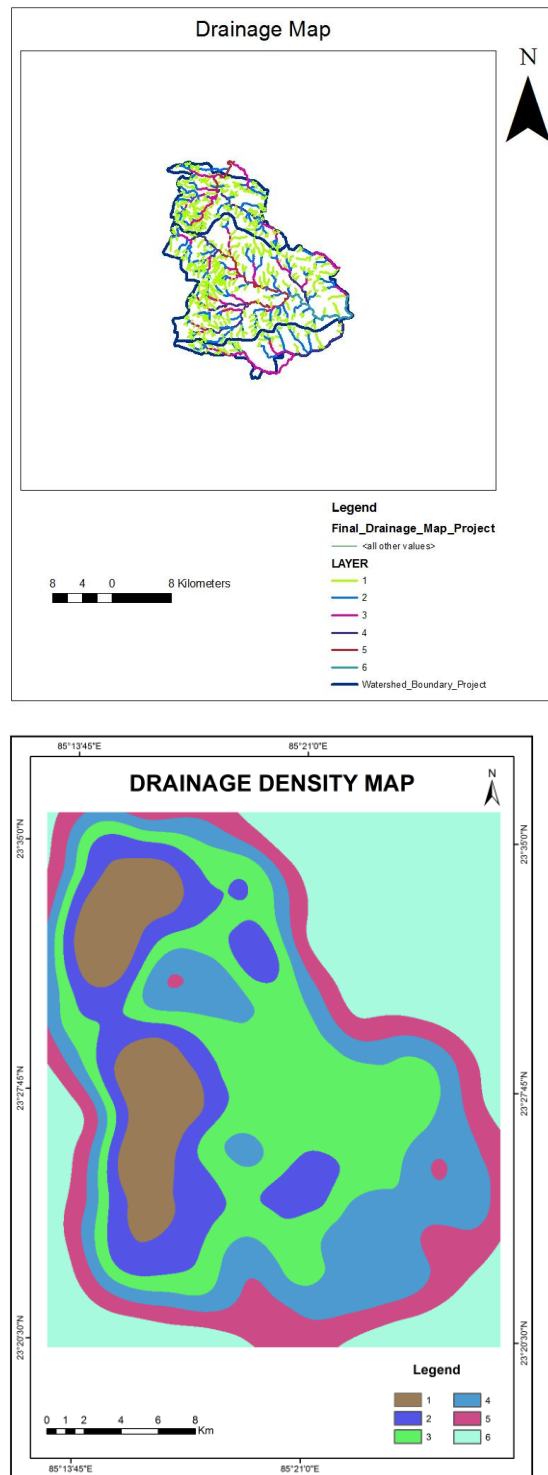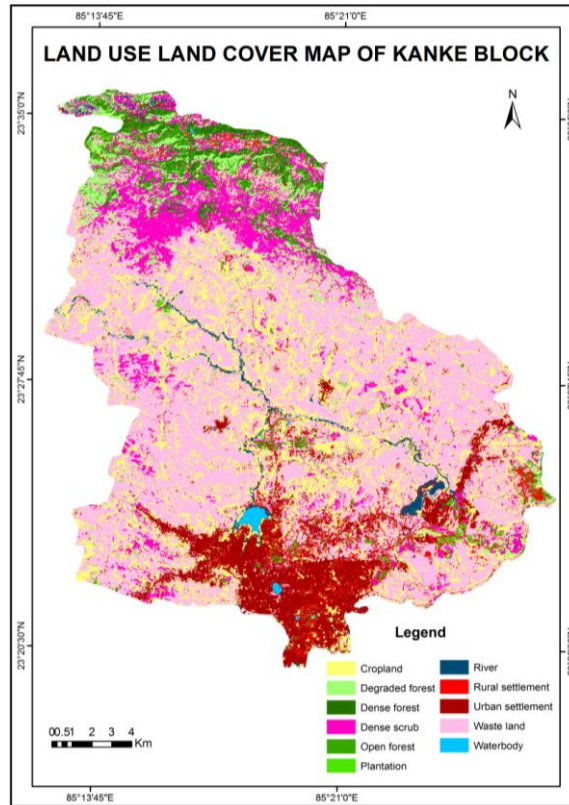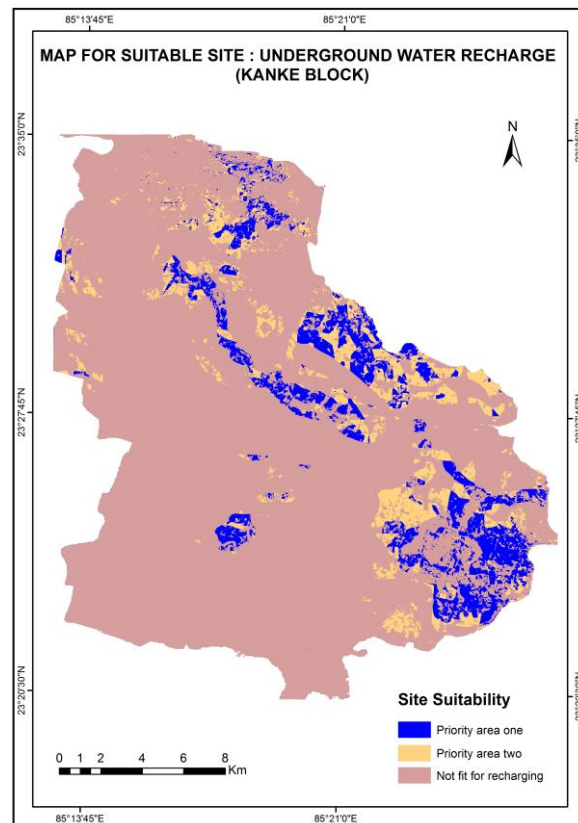*Table 1.1: Comparative Monthly Variation in the Depth to Groundwater (in m) Over the Years 2007 to 2010 in the Three Wells of Kanke Block*

Month	Chauri Basti				Jahaj Kothi				Kanke			
	2007	2008	2009	2010	2007	2008	2009	2010	2007	2008	2009	2010
January	3.27	3.56	4.65	2.78	3.22	3.65	2.80	1.40	3.20	3.34	2.23	1.90
February	3.57	3.28	4.80	3.08	3.78	3.16	2.65	1.46	3.18	3.40	2.55	1.97
March	3.22	3.33	4.92	3.38	3.65	3.20	2.31	2.56	2.53	2.76	2.70	2.80
April	3.32	3.52	4.05	3.30	3.58	3.26	2.83	3.70	2.94	3.28	3.24	3.04
May	3.97	4.80	4.74	3.35	3.72	4.56	2.65	2.68	3.29	4.40	2.70	3.41
June	3.87	1.08	5.95	4.13	1.45	0.84	4.86	4.17	4.65	2.23	3.55	3.04
July	2.89	0.54	4.17	3.96	3.45	1.09	4.05	4.30	2.50	0.97	2.25	1.68
August	1.12	0.65	1.41	2.40	1.26	0.78	1.27	2.10	1.56	0.70	1.53	1.89
September	1,96	1.20	0.92	1.98	1.89	1.40	0.49	1.78	1.93	0.94	0.50	1.30
October	1.54	2.70	2.78	2.56	1.74	1.62	2.63	2.60	1.72	1.63	1.55	1.98
November	2.65	3.41	3.67	3.53	3.02	2.05	3.80	3.78	1.98	1.78	1.58	1.59
December	3.03	4.20	2.48	3.41	3.62	2.53	1.33	3.20	2.30	1.98	1.83	2.10

Table 2.1: Runoff through Different Soil Hydrological Groups of the Area

Soil Hydrological Group	Total Runoff (Q) (mm)	Average Monthly Runoff (mm)
A	56023.02	1807.19
B	63894.58	2061.12
C	77942.93	2514.29
D	83383.60	2689.79

Table 3: *Weightages Assigned to the Different Classes of Parameters Considered*

(a) Different Classes of Geology Including Structure

SI. No.	Lithology/Structural Feature Classes	Weightage
1	Granite gneiss	2
2	Quartz vein	4
3	Quartzite and quartz	3
4	Dolerite	1
5	Laterite	5
6	Fault	6
7	Joint	7

(b) Different Classes of Geomorphology

SI. No.	Geomorphology Classes	Weightage
1	Inselberg	1
2	Pediment inselberg	3
3	Lateritic plain	6
4	Plateau weathered	1
5	Quartz reef	4
6	Water body	8
7	River sand	7
8	Plateau dissected	2

(c) Different Classes of Soils

S. No.	Soil Type	Soil Hydrological Group	Weightage
1	Fine loamy Typic Rhodustalfs	B	3
2	Fine Typic Rhodustalfs	A	4
3	Fine loamy Typic Rhodustalfs	B	3
4	Loamy,lithic Usorthents	C	2
5	Fine Aeric Haplaquepts	D	1

(d) Different Classes of Drainage Density

Value	Drainage Density Class	Weightage
1	Class 1	1
2	Class 2	2
3	Class 3	3
4	Class 4	4
5	Class 5	5
6	Class 6	6

References

[1] Krishna A.P. Remote Sensing Approach for Watershed Based Resources Management Priorities In The Sikkim Himalaya - A Case Study. J. Indian Soc. Remote Sens.1996. 24 (2) 69-83.

[2] Durga Rao K.H.V., et al., 2001: *A Suitable Site: Geographic Information Systems and Remote Sensing Technology.* Making Water Everybody's Business. Centre for Science and Environment, New Delhi, 243-245.

[3] Anbazhagan S., et al., 2001: *Remote Sensing Based Artificial Recharge Studies - A Case Study From Precambrian Terrain, India.* Management of Aquifer Recharge for Sustainability. ISAR-4, Adelaide, A.A. Balkema Publishers, Lisse, 553-556.

[4] Krishna A.P. *Snow and Glacier Cover Assessment in the High Mountains of Sikkim Himalaya.* Hydrological Processes. 2005. 19 (12) 2375-2383.

[5] Saraf A.K., et al. *Integrated Remote Sensing and GIS for Ground Water Exploration and Identification of Artificial Recharge Sites.* Int. J. Remote Sensing. 1998. 19 (10) 1825-1841.

[6] Kumar G.M., et al. *Delineation of Potential Sites for Water Harvesting Structures Using Remote Sensing and GIS.* J. Indian Soc. Remote Sens. 2008. 36; 323-334.

[7] Kumari Nemika, 2011: *An Assessment of Potential Ground Water Recharge Site Using Geoinformatics in Kanke Block, Ranchi District*, M.Tech. Thesis (unpublished), Department of Remote Sensing, BIT, Mesra, India.

[8] Anonymous, 2007: *Manual on Artificial Recharge of Ground Water.* Central Ground Water Board, Ministry of Water Resources, Govt. of India, New Delhi, 198.

[9] Anonymous, 1973: *A Method for Estimating Volume and Rate of Runoff in Small Watersheds.* Technical paper, 149, Soil Conservation Service, USDA- SCS, Washington, D.C., 1973.

[10] USDA-SCS, 1985: *National Engineering Handbook.* Section 4-Hydrology, Washington, D.C.

[11] Durga Rao K.H.V., et al. *Spatial Expert Support System in Selecting Suitable Sites for Water Harvesting Structures- A Case Study of Song Watershed, Uttaranchal, India.* Geocarto International. 2003. 18 (4) 43-50.

Methodology Article   **Open Access**

Application of Thermography Technique for Assessment and Monitoring of Coal Mine Fire: A Special Reference to Jharia Coal Field, Jharkhand, India

J. Pandey[1], D. Kumar[2], R.K. Mishra[1], N.K. Mohalik[1], A. Khalkho[1] and V.K. Singh[1]

[1]Mine Fire Division, Central Institute of Mining and Fuel Research, Dhanbad, Jharkhand, India
[2]Department of Mining Engineering, Indian School of Mines, Dhanbad, Jharkhand, India

Correspondence should be addressed to J. Pandey, jitu.cimfr@gmail.com

Abstract Coal mine fire problem occurs globally and endangering miners' life. It leads to environmental pollution as well as economic loss to the local and regional governance. Surface coal mine fire affected areas are generally detected by thermal survey of an area. Temperature observations through thermometer or thermocouple are used in most cases as traditional monitoring of coal fire. Infrared thermograph technique combination with GPS topography has more advantage over traditional monitoring in terms of efficiency, precision and less costly. A large surface area can be seen, captured, and presented in thermal and visual form in very short interval of time. This paper describes basic principle, monitoring procedure and application of thermography in Jharia Coalfields (JCF) to assess coal mine fire affected areas and strategy to control it.

Keywords *Thermography, Coal Mine Fire, Emissivity, Thermal Image Analysis, IR Scanning*

1. Introduction

Coal is a prime source of energy that fulfils about 70 % fuel requirements in our day to day life [1]. Fire occurrence in this non-renewable natural fuel is posing serious threat to environment in terms of pollution, global warming and economic loss to the industry. Globally, coal fires are reported in USA, Australia, Germany, Spain, Poland, Czech Republic, India, Pakistan, Indonesia, Venezuela and China [2]. However, this problem is more severe in China, USA and India. In India, surface and subsurface fire throughout Jharia Coal Field (JCF) comprises one of the largest mine fire complex in the world [3]. JCF fire is of specific interest and needs attention for safe production of coal and safety of miners. The incidences of coal fire that occur in JCF are mainly due to spontaneous combustion [4].

Detecting coal mine fire is the most important step to decide measures for mitigating and controlling coal fire. Thermal survey is the most common technique used worldwide for several decades. This technique is used for detecting and evaluating, the status and extent of surface and subsurface coal fire. Until 1960s, researchers have used thermocouples and thermometers to assess the coal mine

fire with an advantage of temperature measurements in close proximity. But this method does not produce sufficient data to cover larger area in synoptic view [5]. In case of progress of fire for a larger, unapproachable and unstable area, monitoring by this traditional method becomes very difficult, some time impossible, time consuming and costly.

In view of the above facts, most of researchers prefer the air borne and satellite borne thermal data produced from aerial survey/remote sensing images which make the detection, delineation and monitoring of coal fire easier [6]. The temperature limitation of satellite Landsat-5 TM Band-6 data is 270 K-350K in spectral band 8-14 μm [7]. The spatial resolution of Landsat -5 TM Band 6 and Landsat-7 ETM+ are 120x120m and 60x60m respectively [8]. The Thermal sensor TM band 6 gets saturated (maximum DN value 255 of 8-bit data) at approximately 343-350 K and gives pixel-integrated temperature of about 70^0C only, which is much lower than observed from the field measurement ($>500^0$C) [9]. However, hot spots observed using this technique is unable to distinguish actual coal fires from forest fires, fire in bushes, and fire in soft coal generated by the people residing in the vicinity of the coal field. This often leads to undercounting over a significant amount [1] and [9]. The infrared thermograph, compared to traditional technique has an advantage of good coverage area, non contact type, more-efficient with high precision of temperature measurement [10]. In an electromagnetic spectrum the infrared region varies from 2μm to 13μm wavelength (Figure 1). This wavelength of infrared spectrum is more than that of a visible spectrum [11].
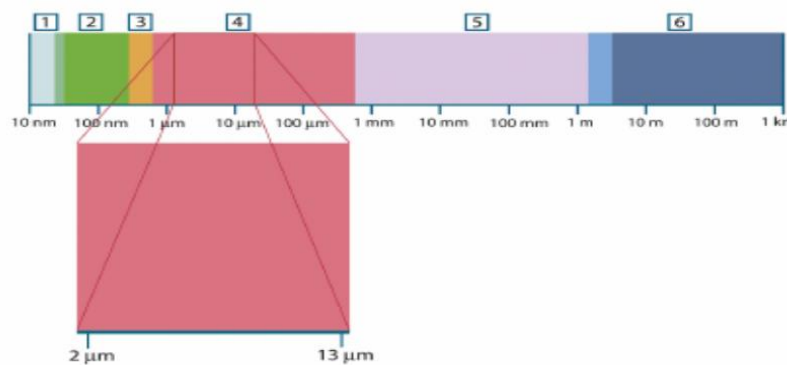

Figure 1: Electromagnetic Spectrum. 1: X Ray, 2: UV, 3: Visible, 4: IR, 5: Microwaves, 6: Radiowaves

A thermography instrument is a thermal pointer or a thermal scanner. The thermal pointer reads the temperature of a specific point whereas a scanner creates the thermal profile of large surface area in visual and thermal form in short interval of time [12]. The infrared system consists of an "infrared energy detector" and a "Monitor". The scanner is an optomechanical device which converts the infrared energy received from an object surface to an electrical signal. These signals are further fed into monitor where it is processed and presented in different forms like simple digital display to indicate temperature level and a video display for thermal profile (Figure 2) [11].
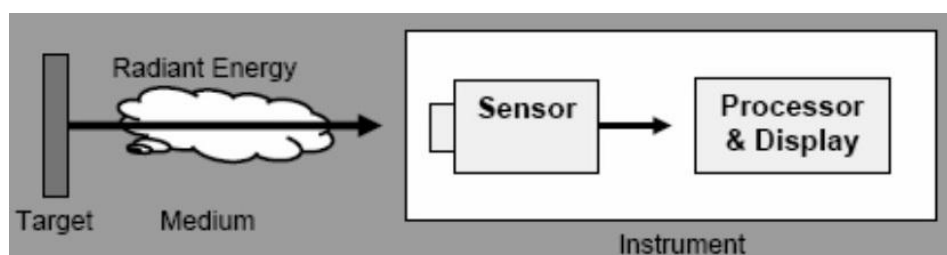

Figure 2: A Schematic Representation Working Principle of Thermal Imaging Camera

Thermographic scanner has facility of software backup for transfer, processing and analysis of the captured image but it cannot detect an object temperature if the medium is separated or covered by glass or polythene material etc. [11]. Therefore, application of thermographic technique to monitor the status and extent of coal mine fire plays a very vital role to diagnose and predict potentiality of this socio-technological problem.

2. Area of Interest

The most complex coal mine fire extending from surface to subsurface subsequent to opencast and deep mining of JCF has been selected for the study. The coal mining in JCF started in 1894 and the massive production of coal on regular basis lead to extension of the mining area. This extension became the reason for spontaneous heating of coal. The first coal fire was observed in 1916 [13], [14], and [15]. JCF is confined between latitudes 23°38' N and 23°52' N and longitudes 86°08' E and 86°29' E extending 38 km from East to West and 19 km from North to South with an area of 450 Sq Km [1, 13].

The total number of fires reported in all Indian coalfields was 196 including 65 fires of JCF, spreading over an area of 17.32 sq km in 1996 reduced to 8.9 sq km after controlled and combated ten fire in 2006 [16, 17]. Due to complex and critical nature of fire problem, about 37 million tons of prime coal have been lost so far and 1860 million tons of coal have blocked and become unwinnable [1, 4]. The subsurface coal fire is maintaining its status for more than five decades and still spreading and endangering hundreds of thousands of lives residing in vicinity of the fire area of JCF (Figure 3) [18].
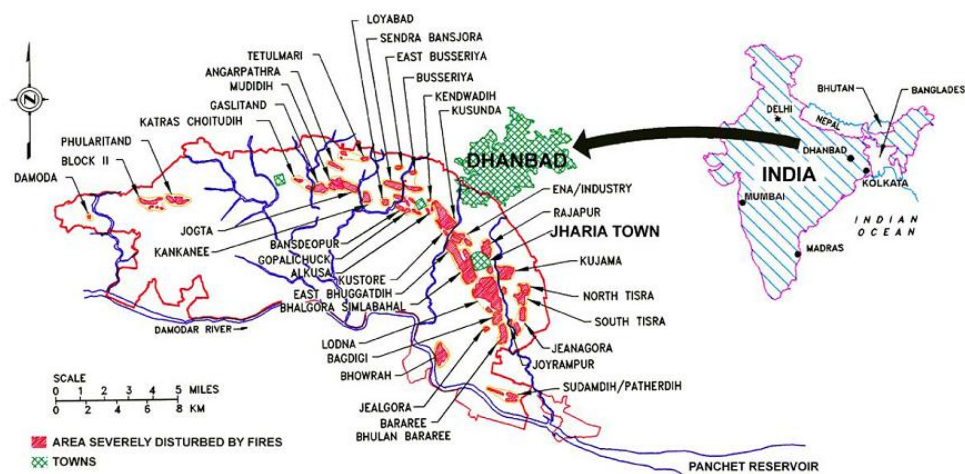
Figure 3: Plan of the Jharia Coalfield and Principal Collieries affected by coal Mine Fires (Reproduced from Michalski, 2004)

3. Thermographic Technique

3.1. Principle

All matters at absolute temperature (0 K) emit electromagnetic radiations continuously which are characteristic of the temperature of the body. The temperature of the earth material can be estimated on thermal radiation. Planck's black body radiation equation relates a spectral radiation and wave length with radiant temperature of an object as given in equation (1) [7].

$$T_{rad} = \frac{hc/k}{\lambda \ln\left[\dfrac{2hc^2\lambda^{-5}}{L_\lambda} + 1\right]}$$

(1)

Where, L_λ = spectral radiance (w/m^2 /sr/μm), λ = wavelength (m), T_{rad}= radiant temperature of the object (K), h = Planck's constant (6.26x10^{-34} J s), c = speed of the light (3x10^8 m/s), k = Boltzman constant (1.38x10^{-23}J/k)

The radiant temperature (T_{rad}) is defined as the equivalent temperature of the black body which would give the same amount of radiation as obtained from a real body. The radiant temperature depends on the actual surface kinetic temperature (T_{kin}) and spectral emissivity (ε_λ) of the material. Spectral emissivity (ε_λ) is the properties of material which control the radiant energy flux. Spectral emissivity (ε_λ) for black body is unity and for most natural material is less than one ranging generally between 0.70 and 0.95. When spectral emissivity of the material is known, kinetic temperature of the object may be obtained using the following mathematical equation (2).

$$T_{kin} = \frac{1}{\varepsilon_\lambda^{1/4}} T_{rad}$$

(2)

The radiant temperature of natural body will thus be less than that for a black body at the same temperature. In thermography technique camera receives radiation from the object itself and from the surrounding reflection via object surface (Figure 4) [11].
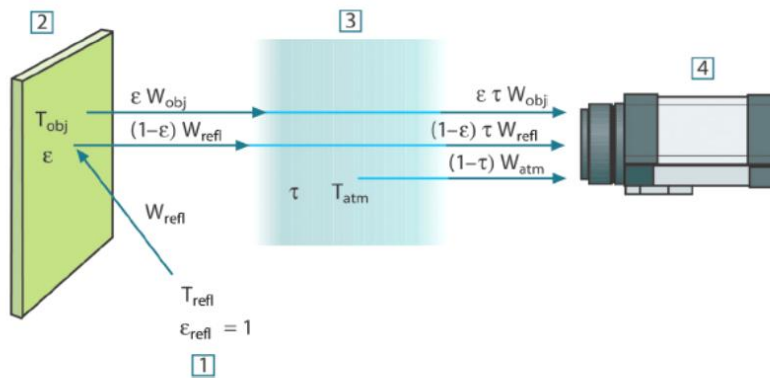
Figure 4: A Schematic Representation of the General Thermographic Measurement Situation.
1: Surroundings, 2: Object, 3: Atmosphere, 4: Camera

The temperature of the object depends upon the factors (i) emission from the object, (ii) reflected emission from the ambient source (iii) emission from the atmosphere. These factors are used to calculate the temperature of the object in FLIR thermal imaging camera in equation (3) [11].

$$U_{obj} = \frac{1}{(\varepsilon - \tau)} U_{tot} - \frac{(1-\varepsilon)}{\varepsilon} U_{refl} - \frac{(1-\tau)}{\varepsilon\tau} U_{atm}$$

(3)

Where, U_{obj} = calculated output voltage for a black body of temperature T_{obj}, U_{tot} = measured camera output for the actual case, U_{refl} = theoretical camera output voltage, U_{atm} = theoretical camera output voltage for blackbody temperature T_{atm} according to the calibration, ε = emittance, $(1-\varepsilon)$ = reflectance of the object, $(1-\tau)$ = emittance of the atmosphere.

For the measurement of thermal anomalies, some object parameters like object emissivity reflected apparent temperature, distance of the object from the camera, relative humidity and temperature of the surrounding (ambient temperature) are required to feed in the camera.

3.2. Data Acquisition and Analysis

Monitoring of coal mine fire is one of the important approaches to know the fire affected area and its extent thereof. Temperature is a direct indicator of coal fire combustion stages and can be used in mineralogical studies, ground geological surveys, as well as remote sensing detection [19]. Thermal monitoring needs temperature distribution at every point of fire affected area for the demarcation of fire zone. The key problem of monitoring is acquiring surface temperature distribution of fire affected area quickly and accurately [10]. The monitoring procedure used for thermographic technique can be divided into three stages as (i) acquiring thermal and visual images (ii) acquiring coordinates of sites using GPS, and (iii) analysis of acquired data.

Thermographic monitoring was conducted in various fire affected mines of JCF using ThemaCAM-P65 infrared thermal imaging camera having adjustable temperature measuring ranges from -20 ^{0}C to +2000 ^{0}C with sensitivity accuracy of ± 2 ^{0}C. The camera have inbuilt lens of 36mm, field of view (FOV) 24°X18° as solid angle and replaceable lenses with 18 mm wide angle lens, 19 mm micro lens and 150 mm close up lens. It includes auto calibration facility for emissivity of different materials. The camera is equipped with storing images, voice comments and text like location, spatial coordinates, surface features etc. and capable for acquiring and displaying visual as well as thermal images on 4" colour monitor with 320X240 pixels size. The acquired images and data can be transferred to computer using USB/ RS232 plug and play connection for fast download and further analysis through Reporter 8.3 Pro software [11].

There is facility of recording the fire areas by connecting DV recorder with camera or using Burst recording technique. It is useful for extensive monitoring over a large area and helpful to periodical monitoring and preparation of thermal profile of the area. All object parameters of thermal camera have been taken care to obtained high temperature precision from acquired data. Analysis of thermo-images will assess the status, extent and direction of fire propagation. The working procedures of this technique have been shown in the flow chart (Figure 5). The thermal and visual images of JCF were taken at various locations of fire affected sites along with their coordinates using GPS. The raw data of the satellite image has been processed using ERDAS 9.1 software. Selected fire locations of JCF are shown in false color composition (FCC) of satellite image (Figure 6). The calculated temperatures of Landsat ETM+ thermal band (Band-6) satellite images having spatial resolution of 60 m were compared with observed field temperature as given in Table 1.
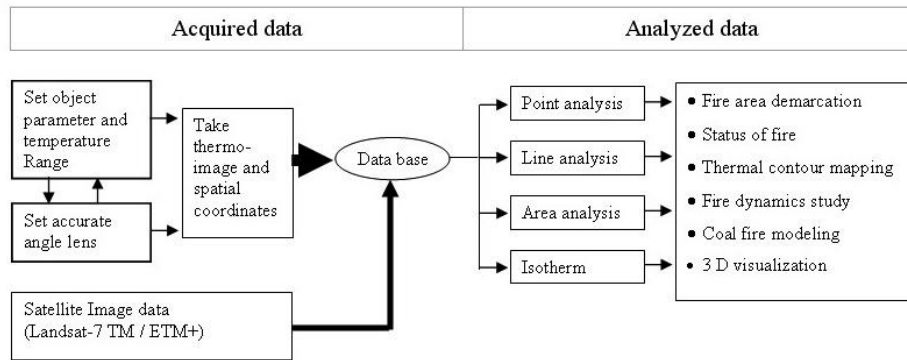
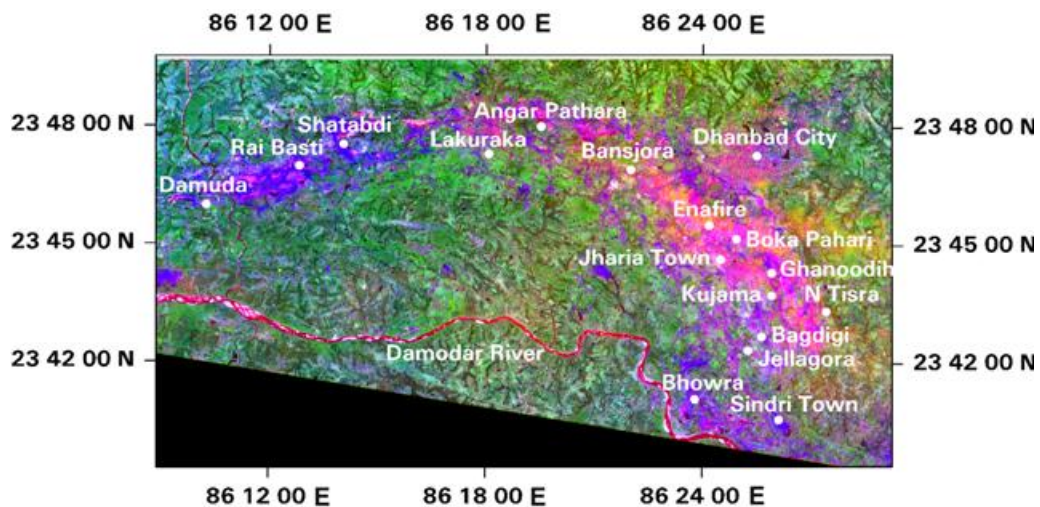**Figure 5:** *Flow Chart of the Monitoring Procedure Used For Acquiring and Analysis of Thermography Technique*

Figure 6: *The Satellite Image of Jharia Coal Field (JCF) In False Color Composition with fire location*

4. Results and Discussion

Thermal survey was carried out at different fire affected locations of JCF using Thermal imaging camera. The observed ground data were also compared with the findings of satellite data at same locations. The significant differences in both the observation were recorded. The obtained temperature of satellite data was very low in comparison to the temperatures obtained by thermal imaging camera (Table 1).

Table 1: *Ground Point Coordinates and Temperatures Taken By G.P.S and Thermal Imaging Camera with Corresponding Satellite Image Temperature of Different Fire Affected Areas of Jharia Coal Field*

Sl. No.	Name of Fire Area	Latitude ($0^0 0^' 0^{''}$ N)	Longitude ($0^0 0^' 0^{''}$ E)	Elevation (m)	Calculated Satellite Image Temp. (^{o}C)	Measured I R camera Temp. (^{o}C)
1.	Ena Fire Project	23 45 35	86 24 10	200	64.80	456
2.	Jai Rampur OCP	23 47 41	86 25 32	220	57.43	375
3.	Boka Pahari(Rajapur)	23 45 13	86 24 55	207	70.44	518
4.	Pandebera Village	23 44 09	86 25 33	167	29.22	65
5.	Ghanoodih Basti	23 44 23	86 25 54	189	46.51	255
6.	Kujama Basti	23 43 48	86 25 53	173	39.59	179
7.	Ghanoodih OCP	23 44 23	86 25 55	192	38.50	167
8.	Jairampur Road	23 43 02	86 25 20	164	38.77	170
9.	Jairampur Village	23 42 55	86 25 18	176	30.13	75
10.	Angar Pathara	23 48 02	86 19 31	195	63.43	441

11.	Tetuliya East- Katras	23 47 42	86 17 00	186	28.76	90
12.	Lodna Basti	23 47 20	86 18 04	192	38.59	168
13.	Lakuraka Basti	23 47 16	86 18 23	188	30.58	80
14.	Tetulia Village	23 47 27	86 17 35	194	30.85	83
15.	Shatabdi OCP (H.R)	23 47 36	86 14 01	209	54.33	341
16.	Shatabdi Dump Fire	23 47 33	86 14 05	209	65.62	465
17.	Shatabadi Mining Area	23 47 39	86 14 38	192	64.44	452
18.	Sendra Bansjora OCP	23 47 42	86 20 53	198	52.79	324
19.	Basjora Colliery	23 46 59	86 22 01	197	39.77	181
20.	Bagdigi OCP	23 42 45	86 45 39	160	61.79	423
21.	South Tisra OCP	23 42 09	86 26 40	197	30.13	79
22.	NorthTisra OCP	23 43 25	86 27 26	194	30.58	80
23.	Damuda B.J. Section	23 46 02	86 10 15	180	38.68	189
24.	Sijua Basti, Damuda	23 46 20	86 10 20	196	30.58	80
25.	Rai Basti	23 47 04	86 12 50	232	45.14	240

H.R.- (Haul Road), OCP- (Open cast project)

The disparity observed between temperatures obtained by remote sensing techniques is due to atmospheric effect, solar reflection and topography etc. [9] and [20]. The maximum temperatures of thermal infrared images and corresponding satellite image found near dwellings area of Boka pahari (Rajapur), Ghanoodih and Kujama 518^0C and 70.44^0C; 167.7°C and 38.59°C; and 179.3°C and 39.59 °C respectively (Figure 7). Children are enjoying the heat during winter season in the fire-affected area without knowing the intensity of fire, stability of ground and emission of obnoxious gases (SO_x, NO_x, CO) along fissures and cracks, which are dangerous for their health and safety. The maximum temperatures at old dump area and at active mining operational bench of Satabdi OCP are 465.7°C and 452.3°C respectively. The thermal and corresponding visual images of Ena fire project and Satabdi OCP showing the difficult mining operation (Figure 8)
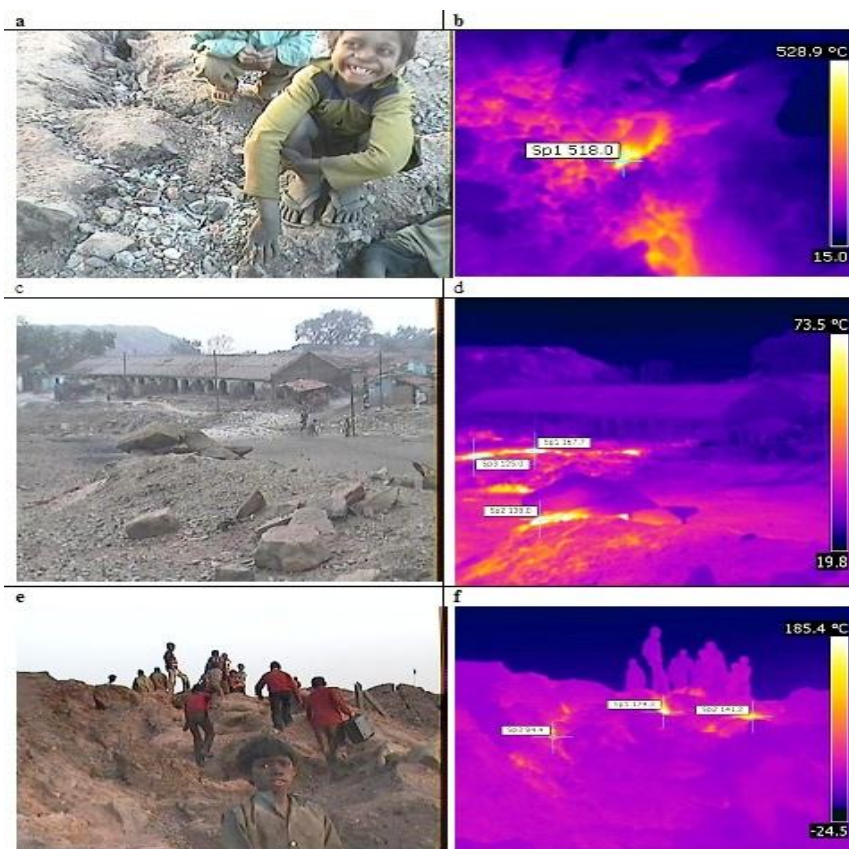

Figure 7: *Visual Image corresponding to Its respective Thermal Infrared Image Showing Maximum Temperature of (a) and (b) Boka Pahari Rajapur OCP (518°C), (c) and (d) Ghanoodih (167.7°C), (e) and (f) Kujama (179.3°C)*
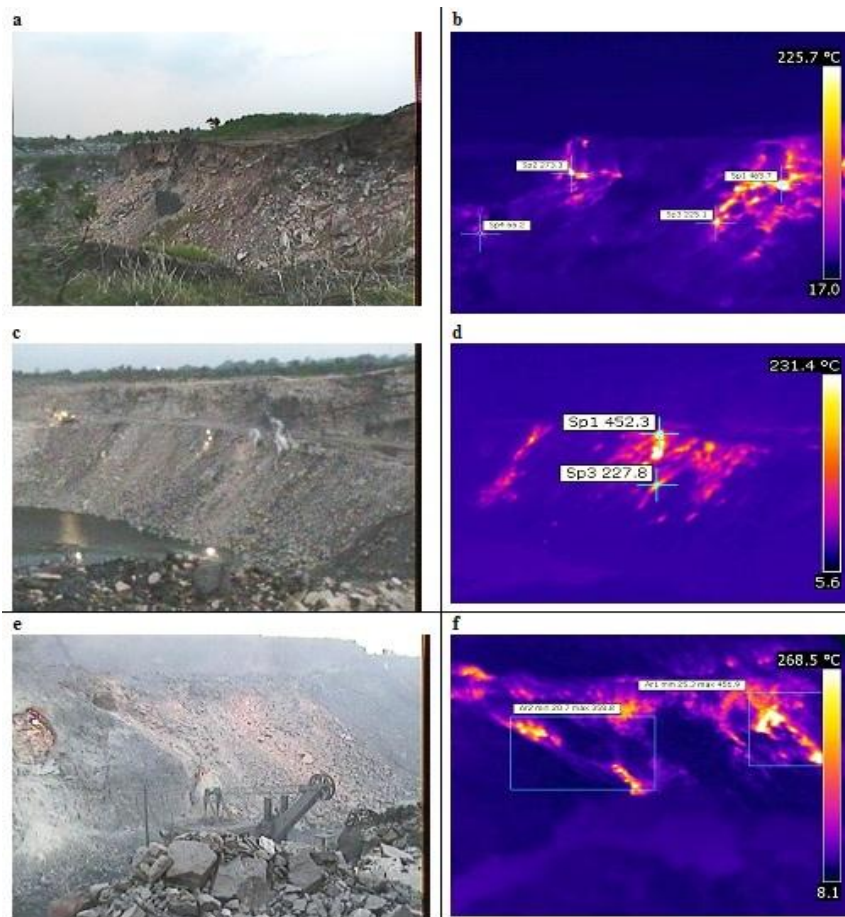
Figure 8: *Visual Image corresponding to its respective Thermal Infrared Image showing maximum temperature of (a) and (b) Satabdi OCP Old Dump Area (465.7°C), (c) and (d) Satabdi OCP Working Bench (452.3°C), (e) and (f) Ena Fire Project Working Bench (465.9°C)*

The analyses of these thermal images have been done using point, line, area, isotherms and trend analysis for interpretations of anomalies. The line analysis of thermal images help to estimate the length of fire affected zone with temperature profile along the line. Temporal monitoring along fixed line will give better result to speculate the direction and rate of fire propagation. Area analysis of a thermal image is giving thermal profile of a selected zone with respect to fire-affected area (Figure 9). Chronological trends analysis of area will be beneficial for determination of fire dynamics, where as isotherm can be used as 3-D visualization of fire area. With the help of result obtained, the status and delineation of fire area can be done more precisely.
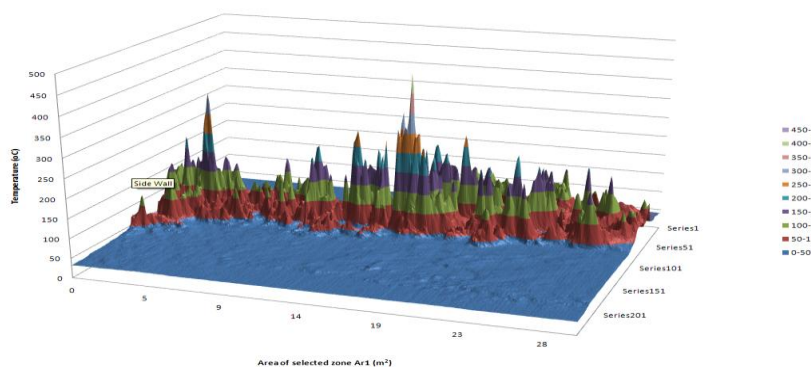

Figure 9: *Area Analysis of a Thermal Image is Giving Thermal Profile of a Selected Zone With Respect To Fire-Affected Area*

5. Conclusion

To assess coal mine fire in JCF at different fire affected area first time thermography monitoring technique was used. Ground level infrared thermographic monitoring has the advantages of being more rigorous, more flexible and less costly than other traditional technique. It will be highly effective for the assessment of coal fire in early stages by temporal monitoring of thermal anomalies. Combining thermography and topography, it is possible to work like remote sensing technique for limited surface area more precisely and effectively. In thermal remote sensing method temperature errors due to atmospheric effect, topography, slope and solar reflection were negligible in thermography. Once anomalies have been determined precisely, the database of an area can be used to determine the fire dynamics, direction and intensity of the fire as well as 3 D modeling. This paper outlined different process of thermography monitoring procedures in different field conditions. It will help to prepare control strategy in fire affected areas in due time. It can also provides an early warning and management information system for future mitigation of coal fire and useful for ground validation of spatial data acquired by the thermal remote sensing.

Acknowledgements

References

[1] V.K. Singh et al., 2007: *Managing Fire in Jharia Coalfields Using Remote Sensing Techniques*. First International Conference on MSECCMI, New Delhi, India, 315-323.

[2] A.Sinha et al., 2005: *Spontaneous Coal Seam Fires: A Global Phenomenon, International Research For Sustainable Control And Management On Spontaneous Coal Seam Fires: Mitigation A Global Disaster*. International Conference, Beijing P.R. China, 42-66.

[3] R.P. Gupta et al. *Landuse Mapping and Change Detection in a Coal Mining Area –A Case Study in the Jharia Coalfield, India.* International Journal of Remote Sensing. 1998. 19 (3) 391-410.

[4] Glenn B. Stracher, et al. *Coal Fires Burning Out of Control Around the World: Thermodynamic Recipe for Environmental Catastrophe*. International Journal of Coal Geology. 2004. 59; 7-17.

[5] Prasun K. Gangopadhayay et al., 2005: *Monitoring of Coal Fire Using Remote Sensing, International Research for Sustainable Control And Management on Spontaneous Coal Seam Fires: Mitigation A Global Disaster.* International Conference, Beijing P.R. China, 351-361.

[6] Anupama Prakash et al. *Design and Implementation of a Dedicated Prototype GIS for Coal Fire Investigation in North China.* International Journal of Coal Geology. 2004. 59; 107-119.

[7] Ravi P. Gupta, 2003: *The Remote Sensing Geology.* 2nd Ed. Springer, Verlag Berlin Heidelberg, Chapter 9, 172, 206.

[8] John R. Jensen, 2005: *Introductory Digital Image Processing.* 3rd Ed. Pearson Prentice Hall, NJ, 47, 60.

[9] R.S. Chatterjee. *Coal Fire Mapping From Satellite Thermal IR Data- A Case Example of in Jharia Coalfield, Jharkhand, India.* ISPRS Journal of Photogrammetery & Remote Sensing. 2006. 60; 113-128.

[10] Yun-jia Wang, 2008: *Infrared Thermography Monitoring and Early Warning of the Spontaneous Combustion of Coal Gangue Pile.* International Archive of Photogrammetery, Remote Sensing and Spatial Information Science, XXXVII, Beijing, 203-206.

[11] User Manual ThermoCAM^{TM} P65, FLIR System. 2006. 185,195.

[12] S.P. Garnaik. *Infrared Thermography: A Versatile Technology for Condition Monitoring and Energy Conservation.* http://www. reliabilityweb.com.

[13] Stanley R. Michalski. *The Jharia Mine Fire Control Technical Assistance Project: An Analysis*. International Journal of Coal Geology. 2004. 59; 83-90.

[14] B.B Dhar, 1996: *Keynote Address on Status of Mine Fires – Trends and Challenges*, In Proceedings of the Conference on Prevention and Control of Mine and Industrial Fires – Trendsand Challenges, Calcutta, India, 1-8.

[15] Zutshi et al. *Indian Coal Vis-A-Vis Spontaneous Heating Problems. Journal of Mines, Metals & Fuels.* 2001, 44 (5) 123-128.

[16] DLR, 2005. *Coal Fire Research – A Sino-German Initiative. World Map of Coal Fires.* German Aerospace Center, Oberpfaffenhofen, Germany. http://www.coalfire.caf.dlr.de/projectareas/world_wide_distribution_en.html

[17] Central Mine Planning and Design Institute Ltd (CMPDIL Ranchi), 2006: *Master Plan for Dealing with Fire, Subsidence and Rehabilitation in the Leasehold of BCCL*, Dhanbad, 1-84.

[18] S.R Michalski et al., 1997: *Investigation of the Jharia Coalfield Mine Fires—India.* Proceedings 14th Annual Meeting of the American Society for Surface Mining and Reclamation, (CD-ROM), Austin, TX.

[19] Zhang Jianmin et al., 2005: *3D Detection and Visualization of Underground Coal Fires*. International Conference, Beijing P.R. China, 410-426.

[20] R.K. Mishra, 2010: *Study of Mine Fire in Jharia Coal Field Using Remote Sensing Techniques*. M. Tech. Thesis, Indian School of Mines Dhanbad, Jharkhand, India, 61-72.

Research Article   **Open Access**

Comparison of MLC and FCM Techniques with Satellite Imagery in A Part of Narmada River Basin of Madhya Pradesh, India

Arun Mondal, Deepak Khare and Sananda Kundu

Department of Water Resources Development and Management, Indian Institute of Technology, Roorkee, India

Correspondence should be addressed to Arun Mondal, arun.iirs@gmail.com

Abstract Landuse and land cover are most important part which is linked with the environment and climate in various ways. This is also important for the modeling of greenhouse gas emissions, carbon balance etc., and is important for understanding the landscape features. The main objective of the present work is to reduce uncertainties in the landuse and land cover pattern. Remote sensing technique is extremely important for the classification purposes by empirical observation and algorithms. In case of present study, a part of Narmada river basin was taken where change in the landuse and landcover was assessed from the Landsat images of the year 2011 with two classification techniques of Maximum Likelihood Classification (MLC) and Fuzzy C-Mean (FCM). The major landuse classes are water body, built-up, vegetation, agricultural land and fallow land. The image has been digitally classified by both MLC and FCM algorithms which have been validated by the accuracy assessment process. The overall accuracy achieved by the FCM was about 84% while with MLC it was about 79%. The Survey of India toposheet was used as the base map for the purpose of geo-correction. FCM was found to be more accurate in comparison to MLC because of its soft classification technique.

Keywords *Landuse, Narmada River Basin, MLC, FCM, Accuracy*

1. Introduction

The landuse change intensity with respect to the population growth of the world has led to such consequences for the environment that resulted in the detail study of these transformations *(Wu et al., 2006)*. Landuse is considered as one of the basic supposition for understanding the global environment changes. Landuse and land cover mapping is an extremely important component, where different parameters are combined together. Remote sensing technology has helped for global information monitoring for the landuse and land cover in the form of spatial, spectral and temporal resolution. This technology has reduced the survey time, availability of latest maps, digital image classification, etc. Since 1972, Landsat satellite data have been used for digital classification for the preparation of landuse classes *(Townshend, 1992; Hall et al., 1995; Lu and Weng, 2007)*. Change in the landuse and land cover was analysed by many researchers like *He et al. (2000) and Zhang et al.*

(2002) who have used multi-temporal satellite images for classifying landuse in the city area of Beijing. Maximum likelihood classification (MLC) is very popular and is used in wide extent throughout the world for extraction of landuse classes *(Huang et al., 2002)*. The MLC classification is a parametric approach where selected classes of signatures are assumed in normal distribution. Some non-parametric types of classification techniques are also there which are considered to have better accuracy for deriving classes *(Kavzoglu and Reis, 2008)*. Some of these well-known non-parametric techniques are Fuzzy C-Mean, Decision Trees, Support Vector Machines (SVM), Artificial Neural Networks (ANN) etc. In fuzzy, a point may be assigned to a particular cluster with its degree of belonging to that particular cluster that is measured from the centroid point of the cluster. So problem of any hard classification can be avoided. Number of studies has been done with the application of fuzzy C-Mean. *Lucieer (2006)* used fuzzy C-Means classifier for estimation of the vegetation units. According to *Foody (1992)*, *Lucieer (2006)* and *Lu and Weng (2007)*, fuzzy technique of classification is important because it can overlap hard classes with the soft technique.

Present study compares the landuse classification techniques of MLC and Fuzzy C-Means to assess the classification accuracy using Landsat satellite imagery. Spatial accuracy was analyzed with the outputs of both the classification techniques in a part of Narmada river basin of Madhya Pradesh of India.

2. Study Area

The study area includes Burhanpur, Barwani, Sehore, Khandwa, Indore, Harda, Dewas, East Nimar and West Nimar districts. It is a part of Narmada river basin of Madhya Pradesh. The area stretches from $21^{°}23'51''$ to $22^{°}54'55''$N and $75^{°}21'41''$ to $77^{°}20'53''$E and covers about 52970 km^2 areas. The region experiences subtropical climate with hot dry summer and a cool dry winter. The rainfall average is about 1370 mm and it decreases from east to west (Figure 1).
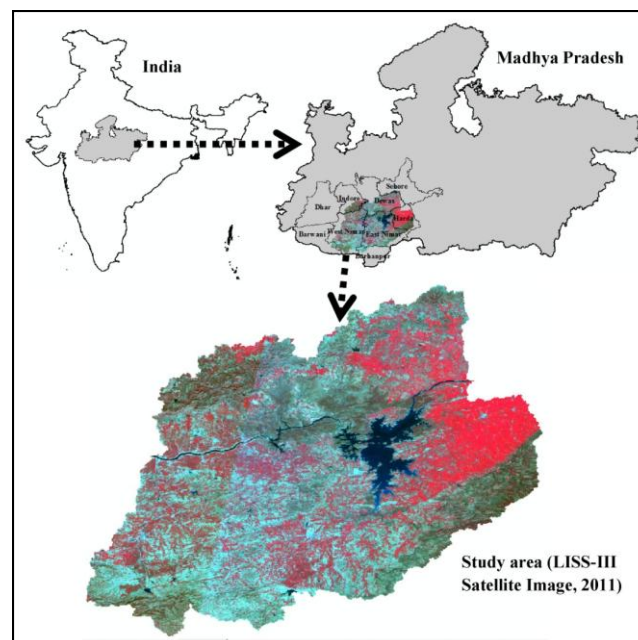

Figure 1: Study Area

3. Data and Methods

For the purpose of classification, Landsat TM satellite imagery was used for applying the methods of Maximum Likelihood Classification (MLC) and Fuzzy C-Mean algorithms. The Landsat TM data of 2011 was used which was corrected geometrically and radiometrically for removing the errors.

Landuse classification of images with the MLC and Fuzzy C-Means were done and accuracy assessment was applied to compare both the techniques.

3.1. Maximum Likelihood Classification (MLC) Technique

MLC is considered as a process to determine known class distribution as the maximum for a given statistic *(Scott & Symons, 1971)*. It is one of the most widely used processes in remote sensing. Here, a pixel having maximum likelihood is assigned to the corresponding class. If there are m numbers of predefined classes, then the class a posteriori probability is given as

$$P(k|x) = \frac{P(k)P(k|x)}{\sum\limits_{i=1}^{m} P(i)P(k|i)}$$

(1)

where P (k) represents the prior probability of class k and P(x | k) is considered as the conditional probability for observing x from the class k (probability density function). For the normal distributions, the likelihood function, P(x | k), is given as following

$$L_k(x) = \frac{1}{(2\pi)^{\frac{n}{2}} \left| \sum_k \right|^{\frac{1}{2}}} \exp\left(-\frac{1}{2}(x - \mu_k)^T \sum\nolimits_k^{-1} (x - \mu_k) \right)$$

(2)

where $x = (x1, x2 \ldots xn)^T$ stands for the vector of a pixel with n number of bands; $L_k(x)$ is the likelihood membership function of x belonging to class k and $\mu k = (\mu_k 1\ \mu_k 2 \ldots \mu_k n)^T$ represents the mean of the kth class;

$$\sum\nolimits_k = \begin{pmatrix} \sigma_{11} & \sigma_{12} & \cdot & \cdot & \sigma_{1n} \\ \sigma_{21} & \sigma_{22} & \cdot & \cdot & \sigma_{2n} \\ \cdot & & \cdot & \cdot & \cdot \\ \cdot & & \cdot & \cdot & \cdot \\ \sigma_{n1} & \sigma_{n2} & \cdot & \cdot & \sigma_{nn} \end{pmatrix}$$

Kth class: is the variance covariance matrix of the class k.   (3)

3.2. Supervised Fuzzy C-Mean Method

Jain and Dubes (1988) give many types of existing clustering techniques where images have been classified by applying supervised classification technique with fuzzy logic. The fuzzy technique gives a natural model where a pixel may have partial membership value corresponding to many land cover categories. This algorithm operates on the basis of iterative minimization of the objective function.

$$J_m(U,v) = \sum_{i=1}^{C} \sum_{k=1}^{N} u_{ik}^m \left\| y_k - v_i \right\|_A^2$$

(4)

Where,

Y = {$Y_1, Y_2 \ldots Y_N$} $\subset R^n$ = the data,
c = number of clusters in Y; $2 \leq c \leq n$,
m = weighting exponent; $1 \leq m < \infty$
U = fuzzy c-partition of Y;   U $\in M_{fc}$
v = ($v_1, v_2 \ldots v_c$) = vectors of centers,
$v_i = (v_{i1}, v_{i2}, .., v_{in})$ = center of cluster i,
$\left\| \ \right\|_A$ = induced A-norm on R", and
A = positive-definite (n x n) weight matrix.

The following constraints are fulfilled by the membership values,

$$0 \leq u_{ik} \leq 1; \text{Where } i \in \{1, \ldots . C\}; k \in \{1, \ldots \ldots . N\} \tag{5}$$

$$\sum_{i=1}^{C} u_{ik} = 1; \qquad k \in \{1, \ldots ., N\} \tag{6}$$

$$\sum_{k=1}^{N} u_{ik} > 0; \qquad i \in \{1, \ldots ., C\} \tag{7}$$

The objective function is the sum of square of Euclidean distances from each input sample and its corresponding cluster centre, and these distances are weighted by the memberships of fuzzy. It is given in the following equations:

$$\hat{v}_i = \left[\sum_{k=1}^{N} u_{ik}^m y_k \right] / \sum_{k=1}^{N} u_{ik}^m \tag{8}$$

$$\hat{u}_{ik} = 1 / \sum_{j=1}^{C} \left[\|y_k - v_i\| / \|y_k - v_j\| \right]^{2/(m-1)} \tag{9}$$

The membership value of each class is dependent on its distance to the centre of the corresponding cluster. Smaller will be the influence of samples having small membership values with greater value of m *(Bezdek et al., 1984)*.

3.3. Accuracy Assessment

Number of methods for accuracy assessment can be found. One common technique is error matrix *(Congalton, 1991; Foody, 2002)*. In this study, overall, producer's and user's accuracy have been calculated. Producer's accuracy is found by dividing the accurate number of sampling points in one class by the total number of points taken from the reference data. For user's accuracy, correct classified points are divided by the total number of points which are already been classified in that particular class.

3.4. Kappa Coefficient

Kappa is a discrete multivariate technique that is used for the measurement of the accuracy of maps and error matrices derived by remote sensing. The Khat statistic is given as

$$\hat{k} = \frac{N \sum_{i=1}^{r} x_{ii} - \sum_{i=1}^{r} (x_{i+} . x_{+i})}{N^2 - \sum_{i=1}^{r} (x_{i+} . x_{+i})} \tag{10}$$

here 'r' is the number of rows in the matrix X_{ij} showing number of observations in row 'i' and column 'j', and X_{i+} and X_{+i} are the marginal totals for the 'i' and I respectively, and N gives the total number of observation *(Lillesand and Kiefer., 2000)*.

Change in the land use and comparison of accuracy of two methods are represented in the given land use classes.

4. Results and Analysis

4.1. Accuracy in Classification

Total of 120 points were taken for accuracy assessment in case of both the classification results. Producer and user accuracy of water body, built-up, dense vegetation, grass land and fallow land are 80%, 77.78%, 76.67%, 83.02%, 73.91% and 66.67%, 77.78%, 79.31%, 81.48%, 77.27% of MLC

technique respectively. In Fuzzy C-Mean tecnique, producer and user accuracy of water body, built-up, vegetation, agricultural land and fallow land are 83.33%, 91.67%, 84.62%, 85.42%, 78.57% and 83.33%, 84.62%, 81.48%, 85.42%, 84.62% respectively (Table 1).

Table 1: Error Matrix

1990					
Class Name	**Reference Totals**	**Classified Totals**	**Number of Correct Points**	**Producers Accuracy (%)**	**Users Accuracy (%)**
MLC (2011)					
Water body	5	6	4	80.00	66.67
Built-up	9	9	7	77.78	77.78
Dense Vegetation	30	29	23	76.67	79.31
Grass land	53	54	44	83.02	81.48
Fallow land	23	22	17	73.91	77.27
Total	120	120	95	……………	…………
Fuzzy C-Mean					
Water body	6	6	5	83.33	83.33
Built-up	12	13	11	91.67	84.62
Dense Vegetation	26	27	22	84.62	81.48
Grass land	48	48	41	85.42	85.42
Fallow land	28	26	22	78.57	84.62
Total	120	120	101	………...	………...

Kappa statistics of the following landuse in MLC are 0.65, 0.76, 0.72, 0.67, 0.72 and in Fuzzy C-Mean they are 0.82, 0.83, 0.76, 0.76 and 0.80 recpectively. The overall kappa statistics and overall accuracy for MLC are 0.70 and 79.17% and in Fuzzy C-Mean they are 0.78 and 84.17% respectively. Thus difference in overall accuracy is 5% between two methods (Table 2 and Table 3).

Table 2: Kappa Statistics

Class Name	MLC (2011)	Fuzzy C-Mean (2011)
Water body	0.65	0.82
Built-up	0.76	0.83
Vegetation	0.72	0.76
Agricultural land	0.67	0.76
Fallow land	0.72	0.80

Table 3: Overall Kappa Statistics and Overall Accuracy

Category	MLC (2011)	Fuzzy C-Mean (2011)
Over all kappa statistics	0.70	0.78
Over all accuracy (%)	79.17	84.17

4.2. Statistics of MLC and Fuzzy C-Mean

Water body area from MLC and Fuzzy C-Mean techniques are about 884 km² and 930 km² respectively. Built-up areas are differing in 3.32% in two methods while difference in area of vegetation is 1.64%. Agricultural land and fallow land is showing difference of 5.72% and 3.82% respectively (Table 4, Figure 2 and Figure 3).

Table 4: Distribution of Area of Different Landuse

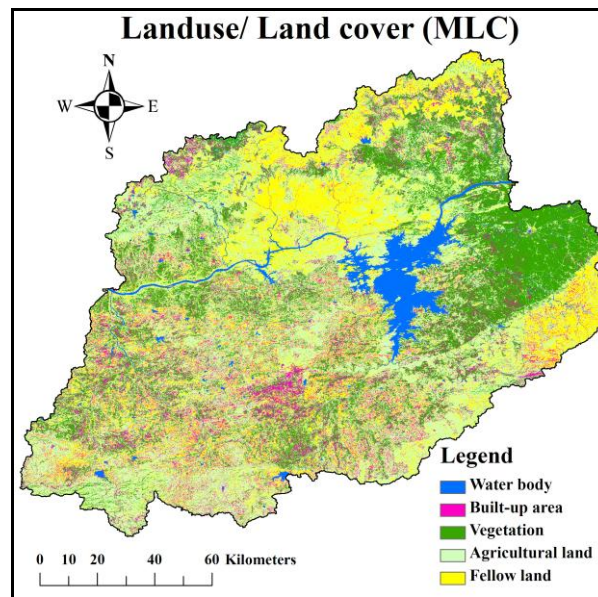| Classes	MLC		Fuzzy C-Mean	
	2011 (Area in km²)	2011 (%)	2011 (Area in km²)	2011 (%)
Water	883.94	4.30	930.42	4.53
Built up	1471.68	7.16	2154.32	10.48
Vegetation	5004.31	24.34	4665.85	22.70
Agricultural land	9518.64	46.30	8341.78	40.58
Fallow Land	3679.42	17.90	4465.63	21.72
Total	20558	100	20558	100

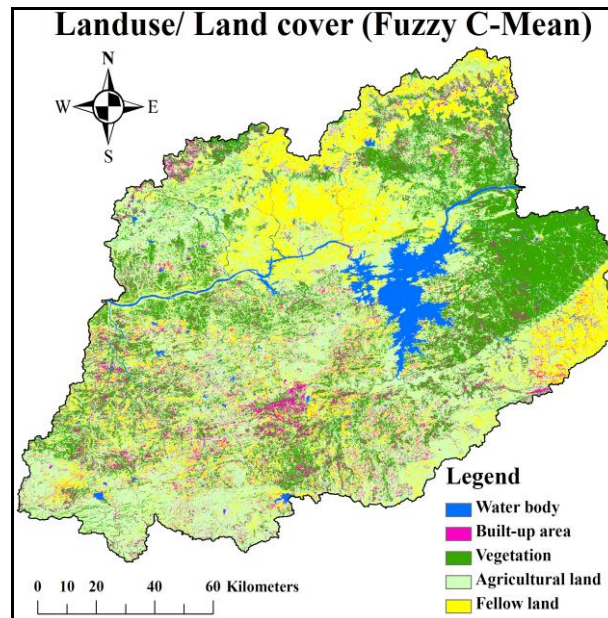*Figure 2: Landuse/ Land Cover Maps from MLC*

Figure 3: Landuse/ Land Cover Maps from Fuzzy C-Mean

Spatial similarity from the outputs of MLC and Fuzzy C-Mean was carried out for each of the landuse classes. 83% of the area has matched i.e. 83% of area is same for both the type of classifications; only 17% of the area has not matched or is different (Figure 4).
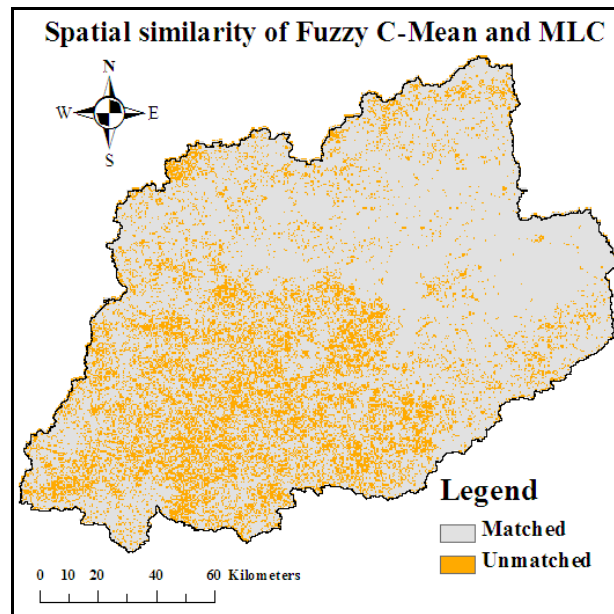

Figure 4: *Spatial Similarity of MLC and Fuzzy C-Mean*

5. Conclusion

Two different types of classification like MLC and Fuzzy C-mean techniques have been applied in a part of Narmada river basin in Madhya Pradesh to identify the more accurate method. Verification with ground observation was done with handheld GPS (Global Positioning System) after classifications to assess the level of accuracy. Level of accuracy has been found to be better in case of Fuzzy C-Mean algorithm than MLC, although the difference in area of the landuse classes is less. 83% of similarity in area was observed in both the methods with only 17% of difference. Nonetheless, Fuzzy C-Mean is considered to be superior to MLC landuse classification because of better accuracy achieved.

Acknowledgement

References

Bezdek et al. *The Fuzzy C-Means Clustering Algorithm.* Computers & Geosciences. 1984. 10 (2-3) 191-203.

Congalton. *A Review of Assessing the Accuracy of Classifications of Remotely Sensed Data* Remote Sensing of Environment. 1991. 37; 35−46.

Foody G.M. *Status of Land Cover Classification Accuracy Assessment.* Remote Sensing of Environment. 2002. 80; 185−201.

Foody G.M. *A Fuzzy Sets Approach to the Representation of Vegetation Continua from Remotely Sensed Data -An Example From Lowland Heath.* Photogrammetric Engineering and Remote Sensing. 1992. 58; 221-225.

Hall F.G., et al. *Status of Remote Sensing Algorithms for Estimation of Land Surface State Parameters.* Remote Sensing of Environment. 1995. 51; 138-156.

He C.Y., et al. *A Study on Landuse/Cover Change in Beijing Area.* Geographical Research. 2000. 20 (6) 679–687.

Huang C., et al. *An Assessment of Support Vector Machines for Land Cover Classification.* International Journal of Remote Sensing. 2002. 23; 725-749.

Jain A., et al., 1988: *Algorithms for Clustering Data.* Prentice-Hall, Englewood Cliffs, NJ.

Kavzoglu T., et al. *Performance Analysis of Maximum Likelihood and Artificial Neural Network Classifiers for Training Sets with Mixed Pixels.* GIScience and Remote Sensing. 2008. 45; 330-342.

Lillesand T.M., et al., 2000: *Remote Sensing and Image Interpretation.* 4th Ed. John Wiley & Sons, Inc., New York.

Lu D., et al. *A Survey of Image Classification Methods and Techniques for Improving Classification Performance.* International Journal of Remote Sensing. 2007. 28; 823-870.

Lucieer A., 2006: *Fuzzy Classification of Sub-Antarctic Vegetation on Heard Island Based On High-Resolution Satellite Imagery.* IEEE Geoscience and Remote Sensing Symposium, 2777-2780.

Scott A.J., et al *Clustering Methods Based on Likelihood Ratio Criteria.* Biometrics. 1971. 27 (2) 387-397.

Townshend J.R.G. *Land Cover.* International Journal of Remote Sensing. 1992. 13; 1319-1328.

Wu Q., et al. *Monitoring and Predicting Land Use Change in Beijing Using Remote Sensing and GIS.* Landscape and Urban Planning. 2006. 78; 322-333.

Zhang Q., et al. *Urban Built-Up Land Change Detection with Road Density and Spectral Information From Multi-Temporal Landsat TM data.* International Journal of Remote Sensing. 2002. 23 (15) 3057-3078.

Research Article   **Open Access**

Hyper Spectral Measurements as a Method for Potato Crop Characterization

Mohamed Aboelghar, Sayed Arafat and Eslam Farag

Agriculture Applications Department, National Authority for Remote Sensing and Space Sciences (NARSS)
El-Nozha El-Gedida, Cairo, Egypt

Correspondence should be addressed to Mohamed Aboelgha, mohamed.aboelghar@gmail.com

Abstract The main objectives of this research is to determine the optimal hyperspectral range and waveband/s in the spectral range of (400–2500 nm) to discriminate between four different varieties of Potato crop (Diamond, Everest, Mondial and Rosetta) that are cultivated in old and newly cultivated lands of Egypt and to propose detailed spectral reflectance characterization for these four varieties which will enable more accurate surveying of these varieties through satellite imagery. Hyperspectral ground measurements of ASD field Spec3 spectroradiometer was used to monitor the spectral reflectance profile during the period of the maximum growth stage of the crop. An average of thirty measurements for each variety was considered in the process. After accounting for atmospheric windows and/or areas of significant noise, a total of 2150 narrow bands in 400–2500 nm were used in the analysis. Spectral reflectance was divided into six spectral zones: blue, green, red, near-infrared, shortwave infrared-I and shortwave infrared-II. One Way ANOVA and Tukey's HSD analysis was used to choose the optimal spectral zone that could be used to differentiate between the four varieties. Then, linear discrimination analysis (LDA) was used to identify the specific optimal wavebands in the spectral zones in which each variety could be spectrally identified. The results of Tukey's HSD showed that NIR is the best spectral zone for the discrimination between the four varieties. The other five spectral zones showed close spectral characterizations between at least two varieties. The results of (LDA) showed the optimal waveband to identify each variety. These results will be used in machine learning process to improve the performance of the existing remote sensing software's to estimate potato crop acreage. The study was carried out in AlBuhayrah governorate of Egypt.

Keywords *Hyper Spectral Data, Potato Discrimination*

1. Introduction

Potato is Egypt's most important export vegetable crop and the second most important (after tomatoes) vegetable crop in economic value (El Tobgy, 1974). Out of an annual production of about 1.2 million tons, over one million are retained for domestic consumption. Average annual per capita consumption of potatoes is about (20-25 kg) (Geddes and Monninkhof, 1984). Therefore, there is a high need for a regular, costly and timely affective process for potato crop acreage estimation and

yield prediction which could be achieved using remotely sensed data. Spectral data from the current generation of Earth orbiting satellites carrying broad-waveband sensors such as Landsat Thematic Mapper (TM), Le Syste me pour l'observation de la terre (SPOT) High Resolution Visible (HRV), and the Indian Remote Sensing (IRS) Linear Imaging Self-Scanning (LISS) have limitations in providing accurate estimates of biophysical characteristics of agricultural crops and vegetation cover (Fassnacht et al., 1997; Weigand et al., 1991; Weigand and Richardson, 1990). These limitations are mainly the low spectral and spatial resolution that makes it difficult to isolate potato crop from the other crop covers in the intensive cultivated lands and of course it is almost impossible to classify the different potato varieties on the national scale. This is in which hyperspectral remote sensing technology could be used to increase the potentiality of the existing satellite image processing software's in classifying potato crops. Also, assessment of potato biophysical and biochemical parameters through hyperspectral remote sensing could be a part of precision agriculture system that will enable more effective potato management process. Hyperspectral sensors measure reflectance in a large number of narrow wavebands, generally with band widths of less than 10 nm. With these narrow bands; reflectance and absorption features related to specific crop physical and chemical characteristics can be detected. Many researches have indicated good relationships between biochemical composition, physical structure, water content, and plant ecophysiological status (Gamon, Pen˜uelas, and Field 1992; Pen˜uelas and Filella, 1998). Spectral determinations have provided an automatic, quick, and non-destructive method of assessing physiological parameters and nutrient levels in crop plants (Hinzman et al., 1986; McMurtrey et al., 1994; Casanova et al., 1998; Diker and Bausch, 2003; Hansen and Schjoerring, 2003). Different hyperspectral remote sensors were used for precision agriculture applications, such as airborne visible infrared imaging spectrometer (AVIRIS), compact airborne spectrographic imager (CASI), multispectral infrared and visible imaging spectrometer (MIVIS), and hyperspectral mapping (HyMapTM) system. These sensors can provide quality images with high spatial and spectral resolutions (Taranik et al., 1993; Fraser, 1998; Treitz and Howarth, 1999; Nolin and Dozier, 2000).

The main objective of the current study is using field hyperspectral measurements to identify the spectral reflectance pattern for four potato varieties. These varieties are quite important for the national export of Potato as well as for the local markets. The final objective is to propose a new method of the assessment of potato biophysical and biochemical parameters that could be a part of precision farming system and finally to propose spectral reflectance pattern that could be used in machine learning process to improve the performance and the accuracy of satellite image processing software's in the estimation of potato acreage and potato yield estimation.

2. Study Area

The study was carried out in the newly reclaimed area of El-Behirah governorate (Nubaria area). The study area is irrigated by center pivot system using underground water. This water is characterized by EC equal 1.5 dSm^{-1}. The climate in this area is arid Mediterranean type with an average annual precipitation of about 10.3 mm and temperature is 25.8 C^o. Generally the soil is a slightly saline where the EC value is about 1.85 dS/m and pH values is about 7.8 and soil texture is sandy.
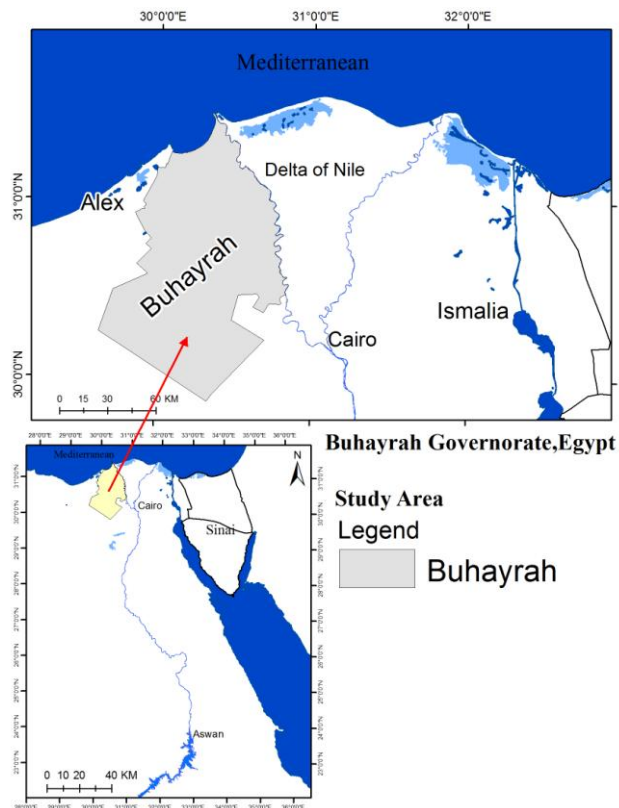
Figure 1: Location Map of Al Buhayrah Governorate

3. Field Hyper Spectral Measurements

The methodology of this work focused on field hyperspectral measurements and statistical analysis for the output measurements in order to choose the optimal spectral zone and wavebands to isolate each variety. As the final objective of this work is presenting information that could be used to increase the accuracy and performance of the existing remote sensing software's in classifying the different varieties in the intensive cultivated lands of the Nile delta. Analytical field spectroradiometer (ASD Field Spec) was used to measure the reflection of the four potato varieties under investigation. The average of thirty points distributed along the study area for each variety was calculated to be used in the study. Measurements were carried out in a full optical spectral range (Visible – Near Infrared – Short Wave Infrared) starting from 350 nm to 2500 nm with 1 nm interval output data. The sampling interval is 1.4 nm at the spectral range (350-1050 nm) while it is 2 nm at the spectral range (1000-2500 nm). These are the intervals which the device is capturing the reflectance. The device automatically performs an interpolation for the data and gives the final data output with (1 nm) interval for the all spectrum range (350-2500 nm). The spectrum characteristics of the device are shown in Table 1. The protocol used for the collection of spectral data is based on measuring radiance from a Spectralon® panel. A designed probe was attached to the instrument's fiber-optic cable to be used to ensure standardized environmental conditions for reflectance measurement. The fiber-optic cable provides the flexibility to adapt the instrument to a wide range of applications. Bare foreoptic 25 degrees used for outdoor measurements resulting circular field of view with 3 cm diameter as measurements were taken at 3 cm height in nadir position (90 degrees) over the measured plants. In the current study, the measurements were performed by holding the pistol grip by hand. As recommended in the instructions of using the device, the Spectralon® was tilted directly towards the sun during optimization.

Table 1: *The ASD Field Spec 3 Specifications*

Spectral Range	350-2500 nm
Spectral Resolution	3 nm : 700 nm 8.5 nm : 1400 nm 6.5 nm : 2100 nm
Sampling Interval	1.4 nm : 350-1050 nm 2 nm : 1000-2500 nm

4. Spectral Reflectance Pattern

Spectral reflectance pattern for the four potato varieties is shown in Figure 2. Reflectance pattern showed the same trend for the four varieties; however, reflectance of Evreast and Diamond was higher than reflectance of Rosetta and Mondial along the whole spectrum. Comparing the reflectance in the different spectral zones for the four varieties showed that the highest spectral reflectance was in infrared spectral zone (700–1300 nm), relatively low reflectance in the spectral zone (1450–1800 nm) while the lowest reflectance was found in the spectral zone (1950-2300 nm). It is noticeable that there is a big similarity in the spectral reflectance pattern between Evreast and Diamond. The reason of this might be the close structure and characterization of the two varieties.
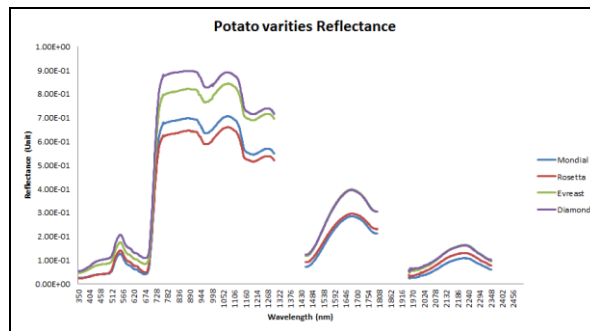

Figure 2: *The Spectral Reflectance Pattern for the Different Crops*

Spectral zones that represent the atmospheric windows (portions of the electromagnetic reflectance that include data noise because of the relative air humidity) were removed. Spectral pattern of each measured sample was identified. Generally, spectral reflectance could be divided into six different spectral portions as follows: blue (350 - 440 nm), green (450 - 540 nm), red (550 - 750 nm), NIR (760 - 1000 nm), SWIR I (1010–1775 nm) and SWIR II (2055–2315 nm).

5. Comparing Standard Deviations from Several Populations

Analysis of variance (ANOVA) methods are presented for comparing means from several populations or processes. While similar methods are occasionally used for comparing several standard deviations, often using the natural logarithm of sample variances as the response variable. There are also a number of alternative procedures that are not based on ANOVA methods that can be used to compare standard deviations. Two of these are described below. Both are highly sensitive to departures from the assumption of normality; consequently, they should be used only after verification that the assumption of normally distributed errors is reasonable. When using ANOVA models with data from designed experiments, a valuable assessment of the assumption of constant standard deviations across (k) factor-level combinations is given by the F-max test The F-max test is used to test the hypotheses (Mason 2003) **(**Equation 1).

$$F_{Max} = \left(\frac{\max(s_i)}{\min(s_i)} \right)^2 \qquad (1)$$

The *F*-statistics in an ANOVA table provide the primary source of information on statistically significant factor effects. However, after an *F*-test in an ANOVA table has shown significance, an experiment usually desires to conduct further analyses to determine which pairs or groups of means are significantly different from one another (Mason, 2003)**.** Tukey's procedure controls the experiment wise error rate for multiple comparisons when all averages are based on the same number of observations. The stated experiment wise error rate is very close to the correct value even when the sample sizes are not equal. The technique is similar to Fisher's LSD procedure. It differs in that the critical value used in the TSD formula is the upper 100α% point for the difference between the largest and smallest of *k* averages. This difference is the range of the *k* averages, and the critical point is obtained from the distribution of the range statistic, not from the *t*-distribution **(**Equation 2**)**.

Two averages $\bar{y}_i$ and $\bar{y}_j$, based on n_i and n_j observations respectively, are significantly different if:

$$\left| \bar{y}_i - \bar{y}_j \right| > TSD$$

Where

$$TSD = q(\alpha; k, v) \left(MS_E \frac{n_i^{-1} + n_j^{-1}}{2} \right)^{\frac{1}{2}} \tag{2}$$

The results of Tukey's HSD test (Figure 3) showed the significancy of the spectral difference between the different varieties along the six spectral zones attached with the general mean of the reflectance for the four varieties, the mean of the reflectance for each variety, the maximum and minmum reflectance values for each variety. Generally, as shown in Figure 3, NIR spectral zone was the best to differetiate between the four varieties with the highest significant difference while red spectral zone was inadequate to differentiate between the four varieties. Only the two spectral zones (NIR) and (SWIR II) showed significant difference between the two varietes (Rosetta and Modial) while three spectral zones (blue, green, NIR) showed significant difference between Diamond and Evreast. In the spectral zones (SWIR I) and (SWIR II), no significant difference was found between Diamond and Evreast while significant difference in these spectral zones was found between these two varieties and the other two varieties.
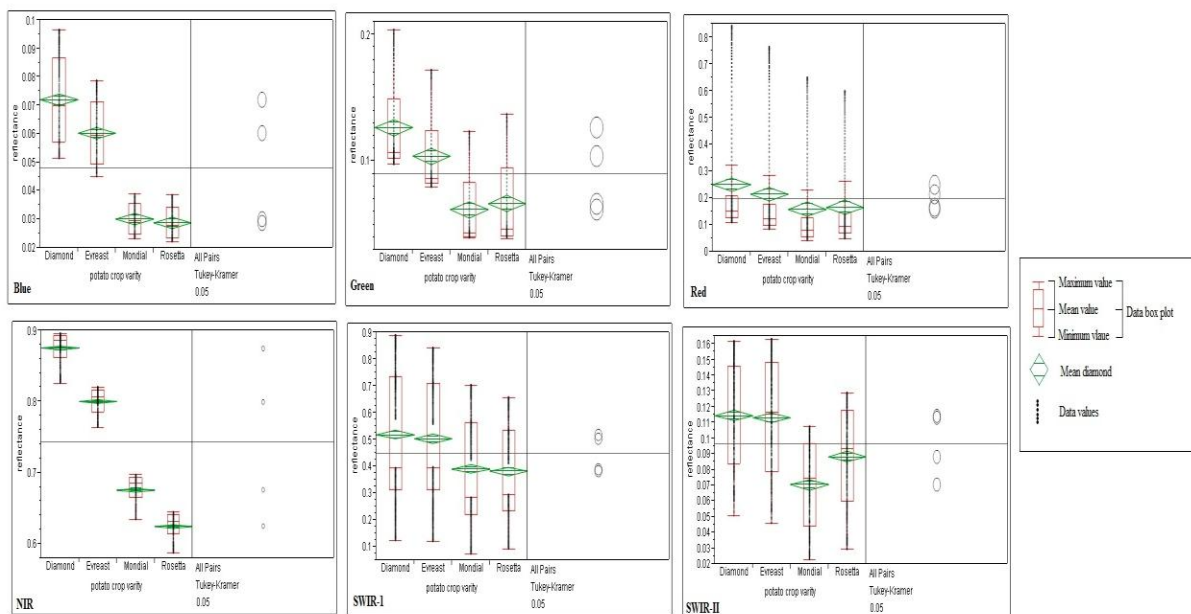

Figure 3: *ANOVA and Tukey's HSD Analysis to Differentiate between the Four Potato Varieties*

6. Linear Discriminate Analysis

Linear Discriminate Analysis (LDA) is a method to discriminate between two or more groups of samples. The groups to be discriminated can be defined either naturally by the problem under investigation, or by some preceding analysis, such as a cluster analysis. The number of groups is not restricted to two, although the discrimination between two groups is the most common approach. Linear Discrimination Analysis (LDA) is a commonly used technique for data classification. LDA approach is explained by Axler 1995. It easily handles the case where the within-class frequencies are unequal and their performance has been examined on randomly generated test data. This method maximizes the ratio of between-class variance to the within-class variance in any particular data set thereby guaranteeing maximal separability. LDA doesn't change the location but only tries to provide more class separability and draw a decision region between the given classes. This method also helps to better understand the distribution of the feature data. In the current study, class-independent transformation type of LDA was performed. This approach involves maximizing the ratio of overall variance to within class variance. It uses only one optimizing criterion to transform the data sets and hence all data points irrespective of their class identity are transformed using this transform. In this type of LDA, each class is considered as a separate class against other classes. In LDA, within-class and between-class scatter are used to formulate criteria for class separability. Within-class scatter is the expected covariance of each of the classes. The scatter measures are computed using equations 3 and 4.

$$Sw = \sum_j Pj \times (\mathrm{cov}_j) \tag{3}$$

Therefore, for the two-class problem,

$$Sw = 0.5 \times \mathrm{cov}_1 + 0.5 \times \mathrm{cov}_2 \tag{4}$$

All the covariance matrices are symmetric. Let and be the covariance of set 1 and set 2 respectively. Covariance matrix is computed using the following equation (5).

$$\mathrm{cov}\, j = \left(x_j - \mu_j\right)\left(x_j - \mu_j\right)^T \tag{5}$$

Then, the between-class scatter is computes using the following equation (6).

$$Sb = \sum_j (\mu_j - \mu_3) \times (\mu_j - \mu_3)^T \tag{6}$$

Sb can be thought of as the covariance of data set whose members are the mean vectors of each class. As defined earlier, the optimizing criterion in LDA is the ratio of between-class scatter to the within-class scatter. The solution obtained by maximizing this criterion defines the axes of the transformed space. As LDA is a class independent type in this study, the optimizing criterion is computed as equation (7)

$$criterion = inv(sw) \times Sb \tag{7}$$

Finally, transforming the entire data set to one axis provides definite boundaries to classify the data. The decision region in the transformed space is a solid line separating the transformed data sets thus equation (8)

$$transforme\_set = transform\_spec^T \times data\_set^T \tag{8}$$

This analysis was carried out to discriminate between the four Potato varieties (Diamond, Everest, Mondial and Rosetta) in order to identify the spectral reflectance pattern of each variety, the optimal waveband to isolate each variety and finally the specific wavelengths that could be used to isolate each variety. Linear discrminant analysis showed the optimal wavebands that could be used to identify each variety. As shown in Table 2, very narrow waveband (714 – 717 nm) was the best to identify Mondial variety while relatively wide spectral range could be used to identify the other three varieties.

Table 2: The Optimal Waveband to Differentiate between the Four Potato Varieties

Variety	Optimal Wavelength Zones (nm)
Everest	712:715/ 1596:1699/ 1700:1754
Diamond	713:1349/1656:1691
Rosetta	350:712/1421:1656/1799:2349
Mondial	714:717

7. Conclusion

Field hyper spectral measurements were used to discriminate between four potato varieties (Everest, Diamond, Rosetta, Mondial). Output measurements were analyzed through two statistical tests to show the best spectral zone and the optimal wavebands to discriminate between the four varieties. Tukey's HSD test indicated that NIR spectral zone was the optimal to differetiate between the four varieties while red spectral zone was inadequate to differetiate between the four varieties. Two spectral zones (NIR) and (SWIR II) showed significant difference between the two varietes (Rosetta and Modial) while three spectral zones (blue, green, NIR) showed significant difference between Diamond and Everest. Linear discrminant analysis showed the unique waveband/s that could be used to isolate each variety. The result of this work is a step forward for better potato crop acreage estimation. The result could be icluded through a machine learning process in the existing image processing softwares to improve crop classification results.

References

Axler S., 1995: *Linear Algebra Done Right*. Springer-Verlag New York Inc., New York.

Casanova D., et al. *Monitoring Rice Reflectance at Field Level for Estimating Biomass and LAI*. Field Crops Research. 1998. 55 (1-2) 83-92.

Diker K., et al. *Potential use of Nitrogen Reflectance Index to Estimate Plant Parameters and Yield of Maize*. Biosystem Engineerung. 2003. 85 (4) 437-447.

El Tobgy H.A., 1974: Contemporary Egyptian Agriculture. Ford Foundation. Beirut, Lebanon.

Fassnacht K.S., et al. *Estimating the Leaf Area Index of North Central Wisconsin Forests Using the Landsat Thematic Mapper*. Remote Sensing of Environment. 1997. 61 (2) 229-245.

Fraser R.N. *Hyperspectral Remote Sensing of Turbidity and Chlorophyll a among Nebraska Sand Hills Lakes*. International Journal of Remote Sensing. 1998. 19 (8) 1579-1589.

Gamon J.A., et al. *A Narrow-Waveband Spectral Index that Tracks Diurnal Changes in Photosynthetic Efficiency.* Remote Sensing of Environment. 1992. 41 (1) 35-44.

Geddes A.M.W., et al., 1984: Report on a Tour of Egypt to Study Potato Production and Marketing. International Potato Center. Lima.

Hansen P.M., et al. *Reflectance Measurement of Canopy Biomass and Nitrogen Status in Wheat Crops using Normalized difference Vegetation Indices and Partial Least Squares Regression.* Remote Sensing of Environment. 2003. 86 (4) 542-553.

Hinzman L.D., et al. *Effects of Nitrogen Fertilization on Growth and Reflectance Characteristics of Winter Wheat.* Remote Sensing of Environment. 1986. 19 (1) 47-61.

Mason R.L, et al., 2003: *Statistical Design and Analysis of Experiments with Applications to Engineering and Science.* 2nd Ed. A John Wiley & Sons Publications.

McMurtrey III, et al. *Distinguishing Nitrogen Fertilization Levels in Field Corn (Zea mays L.) with Active Induced Fluoresing and Passive Reflectance Measurements.* Remote Sensing of Environment. 1994. 47 (1) 36-44.

Nolin A.W., et al. *Hyperspectral Method for Remotely Sensing the Grain Size of Snow.* Remote Sensing of Environment. 2000. 74 (2) 207-216.

Penuelas J., et al. *Visible and Near-Infrared Reflectance Techniques for Diagnosing Plant Physiological Status.* Trends in Plant Science. 1998. 3 (4) 151-156.

Taranik J.V., et al. 1993: *Hyperspectral Technology for Geologic Applications, Better Understanding of Earth Environment.* International Geosciences and Remote Sensing Symposium, (IGARSS). Vol. 2. Tokyo, 917–920.

Treitz P.M., et al. *Hyperspectral Remote Sensing for Estimating Biophysical Parameters of Forest Ecosystems.* Progress in Physical Geography. 1999. 23 (3) 359-390.

Wiegand C.L., et al. *Use of Spectral Vegetation Indices to Infer Leaf Area, Evapotranspiration, and Yield: I. Rationale.* Agronomy Journal. 1990. 82 (3) 623-629.

Wiegand C.J., et al. *Vegetation Indices in Crop Assessments.* Remote Sensing of Environment. 1991. 35 (2-3) 105-119.

Research Article   **Open Access**

Influence of Micro-Climate Parameters on Natural Vegetation – A Study on Orkhon and Selenge Basins, Mongolia, Using Landsat-TM and NOAA-AVHRR Data

Murali Krishna Gurram[1], Oyuntuya Sharavjamts[2] and Nooka Ratnam Kinthada[3]

[1]COWI India Pvt. Ltd., Plot No. 122, Phase-I, Udyog Vihar, Gurgaon, Haryana, India
[2]School of Ecology and Technology Development, Mongolian State University of Agriculture, Mongolia
[3]Dept. of Geoinformatics, AdiKavi Nannaya University, Jayakrishnapuram, Rajahmundry, East Godavari, India

Correspondence should be addressed to Murali Krishna Gurram, murali.krishna.gurram@gmail.com

Abstract A remote sensing study was carried out to map the spatial distribution and intensities of various micro-climate parameters such as surface temperature, surface albedo, precipitation etc., to assess their influence over vegetation health of the region. Remote sensing data pertaining to Landsat-TM and NOAA-AVHRR was used to retrieve the vegetation parameters like NDVI, pasture yield as well as climate parameters like surface temperature and albedo. The study has demonstrated the utility of remote sensing in monitoring the seasonal variations in vegetation growth with respect to meteorological conditions and changes occurring between different periods of same seasons due to change in micro-climate. A direct relationship between micro level variations in the vegetation growth with respect to meteorological conditions in the region was established.

Keywords *Micro-climate Change, NDVI, Landsat TM and NOAA/AVHRR Data*

1. Introduction

Variations in the vigor and pattern of the vegetation manifested over the rangelands and croplands are purely of local character (Lee *et al.,* 2002). Proper identification, classification and mapping of these patterns of high intensive and complex nature requires frequent monitoring as the change in the vigor of the vegetation occurs within a short span of time and mostly depends upon various micro-climatic and terrain conditions. Moreover, change in the vigor differs from one plant species to another. To be able to notice or track, interlink and interpret these changes, observations should be made as frequently as possible i.e., once in every 2-5 days for crops, 2 days for pasture plants on the fenced area and 10 days for pasture plants that grow in the open area. And it is impractical to use any ground based survey techniques for the mapping of the same as they are very time consuming and labor intensive. Studies conducted using remote sensing technology has been proved the best for analyzing such scenarios (Bat-Oyun and Singh, 2005). Importantly, data acquired by the remote

sensing sensors, like, NOAA-AVHRR of high temporal resolution and LANDSAT-TM of relatively high spatial resolution proved to be very effective in determining the patterns of vegetation spreads over a large territory and directly retrieving the parameters such as NDVI, surface temperature and albedo (Oyuntuya *et al.,* 2005). Apart from that, the study is one of the supporting materials for application of remote sensing and comparison of the same results in ecological studies.

1.1. Data Used

Meteorological data parameters, such as temperature and rainfall were obtained from five different stations located in and around the Orkhon-Selenge basin. Meteorological data recorded during 1961-1990 were used for the study. The following table (Table 1) lists the names and location coordinates of the various meteorological stations from where the data pertaining to meteorological parameters were collected.

Table 1: List of Meteorological Stations in the Study Area

S. No.	Name of the Meteorological Stations	Longitude	Latitude
1	Darkhan	105^0 54' E	49^0 28' N
2	Sukhbaatar	106^0 12' E	50^0 14' N
3	Bulgan	103^0 33' E	48^0 48' N
4	Khutag	102^0 42' E	49^0 23' N
5	Baruunkharaa	106^0 40' E	48^0 19' N

NOAA-AVHRR data of 1 km of spatial resolution pertaining to 4 different months starting from May to August between the years 1989-2011 were used for the study. Similarly, multi-temporal data by LANDSAT's Thematic Mapper (TM) sensor of 30 m spatial resolution pertaining to three different years of same season i.e., August 1996, September 2007 and July 2009 were also used for the study. Details of the satellite datasets used for the study are mentioned below.

- NOAA AVHRR data : 1989-2011 (May to September, average of 10 days)
- LANDSAT-TM data : 20th, August 1996; 20th, September 2007 and 24th, July 2009
- Pasture yield : Every 10 days (1989-2011)
- Surface temperature : Average of 10 days (1989-2011)

1.2. Study Area

According to agricultural scientists "Orkhon-Selenge basin" in Mongolia is considered as the land for crop production as it includes all lowlands or hollows between the mountains. The study area encompasses the whole territories of Selenge, Darkhan-Uul, Orkhon and Bulgan aimags (districts) and parts of the Soums Tuv aimag (Figure 1).
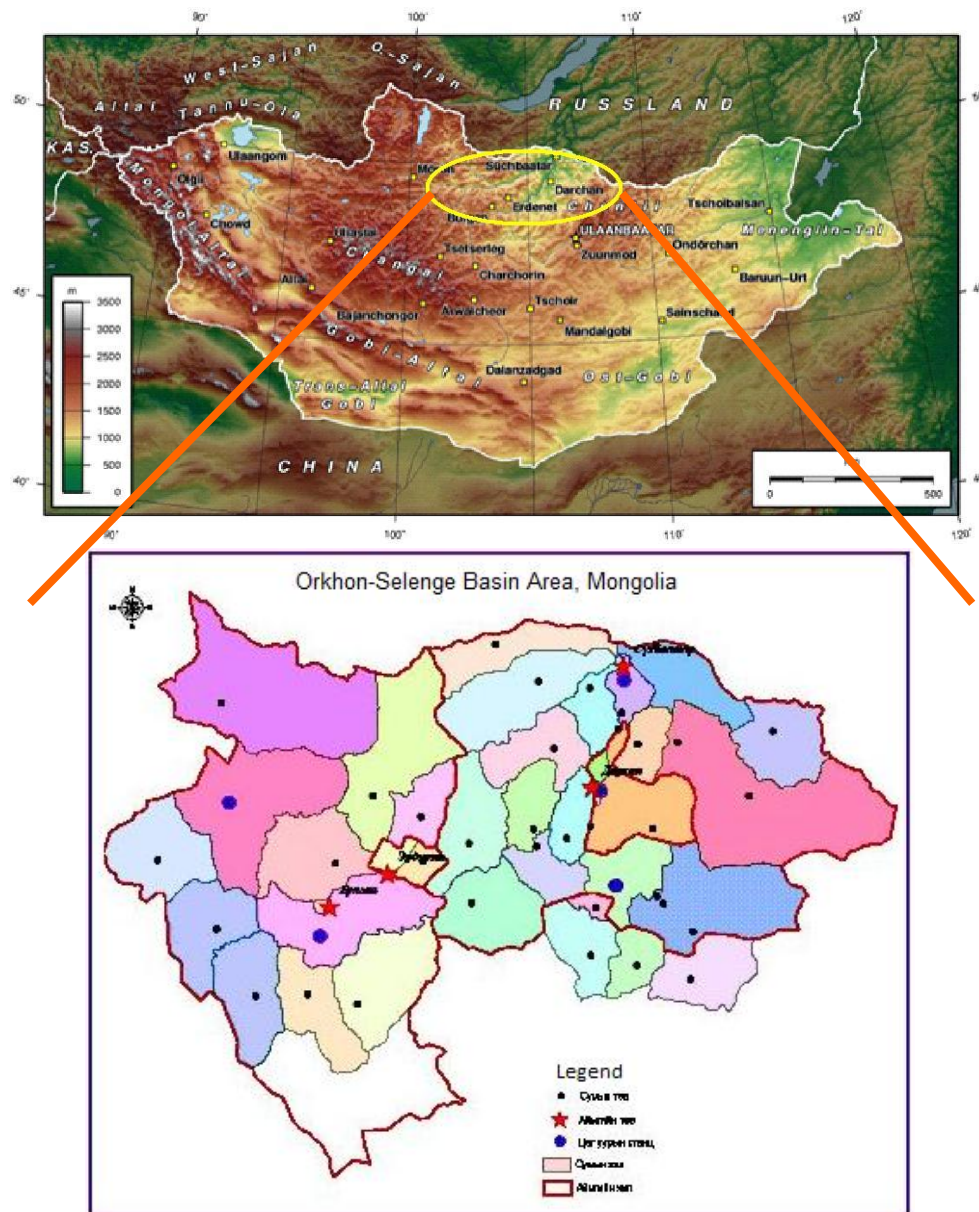
Figure 1: Map Showing the Orkhon-Selenge basin in Mongolia

1.3. Objectives of the Study

The study is aimed at mapping and assessment of various vital land surface parameters, their relationships and patterns using remote sensing in the Orkhon-Selenge basin region.

To accomplish the objectives, the following scenarios were tested:

- Determining the relationship between land surface conditions like NDVI, surface temperature, albedo and meteorological parameters.
- Classification and mapping of the vegetation patterns over a large territory.
- Analyze the patterns of both rangeland vegetation of local character such as crops (observations should be made every 2-5 days), pasture plants on the fenced area (every 2 days) and pasture plants (every 10 days) on open area.

2. Methodology

The study requires key data inputs pertaining to meteorology and vegetation. The methodology mentioned below provides a brief description of the steps involved in collection, processing, retrieval and analysis of the data collected from different sources.

2.1. Data Processing, Retrieval and Analysis

To be able, effectively monitor and map the vegetation types of the entire region, satellite images pertaining to two different sensors of different spatial and temporal resolutions and periods have used for the study. The data acquired by the NOAA-AVHRR of very good temporal resolution, and LANDSAT-TM of relatively higher spatial resolution were used for the study.

2.1.1. NOAA AVHRR Data Processing

In order to retrieve three different vital parameters such as NDVI, Surface temperature and albedo, 10 day interval temporal datasets of NOAA-AVHRR data of August-September during 1989-2011 were used. Particularly, NOAA-AVHRR data is very helpful for mapping the vegetation growth scenarios so that it can keep track of all the changes on a regular basis (Gupta *et. al.,* 1997 & 2001).
The NOAA-AVHRR data sets were geometrically corrected and standard algorithms for atmospheric corrections were applied. NDVI has been calculated as mentioned below:

$$NDVI = (Red - NIR) / (Red + NIR)$$

Subsequently, land surface temperature and pasture yields were calculated to correlate the data with NDVI values.

2.1.2. NDVI vs Pasture Yield

The NDVI values and pasture yield were retrieved to see the relationship between the two and to evaluate the correlation between them (Erdenetseseg and Erdenetuya, 2005). The NDVI values and pasture yield patterns are shown in the Figures 2 and 3 below:
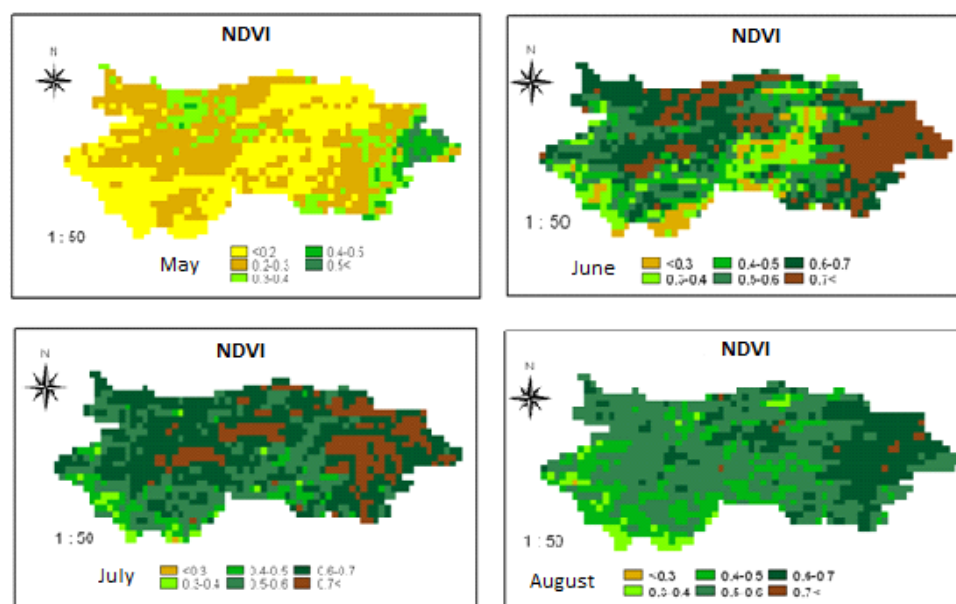

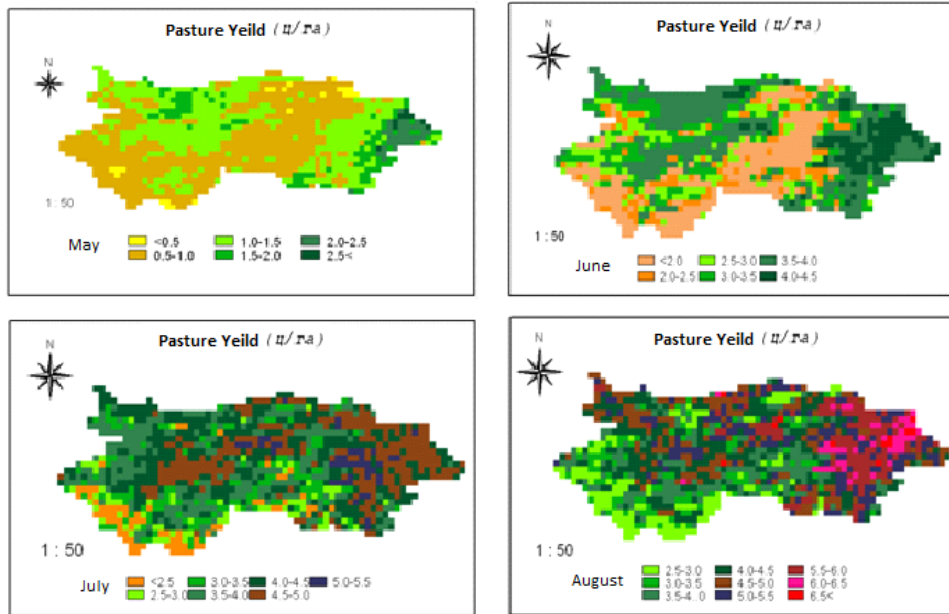*Figure 2: Maps Showing Seasonal Variations in NDVI from May to August*

Figure 3: *Pasture Yield Retrieved from NOAA AVHRR Data*

Regression analysis of NDVI and pasture yield has shown the correlation as shown in the Figure 4 below:
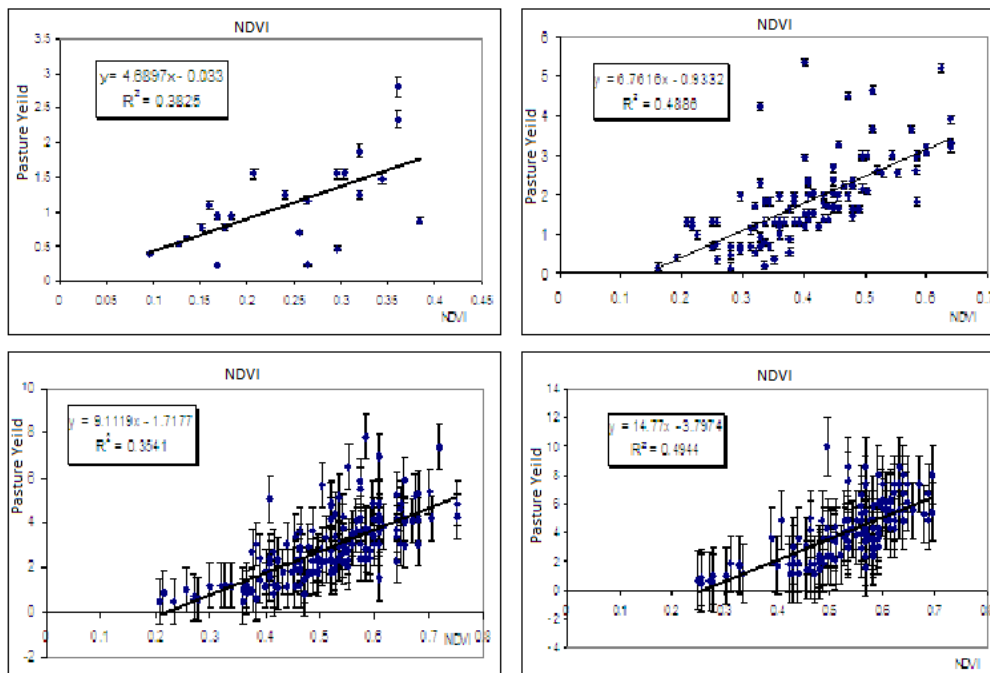

Figure 4: *Regression Curves Showing Relationship between Pasture yield & NDVI*

2.1.3. NDVI vs LST

An attempt was also made to see how NDVI values are correlated with land surface temperature (Azzaya *et al.,* 1998). The following figures (Figure 5 and 6) with results corroborate the relationship between these two parameters.
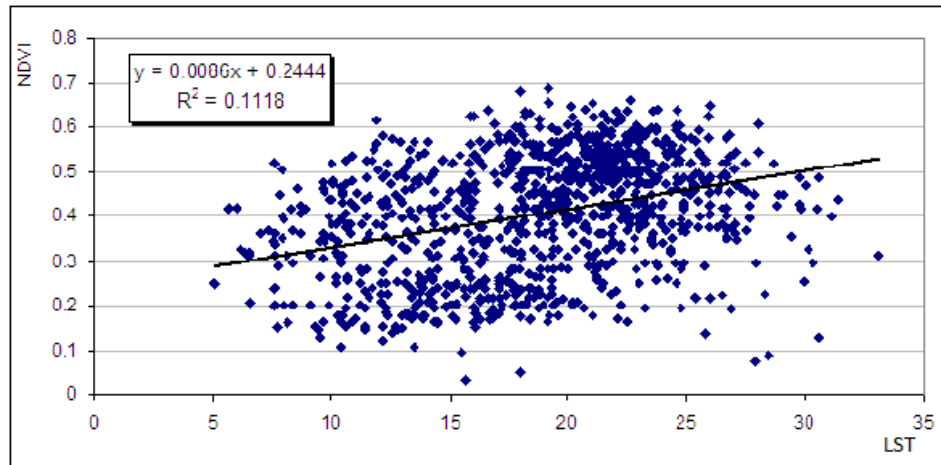
Figure 5: Relationship between LST & NDVI (Vegetation period: from May to September)

Table 1: Correlation between LST & NDVI (Vegetation period: from May to September)

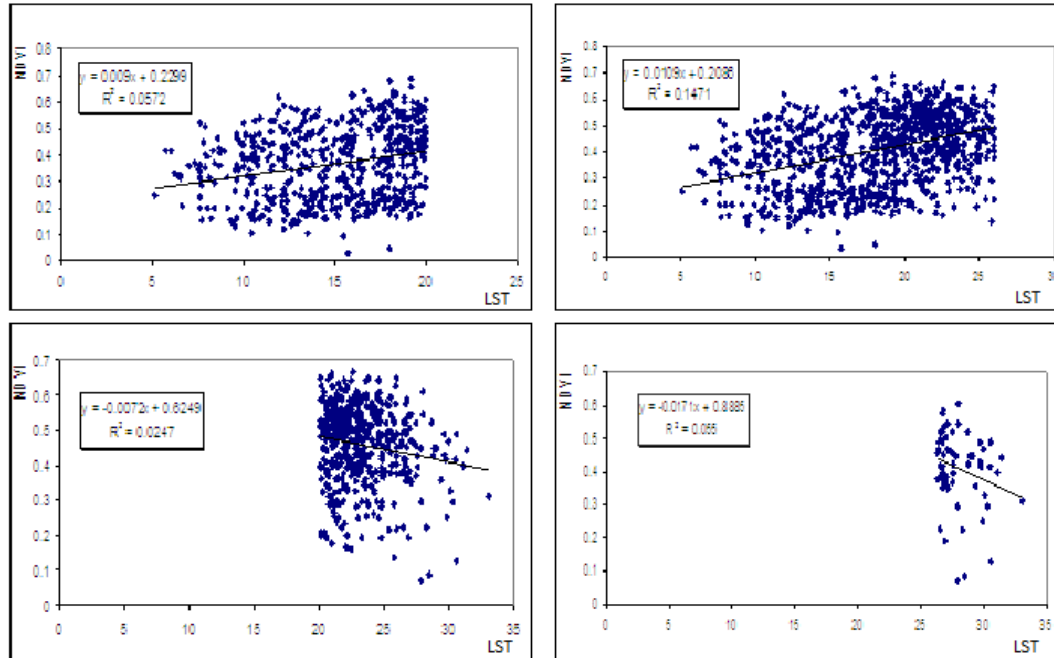| Month	Temperature (in ^{o}C)	NDVI value	Correlation coefficient
May to Sep.	5.1 to 33.1	0.032 to 0.752	0.338
May	7.6 to 25.8	0.032 to 0.536	0.433
Jun.	13.1 to 31.4	0.072 to 0.640	0.101
Jul.	17.8 to 33.1	0.176 to 0.752	-0.184
Aug.	13.3 to 27.5	0.2000 to 0.688	-0.191
Sep.	5.1 to 19.3	0.104 to 0.584	0.137

Figure 6: Regression Curves Showing the Relationship between NDVI and LST

The study investigated the possible use of NOAA AVHRR data for diurnal temperature measurements and mapping of its dynamics. It is determined that the radiant temperature is high on top of high mountain regions with perennial snow cover, sandy, plain, lakes and forest.

2.2. Landsat TM Data Processing

Landsat TM multi temporal datasets were processed to retrieve the NDVI, LST and albedo on high spatial resolution and to generate the land cover theme which is used to correlate with the meteorological and other parameters retrieved from NOAA AVHRR data. Landsat's TM data was also used keeping in mind that it helps in mapping the vegetation patterns at micro-level which is very difficult to identify using the NOAA AVHRR data which is of coarse resolution.

Parameters like NDVI (Figure 7) and surface albedo (Figure 10) were retrieved using the combination of Landsat TM's VIS and NIR bands. Thermal bands (MIR) are used to calculate the land surface temperature or LST (Figure 9) according to the methodology suggested by Prasanjit Dash *et al.* (2001). In addition to this, various land cover classes of the region were delineated using unsupervised classification method with maximum likelihood algorithm. This also helps in the proper identification and classification of different vegetation types which can be used to correlate with other parameters used in the study.
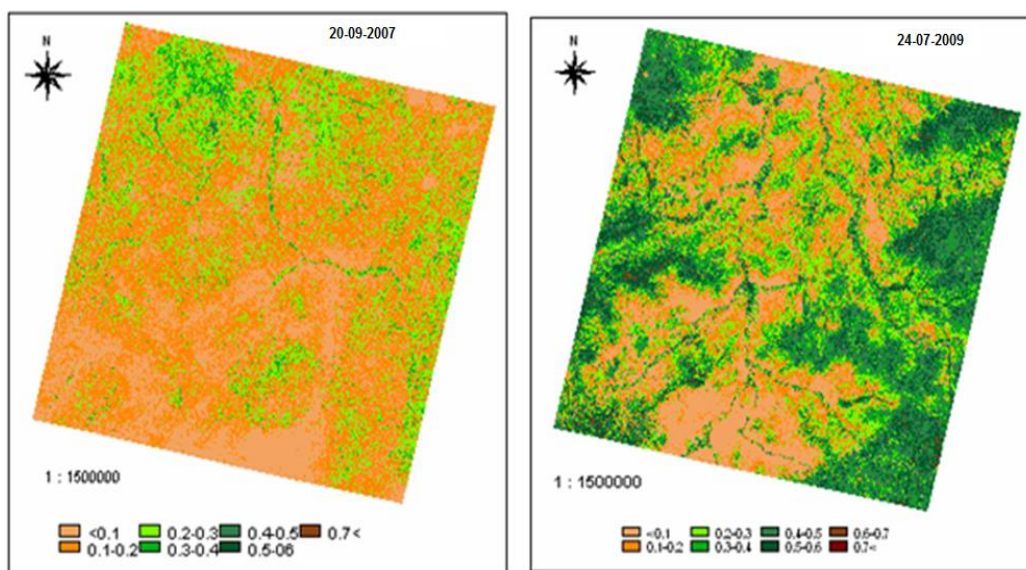
Figure 7: NDVI Derived from the Landsat-TM

Table 4: Variations in the Intensity of NDVI with Respect to Land Use

Land Classes	Date	
	24-07-2009	20-09-2000
Pasture	0.12 to 0.37	0.08 to 0.26
Forest	0.41 to 0.71	0.40 to 0.70
Cultivated area	-0.05 to 0.3	-0.06 to 0.01
Meadow	0.47 to 0.58	0.31 to 0.45
Agriculture area	0.27 to 0.56	0.01 to 0.28

24-07-2009

20-09-2000

Figure 8: *Total Number of Pixels by Each NDVI Class*

Figure 9: *Surface Temperature Classes Retrieved from Landsat-TM*

Table 5: *Surface Temperature Values (^{0}C) Shown by Different Vegetation Classes*

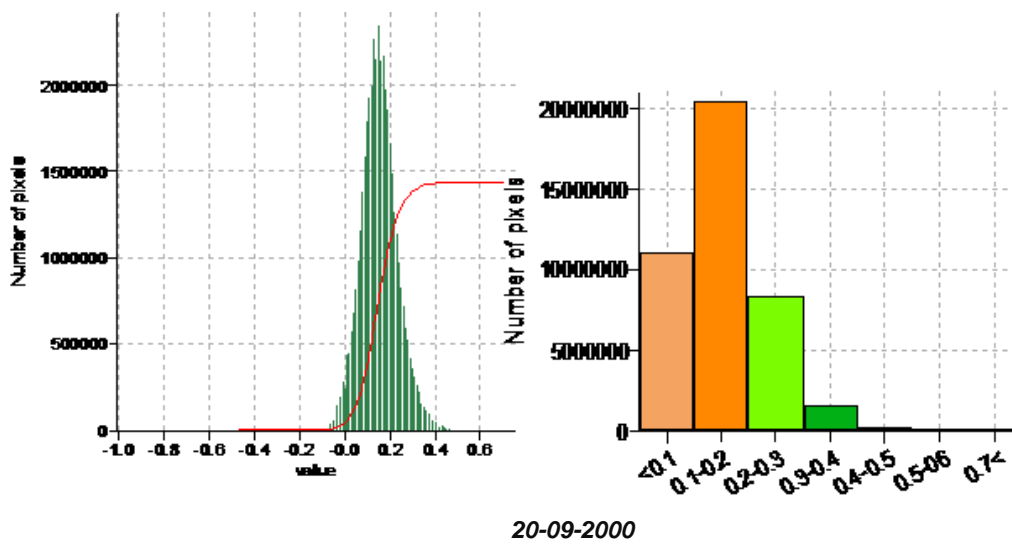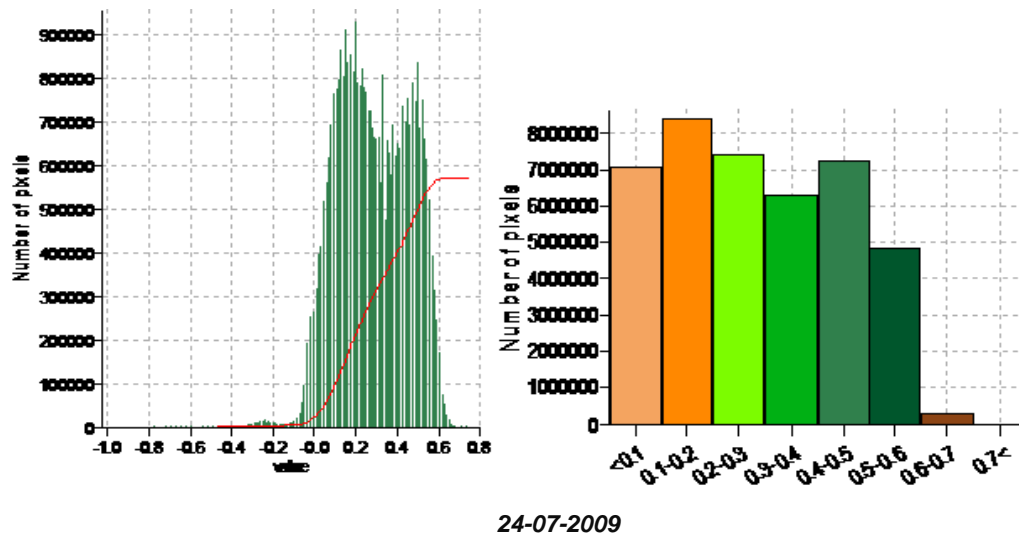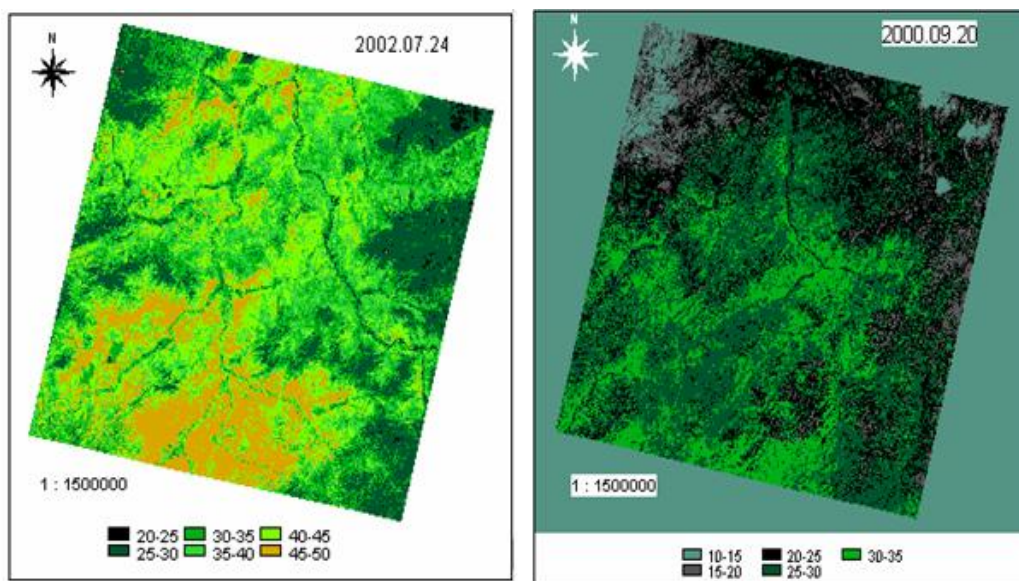| Land Cover	Date	
	24-07-2009	20-09-2007
Pasture	36.3-49.6	27.0-30.7
Forest	27.7-38.5	25.7-27.4
Cultivated area	45.6-50.5	27.2-35.3
Meadow	27.8-36.8	23.5-27.2
Agriculture area	33.4-44.1	24.6-30.1
Lake	27.0-31.4	14.2-22.0
River	27.2-29.1	15.6-22.2
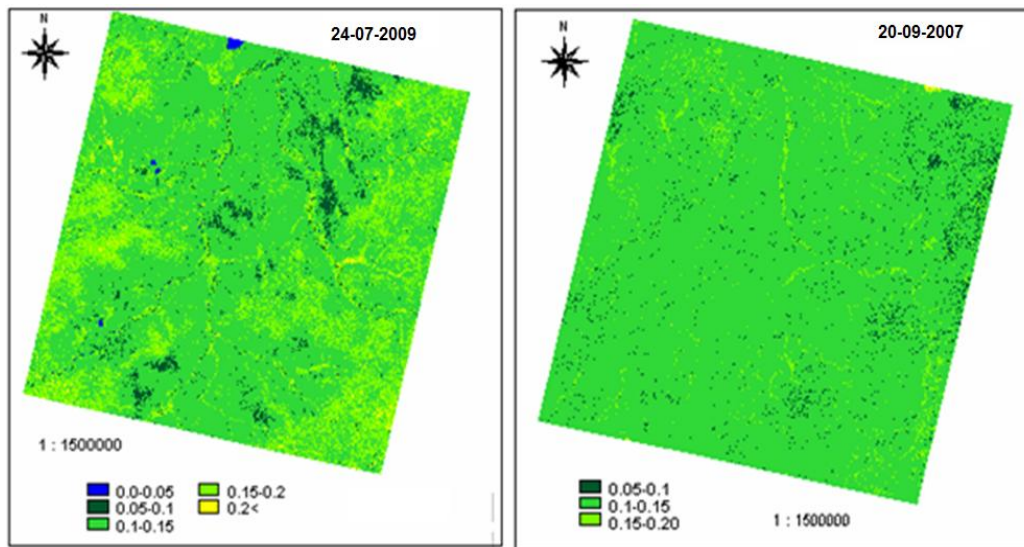
Figure 10: *Mapping of Surface Albedo*

Table 6: *Surface Albedo Values Shown by Different Vegetation Classes*

Land Cover Class	Date	
	24-07-2009	20-09-2007
Pasture	0.098-0.128	0.095-0.135
Forest	0.115-0.166	0.115-0.165
Cultivated area	0.098-0.136	0.119-0.156
Meadow	0.165-0.203	0.128-0.203
Agriculture area	0.128-0.203	0.119-0.156
Lake	0.047-0.097	0.068-0.075
River	0.084	0.031-0.075

3. Results and Discussion

Analysis of meteorological data pertaining to the years 1981-2010 has indicated that the average annual air temperatures during the period was less than zero or between -0.12^{0}C and -1.25^{0}C, while it was -0.36^{0}C at Bulgan station and warmer or 0.01 to 1.0^{0}C at other stations during 1991-2006. These variations in the average annual air temperatures between 0.73 and 1.22^{0}C can be attributed to the changes occurred to local terrain and feature conditions.

It is noticed that, the annual average precipitation in Orkhon-Selenge basin is 339.8 mm; however it is decreased to 6.4 to 43.5 mm during 1991-2006. Variations in monthly average precipitation increased

slightly in all areas during the months of January, May, November and December and decreased or changed drastically during the remaining months. It is decreased by 9.3 to 15.9 mm in other areas during the warmest month of August, while it is increased by 4 to 12.4 mm in Khutag and Bulgan regions.

According to the meteorological conditions observed for one year, the average NDVI values ranged between 0.381 and 0.432 (Figure 4) during vegetation growth period, and for multiple years, there is a slight reduction in NDVI.
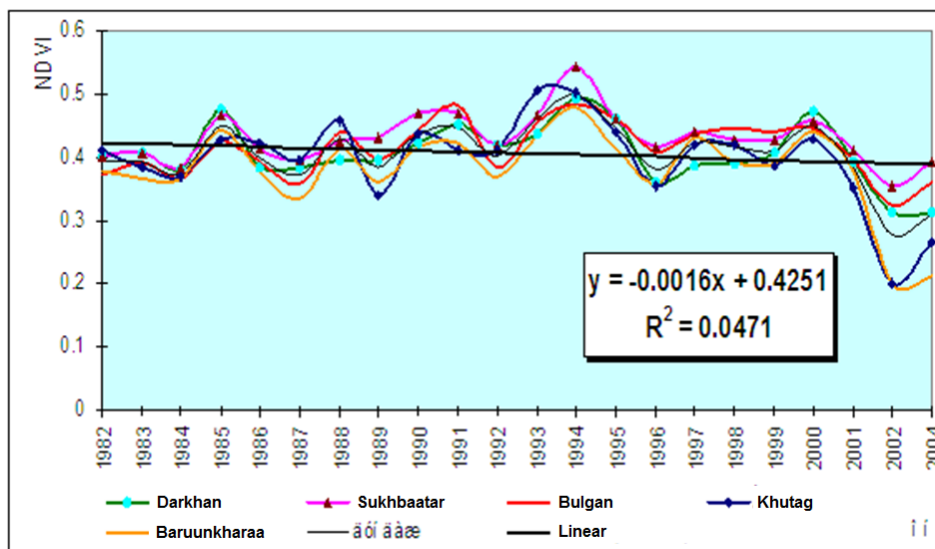

Figure 11: Meteorological Conditions vs NDVI

Depending on the climatic conditions the average NDVI values varied between 0.381 and 0.432 during the vegetation growth period. However, on overall basis the annual average observations have shown a decreasing trend in the NDVI values.

Air temperatures in Orkhan-Selenge basin increased to 0.73-1.22^{0}C in the last 15 years. The annual average air temperatures are above zero and there is a tendency of further warming in the areas other than Bulgan. Total annual precipitation in the region is decreased by 6.4 - 43.5 mm and precipitation received during the warm seasons dropped to 0.6 - 1.3%, with total yearly precipitation accounting for 91.9 - 95.4%.

The vegetation growth in open pastures has shown a positive trend with good or higher correlation coefficient. Based on the NDVI values the vegetation growth in the regions are assessed and mapped accordingly. It is noticed that, increased temperature, prolonged warm seasons and slight decrease in precipitation seems to be favorable for the growth of vegetation. However, such situation is not observed in the study area. Frequent occurrences of unstable climatic conditions, such as, overheating of air and soil during fragile period of plant growth, increase in the precipitation rate and decrease in the frequency of precipitation found to be the reasons for poor vegetation growth.

A positive correlation was found between NDVI and surface temperatures when the temperature is less than 20^{0}C and inverse correlation appeared with the increase in the temperature beyond 20^{0}C. Low humidity and arid conditions with temperatures 20^{0}C can be considered as unfavorable for vegetation growth.

- Depending on the vegetation growth period NDVI values recorded as 0.08-0.37 for pasture, 0.38-0.71 for forest, 0.31-0.59 for river meadow, 0.01-0.7 for crop fields and -0.06 to 0.06 for fallow land. The temperature in a year varies with land types and is highest for fallow land (45.6-50.5^{0}C) and the least for river water (27.2-29.1^{0}C). On the other hand, surface albedo is found to be highest for meadow surface (0.165-0.203) and lowest for water surface (0.047-0.097).

- NDVI found to be high for fallow land compared to pasture, i.e., by 0.2-0.48 which can be consolidated to compare with the primary variety of succession with the biomass, which shows relatively higher productivity.

- There is a positive as well as medium correlation noticed between NDVI and surface albedo, while there is inverse and slight to medium correlation between surface temperature and albedo. It is appropriate to see them together for monitoring terrestrial vegetative patterns.

Table 8: *Table Showing the Relationships between Different Surface Characters*

Date	Indices	NDVI & surface temperature	NDVI & albedo	Albedo & surface temperature
2000.09.20	Case number	14618	664	5777
	Correlation coefficient	-0.26	0.485	-0.099
	Regression equation	$y = -0.0066x + 0.4292$ $R^2 = 0.0694$	$y = 1.9112x + 0.0256$ $R^2 = 0.2351$	$y = -0.0016x + 0.2031$ $R^2 = 0.0097$
2002.07.24	Case number	24217	799	5487
	Correlation coefficient	-0.27	0.38	-0.492
	Regression equation	$y = -0.0071x + 0.5943$ $R^2 = 0.073$	$y = 1.8262x + 0.0848$ $R^2 = 0.1445$	$y = -9E\text{-}05x + 0.1441$ $R^2 = 0.0002$

- Analysis of surface patterns during the years 2006 to 2007 and 2008 to 2009 clearly indicates that there is a degradation of vegetative cover and crop production in the river basin area. The change pattern is shown in the **Figures 12A and 12B**.
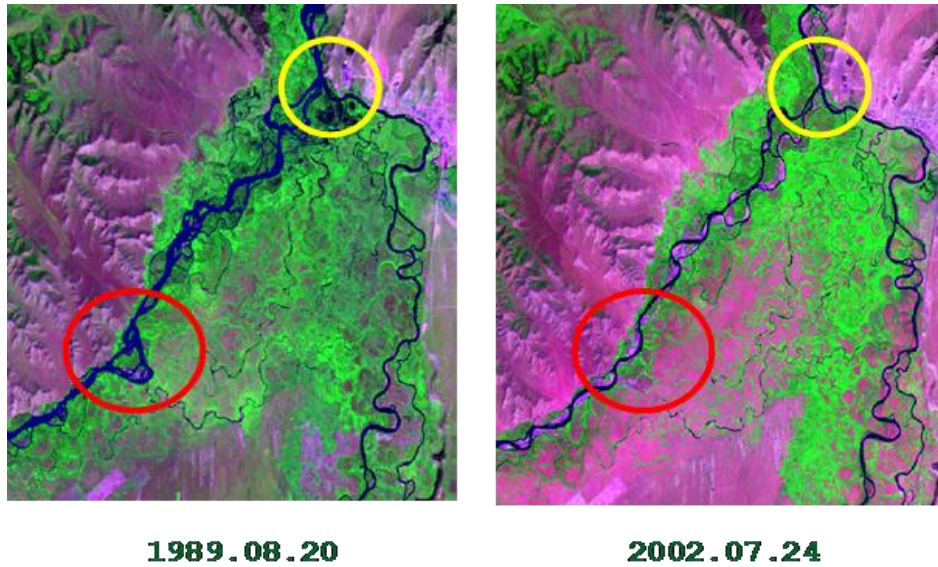
1989.08.20   **2002.07.24**

Figure 12A: Changes Identified along the River Course Areas
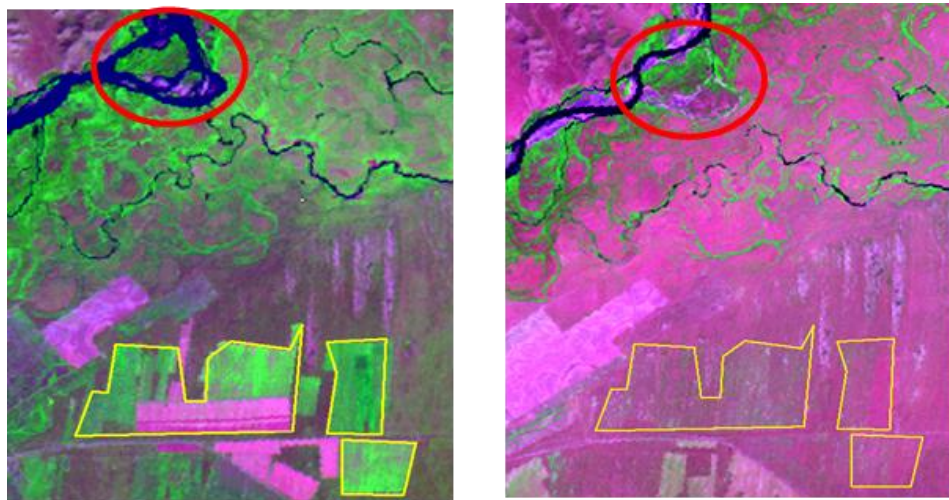
Figure 12B: Changes Identified in the Agricultural Land Use Pattern

4. Conclusion

Remote sensing based analysis highlighted the relationships and influence of land cover parameters vis-à-vis meteorological conditions on micro-climate of the region. NDVI in the open pasture areas have shown a very positive correlation trend with the vegetation suggesting it can be directly used as a measure for mapping and assessment of vegetation growth. NDVI has shown a positive correlation with surface temperatures are less than 20^0C, and at the same time NDVI has shown an inverse correlation when the temperature is more than the 20^0C. Under the low humidity and arid conditions, temperatures are found to be lower than 20^0C which is considered to be unfavorable for vegetation growth. There is a positive and medium correlation found between NDVI and surface albedo. Similarly, there is an inverse and slight to medium correlation found between surface temperature and albedo. Therefore, it is very much essential to take all these parameters into consideration for monitoring the regional surface land cover or vegetation patterns.

References

Azzaya D., et al. *Land Surface Temperature (LST) Estimation Using Satellite Data NOAA-AVHRR over Mongolia.* MNU. 1998. 5; 138.

Bat-Oyun et al. *Drought Assessment over Mongolia Using Remote Sensing and Meteorological Data.* Papers in Meteorology and Hydrology. 2005. 27 (5) 59-68.

Erdenetseseg D., et al. *Application of NDVI/AVHRR/NOAA for the Estimation of Pasture Above-Ground Biomass.* Papers in Meteorology and Hydrology. 2005. 27 (5) 34-37.

Gupta R.K., et al. *The Estimation of Surface Temperature over an Agricultural Area in the State of Haryana and Punjab, India, and Its Relationship with the NDVI, Using NOAA-AVHRR Data",* Int. J. Remote Sensing. 1997. 18; 3729-3741.

Gupta R.K, et al. *Estimation and Validation of Roughness Length, Surface Temperature and Sensible Heat Flux Computed From Remote Sensing (Wifs and NOAA/AVHRR) Data*, Journal Of Agrometeorology. 2001. 3 (1 & 2) 189-215.

Lee R. et al. *Evaluating Vegetation Phenological Patterns in Inner Mongolia Using NDVI Time-Series Analysis.* Int. J. Remote Sensing. 2002. 23 (12) 2505–2512.

Oyuntuya Sh., et al. *The Satellite Based Estimation of Land Surface Energy.* Papers in Meteorology and Hydrology, Mongolia. 2005. 27 (5) 12-20.

Oyuntuya Sh., et al. *Results of Land Surface Processes Using Remote Sensing Technology in Selenge Aimag, Mongolia.* International Conference "Natural Resources and Sustainable Development in Surrounding Regions of the Mongolian Plateau." Ulaanbaatar. 2005. 200-205.

Prasanjit Dash, et al. *Retrieval of Land Surface Temperature and Emissivity from Satellite Data: Physics, Theoretical Limitations and Current Methods.* Journal of the Indian Society of Remote Sensing. 2001. 29 (1 & 2) 23-30.

Research Article   **Open Access**

GIS Based Groundwater Quality Assessment in Tuticorin District Tamilnadu, India

Ramesh Pandian R. and Sashik Kumar M.C.

Department of Civil Engineering, University V.O.C. College of Engineering, Anna University, Tirunelveli Region, Tuticorin, Tamil Nadu, India

Correspondence should be addressed to Sashikkumar M.C., getsashi_kumar@yahoo.com

Abstract Groundwater is widely distributed than surface water and is used for domestic, industrial and agricultural purpose throughout the world. More than 95% of rural population depends on groundwater for all needs. Rapid increase in urbanization and industrialization leads in to deterioration in groundwater quality. In many coastal towns or cities, groundwater seems to be the only source of fresh water to meet domestic, agricultural and industrial needs. But groundwater is under constant threat of saline water incursion, which seems to have become a worldwide concern. Mapping of spatial variability of groundwater quality is of vital importance and it is particularly significant where groundwater is primary source of potable water. In the present study, a detailed investigation was carried out to analyze the spatial variability of groundwater quality for the coastal region of Tuticorin District. Geographical Information System (GIS) based spatial analysis technique has been proven to be a powerful tool to represent the distribution of major ions in the study area. The major water quality parameters such as pH, Electrical conductivity, Total Dissolved Solids, Total Hardness, Calcium, Magnesium, Bicarbonate, Chloride and Sulphate etc. were analyzed. The spatial variation maps of these groundwater quality parameters were derived and integrated through GIS. The final integrated map shows three priority classes such as High, Moderate and Poor groundwater quality zones of the study area and provides a guideline for the suitability of groundwater for domestic purposes.

Keywords *GIS, Surface Water, Groundwater, Spatial Variation, Water Quality, Coastal Region*

1. Introduction

Water is indispensable for the life and it is a very important component for the development of country. Because of the rapidly increasing population, several environmental problems are created which includes groundwater quality degradation. The possibility of groundwater contamination is due to the prevailing drought-prone conditions, the improperly treated and unplanned release of effluents of industry, municipal and domestic into the nearby streams and ponds and the majority usage of groundwater for irrigation are increasing the ionic concentration of the groundwater and making it

more saline. Coastal aquifers constitute an important source of fresh water supply but are often confronted with the problem of seawater intrusion (Lenin et al., 2008). Hence monitoring of groundwater quality has become indispensable. The present study was carried out to evaluate and hydro chemical characteristics of coastal aquifers in Tuticorin District, Tamilnadu. GIS has been applied to visualize the spatial distribution of groundwater quality in the study area. Geographical Information System (GIS) is used for the spatial analysis and it is a powerful tool for representation and analysis of spatial information related to water resources (Rangarajan et al., 2009). A total of 23 groundwater samples were collected and analyzed for various physicochemical parameters in the years 2009 to 2013. The physico-chemical parameters namely pH, Electrical conductivity, Total Dissolved Solids, Total Hardness, Calcium, Magnesium, Bicarbonate, Chloride and Sulphates were analyzed.

2. Description of the Study Area

The study area is located in the coastal tract of southern Tamilnadu. The coastal stretch between Tuticorin and Thiruchendur extends over a distance of about 60 km. Tuticorin is in South Tamilnadu about 540 km south west of Madras (Chennai) and is geographically located in the Gulf of Mannar. The study area is situated in the southeast coast of Tamil Nadu, India and is located between 8°19′ to 9°22′ N latitude and 77°40′ to 78°23′ E longitude covering an area of about 4,590.54 km^2. The location of the study area is shown in Figure 1. Tuticorin city and surrounding areas have considerable presence of industries in several industrial sectors. The study area is chiefly composed of hornblende biotite gneiss, alluvial marine and charnockites in the west (Selvam et al., 2013). The quartzite formations are also found as disseminated patches in the study area. Vaipar, Tambraparani and Karamanaiyar are the major rivers draining the district. All the rivers are ephemeral in nature and run off is generated in heavy rainfall period only. The average annual rainfall of this zone is 877mm. The North-East monsoon contributing to 65.4% of annual rainfall is the major component of recharge into the aquifer. The mean maximum temperature falls in the month of June (37.6^{o}C) and the minimum is seen in January (19.9^{o}C). Evaporation is greater during the months of June, July and August showing the significance of high temperature and radiation. The water quality parameters collected for the study area is shown in Table 1.
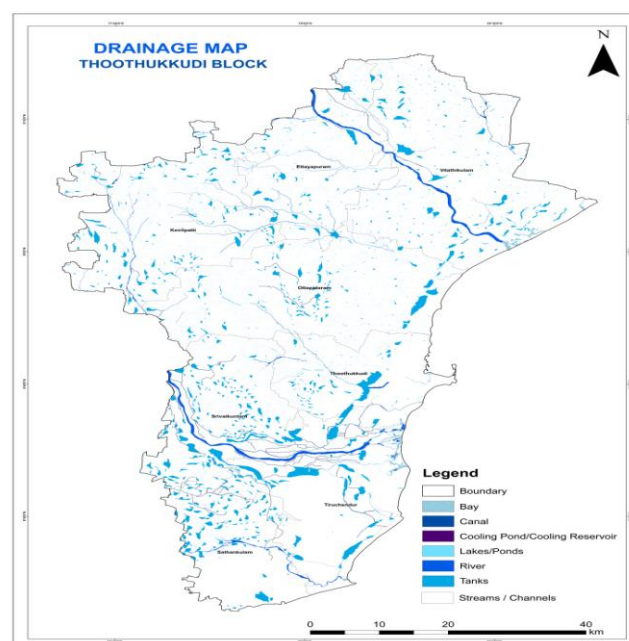

Figure 1: Location Map of Study Area

Table 1: Water Quality Parameters for the Study Area

Sample Location	Latitude	Longitude	pH	EC	TDS	Mg	Ca	HCO3	Cl
Pudukottai	8.752	77.844	8.5	11000	9568	2405.2	497	146	19273
Thoothukudi	8.798	78.12	7.6	1265	1346	89	120	179	569
Kurukusalai	8.928	78.096	7.1	450	312	24.3	68	207	89
Kadambur	8.992	77.853	7.3	230	196	22	46	146	56
Ettayapuram	9.153	77.986	8.5	3563	4562	189	332	656	5698
Vembar	9.106	78.345	8.6	15623	12356	869	265	532	6536
Nagalapuram	9.224	78.147	8.2	5465	6598	798	423	265	3652
Vaippar	9.048	78.256	8.4	12598	21565	2569	568	222	20365
Eppodumventran	9.036	78.042	7.8	9863	11000	422	965	198	4213
Maniachi	8.884	77.886	7.9	2896	3265	196	221	401	2132
Sawyerpuram	8.684	78.027	7.3	199	236	56	98	198	102
Nazareth	8.546	77.952	7.4	569	986	102	56	96	198
Vilathikulam	9.108	78.074	7.9	11235	18659	1986	356	236	16538
Srivaikundam	8.644	77.922	7.1	263	365	63	26	121	102
Kovilpatti	9.211	77.872	7.9	815	1236	96	160	365	212
Karunkulam	8.791	77.869	7.8	265	198	46	36	98	265
Udangudi	8.422	78.0249	7.6	569	1236	56	89	569	465
Tiruchendur	8.491	78.025	8.4	9865	12356	569	265	789	6598
Sathankulam	8.408	78.958	7.5	369	756	56	45	132	102
Ottapidaram	8.856	78.040	7.5	569	986	48	36	98	89
Kayathar	9.089	77.674	7.2	236	362	86	23	145	59
Alwarthirunagari	8.502	77.841	7.1	136	156	46	56	123	39

3. Integration of Spatial and Attribute Database

The groundwater samples were collected from 23 wells and tested for physico-chemical parameters are compared with the permissible limits. The major water quality parameters of the samples were analyzed. The layout map with sample station location in Tuticorin district is shown in Figure 2. The base map of the Tuticorin district is derived from the thematic map collected from Institute of Remote Sensing, Anna University on 1:50,000 scale. The base map was georeferenced and digitized by using MapInfo software and exported to Arc View software for spatial analysis. Spatial interpolation technique through Inverse Distance Weighted (IDW) approach has been used in the present study to delineate the distribution of water pollutants. This method uses a defined or selected set of sample points for estimating the output grid cell value.

4. Results and Discussion

The spatial and the attribute database generated are integrated for the generation of spatial variation maps of major water quality parameters like pH, electrical conductivity, total dissolved solids, total hardness, calcium, magnesium, bicarbonate, chloride and sulphates. Based on these spatial variation maps of major water quality parameters, an integrated groundwater quality map of the study area was prepared using GIS. This integrated groundwater quality map helps us to know the existing groundwater condition of the study area.
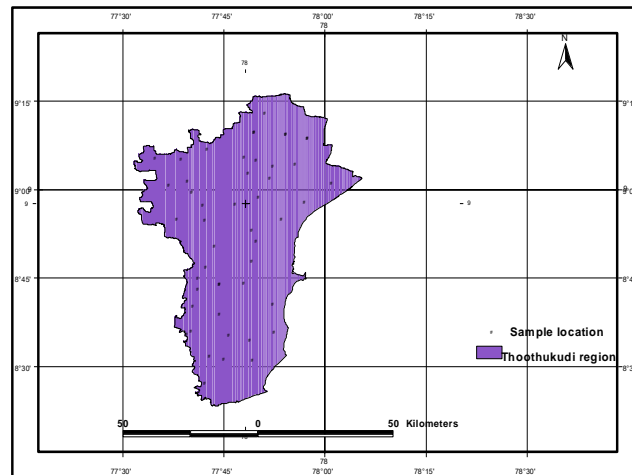
Figure 2: Layout Map with Sample Station Location in Tuticorin District

4.1. pH

pH is one of the important parameters of water and determines the acidic and alkaline nature of water. The pH value of water ranged between 7.1 to 8.6. The pH of the samples was well within the prescribed standards for drinking water. The spatial variation map for pH was prepared and presented in Figure 3.

4.2. Electrical Conductivity (EC)

The salt concentration is generally measured by the determining the electrical conductivity of water. The EC of water samples varies from 136 to 15623 μs/cm. The spatial variation map for Electrical Conductivity (EC) was prepared and presented in Figure 4. From the map it has been observed that very small portion of the study area, the EC value is within the prescribed range. The major portion of the study area is having poor range and northern part is having moderate range of Electrical Conductivity.
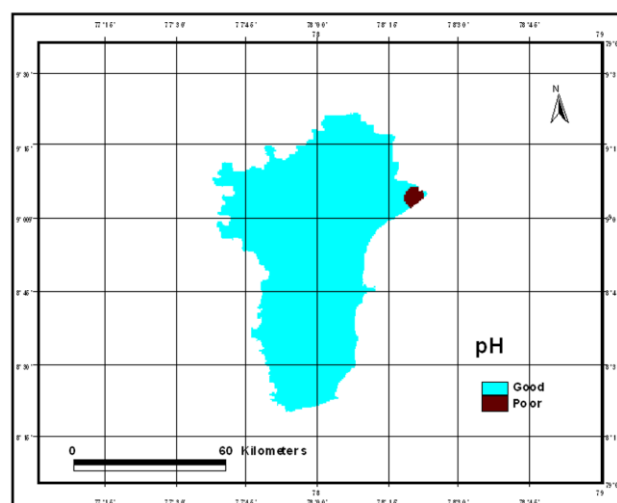

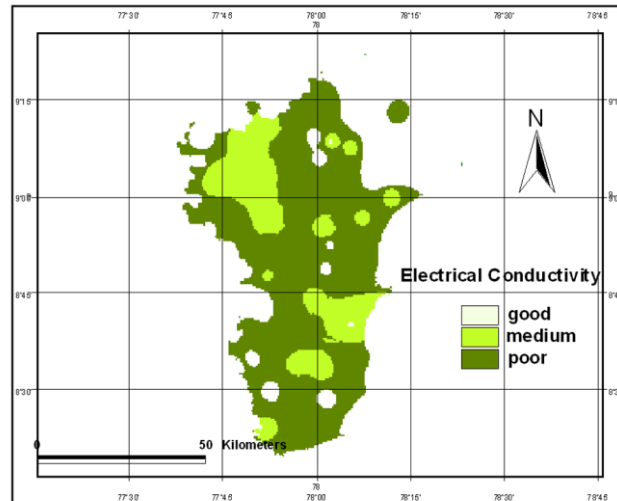*Figure 3: Spatial Variation Map of pH*

Figure 4: *Spatial Variation Map of Electrical Conductivity*

4.3. Total Dissolved Solids

The weight of the residue consisting of pollutants (dissolved ions) left behind after all the water from a water sample is evaporated is a measure of the TDS and gives the general nature of groundwater quality and extent of contamination (Udayalaxmi et al., 2010). The Total Dissolved Solids (TDS) was classified into three ranges (0-500 mg/l, 500-1000 mg/l and >1000 mg/l). The TDS of water samples ranges from 156 to 21565 mg/l. The spatial variation map for TDS was prepared based on these ranges and presented in Figure 5. From the map it has been observed that very small portion of the study area, the EC value is under the good range (0-500 mg/l). The major portion of the study area is having poor range (>1000 mg/l) and northern part is having moderate range (500-1000 mg/l).
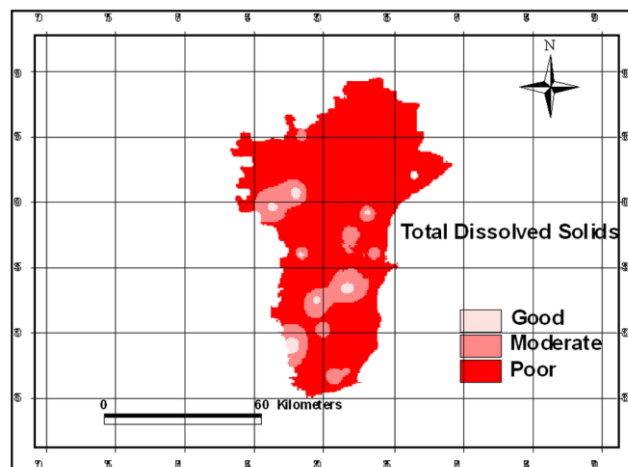
Figure 5: *Spatial Variation Map of TDS*

4.4. Total Hardness

Total hardness, an important property indicating the quality of groundwater is mainly caused by calcium and magnesium cations and is defined as the sum of their concentrations expressed in mg/l. The total hardness was classified in to three ranges (0-300 mg/l, 300-600 mg/l and >600 mg/l) and based on these ranges the spatial variation map for total hardness has been obtained and presented

In Figure 6. Total hardness (TH) of water samples ranges from 145 to 3391 mg/l. From the map it was observed that for major areas, the total hardness value is in the moderate range (300-600 mg/l) and smaller portion having poor and good range.
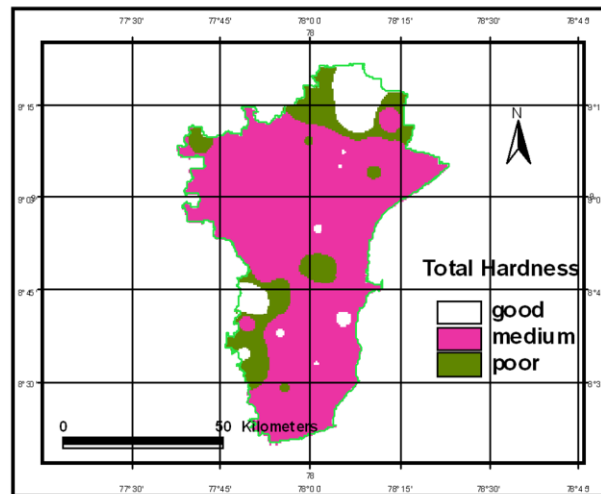
Figure 6: Spatial Variation Map of Total Hardness

4.5. Calcium

Calcium was classified in to three ranges (0-75 mg/l, 75-200 mg/l and >200 mg/l) and based on these ranges the spatial variation map for Calcium has been obtained and presented in Figure 7. Calcium of Water samples ranges from 23 to 965 mg/l. From the spatial variation map, it was observed that Northern part of the study area, the sulphates value is in the poor range ((>400 mg/l). For the Southern part of the study area, sulphate value is in the moderate and only smaller portion is having good range.
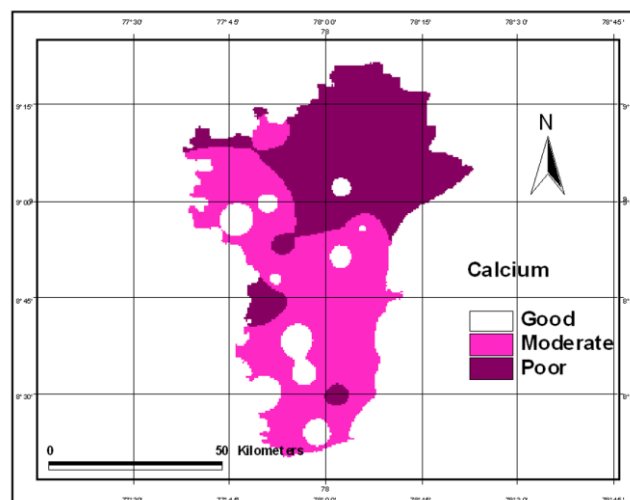
Figure 7: Spatial Variation Map of Calcium

4.6. Magnesium

Magnesium also is one of the abundant elements in rocks. It causes hardness in water. Magnesium concentration of water samples ranges from 22 to 2405.2 mg/l. The spatial variation map for magnesium has been obtained and presented in Figure 8. From the spatial variation map, it was observed that Northern part of the study area, the magnesium concentration is in the poor range. The most part of the study area has moderate range and only smaller portion is having good range.
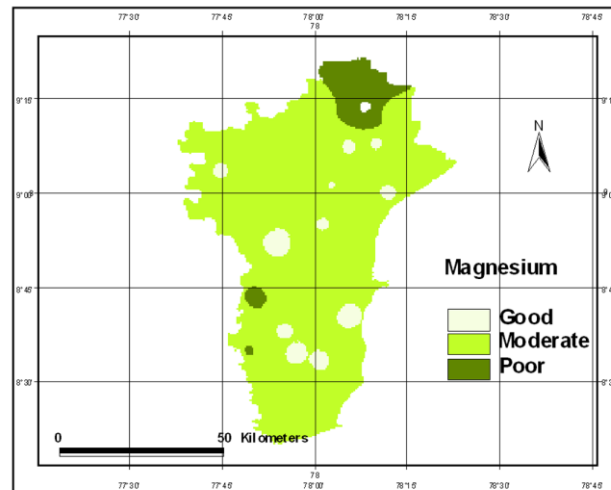
Figure 8: Spatial Variation Map of Magnesium

4.7. Bicarbonate (HCO₃)

Bicarbonate (HCO_3) concentration of water samples ranges from 96 to 789 mg/l. The spatial variation map for Bicarbonate has been obtained and presented in Figure 9. From the spatial variation map, it was observed that most part of the study area is in moderate and poor range and only smaller portion is having good range.
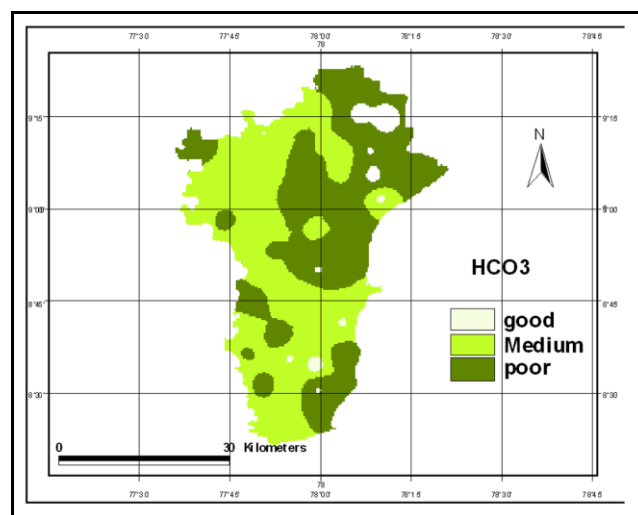
Figure 9: Spatial Variation Map of Bicarbonate

4.8. Chloride (Cl)

Chloride (Cl) concentration of water samples ranges from 56 to 20365 mg/l. The spatial variation map for chloride has been obtained and presented in Figure.10. From the spatial variation map, it was observed that most part of the study area is in the poor range and only smaller portion is having good and moderate range.
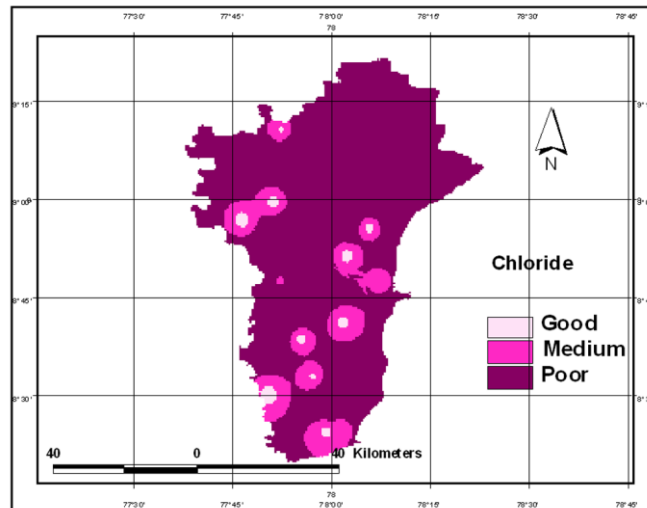
Figure 10: Spatial Variation Map of Chloride

4.9. Sulphates

Sulphates was classified in to three ranges (0-200 mg/l, 200-400 mg/l and >400 mg/l) and based on these ranges the spatial variation map for sulphates has been obtained and presented in Figure 11. Sulphate of water samples ranges from 12 to 1361 mg/l. From the spatial variation map, it was observed that Northern part of the study area, the sulphates value is in the poor range (>400 mg/l). For the Southern part of the study area, sulphate value is in the moderate and good range.

Figure 11: Spatial Variation Map of Sulphate

5. Data Integration Using GIS

The spatial variation map of major groundwater quality parameters were integrated and integrated groundwater quality map of Tuticorin District was prepared and sh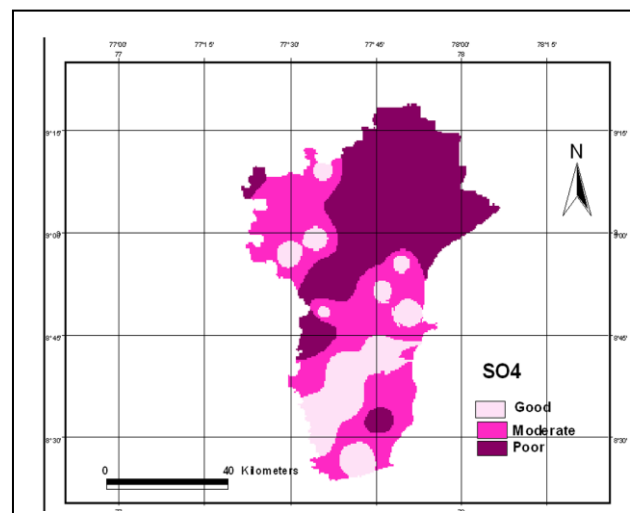own in Figure 12. The integrated map shows the broad idea about good, moderate and poor groundwater quality zones in the study area. The groundwater quality has been classified quantitatively as good, moderate and poor depending on the final weightage values assigned to polygons in the final layer. From the map, it is evident that the groundwater quality in the Northern part of the study area is in the moderate and poor condition while the Southern side of the study area groundwater quality is in the good condition.
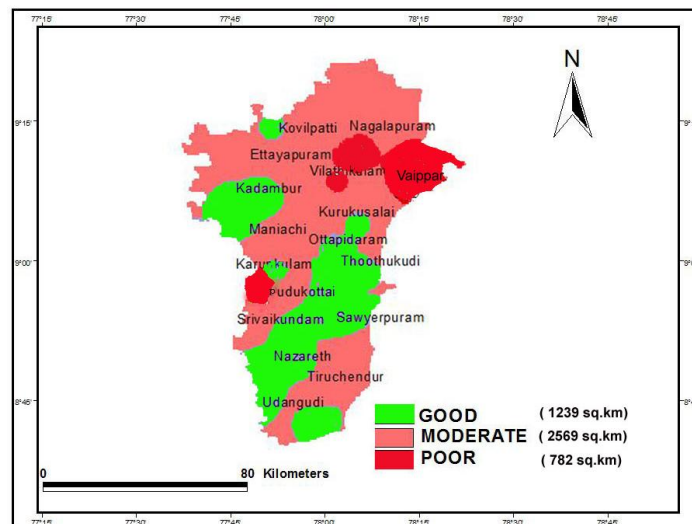
Figure 12: *Spatial Variation Map of Integrated Water Quality*

6. Conclusion

The dependence on groundwater is increasing in many regions because of limited surface water as perennial rivers and frequent failure of monsoon. The groundwater quality is equally important as that of quantity. Groundwater continues to be exploited at ever increasing rates, especially in the rapidly expanding urban areas of the country. The present study has been undertaken to analyze the spatial variation of major groundwater quality parameters such as pH, Electrical conductivity, Total Dissolved Solids, Total Hardness, Calcium, Magnesium, Bicarbonate, Chloride and Sulphates using GIS approach. The groundwater quality of 23 wells randomly distributed in Tuticorin district, Tamil Nadu was selected for the present study. The spatial variation maps of major groundwater quality parameters were prepared and finally all these maps were integrated. The integrated groundwater quality map shows the broad idea about good, moderate and poor groundwater quality zones in the study area.

References

Amer A.M. *Saltwater Intrusion in Coastal Aquifers*. Water Resource Management. 1995. 2; 521–529.

Chidambaram S., et al. *A study on the Hydrogeology and Hydrogeochemistry of Groundwater from Different Depths in a Coastal Aquifer: Annamalai Nagar, Tamilnadu, India*. Environ Geology. 2009. 57; 59–73.

Lenin Kalyana Sundaram V., et al. *Vulnerability Assessment of Seawater Intrusion and Effect of Artificial Recharge in Pondicherry Coastal Region using GIS.* Indian Journal of Science and Technology. 2008. 1 (7) 1-7.

Mondal N.C., et al. *Determining the Interaction between Groundwater and Saline Water through Groundwater Major Ions Chemistry.* Journal of Hydrology. 2010. 388 (1–2). 100–111.

Rangarajan R., et al. *Estimation of Natural Recharge and its Relation with Aquifer Parameters in and Around Tuticorin Town, Tamil Nadu India.* Current Science. 2009. 97 (2) 217–226.

Rajmohan N., et al. *Major Ion Correlation in Groundwater of Kancheepuram Region, South India.* Indian Journal of Environmental Health. 2003. 45 (1) 5-10.

Selvam S. *Use of Remote Sensing and GIS Techniques for Land Use and Land Cover Mapping of Tuticorin Coast, Tamilnadu.* Universal Journal of Environmental Research and Technology. 2012. 2 (4) 233-241.

Selvam S., et al. *Hydro Chemical Characteristics and GIS-Based Assessment of Groundwater Quality in the Coastal Aquifers of Tuticorin Corporation, Tamilnadu, India.* Applied water Science. 2013. 3 (1) 145-159.

Udayalaxmi G., et al. *Geochemical Evaluation of Groundwater Quality in Selected Areas of Hyderabad, A.P., India.* Indian Journal of Science and Technology. 2010. 3 (5) 546-553.

Research Article **Open Access**

Evaluating Impact of Coal Mining Activity on Landuse/Landcover Using Temporal Satellite Images in South Karanpura Coalfields and Environs, Jharkhand State, India

Akshay Kumar and Arvind Chandra Pandey

Department of Remote Sensing, Birla Institute of Technology, Mesra, Ranchi, Jharkhand, India

Correspondence should be addressed to Arvind Chandra Pandey, arvindchandrap@yahoo.com

Abstract This paper investigates the spatio-temporal landuse/landcover changes in South Karanpura coal mine and surrounding areas during the period from 1992 to 2009. Land use/ land cover maps for the year 1992, 2004 and 2009 were generated through the visual interpretation of ETM and IRS-1D LISS-III satellite images with selective field checks. The majority of changes are identified over agricultural land, coal mining area and forests. The study revealed that coal mining area expanded from 10.06 sq. km in 1992 to 21.29 sq. km in 2004 and further diminished to 19.40 sq. km by the year 2009 due to reduction of coal reserve and decline in the coal production indicating 92.84% area increase in coal mining induced landuse changes primarily at the expense of cropland (-38.67%) and dense forest (-71.85%).
Keywords *Remote Sensing, Landuse/Landcover, Coal Mining, Change Detection Statistics*

1. Introduction

Land use refers to man's activities and the various uses which are carried on land whereas land covers refers to natural vegetation, water bodies, rock/soil, artificial cover, and others noticed to the land [10]. Land cover representing the assemblage of biotic and abiotic components on the earth's surface is one of the most crucial properties of the earth system. It reflects the biophysical state of the earth's surface and immediate subsurface, thus embracing the soil material, vegetation, and water. Human activities, especially land use, have changed physical geographical environment greatly, the direct result of which is the changes of land cover [14]. Improper land use practices can adversely affect many natural processes that lead to soil erosion, land degradation, habitat destruction, water pollution and flooding which are often associated with inappropriate agricultural, industrial and urban land use practices. Land is becoming a scarce resource due to population growth and industrialization. Rapid growth of mining activities can also be attributed as one of the reasons for decrease and degradation of land. The mining of natural resources is invariably associated with land

use and land cover changes [10]. Modern techniques of surface mining using heavy equipment can produce dramatic alterations in land cover, both ecologically and hydrologically [15].

Mining of coal both surface and subsurface causes enormous damage to the flora, fauna, hydrological relations and soil biological properties of the systems. Opencast mining, which is being given greater importance for present and future coal mining operations generally, changed the natural topography of the area [5, 13]. Large pits are left after mining and large amounts of overburden material excavated during mining is dumped in the vicinity of the mine sites and continuous rehandling of the overburden dumps further modifies the general landscape of the area. Flow of silt from overburden dumps causes degradation of land and disruption of water flow. Degradation of forests during mining operation is invariably accompanied by an extensive damage and loss to the forest ecosystem and wildlife habitat. The overburden of coal mines when dumped in unmined areas creates mine spoils which ultimately affects the surrounding vegetation.

The use of remote sensing coupled with geographic information systems (GIS) provide the most accurate means of measuring the extent and pattern of such changes in landscape conditions over time [9, 4]. The study on the impact of coal mining on land use changes were carried out by various workers in different parts of the world [5, 6, 11, 13, 14]. Pandey and Nathawat [12] attempted land use land cover mapping in Panchkula, Ambala and Yamunanger districts, Haryana State in India and opinioned that the heterogeneous climate and physiographic conditions in these districts has resulted in the development of different land use/land cover with dominance of agricultural lands.

Studying changes in land-use pattern using remotely-sensed data is based on the comparison of time-sequential data, Change detection using satellite data can allow for timely and consistent estimates of changes in land-use trends over large areas, and has the additional advantage of ease of data capture into a GIS [11]. It also offers the most economical means of assessing environmental impact of the developmental processes, monitoring of bio-species diversity of an ecosystem and generation of suitable action plans for sustainable development [10]. Mining operations, which involve minerals extraction from the earth's crust tends to, make a notable impact on the environment, landscape and biological communities of the earth [3, 1].

The areas under present investigation comprising rich coal reserve of sub-bituminous grade belong to South Karanpura coalfield where mining activity is in progress since 1817. The plateau region with enormous resource potential is badly damaged by coal mining and allied activities. The objective of the present study is to determine the spatio temporal changes in land use / land cover of Patratu region due to coal mining activity in South Karanpura coalfields during the period from 1992 to 2009 by using remote sensing techniques.

2. Study Area

The South Karanpura coal field is located in Ramgarh/Hazaribagh districts of Jharkhand State, India (Figure 1). The study area is situated in Patratu region and comprising about 277 sq. km in the survey of India topographical sheet no. 73 E/6 on a scale of 1:50,000. It is confined between the latitude 23^0 35 N to 23^0 44 N and longitude 85^0 15 E to 85^0 25 E. The South Karanpura coalfield with geological formation belonging to Gondwana system [2] has large reserves of coal suitable for power generation. The main urban settlements in the area are Patratu, Bhurkunda, Saunda, Giddi and Simratanr. Damodar River is the main stream of the area and flows from north-west to south-east with Nalkari River as its main tributary. Coal mining areas are located mainly in the vicinity of Damodar River. Forests cover mainly the hilly terrain and are deciduous and evergreen type whereas agricultural lands are located mainly in the plain areas. The climate of the area is tropical and during summer months the temperature reaches up to 45^0C and in winter it falls to 2^0C. The area receives annual rainfall of 1472 mm with significant seasonal variation.
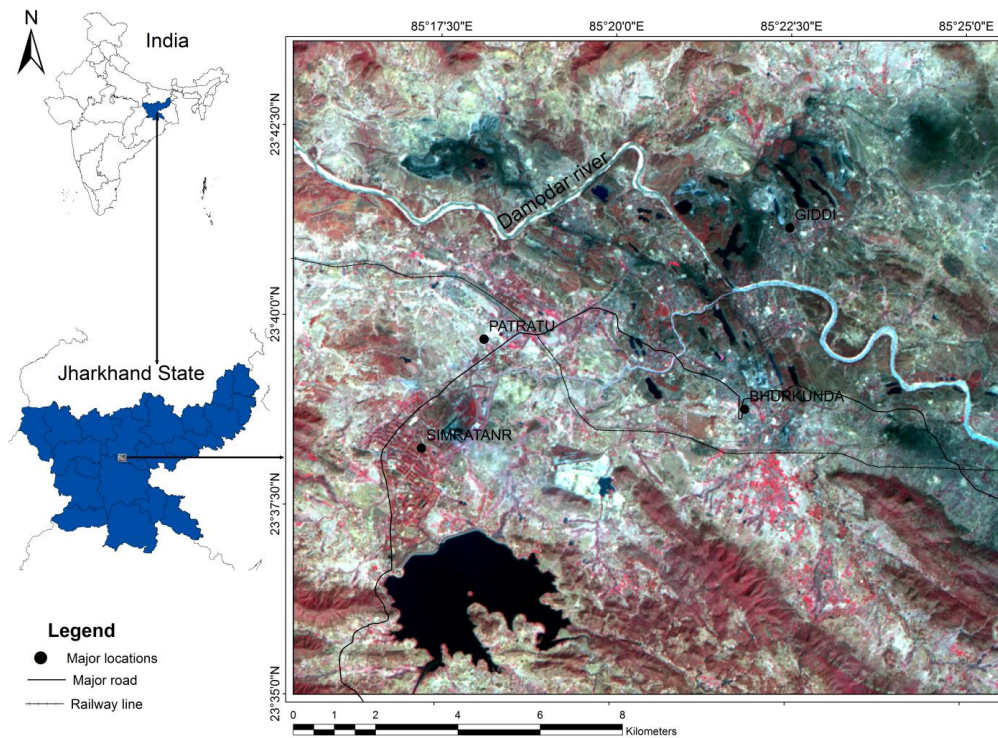
Figure 1: *Location Map of the Study Area and Its Representation on LISS-III Satellite Image in False Colour Composite (FCC). A Large Reservoirs Present In the Area and A Number of Water Bodies Exist Within the Abundant Coal Mines. Dark Grey Tone Represents Coal Mining Area through Which the River Damodar Flows from Northwest to Southeast*

3. Materials and Methodology

3.1. Data

In the present study satellite images covering the study area were acquired for the year 1992, 2004 and 2009. LISS–III data of 2004 and 2009 were obtained from National Remote Sensing Centre (NRSC) Hyderabad, whereas ETM+ data for the year 1992 was obtained from U.S. Geological Survey (USGS) website (http://glovis.usgs.gov). Topographical map of the area, obtained from the survey of India, were used for the ground reference. Survey of India (SOI) topographical map was rectified using geographic latitude-longitude and WGS 84 datum. By using georeferenced topographical map, satellite image were registered using map to image as well as image to image registration procedure. ERDAS imagine software version 9.2 was used for the purpose of georefrencing and registration. Details of satellite data and ancillary data used are given Table 1.

Table 1: *List of Data Used and Their Specifications*

Satellite Data	Path/Row	Date of Acquisition	Spatial Resolution
ETM+	140-044	02 Nov, 1992	30m
IRS P6 LISS-III	105-055	20 Feb, 2004	23.5m
IRS P6 LISS-III	105-055	17 Feb, 2009	23.5m
Topographical map	No. 73E/6	Surveyed 1962	1:50,000 Scale

3.2. Methods

Land use/land cover change information can be obtained by either image-to-image comparison or map-to-map comparison [7]. In the present study, map-to-map comparison was used for land use/ land cover change detection. Temporal satellite images were used for the preparation of landuse/landcover maps. Visual interpretation and image analysis techniques were used to monitor landuse landcover change. Various photographic and geotechnical elements such as tone, texture, shape, size, association, drainage, landform, soil and vegetation etc. are used to identify and delineate the different land use/land cover classes [17]. Image interpretation of satellite data followed by field validation during the year 2010 was done with reference to mapped landuse - landcover categories. By using the satellite data acquired for the year 1992, 2004 and 2009, we determined the spatio - temporal changes in the LU-LC of the region during these periods. In this study the LU/LC categorization was based on LU/LC classification scheme developed by National Remote Sensing Agency [10]. The modification in the categories at level-II was done keeping in view the coal mining activity and related landuse - landcover in the area. The level-II classification were categorized in 17 classes namely urban settlement, industrial settlement, rural settlement, crop land, fallow land, plantation, dense forest, open forest, degraded forest, forest blank, dense scrub, open scrub, barren land, river, reservoir, water body in mine and coal mining area. On screen digitization technique was adopted to digitize the maps using ArcMap software (version 9.3) and further area statistics of various land use categories was calculated.

Land use land cover statistics has used to compute percentage change, trend and rate of LU/LC change between 1992-2004, 2004-2009 and 1992-2009. Table 2 shows area and percent LU/LC change for three periods computed for each land use land cover type. Percent change was computed by comparing the initial (before) and final (after) LU/LC areal coverage according to the following formula:

$$\text{Percent LU/LC Change} = \frac{\text{Present LU/LC area} - \text{Previous LU/LC area}}{\text{Previous LU/LC area}} \times 100$$

Where area is extent of each LU/LC type. Positive values suggest an increase whereas negative values imply a decrease in extent. The detail of the methodology adopted in the study is presented in the methodology flow chart (Figure 2).

4. Results and Discussion

Area under various categories of land use/land cover was obtained satellite image based interpretation from ETM+ data of 1992 (Figure 2), IRS P6 LISS III data of 2004 (Figure 3) and 2009 (Figure 4). Table 2 shows the changes in land use/land cover statistics (in Sq. km and percentage) that have taken place during each study period between 1992, 2004 and 2009. The results of the land use/land cover change statistics are also graphically represented in pie diagram (Figure 6).

4.1. Spatial Distribution of Landuse / Landcover

Land use in an area is the collective outcome of historical responses projecting interrelationship of cultural, ecological and physical environment. Thus land use pattern of a region is an outcome of both natural and socio-economic factors and their utilization by man in time and space. The land use and land cover in the study area exhibit varied patterns due to rapid changes in the relief and geomorphologic landform including marked difference in the climatic condition. The built up area is mainly represented by Patratu, Bhurkunda, Saunda, Giddi and Simratanr. The Hill ranges covering the northeastern parts of the area are densely forested. Damodar River and its main tributary Nalkari River constitute the main streams draining the area. The various categories of landuse – landcover mapped in the area using satellite image of 1992, 2004 and 2009 (Figures 3, 4 and 5) indicated

marked changes in the agriculture and forest areas primarily at the expense of coal mining region. Built up area increased primarily as a coal mining related allied industrial settlement.
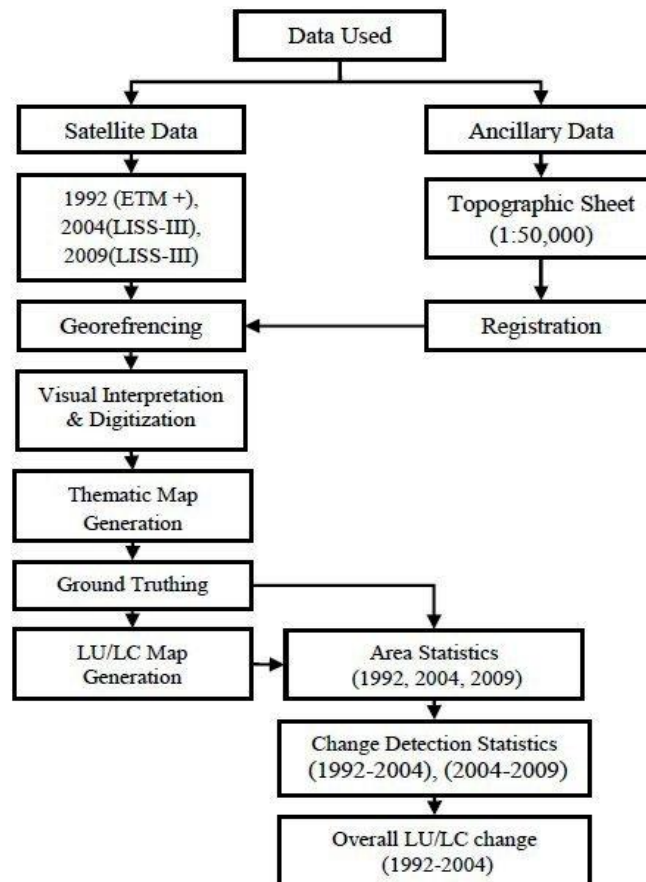
Figure 2: Methodology Flow Chart for the Preparation of Landuse/Landcover Map and Its Change Detection Statistics

The five level-I categories comparing; build up land, agricultural land, forests, wastelands, water bodies and others were further classified into level-II categories i.e. urban settlement, industrial settlement, rural settlement, cropland, fallow land, plantation, dense forest, open forest, degraded forest, forest blank, dense scrub, open scrub, barren land, river, reservoir, water body in coal mine and coal mining area. Temporal changes among various LU/LC categories are discussed below to develop insight about coal mining induced land degradation in the area.

A. *Built up Land* is the land covered by settlements related to the population. The urban sprawl and concomitant growth in population is generally related to decrease in cropland and grassland areas. Built up land is identified on false colour composite (FCC) by its cyan - light grey tone, coarse texture, scattered pattern and irregular outline. Built up land was categorized into three types viz; urban, industrial and rural settlements.

Urban Settlement is comprised of areas with much of the land covered by manmade structures. These are non-linear built up areas covered by impervious structures adjacent to or connected by streets. This cover is related to centers of population. This class usually occurs in combination with, vegetated areas that are connected to buildings that show a regular pattern, such as vegetated areas, gardens etc. and industrial and/or other areas [10]. Hence, all places with a municipality, corporation or cantonment or which are notified town areas and all other places which satisfy the criteria of a minimum population of 5000, at least 75% of whose male working population is non-agricultural and

having a density of population of at least 400 sq. km. are placed under this category. Urban settlement is identified on FCC image by its cyan - light grey tone, coarse texture, scattered pattern and irregular outline. Maps (Figure 3, 4 and 5) shows that urban settlement occupied 9.07 sq. km area (3.25 % of the total study area) in 1992, 11.2 sq. km area (4.03 %) in 2004 and 16.73 sq. km area (6.03 %) during 2009. The increase in settlement area is primarily due to the development of industrial sector which requires residential colonies, industrial buildings, schools, community halls etc.

Industrial Settlement is the area where the human activity is observed in the form of manufacturing along with other supporting establishments of maintenance. Heavy metallurgical industry, thermal, cement, petrochemical, engineering plants etc., are included under this category. Main industrial settlements are located in the central part of the study area in the vicinity of Damodar River and around coal mining areas. Patratu is the main urban and industrial town in the region. It is identified on the FCC image by its regular outer boundary shape, bluish tone and coarse texture. Patratu Thermal Power Station (P.T.P.S.) and Jindal Stell and Power Limited (J.S.P.L.) are the main industries along with a number of small industries like sponge factory, glass factory, cement factory, coal washeries etc. The industrial settlement occupied 3.94 sq. km area (1.39% of the total study area) in 1992, 5.05 sq. km area (1.80%) and 9.32 sq. km area (3.36%) in 2009. The increase in the industrial settlements is due to increase in small coal based industries.

Rural Settlements represent land used for human settlement of size comparatively less than the urban settlements of which more than 80% of the people are involved in the primary activity of agriculture. All the agricultural villages covering 5 hectares area and more are included in this category. Rural settlements are primarily located in the vicinity of forests and within the agricultural lands. The rural settlements covered an area of 6.92 sq. km (2.47 % of the total area) during 1992, 7.84 sq. km (2.81%) during 2004 and 10.13 sq. km (3.65%) during 2009. The rural settlement shows an increase of 3.21 sq. km (1.17%) during 1992 to 2009.

B. *Agricultural Land* may be defined broadly as land used primarily for production of food and fiber. It includes land under crops (irrigated and unirrigated, fallow, plantations etc.).In a broad sense, agricultural lands may be defined as those lands which are cultivated to produce food crops and related activities. Agricultural lands are located in the plain regions and near the peripheral zone of forests. Further agricultural land are categorized in following three classes:

**Cropland*s* *are* the areas with standing crop as on the date of satellite overpass. Cropped areas appear in bright red to red in colour with varying shape and size in a contiguous to non- contiguous pattern with regular - sub regular outline shape. The main crop in the study area is kharif which is monsoon season crop. Cropland covering 45.75 sq. km (16.55 %) area during 1992 was decreased to 32.94 sq. km (11.90 %) area in 2004 and further to 28.06 sq. km (10.11%) in 2009. The land /land cover map (figure 3, 4 and 5) indicated decline in the area under cropland. The total loss of 17.69 sq. km in the cropland was observed during 1992 to 2009 indicating an average loss of 1.04 sq. km area per year. The development of infrastructure, residential complexes of mining industries and power plants resulted in loss of agriculture land. Development of agriculture in other areas is mainly affected by lack of irrigation facilities.

Fallow lands are the lands which are used for cultivation but are temporarily rest, un-cropped for one or more season, but not less than one year and for not more than five years. On the FCC image it was identified by its light brown to light yellow tone, medium to smooth texture having non-contiguous pattern with irregular outline. The area under fallow land category covers 11.00 sq. km (3.95 %) area during 1992, 17.20 sq. km (6.20%) area during 2004 and 12.65 sq. km (4.56 %) area during 2009. The fallow land shows an increase of 6.20 sq. km (0.68 %) area from 1992 to 2004 and subsequently a decrease of 4.55 sq. km area in the period 2004 to 2009. The increase could be attributed to the

loss of crop land which changed to fallow land as a result of the rapid increase in mining activities whereas the decrease reflects the conversion of fallow land into plantation.

Plantation areas are under agricultural tree crops planted adopting agricultural management techniques. These also includes the areas of land use systems and practices wherein cultivation of herbs, shrubs, and vegetable crops are deliberately integrated with agricultural crops mostly in irrigated conditions for ecological and economic reasons. Plantations appear in dark-red to red tone of different sizes with regular and sharp edges indicating the presence of a fence around it. Land use/land cover during 1992 indicates that nearly 40.36% of the area is used for agriculture of which plantation occupies the maximum area (19.86%) followed by crop land (16.55%) and fallow land (3.95%). plantation occupies 54.88 sq. km area (19.86 %) in 1992, 52.40 sq. km area (18.95 %) in 2004 and 30.84 sq. km area (11.11 %) during 2009. It was observed that there was no major changes occurred between 1992 to 2004 period but during 2004 to 2009 substantial decrease of 21.56 sq. km area indicated an average loss of 4.31 sq. km per year in the plantation. This could be attributed illegal eloping of trees by people for fuel wood requirement indicating negative impact of population growth on natural resources.
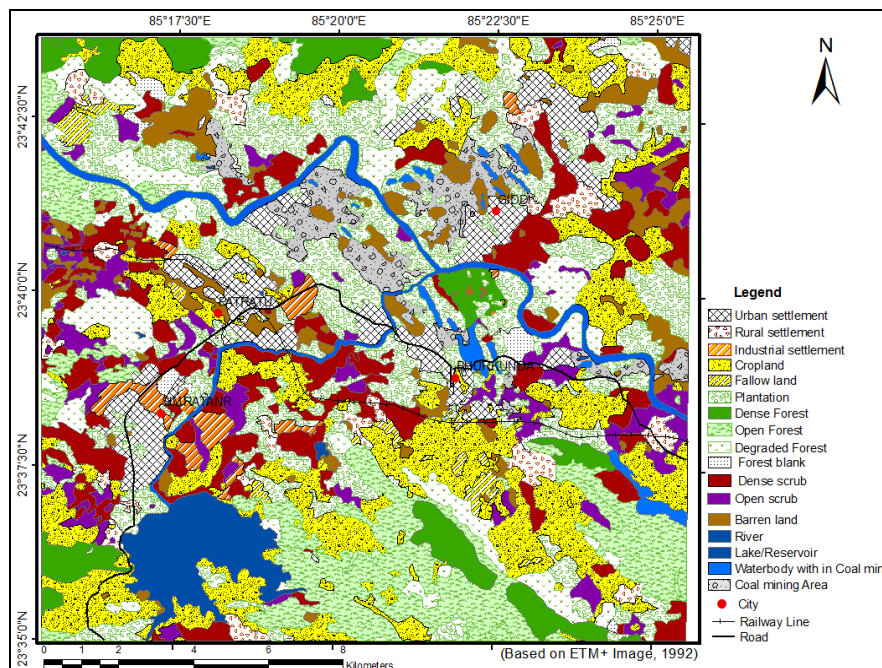
Figure 3: Landuse / Landcover Map Based on ETM+ Image of 02 November, 1992
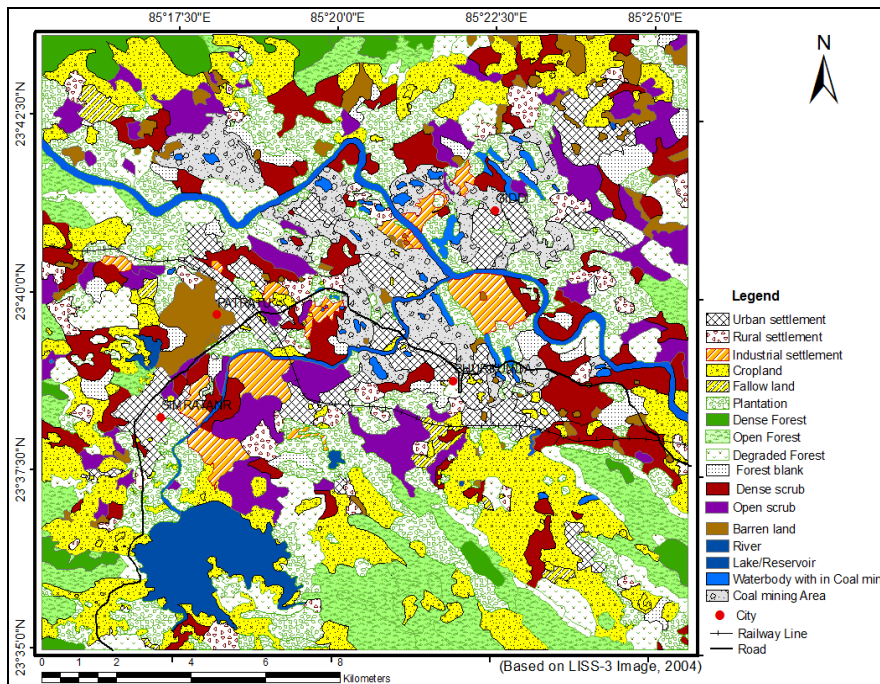
Figure 4: *Landuse / Landcover Map Based On LISS-III Image of 20, February 2004*
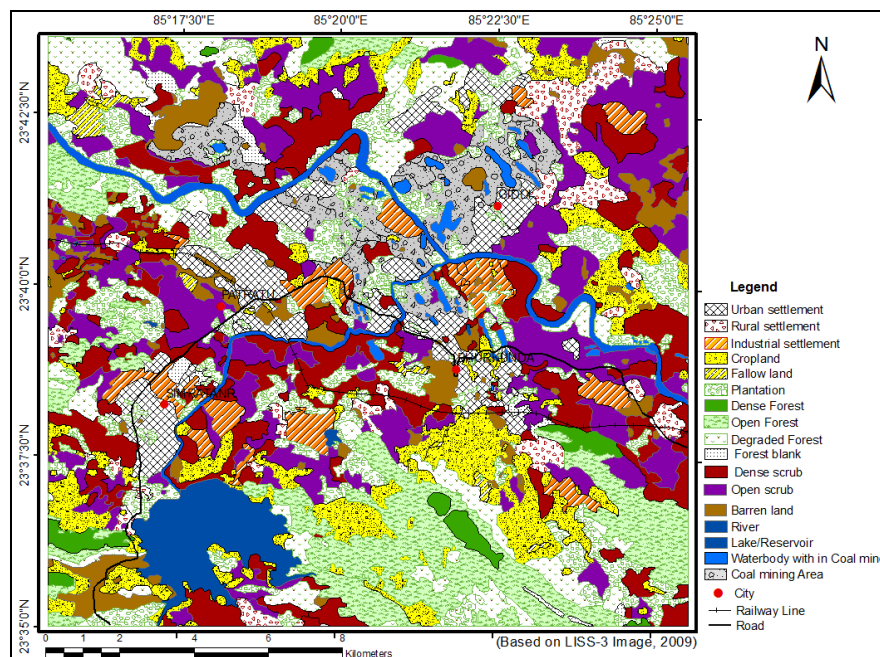
Figure 5: *Landuse / Landcover Map Based on LISS-III Image of 17, February 2009*

C. **Forest** refers to land with a tree canopy cover of more than 10 percent and area of more than 0.5 ha. Forests are determined both by the presence of trees and the absence of other predominant land uses within the notified forest boundaries. The trees should be able to reach a minimum height of five meter [10] within the notified forest boundaries. Forest was classified into three categories on the basis of crown density viz; dense, open and degraded. After observation of percent change analysis, it was found that maximum deforestation occurred in the vicinity of coal mining areas. Forest are divided in four categories, these are:

Dense Forest can be interpreted from the FCC image by its dark red tone, coarse - medium texture, contiguous pattern and regular to irregular shape. The dense forests exhibit crown density of more than 40%. Dense forest covered an area of 14.78 sq. km (5.32 % of the total area) during 1992, 6.60 sq. km (2.36%) of during 2004 and 4.16 sq. km (1.50 %) during 2009. Dense forest shows a decrease of 10.62 sq. km (3.28 %) in area during 1992 to 2009. Most of the coal mining activities are taking place in the vicinity of dense forests because most of the coal resources are located with the hilly terrain covered with forest. Therefore decrease in the area of dense forests is attributed to the removal of trees to initiate coal mining activities and development of mining infrastructure.

Open Forest exhibit crown density in between 40% to 10%. It is easily identified on FCC image by its light red - pinkish colour, smooth - medium texture, contiguous to non contiguous pattern with irregular outline. Open forest covered an area of 27.00 sq. km (9.75 %) in 1992, 26.50 sq. km (9.57%) in 2004 and further decreased to 22.32 sq. km (8.04 %) in 2009. Open forests exhibit overall decrease by 5.32 sq. km during 1992 to 2009. Due to the location of open forests in the peripheral area of dense forest, they are largely affected by human intervention for fuel wood requirement.

Degraded Forest is present mainly in the peripheral zones of the open and dense forests. The occurrence of degraded forests around human settlements indicates their development from degradation of dense and open forests primarily due to human interference in the form of infrastructure development. It occupies an area of 17.45 sq. km (6.29%) in 1992, 19.02 sq. km (6.86%) in 2004 and 18.73 sq. km (6.75%) in 2009 indicating overall increase by 1.28 sq. km during 1992-2009 due to conversion of open into degraded forest.

Forest Blank represents a forest area where the crown density is almost nil, indicating complete destruction of forests in the study area. Forest blanks are mainly located around the active mining areas. Due to mining and related activities about 2.35 sq. km forest cover was harmed forest blank during 1992 to 2004. Deforestation due to mining activity coupled with encroachment of forest areas for agriculture extension as well as clearing of tree for fuel wood requirements by local inhabitants is leading to degradation of forests in the region.

D. *Wasteland* is described as degraded land which can be brought under vegetative cover with reasonable effort and which is currently under utilized and land which is deteriorating for lack of appropriate water and soil management or on account of natural causes. It has limited capability to support life and exhibit less than one-third of their area under vegetation or other cover. Their high spatial occurrence in the vicinity of coal mining zone and related industries clearly depict land degradation due to coal mining activity. Moreover higher levels of wind and water born pollution triggered by mining activity probably leads to shift in the land use practice whereby productive agricultural land are getting degraded and converted to wastelands. Changes in the various categories of waste land are described below:

Dense Scrub possesses shallow and skeletal soils, at times chemically degraded, extremes of slopes, severely eroded and lands subjected to excessive aridity with scrubs dominating the landscape. They have a tendency for intermixing with cropped areas. On the FCC image it can be identified by its pink - light yellow tone, coarse to medium texture scattered pattern and irregular outline boundary. In the study area dense scrub occupied an area of 28.13 sq. km (10.16%) in 1992 and 33.41 sq. km (12.07%) in 2004 which increased to 41.72 sq. km (15.03%) by 2009.

Open Scrub has a similar characteristic as dense scrub except that they possess sparse vegetation or devoid of scrub and have a thin soil covers. It shows an increase of 13.53 sq. km from 26.67 sq. km (9.63%) in 1992 to 33.14 sq. km (11.94 %) in 2009. Open scrubs are mostly located in the plain areas in the south-western parts of the study area.

Barren land occupied an area of 1.95 sq. km (0.67%) in 1992 and 2.57 sq. km (0.90%) in 2004 and increased to 10.66 sq. km (i.e. 3.84%) by 2009. The increase in barren lands was primarily due to the loss of cultivated land as a result of the rapid increase in mining activities in the region.

E. Water Bodies comprises areas with surface water, either impounded in the form of ponds, lakes and reservoirs or flowing as streams, rivers, canals etc. These are seen clearly on the satellite image in blue to dark blue or cyan colour depending on the depth of water. Water bodies are categorized into river and reservoir as described below:

River represent natural course of water flowing on the land surface along a definite channel/slope regularly or intermittently towards a sea in most cases or a lake or an inland basin in desert areas or a marsh or another river. The river Damodar which traverses through the central parts of the study area and flows from WNW to ESE direction is the only perennial river draining the area. Its main tributary is Nalkari River which has been tapped in Patratu reservoir and then joins the Damodar River near Bhurkunda. The land use/land cover maps showed no major changes in river area.

Reservoir is an artificial lake created by construction of a dam across the river specifically for hydro power generation, irrigation, and water supply for domestic/ industrial needs and flood control. The Patratu reservoir located in the south-western part of the area comprised the major water body providing water for domestic and industrial requirement of the region whereas a large number of small water bodies and ash pond are encountered in the coal mining area in the vicinity of Patratu thermal power station. The reservoir showed no major changes during the study period except that its water spread area reduced temporarily meager rain in 2004.

Table 2: Landuse/Landcover (LU/LC) Statistics and its Dynamics during the Study Period

Level-I	Level-II	Year 1992		Year 2004		Year 2009		% Changes in Area in km²		
		Area in (km²)	Area in (%)	Area in (km²)	Area in (%)	Area in (km²)	Area in (%)	1992-2004	2004-2009	1992-2009
Build up land	Urban settlement	9.07	3.25	11.2	4.03	16.73	6.03	23.59	49.24	84.45
	Industrial settlement	3.94	1.39	5.05	1.80	9.32	3.36	28.17	84.55	136.55
	Rural settlement	6.92	2.47	7.84	2.81	10.13	3.65	13.29	29.21	46.39
Agricultural Land	Cropland	45.75	16.55	32.94	11.90	28.06	10.11	-28.00	-14.81	-38.67
	Fallow land	11.00	3.95	17.20	6.2	12.65	4.56	56.36	-26.45	15.00
	Plantation	54.88	19.86	52.40	18.95	30.84	11.11	-4.52	-41.15	-43.80
Forest	Dense forest	14.78	5.32	6.60	2.36	4.16	1.50	-55.35	-36.97	-71.85
	Open forest	27.00	9.75	26.50	9.57	22.32	8.04	-1.85	-15.77	-17.33
	Degraded forest	17.45	6.29	19.02	6.86	18.73	6.75	9.00	-1.52	7.34
	Forest blank	2.34	0.81	1.47	0.5	2.35	0.85	-37.18	59.86	0.43
Waste land	Dense scrub	28.13	10.16	33.41	12.07	41.72	15.03	18.77	24.87	48.31
	Open scrub	26.67	9.63	23	8.30	33.14	11.94	-13.76	44.09	24.26
	Barren	1.95	0.67	2.57	0.90	10.66	3.84	31.79	314.79	446.67

	land									
Water bodies	River	5.73	2.04	5.58	1.99	5.55	2.00	-2.62	-0.54	-3.14
	Reservoirs	8.99	3.22	8.37	3.00	8.93	3.22	-6.90	6.69	-0.67
Others	Water body within mine	2.67	0.93	2.79	0.98	2.60	0.94	4.49	-6.81	-2.62
	Coalmining Area	10.06	3.61	21.29	7.68	19.40	6.99	111.63	-8.88	92.84
	Total	**277.40**	**100**	**277.32**	**99.97**	**277.38**	**100**			

F.   Others category comprises water bodies in abandoned coal mines and active coal mining area. Active mining area exhibit large scale surface excavation for extraction of coal whereas abandoned mining area represents old mines where mining operation ended. This categories represents following two classes:

Water body in coal mine are elongated water bodies measuring up to 1 km in length were located within the mining area. These water bodies are formed due to accumulation of rain water or ground water in the depression areas formed due to mining. Large numbers of such water bodies are located near the confluence of Damodar and Nalkari rivers.

Coal mining areas *are* largely located in the vicinity of Damodar River. Mining pits are interpreted on FCC by its black tone, medium to smooth texture having linear to curvilinear pattern and irregular shape whereas overburden dumps have white to light blue tone coarse to medium texture having contiguous pattern and irregular outer shape. The coal mining area exhibit increase over the years from 10.06 sq. km (3.61% in the total study area) in 1992 to 21.09 sq. km (7.68%) in 2004, at an average rate of 0.91 sq. km per year. It is interesting to note that coal mining area witnessed reduction during the period of 2004(21.09 sq. km) to 2009 (19.40 sq. km) as areas of abundant mines were largely converted into water bodies with in coal mine areas. The reduction in coal mining area indicate diminishing coal reserves in the area and decline in the coal production as large numbers of mines are now abundant and filled with water. A large part of the area classified under mining area have mining dump which form large heaps of dumping materials attaining height of about 30-50 meter above ground level. Ghosh [5] emphasized that the consequences of mining activities leads to the change in the natural topography of the region.

The land use/land cover distribution during the year1992, 2004 and 2009 was assessed. Area under forests and coal mining were calculated. Forest area which was 61.57 sq. km in 1992 (22.17%) reduced to 53.59 sq. km in 2004 (19.29%) and further reduced to 47.56 sq. km (17.14%) by the year 2009. Thus apparent decrease in forest cover is 2.88% during the 1992-2004 and 2.15% during 2004-2009 (Table 2). Prakash and Gupta [11] studied the land use/land cover changes of Jharia coal field of India and reported gradual change in land cover that pose a serious threat to the vegetation present in the area due to prominent mining. Koster and Slob [6] and Schejbal [14] have reported loss of plant vegetation and growth due to haphazardly spread out of waste materials in coal mining areas due to unhealthy environmental conditions. It was observed that major loss of forest areas occurred in the vicinity of coal mining region. Complete destruction of forests was observed in certain coal mines also because of agriculture extension into forest area and due to clearing of tree for fuel wood requirement of local inhabitants coupled with reduced regeneration of vegetation due to environmental pollution. Similarly the coal mining area which was 10.06 sq. km in 1992 (3.6%) increased to 21.29 sq. km in 2004 (7.68%) but reduced to 19.40 sq. km (6.99%) by the year 2009 (Table 2). The spread of coal mining activity leads to total destruction of forest cover within the mine area and also leads conversion of surrounding agricultural lands into wastelands dominated by open and dense scrub. Rathore and Wright [13] and Prakash and Gupta [11] remarked that mining and land use/land cover changes were correlated to each other.
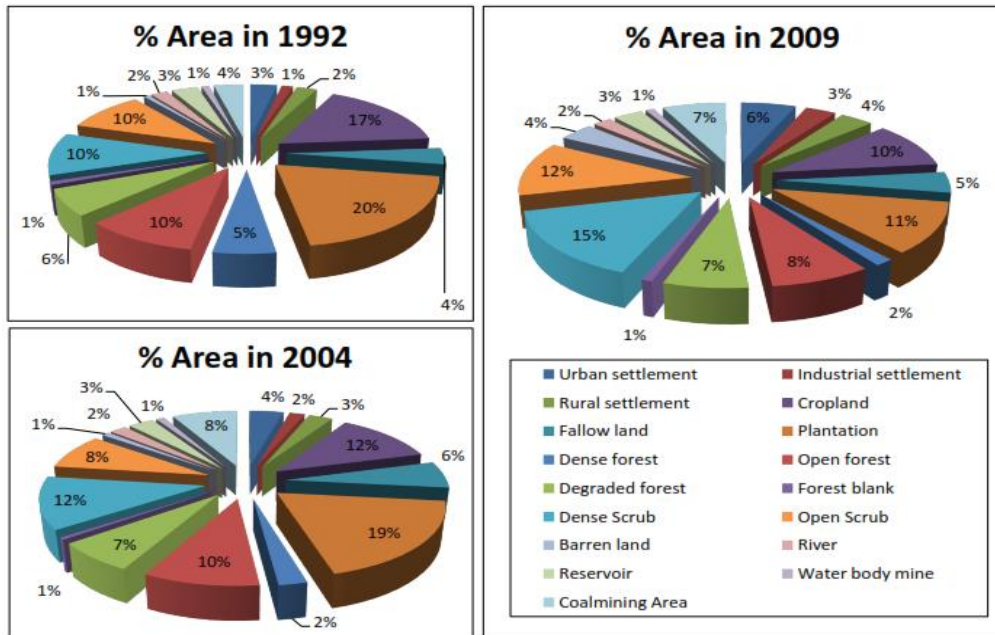
Figure 6: Pie -Chart Showing the % Area over the Three Periods (1992, 2004 & 2009)

From Table 2, it is apparent that built-up land shows positive change in all the periods. Urban settlement indicated an increase by 23.59% and 49.24 % during 1992 to 2004 and 2004 to 2009. The overall percentage change during 1992-2009 was 84.45%. The Industrial settlement showed gradual percentage change during 1992 - 2004. It indicated 84.55% increase in this period due to increase in the number of allied industries in this area. The overall area change was 136.55% during the period from 1992 to 2009. This is a clear indication of increase in population and infrastructure development in the area during this period. The land use/land cover change analysis of indicates that there was conversion and associated decrease in dense forest to open forest and open forest to mining areas in temporal domain. During the initial stage, mining was carried out mostly in dense forest areas of the region and these forests got fragmented and now exist as open forest. The conversion of dense forest into open forest or degraded forest also indicated decreasing trend. It was found that 55.35% dense forest area was converted to open forest and 1.85% open forest to degraded forest during 1992 to 2004. Whereas during 2004 to 2009 the conversion of dense forest area was 36.97% and over all conversion was 71.85%. Destruction of forests during mining operation was invariably accompanied by an extensive damage to the ecosystem. The overburden from coal mines when dumped in unmined areas creates mine spoils which ultimately affects the surrounding vegetation.

Wasteland recorded both positive and negative change over the years. Scrublands occur in small scattered patches in the entire area. In 1992 to 2004 the total percentage change area of dense scrub was 18.77% whereas open scrub indicated negative percentage area change (-13.76%). Further both categories indicated positive percent area change during the period 2004 to 2009. Dense scrub indicated 24.87% and open scrub indicated 44.09 % area change in this period. Overall during 1992 to 2009 the dense scrub indicated 48.31% and open scrub indicated 24.26% area increase (Table 2). Barren land exhibited 31.79% increase during 1992 to 2004. Further indicated rapid increase to 314.79% during 2004 to 2009 with an overall change of 446.67% area. Huge watershed formation in the area therefore can be attributed to human activities, which primarily include, mining activities along with over grazing, fire wood extraction etc. Mining activities increased over the year and huge amount of mining waste like overburden were dumps on surrounding land which destroyed the quality of soil and decreased their productive capacity turning them to barren land. The percentage changes of all categories are graphically represented in bar diagram (Figure 7).
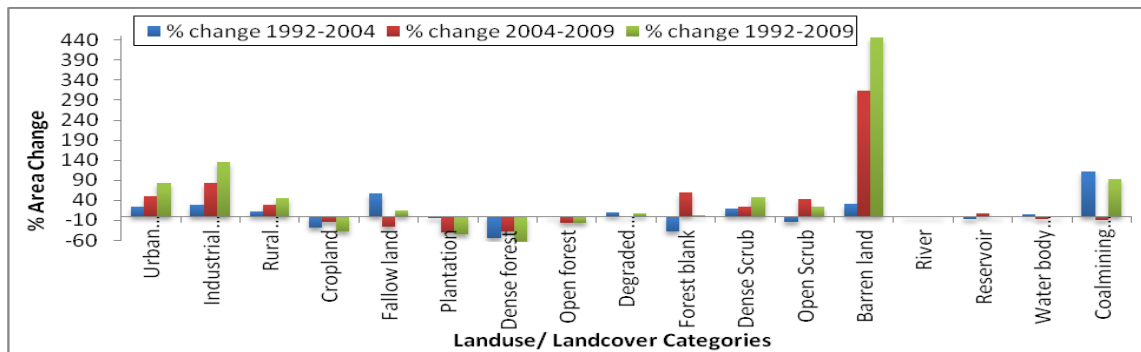
Figure 7: Percentage Change in Area under Various Land Use/Land Cover Categories

Area under water bodies recorded a negative change although very minimal in nature. Whereas feature class under rivers indicated no significant change during the entire period. During 1992 to 2004 period it indicated 2.62%, change whereas in subsequent periods (2004 to 2009 and 1992 to 2009) percentage area change was 0.54% and 3.14% respectively. This indicates that coal mining and allied activities doesn't have much influence on perennial river system. Cropland exhibit reduction over the period due to increase settlement and mining activity. Cropland area decreased by 28% during 1992 to 2004 and further reduced by 14.81% in subsequent period (2004 to 2009). Fallow land indicated both increasing and decreasing trend in subsequent period as It shows 56.36% area increase during 1992 to 2004 contrary to reduction by -26.45% during 2004 to 2009. Plantation indicated substantial decrease in the later periods (2004 to 2009; -41.15%). On compared to earlier periods (1992 to 2004; -4.52 %) such draping reduction in plantation in the recent periods indicate reclass mining activity within green belts. The feature class under others includes water body with in coal mines and coal mining area. The class Water bodies within the abundant and active coal mines indicated no significant change since 1992 although the areas under coal mining have increased considerably during 1992-2009. The recent area change in coal mining region during 1992 to 2004 was 111.63% indicating expansion by double in size in 1992. Minor expansion (8.88%) during 2004 to 2009 reflects over expansion if mining activity in the past beyond the full exploitation capacity.

5. Conclusion

The remote sensing techniques proved its potential in generating accurate spatio- temporal area statistics of LU/LC and its dynamics in the coal mining areas. With the onset of mining operation, considerable area under dense forest was degraded to open forest as well connected to area such as settlement, roads and scrublands. Due to mono cropping agricultural practice in the region the local people also inclined towards the mining activities thereby most of the agricultural lands were converted into mining areas. It was analysed that major loss in forest areas occur in the vicinity of active coal mining regions and there was not much impact on the scrublands and non-forest areas of the region due to mining. Total destruction of forest cover was noted in certain coal mines. At places the forest cover was reduced due to agriculture extension into forest area and due to clearing of tree for fuel wood requirement of local inhabitants coupled with reduced regeneration of vegetation due to environmental pollution. The coal mining area which was 10.06 sq. km in 1992 (3.6%) increases to 21.29 sq. km in 2004 (7.68%) and further diminished to 19.40 sq. km (6.9%) by the year 2009. The spread of coal mining activity in the region leads to total destruction of forest cover within the mine area and also leads conversion of surrounding agricultural lands into wastelands dominated by open and dense scrub. There is an urgent need to increase the forest cover of the area to sustain ecological balance in the region. Similarly degradation of land envisages the need for adoption of proper land management practices. Meticulous long term land use planning is of paramount importance for the sustained and proper use of the available land and water resources in the mining and adjoining regions.

The present study on landuse - landcover mapping and its dynamics would certainly provide meaningful insights on changing dynamics of land emphasizing impact of coal mining activity on land degradation in the area.

Acknowledgments

References

[1] Bell F.G., et al. *Environmental Impacts Associated With an Abandoned Mine in the Witbank Coalfield, South Africa.* International Journal of Coal Geology. 2001. 45; 195-216.

[2] CIL, 1993: *Coal Atlas of India*, Central Mine Planning and Design Institute, Coal India Limited, Calcutta, India.

[3] Down C.G., et al. *The Environmental Impact of Mining.* London. Applied Science. 1977.

[4] DeFries R., et al. *Global and Regional Land Cover Characterization from Satellite Data; an Introduction to the Special Issue.* International Journal of Remote Sensing. 2000. 21 (6&7) 1083-1092.

[5] Ghosh R. *Mining in Jharia Coal Field, Eastern India: An Estimation of Its Impact Index.* Journal Geological Society of India. 1989. 33; 353-360.

[6] Green K., et al. *Using Remote Sensing to Detect and Monitor Land-Cover and Land-Use Change.* Photogrammetric Engineering and Remote Sensing. 1994. 60; 331–337.

[7] Koster R.D., et al. *An Application of a Geographic Information System for the Purpose of Mining and Rehabilitation Planning In the Karvina District, Czech Republic.* Memoir of the Centre of Engineering Geology in the Netherlands, No. 116, Delft University of Technology. 1994. 7-79.

[8] Miller A.B., et al. *An Analysis of Land Cover Changes in the Northern Forest of New England Using Multitemporal LANDSAT MSS Data.* International Journal of Remote Sensing. 1998 2 (19) 215-265.

[9] NRSA, 2012: *National Land Use Land Cover Mapping using Multi-temporal Satellite Data.* Technical manual (2nd Cycle), Document Control No. RSC-RSAA-LRUMG-LUCMD-Mar-12-TR-392.

[10] Prakash A., et al. *Land-Use Mapping and Change Detection in a Coal Mining Area - A Case Study in the Jharia Coal Field, India.* International Journal of Remote Sensing. 1998. 3 (19) 391-410.

[11] Pandey A.C., et al., 2002: *Land-Use Land-Cover Mapping Through Digital Image Processing of Satellite Data – A Case Study from Panchkula, Ambala and Yamunanger Districts, Haryana State, India.* MAP ASIA 2002 Proc., Bangkok.

[12] Rathore C.S., et al. *Monitoring Environmental Impacts of Surface Coal Mining*, International Journal of Remote Sensing. 1993. 14; 1021-1042.

[13] Schejbal C., 1995: *Problems of Mines Closure and Reviving of Landscape in the Mining Area*, Proceedings of the International Conference, Beijing, China, 681-691.

[14] Simmons, J.A., et al. *Forest to Reclaimed Mine Land Use Change Leads to Altered Ecosystem Structure and Function.* Ecological Applications. 2008. 18; 104−118.

[15] Turner II B.L, et al., 1990: *The Earth as Transformed by Human Action: Global and Regional Changes in the Biosphere over the Past 300 Years. Cambridge*: Cambridge University Press, 732.

[16] T.M. Lillesand et al., 2004: *Remote Sensing and Image Interpretation.* 5th Edition, John Wiley, New York.

Research Article **Open Access**

Landslide Hazard Zonation of Lunglei Town, Mizoram, India Using High Resolution Satellite Data

R.K. Lallianthanga and Z.D. Laltanpuia

Mizoram Remote Sensing Application Centre, Science & Technology, Planning Department, Aizawl, Mizoram, India

Correspondence should be addressed to R.K. Lallianthanga, rklthanga@yahoo.com

Abstract Immature geology coupled with heavy rainfall is the main causes of slope instability resulting in landslides in the hilly regions of north-east India including Mizoram. The occurrence of landslide is more frequent within the township where anthropogenic activities are taking place. The present study has been taken up to study the landslide prone areas of Lunglei town using high resolution satellite data. Various thematic layers, namely, lithology, geological structures, slope morphometry, geomorphology and land use/land cover were prepared using Satellite Remote Sensing and Geographic Information System (GIS) techniques. The various parameters were classified, ranked and weighted according to their assumed or expected importance in inducing slope instability based on apriori knowledge of the experts. A heuristic method has been applied for the assignment of ranks and weights. Finally, landslide hazard zonation map is prepared showing five hazard classes ranging from very low hazard to very high hazard. The landslide hazard zonation map prepared in the present study will be useful for carrying out mitigation programmes as well as for planning and implementation of future developmental schemes within the town.

Keywords *GIS, Landslide Hazard Zonation, Lunglei, Remote Sensing*

1. Introduction

Landslide is the most frequently occurring geo-environmental hazard in the hilly Himalayan regions. It can cause damage in the road sector and residential areas [1]. It becomes a disaster causing destruction of lives and properties when it occurs within the township or other human habitations [2]. Geologically, Mizoram is a part of Tripura-Mizoram miogeosyncline, which in turn belongs to the broad Assam-Arakan geosynclinal basin. The area is represented by a repetitive succession of argillaceous and arenaceous sediments of Palaeogene-Neogene age. The general trend of the rock formations is N-S with dips varying from 20° to 50° either towards east or west [3]. The sediments of Mizoram are divided into Barail, Surma and Tipam Groups [4].

Lunglei town has been experiencing a fast growth in urbanization. Various developmental activities are being taken up without sufficient consideration of the existing slopes instabilities. This coupled with heavy rainfall, soft nature of the sediments, topography and complex structural disposition leads to manifold increase in the incidence of landslides in the region [5]. Though these movements cannot be stopped from occurring, their effect can be minimized through suitable mitigation measures for reducing their frequency and severity [6].

Reports on landslide studies within Lunglei town in particular, and Mizoram in general, are very meager. Geo-environmental appraisal of Lunglei town and its surroundings was undertaken by the Geological Survey of India [7]. The geology, geomorphology, soil, hydrology and slope morphometry within the town were studied in detail. LHZ mapping and slope stability studies for the town at 1:25,000 scale had been carried out by the Geological Survey of India [8], and concluded that systematic urban planning may be done considering the slope instability factor of the hill slopes identified through successive meso and micro-level landslide hazard zonation studies. Subsequently, meso scale LHZ and slope stability studies around Lunglei town at 1:10,000 scale had been undertaken by the Geological Survey of India [9] following BIS guidelines and incorporating more detailed input factors. Tiwari *et al.* [10] have done exhaustive work on LHZ mapping along Hrangchalkawn-Rotlang road section and, Hnahthial - Hrangchalkawn road section at 1:50,000 scales, where in some parts of Lunglei town area was covered in these two studies.

In recent years, with the advent of Remote Sensing and GIS techniques, landslide hazard zonation studies have become more advanced and operative [11]. The techniques have opened new perspectives for carrying out evaluation, management and monitoring of natural hazards with better results and more economical measures than is possible with conventional methods. Landslide Hazard Zonation (LHZ) using Remote Sensing and GIS techniques have been conducted in Bhagirathi Valley [12], Uttaranchal and Himachal Pradesh [13], Darjeeling Himalaya [14], Sikkim Himalaya [15], Aizawl town [16], Dikrong river basin [17], Kohima town [11], Kullu District [2], South Sinai, Egypt [18], Giri Valley [19], Nilgiri district [20], Serchhip town [21] and Mamit town [22]. It has been proven from the previous studies that high resolution satellite data are useful for micro-level landslide hazard zonation in hilly areas. Keeping all these in mind, landslide hazard zonation mapping of Lunglei town at 1:5,000 scale was taken up for undertaking mitigation measures, and to identify suitable areas for future developmental activities within the town.

2. Materials and Methods

2.1. Study Area

Lunglei town is the second largest settlement of Mizoram with an area of 55.08 sq. km. It is the administrative headquarters of Lunglei district, and is located between 92° 42′ 45" E to 92° 50′ 05" E longitudes and 22° 48′ 18" N to 22° 56′ 55" N latitudes. It falls under Survey of India toposheet No. 84B/09 and 84B/13. It is linked by National Highway 54 with Aizawl, the state capital of Mizoram at a distance of 235 km. The entire district is under the direct influence of south west monsoon, with average annual rainfall of 2527.70 mm (23). Location map of the study area is shown in Figure 1.

2.2. Data Used

Quick bird satellite imagery having spatial resolution of 0.8 m were used as the main data. Indian Remote Sensing Satellite (IRS-P5) stereo-paired Cartosat-I data having spatial resolution of 2.5 m was also used to generate Digital Elevation Model (DEM) of the study area, from which contour map is subsequently generated. In addition, Survey of India

(SOI) topographical maps and various ancillary data were also referred. Ground truth survey was conducted to verify maps and incorporate relevant ground information.
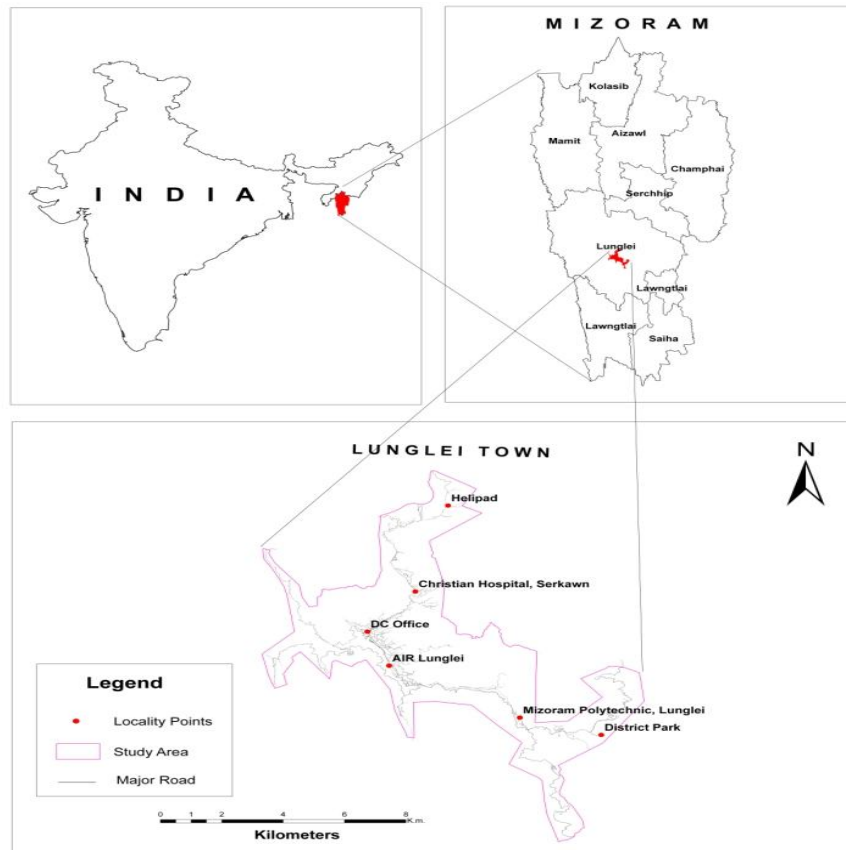
Figure 1: Location Map of the Study Area

2.3. Thematic Layers

The following thematic layers have been prepared using standard Remote Sensing and GIS techniques, and were utilized as parameters for giving weightage for different landslide hazard classes.

2.3.1. Land Use/ Land Cover

Land use/land cover is an indirect indication of stability of hill slopes because it controls the rate of weathering and erosion of the underlying rock formations. The study area is divided into six land use/land cover classes, viz., heavy vegetation, light vegetation, built-up, scrubland, barren/No vegetation and water body. The areas covered by heavy vegetation are found to be least susceptible to landslide. Hence, heavy vegetation class is assigned low weightage value. Barren Land and Built-Up areas are more prone to landslide than those of other classes and are given high weightage values. The statistics of land use/land cover is shown in Table 1, and the map is shown in Figure 2.

Table 1: *Land Use/ Land Cover Statistics*

Land Use Class	Area (in Sq. Km.)	Percentage
Heavy Vegetation	10.19	18.51
Light Vegetation	7.57	13.74
Built up	4.35	7.90
Scrubland	28.42	51.59
Barren/No Vegetation	4.52	8.21
Water Body	0.02	0.04
Grand Total	**55.08**	**100.00**

2.3.2. Slope

Slope is one of the important factors of landslide incidences. Landslides are more prevalent in the steep slope areas than in moderate and low slope areas [15]. The western aspects of the middle and the northern parts of the study area are characterized by very steep slope. Besides, steep hillside slopes are also noticed in few places. The eastern parts of the study area, on the other hand, are characterized by low and gentle slope. The slopes of the area are represented in terms of degrees, and are divided into five slope facets, viz., 0-10, 10-20, 20-40, 40-60 and above 60 degrees. Weightage values are assigned in accordance with the steepness of the slope, where steeper slope has higher weightage value than gentler slope. The slope statistics is given in Table 2, and slope map is shown in Figure 3.

Table 2: *Slope Statistics*

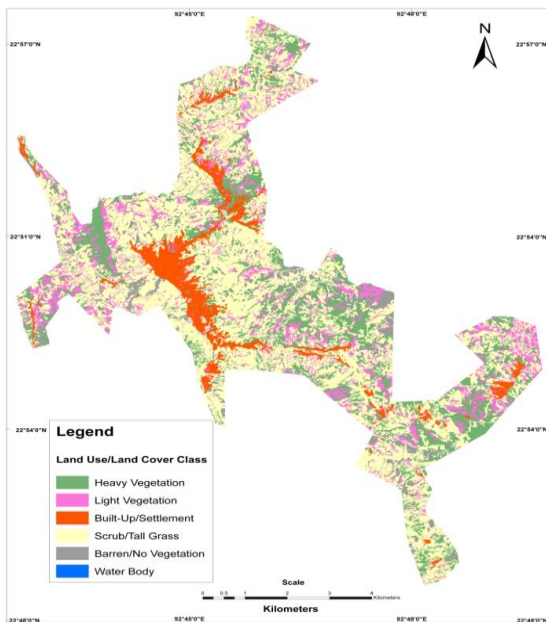| Degree of Slope	Area (in Sq. Km.)	Percentage
0-10	2.64	4.80
10-20	2.40	4.35
20-40	18.51	33.60
40-60	30.52	55.41
>60	1.01	1.84
Grand Total	**55.08**	**100.00**

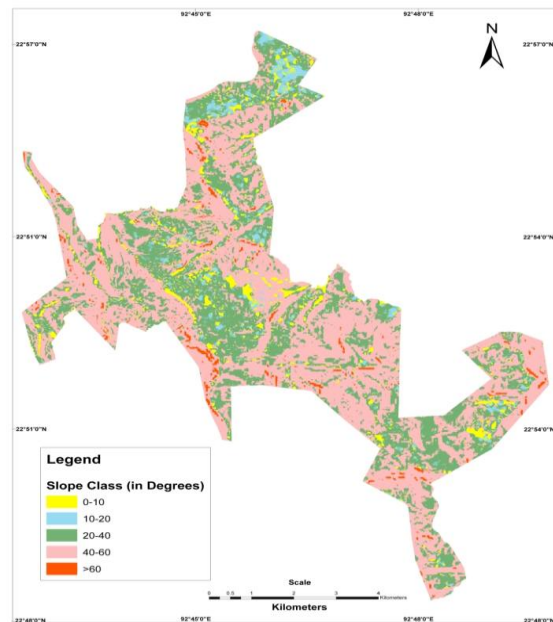**Figure 2:** *Land Use/Land Cover Map of the Study Area*

Figure 3: *Slope Map of the Study Area*

2.3.3. Geomorphology

The study area comprises of highly dissected, undulating and moderately sloping structural hill ranges, with height ranging from 800m to 1500m above mean sea level. Some of the hillocks are highly dissected with sharp ridges and steep slopes, whereas some areas are characterized by gentle and low dissected hillocks. This indicates that the topography is immature. A limited number of flat lands are mostly confined along the streams and between the spurs. Geomorphologically, the whole area is divisible into high structural hill, medium structural hill, low structural hill and valley fill. High elevated areas are more susceptible to landslide than low elevated areas. The statistics of geomorphology is given in Table 3 and geomorphological map of the study area is shown in Figure 4.

Table 3: Geomorphology Statistics

Geomorphic Unit	Area (in Sq. Km.)	Percentage
High Structural Hill	3.67	6.67
Medium Structural Hill	39.63	71.94
Low Structural Hill	11.67	21.18
Valley Fill	0.12	0.21
Grand Total	**55.08**	**100.00**

2.3.4. Lithology

The study area is composed of rocks of middle bhuban and upper bhuban formation of surma group [9]. It exposes limited rock types, viz. sandstones, shales and siltstones, and their intermixtures in varying proportions [3]. The middle bhuban formation is conformably underlain by the upper bhuban formation with gradational and transitional contact. The middle bhuban formation is mainly argillaceous with shale as the dominant rock type. It consists of assemblage of shale, siltstone, sandy shale and clayey bands with subordinate amount of sandstones. The upper bhuban formation is mainly arenaceous with sandstone as the dominant rock type. It comprises of sandstone with subordinate amount of shale, siltstone with occasional clay bands. Six litho-units have been established for the study area purely based on the exposed rock types of the area. These are named as sandstone, shale-sandstone, siltstone-shale, shale-siltstone, crumpled shale and gravel-silt unit. It may be noted that the demarcation and correlation of the two formations is extremely difficult owing to more or less uniform lithological characters and absence of marker horizons and index fossils [24]. For the occurrence of landslide, crumpled shale unit is the most susceptible rock type, followed by shale-siltstone unit. In accordance with this, weightage values are assigned for each of the rock types. The statistics of lithology is given in Table 4.

Table 4: Lithological Statistics

Rock Types	Area (in Sq. Km.)	Percentage
Sandstone	5.70	10.35
Shale-Sandstone	9.84	17.86
Siltstone-Shale	17.05	30.95
Shale-Siltstone	21.58	39.18
Crumpled Shale	0.79	1.43
Gravel-Silt	0.13	0.23
Grand Total	**55.08**	**100.00**

2.3.5. Geological Structure

Structurally, the study area is represented by a NW-SE trending of the eastern limb of Lunglei anticline. The beds generally trend N-S to roughly NNW-SSE and dip on either side from 20° to 65°

with local variations. Besides bedding planes, two to three sets of joints have been noted [10]. The lineaments are well distributed within the study area, and are oriented in various directions. Few faults of small magnitude have been identified which are mostly transverse/oblique in disposition. The geological map is shown in Figure 5.

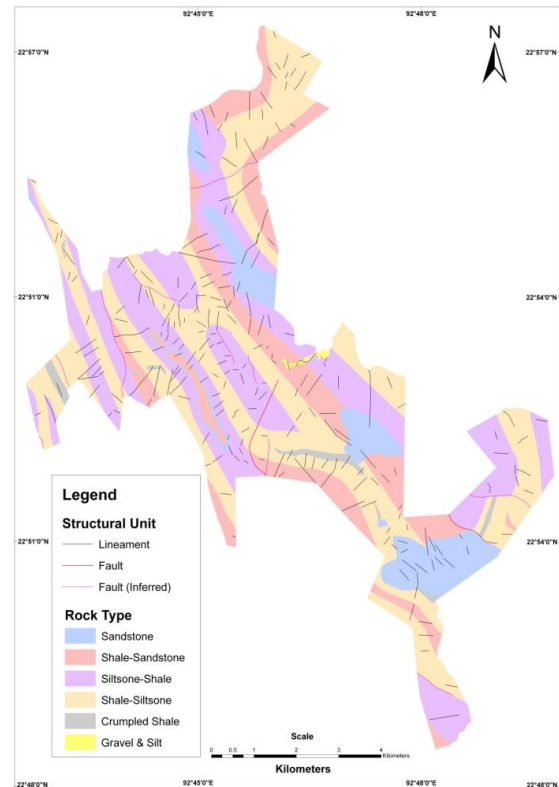**Figure 4:** *Geomorphology Map of the Study Area*   **Figure 5:** *Geological Map of the Study Area*

2.4. Data Analysis

Landslide Hazard Zonation was carried out by ranking of various causative factors operative in a given area based on their influence in initiation of landslides. The heuristic method is , therefore, used in the present study.

The first step involves selection of causative factors of slope instability in the area of interest. Consequently, five causative factors viz., lithology, structure, slope morphometry, geomorphology and land use/land cover were considered in the present study. Each causative factor was converted to a thematic map. Each parameter is carefully analysed so as to establish its relation to landslide susceptibility. The relative importance of each parameter for landslide is evaluated according to subjective opinion based on the *apriori* knowledge of the experts. Accordingly, rank values were assigned to each parameter, starting from 1 to 100, with 1 and 100 being the least and the most important in inducing landslides respectively. Among the various causative factors considered, slope is found to be the most influencing factor for slope instability within the study area. Hence, the highest rank value was assigned to it. Similarly, different rank values were assigned to the remaining parameters based on the relative importance towards landslide occurrence. The sum of the ranks of all parameters equals 100.

Each parameter was classified into a number of classes based on the relative influence of slope instability. Each class was assigned an ordinal rating (weight) from 0 to 10. The weight values of each class within a parameter were attributed on the basis of its importance in causing mass movements. For example, in the lithology layer, the crumpled shale unit offers more chance of slope failure than

the hard and compact sandstone unit. Similarly, areas located within the vicinity of fault zones and other geological structures are more vulnerable to landslides and other mass movements. For this, areas 50 m on both sides of all the lineaments including faults are buffered. Likewise, due considerations are given for the relation between landslides and other classes of a parameter, and different weight values were assigned accordingly. Summation of these attribute value were then multiplied by the corresponding rank value to yield the different zones of landslide hazard. The distribution of ranks and weights for different parameters and their classes are given in Table 5, and the flowchart for methodology is shown in Figure 6.
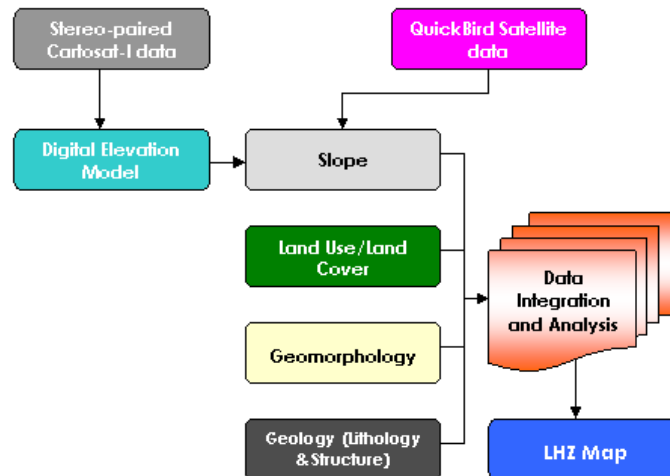
Figure 6: *Flowchart for Methodology*

Table 5: *Parameters and Their Ranking in Terms of Their Influence to Landslides*

Parameter	Rank	Category	Weight
Land Use / Land Cover	15	Heavy Vegetation	3
		Light Vegetation	5
		Built-up	8
		Scrubland	6
		Barren/No Vegetation	7
		Water Body	0
Slope Morphometry (in degrees)	35	0-10	2
		10-20	4
		20-40	6
		40-60	8
		> 60	5
Geomorphology	10	High Structural Hill	4
		Moderate Structural Hill	3
		Low Structural Hill	2
		Valley Fill	0
Lithology	25	Sandstone Unit	4
		Shale-Sandstone Unit	6
		Siltstone-Shale Unit	8
		Shale-Siltstone Unit	9
		Crumpled Shale Unit	10
		Gravel-Silt Unit	7
Geological Structure	15	Length of Buffer distance on either side	8

3. Results and Discussion

Combining all the controlling parameter, and by giving different weightage value for all the themes, the final LHZ map is prepared on the scale of 1:5,000. The area statistics of the landslide hazard zones are given in Table 6 and the landslide hazard zonation map of the study area is shown in Figure 7.

Table 6: LHZ Statistics

Hazard Zone	Area (in Sq. Km.)	Percentage
Very High Hazard Zone	1.01	1.85
High Hazard Zone	7.67	13.92
Moderate Hazard Zone	19.76	35.87
Low Hazard Zone	17.05	30.95
Very Low Hazard Zone	9.57	17.37
Water Body	0.02	0.04
Grand Total	**55.08**	**100.00**

The area is categorised into 'Very High', 'High', 'Moderate', 'Low' and 'Very Low' hazard zones, and are described below:

Figure 7: LHZ Map of the Study Area
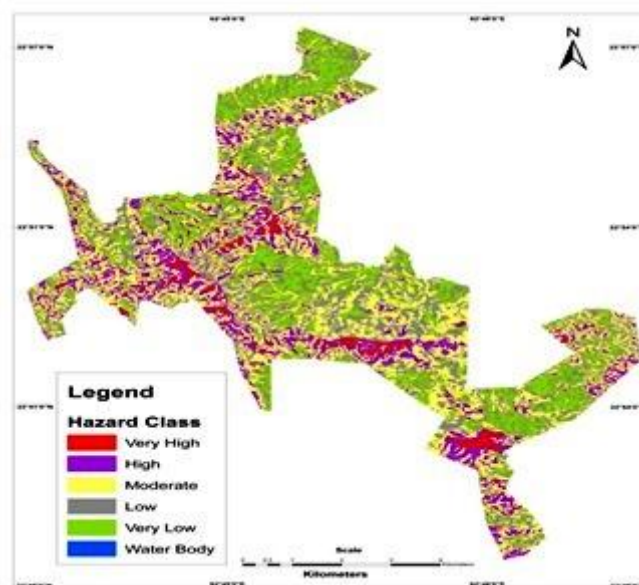
3.1. Very High Hazard Zone

This zone is highly unstable, and is at a constant threat of landslides, especially during and after an intense spell of rain. This zone has steep slopes with loose and unconsolidated materials, and also areas where active landslides had occurred. This zone is dispersed in few places as found in eastern side of Bazar Veng along parallel road, part of Zohnuai and Serkawn area, Zotlang (below Tourist Lodge) and Rahsi Veng – Sazaikawn road (below Sap tui). It is also found scattered in small patches along Luangmual – Sazaikawn road below Chanmari and Lunglawn. The Lower part of Theiriat locality along Aizawl road also falls within the very high Hazard Zone. It also includes areas where unplanned quarrying, such as Vawngzawl quarry, road cutting and other human activities are actively undertaken. In addition, it is also found along the streams where toe-erosional activities are constantly

taking place and also in other parts of the town area in small pockets. The vegetation in this zone is generally scarce. The rocks exposed are characterized by numerous bedding and joint planes which facilitate the chance of sliding down along the slope. This zone constitutes an area of 1.01 sq. km and forms 1.84% of the total study area.

It is recommended that no human induced activity be undertaken in this zone. It will be difficult to develop economically and socially acceptable remedial measures which can prevent recurrence of the hazard. Hence, such areas have to be entirely avoided for settlement or other developmental purposes.

3.2. High Hazard Zone

This zone includes areas where the probability of sliding the debris is at a high risk due to weathered rock and soil debris covering steep slopes which when disturbed are prone to landslides. Many of the pre-existing landslides occurred within this zone. Besides, this zone includes some areas where the dip direction and slope direction, which are usually very steep, are the same. This rendered them susceptible to sliding along the slope. Several lineaments, fractured zones and fault planes also traverse the high hazard zone. Areas, which experience constant erosion by streams because of the soft nature of the lithology and loose overlying burden, also fall under this class. The High Hazard Zone is distributed in many parts of the town area. It always surrounds the Very High Hazard Zone. This zone is found in Rahsi Veng, College Veng, Hauruang, Theiriat, eastern side of Bazar Veng, etc. Vegetation is generally either absent or sparse. The High Hazard Zone is also found along the intersection of steep slope with road cutting. This zone occupies an area of 7.67 sq. km which is 13.92% of the total study area.

Allocation and execution of major housing structures and other projects within this zone should be discouraged. If unavoidable circumstances compel the execution of such activity, precaution should be taken in consultation with the geological experts. Unless immediate action plans are implemented, this zone will soon deteriorate to the critical situation.

3.3. Moderate Hazard Zone

This zone is generally considered stable, provided its present status is maintained. It comprises areas that have moderately dense vegetation, moderate slope angle and relatively compact and hard rocks. Although this zone may include areas that have steep slopes (more than 45 degree), the orientation of the rock bed or the absence of overlying loose debris and human activity may make this zone less hazardous. The Moderate Hazard Zone is distributed in various parts of the study area. Several parts of the human settlement also come under this zone. This zone covers an area of 19.76 sq. km. and occupies 35.87% of the total study area.

Although this zone is generally considered stable, it may contain some pockets of unstable zones in some areas. Such areas need to be identified on the ground and suitable mitigation measures should be undertaken. It is recommended that human activity that can destabilize the slope and trigger landslides should not be undertaken within this zone. Although this zone comprises areas which are stable in the present condition, future land use activity has to be properly planned so as to maintain its present status.

3.4. Low Hazard Zone

This zone includes areas where the combination of various controlling parameters is not having adverse influence on the stability of the slope. In other words, this zone comprises areas where the chance of slope failure is low or unlikely to occur by virtue of its present environmental set up.

Vegetation is relatively dense, except in some areas. Although some of the areas may be covered with soft and unconsolidated sediments, the slope angles are generally low, about 30 degrees or below. Flat lands and areas having low degrees of slope fall under this class. This zone is mainly confined to areas where anthropogenic activities are less or absent, and are mainly distributed along the periphery of the study area. This zone covers an area of 17.05 sq. km. and forms 30.96% of the total study area.

No evidence of slope instability is observed and mass movement is not expected within this zone. Therefore, this zone is suitable for carrying out developmental schemes. Developmental activities are considered safe to be carried out within this zone.

3.5. Very Low Hazard Zone

This zone generally comprises areas covered by dense vegetation and is mostly located away from human settlement. In addition, it includes valley fill and other flat lands. Therefore, it is assumed that this zone is free from the present and future landslides. The dip direction of the rocks and slope angles are fairly low. Although the lithology may comprise of soft rocks and overlying soil debris in some areas, the chance of slope failure is minimized by low slope angle and vegetative cover. This zone covers an area of 9.59 sq. km., and forms 17.41% of the total study area.

As far as slope instability is concerned, developmental activities of any kind can be safely carried out within this zone. Most of the areas within this zone can be allocate for major housing structures without hesitation.

4. Conclusion

In the present study, it is observed that human activities coupled with natural factors like lithology, slope, geological structure, rainfall, etc. have caused some parts of Lunglei town highly prone to landslides. In this situation, it is necessary to have proper mitigation plan for future developmental activities particularly in the areas falling under Very High and High hazard zones. The study also revealed that there are many stable areas where developmental activities can be taken up.

It has been proven that, a combination of Quickbird imagery for interpretation and Cartosat-I stereo data for DEM and slope generation, supported by detailed ground truthing can be utilized for producing reliable large scale geological map and landslide hazard zonation map with high accuracy in the hilly areas. The outcome map of this study will therefore, be a useful database for undertaking mitigation measures, and also for selecting viable sites for carrying out future developmental operations within the town.

5. Acknowledgements

References

[1] Gurugnanam B., et al. *GIS Based Weighted Overlay Analysis in Landslide Hazard Zonation for Decision Makers Using Spatial Query Builder in Parts of Kodaikanal Taluk, South India*. Journal of Geomatics. 2012. 6(1) 49.

[2] Chandel et al. *RS & GIS Based Landslide Hazard Zonation of Mountainous Terrains. A Study from Middle Himalayan Kullu District, Himachal Pradesh, India.* International Journal of Geomatics and Geoscience. 2011. 2(1) 121-132.

[3] Tiwari R.P., et al. *Landslide Hazard Zonation – A Case Study Along Hnahthial – Hrangchalkawn Road Section, Lunglei District, Mizoram.* Proceedings of International Conference on Disaster and Management, Tezpur University. 1997. 461-478.

[4] Anonymous. *Geology and Mineral Resources of Manipur, Mizoram, Nagaland and Tripura*, Geological Survey of India, Miscellaneous Publication No. 30, Part IV. 2011. 1 (2) 30-35.

[5] Tiwari R.P., et al. *Landslide Hazard Zonation along Rotlang – Tuichawng Road Section, Lunglei District, Mizoram*. Status of Landslides in North-East India & Natural Disaster Management (Ed., Prof. G.D. Sharma). 1998. 9-24.

[6] Mehrotra G.S., et al. *Landslide Hazard Zonation – A Guide for Future Planning and Development of Himalaya (Abstr.)*, Proceedings of the Indian Geological Congress. 1993. 103-104.

[7] Jaggi G.S. *Geo-Environmental Appraisal of Lunglei Town and Its Surroundings, Lunglei District, Mizoram. Progress Report for the Field Session 1986-1987,* Geological Survey of India, North Eastern Region, Shillong. 1989.

[8] Kumar Pankaj, 2007: *Landslide Hazard Zonation and Slope Stability Studies around Lunglei Area, Mizoram.* Progress Report for the Field Session 2005-06 (Unpublished)*,* Geological Survey of India, North Eastern Region, Shillong.

[9] Kumar et al. *Report on Meso Scale Landslide Hazard Zonation and Slope Stability Studies Around Lunglei Town, Mizoram,* Progress Report for the Field Session 2006-07 (Unpublished), Geological Survey of India, North Eastern Region, Shillong. 2008.

[10] Tiwari R.P., et al. *Landslide Hazard Zonation Mapping along Hrangchalkawn – Rotlang Road Section, Lunglei, Mizoram.* Proceedings of the ISEG Symposium on Modern Practices in Geotechniques, Lucknow. Journal of Engineering Geology. 1996. XXIV: 257-269.

[11] Hiese et al. *Landslide Hazard Zonation Mapping of Kohima Town.* Indian Landslides. 2010. 3 (2) 41-46.

[12] Gupta R.P., et al. *Landslide Hazard Zonation in a Part of Bhagirathi Valley, Garhwal Himalayas, Using Integrated Remote Sensing-GIS*. Journal of Himalayan Geology. 1999. 20 (2) 71-85.

[13] Anonymous. *Landslide Hazard Zonation Mapping in the Himalayas of Uttaranchal and Himachal Pradesh States using Remote Sensing and GIS Techniques* (Unpublished), National Remote Sensing Agency, Dept. of Space, Govt. of India, Hyderabad. 2001.

[14] Sarkar, S. et al. *An Integrated Approach for Landslide Susceptibility Mapping Using Remote Sensing and GIS.* Photogrammetric Engineering and Remote Sensing. 2004. 70 (5) 617-625.

[15] Sharma, A. K., et al. *Landslide Hazard Zonation of Gangtok Area, Sikkim Himalaya Using Remote Sensing and GIS Techniques*. Journal of Geomatics. 2011. 5(2) 87-88.

[16] Lallianthanga R.K. et al. *Landslide Hazard Zonation of Aizawl Town using Remote Sensing and GIS Techniques – A Qualitative Approach.* Bulletin of National Natural Resources Management System (B), Dept. of Space, Govt. of India, Bangalore. 2008. 32; 47-55.

[17] Pandey A., et al. *Landslide Hazard Zonation using Remote Sensing and GIS: a Case Study of Dikrong River Basin, Arunachal Pradesh, India*. Environmental Geology. 2008. 54 (7) 1517-1529.

[18] Arnous et al. *Integrated Remote Sensing and GIS Techniques for Landslide Hazard Zonation: A Case Study Wadi Watier Area, South Sinai, Egypt*. Journal of Coastal Conservation. 2011. 15 (4) 477-497.

[19] Negi R.S., et al. *Landslide Hazard Zonation using Remote Sensing and GIS: A Case Study of Giri Valley, District Sirmaur, Himachal Pradesh*. International Journal of Environmental Science. 2012. 1 (1) 26-39.

[20] Nithya S., et al. *An integrated Approach with GIS and Remote Sensing Technique for Landslide Hazard Zonation.* International Journal of Geomatics & Geosciences. 2010. 1(1) 66-75.

[21] Lallianthanga R.K., et al. *Micro-level Landslide Hazard Zonation of Serchhip Town, Mizoram, India Using High Resolution Satellite Data*. Science Vision. 2013. 13 (1) 14-23.

[22] Lallianthanga R.K., et al. *Landslide Hazard Zonation of Mamit Town, Mizoram, India using Remote Sensing and GIS Techniques*. International Journal of Geology, Earth and Environmental Sciences. 2013. 3 (1) 148-194.

[23] Anonymous. Meteorological Data of Mizoram. Mizoram Remote Sensing Application Centre, Aizawl, Mizoram. 2012. 43-45.

[24] Anonymous. *Environmental Studies of Lunglei Town Using Remote Sensing and GIS*, Mizoram Remote Sensing Application Centre, Aizawl, Mizoram. 2008.

Cloud Publications

Research Article   **Open Access**

ASTER DEM Based Studies for Geological and Geomorphological Investigation in and around Salbardi Fault of Betul District (M.P.) and Amaravati District (M.S.), India

B.S. Manjare and Suyog Anil Jagtap

Department of Geology, RTM Nagpur University, Nagpur, Maharashtra, India

Correspondence should be addressed to Suyog Anil Jagtap, suyog.jagtap@gmail.com

OPEN ACCESS

Abstract The Salbardi and adjoining area are one of the important elements of the Son Narmada Tapti Lineament. Digital elevation models (DEMs) are more and more used for visual analysis of topography, landforms, as well as modeling of surface processes. DEM of study area is generated from ASTER DEM data of 30m resolution with using software ARC GIS 9.3. The analysis of the remote sensing data with conventional studies and sufficient ground truth information makes probable to recognize and delineate the various ground features such as geology, structures, geomorphological features and their characters. This study is an attempt to delineate the geomorphology in and around Salbardi and adjoining area of Madhya Pradesh and Maharashtra states, using integrated approach of Remote Sensing and GIS techniques especially ASTER DEM by observing the elevation, aspect, slope, lineament, and shaded relief of images. DEM has been an excellent supplementary information database for interpretations in the present study area along with other data.
Keywords *ASTER DEM, GIS, Geomorphology, Remote Sensing*

1. Introduction

Digital elevation models (DEMs) is a digital representation of the topographical surface. It is used for visual interpretation, analysis of topography, landforms, lithology as well as modeling of surface processes. In the present scenario, GIS is being used in various purposes such as evaluation of surface features for geological and geomorphological studies. The modern computer technologies may provide additional tools for geological and geomorphological mapping which may improve better agreement of determined geological units with the terrain topography. One of such tools of GIS is the Digital Elevation Model (DEM) which can serve both as information source for finding geological boundaries, controlling elevations, and at the same time play important role in preparation of the base map as well as various surficial thematic maps (S., Ostaficzuk, 2005). It is also used for many purposes like providing flood and landslide risk zone, highways and corridor selection including cut

and fill estimation etc. These data are also good for geological interpretation particularly in terms of geomorphology, rock type and structure (Sarapirome et al., 2002).

2. Study Area

The study area lies in the Survey of India toposheets no. 55k/2, 55/k3, 55G/14, 55G/15 and bounded by latitude and longitude 21^0 20' to 21^0 35' E and 77^0 45' to 78^0 10' N respectively. The area from the present study divided in to two parts i.e. one part comes under the state of Maharashtra and other falls under the state of Madhya Pradesh. The proposed study area is one of the important elements of the Tapti-Purna lineament which in turn is a major component of SONATA (Son-Narmada-Tapti Lineament), straddling across the Indian shield in ENE-WSW direction (Acharyya et al., 1998). The fault at the junction of Tapti Grabben and Satpura Horst is termed as Satpura foot hill fault and is the most active element of the system (Ravi Shankar, 1995).

Auden (1949) had guessed the through of this fault to be anywhere between 1800-1400 m in Gawilgrah region. This is a regional feature which can be traced throughout the proposed area and extend in either direction for considerable distance. It was variously described as Gawilgrah fault, Ellitchpur fault and Salbardi fault in different stretches (Rajurkar, 1992; Saxena, 1984). The vertical through or displacement across the fault junction of the Tapti grabben and Satpura horst was measured to about 1000mt at Salbardi of this 425 meters appears to be quaternary component (Ravi Shankar, 1992). The northern contacts of Proterozoic rock with Upper Gondwana with that of Deccan trap and with Gondwana are faulted. It is an ENE-WSW trending fault and known as Salbardi fault (Ravi Shankar, 1994).This fault is most probably the eastern continuation of well known Gavilgrah/Elichpur fault (Rajurkar 1981).
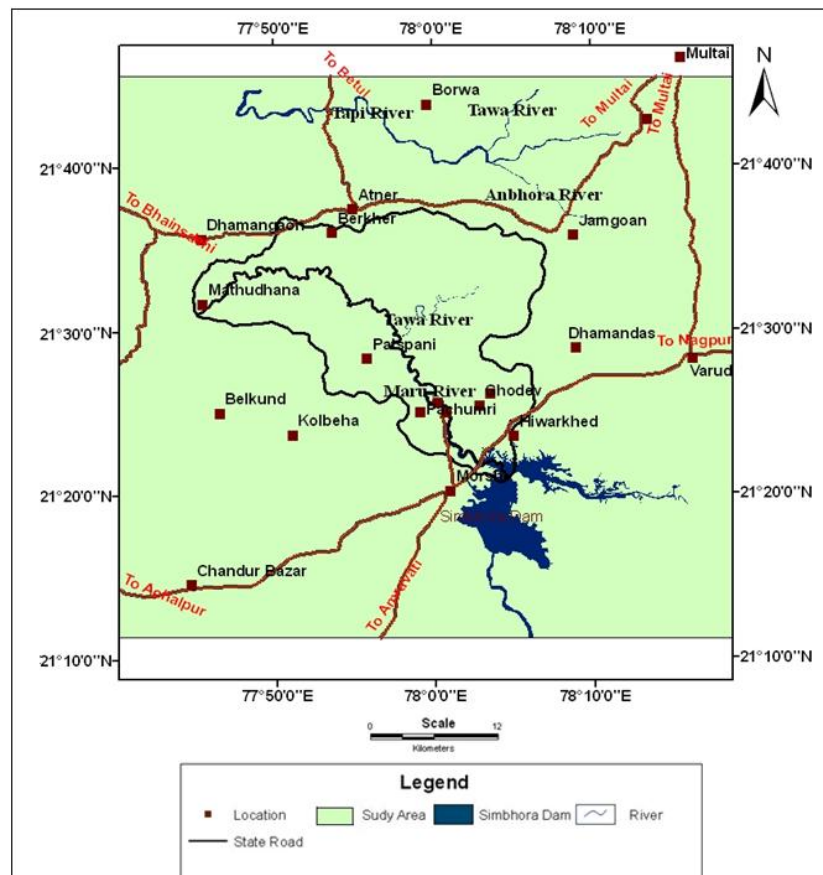

Figure 1: Location Map of the Study Area

3. Materials and Methodology

3.1. Data Used

a. ASTER DEM 30m (USGS/NASA ASTER DEM data), available from
   http://www.gdem.aster.ersdac.or.jp
b. ERDAS IMAGINE 9.2
c. ARC GIS 9.3

3.2. Methodology

The input data is used as ASTER DEM 30m with resolution for the present study area. DEM map is representing the altitude of the study area ranging from 282 to 1138 mt amsl. Aspect map which is generated in ARC GIS 9.3 software from the input data to know the topographical slope direction and geological features of the area. Slope map is also generated to know the intensity of slope. Slope of the study area has been classified into seven classes as per the IMSD guidelines (NRSA, 1995). The area constitutes 0 to more than 35% slope. Most of the area falls into 0-1% i.e. nearly level and 1-3%. High slope is observed in the northern part, western part and southwestern part of the study area (Figure 4).
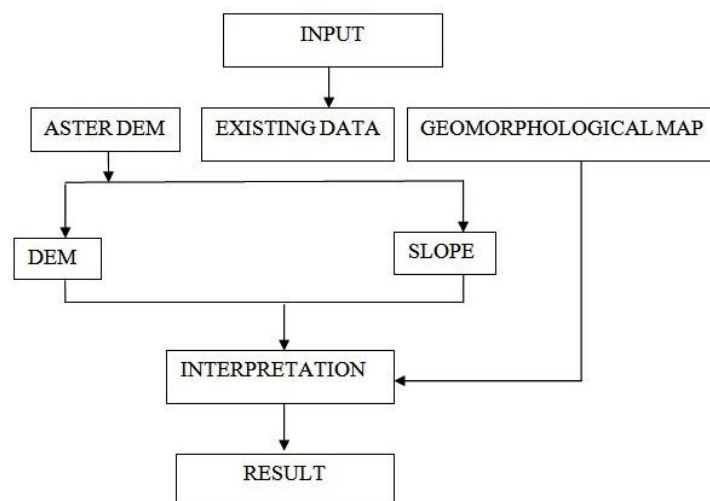

Figure 2: Flow Chart Showing Methodology

4. Interpretation

Digital elevation models suggest the most widespread methods for extracting important elevation and topographic information. DEMs are used for visual analysis of topography, landscapes and landforms other than modeling of surface processes (Welch 1990). Currently Digital elevation models (DEMs) is considered as the main resource for the extraction of various geomorphologic and topographic features depending on their elevation, spatial distribution and deviations (Felicisimo 1994). Digital Elevation Model (DEM), Digital Elevation Data (DED), Digital Terrain Data (DTD) (Campbell 2002) or Digital Terrain Model (DTM) all consists of different arrangements of individual points of x (east-west direction) and y (north-south direction) coordinates of horizontal geographic positions. Z is the vertical elevation value that is relative to a given datum for a set of x, y points (Bernhardsen 1999, Bolstad and Stowe 1994, Welch 1990). They composed of samples array of elevations for a number of ground locations at equally spaced intervals (USGS 1990).

DEM of the study area indicates that the slope trends towards north from south. Shaded relief images can help to identify the information about geomorphometric features, rock types and structures of an area. From the shaded relief images, the geomorphometric features which is described as extent, tone, textures, size, shape, height, variation of slope and aspect on the surface can be identified (Figure 3). Geological structures look like a series of curvilinear features from southwest to northeast alternate banded appearance of soft and hard rocks. The data deciphers that in the southwestern part of the study area constitute hills like structures as identified, which may be of hard rocks like felspathic gneiss, etc. Tributaries are following the soft rocks, merging and making a form of river. A river flowing from north to south direction is totally structural controlled (a clear view of the river can be seen in (Figure 1). In northwest part of the study area another river has been identified with the help of the generated data. Northern part of study area has a sudden change in the topography is rugged (Figure 3).
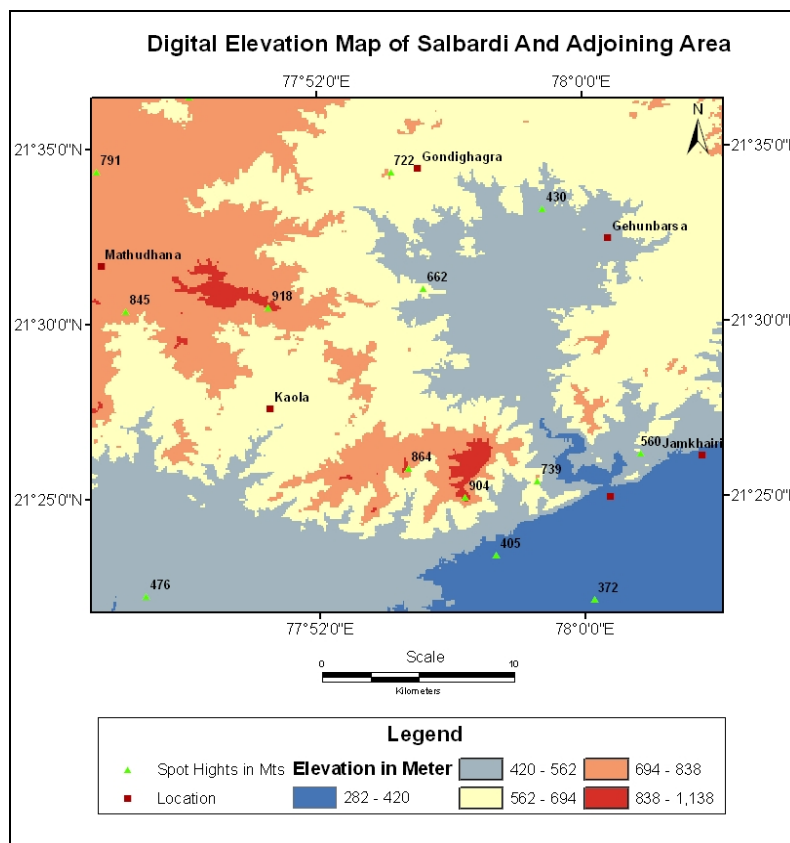

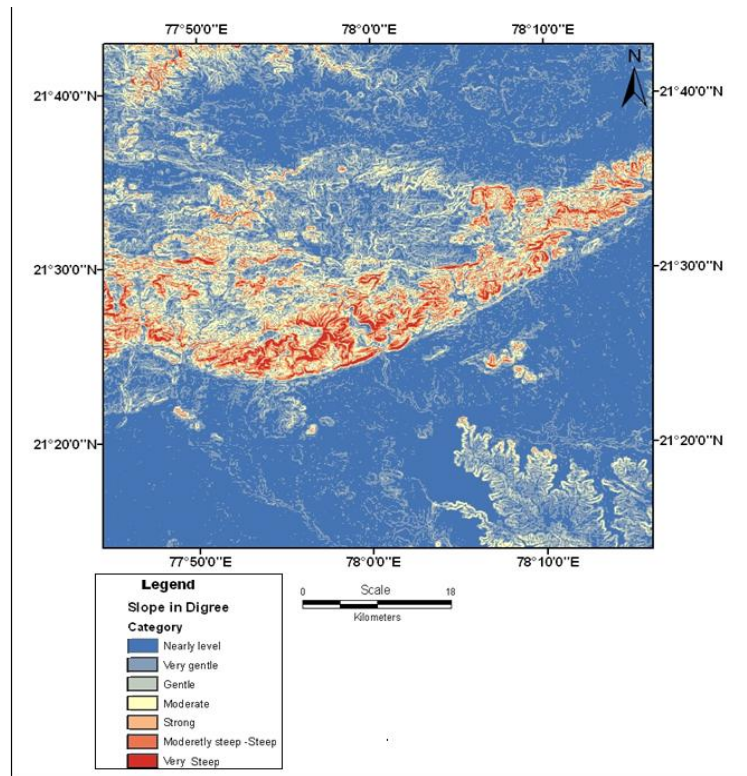***Figure 3:*** *DEM Map of Study Area*

Figure 4: *Slope Map of the Study Area*

In the study area, the slope values vary from 0 to 42º. The slope values have been categorized in to seven groups like 0-1, 1-3, 3-5-10, 5-10, 10-15, 15-35 and above 35º with slope class namely nearly level, very gently, gentle, moderate, strong moderate, steep to steep, very steep respectively (Figure 4). Steep slopes to moderately steep slope are observed in hill top plain/dissected plateau and valley fill zones covering 15% of the total area and rest are nearly level, very gently, gentle to moderate category out of 4572 sq Km. Topography relates to the local and regional and gives an idea about general direction of the slope and direction of the study area that influence the whole topography of the area.

5. Conclusion

DEM and satellite data can be used for visualization and interpretation of the area in terms of geology and geomorphology. In geological investigation we can delineate the changes in structures of the area and in the geomorphological features. We can identify the geomorphological features like lineaments, faults, fractures but not in details. DEM data, however cannot be ignored altogether as it can be very useful in giving an overview of the geology and geomorphology of any area especially where any other data.

Slope is the most important and specific feature of the earth's surface form. The Salbardi and adjoining region experiences a fully developed slope profile that includes slope classification and slope elements. The slope classification was adopted by NRSA, 1995 which is more convenient for the better interpretation and analysis of the slope for the study area. The slope elements in a complete sequence i.e. from the crests to pediments have been observed in the fully developed hilly slope near Salbardi and Jamkhari village. The slope map papered in degree form with their elements. In the study area the different slope elements have been observed.

References

Acharyya S.K., et al. *Tectonothermal History of the Central Indian Tectonic Zone and Reactivation of Major Faults/Shear Zones*. J. Geol. Soc. India. 2000. 55; 239-256.

Auden J.B. *Geological Discussion of the Satpura Hypothesis*. Proc. Natl. Inst. Sci. India. 1949. 15; 315–340.

Bernhardsen T., 1999: Geographic Information Systems: An Introduction. 2nd Ed. John Wiley and Sons, Inc., New York.

Bolstad P.V., et al. *An Evaluation of DEM Accuracy: Elevation, Slope, and Aspects*. Photogrammetric Engineering and Remote Sensing. 1994. 60 (11) 1327-1332.

Campbell L.B., 2002: Introduction to Remote Sensing. 3rd Ed. The Guilford Press, New York.

Felicísimo A.M. *Parametric Statistical Method for Error Detection in Digital Elevation Models*. ISPRS Journal of Photogrammetry and Remote Sensing. 1994. 49 (4) 29-33.

NRSA, 1995: Integrated Mission for Sustainable Development, Technical Guidelines, National Remote Sensing Agency, Hyderabad.

Ostaficzuk S., 2005: *The Current Role of Geological Mapping in Geosciences*. Springer, Netherlands, 89-96.

Rajurkar S.T., 1981: *Photographic Interpretation of Upper Wardha Project and Surrounding Area Wardha, Amravati and Betul Districts*. Geol Suvy. India. 69-292.

Ravi Shankar. *Structural and Geomorphological Evolution of SONATA Rift in Central India on Response to the Himalayan Uplift*. Pal. Soc. Ind. 1992. 38; 17-30.

Ravi Shanker. *Geothermal Regime of the Son–Narmada–Tapti Lineament Zone*. Geological Survey of India Special Publication. 1995. 10; 213-248.

Sarapirome S., et al., 2002. Application of DEM Data to Geological Interpretation: Tho Pha Phum Area, Thailand. 23rd Asian Conference on Remote Sensing, Birendra International Convention Centre, Kathmandu, Nepal.

Saxena R.K. Geothermal Investigation of Salbardi around Hot Spring Area, Dist. Betul (M.P) and Amravati Maharashtra. Geol. Surv. Ind. F.S. 1981-82.

USGS, 1990: U.S. Geodata: Digital Elevation Models. National Mapping Program, Technical instructions, Data Users Guide 5. Department of the Interior: United States Geological Survey (National Mapping Division).

Welch R. *3-D Terrain Modeling for GIS Applications*. GIS World. 1990. 3 (5) 26-30.

Research Article   **Open Access**

Selection of Potential Sites for Solar Energy Farms in Ismailia Governorate, Egypt using SRTM and Multicriteria Analysis

Hala Adel Effat

Division of Environmental Studies and Land Use, National Authority for Remote Sensing and Space Sciences, NARSS, Cairo, Egypt

Correspondence should be addressed to Hala Adel Effat, haeffat@yahoo.com

Abstract Egypt is known to be one of the most optimal locations in the world for solar energy production. Solar energy can provide a great opportunity for sustainable development and population redistribution in its vast deserts. Ismailia Governorate encompasses the Suez Canal which in turn possesses high development potentiality. The objective of this paper is to identify optimum sites for constructing solar energy plants in Ismailia Governorate. To achieve this objective, two interrelated steps have been applied in this research. First, remote sensing including satellite data from SPOT-4 was used to derive land use/land cover map of the study area. Also, Shuttle Radar Topography Mission (SRTM) and Digital Elevation Model (DEM) were used to model the aspect angles map and to model the global solar radiation map for the study area. The global insolation (direct and diffuse radiation, WH/m2) shows where the highest amounts of solar radiation are. Second, a Spatial Multicriteria Evaluation (SMCE) model was designed. Various criteria were used in this study, including meteorological (global insolation); terrestrial (the aspect); economic (distance from power lines, main roads and populated area). The Analytical Hierarchy Process (AHP) was used for calculation of the criteria weights. A weighted overlay was used to produce a suitability index map for solar energy power. Few sites were selected based on high suitability index values and area of a site. The methodology proves to be promising for creating zoning maps for developing solar energy infrastructures in the region.

Keywords *Egypt, Ismailia, Solar Radiation, Spatial Multicriteria Evaluation, Shuttle Radar Topography Mission, Site Selection*

1. Introduction

Selection of a suitable site is based on a set of criteria mainly depending on the local conditions of its surrounding environment. This fact applies on the problem of site selection for suitable solar farms. The varying atmospheric conditions (clouds, dust, pollutants) further modify the availability of solar irradiation within years and even days. Atmospheric conditions not only reduce the quantity of insolation reaching the Earth's surface but also affect the insolation quality by scattering and

absorption of incoming light and altering its spectrum. While average insolation data offer an insight into solar energy potential on a regional scale, locally relevant conditions such as surrounding terrain may significantly influence the solar energy potential in a specific site (Hofierka and Cebecauer, 2008). In addition, some economic and social criteria participate in the evaluation of the lands. Example of such criteria is the proximity of the selected site to power transmission lines or converting stations and the proximity to main roads or populated areas.

Multicriteria Evaluation (MCE) is widely used as a spatial analysis tool in energy evaluation and environmental fields. Such methods are frequently integrated in GIS, to select the best site for a certain activity. It is thus possible to obtain continuous suitability maps, and thus provide an optimal framework for the integration of the environmental, economic, and social factors that affect land suitability for a certain use. Among the various MCE techniques that can be applied to the evaluation of land suitability, is the Analytical Hierarchy Process (AHP) method (Saaty, 1980) such method represents a specific problem by means of the hierarchical organization of criteria, and afterwards uses comparisons to establish weights for criteria and preference scores for classes of different criteria, based on user judgment. Recent developments in GIS have led to significant improvements in its capability for decision making processes in land allocation and environmental management, among which multi criteria evaluation (MCE) is one of the most important procedures (Janssen and Rietveld, 1990; Jankowski, 1995). (Arán-Carrión et al., 2007) used Multicriteria Evaluation (MCE) and geographic information system (GIS) to select the optimal location of grid connected photovoltaic power plants in North of the Granada Province. (Jiang, 2007) used the AHP and analyzed the suitable and low cost sites for industrial land using SMCE in Panzhihua, China. GIS and AHP were also used together for land suitability analysis for urban development in the studies conducted by (Aly et al., 2005; Mohammad et al., 2006; Cerreta and Toro, 2012). (Janke, 2010) used MCE and GIS to model solar and wind farms in Colorado. (Aydin et al., 2010) conducted a GIS-based environmental assessment of wind energy systems for spatial planning in Western Turkey.

2. Description of the Investigated Area

Ismailia Governorate is located between latitudes 30° 13´ and 31° 10´ North and longitudes 31° 48´ and 32° 50´ East, covering an area of 5067 square kilometers, equivalent to 0.5% of the total Egyptian territory (Figure 1). Population counts are 896,000 capita for 2006 which is equivalent to 1.2% of total population in Egypt (GOPP, 2007). The Governorate has five administrative divisions namely, Ismailia, Fayed, El Tell El Kebeir, El Kantara Shark and El Kantara Gharb. The main capital city is Ismailia city. Six towns in addition to a hierarchy of villages reaching a total of 30 units constitute the populated areas. The landcover are bare desert with some cultivated and newly reclaimed lands and established fish farms in addition to the lakes, the Suez Canal and urban areas. The climate and soil conditions promote the Governorate as Egypt's significant fruits and vegetables producer. Its location as the hub-city for the Suez Canal region puts it at cross roads to Cairo, Suez, Port-said and Sinai. In addition, the Egyptian Government has plans for developing the Suez Canal Region as an international navigation and trade center. Such development potentials necessitated the evaluation and exploration of the region for renewable energy resources such as solar energy potentiality.

2.1. Geology

The land of Ismailia Governorate is mainly formed of gravelly plain extending northwards until reaching the Mediterranean coast. The area is drained by a large dry valley called Wadi Tumaylat, which forms an old arm of the Nile Delta ending near Ismailia. Such valley is a sandy depression located west of Ismailia and extends for 52 kilometers from west to east. The north of Wadi Tumaylat spread Plio Pleistocene deposits of gravel and sand forming the island of Tell El-Kebir.

2.2. Climatic Conditions

Ismailia Governorate enjoys an ideally moderate climate, with the sun shines most of the year an average of about 10 hours daily. Rainy days are few, and the north wind blowing from Europe cools of the weather in the study area even in summer (June to August). (Table 1) gives the monthly averages of some climate elements measured at Ismailia Meteorological station during the period 1961 to 1968 (Egyptian Meteorological Authority, 2005). This station is located at latitude 30° 35´ North and longitude 32° 14´ East.
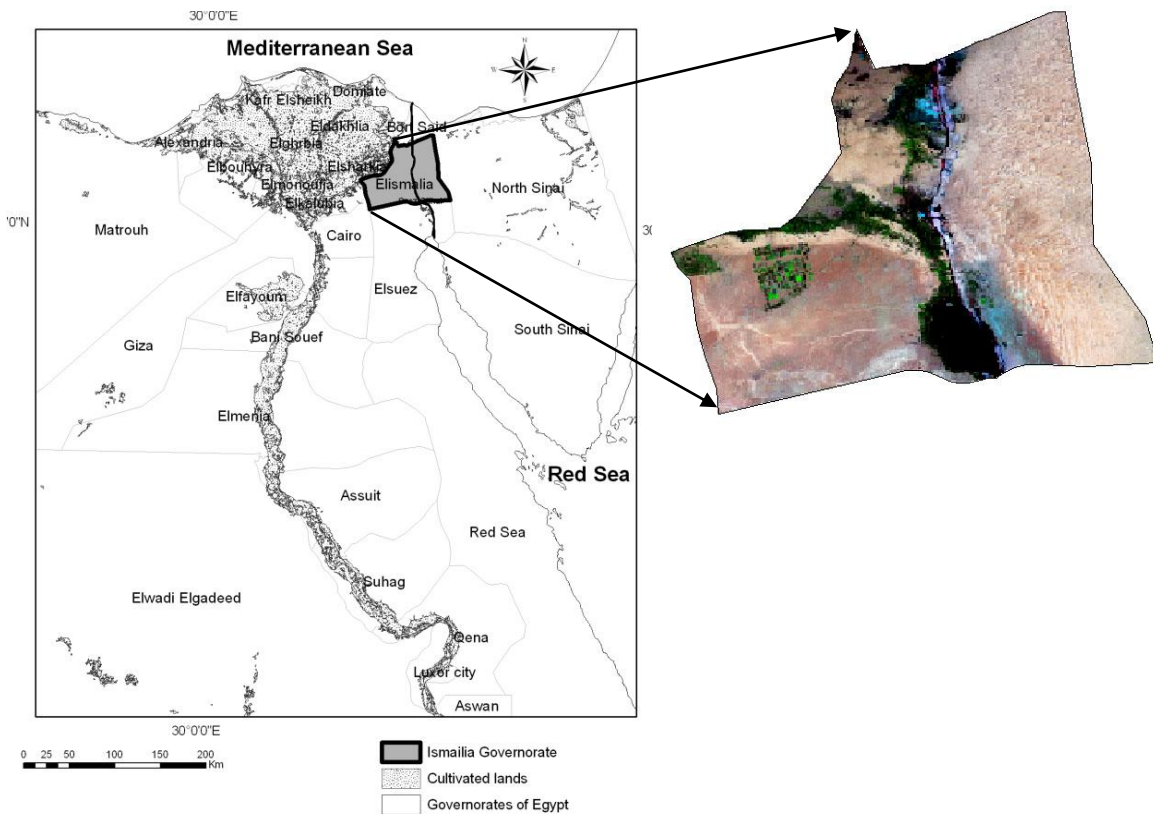
Figure 1: *Location of Ismailia Governorate*

Table 1: *Monthly Average of Some Climatic Elements at Ismailia Station*

Month	Max. Temp. °C	Min Temp.	Relative Humidity (%)	Rainfall mm/month	Sunshine Hrs.
January	19.6	7.9	66	7.2	9
February	20.9	8.5	61	6.2	8
March	23.5	10.3	59	6.8	9.5
April	28.3	13.6	53	1.7	10.5
May	31.8	16.5	50	1.3	11
June	34.6	19.5	53	0.0	12
July	35.9	21.9	57	0.0	12.5
August	35.7	22.1	59	0.0	11.5
September	33.5	20.3	61	0.0	10.5
October	30.3	17.4	63	1.5	9.5
November	25.8	13.3	65	3.9	8.5
December	21.1	9.4	67	4.7	7.5

2.3. Sunshine Duration

Sunshine duration is defined as the sum of sub-period for which the direct solar radiation is intense enough to cast distinct shadow, i.e. the direct solar irradiance exceeds 120 W/m3. Its unit is evidently time (hours) and it is measured to the nearest 0.1 hours. Sunshine duration at Ismailia, the monthly mean of the bright sunshine duration reaches up to 10 hours (Egyptian Meteorological Authority, 2005).

3. Data Sources

Two primary data sets were used to model the solar energy potential sites as follows:

A. **SRTM Data:** The Shuttle Radar Topography Mission (SRTM) data acquired by space shuttle Endeavour mission in 2001 by C-band SAR interferometry instrument were used in this study. The data was processed by NASA and the USGS SRTM data was used to model the area solar radiation map and the aspect angles map using ESRI ArcGIS 9.2 spatial analyst modules.

B. **SPOT-4 Data:** SPOT-4 is a French Earth Observation satellite that was launched in March 1998 at an altitude of 810 km. SPOT scenes are typically 60x60 km for vertical viewing, or 60 km by up to 80 km for oblique viewing. SPOT-4 is characterized by multispectral data represented by 4 bands covering green, red, near infrared and shortwave infrared portions spectrum, with 20 m spatial resolution, in addition to a single panchromatic band acquired in the wavelength region from 0.62 to 0.68 μm with 10 meter spatial resolution. SPOT-4 images acquired in 2010. The rectified images were mosaiced and classified in ERDAS Imagine software to derive the land-use / land-cover map. Such map was reclassified into a binary map to create the land cover constraints map.

C. **Maps:** The topographic map published by the Egyptian General Survey Authority (1989) scale 1:50,000 was scanned, geometrically corrected and used to extract the roads, power lines by on-screen digitizing. The roads were further updated from SPOT-4 imagery acquired in 2010. All data were projected to WGS-84 of the Universal Transverse Mercator System (UTM) of geographic coordinates, and were resample to 100 m resolution and used in the present study. A conceptual flow chart for the methodology is shown in (Figure 3).

4. Methods

Planning for solar energy usually entails the consideration of a number of interrelated factors. For studying such factors, the following materials have been acquired, collected, processed by adequate methods and a Spatial Multicriteria Evaluation model was designed.

4.1. Identification of the Criteria

Climate criteria are the most important for the decision rule since they define the electricity production capacity of the photovoltaic power plant. Next come Orography, whose importance mainly depends on the aspect angles (orientation) and land slope. The milder the slopes are, the greater the importance of this type of area since the most suitable sites are those where the ground is flat and oriented towards the south. For the investigated region, most lands are flat or mild slopes, thus only the aspect was considered. Accessibility factors were also considered in the site selection. Such factors are identified through the location criteria and help in identifying feasible sites for a solar farm. Factors such as proximity to power lines, main roads and populated areas are vital factors for the site selection. Land constraints were derived by masking out the water bodies, cultivated lands, urban

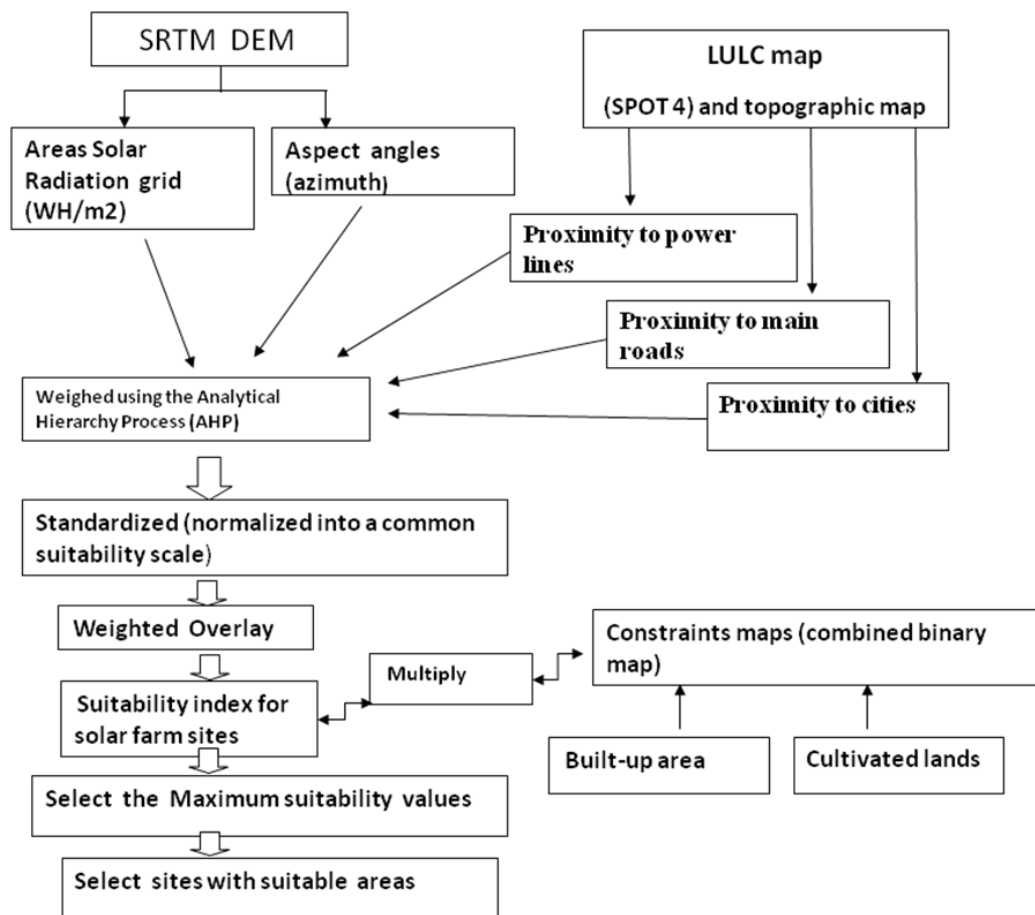areas, wetlands and sabkahs from the land use-land cover map. Criteria are described in the following section:

Figure 2: *Conceptual Chart for the Applied Methodology*

4.1.1. Solar Radiation Mapping

The solar radiation module in ESRI Spatial Analyst was used in this study to calculate the direct, diffuse and total global radiation map using SRTM digital elevation model. Topography is a major factor that determines the spatial variability of insolation (incoming solar radiation). Variation in elevation, orientation (slope and aspect), and shadows cast by topographic features all affect the amount of insolation received at different locations. Insolation originates from the sun, is modified as it travels through the atmosphere, is further modified by topography and surface features, and is intercepted at the earth's surface as direct, diffuse, and reflected components. Direct radiation is intercepted unimpeded, in a direct line from the sun. Diffuse radiation is scattered by atmospheric constituents, such as clouds and dust. Reflected radiation is reflected from surface features. The sum of the direct, diffuse, and reflected radiation is called total or global solar radiation. The solar radiation analysis tools, in the ESRI Spatial Analyst extension, were used to map and analyze the effects of the sun over a geographic area for specific time periods. It accounts for atmospheric effects, site latitude and elevation, steepness (slope) and compass direction (aspect), daily and seasonal shifts of the sun angle, and effects of shadows cast by surrounding topography. The solar radiation analysis tools calculate insolation across a landscape or for specific locations, based on methods from the hemispherical view shed algorithm developed by (Rich, 1990; Rich et al., 1994) as further developed by (Fu and Rich, 2000) The total radiation is calculated as the sum of the direct and diffuse radiation. The total amount of radiation calculated for a particular location or area is given as global radiation.

The calculation of direct, diffuse and global insolation is repeated for each feature location or every location on the topographic surface producing insolation maps for an entire geographic area. The solar insolation equations are described as follows (ESRI Spatial Analyst):

$$Dir_{\theta,\alpha} = S_{Const} * \beta^{m(\theta)} * SunDur_{\theta,\alpha} * SunGap_{\theta,\alpha} * \cos(AngIn_{\theta,\alpha}) \quad .... (1)$$

Where

S_{cons} : Solar flux (constant) (1376 W/m2)

$\beta^{m(\theta)}$: The transmissivity of the atmosphere (av. Of all wavelength) for the shortest path in the direction of the zenith,

$SunDur_{\theta,\alpha}$: The time duration represented by the sky sector. For most sectors, it is equal to the day interval multiplied by the hour interval.

$SunGap_{\theta,\alpha}$: The gap fraction of the sun sector.

$AngIn_{\theta,\alpha}$: The angle of incidence between the centroid of the sky sector and the axis normal to the surface.

$$Dif_{\theta,\alpha} = R_{glb} * P_{dif} * Dur * SkyGap_{\theta,\alpha} * Weight_{\theta,\alpha} * \cos(AngIn_{\theta,\alpha}) \quad .... (2)$$

Where

R_{glb} : The global normal radiation

P_{dif} : The proportion of global normal radiation flux that is diffused. Typically it is approximately 0.2 for very clear sky conditions and 0.7 for very cloudy sky conditions.

Dur : The time interval for analysis.

$SkyGap_{\theta,\alpha}$: The gap fraction (proportion of visible sky) for the sky sector.

$Weight_{\theta,\alpha}$: The proportion of diffuse radiation originating in a given sky sector relative to all sectors.

$AngIn_{\theta,\alpha}$: The angle of incidence between the centroid of the sky sector and the intercepting surface.

Global radiation (Globaltot) is calculated as the sum of direct (Dirtot) and diffuse (Diftot) radiation of all sunmap and skymap sectors, respectively.

$$Global_{tot} = Dir_{tot} + Dif_{tot} \quad .... (3)$$

The solar radiation maps are shown in Figure 3.

4.1.2. Aspect Angle

Shuttle Radar Topography Mission digital elevation model was used to derive the aspect angle in azimuth for the investigated area. The aspect is expressed in positive degrees from 0 to 359.9, measured clockwise from north. For the geographical location of the investigated region (in Northern Hemisphere), the southern direction is the best in receiving solar radiation, the south-west and south-east are the second and third best respectively (Figure 4).

4.1.3. Proximity to Power Lines

Proximity of a site for the solar plant to a power supply line is considered an economic factor. It reduces the cost of installation and creation of a new infra-structure. A distance function (multiple buffers) was used to calculate the distance from the power lines (Figure 5a).

4.1.4. Proximity to Main Roads

Proximity of a solar plant to a main road is considered an economic factor. A distance function (multiple buffers) was used to calculate the distance from the main roads after considering a road buffer area of 200 meters. (Figure 5b)

4.1.5. Proximity to Cities

Proximity of a site for the solar plant to a populated area is considered an economic factor. A buffer zone (2 kilometers) was used around the cities and towns as a constraint. A distance function (multiple buffers) was used to calculate the distance from the main cities (Figure 5c).

4.2. Constraints Criteria

The land use -land cover map was derived by supervised classification of SPOT-4 satellite image (Figure 6a). Constraints (unsuitable cells) are cultivated lands, built-up areas buffers, natural vegetation areas and road buffers. Such classes were excluded from the lands considered for developing a solar farm (Figure 6b).

4.3. Criteria Weighting

For suitability analysis it is necessary to give a relative weight for each of the participating criteria as per their relative importance in the desired development. Analytical Hierarchy Process (Saaty, 1997) was used to assign weights to each criterion, factor, and indicator, and thus determine their relative importance in the final decision adopted within the model. The method is based on pair-wise comparison within a reciprocal matrix, in which the number of rows and columns is defined by the number of criteria. Accordingly, it is necessary to establish a comparison matrix between pairs of criteria, contrasting the importance of each pair with all the others. Subsequently, a priority vector was computed to establish weights (wj). These weights are a quantitative measure of the consistency of the value judgments between pairs of factors (Saaty, 1992). Satty's scale of measurement is used as follows:

$S = \{1/9, 1/8, 1/7, 1/6, 1/5, 1/4, 1/3, 1/2, 1, 2, 3, 4, 5, 6, 7, 8, 9\}$

A pairwise comparison matrix was designed. The comparisons ratings are provided on a nine-point continuous scale, which was proposed by (Eastman, 1995). The comparisons ratings and factors were discussed with experts and the pairwise comparison matrix was constructed based on (Table 2a). If we call that weight aij, and use that scale of comparison and if the relative weighting is a23 = 3/1, then the relative importance of attribute 3 with regard to 2 is its reciprocal a 32 = 1/3. This process generated an auxiliary matrix in which the value in each cell is the result of the division of each value judgment (aij) by the sum of the corresponding column. Finally, the average of the normalized values of rows was obtained, which corresponds to the priority vector (wj). This was normalized by dividing each vector value by n (the number of vectors), thus obtaining the normalized overall priority vector, representing all factor weights (wj). For estimating consistency, it involves the following operations:

a. Determination of the weighted sum vector by multiplying matrix of comparisons on the right by the vector of priorities to get a new column vector. Then divide first component of new column vector by the first component of priorities vector, the second component of new column vector by the second component of priorities vector, and so on. Finally, sum these values over the rows.

b. Determination of consistency vector by dividing the weighted sum vector by the criterion weights. Once the consistency vector is calculated it is required to compute values for two more terms, lambda (λ) and the consistency index (CI). The value for lambda is simply the average value of the consistency vector.

The calculation of CI is based on the observation that λ is always greater than or equal to the number of criteria under consideration (n) for positive, reciprocal matrices and λ=n, if the pairwise comparison

matrix is consistent matrix. Accordingly, λ-n can be considered as a measure of the degree of inconsistency. This measure can be normalized as follows:

$$CI = (λ-n) / (n-1) \ldots\ldots\ldots\ldots (1)$$

The term CI, referred to as consistency index, provides a measure of departure from consistency. To determine the goodness of CI, AHP compares it by Random Index (RI), and the result is what we call CR, which can be defined as:

$$CR = CI/RI \ldots\ldots\ldots\ldots\ldots (2)$$

Random Index is the CI of a randomly generated pairwise comparison matrix of order 1 to 10 obtained by approximating random indices using a sample size of 500 (Saaty, 1980), Table 2b shows the value of RI sorted by the order of matrix.

Table 2a: Saaty's Nine-Point Weighting Scale

Intensity of Importance	Description	Suitability Class
1	Equal importance	Lowest suitability
2	Equal to moderate importance	Very low suitability
3	Moderate importance	Low suitability
4	Moderate to strong importance	Moderately low suitability
5	Strong importance	Moderate suitability
6	Strong to very strong importance	Moderate high suitability
7	Very strong importance	High suitability
8	Very to extremely strong importance	Very High suitability
9	Extremely importance	Highest suitability

The consistency ratio (CR) is designed in such a way that if CR < 0.10, the ratio indicates a reasonable level of consistency in the pairwise comparisons; if, however, CR > 0.10, then the values of the ratio are indicative of inconsistent judgments. In such cases one should reconsider and revise the original values in the pairwise comparison matrix.

Table 2b: Random Index

Order Matrix	1	2	3	4	5	6	7	8	9	10
R.I.	0.00	0.00	0.58	0.9	1.12	1.24	1.32	1.41	1.45	1.49

4.4. Standardization of Criteria

In this step the criteria are placed in either minimization or maximization functions. Solar radiation indicators were classified using equal intervals between the maximum and minimum values and are distributed in homogenous intervals. For the Aspect criterion, the standardization was done by classifying the aspect map into the azimuth main directions (Table 6). The economic criteria of proximity to roads, power lines and populated areas data were minimization criteria (the less values the better). Such criteria maps were classified using equal intervals into ten classes using equal intervals between the maximum and minimum values (Table 7). All classified criteria attributes were recoded into a suitability scale ranging from 1-10.

4.5. Combining the Criteria Maps

The simple additive weight method was used to combine the criteria and constraints to yield the suitability map as follows:

Suitability map = ∑ (factor map * weight) Π (constraint map)

The result was also normalized and reclassified. Figure 6 shows the suitability map that was obtained.

4.6. Selection of Potential Sites

A condition rule was used to select some potential sites for constructing solar energy farms. The sites should have a maximum suitability value from 7-9 and should have an area between 1-2 square kilometer.

5. Results and Discussion

Results obtained from each of the above described methodology are given in brief description in the following section.

5.1. The Solar Maps

The diffuse radiation, direct radiation and global Solar Radiation maps result of running ESRI Spatial Analyst solar module are depicted in Figures 3a, 3b and 3c respectively.
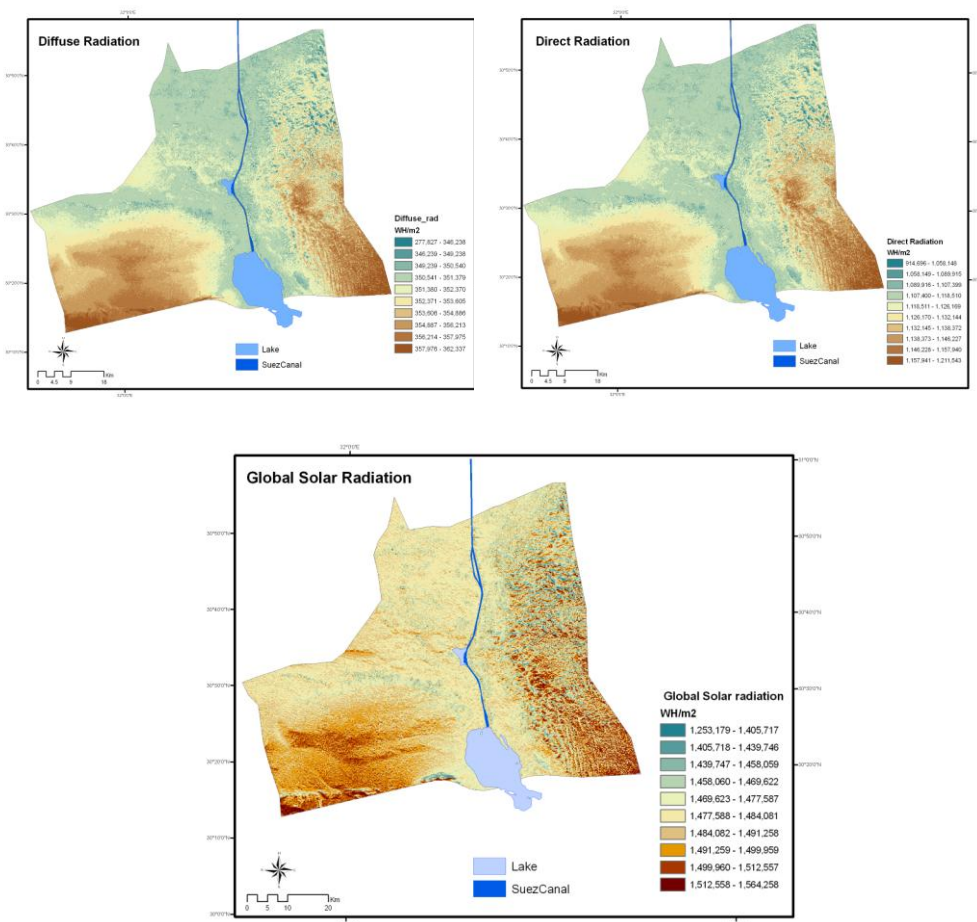

Figure 3: a) Diffuse radiation b) Direct radiation. c) Global Solar Radiation

5.2. Aspect Map

Aspect map describes the direction in azimuth for land slope angles. Aspect produced from SRTM digital elevation model is shown in Figure 4.

Figure 4: *Aspect Angles Map*
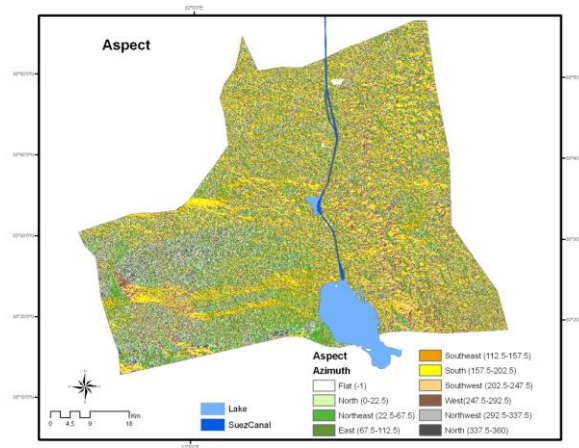
5.3. Proximity Maps

The proximity maps are the results of running the distance functions in ESRI Spatial Analyst Proximity to power lines, main roads and cities are shown in Figures 5a, 5b and 5c respectively.
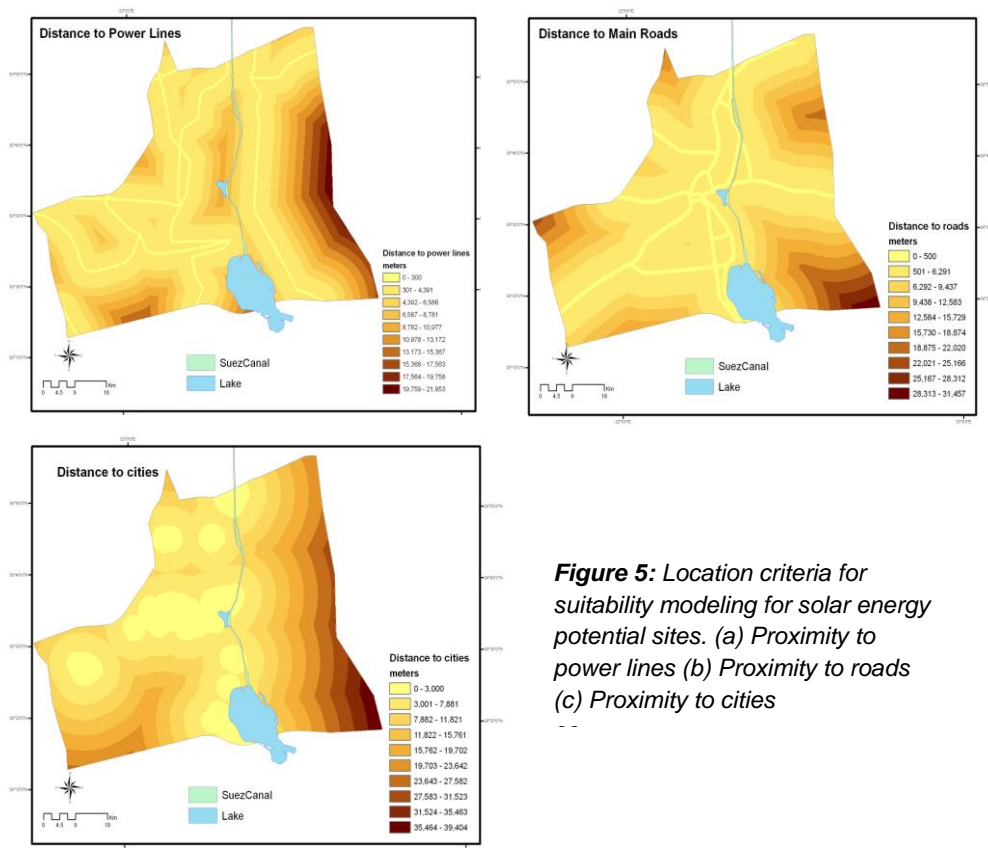

Figure 5: *Location criteria for suitability modeling for solar energy potential sites. (a) Proximity to power lines (b) Proximity to roads (c) Proximity to cities*

5.4. Constraints Map (Exclusion Zones)

The land cover map derived by classification of SPOT-4 image and the land cover constraints map are shown in Figures 6a and 6b respectively.
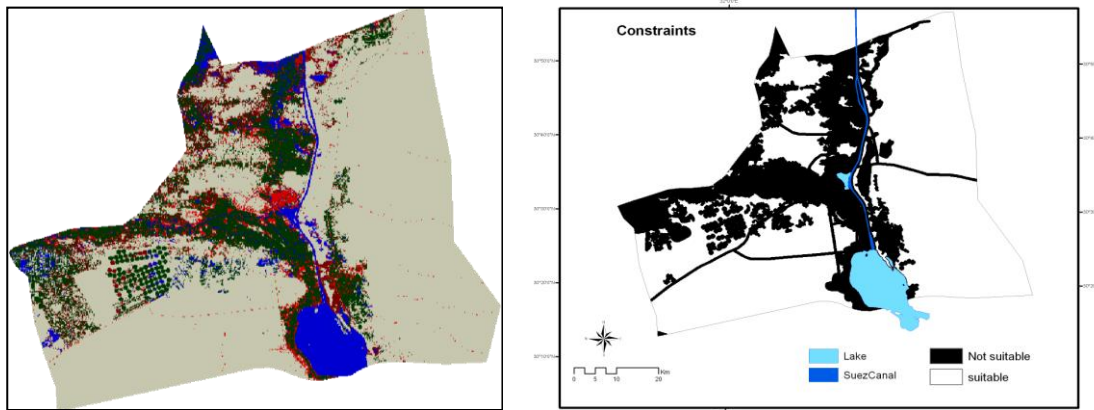

Figure 6: *(a) Land Use-Land Cover Result of Supervised Classification of Spot- 4 (b) Constraints Map Derived From the Land Use-Land Cover*

5.5. Pairwise Comparison Matrix and Calculation of Criteria Weights

Results of the pairwise comparison matrix are shown in Tables 3, 4 and 5.

Table 3: *Pairwise Comparison Matrix*

Pairwise Comparison Matrix					
	Solar Radiation	Aspect	Distance to Power Lines	Distance to Roads	Distance to Cities
Solar Radiation	1	2	4	5	6
Aspect	0.50	1	2	2.5	3
Distance to Power Lines	0.25	0.50	1	1.25	1.50
Distance to Roads	0.20	0.40	0.80	1	1.20
Distance to Cities	0.17	0.33	0.67	0.83	1
Total	**2.11**	**4.23**	**8.46**	**10.58**	**12.7**

Table 4: *Normalized Pairwise Comparison Matrix*

Normalized Pairwise Comparison Matrix					
	Solar Radiation	Aspect	Distance to Power Lines	Distance to Roads	Distance to Cities	Weight
Solar radiation	0.473	0.472	0.473	0.473	0.472	0.47
Aspect	0.237	0.237	0.236	0.237	0.236	0.24
Distance to power lines	0.118	0.118	0.118	0.118	0.118	0.12
Distance to roads	0.094	0.094	0.095	0.094	0.095	0.09
Distance to cities	0.078	0.079	0.079	0.078	0.079	0.08
Total	**1.00**	**1.00**	**1.00**	**1.00**	**1.00**	**1.00**

Table 5: *Calculation of the Consistency Vector*

Criteria	Weight Sum Vector	Consistency Vector
Solar Radiation	[(1)(0.47)+(2)(0.24)+(4)(0.12)+(5)(0.09)+(6)(0.08)]	2.4 / 0.47 = 5.10
Aspect	[(0.5)(0.47)+(1)(0.24)+(2)(0.12)+(2.5)(0.09)+(3)(0.08)]	1.42/0.24 = 5.91
Distance to Power Lines	[(0.25)(0.47)+(0.50)(0.24)+(1)(0.12)+(1.25)(0.09)+(1.5)(0.08)]	0.589 / 0.12 = 4.9
Distance to Roads	[(0.2)(0.47)+(0.4)(0.24)+(0.8)(0.12)+(1)(0.09)+(1.2)(0.08)	0.478 / 0.09 = 11.28
Distance to Cities	[(0.17)(0.47)+(0.33)(0.24)+(0.67)(0.12)+(0.83)(0.09)+(1)(0.08)	0.392/ 0.08 = 4.9

5.6. Calculation of Lambda

(λ) (Average of Consistency vectors) = (total consistency vectors / n) ………………equation (3)
(λ) = (5.10 + 5.91 + 4.9 + 5.31 + 4.9) /5 = 5.22
λ should be equal or greater than the number of criteria under consideration. The value calculated above satisfies this condition.

b) Calculation of CI

CI = (λ-n) / n-1   ....equation (4)
CI = (5.22-5) / (5-1) = 0.22/4 = 0.055

Calculation of CR

CR = CI/RI ....equation (5)
RI = 1.12 for n =5
CR = 0.055 / 1.12 = 0.049

CR (= 0.049) <0.10 indicated a reasonable level of consistency in the pairwise

Comparison matrix used for the weight calculation.

5.7. Standardization of the Criteria Maps

Table 6: *Standardized Solar and Aspect Criteria Attributes*

Suitability Scale	Solar Radiation (WH/m2)	Aspect (Azimuth)
1	1,253,179 - 1,405,717	327.1 – 360 (North)
2	1,405,717 - 1,439,746	22.1 - 67 (North East)
3	1,439,746 - 1,458,059	67.1 – 112 (East)
4	1,458,059 - 1,469,622	292.1 – 337.5 (North West)
5	1,469,622 - 1,477,587	-
6	1,477,587 - 1,484,081	-
7	1,484,081 -1,491,258	247.1 – 292 (South West)
8	1,491,258 - 1,499,959	112.1 – 157 (South East)
9	1,499,959 - 1,512,557	247.1 - 292 (South West)
10	1,512,557 -1,564,258	157.1 - 202 (South)
10	-1 - 0	Flat lands

Table 7: Standardized Economic Criteria Attributes

Suitability Scale	Distance to Power lines (meters)	Distance to Main Roads (meters)	Distance to Urban Areas (meters)
0	0 - 300	0 - 500	0 - 3, 000
9	301 - 4,391	501 - 6,291	3001 - 7,881
8	4,392 - 6,586	6,292 - 9,437	7,882 - 11,821
7	6,587 - 8,781	9,438 – 12,583	11,822 -12,584
6	8,782 - 10,977	12,584 – 15,729	12,584 - 15,729
5	10,978 -13,172	15,730 – 18,874	15,730 – 18,874
4	13,173 -15,367	18,875 – 22,020	18,875 – 22,020
3	15,368 - 17,563	22,021 – 25,166	22,021 – 25,166
2	17,563 - 19,758	25,167 – 28,312	25,167 – 28,312
1	19,759 - 21,953	28,313 – 31,457	28,313 – 31,457

5.8. Weighted Overlay

The obtained spatial decision model is the result of crossing information from a series of layers regarding weather, environmental, topographic and location, as well as excluding some constraints (e.g. natural vegetation, cultivated land, urban areas), where a decision methodology (Multicriteria Evaluation and Analytical Hierarchy) has been followed. The suitability index map (of grid values ranging from 1-9) is shown in Figure 7. Large zones of high grid values 7, 8 and 9, mean that there are plenty of suitable areas to build photovoltaic power plants. The suitability map reflects the carrying capacity of the land for hosting solar energy farms. Excluded areas are not considered in this assessment as these are cultivated or urbanized lands. The result shows that large desert areas of highly suitable locations (8-9) are spatially distributed all over the image. Most suitable lands with large areas spread in the south-west bank of the Suez Canal. This is logic due to the nature of the flat desert lands which receives large numbers of sun hours and high level of global irradiation and its proximity to power lines, main roads and cities. In the Eastern bank of the Suez Canal, the same class exists in flat and gentle slopes lands with southern orientation (aspect) yet, with less areas due to low density of power transmission networks and main roads where most cities in the governorate are located in the western bank of the canal. The south eastern region of the study area receives high irradiation quantity. If the area is to be developed and the infrastructure improved in the future, the carrying capacity (suitability values) is expected to increase and more highly suitable areas would emerge in the eastern bank of the Suez Canal.
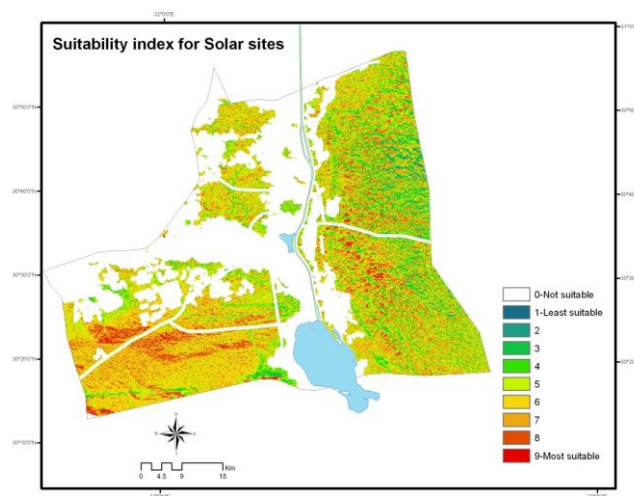

Figure 7: Suitability Index Map Result of the Weighted Overlay Model

5.9. Potential Sites for Solar Farms

Thirteen optimum locations for solar stations were selected from the suitability index (Figure 8). Details of such locations are shown in Table 8. Such locations fulfill the five model criteria in addition to the two selection criteria (the first is the suitability value and the second is the site area).

Table 8: Areas of Potential Sites for Solar Farms

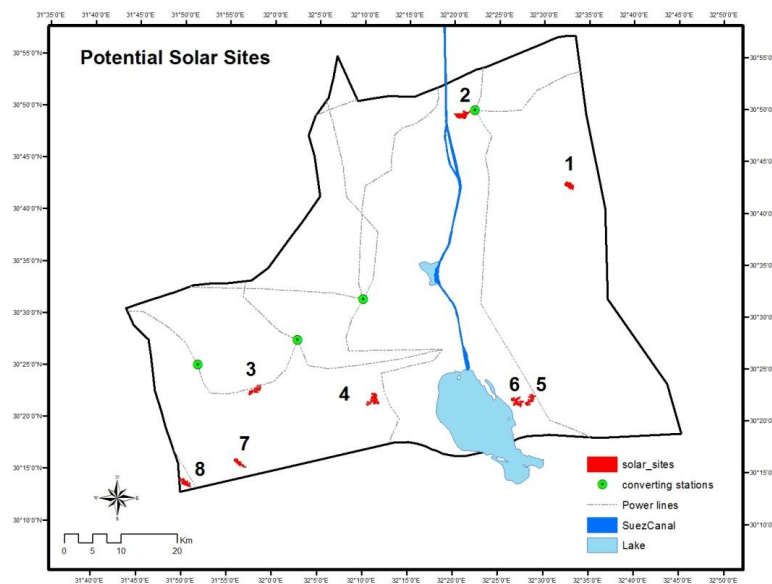| Site Numbers	Suitability Values	Area in Square Meters
1	7	1,130,242
2	7	1,974,183
3	7	1,184,334
4	8	1,913,135
5	7	1,240,840
6	7	1,485,743
7	8	1,012,124
8	8	1,191,839

Figure 8: Location of the Potential Sites for Solar Farms in Ismailia Governorate

6. Model Validation

Model validation was done to guarantee if the model offers reliable representations of the system it represented (Arán-Carrión et al., 2008). Validation was done as follows:

   a) The landcover classification image was verified by checking the accuracy of the pixels using a high resolution image.
   b) Visual comparisons were performed between the resulting suitability index values and the highest values in the criteria images.
   c) Selected optimum sites locations were overlaid on a high resolution image to verify the location has no constraints.

7. Conclusion

1) The selection of suitable sites for solar energy farms in Ismailia Governorate is based on a number of interrelated factors of geography, climate and land use-land cover. For studying such factors, remote sensing (SPOT-4 and SRTM) and GIS techniques were used and a Spatial Multicriteria Evaluation (SMCE) model was designed.

2) Integration of the interpreted data obtained from a series of layers regarding environmental and topographic features and land cover resulted in developing a spatial decision model. The study produced a suitability index map with plenty of suitable zones to construct grid-connected photovoltaic power plants. This is mainly because the Ismaila Governorate has almost flat and gentle slopes topography, and enjoys most sun radiation hours in a year period.

3) It is concluded that Spatial Multicriteria evaluation analysis managed to solve the site selection problem and fulfill the objective of the study. It considered the most effective criteria, i.e. climate and orography, and their relative importance in the decision making. Such decisions support tool studied need more attention from both researchers and decision makers.

References

Arran-Carrion J., et al. *Environmental Decision-Support Systems for Evaluating the Carrying Capacity of Land Areas: Optimal Site Selection for Grid-Connected Photovoltaic Power Plants*. Renewable and Sustainable Energy Reviews. 2007. 12; 2358-2380.

Aly M.H., et al. *Suitability Assessment for New Minia City, Egypt: A GIS Approach to Engineering Geology,* Environment and Engineering Geoscience. 2005. 3; 259-269.

Aydin N.Y., et al. *GIS-Based Environmental Assessment of Wind Energy Systems for Spatial Planning: A Case Study from Western Turkey.* Renewable and Sustainable Energy Reviews. 2010.14; 364–373.

Cerreta M., et al. *Urbanization Suitability Maps: A Dynamic Spatial Decision Support System for Sustainable Land Use.* Earth System Dynamics. 2012. 3; 157–171.

National Centre for Space Studies (CNES), SPOT Image, Toulouse, France, 1998: SPOT 4 Image. http://www.astrium-geo.com/

Eastman, J.R., et al. *Raster Procedures for Multi-Criteria/Multi-Objective Decisions.* Photogrammetric Engineering & Remote Sensing. 1995. 61 (5) 539-547.

Egyptian Meteorological Authority, 1996: *The Climate Atlas of Egypt.* Egyptian Meteorological Authority, Cairo, Egypt.

ESRI, 1996: *Working with the ArcView Spatial Analyst.* Environmental Systems Research Institute, Inc., Redlands, California, USA.

Fu P., et al., 2000: *The Solar Analyst 1.0 Manual.* Helios Environmental Modeling Institute (HEMI), USA.

General Organization for Physical Planning, 2007: *The Environmental Vision of the Strategy of Urban Development in Egypt.* Online Published Report. GOPP, Cairo, Egypt.

Hofierka J., et al. *Spatially Distributed Assessment of Solar Resources for Energy Applications in Slovakia*. Acta Facultatis Studiorum Humanitatis et Naturae Universitatis Prešoviensis. Prírodné vedy, Folia Geographica. 2008. 12; 97-114.

Janssen, R., et al., 1990: *Multi-Criteria Analysis and Geographical Information Systems: An Application to Agricultural Land Use in the Netherlands*. Geographical Information Systems for Urban and Regional Planning. Kluwer Academic Publisher, the Netherlands, 129-139.

Jankowski P. *Integrating Geographical Information Systems and Multiple Criteria Decision Making Methods.* International Journal of Geographic Information Science. 1995. 9; 251-273.

Jiang, J., 2007: *Analysis of the Suitable and Low-Cost Sites for Industrial Land Using Multi Criteria Evaluation: A Case of Panzhihua, China*. Master's of Science Thesis in Geoinformatics. School of Architecture and the Built Environment Royal Institute of Technology, Stockholm, Sweden.

Janke J.R. *Multicriteria GIS Modeling of Wind and Solar Farms in Colorado*, Renewable Energy. 2010. 35; 2228-2234.

Mohammad, A.M., et al. *Integrating GIS and AHP for Land Suitability Analysis for Urban Development in a Secondary City of Bangladesh*. J. Alam Bina. 2006. 8; 1-19.

Military Survey Department, 1995: *The Topographic Map of Egypt, Scale 1:25,000*. Cairo, Egypt.

Rich P.M., 1990: *Characterizing Plant Canopies with Hemispherical Photographs. In: N.S. Goel and J.M. Norman (Eds*), Instrumentation for Studying Vegetation Canopies for Remote Sensing In Optical And Thermal Infrared Regions. Harwood Academic Publishers, Newark, New Jersey, United State, 360

Rich P.M., et al. 1994: *Using View Shed Models to Calculate Intercepted Solar Radiation: Applications In Ecology.* American Society for Photogrammetry and Remote Sensing Technical Papers, 524-529.

Saaty T. *A Scaling Method for Priorities in Hierarchical Structures*. Journal of Mathematical Psychology. 1997. 15; 234-281.

Saaty T.A., 1992: *Decision-Making for Leaders*. 2nd Ed. RWS Publication, Pittsburgh, USA.
United States Geological Survey (USGS), *Shutle Radar Topography Mission*.
http://seamless.usgs.gov

Short Communication   **Open Access**

Structural Evolution of Mainpat Plateau, Surguja District, Central India

S.H. Adil[1], V.N. Patel[1], R.K. Trivedi[1], S.K. Gupta[1] and R.B. Golekar[2]

[1]Department of Applied Geology, Dr. H.S. Gour Central University, Sagar, Madhya Pradesh, India
[2]Department of Applied Geology, North Maharashtra University, Jalgaon, Maharashtra, India

Correspondence should be addressed to S.H. Adil, adilsh@rediffmail.com

Abstract The Mainpat Plateau falls in Surguja district in Chhattisgarh state, India. It is located in Survey of India toposheet numbers 64 N/1, N/5 and N/6 lying between longitudes E83°08' to 83°25' and latitudes N22°41' to 22°55'. General elevation of the Plateau is around 1060 m msl. The Mainpat Plateau as a whole is a mesa landform; rising more than 450 m high from the foothills, and consisting of Archaeans (granite-gneisses, phyllite, etc.), Gondwanas and Deccan basalt. Archaeans found at the foothills are overlain by the Gondwanas at the western escarpment, and covered by basalt at the top. The Central Indian Craton (CIC) has four major NE-SW trending major lineaments. In which northern most lineament separates Bundelkhand granite and Vindhyan basin. In the south of this lineament another one major lineaments separates Vindhyans with Gondwanas. In further south major shear zone marked by lineament passing through Mainpat plateau. A lineament followed by Son and Tapti valley lies in the south of study area. Different parts (plateaus) of Surguja area belong to the Central Indian Craton (CIC). CIC is bounded by folded belts: (i) Raigarh folded belt to the east (ii) Delhi folded belt to the west (iii) Indogangetic plain to the north and (iv) Eastern Ghat Mobile Belt to the south.
Keywords *Deccan Traps, Maipat Plateau, Structural Evolution, Surguja District India*

1. Introduction

The area of study Mainpat Plateau falls in Surguja district in Chhattisgarh state, India. It is located in the Survey of India toposheet numbers 64 N/1, N/5 and N/6 lying between longitudes E83°08' to 83°25' and latitudes N22°41' to 22°55'. The plateau is located about 45 km SSE of Ambikapur, the District Headquarter of the Surguja. The area is conveniently approachable in all seasons by well connected by road, from the District Headquarter (45 km) and that reaches up to the top of the plateau. The nearest rail head is Bishrampur (SE Railway) situated at a distance of 65 km from the study area and nearest airports is Raipur (Chhattisgarh) and Ranchi (Jharkhand). Sitapur is the main townships and subdistrict headquarters 28 km from the study area.

The study area is occupied by Mainpat plateau which is covered by Deccan Traps. The average height of the plateau is 1080 m and maximum height is 1165 m above MSL at Parpatia village on Mainpat in the western side of the plateau. The top of the whole plateau is covered by laterite and bauxite. Laterite and bauxite is the residual product of extreme chemical weathering of preexisting aluminous rocks under favorable geomorphic, climatic and hydrogeological conditions. On Mainpat plateau, the basalts of Deccan volcanism are the rock which had undergone chemical weathering. Mobility of an element is a function of solubility, supportive phenomenon and translocation (Dennen *et al.*, 1977). The highly mobile and soluble constituents like Si, Mg, Ca, Na and K are leached out from basalt and least mobile chemical constituents like Al, Fe and Ti remain in place. This geochemical processes of lateritisaton and bauxitisation can be summarized as a selective mobilization, leaching and partial re-precipitation going hand in hand with hydration of the elements that remain in the weathering profile. It is, therefore, quite essential to study the geochemistry of parent rock and residue in respect of major and trace elements which will ultimately lead to understanding the process of lateritisaton/bauxitisation in that particular area (Figure 1). The plateau has a dendritic drainage pattern of its streams because of the undulating flat nature of plateau top. Otherwise it is showing a radial drainage pattern from its slopes.
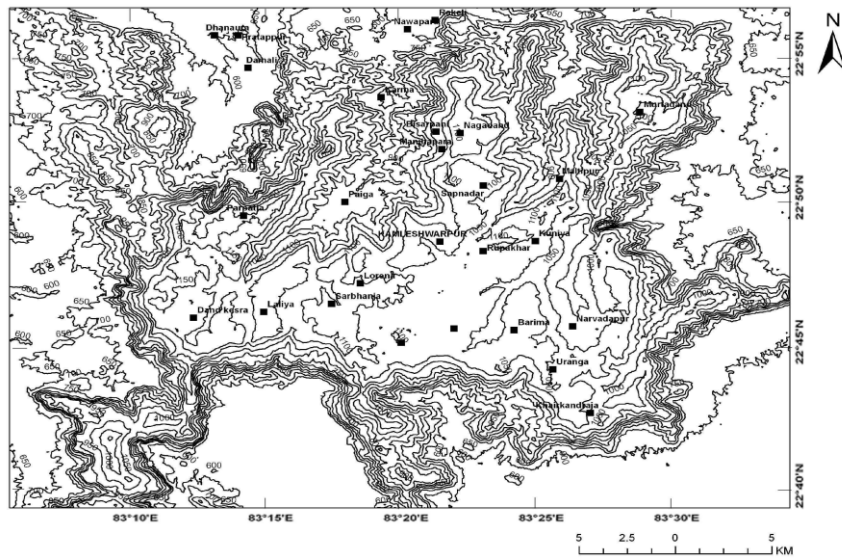

Figure 1: Contour Map of Around Mainpat Plateau, Surguja District

2. Regional Geology

Regionally, the area comprises predominantly the rocks of Precambrian and Gondwana Supergroup. The Metasedimentary rocks (Sausar Group) are characterized by pilots, quartzite, chlorite schist, quartz chlorite schist, quartz sericite schist and intra-formational conglomerate etc. The entire succession is equivalent to Sausar Group. The phyllite and schist sequence is occasionally intruded by amphibolite/dolerite dykes. In the area rocks occurring in and around Lakshmanpur belong to the Surguja metamorphic belt, which is the western extension of the Chhotanagpur Gneissic Complex (Majumdar, 1998). In contrast to the Sausar group of rocks, these metamorphoses comprise quartzites, schist, crystalline carbonate and Calc silicate rocks older metamorphic; metagreywacke, conglomerate, phyllite and amphibolite (Mulay, 1968) of Precambrian age (Figure 2). These are followed by granitoids comprising genesis complex and granites. The gneissic complex includes biotite gneiss, porphyritic microcline biotite gneiss, albite-oligoclase gneiss and hornblende gneiss. Granite and granodiorite occur as small plutons intruding the gneissic meta-sediments (Mulay, 1968). Pegmatite, aplite and quartz veins occur within the above rocks. The metamorphites and granitoids are overlain by lower Gondwana sequence.

The Gondwana Super Group rocks rest uncomfortably over the metamorphites and granites (Table 1).

Table 1: Stratigraphic Succession of the Study Area

| Period	Supergroup/ Group	Litho-Units
Recent to Sub-Recent		Alluvial soil, Laterite and Bauxite
Upper Cretaceous to Lower Paleocene	Deccan Trap	Basaltic flows
Cretaceous	Lameta	Earthy Greenish to White Sandstone
upper Carboniferous to Lower Cretaceous	Barakar	Coarse grained sandstone with Coal Seams, Fine grained sandstone, siltstone, green Shale
	Talchir	
Middle to upper Carboniferous	Gondwana	Conglomerate, sandstone
Precambrian	Chhattisgarh	Granite-gneiss, phyllite, quartzite etc.
Archaean	Basement	Granite/Gneiss, Phyllite, Quartzite, Acid and Basic intrusions
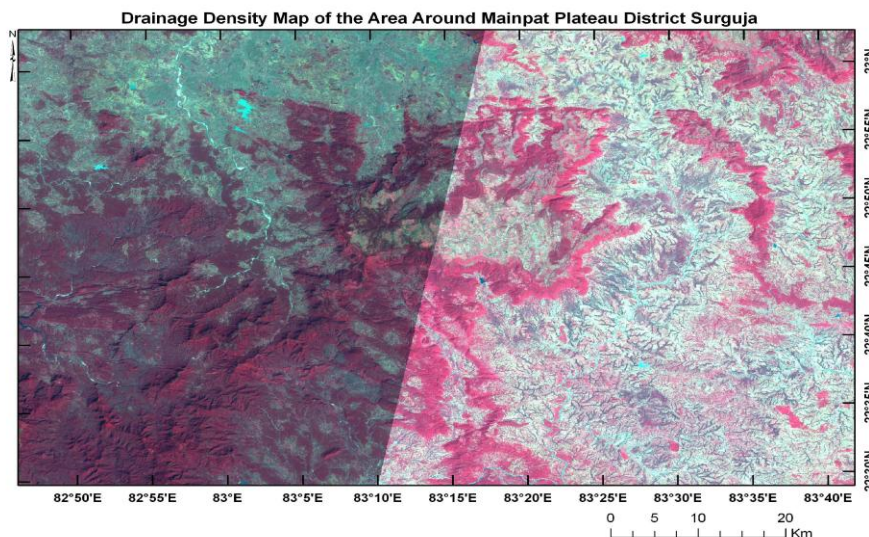
Figure 2: Drainage Density Map of Around Manipat Plateau, Surguja District

3. Lineament Pattern

Different pats (plateaus) of Surguja area belong to the Central Indian Craton. The Mainpat plateaus area also belong to the Central Indian Craton is bounded by folded belts: (i) Raigarh folded belt to the east (ii) Delhi folded belt to the west (iii) Indogangetic plain to the north, and (iv) Eastern Ghat Mobile Belt to the south. Stratigraphically, Central Indian Craton (CIC) consists of older granitic and/or gneiss complex, mid- to neo- Proterozoic sedimentary sequences, Paleozoic to Mesozoic sedimentary sequences and younger basaltic flows. Bauxitic/lateritic plateaus of Surguja area developed over Deccan trap basalt, which conformably overlies on Gondwana sequence. Talchir boulder bed marks the older-most unit of Gondwana sequence which uncomfortably rest on older granites. The regional geotectonic units include lower Proterozoic Chhotanagpur Gneissic Complex (CGC) and metasediments of Gangpur Group of rocks in north-central part, the middle-upper Proterozoic rock of Chhattisgarh Supergroup in the southern part, lower Gondwanas along NW- E trending and Lameta-Deccan Traps in northern western part (Figure 3).
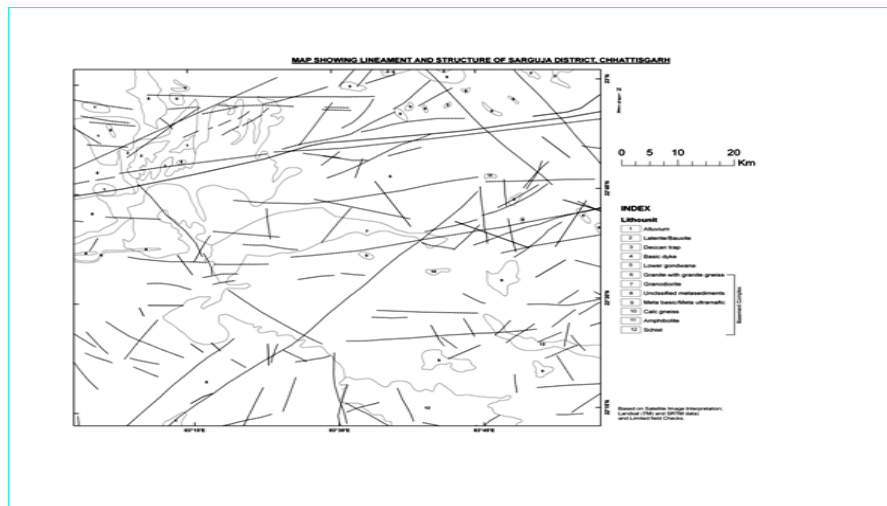
Figure 3: Lineament and Structural Map of Surguja District in Chhattisgarh, India

4. Structural Setup

The Central Indian Craton (CIC) has four major NE-SW trending major lineaments. In which northern most lineament separates Bundelkhand granite and Vindhyan basin. In the south of this lineament another one major lineaments separates Vindhyans with Gondwanas. In further south major shear zone marked by lineament passing through Mainpat plateau. A lineament followed by Son and Tapti valley lies in the south of the study area.

Major structural elements include the Tapti lineament and related fractures and shear (Tanshear) passing through the northern part of the area. Major lineaments are trending in E-W direction; NE-SW and NW-SE trending lineaments were also observed. Major shear zones between 22°20'-22°40' latitudes are associated mineralization in the area. The western part of the Tapti Lineament zone is thoroughly studied with a field check along lineament, fault and fractures (Mishra *et al*., 2008).

However, basic rocks are seen in the NE of Bandana, north of Bagicha, east of Kuramkela, north of Retva, north-west of Poprenga, east of Tatkela, east and south of Batuali, north-west of Saraswatipur, north of Phuldih and east of Nankana village. Mainpat Plateau is tectonically uplifted about 450 m from the general ground level. The general elevation of the Plateau is around 1060 m msl. The Mainpat Plateau as a whole is a mesa landform, rising more than 450 m high from the foothills.

5. Conclusion

Based on an aerial photo and satellite image interpretation, four major lineament trends are identified in the area i.e. N - S, E - W, NNW - SSE and NE - SW.

Acknowledgments

References

Dennen W.H., et al. *Geology and Geochemistry of Bauxite Deposits in the Lower Amazon Basin.* Econ. Geol.1977. 72; 82-89.

Mazumder S.K., 1998: Geology of the Chhotanagpur Gneissic Complex – A perspective, in M. S. Krishnan Birth Cent. Sem., Geological Survey of India, 112-114.

Mulay V.V., 1968: Geology in Parts of Kusmi and Ambikapur Tehsils, Surguja District, M.P. Unpub. Pro. Rep. GSI, FS.

Mishra B.K., 2008: Regional Search for Lamproite/ Kimberlite in Tapti Lineament Zone in Raigarh, Jashpur and Surguja Districts of C.G., Unpub. Rep. Geol. Surv. Ind., F.S.

Research Article   **Open Access**

Water Management Problems Associated with Urban Sprawl in Gharbia Governorate, Egypt Using Remote Sensing and GIS

Salwa F. Elbeih[1], Adel A. Shalaby[2] and Ahmed M. Bahy El Deen[1]

[1]Engineering Applications and Water Division, National Authority for Remote Sensing and Space Sciences (NARSS), Egypt
[2]Environmental Studies and Landuse Division, National Authority for Remote Sensing and Space Sciences (NARSS), Egypt

Correspondence should be addressed to Salwa F. Elbeih, saelbeih@narss.sci.eg, saelbeih@gmail.com

Abstract Urban sprawl is one of the major problems that evolved in the Nile Delta as a result of the deficiency in the security system after the 25th of January revolution in Egypt in 2011. This problem not only threatens the limited fertile lands but also influences the water distribution regime in these areas. For this purpose, three types of satellite images were employed; i.e. Landsat Thematic Mapper (TM) 1990, Egyptsat-1 2010 and SPOT 5–2011, to study the urban sprawl and its impact on the agricultural land and water distribution management in Gharbia Governorate. Maximum likelihood supervised classification and post classification change detection techniques were applied for monitoring the urban sprawl in this study area. The accuracy of the classification results was assessed using a 1992 topographic map. Using ancillary data, visual interpretation and expert knowledge of this area through GIS further refined the classification results. Combining the soil and land capability maps, on one hand, and the urban thematic layers, on the other hand, using GIS, made it possible to point out the risk of urban expansion on the expense of the highly capability class. During the period of (1990–2011), the highly capable soils decreased from 1710.75 km^2 in 1990 to 1610.22 km^2 in 2011. A total of 1.5 km^2 of urban areas was recently constructed after 2010 inside the 500 m buffer zone around the (10–25 m) width canals. A water management index is calculated which decreased as a result of the urban sprawl on a 500 m buffer zone around the irrigation canals.

Keywords *Gharbia, Urban Sprawl, Water Management, Remote Sensing, GIS*

1. Introduction

In one of their most recent reports, the United Nations Population Division projects the world population to reach 9.3 billion persons by 2050, that is, 2.3 billion more than in 2011. In the same report, the population of Egypt is expected to reach 100,909 million for the year 2025 and 123,452 million for 2050 (United Nations, 2011). According to the population clock device, the number of

Egypt's population at home arrived 84 million people at the first of March 2013 (Al-Ahram Gate, 2013).

Desert and uninhabited lands represent about 95% of the total area of Egypt. However, the majority of the population is concentrated around the River Nile. This unbalanced distribution causes serious social and economic problems. Accurate and up-to-date land cover change information and irrigation distribution networks are necessary to understand both human causes and environmental consequences of such changes. Therefore, determining the trend and the rate of land cover conversion and water distribution are necessary for the development planner in order to establish rational land use policy.

Urban Sprawl is an unplanned outgrowth which may have negative impacts on the land resources and economy. It can be defined as the scattering of new development areas on isolated tracts, separated from other areas by vacant land (Ottensmann, 1977). Over a specific geographic area, water-efficient land development can save significant quantities of water while less efficient land development sprawl often results in wasteful use. Urban sprawl clearly affects water consumption.

Urban sprawl on the agricultural lands is one of the negative outcomes that happened due to lack of the security regime during and after the Egyptian revolution that began on the 25th of January 2011. During the 18 days of the revolution thousands of feddans of highly fertile and cultivated lands were illegally converted to built-up areas. During this period, monitoring reports, issued by the Directorate of Land Protection Department of Agriculture in Gharbia Governorate Egypt, showed high evidence of urban encroachment on the agricultural centers. This urban encroachment was more than 12,000 cases during the period from 25th of January to 31st of March 2011. This phenomenon is very obvious in Gharbia Governorate and according to this report; Zifta center was ranked as the first followed by Santa and Qotour (Ahram Masaii, 2011).

This practice will not only decrease the areas of the fertile lands but will also decrease Egypt's exports from vegetables and fruits and hence add a lot of burden on the Egyptian economy. In addition, building on some agricultural lands will hinder the fair water distribution to the rest of the agricultural lands due to the presence of a concrete obstacle in the path of the water way to the neighboring lands. One of the negative outcomes of building on cultivated lands is that the area negatively influenced by this built-up area is 4 to 6 times the area of the actual area of the building. That is because the building forms a shadow around it which is reflected on the productivity of the cultivated plants. Also this unofficial building represents a stealing to the government properties in part of the road and land and hence influences the safety of the inhabitants.

According to (Belal and Moghanm, 2011), the main type of human induced land degradation in Gharbia Governorate is urbanization during the period from 1972 to 2005. In the year 2005, extra urbanized area covered 5639.57 feddans as 7.15% of the total area, while the cultivated area decreased by 5659.4 feddans as 7.17 % of the total area (Belal and Moghanm, 2011). In Qalubiya Governorate, a considerable increase in urban settlements has taken place at the expense of the most fertile land. The built-up areas in the governorate increased from 89.96 km^2 in the year 1992 to 124.54 km^2 in 2001 and to 241.86 km^2 in the year 2009. During the study period the total urban area increased by 151.9 km^2 with a rate of 8.9 km^2 per year (Shalaby et al., 2011).

Gharbia Governorate represents the highest in the urban sprawl on the agricultural lands but at the same time the least in the number of buildings failure. That is attributed to the family nature of these buildings (that is not for investment purposes) and the less number of floors compared to other main governorates according to H. Allam (Personal communication).

The temporal dynamics of remote sensing data can play an important role in monitoring and analyzing land cover and land use changes. Supervised classification and post-classification change detection techniques will be applied to map land cover and land use changes in the study area. The objectives of this study are to: investigate the urban sprawl and its impact on agricultural land through integrating remote sensing and GIS, and study the negative impacts of these new buildings on the water distribution system to the neighboring lands. These two objectives mainly focus on the conditions after the 25th of January revolution in Gharbia Governorate.

2. Study Area

Gharbia Governorate is chosen for investigation due to the availability of some governmental information and reports on the urban sprawl over the agricultural lands during the 25th of January revolution in 2011. Gharbia Governorate is located between latitudes 30°45′ and 31°18′ East and longitudes 30°34′ and 31°09′ North in the middle of the Nile Delta between Damietta and Rosetta branches, (Figure 1). The total area of Gharbia Governorate is 1951.1 km², 82 % of which are cultivated lands (CAPMUS 2012). The population of Gharbia was 4.09 million inhabitants in 2007 (IDSC 2009). The governorate is subdivided into eight administrative districts: Tanta, El-Mahala El-Kobra, Zefta, Kafr El Zayat, Alsanta, Samanoud, Kotor and Basioun (Figure 1). The main economic activity in the governorate is cultivation in addition to textile, oil and soap industries. Tanta (the capital of the governorate) and El–Mahalla El–Kobra (the main center for textile industry) are taken as two examples for the land cover / land use and water management studies in this research.

Gharbia Governorate is characterized by the climate of the Mediterranean Sea with hot arid summer and little rainy winter. The mean temperatures are especially high in the dry season where they range between 24° and 31°C with an average temperature of 22°C and the difference between the average temperature in summer and winter is 6°C (Climatological Normal for Egypt, 2011). Based on the USDA (2010), the soil temperature regime of the studied area is defined as Thermic and soil moisture regime as Torric.

The main irrigation canals in the governorate are: Bahr Shibin, Tirat Al – Bajuriyyah, Tirat Al – Qasid, Tirat Al – Jafariyyah, Bahr Nashart, Tirat Al – Atf, Tirat As – Sahil, Tirat Al – Ninaiyyah, Ar - Rayyah Al – Abbasi and Al - Rayyah Al – Menoufi. The irrigation canals of more than 25 m width exhibit a total length of 212.8 km, while those of 10-25 m width attain a total length of 350.7 km.

Concerning the dominant geologic units, the Quaternary Nile Silt is the dominant unit in the whole governorate.

Only two sub-great soil groups exist in Gharbia Governorate (i.e. Vertic Torrifluvents and Typic Torrifluvents). Most of the governorate soils are exhibited by the Vertic Torrifluvents sub-great group that have cracks and slickensides or wedge-shaped aggregates, as they cover an area of 1889.1 km^2 representing 96.9% of arable land. The Typic Torrifluvents sub-great group covers 60.6 km^2, representing 3.1% of the soils aligned along the eastern and western borders of the governorate.

3. Materials and Methods

3.1. Data Sets

The materials used in this research are:

- Three Egyptsat-1 images acquired on the 31st of May and 2nd of July 2010;
- Two SPOT 5 images (Path 110-111/Row 288) acquired on the 16th and 17th of March 2011;
- Two Landsat TM images (Path 176-177/Row 39) acquired in 1990;

- Soil map of Egypt (1982) scale 1:100,000;
- Topographic maps (1992) scale 1: 50,000;
- The detailed irrigation network of the governorate obtained from the 1992 topographic map;
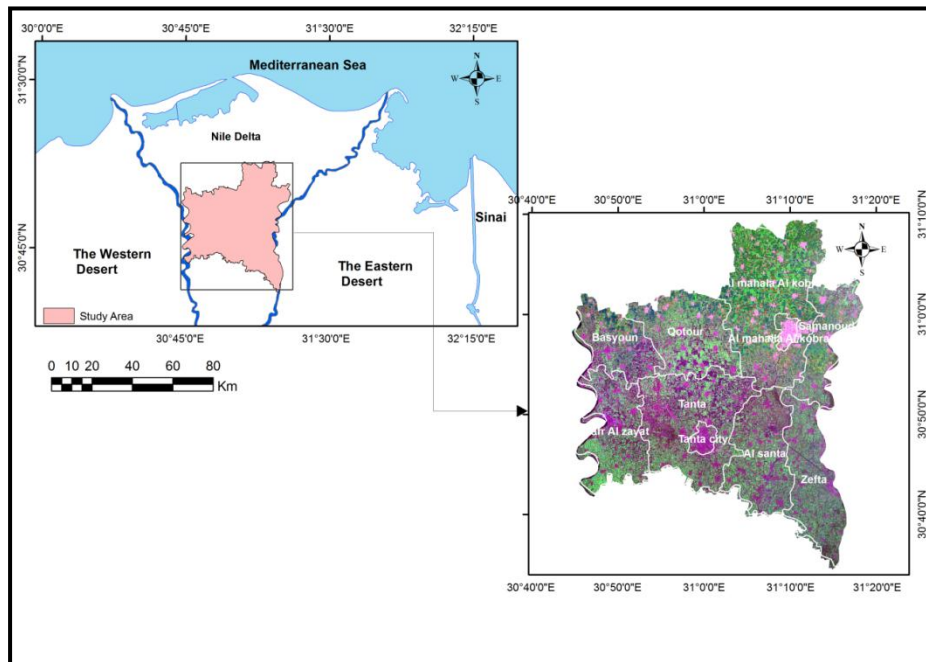- The 2012 administrative boundary of Gharbia Governorate.

Figure 1: *Location Map of the Gharbia Governorate on Egypt Map (left), Landsat ETM+ Image of Gharbia Governorate (FCC 1, 2, 3) to the Right*

Table 1 shows the specifications and details of the used satellite images.

Table 1: *Specifications of Landsat TM, Egyptsat-1 and SPOT 5 Images*

Band	Spatial Resolution (m)			Spectral Resolution (μm)		
	Landsat TM	Egyptsat-1	SPOT 5	Landsat TM	Egyptsat-1	SPOT 5
1	30	7.8	2.5	0.45 – 0.52	0.51-0.59	0.51-0.73
2	30	7.8	10	0.52 – 0.60	0.61-0.68	0.5–0.59
3	30	7.8	10	0.63 – 0.69	0.80-0.89	0.61–0.68
4	30	7.8	10	0.76 – 0.90	0.50-0.89	0.79–0.89
5	30	39.5		1.55 to 1.75	1.1-1.70	
6	120			10.40 to 12.5		
7	30			2.09 to 2.35		

These satellite images were used to calculate the changes in the urban areas that occurred between the years 1990 and 2011. The two consecutive dates of 2010 and 2011, where chosen based on several governmental reports after the 25th of January 2011 revolution emphasizing the presence of severe urban encroachments on the fertile lands in the governorate.

3.2. Methodology

The methodology applied in the present study is composed of the following steps: (1) conversion of raster data to vector format, (2) generation of thematic layers, (3) supervised image classification, (4) production of digital soil maps, (5) urban sprawl detection and (6) creation of buffer area around irrigation canals.

3.2.1. Conversion of Data to a Vector Format

Topographic maps and soil maps were converted to a vector format by digitization of the existing hard copy maps into the required classes compatible with the present study objectives.

3.2.2. Generation of the Thematic Layers

Generation of the thematic layers of information involves digital image processing of remote sensing data and further processing of existing maps for extraction of the required information.

- Various standard digital processing image processing techniques have been adapted to the three image sets (Table 1). These processes are applied to enhance the information in the images and to facilitate the extraction of information and involve:

a. Geometric correction of each image using a shape file that includes the main intersecting linear features in the images.
b. Contrast stretching of individual bands to improve the interpretability of different features
c. Generating a False color composite (FCC): bands (3, 4, 7) for Landsat TM, bands (1, 2, 3) for Egyptsat-1 and bands (2, 3, 4) for SPOT 5. This process highlights the land use, vegetation cover, soil types and irrigation network.
d. SPOT 5 2.5 m resolution image obtained from the fusion of the 2.5 m panchromatic image and the three 10 m multispectral images.
e. The two Landsat TM images have been mosaiced and a subset of the governorate has been obtained. The subset of Landsat TM (bands 3, 4, 5) was further rectified to a UTM map projection using image to image registration method and was resembled to a pixel size of 10 m, using nearest neighborhood.

3.2.3. Creation of Urban Areas Thematic Layer

That is the backbone for this research; that is the creation of urban areas thematic layer using the supervised image classification technique. A thematic map shows the spatial distribution of identifiable earth surface features where it provides an informational description over a given area rather than a data description (Schowengerdt, 2007). This step involves the following secondary steps:

- A number of target classes required to be delineated from the scene must be put in mind. Such a set is called a classification scheme (or a classification system).
- Training the classifier: In order to classify an image into categories of interest, the classification algorithm needs to be trained to distinguish those categories from each other. Representative category samples known as training samples are used for this purpose. After the classifier is trained to recognize the different categories, the "rules" that were developed during training are used to label all pixels in the image as one or more of the training categories. In this research, the training of a classification algorithm is supervised in which the prototype pixel samples are already labeled by virtue of ground truth, existing maps or photo interpretation (Schowengerdt, 2007). From the training samples, three signatures are obtained from the whole scene; urban areas, cultivated lands and water bodies. Table 2 shows the number of pixels assigned to each signature with its corresponding color.

Table 2: Signatures Names, Color and Count of Each Class

Class No.	Signature Name	Color	Count
1	Urban Areas		87
2	Cultivated lands		93
4	Water Bodies		17

- Next, was the supervised classification of each image based on the collected signatures into: urban areas, water bodies and, cultivated lands using Envi 4.8 software.
- Conversion of all raster data to a vector format using Envi 4.8.
- Post classification process involves:

a- Editing of the output urban features to match with the actual features in the study area. In other words, this step mainly depends on the visual interpretation by assigning each feature its correct class (urban-water-cultivated).

b- Topology building for the urban areas features for the years 2010 and 2011 with the two following rules:
  - Each feature of 2010 must be covered by a 2011 feature with an exception where an urban area or a building in 2010 is removed (exception).
  - Each urban area from each year must not intersect with another urban area from the same year.
  - The final thematic maps for the urban areas for the years: 1990, 2010 and 2011 were produced as shown in Figure 2.

c- Accuracy assessment using 100 points from existing land use maps. To increase the accuracy of land use classification, ancillary data and results of visual interpretation were integrated with the classification result using GIS.

3.2.4. Production of the Digital Soil Map

The soil map of the study area was extracted from the available soil map of Egypt produced by the Academy of Scientific Research and Technology (ASRT 1982). The original nomenclature of soil order, suborders and sub-great groups has been updated according to the latest American Soil Taxonomy of USDA (2010). The transformation of the soil map (produced in 1982) into a digital format was done. On-screen digitizing was used to convert hardcopy into vector formats ArcGIS 9.2.

3.2.5. Urban Sprawl Detection

The success of the change detection especially between the two close dates of 2010 and 2011 depends on both the amount and nature of change and success of the image preprocessing and classification procedure. If the nature of the change within a particular scene is either abrupt or at a scale appropriate to the imagery collected then change should be relatively easy to detect; problems occur only if spatial change is subtly distributed and hence not obvious within any image pixel (Milne 1988). In the case of the study area and its conditions with respect to the abrupt changes that happened during the 2011 revolution, changes in urban areas were easily detected. This urban sprawl between 1990 and 2011 was normal compared to that between 2010 and 2011.

3.2.6. Water Management

Based on the irrigation network of the governorate, canals are categorized according to their width; i.e. more than 25 m, 10 to 25 m and 5 to 10 m (Figure 3). This step was used for the evaluation of the water management and distribution in the study area.

The water distribution was negatively influenced by the unplanned (spontaneous) buildings especially in a buffer zone of a chosen distance of 500 m around the (10 to 25 m width) canals.
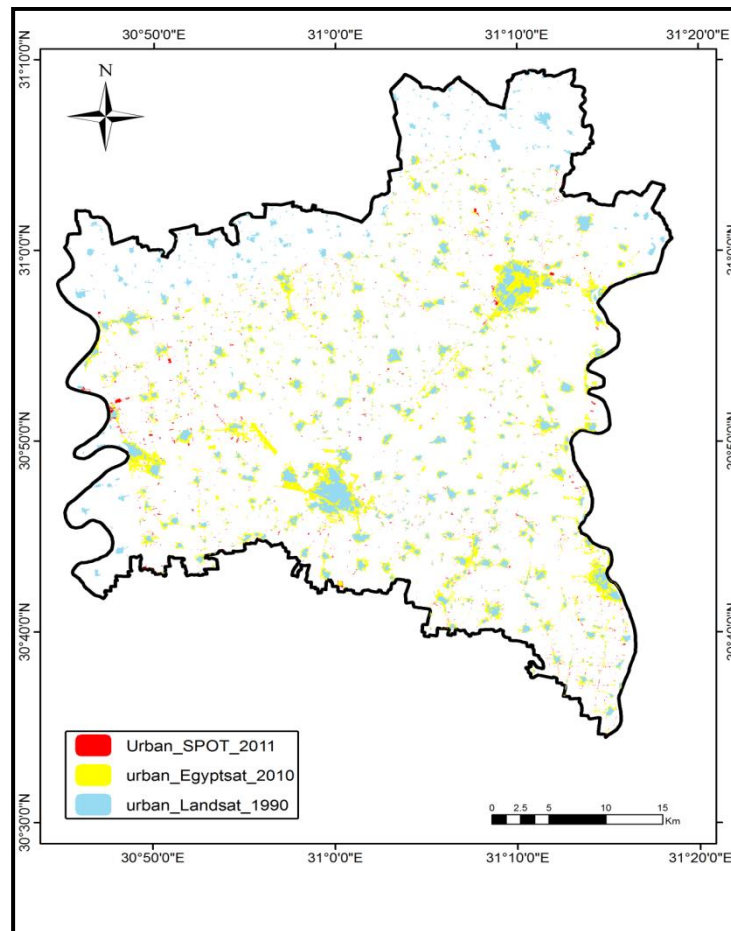

Figure 2: Urban Areas in 1990, 2010 and 2011 of Gharbia Governorate

4. Results and Discussion

4.1. Urban Sprawl

The population of Gharbia Governorate has increased from 3.93 million to 4.38 inhabitants between 2004 and 2011 at an annual rate of 75,593 inhabitants per year (CAPMUS 2012). From the present study, it was found that the total loss in arable land between 1990 and 2011 was 107.95 km^2 due to urbanization, that is, with a rate of 5.15 km^2 per year. With this rate of population growth it is expected that the population of the governorate will reach about 7336684.57 by the year 2050, consequently urban expansion may increase by about 200.05 km^2. To overcome this serious problem, the rate of population growth must be decreased and new urban areas must be established outside the Nile Delta to accommodate the expected population growth.

Change detection results between 1990 and 2011 showed that the built-up areas of the governorate increased from 102.67 km^2 in 1990 to 202.18 km^2 in May 2010 to 210.63 km^2 in March 2011 (Figure 2). During this period the total urban area increased by 107.95 km^2 with an average rate of 5.15 km^2/year (Table 3). Between May 2010 and March 2011 the increase in urban areas was 8.45 km^2/year (Figure 4) which is more than the yearly average rate and this could be due to the absence of security authorities during the 25th of January revolution.
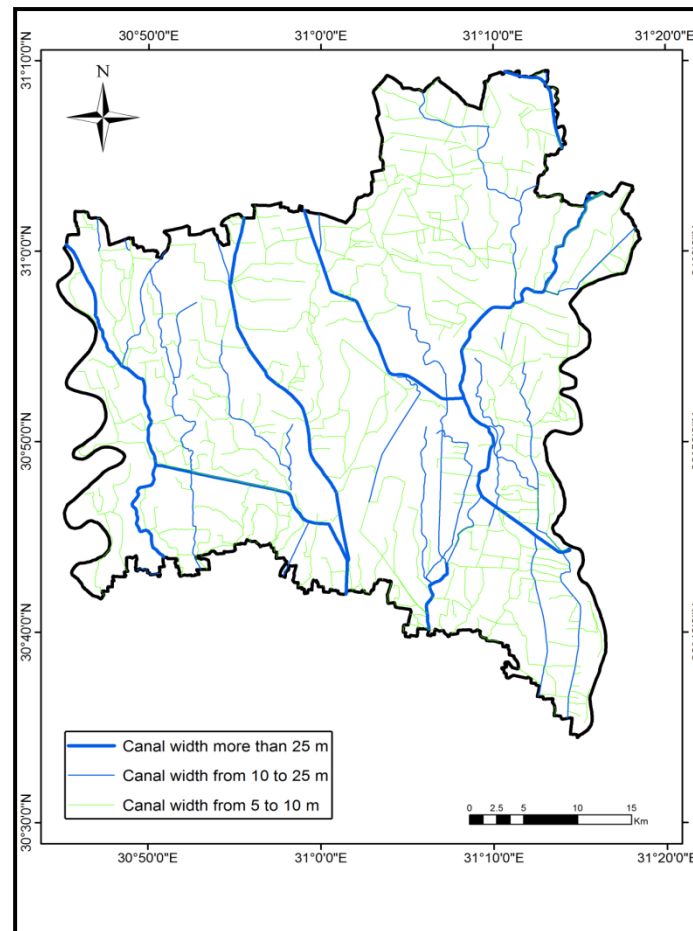
Figure 3: *The Irrigation Network of Gharbia Governorate*

According to a report published by the central directorate for land protection (Ministry of Agriculture and Land Reclamation) in April 2013, the number of encroachments on agricultural lands in Gharbia Governorate from 25/1/2011 to 1/4/2013 is 70752 cases with a total area 13.43 Km^2 that is about 6.2 Km^2/year. These cases are classified into simple (4.41 Km^2), medium (3.22 Km^2) and severe (4.56 Km^2) cases. From the 70752 cases, 4156 cases were removed with a total area of 1.22 Km^2 and the rest 66596 cases with a total area of (12.21 Km^2) still unremoved.

Districts most influenced by this increase are Al-Mahalla and Tanta which are the main economic districts in the governorate. Integrating remote sensing and GIS provided valuable opportunities for analysis of the output spatial data. In these two districts, during the period from 1990 to 2011, the total urban expansion was estimated to be 36.9 km^2 at a rate of 1.76 km^2/year (Table 4). Figure 5 shows the change in urban settlements in Mahalla and Tanta from 1990 to 2011.

4.2. Soil

The soil map of Gharbia Governorate demonstrates that only two sub-great groups are presented in the whole area. The *Vertic Torrifluvents* sub-great group dominates the soil types, covering an area of 1710.75 km^2 (87.7% of the governorate). The *Typic Torrifluvents* sub-great group covers limited patches within the alluvial landscape, exhibiting 109.57 km^2 (5.6%).
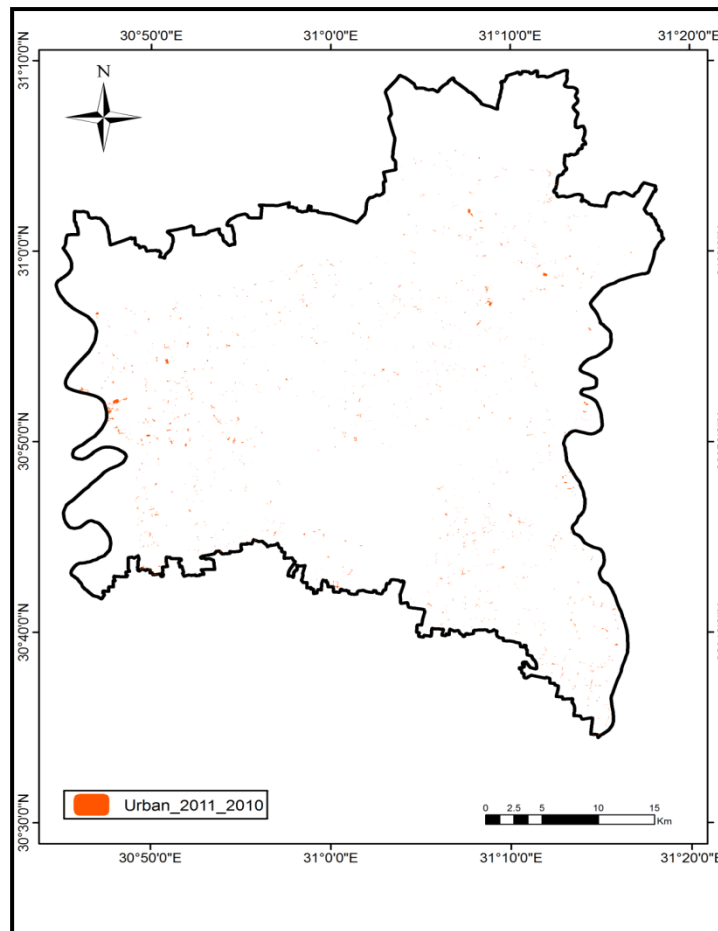
Figure 4: Difference in Urban Settlements between 2010 and 2011

The visual interpretation gave a general idea about the forms of land cover changes over the investigated period. Many urban areas were erected recently, especially near the main cities such as Al-Mahalla and Tanta, at the expense of the most fertile soils. The overlaying of the visual interpretation over the classification result led to the increase in the overall accuracies by about 10%. A standard overall accuracy for land cover and land use maps is set between 85% (Anderson et al., 1976) and 90% (Lins and Kleckner, 1996). In this study the overall classification accuracy was found to be 93% for 1990, 94.3% for 2010 and 96.4% for 2011. The differences in the accuracies of the classification of the three different images could be attributed to the specification of Landsat TM, Egyptsat-1 and SPOT 5 where the SPOT 5 images have the highest spatial resolution.

The urban areas are overlaid on top of the soil capability map to show the extent of urban areas on the expense of agricultural land (Figures 6 to 8).

Remote sensing data and GIS provide opportunities for integrated analysis of spatial data. Cross-tabulation performs image cross-tabulation in which the categories of one image are compared with those of a second image and tabulation is kept for the number of cells in each combination.

Urban sprawl between 1990 and 2011 was mapped and overlaid on the soil map of the study area (Figure 2). The statistical data about the spatial urban changes from 1990 to 2011 are illustrated in Tables 3 and 4 and Figure 9.
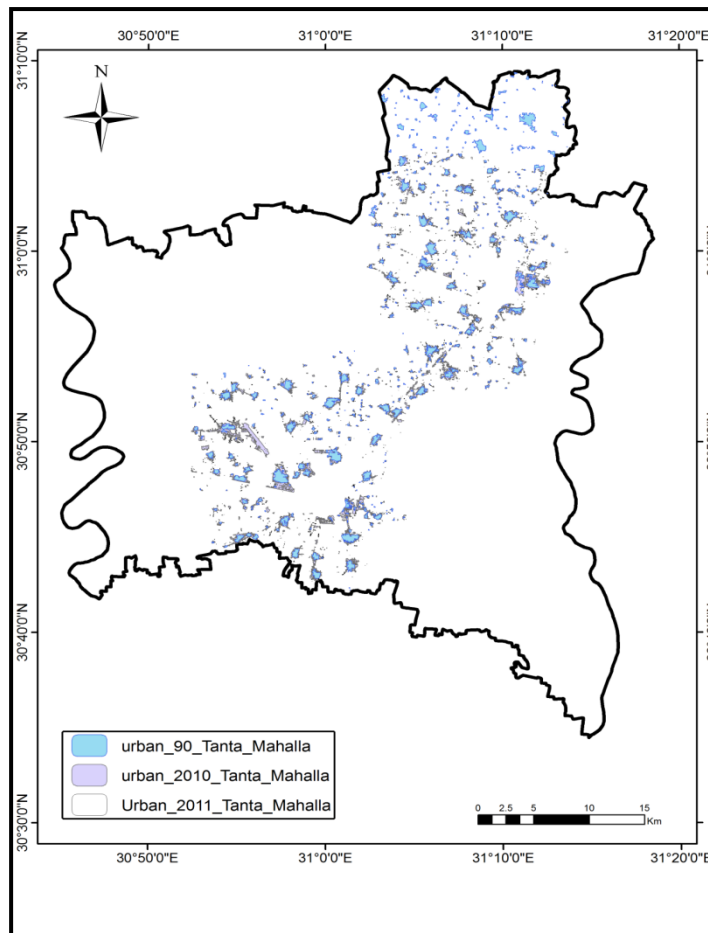
Figure 5: *Urban areas of Tanta and Mahalla between 1990 and 2011*

Table 3: *Urban Settlement Changes of Gharbia Governorate from 1990 to 2011, Areas in Km²*

Taxonomic Unit	1990	2010	2011	Changes between 1990 and 2010	Changes between 1990 and 2011	Changes between 2010 and 2011
Built Up Areas	102.67	202.18	210.63	99.50	107.95	8.45
Water	27.55	27.55	27.55	0.00	0.00	0.00
Vertic Torrifluvents	1710.76	1618.00	1610.22	-92.76	-100.53	-7.77
Typic Torrifluvents	109.5683	103.0557	102.3816	-6.51	-7.19	-0.67

Table 4: *Urban Settlement Changes of Tanta and Al-Mahalla Districts from 1990 to 2011, Areas in km²*

Taxonomic Unit	1990	2011	Change between 1990 and 2011
Built Up Areas	33.29	70.19	36.9
Vertic Torrifluvents	699.3	653.72	-45.58
Typic Torrifluvents	25.51	24.26	-1.25

In terms of land capability classification, the high capable soils (Class I), which are the best in nearly all respects for both agricultural production and nonagricultural uses, decreased from 1710.75 km^2 in 1990 to 1618.0 km^2 in 2010 and to 1610.22 km^2 in 2011. The moderate capable soils, that have some limitations that reduce the choice of plants or require moderate conservation practices, decreased from 109.57 km^2 in 1990 to 103.06 km^2 in 2010 and to 102.38 km^2 in 2011.

Urbanization had spread in the whole governorate especially near Al-Mahalla and Tanta. In these two districts, during the period 1990–2011, the total urban expansion was estimated to be 36.9 km^2, with most of this expansion being at the expense of the most fertile soil (Vertic Torrifluvents).

The existence of a law that forbids construction on agricultural land did not prevent the unplanned urban invasion over the fertile land. This kind of unplanned urban expansion has severe consequences causing many social and health problems. This is caused by inappropriate infrastructure including roads and sewage systems as well as clean water unavailability.

Fragmentation and dispersal of the agricultural land is a major characteristic of the Egyptian agriculture. Fragmentation indicates a small size of the production unit. Dispersal means the distribution of holding into scattered plots within the same village or in other villages within the same district. (Kruseman and Vullings, 2007) reported that more than 80% of the landholdings in Egypt are currently less than six acres and it is expected to be less than four acres by 2025. Fragmentation and dispersal of landholdings are caused by overpopulation and the system of inheritance with a relatively constant area of the agricultural land which lead to a sequential partition of the land. Fragmentation and dispersal of the agricultural landholding have a negative impact on the rate of growth in the agricultural sector. This is evident by the difficulty in implementing modern agricultural techniques leading to the high cost of agronomic practices and the low efficiency of agricultural labour (Farah, 1967). Therefore, fragmentation led to the loss in the cultivable land due to the fact that part of it is used for building, irrigation, drainage and passages around and inside small holdings. Land fragmentation affects the land ownership where there is a loss of about 20% of land use in irrigation canals and partition between the farms (Kruseman and Vullings, 2007). Fragmentation of the farm size reduces the potential financial returns and increases the value of land for non-agriculture purposes.

4.3. Water Management and Irrigation

Surface water management in the governorate and how it is negatively influenced by the urban sprawl especially after the 2011 revolution is studied. A buffer zone of 500 m was chosen around the secondary canals (10–25 m width). This buffer distance was chosen for studying how the buildings in this buffer area will represent an obstacle for water to reach the distant lands. Examples of these canals are: Tirat Umar, Tirat Shirshabah, Tirat Manyal At–Tawil, Tirat Bahr Sayf and Tirat Al-Hayatim.

Figure 10 shows the total urban area in the 500 m buffer zone around the secondary canals which is estimated to be: 16.08, 35.99 and 37.7 km^2 for the years 1990, 2010 and 2011 respectively. This means that this area has increased due to the unplanned urbanization and hence is subject to poor water management. These buildings represent an obstruction that will delay (interrupt) the water distribution to the farmers especially those at the end of the canals.
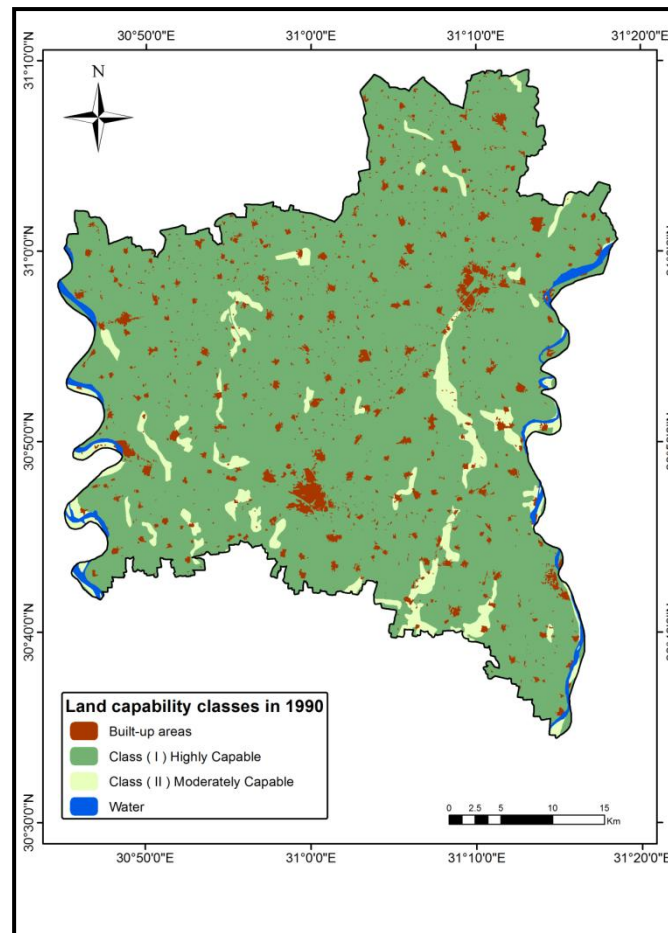
Figure 6: Urban Settlements, Extracted from TM Image of 1990, Overlaid on Soil Capability Map

In order to evaluate the efficiency of the water distribution system to the cultivated lands, an index is set. This index is defined as the ratio between the total length of secondary canals (10–25 m width) in km (estimated to be 320.35 km) and the total area of cultivated areas in km^2 within the 500 meter buffer zone. The increase in the urban areas reflects a decrease in the cultivated land and hence the higher the value of this index, the lower the water management is. Accordingly, it was found that in 1990 the agricultural lands in Gharbia Governorate were managed better compared to those in 2010 and 2011 (Table 5). Similarly, for Tanta and Mahalla districts, the total urban area in the 500 m buffer zone around the secondary canals is estimated to be: 5.41, 11.05 and 11.47 km^2 for the years 1990, 2010 and 2011 respectively. Also, the water management index values reflect similar conditions to those found in the governorate as a whole (Table 6).
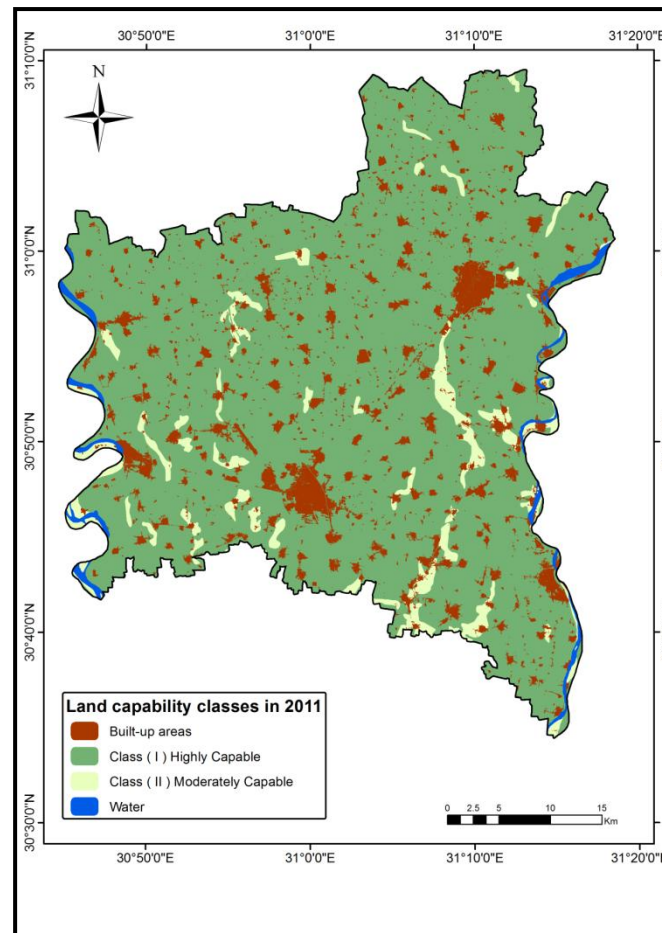
Figure 7: *Urban Settlements, Extracted from Egyptsat-1 Image of 2010, Overlaid on Soil Capability Map*

Table 5: *Water Management Index in Gharbia Governorate in 1990, 2010 and 2011*

Year	Urban Area in the 500 M Buffer Zone (Km^2)	Water Management Index Value	Water Management
2011	37.74	8.49	Low management
2010	35.99	8.89	Low management
1990	16.08	19.92	High management

Table 6: *Water Management Index in Tanta and Al-Mahalla districts in 1990, 2010 and 2011*

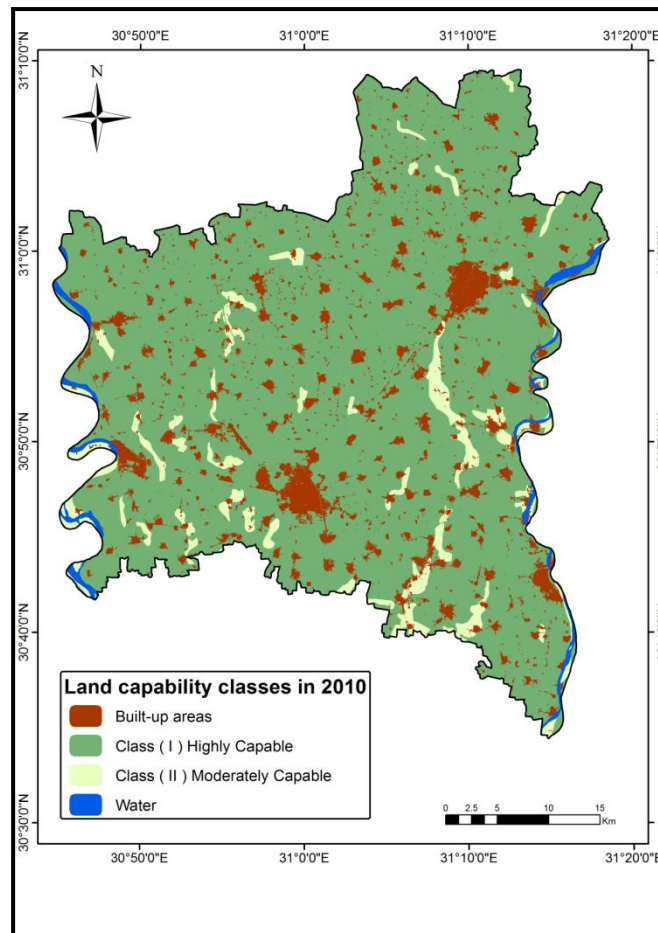| Year	Urban Area in the 500 M Buffer Zone (Km^2)	Water Management Index Value	Water Management
2011	11.47	7.67	Low management
2010	11.05	7.96	Low management
1990	5.41	16.26	High management

Figure 8: *Urban Settlements, Extracted from SPOT 5 Images of 2011, Overlaid on Soil Capability Map*
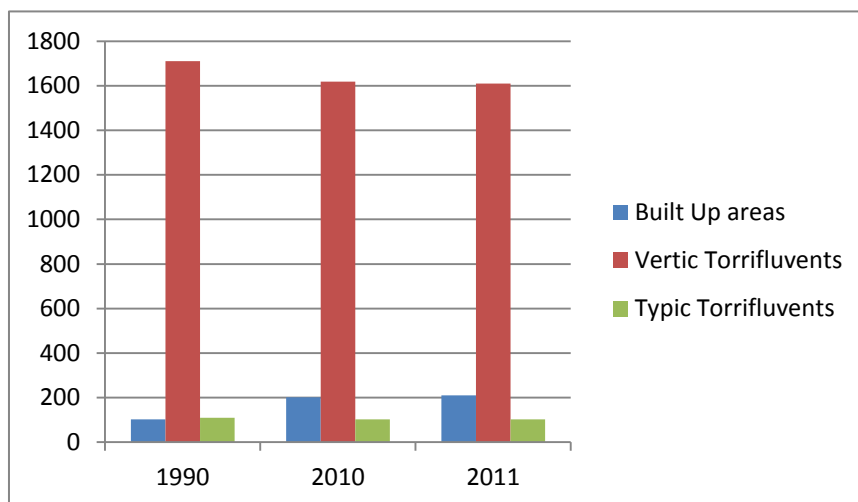

Figure 9: *Trends of Soil Types and Built Up Areas Changes in the Governorate*
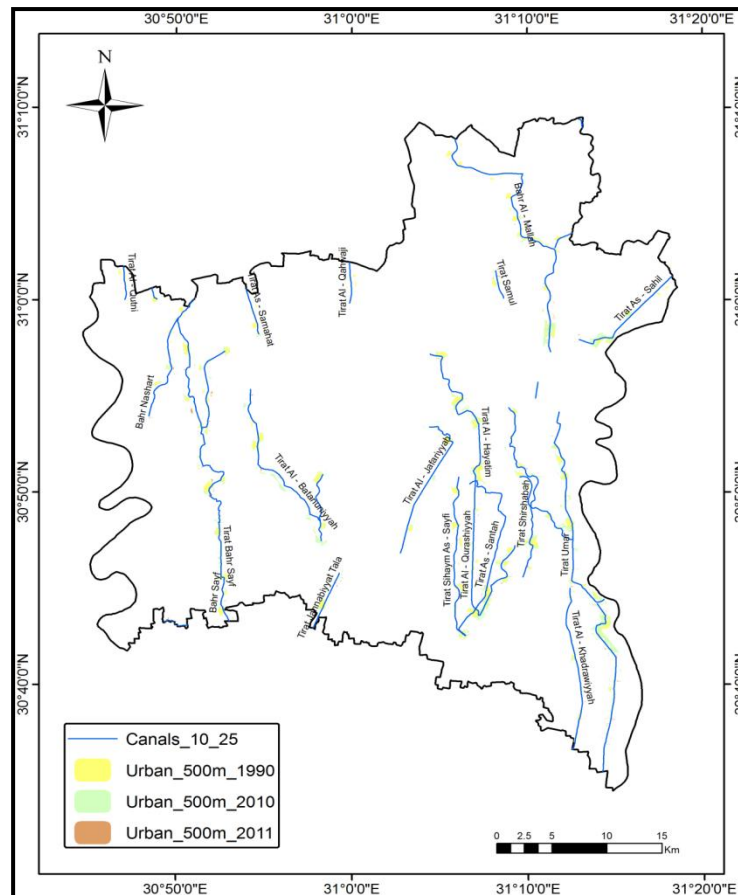
Figure 10: *The Urban Areas in a Buffer Distance of 500 m around the Canals (10 –25 m width) from 1990 to 2011*

Consequently, the negative outcomes of the urban sprawl could be summarized as direct and indirect outcomes as follows:

- Water management index in the cultivated lands in the buffer zone around the secondary canals reflects the negative impacts of increasing the urban areas on the expense of the highly fertile lands.

- Inhabitants will tend to dispose their municipal wastes directly in the canals without any treatment and hence will represent a hazard especially that this water is used to irrigate their cultivated lands.

- The location of these buildings and houses without any system of solid waste disposal and / or absence of an efficient disposal network unquestionably will influence the water quality of these irrigation canals.

- The influence of the building height on the plant productivity of the surrounding lands (as mentioned before in the Introduction section).

- Some inhabitants will tend to construct some primitive pipes to convey water from the canals to their lands after being obstructed by the newly constructed houses. These pipes are not well designed and their materials do not follow any quality control legislation and hence may lead to water leakage from them to the groundwater table. This will cause a rise in the

groundwater table and hence soil salinization and water logging and finally the soil is degraded and its productivity of certain types of crops will be reduced.

5. Conclusion and Recommendations

The main objective of this research was to study the influence of urban sprawl on the agricultural lands and how it also influenced the water distribution regime in Gharbia Governorate. Integrating visual interpretation with supervised classification was found to increase the overall accuracy by 10 %. The study area witnessed a severe land cover change as a result of urbanization due to the double influence of population growth and lack of security especially during the beginnings of 2011. A considerable increase in urban settlements has taken place at the expense of the most fertile lands in the governorate. Water management was negatively influenced by building in the 500 m buffer zone around the (10-25 m width) canals. Integrating remote sensing and GIS provided valuable information on the nature of land cover changes and its impact on irrigation network.

Urbanization on the expense of fertile soils and irrigation network is mainly due to rapid population growth and lack of strict rules that prohibits such types of encroachment. Detailed socioeconomic studies are needed to preserve the precious and limited lands and also to protect the water ways from the expected pollution resulting from such behaviour.

Finally, it can be concluded that urban sprawl over cultivated lands will have lots of negative outcomes compared to those built in urban areas.

It is recommended to:

- Increase the allowable buffer area around the main and secondary canals which mainly depend on the irrigation water directly from the irrigation network.

- Provide scientific advice in the form of agricultural guidance brochures or TV films to inhabitants. These advertising materials will help them to understand the problem and its outcomes on both the short and long terms.

- Fix a minimum buffer distance around the irrigation canals to build in. This distance must not be less than 500 m so that the water courses will be completely protected from pollution.

- More care to guidance brochures by videos to illiterates, websites, capacity building, field days, workshops, NGO repair, and informants training to deliver scientific information in an easy and clear way.

Acknowledgments

References

Belal A.A., et al. *Detecting Urban Growth using Remote Sensing and GIS Techniques in Al Gharbiya Governorate, Egypt*. The Egyptian Journal of Remote Sensing and Space Sciences. 2011. 14 (2) 73-79.

Adel A. Shalaby et al. *Urban Sprawl Impact Assessment on the Agricultural Land in Egypt using Remote Sensing and GIS: A Case Study, Qalubiya Governorate.* Journal of Land Use Science. 2012. 7 (3) 261-273.

Ahram Masaii, 2011: 12*,000 Case of Encroachment on Agricultural lands in Gharbia since 25 January*. Ahram Masaii, 7229. http://massai.ahram.org.eg/News/30812.aspx (In Arabic).

Al-Ahram Gate, 2013: *Egypt's Population of 92 Million People with Early March 8 Million of them abroad and Males Superior to Females*, 27 February, http://gate.ahram.org.eg/News/314323.aspx.

Anderson J.R., 1976: *A Land-Use and Land Cover Classification System for Use with Remote Sensor Data.* US Geological Survey Professional Paper 964, Washington, DC.

ASRT, 1982: *Soil Map of Egypt.* Final Report. Academy of Scientific Research and Technology (ASRT) Cairo, Egypt.

CAPMUS, 2012: *Central Agency for Public Mobilization and Statistics.* www.capmas.gov.eg.

Climatologically Normal for Egypt, 2011: the Normal for Gharbia Governorate Station, (1960 – 2011), Ministry of Civil Aviation: Meteorological Authority, Cairo, Egypt.

Farah A.F., 1967: *Fragmentation in the Egyptian Farms: Dimensions of the Problem and Planning for Remedy.* Internal Memorandum No. 794. The National Planning Institute (NPI), Cairo, Egypt.

IDSC, 2009: *Egypt's Description by Information 2009*. Years of Development. 8th Ed. The Egyptian Cabinet Information and Decision Support System.

Kruseman G., et al., 2007: *Rural Development Policy in Egypt Towards 2025; Targeted Conditional Income Support: A Suitable Option?* Alterra Rapport 1526 ISSN 1566-7197
http://www.upehc.org/documents/Rural Development Policy in Egypt Towards 2025.pdf

Lins K.S., et al., 1996: *Land Cover Mapping: An Overview and History of the Concepts.* In: Gap Analysis: A Landscape Approach to Biodiversity Planning. American Society for Photogrammetry and Remote Sensing, Bethesda, Maryland, 57-65.

Milne A.K., 1988: *Change Detection Analysis Using Landsat Imagery a Review of Methodology*. In: Proceedings of IGARSS 88 Symposiums, Edinburgh, Scotland, 541–544.

Ottensmann J.R. *Urban Sprawl, Land Values and the Density of Development*. Land Economics. 1977. 53 (4) 389–400.

Schowengerdt R.A., 2007: *Remote Sensing Models and Methods for Image Interpretation.* 3rd Ed., Elsevier, Amsterdam, Netherlands.

United Nations, Department of Economic and Social Affairs, Population Division, 2011*: World Population Prospects: The 2010 Revision, Highlights and Advance Tables*. ESA/P/WP220.

Research Article　　　　　　　　　　　　　　　　　　　　　**Open Access**

Terrestrial Laser Scanning: Application for Measuring of Structures Information in Geological Outcrops

Marcelo Kehl de Souza[1], Maurício Roberto Veronez[1], Francisco M. W. Tognoli[1], Luiz Gonzaga da Silveira Jr. [2], Leonardo Campos Inocencio[1], Reginaldo Macedônio da Silva[1] and Rudi César Comiotto Modena[1]

[1]Graduate Program on Geology, Vale do Rio dos Sinos University (UNISINOS), São Leopoldo, Brazil
[2]Graduate Program on Applied Computer Science, Vale do Rio dos Sinos University (UNISINOS), São Leopoldo, Brazil

Correspondence should be addressed to Marcelo Kehl de Souza, marcelo.k.souza@gmail.com

Abstract This study aimed to build a workflow to survey geological planar structure geometries using light detection and ranging technique. The study covered a field survey with the determinations of plane attitude using compass, clinometers, and digital images through light detection and ranging technique. Three methods were used to compute the selected planes into the point cloud, namely, three points, planar regression, and moment of inertia analysis. The methods were evaluated and compared with traditional methods of measurement (compass and clinometers). The evidence shows that the three-point method is quick and simple; however, it does not have any tool for quality analysis. Planar regression method proves to be effective and has tool for analyzing the degree of fit to the calculated plane. The Moment of Inertia provides degree of fit and reliability analysis to the calculated plane.

Keywords *LIDAR, Serra Geral Formation, Fracture Orientation*

1. Introduction

Geology has increasingly employed digital techniques for collecting spatial data with high resolution and, therefore, great accuracy in the generation of 3D geological models, which enable more detailed quantitative analysis [1].

One of the techniques that have been deployed into the geological activity is the use of terrestrial laser scanner (TLS). TLS is able to acquire a point cloud which can be incorporated into the analysis and interpretation of field data [1]. In addition, 3D outcrop models may be used virtually with the support of visualization techniques, making it easier by contributing to cost reduction and planning

fieldwork, allowing the acquisition of measurements of geological structures safely in areas of hard access [2].

TLS has become increasingly popular in geomorphologic studies [3-10]; however, its application in parametric/geometric study of outcrops still needs to be improved. These improvements are related, directly, to the identification and interpretation of geological features, as well as the parameterization of structures in digital outcrop models (DOMs), generated from a dense cloud of three-dimensional points.

In outcrops of hard access, where there is the interference of magnetic fields in deposits of magnetic mineral, that is, magnetite, ilmenite, pyrrhotite, and so on; traditional methods (compass and clinometers) may lead to errors, making it difficult and distorting the generation of geological models. Therefore, it is necessary to build a methodology for planning, collecting and processing data for geometric data modeling of geological structural plans with the use of TLS.

The study aims to build a workflow for survey geological planar structure geometries using LIDAR technique. For this purpose, three methods are applied and compared, namely, three points (3P), planar regression (PR), and moment of inertia analysis (MI), for the characterization of planar geological structures using the point cloud.

2. Literature Review

The characterization of outcrop surface is related to many geological applications, such as the slope stability analysis [7, 8], studies of analog outcrops of hydrocarbon reservoirs [11-16], DOM interpretations [17-19] and studies of fractured rocks [4, 7, 14, 20, 21].

For featuring high resolution in the generation of 3D point cloud, TLS is effective in getting measurements that make the process of interpretation of geological structures easier [17, 22], as well as measurements of planes for geological structural studies [7, 10].

There are some methods of getting the orientation of a plane from a point cloud [7, 23-25]. The first is to select three points in the georeferenced point cloud and calculate both the dip direction and the dip [7]. The second, called moment of inertia analysis (MI), consists in finding the maximum moment of inertia axis, pole to the best-fit plane, estimating the moment of inertia of a set of data points [25]. It is assumed that, to estimate the moment of inertia of a set of points, the best-fit plane passes through the point of coordinates: $\bar{x}, \bar{y}$, and $\bar{z}$, the center of mass of the nodes. From the calculation of the vectors that connect the center of mass to each node, the orientation matrix T is made:

$$T = \begin{bmatrix} \sum l_i^2 & \sum l_i m_i & \sum l_i n_i \\ \sum m_i l_i & \sum m_i^2 & \sum m_i n_i \\ \sum n_i l_i & \sum n_i m_i & \sum n_i^2 \end{bmatrix}$$

From the symmetric matrix T, the eigenvectors (v_1, v_2, v_3) and the corresponding eigenvalues $(\lambda_1, \lambda_2, \lambda_3)$ can be found [26]. The eigenvector v_1 is associated with the orientation of maximum density of vectors. The eigenvector v_3 is associated to the minimum density of vectors, the highest moment of inertia, and therefore, the pole of best-fit plane.

The third method calculates the orientation of a plane through the points used in the method called planar regression (PR) [24, 25]. The equation of best-fit plane, in this method, is expressed by the regression planar:

$$Z = b_0 + b_1 X + b_2 Y$$

The matrix below is made to find the coefficients b_0, b_1, b_2 of an n number of captured points:

$$
\begin{bmatrix}
n & \sum\limits_{i=1}^{n} x_i & \sum\limits_{i=1}^{n} y_i \\
\sum\limits_{i=1}^{n} x_i & \sum\limits_{i=1}^{n} x_i^2 & \sum\limits_{i=1}^{n} x_i y_i \\
\sum\limits_{i=1}^{n} y_i & \sum\limits_{i=1}^{n} x_i y_i & \sum\limits_{i=1}^{n} y_i^2
\end{bmatrix}
\begin{bmatrix}
b_0 \\ b_1 \\ b_2
\end{bmatrix}
=
\begin{bmatrix}
\sum\limits_{i=1}^{n} z_i \\
\sum\limits_{i=1}^{n} x_i z_i \\
\sum\limits_{i=1}^{n} y_i z_i
\end{bmatrix}
$$

where x_i, y_i, z_i are the coordinates of the selected points of the plane. The coefficients b_0, b_1, b_2 can be found either by Cramer's theorem or by Gaussian elimination. According to the coefficients (vector normal to the plane) the dip direction and the dip are determined.

The concepts degree of fit and reliability define the quality of the orientation measurements produced from the points [25]. The degree of fit is inversely proportional to the distance of the nodes. The reliability is associated with the stability of the method.

In the PR, the degree of fit of the plane is found through the correlation coefficient R^2, which is the relation among the variables [24], expressed by the following:

$$
R^2 = \frac{\left[\sum (z_i - \bar{z})(\hat{z}_i - \bar{\hat{z}}) \right]^2}{\sum (z_i - \bar{z})^2 \sum (\hat{z}_i - \bar{\hat{z}})^2}
$$

$$
\hat{z}_i = b_0 + b_1(x_i - \bar{x}) + b_2(y_i - \bar{y})
$$

In the MI, the degree of fit and reliability can be obtained through the ratio between the eigenvalues of the matrix orientation [26]. The degree of fit is defined by the ratio between the eigenvalue one (λ_1) and eigenvalue two (λ_2), according to the equation:

$$
M = \ln(\lambda_1 / \lambda_3)
$$

The higher is the value of M, the shorter is the distance between the best-fit plane and the nodes. However, a good fit plane does not necessarily correspond to good quality in the orientation. For reliability in the orientation measurement, the nodes need to be as far as possible from the collinearity and as far as possible from the center of mass. The ratio between the eigenvalues of the orientation matrix, in the analysis of the moment of inertia, provides the degree of collinearity of points, the reliability of the best-fit plane, expressed by the following:

$$
K = \ln(\lambda_1 / \lambda_2) / \ln(\lambda_2 / \lambda_3)
$$

3. Material and Methods

To carry out this research, the equipment used was 3D Terrestrial Laser Scanner ILRIS- from OPTECH, Receptor GPS- Topcon Model Hiper Lite RTK and compass with clinometers.

The study was conducted in a quarry (Figure 1a), located in the town of Estância Velha in the State of Rio Grande do Sul, Brazil (UTME = 485685 m; UTMN = 6722017 m; Zone 22S, SIRGAS2000).
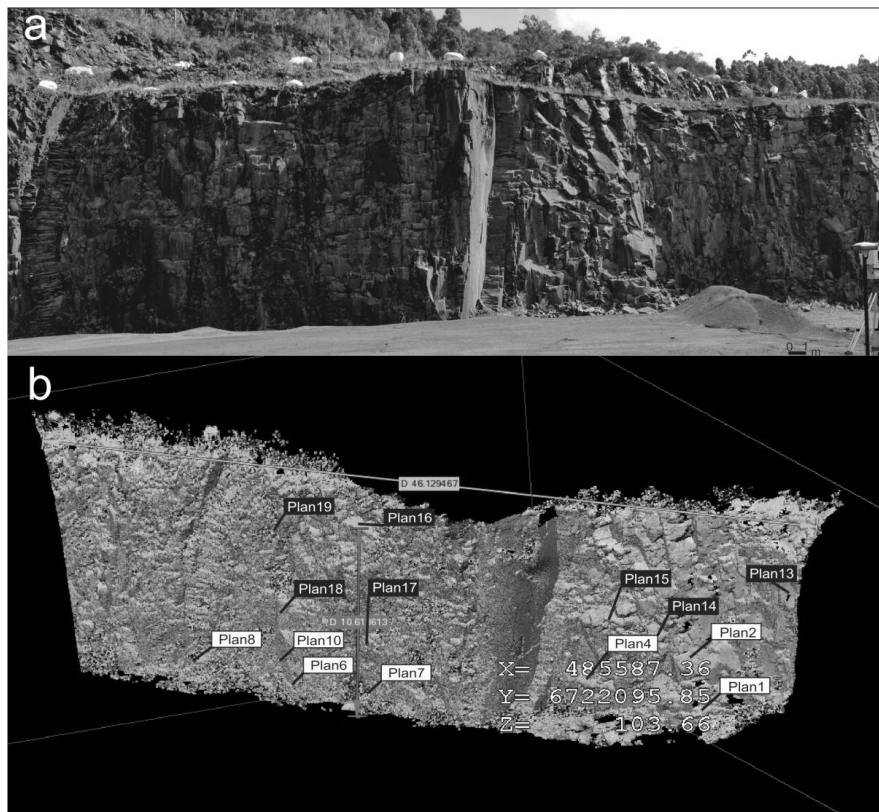
Figure 1: *a) Picture of Study Area. b) Georeferenced Point Cloud. The IMInspect Module of the Polyworks Program was used to Obtain Measurements, in Meters, in the Outcrop. The Planes Marked in White is Planes Measured by Compass and Clinometers, the Orientations of Which were computed with three techniques: 3P, MI, and PR. The Planes Marked in Black, of Hard Access, were Computed with the Three Techniques.*

The quarry lies on the first basaltic floods of the southern edge of the Paraná Basin [27]. The wall of the quarry is composed of a basaltic flood of approximately 40 meters thick located in a valley between two massive Aeolian dunes of the Botucatu Formation [28] (Figure 1a). Superimposed on these volcanic rocks, an interflood dune, with up to 27 meters thick, was formed, slightly hidden by small basaltic flood that came from the north [28].

The scans were performed in two selected locations with 30% overlap, with a 20-millimeter point spacing and an average distance of 33 meters from the outcrop. In the stage of data processing, the point clouds generated by the TLS had to be georeferenced.

For georeference it was necessary to define a reference point near the outcrop. In that place a scan coordinate was performed for 2 hours by GPS. With the aid of GPS Rover 2 stations were positioned for the TLS survey. The coordinates of reference point and TLS stations were imported to IMALign module in Polyworks software. The point clouds, in this module, were moved to the correct station, merged and georeferenced.

The planes are identified and marked directly on the point cloud (Figure 1b). To calculate the orientation of fracture planes, the three methods mention above were used: 3P, MI, and PR.

4. Results and Discussion

The point cloud obtained from the LIDAR technique has a total of 6.1 million georeferenced points in the UTM-SIRGAS2000 coordinate system, producing the first result of the technique (Figure 1b). The

point cloud can be positioned at points of view that field work does not allow, either for the dimensions of the outcrop or for safety reasons.

The poles of the planes measured, 30 measurements in each plane, with compass and clinometers, were plotted on stereographic projection of the equal area (Figure 2).
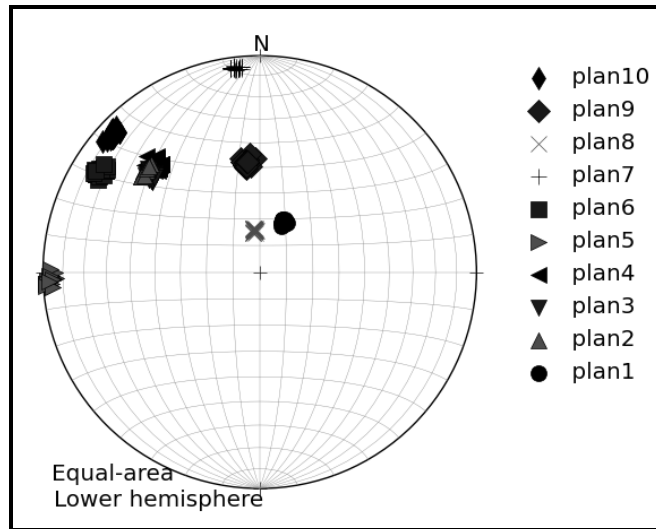

Figure 2: Poles of the Planes Measured Using a Compass and Plotted on Projection of the Equal Area

In the comparison made between the orientations of fracture planes using a compass and a clinometers and the three methods (3P, MI, and PR) conducted in this study; the evidences how's differences in the dip direction of 5.9 degrees, 2.4 degrees, and 3.1 maximum, respectively (Figure 3).
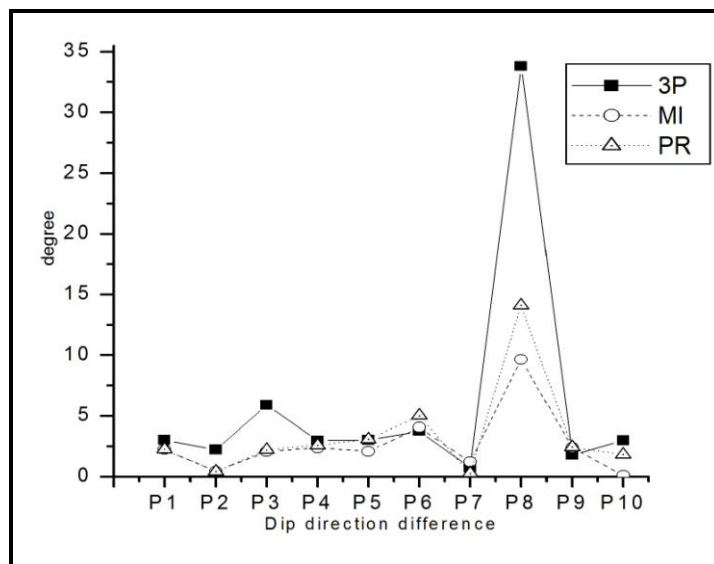

Figure 3: Graph Showing the Difference between the Averages of Measurements of Dip Direction in the 10 Fracture Planes Carried Out Using a Compass and the Measurements Calculated by the Three Techniques: 3P, MI, and PR in Degrees

In the comparison made with the dip angle, the maximum differences were as follows: 5.4, 2.3, and 4 degrees, respectively, for 3P, MI, and PR (Figure 4).
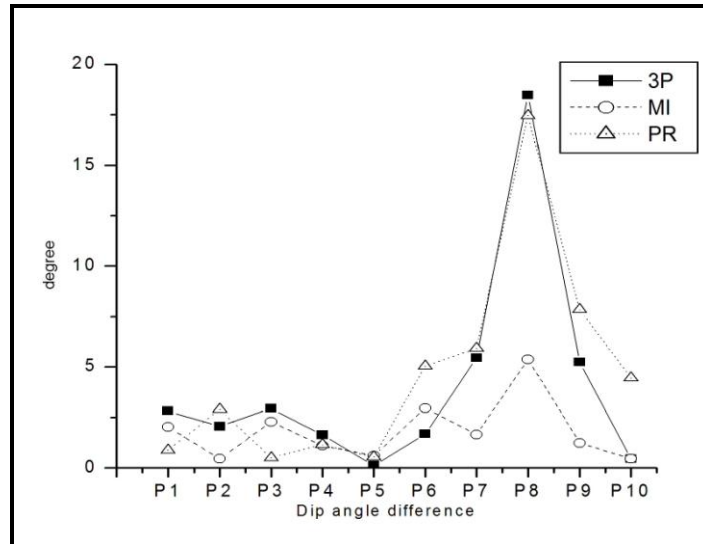
Figure 4: *Graph of the Difference between the Averages of the Measurements of Dip Angles of 10 Fracture Planes Carried Out Using an Inclinometer and the Measurements Calculated by the Three Techniques: 3P, MI, and PR, in Degrees*

The planes that PR (Figure 5) and MI (Figure 6) identified as low degree of fit and low reliability were excluded from that comparison. Measurement accuracy of 8 and 4 degrees of, respectively, dip direction and dip are suitable for the purpose of geotechnical studies [10].
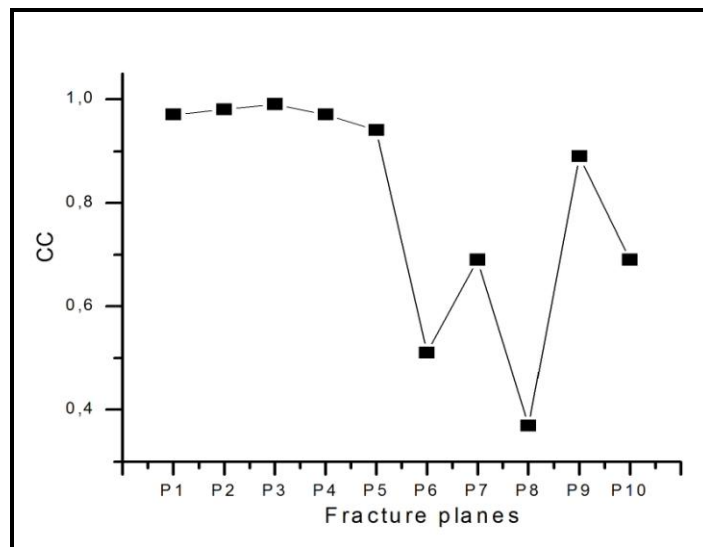
Figure 5: *Graph of the Correlation Coefficient (CC) of the Planes Calculated by Planar Regression*

Some planes stood out in the graphics of point spatial distribution, according to the ratio between the eigenvalues (Figure 6). The plane 8, in particular, shows bad ratios in M and K in the MI. Good best-fit planes produce values higher than 4 for M and values lower than 0.8 for K [25]. It was perceived that the plane 8 is occluded because of obstacles for the TLS, resulting in a selection of points that are not representative of the plane to be measured.

Figure 6: *Graph of Point Spatial Distribution According to the Ratio between the Eigenvalues. With the Ratios of Fit Degree (M) and Reliability of the Measurements (K) of the Computed Planes in the MI Method.*
Source: Adapted from [26]

Plane 6 showed a low degree of fit in both PR (correlation coefficient) and the MI (ratio M). The photograph of the plane in Figure 7 shows the smooth curved surface.
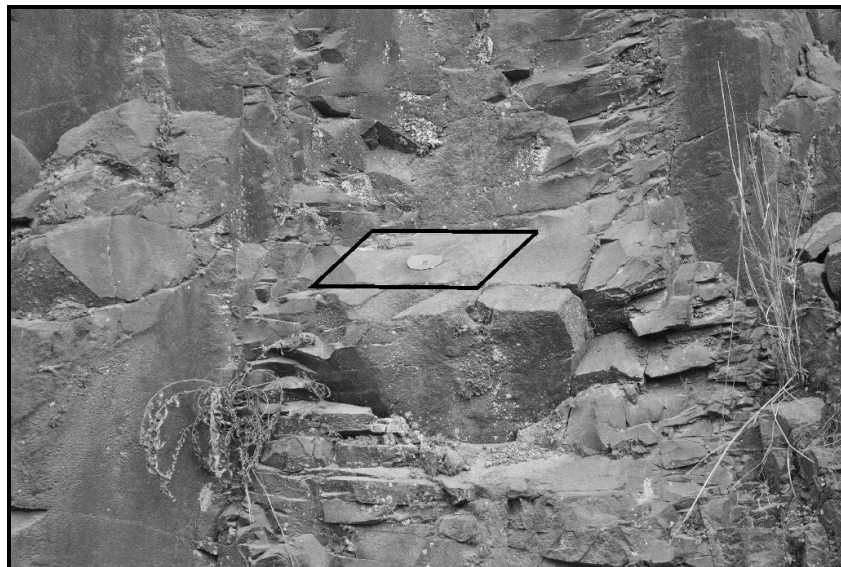
Figure 7: *Plane 6; The Photograph of the Plane Shows the Irregular Surface*

Calculations on dip direction (Figure 8a) and dip (Figure 8b) were carried out for 10 planes of hard access with the methods 3P, MI, and PR.

(A)

(B)
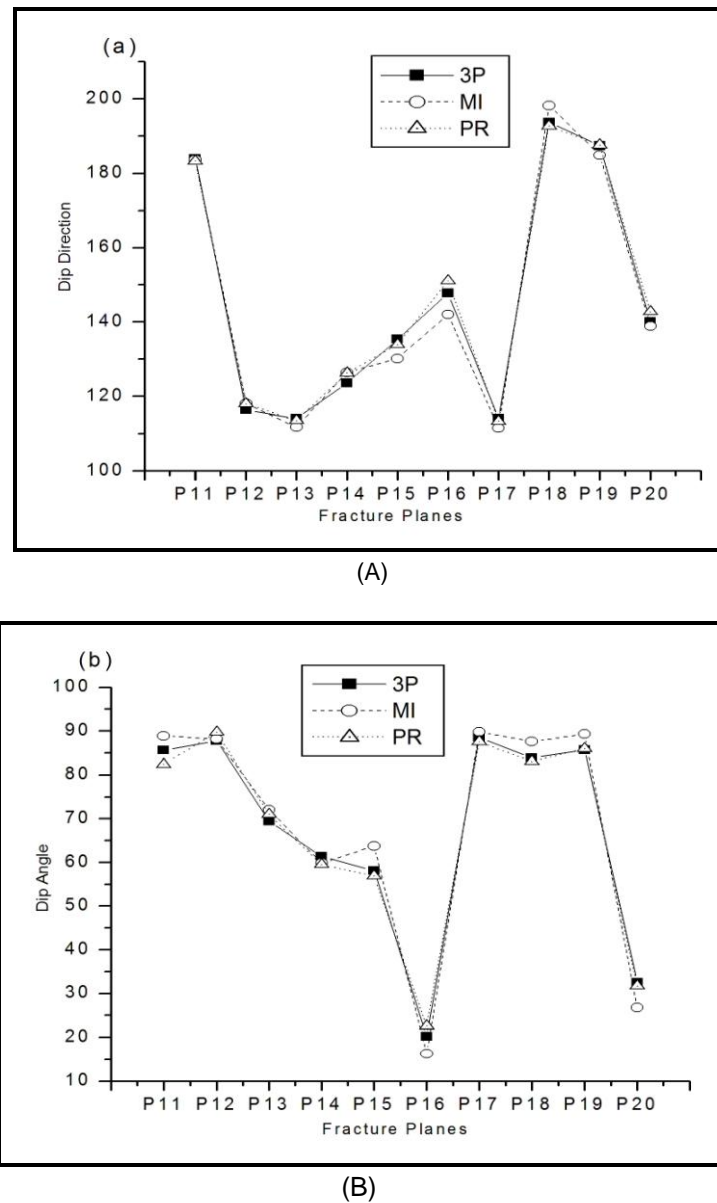
Figure 8: Graph of the Measurements of Dip Direction (A) and Dip Angles (B) of 10 Fracture Planes of Hard Access, in Degrees

Three planes of hard to access stand out: plane 15 (M < 4), plane 16 (K > 0.8), and plane 20 (M < 4 and K > 0.8) (Figure 9). Plane 15 features a curved surface, and plane 16 features low dip angle and is on the top of the outcrop; besides, it presented a point cloud twice bigger than the one setting in scanning. It is advisable, for surveying with TLS in these situations, if possible, to make way between the equipment and the outcrop. Finally, the plane 20 features a rough surface.
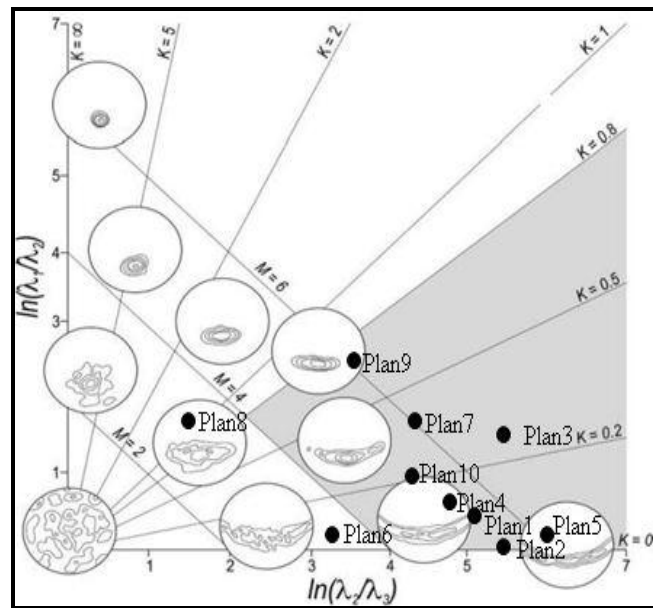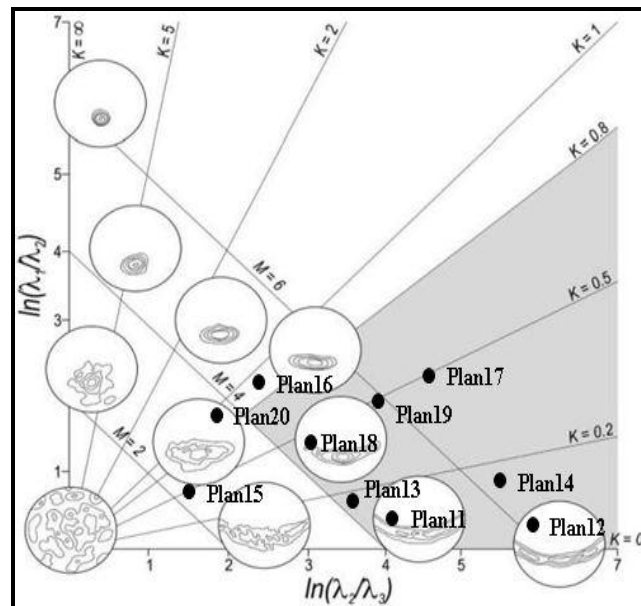
Figure 9: *Graph of Point Spatial Distribution According to the Ratio between the Eigenvalues. With the Ratios of Degree of Fit (M) and Reliability of the Measurements (K) of the Planes of Hard Access Computed in the MI Method.*
Source: Adapted from [26]

5. Conclusion

The processing of point cloud generated by the LIDAR technique was performed using three different methodologies: 3P, MI, and PR. The 3P method is quick and simple to measure planar geological structure orientation; however, it does not have any tool for quality analysis. The two methods, MI and PR, prove to be effective in calculating the orientation of planes from selected points of a point cloud. Both feature a tool for analyzing the degree of fit of selected points to the calculated plane. Although, MI, besides presenting minor measurement differences when compared with traditional methods, provides the quantitative measurement of the point spatial distribution, proving to be an efficient tool for processing the orientation of planes from points. This work shows that appropriate methods of LIDAR surveying and processing point cloud can provide realistic characterizations of the orientation of planar geological settings with a degree of fit and reliability.

Acknowledgment

References

[1] S.J. Buckley, J.A. Howell, H.D. Enge and T.H. Kurz. *Terrestrial Laser Scanning in Geology: Data Acquisition, Processing and Accuracy Considerations.* Journal of the Geological Society. 2008. 165; 625-638.

[2]   S.J. Buckley, H.D. Enge, C. Carlsson and J.A. Howell. *Terrestrial Laser Scanning for Use in Virtual Outcrop Geology.* Photogrammetric Record. 2010. 25; 225-239.

[3]   J. Armesto, C. Ordonez, L. Alejano and P. Arias. *Terrestrial Laser Scanning Used to Determine the Geometry of a Granite Boulder for Stability Analysis Purposes.* Geomorphology. 2009. 106; 271-277.

[4]   M.I. Olariu, J.F. Ferguson, C.L.V. Aiken and X.M. Xu. *Outcrop Fracture Characterization Using Terrestrial Laser Scanners: Deep-Water Jackfork Sandstone at Big Rock Quarry, Arkansas.* Geosphere. 2008. 4; 247-259.

[5]   A. Abellán, J.M. Vilaplana and J. Martínez. *Application of a Long-Range Terrestrial Laser Scanner to a Detailed Rockfall Study at Vall de Núria (Eastern Pyrenees, Spain)*. Engineering Geology. 2006. 88; 136-148.

[6]   S. Nagihara, K.R. Mulligan and W. Xiong. *Use of a Three-Dimensional Laser Scanner to Digitally Capture the Topography of Sand Dunes in High Spatial Resolution*. Earth Surface Processes and Landforms. 2004. 29; 391-398.

[7]   A. Nagalli, A. Pio Fiori and B. Nagalli. *Método Para Aplicação De Escâner a Laser Terrestre Ao Estudo Da Estabilidade De Taludes Em Rocha.* Revista Brasileira de Geociências. 2011. 41 (1) 56-67.

[8]   S. Slob, B. Van Knapen, R. Hack, K. Turner, J. Kemeny and Trb*. Method for Automated Discontinuity Analysis of Rock Slopes with Three-Dimensional Laser Scanning.* Geology and Properties of Earth Materials. 2005. 187-194.

[9]   M.A. Pearce, R.R. Jones, S.A.F. Smith, and K.J.W. McCaffrey. *Quantification of Fold Curvature and Fracturing using Terrestrial Laser Scanning*. Aapg Bulletin. 2011. 95; 771-794.

[10] M. Sturzenegger and D. Stead. *Close-Range Terrestrial Digital Photogrammetry and Terrestrial Laser Scanning for Discontinuity Characterization on Rock Cuts.* Engineering Geology. 2009. 106; 163-182.

[11] D. Garcia-Selles, O. Falivene, P. Arbues, O. Gratacos, S. Tavani and J.A. Munoz. *Supervised Identification and Reconstruction of Near-Planar Geological Surfaces from Terrestrial Laser Scanning*. Computers & Geosciences. 2011. 37; 1584-1594.

[12] J.K. Pringle, J.A. Howell, D. Hodgetts and A.R. Westerman. *Virtual Outcrop Models of Petroleum Reservoir Analogues: A Review of the Current State-of-the-Art.* First Break. 2006. 33-42.

[13] R.M. Phelps and C. Kerans. *Architectural Characterization and Three-Dimensional Modeling of a Carbonate Channel-Levee Complex: Permian San-Andres Formation, Last Chance Canyon, New Mexico, USA.* Journal of Sedimentary Research. 2007. 77; 939-964.

[14] D. Kurtzman, J.A. El Azzi, F.J. Lucia, J. Bellian, C. Zahm and X. Janson*. Improving Fractured Carbonate-Reservoir Characterization with Remote Sensing of Beds, Fractures, and Vugs.* Geosphere. 2009. 5; 126-139.

[15] A. Rotevatn, S.J. Buckley, J.A. Howell and H. Fossen*. Overlapping Faults and their Effect on Fluid Flow in Different Reservoir Types: A LIDAR-Based Outcrop Modeling and Flow Simulation Study.* Aapg Bulletin. 2009. 93; 407-427.

[16] H.D. Enge, S.J. Buckley, A. Rotevatn and J.A. Howell. *From Outcrop to Reservoir Simulation Model: Workflow and Procedures.* Geosphere. 2007. 3; 469-490.

[17] E.P. Baltsavias, E. Favey, A. Bauder, H. Bosch and M. Pateraki. *Digital Surface Modeling by Airborne Laser Scanning and Digital Photogrammetry for Glacier Monitoring.* Photogrammetric Record. 2001. 17; 243-270.

[18] J.A. Bellian, C. Kerans and D.C. Jennette. *Digital Outcrop Models: Applications of Terrestrial Scanning Lidar Technology in Stratigraphic Modeling*. Journal of Sedimentary. 2005. 75; 166-176.

[19] R.M. Silva, L.C. Inocencio, L. Jacobi, D. Lamberty, F.M. Tognoli and M.R. Veronez; 2012: *LIDAR for Visualization of 3D Geological Models*. Coordinates.

[20] J.A. Bellian, R. Beck and C. Kerans. *Analysis of Hyperspectral and Lidar Data: Remote Optical Mineralogy and Fracture Identification.* Geosphere. 2007. 3; 491-500.

[21] R.R. Jones, S. Kokkalas and K.J.W. McCaffrey. *Quantitative Analysis and Visualization of Nonplanar Fault Surfaces Using Terrestrial Laser Scanning (LIDAR)-The Arkitsa Fault, Central Greece, as a Case Study.* Geosphere. 2009. 5; 465-482.

[22] I. Fabuel-Perez, D. Hodgetts and J. Redfern. *A New Approach for Outcrop Characterization and Geostatistical Analysis of a Low-Sinuosity Fluvial-Dominated Succession Using Digital Outcrop Models: Upper Triassic Oukaimeden Sandstone Formation, Central High Atlas, Morocco.* Aapg Bulletin. 2009. 93; 795-827.

[23] Q. Feng, P. Sjögren, O. Stephansson, and L. Jing. *Measuring Fracture Orientation at Exposed Rock Faces by Using a Non-Reflector Total Station.* Engineering Geology. 2001. 59; 133-146.

[24] A.K.L. Kwong, H. Kwok and A. Wong, 2007: *Use of 3D Laser Scanner for Rock Fractures Mapping.* Presented at the FIG Working Week, Hong Kong, China.

[25] O. Fernández. *Obtaining a Best Fitting Plane Through 3D Georeferenced Data.* Journal of Structural Geology. 2005. 27; 855-858.

[26] N.H. Woodcock. *Specification of Fabric Shapes Using an Eigenvalue Method.* Geological Society of America Bulletin. 1977. 88; 1231-1236.

[27] W. Wildner, F.V. Orlandi and L.E. Giffoni; 2011: *Excursão Virtual aos Aparados da Serra, RS/SC : Aspectos Geológicos E Turísticos Cânions Do Itaimbezinho e Fortaleza*. http://www.cprm.gov.br/Aparados/index.htm.

[28] H.T. Frank, 2008: *Gênese e Padrões de Distribuição de Minerais Secundários na Formação Serra Geral (Bacia do Paraná).* M.S. Thesis, Instituto de Geociências, Universidad Federal do Rio Grande do Sul, 322.

Research Article   **Open Access**

Assessment of Meteorological Drought for Chittar Sub-basin Using Geographical Information System

M.C. Sashikkumar and O. Ganesh Babu

Department of Civil Engineering, University V.O.C College of Engineering, Anna University, Tirunelveli Region, Tuticorin, Tamil Nadu, India

Correspondence should be addressed to M.C. Sashikkumar, getsashi_kumar@yahoo.com, oganeshbabu@gmail.com

Abstract Drought is a normal feature of the climate and its recurrence is inevitable. Droughts occur due to failure of monsoons over a region. Within a short period of time, the amount of moisture in soils begin to decrease which then leads to decrease in flow of rivers, water levels in lakes, reservoirs and wells after several weeks or months. As the economy of our country is often gripped with the gamble of monsoons, studies regarding drought become inevitable. Drought is caused due to deficiency of water that depends on rainfall, which falls in uneven pattern across the country. Hence, an attempt is made in the present study to analyse rainfall status and assess the drought severity of Chittar sub-basin in meteorological aspect using Geographical Information System (GIS). GIS provides tools to incorporate spatial and temporal variations of water resources data. The assessment of drought severity in the meteorological context was carried out by India Meteorological Department (IMD) method. Meteorological drought risk index for each rainfall station the sub-basin was calculated by frequency analysis. Spatial interpolation of meteorological drought risk index was mapped in Arc view GIS 3.2a software. The meteorological drought risk maps help the administrators and planners to plan various alternative measures to overcome the drought and its impacts.

Keywords *Drought, GIS, IMD, Sub-basin*

1. Introduction

Drought is a factor of uncertainty, which affects country's agriculture and economy. Periodic droughts pose serious limitations to nation's efforts towards agricultural self-efficiency. Drought is generally viewed as a sustained and regionally extensive occurrence of below average natural water availability, either in the form of rainfall, river runoff or ground water. All droughts originate from a significant reduction in precipitation extended over a season or longer and result in water deficit. It is to be realized that there is a need to develop a complete drought assessment procedure, which would consider all aspects of drought causing parameters. Drought continues to be a factor of uncertainty in Indian agriculture in spite of significant scientific and technological developments. Drought in India

has been considered mainly from meteorological point of view. As the basic factor for drought is deficiency of water, which depends on rainfall, it is aimed to analyse long-term rainfall data and to assess the drought severity of Chittar sub-basin of Thamiravaruni River basin, Tamil Nadu in meteorological aspect using GIS. Geographical Information System provides tools to incorporate spatial and temporal variations of water resources data.

2. Materials and Methods

2.1. Study Area

Chittar sub-basin of Thamiravaruni basin has been chosen for the present study since it has many dry regions within the perennial river basin. Thamiravaruni irrigation system is the one of the major systems in Tamil Nadu with a command about 77,500 ha irrigating Tirunelveli and Thoothukudi districts. Chittar River is the largest tributary of the Thamiravaruni River. It lies between $8^0 45'$ N and $9^0 15'$ N Latitudes and between $77^0 10'$ E and $77^0 50'$ E Longitudes. The eastern part of the sub-basin is generally plain with the lowest elevation of about 60 to 80 m above MSL and the slope ranging from is less than 1%, whereas in the west, the topography is undulating plains and the slope ranges from 1 to 3%. The high hills of the Western Ghats mark the western boundary of the sub-basin. The climate of the sub-basin is generally semi-arid. The maximum temperature ranges between 30°C to 37.5°C and the minimum temperature between 20°C to 27°C. The months of March, April, May and June are hottest depending on the location within the basin, and the cooler months are November, December and January. The index map of the Chittar sub-basin is shown in Figure 1.
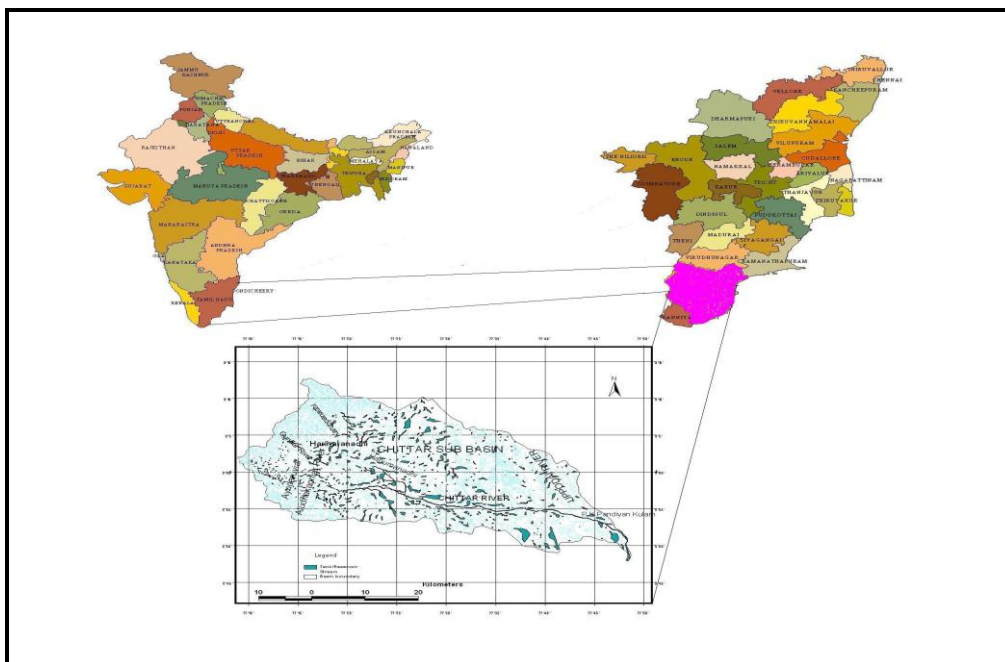
Figure 1: Index Map of Chittar Sub-basin

2.2. Rainfall Analysis

Rainfall is a main factor, which is responsible for vegetation, hydrology and it is particularly most important to agriculture. Thirty years of monthly rainfall data from 15 rain gauge stations in Chittar sub-basin were collected from Ground Water Division, PWD. The statistical parameters like mean, standard deviation, co-efficient of variation, skewness and kurtosis were identified. Rain gauge location map of Chittar sub-basin is shown in Figure 2.
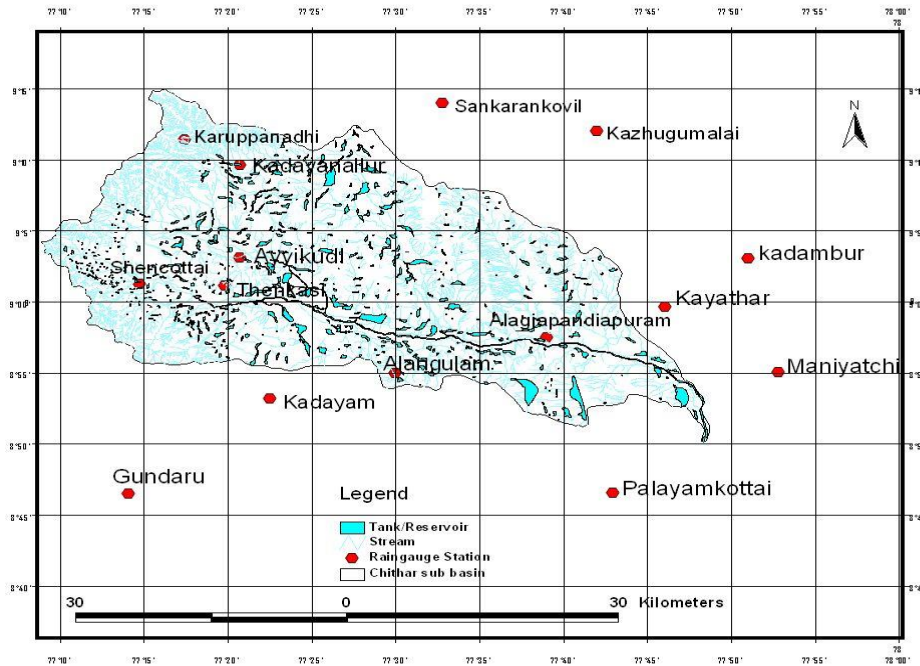
Figure 2: *Rain Gauge Location Map of Chittar Sub-basin*

2.3. Meteorological Drought Assessment

Meteorological drought is a situation when there is a significant decrease in precipitation from the normal over an area [1]. Among various methods, the IMD method is a simple and widely used one, which will give a preliminary idea about the drought condition of an area. In this method, drought is assessed on the basis of percentage deviation of rainfall from the long-term annual mean rainfall [2]. The percentage deviation (D_i) given by:

$$D_i = \frac{P_i - \overline{P}}{\overline{P}}$$

Where, P_i is the annual rainfall in the year i; and $\overline{P}$ is the long term annual mean rainfall.

IMD classification of drought is based on the deviation of rainfall which is given in Table 1.

Table 1: *IMD Classification of Drought*

Sl. No.	Range of D_i	Classification of Drought	Category
1	>0	M0	No drought
2	0 to –25	M1	Mild drought
3	-25 to –50	M2	Moderate drought
4	< -50	M3	Severe drought

The drought severity classes were found out for each rain gauge station on a yearly basis. The frequency of various classes of drought severity for each station was found out. The weight ages 0, 1, 2, and 3 are assigned to drought severity classes of no, mild, moderate and severe droughts respectively [3]. The meteorological drought risk index of each station is found out by multiplying the frequency of each class of drought severity by the corresponding weight age. The spatial distribution of drought risk was found out using the nearest neighborhood analysis in GIS [4].

3. Results and Discussion

The spatial pattern of drought risk of a basin can be analysed easily with the help of drought risk maps in GIS environment. This information will help the district authorities in prioritising areas for mitigating the effects of drought. The meteorological drought was quantified by taking into account the long-term drought severity or intensity and duration. Drought risk area mapping was then carried out in GIS environment. The results of this analysis are presented below.

3.1. Analysis of Rainfall Data

The statistical analysis was carried out for annual rainfall data to identify statistical parameters like mean, standard deviation, co-efficient of variation, skewness and kurtosis. The results obtained from this analysis are presented in Table 2. The average precipitation for the basin is 833 mm. The Kadambur Station has very low coefficient of variation of 23.95% and Kayathar has high variation of 52.82%. The coefficient of variation increases with increase in aridity. Also it indicates that many dry years and a few wet years in the study area leading to the identification of drought proneness. The parameters such as skewness and kurtosis were also estimated. The result indicates that all the rain gauge stations have positive skewness except Alagiapandiapuram and Kadayam which is negative skew. Most of the data have values above the mean. Negative skewness has huge influence on this parameter, which indicates the true homogeneity of drought condition. Usually annual precipitation data are highly skewed due to insufficient rainfall during non-monsoon periods. Analysis of rainfall data shows that there were many dry years and few wet years. The degree of skewness gradually increases as the climate becomes drier.

Table 2: Statistical Parameters for Annual Rainfall Data in Chittar Sub-basin

Sl. No.	Name of Rain Gauge Stations	Annual Average (mm)	Standard Deviation (mm)	Co-efficient of Variation (%)	Skewness	Kurtosis
1	Alagiyapandiapuram	626.03	282.80	45.17	-0.40	-0.19
2	Alangulam	743.6	219.70	29.55	0.55	0.3
3	Ayyakudi	674.0	227.97	33.82	0.27	-0.37
4	Gundaaru	1788.3	513.76	28.73	0.75	0.02
5	Kadambur	744.93	178.41	23.95	0.94	1.23
6	Kadayam	841.8	382.7	45.46	-0.01	-0.17
7	Kadanallur	737.10	277.29	37.62	1.29	3.5
8	Karuppanadhi	673.3	220.42	32.74	1.22	3.02
9	Kayathar	587.0	310.03	52.82	0.90	2.28
10	Kazhugumalai	742.13	200.13	26.97	0.34	-0.66
11	Maniyatchi	690.74	345.91	50.08	0.41	0.46
12	Palayamkottai	720.2	201.5	27.98	0.22	-0.46
13	Sankarankoil	674.9	242.93	35.99	0.63	-0.44
14	Shenkottai	1536.9	554.81	36.10	0.72	-0.37
15	Tenkasi	904.8	306.14	33.84	0.92	1.82
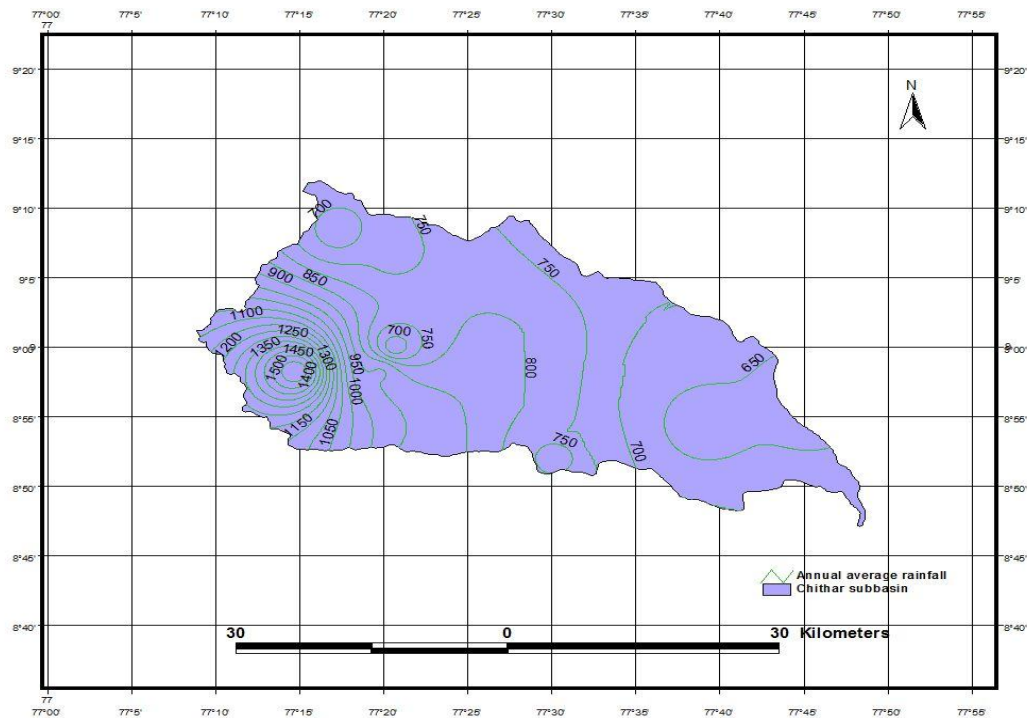
Figure 3: *Spatial Distribution of Annual Rainfall of Chittar Sub-basin*

3.2. Meteorological Drought Assessment

Drought assessment has been carried out for all the fifteen stations. The results shows that many blocks were affected by moderate and severe drought condition during the years 1982, 1986, 1989, 1999 and 2001. The drought severity values of all the stations were exported from MS Excel to Map/Info GIS to generate drought severity maps. Figures 4, 5 and 6 indicate the drought severity (block wise) for the years 1989, 1999 and 2001 respectively during which the basin had experienced severe drought conditions. From the Figure 4, it is observed that during the year 1989, all the blocks of the basin were affected by rainfall deficiency except Alangulam. Blocks such as Shenkottai, and part of Thenkasi, Ayyikudi are exposed to no drought. It can be seen from Figure 5, it is observed that during the year 1999, all the blocks of the basin were affected by rainfall deficiency except Karuppanadhi and some parts of Ayyikudi. Blocks such as Shenkottai, and part of Thenkasi are exposed to no drought. Moderate drought prevailed in Kayathar, Kadayanallur, Mannur, Alangulam of Chittar sub-basin. It can be seen from Figure 6 that during the year 2001, most of the blocks were affected by drought with severity class ranging from mild to severe. Parts of Mannur, Kayathar and some part of Ayyikudi, were severely affected.

Figure 4: *Drought Severity of Chittar Sub-basin During 1989*

Figure 5: *Drought Severity of Chittar Sub-basin During 1999*

Figure 6: *Drought Severity of Chittar Sub-basin During 2001*

3.3. Meteorological Drought Risk Mapping

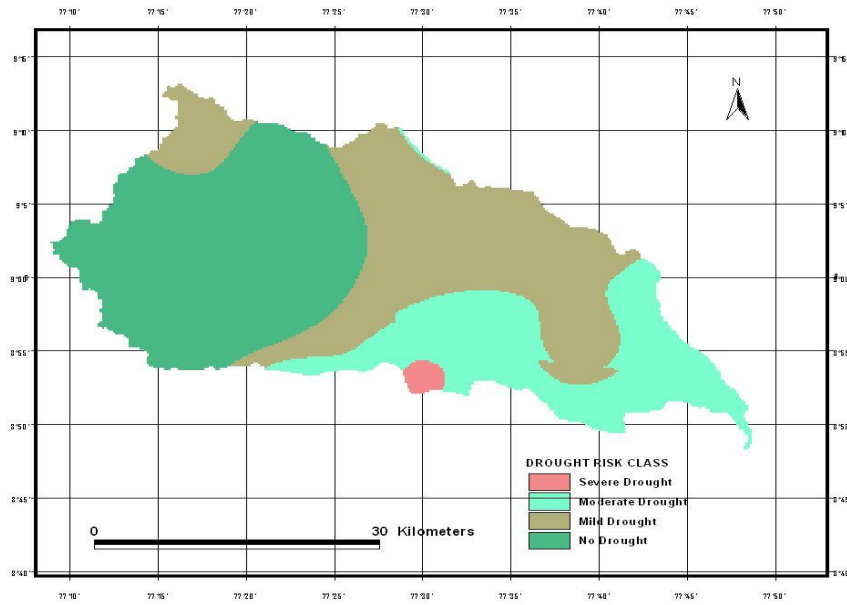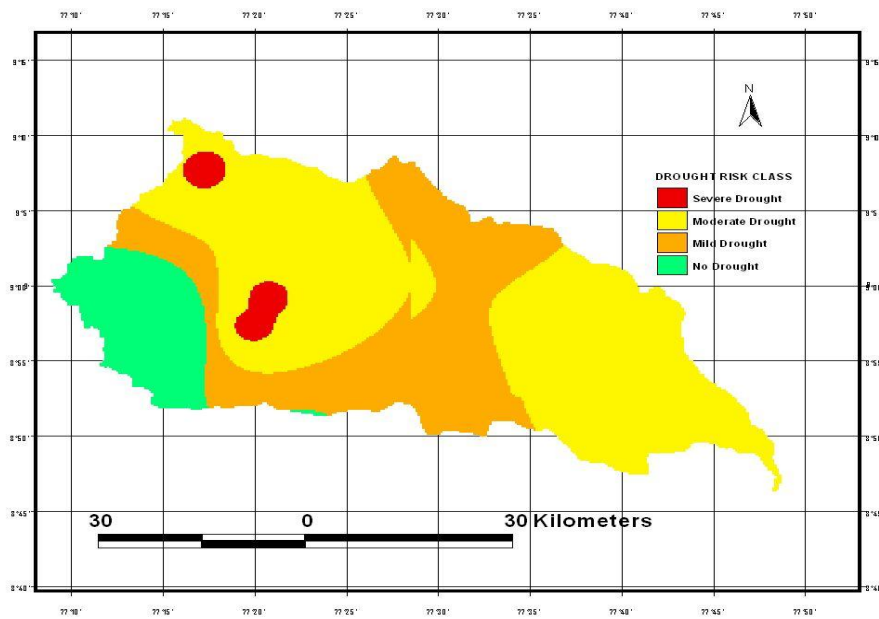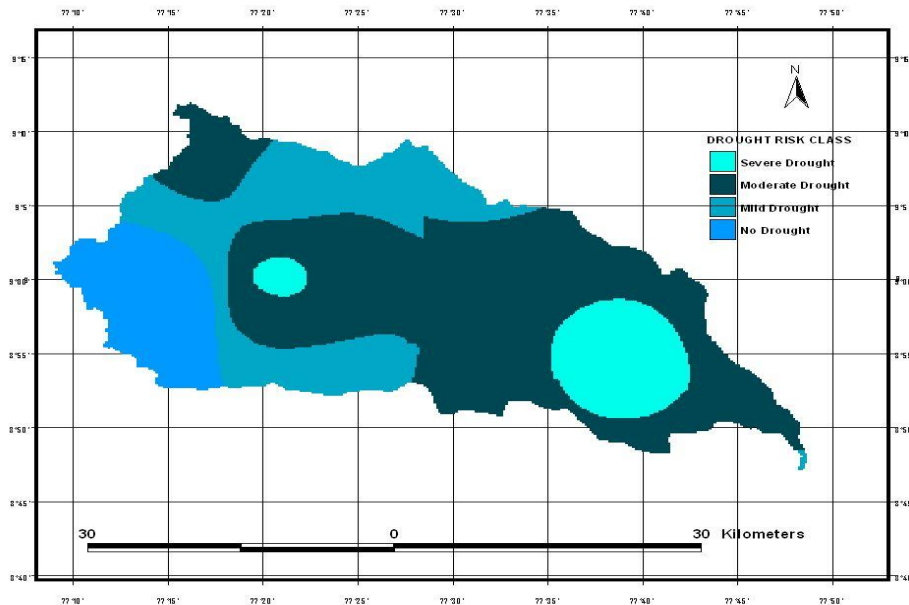Meteorological drought risk index was developed by frequency analysis based on thirty years rainfall data and the results are shown in Table 3. The drought risk index ranges from 1.00 at Gundaru to 2.84 at Kayathar. Four drought risk classes were delineated based on the range of drought risk index. The spatial interpolation of meteorological drought risk index was carried out using Arc view GIS 3.2a. The meteorological drought risk map for Chittar sub-basin is shown in Figure 7. In general, as the blocks surrounding the Western Ghats receive very good rainfall, they are very less prone to meteorological drought risk than other regions. As the distance of blocks from Western Ghats increases, the rainfall decreases. As a result, the drought proneness gradually increases towards East, which can be clearly noticed in the risk map. As Tenkasi and Senkottai are shielded by Western Ghats, they are very less prone to meteorological drought risk. Part of Kadaiyanallur, Kilpavur, Alangulam, Kurivikulam, Shenkottai and Kayattar blocks are under moderate drought risk status. Northern and tail end blocks such as Sankarankovil, Ottappidaram, Karuppanadhi, Karunkulam, part of Manur, and Kayattar are liable to severe drought risks. During heavy rainfall periods, considerable runoff flows to sea, which may be conserved by recharging; to feed the drought affected tail end blocks in this basin.

Table 3: *Meteorological Drought Risk Assessment in Chittar Sub-basin*

Sl. No.	Name of Raingauge Station	Annual Average Rainfall (mm)	No Drought	Mild	Moderate	Severe	Drought Risk Index	Drought Risk Class
1	Alagiyapandiapuram	626.03	0.2	0.4	0.2	0.2	2.4	Moderate
2	Alangulam	743.6	0.25	0.35	0.35	0.05	2.2	Moderate
3	Ayyakudi	674.0	0.16	0.39	0.29	0.16	2.45	Moderate
4	Gundaaru	1788.3	1.00	0.00	0.00	0.00	1.00	Very Mild
5	Kadambur	744.93	0.30	0.48	0.22	0.00	1.92	Mild
6	Kadayam	841.8	0.52	0.23	0.13	0.13	1.89	Mild
7	Kadayanallur	737.10	0.28	0.28	0.36	0.08	2.24	Moderate
8	Karuppanadhi	673.3	0.10	0.38	0.35	0.17	2.59	Severe

9	Kayathar	587.0	0.16	0.13	0.42	0.29	2.84	Severe
10	Kazhugumalai	742.13	0.36	0.48	0.16	0.00	1.8	Mild
11	Maniyatchi	690.74	0.32	0.45	0.16	0.07	1.98	Mild
12	Palayamkottai	720.2	0.29	0.36	0.23	0.13	2.22	Moderate
13	Sankarankoil	674.9	0.16	0.32	0.39	0.13	2.49	Moderate
14	Shenkottai	1536.9	0.94	0.06	0.00	0.00	1.06	Very Mild
15	Tenkasi	904.8	0.55	0.26	0.16	0.03	1.67	Mild
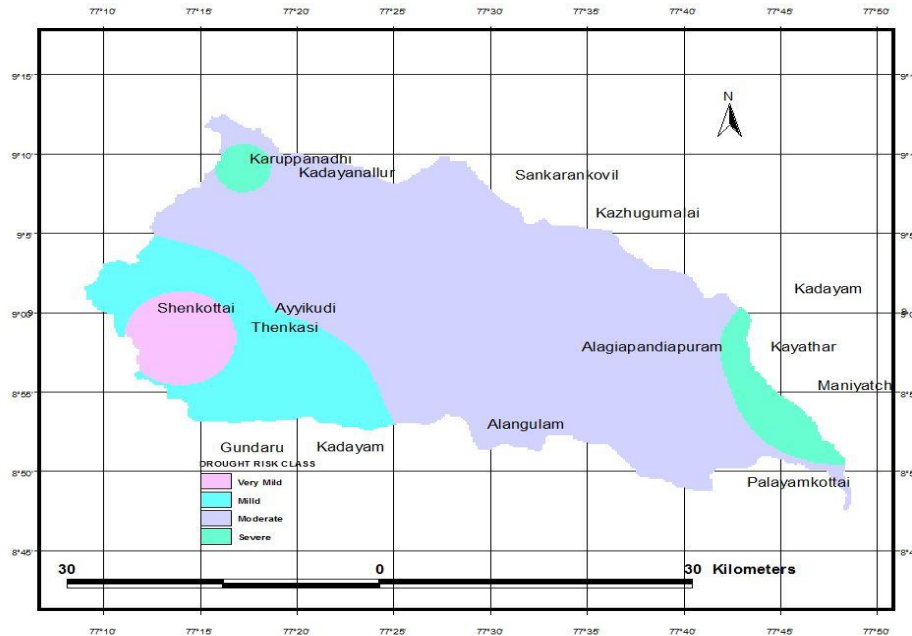
Figure 7: *Meteorological Drought Risk Map of Chittar Sub-basin*

4. Conclusion

Drought is a period of drier than normal conditions that results in deficient water related problems. The consequences of drought range from water supply shortages and crop losses to famine and human abandonment of geographic regions. Drought risk area evaluation is inevitable for taking up the proactive approach of mitigating the drought. The historical occurrence of droughts and their intensity, duration and spatial extent are of great concern for evaluating the risk. In the present study, an attempt is made to quantify meteorological drought risk index. Geographical Information System provides tools to incorporate spatial and temporal variations of water resources data. Rainfall analysis was carried out to find out the variation in space and time for Chittar sub-basin. The assessment of drought severity in the meteorological context was carried out by India Meteorological Department method. IMD is a simple methodology to assess meteorological drought severity of a region. A meteorological drought risk index was developed using the frequency of different classes of drought severity ascertained by this method. Meteorological drought has occurred in the basin once in every 3 to 5 years. Meteorological drought risk area map indicates that except the western blocks of the basin, almost all the other blocks of the basin need urgent drought proofing measures. Evaluations of droughts would help the water resources managers to plan and execute the drought mitigation measures. This will also be very useful to take effective long-term drought proofing measures for the regions that are constantly affected by drought.

References

[1] Dracup J.A., Lee K.S., and Paulson E.G. *On the Definition of Droughts.* Water Resource Research. 1980. 16 (2) 297-302.

[2] Herbst P.H., Bredenkamp D.B., and Barker H.M.G*. A Technique for the Evaluation of Drought from Rainfall Data.* Journal of Hydrology. 1966. 4; 264-272.

[3] T. Murali Krishna, G. Ravikumar and M. Krishnaveni*. Remote Sensing Based Agricultural Drought Assessment in Palar Basin of Tamil Nadu State, India.* Journal of Indian Society of Remote Sensing. 2009. 37; 9-20.

[4] Sharma T.C. *A Drought Frequency Formula.* Journal of Hydrological Sciences. 1997. (6) 803-814.

Research Article **Open Access**

Modern Geomatical Applications for Cadastral Reform: The Italian Case

Gabriele GARNERO[1] and Flavio Celestino FERRANTE[2]

[1]University and Polytechnic of Turin - DIST (Interuniversity Department of Regional and Urban Studies and Planning) Torino, Italy
[2]Revenue Agency- Central Directorate for Cadastre and Cartography, Roma, Italy

Correspondence should be addressed to Gabriele GARNERO, gabriele.garnero@unito.it

Abstract The recent introduction of the IMU (Municipal Property Tax) in Italy has highlighted the vexed question of inequality existing in cadastral appraisal systems. This article outlines the methods and activities, in the field of mapping, supporting of the important process of renewal of the entire cadastral system. It describes the technology and spatial data currently available that can assist in setting up complex issues of reforming appraisal system and, more generally, in the processes against tax evasion in real estate. This paper aims to offer a contribution to the documentation and comprehension of geo-referenced data of the real estate in Italy and processing and analysis tools. The contribution is related to both the hypothesis of a reform of the cadastral appraisal system and, more generally, to the fight against tax evasion in real estate, and to the regular institutional Agency's (*Agenzia del Territorio* – AdT) activities recently incorporated in the "Agenzia delle Entrate". We will discuss AdT data and the technologies of the Agency; then the data and technologies outside the domain of the Agency, but closely related to and interoperable with the first one.
Keywords *Cadastral Surveying, Land Management, Oblique Images, Cadastral GIS*

1. Introduction

In support of the important process of renewal of the entire cadastral Italian system, the principles and criteria relevant for this paper are listed below:

- territorial and functional segmentation of the real estate market;
- use of statistical functions expressing the relationship between the market value, location and positional features and building assets for each destination cadaster and for each geographical area;
- use of "per square meter" as a measurement of urban real estate.

As can be seen from the principles and the above operational criteria, the data concerning the geo-localization of properties in relation to the urban context and to the characteristics of manufactured building play a fundamental role in the revision process, for the correct determination of cadastral appraisal systems and for the time and resources needed for their acquisition. To effectively address these challenges, we need a precise, complete and qualified knowledge of Italian real estate. The AdT manages, on behalf of the State, the real estate information system in Italy, in terms of identification, description of the technical characteristics and economic evaluation and registration of rights. The geo-localizing of real estates is based on the cadastral mapping system.

Since 1960, the Cadaster, as an official cartographic body of the State, is responsible for the management of cadastral maps and especially its continuous updating. The mapping system of the Cadaster is now complete and relatively uniform, throughout the country; it is based on large-scale mapping and entirely managed in vector format, and it is connected to the administrative and census archives through a unique identifier for the entire national territory, consisting of the number of parcel.

The system is now integrated with high-resolution digital ortho imagery and road graphs, but the real strength is its updating system. The inextricable link between the technical component of the map and the legal and administrative-census component, represented by the register identifier (parcel number), must be constantly updated and aligned in both archives throughout all stages of preservation, in order to make effective land registry information in all tax, civil and land governance proceedings [20].

In the more general framework, for the exchange of information with other local authorities where the Cadastral database is characterized by a great potential, in order to meet the needs of territorial knowledge, punctual and prompt updating of archives by automated and standardized procedures is essential to ensure the constant updating and synchronization of information provided by the various cadastral archives [12, 13].

To cope with the amount of more than 600,000 updating acts presented every year at the provincial offices of the Cadaster handling an average of 1,500,000 parcels, in order to eliminate any possible subjectivity in technical examination of documents, the updating system of maps and census data of Land cadaster (*Catasto dei Terreni*) has been fully automated by a computer procedure called *"Pregeo10"* [6, 8]. The new updating system, developed by the Agency with the active participation of concerned National Boards of Professional Associations, is entered into force throughout the country on October 15, 2009. This important goal qualifies the Italian Cadaster as Public Administration type 2.0 [18, 19].

2. The Ortho Imagery Produced by Agea & Identification of Unknown Buildings in the Cadaster

In the context of spatial information available throughout the Country, the ortho imageries produced by *Agea* (*Agenzia per le Erogazioni in Agricoltura*) certainly occupy an important position in the context of the checks provided by the Community regulations for the management of the contributions granted under the CAP (Common Agricultural Policy).

Agea is responsible, according to Decree no. 99/2004, of the coordination and management of the SIAN - National Agricultural Information System, where a full aero-photogrammetric coverage is provided every three years throughout the entire national territory and the production of the cultivation themes based on cadastral maps, in regard of agricultural land.

The Decree 82/2005 (Digital Administration Code) establishes the principle of the "reuse" of the data generated by each Public Administration and their accessibility, through appropriate agreements, by other administrations concerned.

Since 2010, in order to optimize its aspects related to the reuse of ortho imageries, the planning of survey programs has changed. It now becomes on a regional basis rather than provincial, and opens the possibility for the concerned administrations, to acquire jointly to *Agea* ortho imagery with the ground pixel resolution 20 cm instead of 50 cm institutionally provided: this increase in resolution, in case it would be implemented, will start from the next three years 2014-2016 and will lead to a real improvement in the possibilities of using the ortho maps produced within the SIAN for real estate updating.

The ortho images with ground pixel resolution of 20 cm would allow to determine with greater accuracy the positional and close range parameters properties and, consequently, to refine the appraisal of urban housing units, considerably limiting the direct intervention on the ground.

In the broader context of the fight against tax evasion, the AdT has undertaken a long series of actions aimed to identify potential evasion in real estate projects with high technological contents. In the recent past, according to the provisions of the Finance Act of 2007, the AdT has undertaken a significant project to "identify the buildings unknown by the Cadaster".

The project, characterized by an advanced technology, was prepared in collaboration with AdT, *Agea* and *Sogei* (*Società Generale di Informatica*) and is an example of cooperation and integration between information systems of Public Administrations. Thanks to a special agreement signed in May 2007, the agencies have identified the common ground where their skills might find useful synergies for the government and citizens, in the general interest of the State.

In order to achieve this goal, a general survey of the whole country has been carried out, with the exception of the Autonomous Provinces of Trento and Bolzano. The local survey was carried out through the integration of cadastral maps in vector format with digital high-definition color ortho imagery, the Digital Terrain Model (DTM), the Digital Surface Model (DSM) and near-infrared images [11]. The first step, carried out on the basis of the DTM and DSM, has involved the automatic identification of existing land features; these were then classified, first in relation to the height and then with the aid of near infrared images: it was possible to discriminate the vegetation from other artifacts, thus identifying buildings in automatic mode.

The spatial intersection, between polygons related to objects on the ground identified and the polygons of the buildings, present in the cadastral maps allowed to highlight the parcels on which buildings were found which are not present in the cadastral maps.

The results obtained were then subjected to systematic quality control, performed through the conventional photo-interpretation on the same digital high resolution ortho photos (pixels 50 cm), in order to eliminate errors that an automated process at industrial level inevitably entails, especially in relation of the "quality" of the used data.

The final product of the activity, carried out in synergy with *Agea,* consists of a list of the parcels on which buildings were found which are not present in the maps of the Cadaster; the list of the parcels was then intersected with the data of the various cadastral archives. This operation has eliminated, from the initial parcels, the ones known in the Land cadaster, as in other internal records.

The project, which began in mid-2007, was concluded in the early 2010 and has identified over 2,000,000 parcels on which there are unknown buildings. Among the positive effects of this project, the full availability for the Cadaster, of the high-definition ortho imageries immediately integrated with the cadastral maps in their systems must be highlighted, for the development of important projects, not least for the reform of the Cadaster.

According to the current provisions of law (Decree Law 78/2010, Art. 19, Paragraph 12), from 1 January 2011, the AdT, on the basis of new information related to technical and administrative checks, remote sensing and ground surveys must provide to start the constant monitoring of the territory by identifying, in collaboration with municipalities, other buildings not declared in the Land Cadaster. In order to achieve these statutory provisions and to make a more effective investigation, the AdT is considering the possibility of making use of advanced technological solutions such as aerial images acquired by oblique sensors, as explained in the following paragraphs.

3. Applications Relating to the Use of Google Earth and Microsoft Virtual Earth

The diffusion of shared *web* tools providing completely free of charge repertoires of dynamic aerial and satellite imagery on a global scale is now well established: the basics of *Google Earth* and *Microsoft Virtual Earth.* We all quickly learned to know and use for no professional applications are becoming real integrated tools proposed as a *repository* of spatial information not limited to data entered in network by the managers of the system, but as instruments in which it is possible to integrate and share information in different ways [3, 7].

Recently, this potential has been extended to the world of geographic information systems, with the opportunity to integrate local databases with remote *databases* of images: the instrument is of great interest for the study of territorial and landscape issues, given the integration of GIS tools already widely used in the field, and good image quality and potentially continuously updated, allowing a careful reading of the territory and its modifications [5]. Its implementation in the GIS also allows an active participation in the process of spatial analysis, with the option to extract data interpreted from the images in vector and/or alphanumeric geographic databases. There have already been numerous studies [2, 14, 17] on the possibilities of use of these innovative supports in the processes of territorial and landscape analysis, in order to identify the scale threshold beyond which the basics in subject no longer constitute a support geometrically reliable.

Virtual Earth and *Google Earth* are using a reference system that, at least in Italy, is not employed in other applications: the system *3785 - Web Mercator WGS84,* as codified in *EPSG Geodetic Parameter Dataset.* EPSG (*European Petroleum Survey Group*), an agency currently included in *OGP Surveying and Positioning Committee*, body of the *International Association of Oil & Gas Producers* (OGP) which provides to maintain and to issue a worldwide database of cartographic and geodetic reference systems and their transformation parameters.

For the purpose of this paper, the geo-referenced images of *Google Street View* implemented within *Google Maps* and *Google Earth* are particularly useful providing panoramic views of 360° horizontally and 290° vertically along the streets (at a minimum distance of 10-20 meters apart) and allows users to view portions of cities around the world at ground level.

Introduced in May 2007, the service *Street View* is active in Italy from October 2008; especially in 2009, there has been a rapid increase of the streets served: the cover is shown dragging an orange man ("*Pegman*", present in task bar) and placing him in a point on the road, in order to activate the corresponding panoramic photography. To carry out the photos, *Google Street View* uses special cameras (the *Dodeca 2360*, equipped with 11 objectives and produced by the Canadian company *Immersive Media*) located on the roof of cars. Pedestrian areas, parks and roads, bicycles are used instead of the specially equipped vehicle: the service is now extended to most of the main roads and urban streets of many large and small urban centers, with a coverage extended to all Italian regions, the coverage of the updated service is available *online* at
http://www.google.com/help/maps/streetview/learn/where-is-street-view.html

It is clear that the ability to view, at least, the street fronts of the areas already served by the service, can be of immediate and quick use in order to allow users a first visual access to the extrinsic characteristics of the buildings and surrounding areas.

4. Oblique Photogrammetry

On the national market, several companies are operating, able to realize, in addition to traditional nadir ones, photogrammetric surveys performed with sets of cameras arranged so as to capture the territory features with oblique angles, so as to give priority to the acquisition of the facades of buildings [14].

The industrial solutions going under the name of *Pictometry®*, *Midas®* of *Track'air*, *iOne®* of *Visual Intelligence* , ..., involve the use of survey systems consisting of several cameras rigidly connected to each other, mounted on a single support on which the inertial sensor is applied (IMU) for the acquisition of the angular components of the image.

In *Pictometry* and *Midas* systems there are 5 cameras, 4 of them are installed with an inclination of 40-45° from the vertical, according to the four directions of view and perpendicular to each other (forward, backward, left and right); the fifth chamber is installed as the traditional photogrammetric cameras in order to capture the territory flown over from the zenith. Frames are triggered simultaneously and are therefore five images that share the same instant. The *tools* available allow, as well as to manage the large mass of data in navigation environments from the base ortho image, to make queries and quantitative measurements on the plano-altimetric size of buildings, thus providing the operators with performing tools for the analysis and check of buildings.

As known to the authors, aerial oblique images are currently available, throughout the national territory, of all the provincial capitals and major towns with a population of over 50,000 inhabitants, with photos from 2005 (Figure 1).

Figure 1: Oblique Sensors Integrated into the Process of Photogrammetric Surveys

Furthermore, during 2010 and 2011, the Autonomous Region of Sardinia has arranged for services relating to the contract for the capturing oblique images of the historical centers: all urban centers have been acquired, with technology *Pictometry* and with ground pixel resolution of the order of magnitude of 5 cm, so as to document the landscape context in which the centers ("*centri matrice*") are located and to highlight morphological and settlement differences between centers, with particular reference to the morphology of the plains, hills, mountains, coast, slope, etc. (Figure 2).
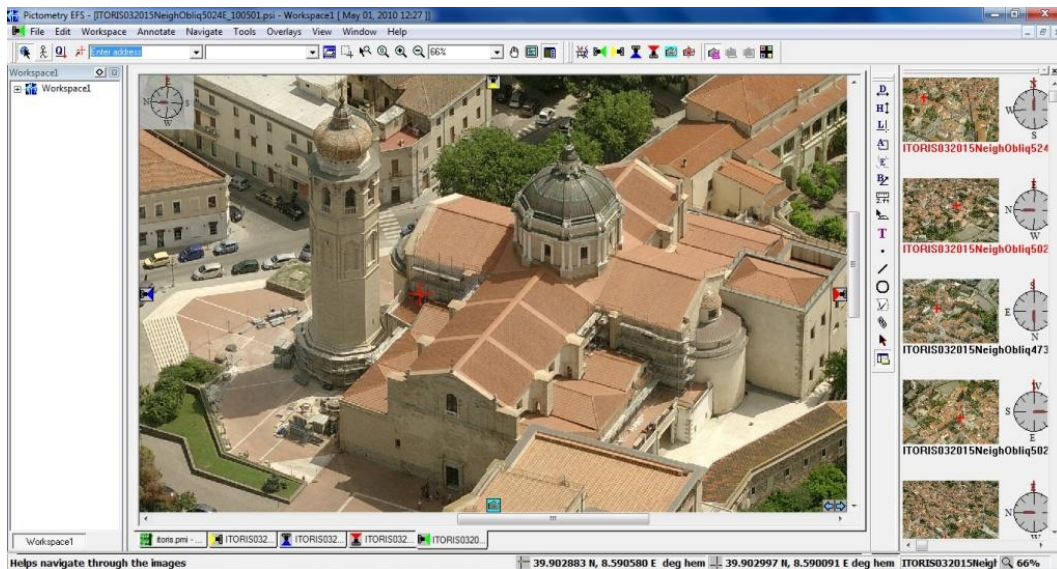

Figure 2: Consultation of Oblique Images of a Center of the Sardinia Region

The set of nadir and oblique photos allow to better understand the way in which these centers have developed, and to pick up the different building types through the analysis of the fronts of buildings and the internal parts, as well as to highlight the issues concerning the restoration and renovation of fine buildings, with a purpose of monitoring the territory, from the urban point of view in relation to the city center and the surrounding buildings.

The high definition allows documenting the current state of the buildings and road plots, so as to permit the establishment of a photographic support to institutional planning and regulation of the land [9, 10].

From the above, it therefore appears that the availability of already realized oblique images, relatively recent and, as previously described, directly relatable with cadastral maps with the technology to be described later, is not negligible, as it is likely to cover not less than 70% of built areas, so it is reasonable to hypothesize the development of this asset of information for the previously explained purposes*,* reasonably quickly, so as to avoid the natural obsolescence of the same.

Among the technologies readily available, the system BLOM-urbex allows you to integrate the cadastral maps with Orthophoto, displayed in the center of the screen, while the side shows the oblique images related to the same area. But it is still difficult, especially in city centers and in particular in those with complex morphology, to univocally identify the selected perspective views of the building on the cadastral map of which we want to know the characteristics. This ambiguity is resolved with the technology that will be discussed later, on the occasion of the description of 3D models of buildings.

Many have also considered the possibility of integrating photogrammetric surveys performed by *Agea*, already mentioned above, with at least 2 oblique cameras, in order to obtain, at the same time the acquisition of frames for ortho imagery and oblique images to be used for applications in the built environment [15]. Such surveys, if systematically realized, cannot of course be compared to the ones especially produced as oblique, because of the obvious shortcomings relative to the scale and therefore the size of the pixels, of insufficient capture directions and consequent deficiencies of information, with directions of building profiles completely excluded from the acquisition.

Anyway it is correct to consider that such possibilities, which should be produced with very low costs because of the simultaneity with the primary observations, could be profitably used in contexts outside the city, where there are less issues of mutual coverage between buildings and where it is not and, it cannot be economically feasible an oblique survey in canonical way.

In the economic context characterizing the present time, however is natural to consider the exploitation of what is available and usable with what can be achieved with sustainable costs, so as to ensure the economic feasibility to what is necessary to achieve the objectives.

5. Surveys with UAV

The only identification and documentation of the extrinsic characteristics of buildings could be obtained also with instruments of decidedly lower performance and less expensive than those described above as, for the applications in question, a metric quality is not required in order to perform measurements and quantitative estimates, but rather a good photographic quality that allows the operator to identify photographically all or most of the features to be detected in an inspection in the countryside, or at least to limit the visits to the controversial cases [4].

There is thus an increasing interest in the possibility of using pseudo-amateur photographic equipment on board of unmanned aircraft, technically defined *drones* or UAV (*Unmanned Aerial Vehicle*); this means aircraft with varying size from ones for military applications to small toy model aircraft.

The availability of GNSS positioning systems sufficiently precise can be obtained with very small size and weight, together with the existence of microscopic accelerometers and gyro sensors with MEMS technology, with software controlled now generally available in *open source*, opens new possibility of realization of systems for the acquisition of digital images on board of aircraft of various sizes [1].

The recent regulations issued by ENAC (*Ente Nazionale Aviazione Civile* - National Agency for Civil Aviation) NI-008-2012, dated August 2, 2012, defines precisely the activities of so-called mini-and micro-UAVs (respectively weighing less than 20 and 5 kg) and at up to a limit of 150 kg in respect of activities which, though still described as "experimental", can obviously have interesting professional consequences.

In the near future, it will also be possible to perform low altitude surveys, with tools like APR (*Aircraft in Remote Steering*), to recover photogrammetric information that would not be acquired through inspection, both for lack of access and for economic reasons.

6. Technology for the Virtual Reconstruction of Built Areas

The availability of information already acquired and also the possibility that other acquisition channels are activated, for large parts of the territory as for decidedly sub-regional context, allows defining a profitable use of these observation methods within the cadastral issues, even in relation to the availability of technologies that can be easily *customized* for these specific needs.

An operator setting himself the aim of verifying the extrinsic characteristics of buildings using aerial oblique images, should be able to operate in a dedicated software, which allows him to see the cadastral map integrated with the ortho image, and should be able to see oblique images with the help of software minimizing the possibility of misidentification of the building while synchronizing the oblique view on the building pointed on the map.

To this aim, in addition to the customization of the environments of consultation of the oblique images which we have been previously shown, the implementation is now feasible, albeit in a simplified mode, of a *3D City Model* dedicated to cadastral applications (Figure 3).

This term is technically defined as a consultation environment in which the buildings are reconstructed geometrically as solid and whose faces are "draped" from the information available on the radiometric frames: in this way the user forgets the frames and finds a virtual model reconstructed on which he can perform the observations or possibly measurements.

The construction of the *3D City Model* has long been present within the geomatic products available on the market, but only the recent improvements in the techniques of autocorrelation allow planning of generation processes achievable in entirely automatic mode, with consequent reduction of costs of production and therefore openings to more generalized use.
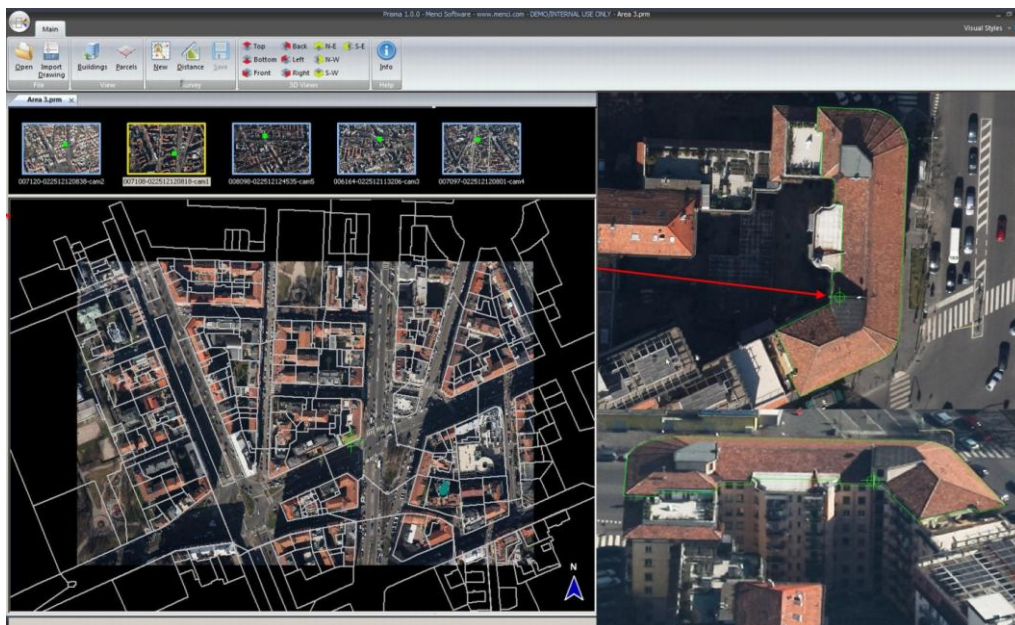
Figure 3: Prototypal Realization of a 3D City Model using an Oblique Midas (Property Blom CGR) Survey with Menci Software Technology on the City of Milan

Of course, once available for this aims, the performed basic may be exploited and also used for different purposes; for example, for the integrated protection and control, in municipal databases on in others various applications [16].

7. Integration of GIS Technology and Data Inside and Outside the Domain of AdT

As shown in the Introduction, it appears how for the implementation of plans of cadastral surveys reforming, geographic data (cadastral maps, orthoimagery, LiDAR data, oblique images captured by sensors, road graphs, real estate zoning, ...) and alphanumeric (cadastral DB, real estate DB, …) knowledge are strategic.

The effective exploitation of all these information components in a suitable environment that can integrate and correlate data from different sources is essential for the success of the project of reforming the estimate of the Building cadaster.

The environment able to integrate geographical and alphanumeric data along with the technologies, as known, is the GIS (*Geographic Information System*). For issues related to the reform of the Cadaster, GIS platforms allow for example to correlate data of the Urban Building Units (UIU) directly to the cadastral map: the operator can perform precise analyzes or statistics of any attribute of UIU (value/rent, classification, consistency, …) and represent reports on cadastral maps which, when suitably integrated with the high resolution orthophotos, allows to correlate the data position and/or overlooking with classification or consistency of the data of UIU.

The Figure below shows, for example, on the cadastral map integrated with the orthophotos, reports of a statistical analysis conducted on the data of classification of the Urban Building Units of a central area of Rome, a comparison between the statistical data of classification of building units both those within the same building and those in the same area of study, highlighting some of the inequalities in classification that the cadastral survey review should cancel or at least reduce (Figure 4).
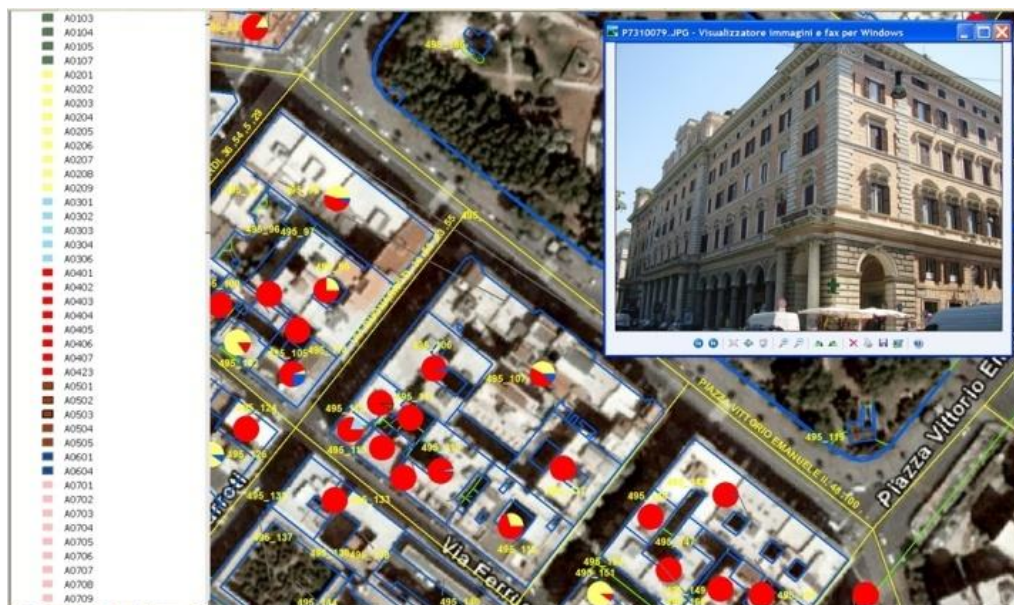
Figure 4: Cadastral Maps Integrated with Orthophoto Maps and Graphs - Results of the Analysis on Spatial Data "Classification" of Urban Building Units

It is thus possible to integrate and analyze, on the same GIS platform, data relating to the characteristics of the extrinsic buildings: such information can be effectively drawn from close-up images of the sensors acquired simultaneously with the nadir images and allows, as indicated, relating the buildings fronts with "buildings' polygons" represented on the cadastral map, without any ambiguity.

8. Conclusion

The data on the position, the prospect and those relating to the extrinsic characteristics of the building, allow to effectively implement the estimation algorithm for the value of the building and severely limiting the direct intervention on the ground, with an obvious containment of time and costs.

The assumed GIS platform is crucial in analysis and management of data, in preparation for the estimation of property values, but it becomes particularly strategic in the final phase of the process, that is, when it comes to review and harmonize values and UIU rents of neighboring buildings belonging to different areas characterized by different values of the real estate market or to different municipalities or even to different provinces or regions.

It seems appropriate to point out, in conclusion, that, regardless of the technology platform, the effectiveness of the results depend strongly on the data quality (completeness, consistency, accuracy, updating, positional accuracy, etc.), especially by their degree of correlation in various archives.

References

[1] Astori, B., Guzzetti, F., Pinto, L. (1996): *Studio sperimentale sull'uso di metodologie avanzate di ripresa, per la costruzione di carte a grande-media scala.* Bollettino Di Geodesia e Scienze Affini. 55 (4) 313-374.

[2] Bennett, R., Kalantari, M., Rajabifard, A. R. (2010): *Let the Dialogue Begin Beyond Cadastre 2014.* GIM International. 24 (7) 25-27.

[3] Chiabrando, R.; Garnero, G.; Godone, D. (2008): Basi dati condivise per l'analisi e la progettazione territoriale: Google Earth e Virtual Earth cambiano le prospettive sulla gestione dei dati territoriali, Congresso AIIA 2008: Segni dell'uomo e trasformazioni del paesaggio: analisi storica e prospettive di valorizzazione. Marina di Pisticci (MT).

[4] Cicibas, H.; Demir, K.A., Gunal, M.M.; Arica, N. (2012): *A Simulation Model for Analysing Unmanned Aerial Vehicle Flight Paths.* 24th European Modeling and Simulation Symposium, EMSS 2012, 543-548.

[5] Dragićević, S., Li, S., Brovelli, M., Veenendaal, B. (2011): *Pervasive Web Mapping, Geoprocessing and Services*; Transactions in GIS. 15 (2) 125-127.

[6] Ferrante F. (2010): *Il sistema di aggiornamento della cartografia catastale.* Un tesoro Ritrovato, Cangemi Editore.

[7] Ferrante F. (2009): L'integrazione del catasto con Google Earth, Google Maps e Street-View, Territorio Informa, gennaio/marzo 2009.

[8] Ferrante F. (2009): Il nuovo sistema di aggiornamento del Catasto dei Terreni, Rivista dell'Agenzia del Territorio, n. 2/2009.

[9] Garnero, G.; Cogoni, A. (2012) Activity at *Low Altitude Photography in Urban Agglomerations of Sardinia and its Architectural Context, in Planning Support Tools: Policy Analysis, Implementation and Ev*aluation. Proceedings of the Seventh International Conference on Informatics and Urban and Regional Planning INPUT 2012, Franco Angeli, Milano.

[10] Garnero, G.; Corrias, A.; Manigas, L.; Zedda, S.V.: *VGI, Augmented Reality and Smart Web Application: Projects of Development in the Territory of the Sardinia Region.* In B. Murgante et al. (Eds.): ICCSA 2013, Part IV, LNCS 7974, Springer, Heidelberg, 77-92.

[11] Godone, D.; Garnero G. (2013): *The Role of Morphometric Parameters in Digital Terrain Models Interpolation Accuracy: A Case Study.* European Journal of Remote Sensing. 46; 198-214.

[12] Grecea, C., Bala, A.C., Herban, S. (2013): *Cadastral Requirements for Urban Administration, Key Component for an Efficient Town Planning*. Journal of Environmental Protection and Ecology. 14 (1) 363-371.

[13] Groot R. (2001): *Reform of Government and the Future Performance of National Surveys*. Computers, Environment and Urban Systems. 25 (4-5) 367-387.

[14] Habbecke, M.; Kobbelt, L. (2012): *Automatic Registration of Oblique Aerial Images with Cadastral Maps*. Lecture Notes in Computer Science (Including Subseries Lecture Notes in Artificial Intelligence and Lecture Notes in Bioinformatics), 6554 LNCS (PART 2), 253-266.

[15] Kraus K. (1994): Fotogrammetria (trad. italiana di S. Dequal), Ed. Levrotto e Bella, Torino.

[16] Minucciani, V.; Garnero, G. (2013): *Available and Implementable Technologies for Virtual Tourism: A Prototypal Station Project*. In B. Murgante et al. (Eds.): ICCSA 2013, Part IV, LNCS 7974, Springer, Heidelberg, 193-204.

[17] Van Oosterom P. (2013): *Research and Development in 3D Cadasters,* Computers, Environment and Urban Systems. 40; 1-6.

[18] Rajabifard, A., Williamson, I., Steudler, D., Binns, A., King, M. (2007): *Assessing the Worldwide Comparison of Cadastral Systems*. Land Use Policy. 24 (1) 275-288.

[19] Steudler, D., Rajabifard, A., Williamson, I.P. (2004): *Evaluation of Land Administration Systems*. Land Use Policy. 21 (4) 371-380.

[20] Zhao Y. (2010): *One Map-Based Land Information System- Towards E-Government for Land Management*. Proceedings of the International Conference on E-Business and E-Government, ICEE 2010, 687-690.

Research Article   **Open Access**

Drought Analysis Using Digital Image Processing & Meteorological Data

Surendra Singh Choudhary, P.K. Garg and S.K. Ghosh

Department of Geomatic Engineering, Indian Institute of Technology, Roorkee, Uttarakhand, India

Correspondence should be addressed to Surendra Singh Choudhary, surendra2060@gmail.com

Abstract Meteorological drought is simple absence/deficit of rainfall from the normal. It is the least severe form of drought and is often identified by sunny days and hot weather. Importance of time scale when accessing different types of drought, meteorological drought depends on precipitation deficit and duration of period with precipitation deficit. This study demonstrates observed meteorological based drought indices such as Normalized Deviation (ND), De Martonne's Index (I_A)**,** Pluvothermic Quotient (PQ), Negative Moisture Index (NMI) and Standard Precipitation Index (SPI) values were interpolated to get the spatial pattern of meteorological based drought. Crop yield and production trend was plotted and an equivalent Normalized Difference Vegetation Index (NDVI) threshold was identified to get the agricultural drought risk in Jodhpur district, where the occurrence is high in Jodhpur district. Monthly rainfall data from six stations were used to derive the Standardized Precipitation Index (SPI). The Landsat-7 ETM+ and Landsat-5 TM satellite sensor data was used for calculating Brightness Temperature (BT), Land Surface Temperature (LST). BT was converted to the Vegetation Condition Index (VCI) and the Temperature Condition Index (TCI), which are useful indices for the estimation of vegetation health and drought monitoring. The analysis was carried out for a period of 21 years (1991–2011) and from the SPI analysis it is found that in 2002 all of the area under study was affected by drought with greater intensity, can be classified as extreme and severe drought conditions.
Keywords *NDVI, BT, TCI, LST, DEM, Crop Yield, Production*

1. Introduction

Drought is a climatic anomaly, characterized by deficient supply of moisture, resulting either from sub-normal rainfall, erratic rainfall distribution, higher water need or a combination of the entire factors (Bhalme and Mooley, 1980). The escalating impact of drought has increasingly drawn the attention of scientists, planners and society. The vulnerability to drought in relation to the increasing needs of the growing population has become a point of great concern, especially at the food front. Drought is considered the most complex but least understood of all natural hazards, affecting more people than

any other hazard. Drought is a normal feature of climate and its recurrence is inevitable (Mishra and Desai, 2005).

Different definitions of drought have been proposed from time to time depending on the moisture needs for specific human activities and subject of interest. In current hydrological literature, devising a suitable universal definition of drought has become a difficult task (Yevjevich, 1967; Dracup et al., 1980b). (Cole, 1933) has defined drought as a period of at least 15 consecutive days none of which had rainfall of 2.5 mm or more. According (Hoyt, 1936), there is a drought when annual rainfall is less than 85% of normal. (Ramdas, 1960) has defined drought as a situation when rainfall is deficient by twice of its mean deviation. (Konstantinov, 1968) believed that drought should be studied using an analysis of deficit of evapotranspiration, which defined as the difference between the potential and the real evapotranspiration. (Palmer, 1965) has defined drought at a given location, as a period of time, lasting months or years, during which the actual moisture supply consistently falls short of the climatically expected moisture supply. (Dracup et al., 1980a) has defined drought as a period of time (month/year) with rainfall/runoff below a mean truncation level which is derived from long term rainfall/runoff series. Variables which are used either alone or in combination for defining drought are rainfall, temperature, humidity, evaporation from free water, transpiration from plants, soil moisture, wind, stream flow and wind conditions. Drought is difficult to detect and monitor for three reasons: (1) it develops slowly, and the onset and end are indistinct; (2) it is precisely and universally defined and (3) its impact is non-structural and often spreads over a very large area (Wilhite, 2000).

The global climate change is characterized by increase in surface temperatures to the tune of 0.6±0.2°C over the twentieth century and with a projected rise in the range of 13.5°C by 2100 (Houghton et al., 2001). Climate change is expected to change the existing vulnerability profile of India (O'Brien et al., 2004). The studies on the past climate indicated an increase in the temperatures to the tune of 0.57°C per 100 years (Kumar et al., 1994; Singh et al., 2001). Some studies identified decadal departures above and below the long time average rainfall alternatively for three consecutive decades (Kothyari and Singh, 1996). The most notable climate change implication for the vulnerable India is the frequent occurrence of drought. It is therefore important for scientific community to carry out enhanced preparedness with due emphasis to the community based preparedness planning, review the existing monsoon and drought prediction methodologies, and establish drought monitoring and early warning systems in association with a matching preparedness at the input level.

Arid Rajasthan is characterized by limited seasonal precipitation with erratic distribution, high atmospheric temperature that has large diurnal and seasonal variation, strong insolation and persisting wind regime. Consequently, there are high crop water requirements. The weather conditions remain too dry, even in normal years, for most part of the year and are inhospitable for successful crop growth (Rao, 2009).

Sowing rains have also been found to occur at times as early as 1st week of June in the eastern part and 2nd week of June in the western part. Such early or late commencement of sowing rains lead to large variability in year to- year crop productivity. The assured crop growing period in western Rajasthan varies from 25 to 90 days under shallow soils and 35 to 105 days under deep soils (Rao *et al.*, 1994).

Relative humidity in the region is often less than 30% during summer months, but gradually increases to 80% by monsoon and then decreases from October onwards, following the withdrawal of the monsoon. Low humidity, combined with strong wind regime, leads to advection, a phenomenon that causes evaporation loss more than the energy actually available through solar radiation. (Rao, 2009).

2. Various Meteorological Drought Indices

(i) **Normalised Deviation (ND)** (Nagarajan, 2003)

It is defined on the basis of degree of dryness (in comparison to normal or average amount) and duration of the dry period. It is the departure of actual precipitation to average amount of monthly, seasonal or annual rainfall. It lies between -1 to +1, negative indices deficit rain. Following equation gives the relationship between ND and precipitation:

$$ND = \frac{P_{total} - P}{P} \qquad (2.2)$$

Where, P_{total} is the total precipitation in mm for a year and P is the average annual rainfall.

(ii) **Dryness Index (I_d)** (Nagarajan, 2003)

It gives the relation between temperature and precipitation of the region and is given by following equation.

$$I_d = \frac{56 \log_{10} 120T}{P} \qquad (2.3)$$

Where T is average annual temperature 0^0C and P is the average annual precipitation in mm. It is classified as arid extreme if I_d greater than 72, arid moderate if I_d between 50 and 71 and arid mild if I_d less than 50.

(iii) **De Martonne's Index (I_A)**

De Martonne's Index gives the relationship between precipitation and temperature, and is given by following equation.

$$I_A = \frac{P}{T - 10} \qquad (2.4)$$

For true desert I_A is less than 5, for arid zone I_A is between 5 and 10, for semi-arid zone I_A is between 20 and 30 (Nagarajan, 2003).

(iv) **Pluvothermic Quotient (PQ)**

Pluvothermic Quotient brings out the relationship among parameters such as precipitation and temperature and is given by the following equation.

$$PQ = \frac{100 * P/(T_M + T_m)}{(T_M - T_m)} \qquad (2.5)$$

Where, T_M is average maximum temperature in the hottest month and T_m is average minimum temperature in the coldest month. When PQ is less than 40, it is desert, if PQ lies between 60 and 100, it is semi-arid and PQ is greater than 300 for humid zone (Nagarajan, 2003).

(v) **Arid Anomaly Index (AI)** (Nagarajan, 2003)

Arid anomaly gives the expression of water deficiency by the plants and is given by following Equation.

$$AI = 100 \left(PE - \frac{AE}{PE} \right) \qquad (2.6)$$

Where, PE is potential evapotranspiration, AE is actual evapotranspiration. As per IMS standards, for mild arid region AI lies between 0 and 25, for moderate arid region the value of AI lies between 26 and 50 and severe if AI is greater than 50.

(vi) Negative Moisture Index (Bhalme and Mooley Index) NMI

This index is also known as Bhalme and Mooley index. This index values are classified between normal to extreme drought by Palmer's drought intensity classification, and is given by following equation.

$$\text{NMI (M)} = \frac{100 \left(P_{mtotal} - P_{mmean} \right)}{e} \qquad (2.7)$$

Where, P_{mtotal} is total monthly precipitation, P_{mmean} is monthly mean precipitation over M years of observation, m denotes month under consideration and e is the standard deviation. The NMI values are classified between normal to extreme drought by palmer's drought intensity classification (Nagarajan, 2003).

(vii) Palmer Drought Severity Index (PDSI) (Palmer, 1965)

PDSI is soil moisture algorithm. This index is calibrated for homogeneous area and not for mountainous areas. It could be compared between locations and months. PDSI involving for steps which are hydrological accounting, climatic coefficients, climatically approximate for existing conditions (CAFEC) value and moisture anomaly index. Following equation gives an empirical expression to measure drought severity.

$$X_j = 0.897 X_{j-1} + \frac{Z_j}{3} \qquad (2.8)$$

Where, Z_j represents values of moisture anomaly index for the dry intervals and X_j represents the values of PDSI for j^{th} month.

The Palmer is a soil moisture algorithm calibrated for relatively homogeneous regions. Many U.S. Government agencies and states rely on the Palmer to trigger drought relief programs. Values of palmer classification for various conditions of drought are given in Table 1. The first comprehensive drought index developed in the United States. Palmer values may lag emerging droughts by several months; less well suited for mountainous land or areas of frequent climatic extremes built-in time scale that can be misleading.

(viii) Standardized Precipitation Index (SPI)

The Standardized Precipitation Index (McKee et al., 1993) has been applied to quantify monthly precipitation deficit anomalies on multiple time scales (1-month) for the period during 1991–2011. Computation of the SPI involves fitting a gamma probability density function to a given frequency distribution of precipitation for a given station. The SPI represents a statistical *z*-score or the number of standard deviation (following a gamma probability distribution transformation to a normal distribution). Above or below that an event is demarcated with reference to mean (Edward and Mckee, 1997). The values of SPI between $1 > Z > -1$ shows the near normal precipitation event. Further the *z*-score −1 or less indicates the drought events. When the value of *z*-score goes lower than −1.5, it indicates of severe drought condition. The estimated values of SPI (*z*-score) for one month time scale

revealed that the extreme dry events with *z*-scoreless than −2 are mostly experienced in the month of May. SPI values are shown in Table 2.

Table 1: Palmer Classifications

Palmer Classifications	
Values	**Indicator**
4.0 or more	Extremely Wet
3.0 to 3.99	Very Wet
2.0 to 2.99	Moderately Wet
1.0 to 1.99	Slightly Wet
0.5 to 0.99	Incipient Wet Spell
0.49 to -0.49	Near Normal
-0.5 to -0.99	Incipient Dry Spell
-1.0 to -1.99	Mild Drought
-2.0 to -2.99	Moderate Drought
-3.0 to -3.99	Severe Drought
-4.0 or less	Extreme Drought

Table 2: Standardized Precipitation Index (SPI) (McKee et al., 1993)

SPI	Classification	Probability (%)
2.00>	Extremely Wet	2.3
1.50 to 1.99	Very Wet	4.4
1.00 to 1.49	Moderate Wet	9.2
0 to 0.99	Mildly Wet	34.1
0 to -0.99	Mild Drought	34.1
-1 to -1.49	Moderate Drought	9.2
-1.50 to -1.99	Severe Drought	4.4
-2.00<	Extreme Drought	2.3

The transformation of original precipitation values (for any specified time period) in to the Standard Precipitation Index has the intent of:

(i) Shifting the mean of the data to have a transformed mean of zero;
(ii) Shifting the standard deviation of the data to have a transformed value of 1.0;
(iii) Reducing the skew existing in the data towards zero.

When these goals have been achieved, the resultant Standard Precipitation Index may be calculated as-

$$\text{Mean} = \bar{X} = \frac{\sum X}{N}, \tag{2.9}$$

Interpretable as a standardized (or Z) scope with a mean of zero and standard deviation of 1.0.

$$s = \sqrt{\frac{\sum(X-\bar{X})}{N}} \tag{2.10}$$

$$\text{Skew} = \frac{N}{(N-1)(N-2)}\sum\left(\frac{X-\bar{X}}{s}\right)^2 \tag{2.11}$$

Second, the precipitation data are transformed by the log normal (ln) and the mean of those values is computed. Those transformed value are further described by the constant U, shape and

$$\text{Log mean=}\bar{X}_{ln} = \frac{\ln(X)}{N} \tag{2.12}$$

$$U = \ln(X) - \bar{X}_{ln} \tag{2.13}$$

$$\text{Shape=}\beta = \frac{1}{4U}\left[1 + \sqrt{\frac{4U}{3}}\right] \tag{2.14}$$

$$\text{Scale=}\alpha = \frac{\bar{X}}{\beta} \tag{2.15}$$

Third, the log values are transformed by gamma distribution, incorporating the shape and scale values:

Cumulative Gamma transform=

$$G(x) = \frac{1}{\alpha^{\beta}\Gamma\beta}\int_0^x x^{\beta-1}e^{-\frac{x}{a}}dx \tag{2.16}$$

The example employs Excel spreadsheet functions, where available, other spreadsheet program have similar function that produce identical values.

T transform=

$$t = \sqrt{\ln\left[\frac{1}{X_g}\right]} \text{ where } X_{g \leq} 0.5 \tag{2.17}$$

$$\text{Or, } t = \sqrt{\ln\left[\frac{1}{1-X_g}\right]} \text{ where } X_g \leq 1.0 \tag{2.18}$$

First, the precipitation data are described as to their mean, standard deviation and skew:
Then, the gamma transformed values are again transformed, with different formulae according

$$\text{SPI} = -\left[t - \frac{C_0 + C_1 t + C_2 t^2}{1 + d_1 t + d_2 t^2 + d_3 t^3}\right] \text{ where, } X_g \leq 0.5 \tag{2.19}$$

$$\text{Or, SPI} = +\left[t - \frac{C_0 + C_1 t + C_2 t^2}{1 + d_1 t + d_2 t^2 + d_3 t^3}\right] \text{ where, } X_g \leq 1.0 \tag{2.20}$$

To the magnitude of the gamma transformed values:

Fifth, the Standard Precipitation Index results from the t transformations, with different formulae according to the magnitude of the gamma transformed values:

Where, C_0 = 2.515517
C_1 = 0.802853
C_2 = 0.010328
d_1 = 1.432788
d_2 = 0.189269
d_3 = 0.001308

3. Study Area

The study has been carried out in Bhopalgarh Tehsil which is one of the promising and drought prone Tehsils among nine Tehsils of Jodhpur district. It lies between 26°28'22″ and 26°42'21″N and between 73°10'30″ and 73°26'40″E catchment covering an area of about 273km^2. The topography of the area is undulating. The climate in the region is characterized by a significant dry season from November to May, which sometime extends in dry years up to June. The average temperature experienced by the State is January to March is 5-25°C, April to June is 35-45°C, July to September is 30-40°C and October to December is 20-30°C (www.mapofindia.com).

The area has semi-arid climate, comprising of undulating terrain, dry land cultivation (mostly rained) and barren (scrub) land to a larger extent, fallow and degraded grazing lands. The average rainfall is 320 mm based on 1901-2012 years rainfall data. In contrast, the average annual rainfall in the study area for the period from 2000 to 2002 was only 202 mm. This area is prone to water scarcity and thus, drought-like conditions prevail. The major land use/land cover includes mixed cropland which are rain fed, water tanks, vegetation which includes outcropped and plantation, barren land consisting of poor to no vegetative cover and rocky surface. The majority of irrigation wells got dried up and groundwater is over-exploited.

4. Methodology

4.1. Required Data

The data required for the study has been procured from various sources.

4.1.1. Satellites Data

Table 3 shows pre-processed multi-temporal satellite images from the Landsat-7 and sensor ETM+ sensor.

Table 3: Satellite Images from the LANDSAT-7 and ETM+ Sensor
(www.earthexplorer.usgs.gov)

S. No.	Satellite	Sensor	Path-Row	Dates
1.	LANDSAT-7	ETM+	149-42	20.04.2000
2.	LANDSAT-7	ETM+	149-42	29.10.2000
3.	LANDSAT-7	ETM+	149-42	12.05.2002
4.	LANDSAT-7	ETM+	149-42	03.10.2002
5.	LANDSAT-7	TM	149-42	11.06.2010
6.	LANDSAT-7	TM	149-42	02.11.2010
7.	CARTOSAT	PAN	149-42	05.06.2010

Process of different operations of meteorological data, satellites data is presented in Figure 1.

4.1.2. Meteorological Data

Meteorological temperature and precipitation data of all months and 21 years are shown in Tables 4 and 5 respectively.

Table 4: *Average Temperature and Precipitation Data*
(Source: www.imd.gov.in)

Months	Temperature (°C)			Precipitation (mm.)
	Normal	Warmest	Coldest	Normal
January	14.3	23.0	5.6	0
February	17.1	25.5	8.8	10
March	23.4	31.8	15.0	10
April	30.2	38.2	22.1	0
May	34.3	41.7	26.8	20
June	35.2	41.6	28.8	30
July	32.8	37.8	27.7	60
August	31.7	36.6	26.8	50
September	30.7	36.7	24.7	30
October	27.7	36.2	19.1	0
November	21.5	30.7	12.1	0
December	16.1	25.3	6.9	0

Table 5: *Temperature and Precipitation Data of 21 years*
(Source: www.tutiempo.net/en/climate/jodhpur)

Years	Total Precipitation (mm)	Total Precipitation in May (mm)	Average Minimum Temperature of January (°C)	Average Maximum Temperature of May (°C)	Average Temp of May (°C)
1991	185	0	8.1	40.4	34
1992	380	7.4	8.8	41.6	34.6
1993	170	7.2	9.3	42.6	35.15
1994	340	3.2	11.2	42.3	34.8
1995	398	2.3	8.2	42.3	34.9
1996	443	49	10.3	39.9	32.9
1997	387	0	9.2	39	31.95
1998	431	0	9.6	43.1	35.35
1999	309	10.6	8.9	40.6	33.75
2000	303	4	9.8	41	34.45
2001	397	40.89	8.9	41.1	34.8
2002	198	0	9.4	43.4	36.4
2003	398	0	10.6	41.6	34.6
2004	299.4	0	10.9	41.2	34.7
2005	285	11.43	8.5	40.7	33.7
2006	268	0	8.7	41.7	35.5
2007	326	0	10.3	41.6	34.9
2008	557	56.9	9.7	38.6	32.4
2009	197.6	0	12.2	42.7	35.7
2010	494	0.51	10.5	43.3	36.6
2011	550	5.59	8.8	41.1	34.7
AVG	348.381	9.47714	9.61429	41.419	34.5643
MAX	557	56.9	12.2	43.4	36.6
MIN	170	0	8.1	38.6	31.95
STDEV	112.218	17.0838	1.06362	1.30024	1.16288

4.2. Software Required

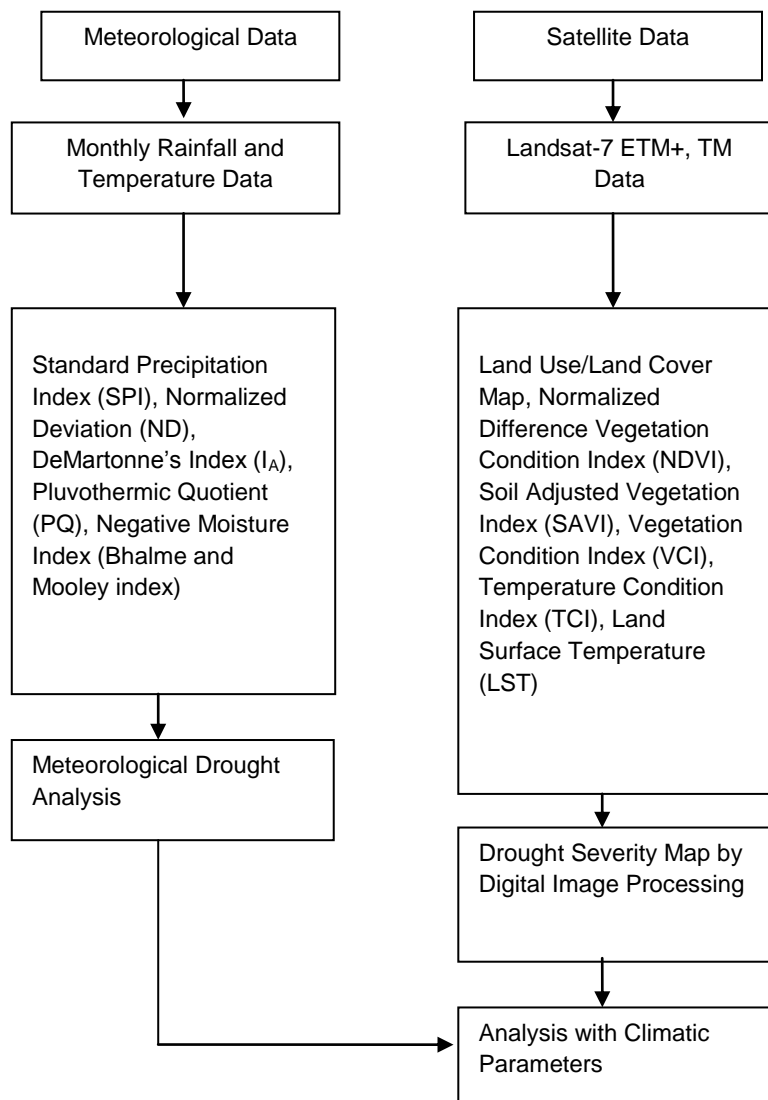Software used to carry out different image processing operations is ERDAS and ARC GIS.

Meteorological Data	Satellite Data
Monthly Rainfall and Temperature Data	Landsat-7 ETM+, TM Data
Standard Precipitation Index (SPI), Normalized Deviation (ND), DeMartonne's Index (I_A), Pluvothermic Quotient (PQ), Negative Moisture Index (Bhalme and Mooley index)	Land Use/Land Cover Map, Normalized Difference Vegetation Condition Index (NDVI), Soil Adjusted Vegetation Index (SAVI), Vegetation Condition Index (VCI), Temperature Condition Index (TCI), Land Surface Temperature (LST)
Meteorological Drought Analysis	Drought Severity Map by Digital Image Processing
	Analysis with Climatic Parameters

Figure 1: Flow Chart of Steps of Methodology

4.3. Geo-referencing of Satellite Data

Landsat satellite data have been checked for radiometric error, and are georeferenced with respect to the Survey of India topographic maps. Pre-processing, such as geometric and radiometric correction were necessary before the analysis, in order to reduce the radiometric distortion in multi-date images. Second order polynomial transformation was used to achieve higher accuracy in georeferencing. This polynomial requires 6 or more ground control points (GCPs) for geometric rectification of satellite data. To ensure better geometric fidelity of the images minimum of 20 GCPs, well distributed spatially, have been used for each satellite image.

UTM North 84 projection system and UTM zone 43 (Range 72˚E–78˚E) have been used for geo-referencing of Landsat satellite images.

4.4. Development of Land Use/Cover Map

All 7 bands have been used to obtain land use classes by adopting supervised classification using ERDAS Imagine software. Land use maps were generated by maximum likelihood method. Since the study area has a mixed cropping pattern, only crop land is identified in particular. Water and moistened water body are also very distinctly identified. Barren land has a limited ability to support life, and therefore it is also easily identifiable. The rocky outcrops and vegetation cover are mixed. The five classes considered for the study area are; Built-up area, Waste/Barren land, Agriculture, Sandy and Water. Classification accuracy assessments was done with field knowledge, visual interpretation and also referring the Google Earth Images.

4.5. Generating Vegetation Indices

A number of vegetation indices based on remote sensing data have been used to monitor vegetation, with the most widely adopted being the normalized difference vegetation index (NDVI) (Tucker, 1979).

(A) Derivation of NDVI and SAVI Images

From geo-referenced images, a series of new data are generated viz., Normalized Difference Vegetation Index (NDVI), Soil Adjusted Vegetation Index (SAVI). NDVI calculation was performed to extract vegetation index values, which were used as the main indicator for determining drought impact. For this study, NDVI images were generated for each of pre and post-monsoon images. The data used in compiling the NDVIs closely related to the radiation absorbed and reflected by vegetation in the photosynthetic processes. Green and healthy vegetation reflects much less solar radiation in the visible (red) compared to those in the near-infrared (NIR). More importantly when vegetation is under stress, the band red value may increase and the band NIR value decrease.

(B) Derivation of VCI Image

The Vegetation Condition Index (VCI) is a measure of the amount and vigor of vegetation at the surface. The reason VCI is related to vegetation is that healthy vegetation reflects very well in the near infrared part of the spectrum. Green leaves have a reflectance of 20 % or less in the 0.5 to 0.7µm range (green to red) and about 60 % in the 0.7 to 1.3µm ranges (near infrared).

(C) Land Surface Temperature

Land surface temperature was computed for each pixel following steps given in Figure 2.

For all the calculations at pixel level, models were developed using Spatial Modeler module of ERDAS Imagine. Vegetation affects the latent thermo flux of the surface intent to the atmosphere through the evapotranspiration. Lower LST (except water bodies) is usually measured in areas with higher NDVI values
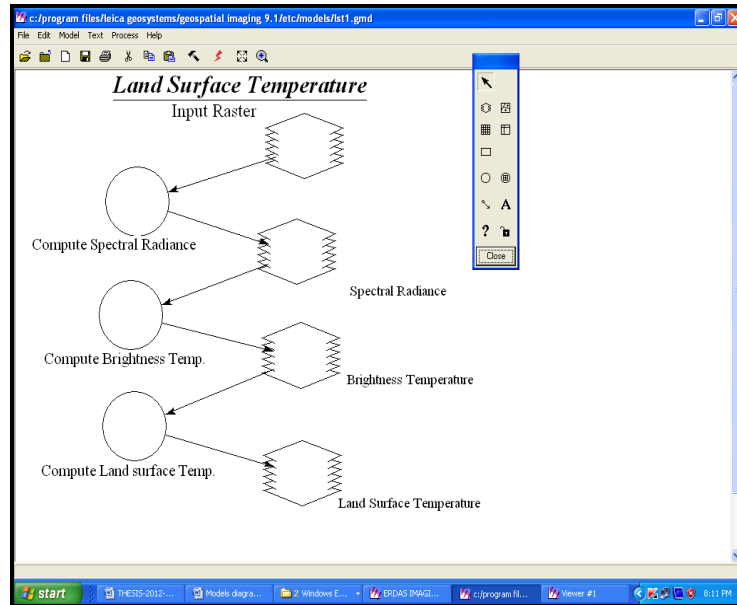
Figure 2: *Process to Determine Land Surface Temperature using ERDAS Imagine Software*

(D) **Temperature Condition Index**

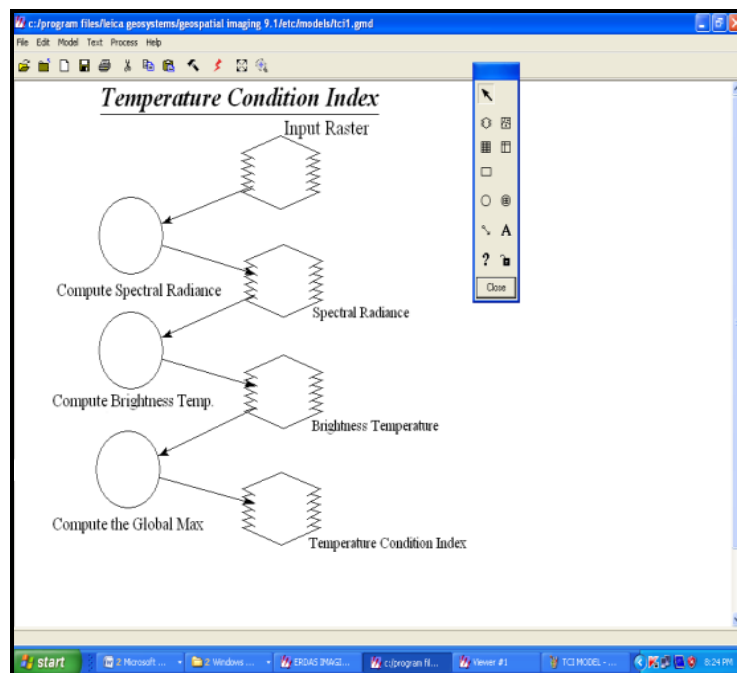Temperature condition index images are generated by procedure given in Figure 3.

Figure 3: *Procedure to Determine Temperature Condition Index*

4.6. Generation of Drought Severity Map

Systematically procedure of generate drought map of drought year is shown in Figure 4. It is necessary that the thematic layers be ranked depending upon the importance of the parameter that influence drought. In order to overcome the difficulty of subjectively and biasness with respect to

ranking of parameters by direct methods, Saaty's pair-wise comparison method which uses statistical concept is used.

Table 6: *Pair Wise Comparison Matrix*

Option Matrix for Criterion of Drought							
Pair-Wise Comparison of Option Against Criterion	**NDVI**	**SAVI**	**VCI**	**LST**	**TCI**	**Geometric Mean of Rating Against Criterion**	**Option Priority Vector for Criterion**
NDVI	1	1.5	0.5	2	2.5	1.5	0.22
SAVI	0.67	1	0.33	1.33	1.66	0.998	0.147
VCI	2	3	1	4	5	3	0.443
LST	0.5	0.75	0.25	1	1.25	0.75	0.11
TCI	0.4	0.6	0.2	0.4	1	0.52	0.076
Total						6.768	

The pair-wise comparison method consists of generation of pair-wise comparison matrix, criteria ranking and estimation of consistency ratio. Table 6 gives pair-wise comparison matrix (6*6) of the criterion parameters. Pair-wise comparison method allows the more important criteria to always come before the less important criteria to provide ease in finalizing intensity of importance.
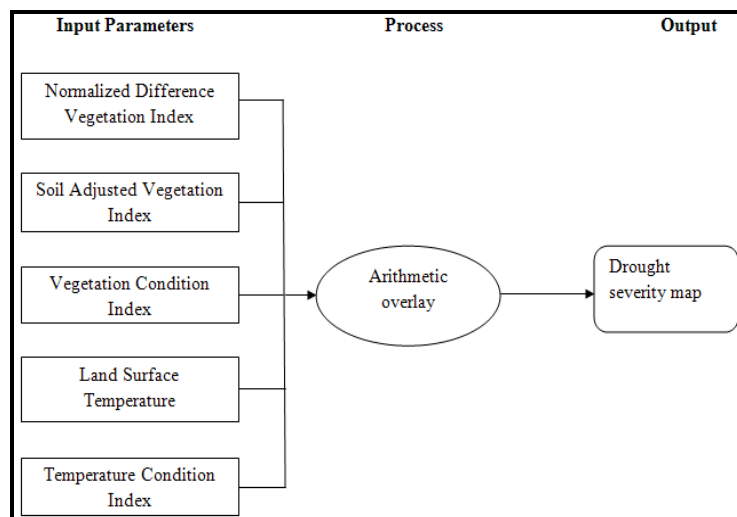

Figure 4: *Schematic Diagram of Generation Drought Severity Map*

5. Results

5.1. Meteorological Drought Indices

Values of meteorological indices generated are shown in Table 7. Variation in meteorological drought indices values are shown in Figures 5 and 6.

Table 7: Calculated Values of Different Drought Indices

Years	Norm. Dev (ND)	PQ	DeMartonne's Index (I$_A$)	NMI (M)
1991	-0.469	22.2387	7.70833	-55.475
1992	0.09076	21.0742	15.4472	-12.159
1993	-0.512	20.1578	6.75944	-13.329
1994	-0.0241	20.9382	13.7097	-36.743
1995	0.14243	20.2306	15.9839	-42.011
1996	0.2716	23.4455	19.345	231.347
1997	0.11085	24.2544	17.631	-55.475
1998	0.23715	19.7333	17.002	-55.475
1999	-0.113	22.2019	13.0105	6.57265
2000	-0.1303	21.9804	12.3926	-32.061
2001	0.13956	21.6386	16.0081	183.875
2002	-0.4317	19.4063	7.5	-55.475
2003	0.14243	21.5289	16.1789	-55.475
2004	-0.1406	22.0686	12.1215	-55.475
2005	-0.1819	21.9904	12.0253	11.4311
2006	-0.2307	20.9464	10.5098	-55.475
2007	-0.0642	21.4458	13.0924	-55.475
2008	0.59882	24.958	24.8661	277.59
2009	-0.4328	20.8057	7.68872	-55.475
2010	0.41799	19.7423	18.5714	-52.489
2011	0.57873	21.6148	22.2672	-22.753
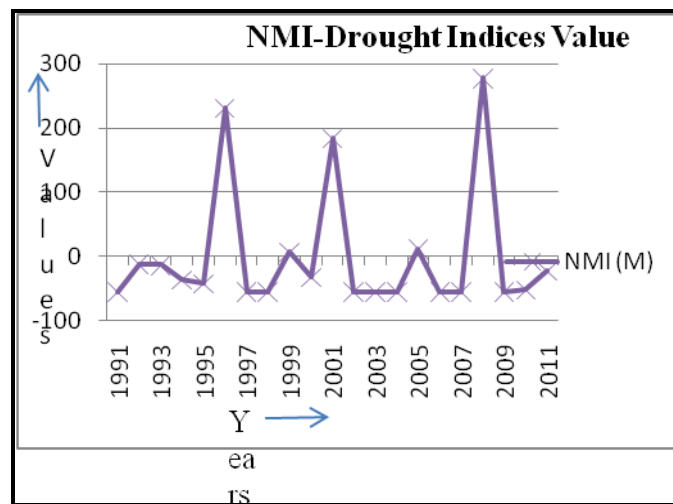
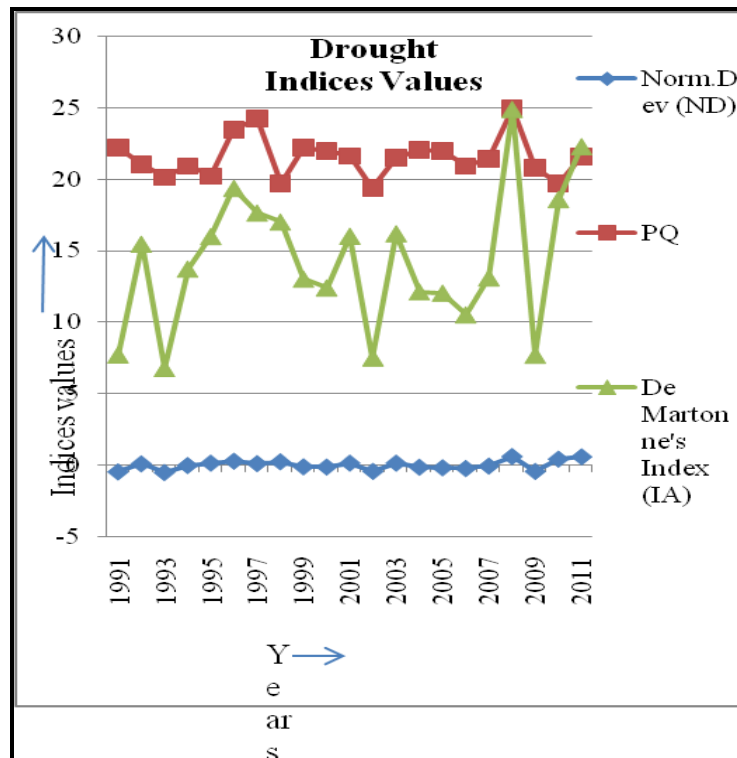*Figure 5: NMI Drought Indices Values and Years*

Figure 6: Different Drought Indices values and Years

Calculation procedure to determine Standard Precipitation Index (SPI) is shown in Table 8 and variations of SPI of pre-monsoon month May with years are given in Figure 7. SPI is only dependent on rainfall data of particular month of particular year.

From above three figures, values of Standard Precipitation Index (SPI), Negative Moisture Index (NMI), Normal deviation (ND), Pluvothermic Quotient (PQ) are less in years 2000, 2002 and 2010 as compared to other years. Values of DeMartonne's Index (IA) are so high in these years as compared to other years. This variation indicates drought condition. Accordingly, drought can be classified in different categories.

Table 8: Find out Standard Precipitation Index

Years	Precipitation of May	Ln of Precipitation	U	β	Scale(α)	Gamma	t	SPI
1991	10	2.302585	0.186798	2.006265	6.154771	0.356276	1.015899	0.24432
1992	7.4	2.00148	2.00148	0.328956	37.53721	0.002297	2.464963	-1.66546
1993	7.2	1.974081	1.974081	0.332101	37.18176	0.001531	2.545908	-1.76107
1994	3.2	1.163151	1.163151	0.482598	25.5867	1.76E-08	4.225548	-3.64699
1995	2.3	0.832909	0.832909	0.616461	20.03062	3.1E-09	4.426301	-3.8644
1996	49	3.89182	3.89182	0.210567	58.6421	1	0	2.515517
1997	4.5	1.504077	1.504077	0.401597	30.74746	1.12E-06	3.70171	-3.0736
1998	4.6	1.526056	1.526056	0.397502	31.06422	1.54E-06	3.658293	-3.02562
1999	10.6	2.360854	2.360854	0.293771	42.03302	0.180612	1.308206	-0.18856
2000	4	1.386294	1.386294	0.425515	29.01919	2.2E-07	3.915132	-3.30838
2001	40.89	3.710886	3.710886	0.217224	56.84497	1	0	2.515517

2002	4.8	1.568616	1.568616	0.389866	31.67271	2.89E-06	3.571086	-2.929
2003	7.9	2.066863	2.066863	0.321752	38.37775	0.005872	2.266619	-1.4282
2004	9.4	2.24071	2.24071	0.30442	40.56265	0.053878	1.709104	-0.73143
2005	11.43	2.436241	2.436241	0.287565	42.94022	0.326851	1.057474	0.180179
2006	8.9	2.186051	2.186051	0.309606	39.88325	0.028271	1.888366	-0.96128
2007	5.1	1.629241	1.629241	0.379606	32.52871	7.26E-06	3.439839	-2.78294
2008	56.9	4.041295	4.041295	0.20546	60.0999	1	0	2.515517
2009	1.4	0.336472	0.336472	1.240666	9.952802	3.69E-07	3.848603	-3.23538
2010	4.2	1.435085	1.435085	0.41518	29.74156	4.24E-07	3.830709	-3.21571
2011	5.59	1.720979	1.720979	0.365316	33.80113	3.02E-05	3.22593	-2.54307
MEAN	12.3481							
STDIV	15.74967							
SKEW	2.181304							
	Log mean	2.115787						
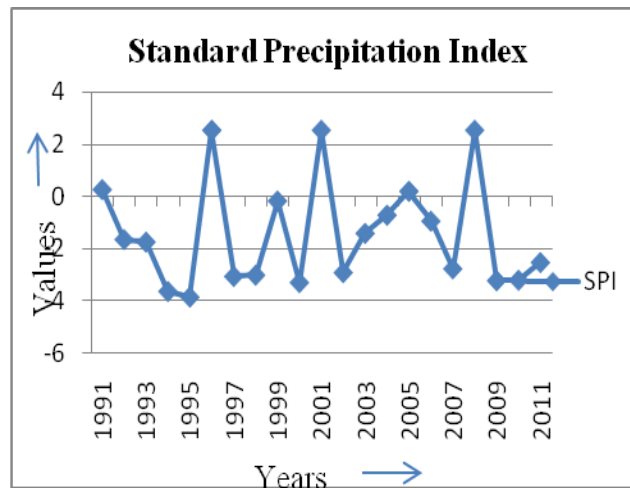
Figure 7: *Standard Precipitation Index*

5.2. Land use /Land cover map

Land use land cover classes of study area of pre and post-monsoon are shown in Table 9.

Table 9: *Land Use Land Cover Area of Pre and Post-Monsoon*

		Pre-monsoon Area (Km^2)			Post-monsoon Area (Km^2)		
S. No.	Class	2000	2002	2010	2000	2002	2010
1	Build up area	2.2	2.32	3.01	2.322	2.45	3.71
2	Sandy area	141.6	230	154.84	196.4	169.19	138.1
3	Waste/Bare area	122.6	34.87	111.0155	43.3	70.432	106.2
4	Agriculture area	6.2	5.9	2.8891	28.02	26.5234	21.1
5	Water	0.12	0.66	0.76	2.3	3.72	3.21

From this table, it is seen that waste land and sandy area is increasing whereas water and agriculture areas are decreasing. Drought is also found to have more intensity in year 2010 as compared to other years.

5.3. Normalized Difference Vegetation Index (NDVI)

Normalized difference vegetation Index (NDVI) of Landsat ETM+ and TM satellite images of pre and post monsoon of 2000, 2002 and 2010 years were generated. Variations of NDVI are shown in Figure 8.

NDVI value range has been divided into four categories (i) -1 to -0.5 for severe drought, (ii) -0.5 to 0.0 for moderate drought, (iii) 0.0 to +0.5 mild drought and (iv) +0.5 to +1 no drought. Accordingly, NDVI values between -0.3617 to 0.6 of study area has been classified as moderate drought, mild drought, and no drought, respectively.
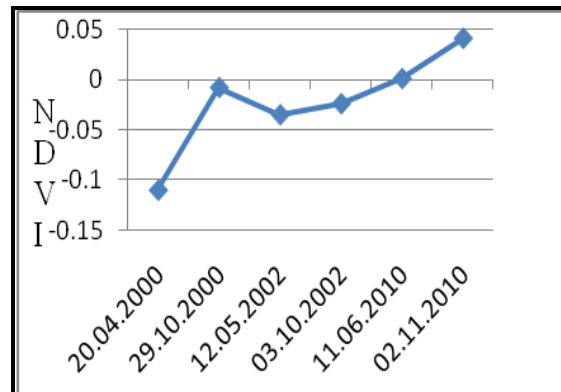
Figure 8: Mean values of NDVI

5.4. Difference of Pre and Post-Monsoon Images

The next step was to calculate the difference between NDVI acquired for each pre and post-monsoon for years, 2000 and 2002.
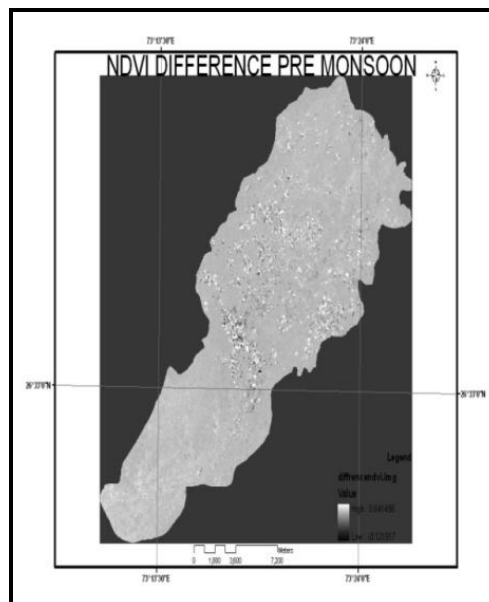
Figure 9: Difference of NDVI Images of Pre-Monsoon (2000-2002)

The purpose was to detect NDVI change between normal and drought conditions.
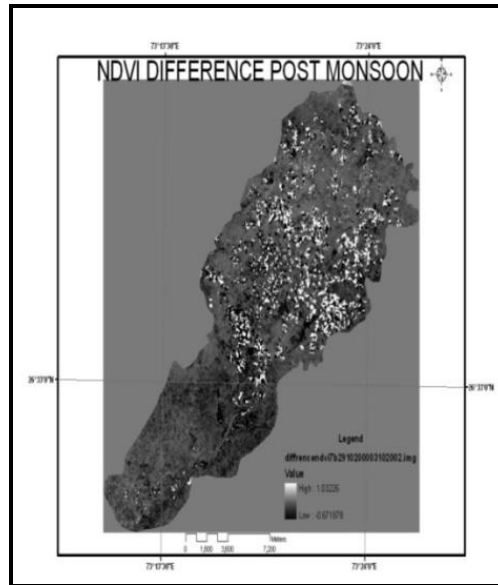
Figure 10: Difference of NDVI Images of Post-Monsoon (2002-2002)

If difference values are positive then area is less affected by drought, if value is zero then there is no change in drought condition and if value is negative then there is significant change in drought conditions. Difference of NDVI of pre-monsoon is shown in Figure 9 and post-monsoon shown is in Figure 10.

5.5. SAVI Images

Range of SAVI values computed from satellites images are shown in Table 10.

Table 10: SAVI Values of Landsat Images

Date	Min	Max	Mean
20.04.2000	1.1692	1.5659	1.391
29.10.2000	1.14	2.108	1.492
12.05.2002	1.3428	1.868	1.465
03.10.2002	1.243	2.5	1.496
11.06.2010	1.193	2.1	1.499
02.11.2010	1.27	1.9695	1.541

5.6. Vegetation and Temperature Condition Indices

VCI is derived from NDVI images and TCI from brightness temperature. It shows a relationship between temperature and vegetation.
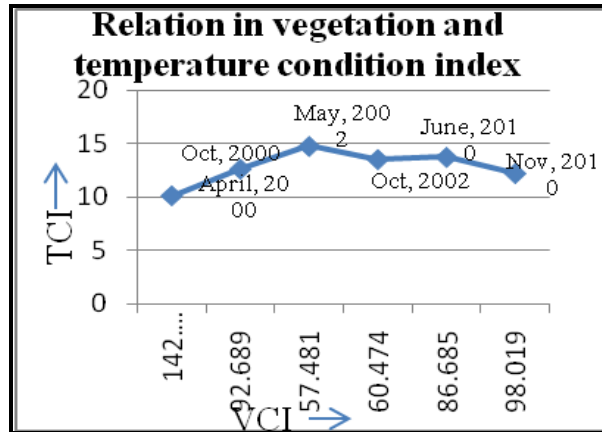
Figure 11: Relation in VCI and TCI

VCI value is high where TCI value is low; it means dense vegetation helps to lower down the temperature. Variations in TCI and VCI value over three years are shown in Figure 11 indicate that both are reciprocal to each other.

5.7. Land Surface Temperature

Land surface temperature values of study area were computed from satellites images. Variation of mean LST values is shown in Figure 12.
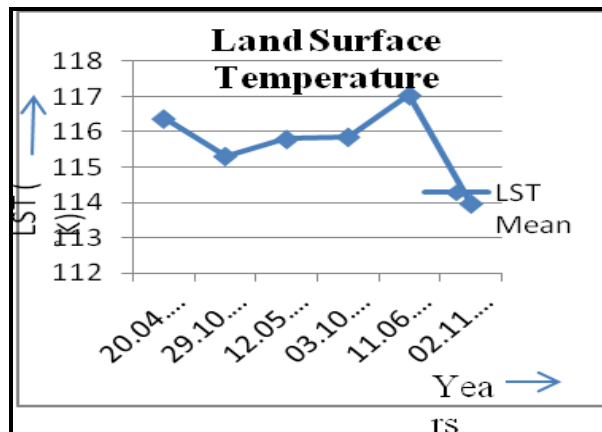

Figure 12: Variation of Land Surface Temperature Index Values

More than 200 points are selected randomly on the LST image and corresponding NDVI values are obtained to find the correlation between LST and NDVI. The correlation coefficient so obtained between LST and NDVI is found as -0.79. This clearly indicates that the LST is strongly and negatively correlated with NDVI. Hence areas with least vegetation cover are expected to experience more temperature and more drought condition.

5.8. Drought Severity Map

Drought severity map of pre-monsoon of year 2000, 2002 and 2010 are shown in Figures 13, 14 and 15, respectively.
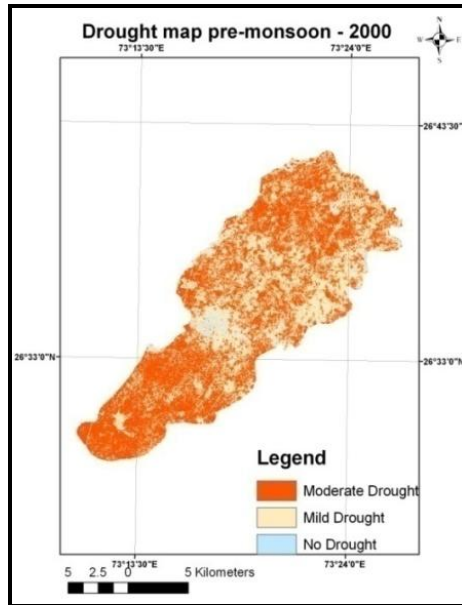
Figure 13: Generated Drought Severe Map of Pre-Monsoon of Year 2000

These maps are generated by arithmetic overlay process already described in Figure 14. Area of various drought classes is shown in Table 11.
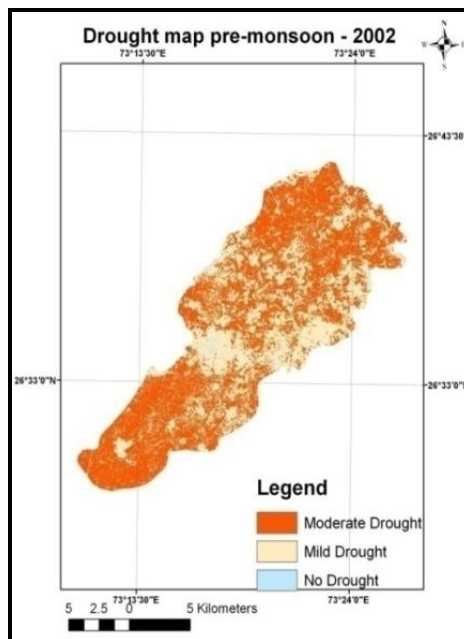

Figure 14: Generated Drought Severe Map of Pre-Monsoon of Year 2002

Relationships of drought (Moderate and Mild) with crop production, yield and land use land cover for year 2000, 2002 and 2010 are shown in Figures 13, 14 and 15, respectively.
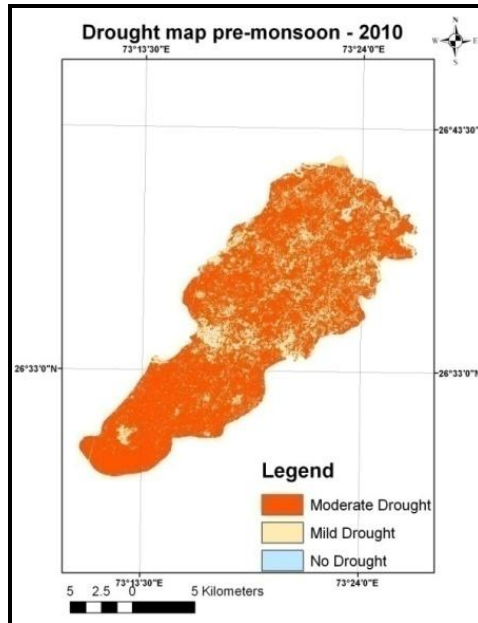
Figure 15: Generated Drought Severe Map of Pre-Monsoon of Year 2010

Table 11: Area of Drought Classes of Pre-Monsoon

S.No.	Drought Category	Year-2000 Drought Area (Km^2)	Year-2002 Drought Area (Km^2)	Year-2010 Drought Area (Km^2)	Changes in area of 10 years (Km^2)
1.	No Drought	6.51	4.24325	2.037	-4.4
2.	Mild Drought	117.65	113.1	61.14	-56.5
3.	Moderate	147.93	154.78	208.99	61.06
Drought area		265.58	267.88	270.14	4.56
Total area		272.1	272.12	272.17	00
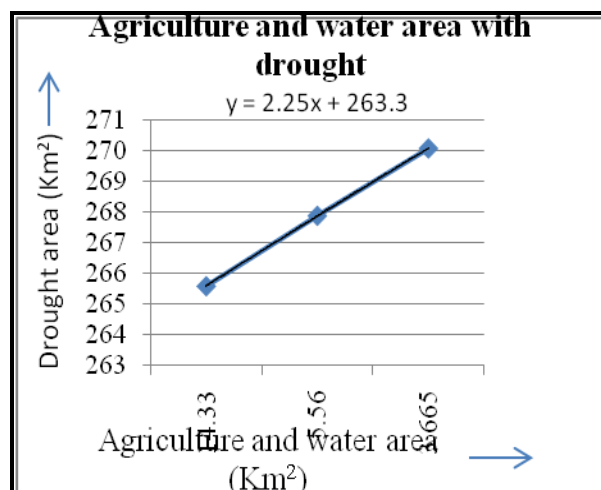
Figure 16: Variation of Agriculture and Water with Drought

6. Discussion

(i) The analysis of Landsat images of pre and post-monsoon of years 2000, 2002 and 2010 revealed that land use and land cover of the catchment of study area has changed over 10 years.

(ii) Meteorological analysis data illustrate that NMI values of years 2000, 2002, 2009, 2010 are more negative compare to others.

(iii) Normalized deviation (ND) has negative values of years 2000, 2002 and 2010 these shows drought years.

(iv) All other meteorological indices have less positive values for these three years.

(v) Standard Precipitation index (SPI) also show negative values for years 2000, 2002, 2010.

(vi) The results of drought and NDVI study illustrate that vegetation condition can be used as indicator for drought condition of an area. NDVI can be used as the main indicator to evaluate drought.

(vii) Difference images of NDVI show drought conditions. In these images, if difference values are positive then area is less affected by drought, if difference values are zero the area is not affected by drought, and if difference values are negative then the area has affected by drought.

(viii) VCI and TCI are inversely proportional to each other. Values of VCI are very low in post monsoon of 2002 and very high TCI in pre-monsoon of 2002.

(ix) From the LST image it was observed that highest temperatures of about 302°K exist in urban built up areas and other impervious areas, and lowest temperatures of about 289°K exist in vegetative areas.

(x) Indices derived from the thermal bands, such as LST and the TCI have a higher sensitivity to drought conditions than indices derived from the visible bands, such as the NDVI, VCI and SAVI.

(xi) From LST images, it is clearly understood that surface temperature is more in urban area as compared to rural areas. Also the study shows that the LST is strongly and negatively correlated with NDVI.

(xii) Low rainfall is usually the cause of drought, but high temperatures may also be involved. Drought as related to precipitation may be a result of several growing days without precipitation, low seasonal precipitation, or abnormally low annual precipitation approximately 303 and 198 mm for year 2000 and 2002, respectively.

(xiii) In drought area map, mild drought is high in 2000 and less in 2010, Area of moderate drought in 2010 is high and low in 2000 and total area affected by drought is more in 2010.

7. Conclusion

The following are the significant conclusions that have been drawn by way of having achieved the overall objectives of this research study.

(i) Area of drought is less in 2000 more in 2010 value of difference is 4.56 km^2. It means intensity of drought has increased in ten years.

(ii) Land surface temperature values of build up area, sandy area, waste land, agriculture, water have been found in decreasing order.

(iii) Sandy and waste land area has increased 1.655 km^2 and agriculture and water area is decreased 2.671 km^2 in 10 years from 2000 to 2010.

(iv) Meteorological data deficient are main causes of all types of drought.

Recommendations for Future Work

The study has identified an approach by which drought can be identified using remote sensing and GIS. The drought maps are of great importance as they can be used subsequently for preparing action plan for providing relief measures to drought affected areas. Thus, the future direction of research can be enumerated as follows:

a. Prioritization of critical parameters related to drought condition;
b. Preparation of short and long term action plans;
c. Definition of a well defined drought classification based on numeric indices.

Acknowledgements

References

Bhalme H.N. and Mooley D.A. *Large-Scale Drought/Floods and Monsoon Circulation*. Mon. Weath. Rev. 1980. 108; 1197.

Cole H.S. *Drought in Arhansas*. Monthly Weather Review. 1933. 61 (5) 129-40.

Dracup J.A., Lee K.S. and Paulson E.G. Jr. *On The Definition of Droughts*. Water Resource Research. 1980. 16 (2) 297-302.

Dracup J.A., Lee K.S. and Paulson E.G. Jr. *On the Statistical Characteristics of Drought Events*. Water Resources Research. 1980. 16 (2) 289-296.

Hoyt J.C., 1936: Drought of 1930-1934. U.S. Geological Survey Water Supply. 608; 106.

Konstantinov A.R. 1968: *Isparanije v prirode (Evapotranspiration in Nature).* Gidrometeoizda, Leningrade, 532.

Mishra A.K. and Desai V.R. *Spatial and Temporal Drought Analysis in the Kansabati River Basin, India.*Int River Basin Management. 2005. 3 (1) 31-41

Palmer W.C., 1965: Meteorological Drought. U.S. Weather Bureau Research. 45, 58.

Ramdas L.A., 1960: *Crops and Weather in India*. Indian Council of Agricultural Research, New Delhi, 127.

Tucker C.J. *Red and Photographic Infrared Linear Combinations for Monitoring Vegetation*. Remote Sensing of Environment. 1979. 8; 127-150.

Wilhite D.A. *Drought as a Natural Hazard: Concepts and Definitions*. Drought: A Global Assessment. W.D.A. Routlegde. 2000. 1; 1-3.

Yevjevich V.M., 1967: *An Objective Approach to Definitions and Investigations of Continental Hydrologic Droughts*. Hydrol. Pap. 23, Colorado State Univ. Fort Cllins.

Rao A.S., 2009: *Climate Variability and Crop Production in Arid Western Rajasthan*. Central Arid Zone Research Institute, Jodhpur, India, 48-61.

Rao A.S., Ramakrishna Y.S. and Venkateswarlu J. *Determination of Crop Growing Period in Arid and Semi-Arid Regions of Rajasthan*. Annals of Arid Zone. 1994. 33; 229-231.

Cloud Publications

Research Article

Open Access

GIS Analysis of Peri-Urban Agricultural Land Encroachment in (FCT), Nigeria

Etim N.E.[1] and Dukiya J.J.[2]

[1]82 D, Godwin Abbe Avenue, Ewet Housing Uyo, Akwa Ibom State, Nigeria
[2]Department of Urban and Regional Planning, Federal University of Technology, Minna, Nigeria

Correspondence should be addressed to Dukiya J.J., duksat2000@futminna.edu.ng; duksat2000@yahoo.co.uk

Abstract Population explosion, globalization of the economy and the technological advancement of man are responsible for major modern-day transformations in the nature and flow of the Earth ecology, which has a very broad historical background that dates back to ancient times. Presently, the fast urban growth in Nigeria has affected approximately 400,000 hectares of vegetative cover. In the Kuje area council, the increases in urbanization and sprawling pattern of development in Abuja have culminated into the quick disappearance or total transformation of fertile agricultural sites into peri-urban development. This study use questionnaire administration in the ten wards of the area council and multitemporal images of Landsat TM and Nigeria Sat-1 over a period of 35 years (1975–2010) to assess the level of urban encroachment on agricultural lands and displacement of farmers in Kuje area council. The study reveals that urban encroachment into agricultural lands is alarming at the rate of 15.7 Km^2 annually, and a total of 509 Km^2 of agricultural land have been lost to urbanization within the 35 years under review. It is therefore recommended among other things that land management in the area council should be incorporated into the existing Abuja Geographical information System (AGIS) for effective sustainable human development.

Keywords *Agricultural Land, Encroachment, GIS, Peri-Urban, Remote Sensing and Urbanization*

1. Introduction

The activities of man and not the forces of nature are responsible for major modern-day transformations in the nature and flow of the Earth, which has a very broad historical background that dates back to ancient times (Yang and Lo, 2003). This situation has also been aggravated by population explosion, globalization of the socio-economic sector and the technological advancements. Comprehending all the activities and social actions that move them is critical to modeling, forecasting and understanding of universal, regional and local changes in the environment and likewise for the management and response to these changes (Turner and Williams, 1994).

Settlements refer to the occupation of land for man's modification of the natural surroundings through myriad developmental activities. The United Nations (2008) once predicted that by the year 2000, approximately 24 million hectares of cropland globally would be changed to metropolitan purpose. Projections by the United Nations suggested that global population of cities would increase exceeding one billion populace between the years 2010 to 2025, whereas the population of local areas would scarcely increase, see Figure 1.
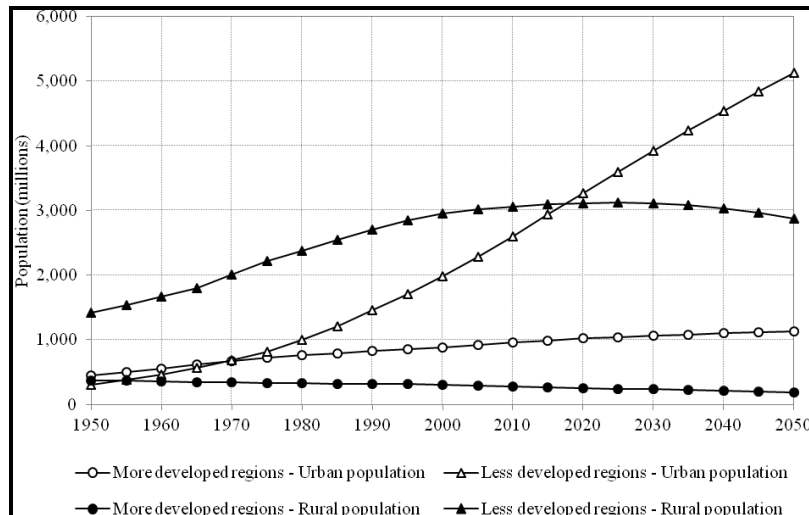
Figure 1: *Urban and Rural Populations by Development Group, 1950-2050*
Source: World Urbanization Prospects; the 2011 Revision

There exist some elements of land use management adaptations from agricultural to none-agricultural uses, the set of laws that are intended to control this are most times shunned by decision makers and property developers (Hardoy *et al.,* 2001). In the Kuje area council, the increases in urbanization and sprawling pattern of development from Abuja have culminated into the quick disappearance or total transformation of fertile agricultural sites to peri-urban development. Although urbanization contributes to national socioeconomic development, the rate of change makes it impossible for government at all levels to meet the needs of basic urban life like food and housing; hence the encroachment on major agricultural lands, (Ekpeyong, 2006). This is particularly visible in Kuje Area Council of the FCT, where agricultural land is disappearing each year, as a result of urbanization occasioned by the growth of the Federal Capital Territory (FCT).

1.1. Review of Literatures

More than fifty percent of land surface free from ice have been translated or considerably altered by the activities of man for the past 10,000 years (Population Reference Bureau, 2001; Mittermerier *et al.,* 2003). This is as a result of the natural and pressure from diverse anthropogenic actions like urbanization and urban sprawl, deforestation, mineral exploitation, intensive agriculture etc. (FAO, 2003; Sarma *et al.,* 2008; Njomo, 2008).

By the year 1900, 14% of the population of the earth were residing in metropolitan areas (UNCHS, 1996) and this percentage of people is rapidly on the increase and presently more than 60% of the people are residing in metropolitan areas (Ifatimehin and Musa, 2008). The continent of Africa is experiencing the fastest pace of urban growth at a pace of approximately 67% in comparison with developing and developed nations (Cohen, 2004).

Presently, the fast urban growth in Nigeria is affecting approximately 400,000 hectares of vegetative cover every year (Adesina, 2005). (Kramer *et al.,* 2008) and (Heimlich and Anderson, 2001) have

both observed that urban growth encourages sprawl blueprint, which most of the time possess negative effects on the ecology of the region, particularly in vegetative and hydro-geomorphology. Food security according to FAO (2006) 'exist when every human, whatever the time, possess both economic and physical access to adequate, secured and wholesome food to meet up the standard dietary requirements and choice of food they prefer for a vibrant and vigorous living'. The transformation of agricultural lands to other land uses is a threat to food security, for instance, in one of the Chilean city, about 1,734 hectares of wetlands and 1,417 hectares of agricultural land were transformed into residential areas between the years 1975 to 2000 (Kwasi, 2004). While in Accra (Ghana), it is estimated that 2,600 hectares of agricultural land are converted every year and similar patterns were observed in China and Indonesia (Lambin *et al.,* 2003). Alabama, Arkansas, Illinois, Mississippi, New York and California are at the top among the states in USA that have lost most proportion of their prime arable lands over the past five years, (Ralph, 2008). Approximately 400,000 hectares of arable land have been taken over by Urban sprawl annually, (Jiang *et al.,* 2007).

In modern day land management, satellite sensors like the Advanced Very High Resolution Radiometer (AVHRR), the French Spot System and Landsat Thematic Mapper (TM) have been used efficiently for the measurement of biomass burning, deforestation and other land use transformation, (Tucker *et al.,* 1991; Skole and Tucker, 1993; Sellers *et al.,* 1995). For instance, one approach adopted by the US Defence Meteorological Satellite Programs Operational Line Scan System (DMS/OLS), is the use of night-time satellite data sets as a procedure for the detection of metropolitan land use encroachment and integrating these data sets together with maps of soils to approximate the impending effect of urban growth on fundamental soil resources, (Elvidge, *et al.,* 1997; Kramer, 1994).

In Nigeria also, since Abuja became the country's Federal Capital Territory in 1976, series of studies have been carried out to determine the rate and extent of urbanization. (Ujoh *et al.*, 2010), specifically used Remote Sensing data, Geographical Information Systems (GIS) techniques, and ground data to estimate annual rate of urban sprawl in Abuja. The data set from Landsat TM, Landsat ETM and Nigeriasat-1 satellite data for 1987, 2001 and 2006, respectively, revealed that the annual rate of urban sprawl was 10.6 km^2 over a 19-year period (1987 and 2006). According to them, this resulted into land degradation that includes widespread alteration in the land use/land cover of Abuja environment. Similar results were reported by (Riebsame *et al.*, 1994; Twumasi *et al.*, 2004; Kelarestaghi *et al.*, 2006; Ifatimehin, 2006, 2008). The extent and rate of LU/LC changes of the Abuja city poses a significant regional threat to the national environment sustainability. Other studies in urban encroachment on vegetation/agricultural land include: El-shakhs and Amirahmadi, 1993; Brockherhoff, 2000; UN, 2004; Cariboni, 2002; and Bojle, 2005.

1.2. Aim and Objectives of Study

This study is aimed at assessing the level of Abuja's urban encroachment on agricultural land in Kuje Area Council of FCT in view of the food security challenges in the country. The Specific Objectives are:

    i. To analyze and map the landuse/landcover of the area over a period of 35 years,
    ii. Determine the rate, nature and direction of encroachment in the area,
    iii. Estimate the land use changes and its effect on agriculture land during the time period.

2. Methodological Approach

In this study primary and secondary data were used to ascertain the level of urban encroachment on agricultural land and productivity. The primary data include the use of two sets of questionnaire administered to the professionals in Land Administration in FCT and the residents within the wards of the Area Council, while oral interviews was conducted on the 10 Ward heads. A total of Seven

hundred and eighty-three (783) questionnaires were administered constituting 0.2% of the total population of Kuje Area Council as projected from the census figures of National Population Commission of 2006 as indicated in Table 1.

Table 1: Questionnaire Distribution in Per Ward Kuje Area Council

Ward	No of Respondents
Kuje Central	250
Gaube	100
Rubochi	85
Chibiri	75
Kujekwa	60
Kwaku	47
Gwadubada	43
Yenche	43
Gudukeria	40
Kabi	40
Total	783

Source: Author's Field Work, 2012

2.1. Secondary Data

Secondary data were also used for the change detection in land uses, these are basically satellite imageries and maps obtained from relevant agencies as displayed in Table 2.

Table 2: Imagery Data Types and Sources

Data	Year	Resolution	Acquisition Source
Landsat TM (Multispectral)	1975, 1980, 1985	30 meters	National Centre for Remote Sensing (NCRS), Jos.
Landsat ETM+ (Multispectral)	1990,1995,2000	30 meters	National Centre for Remote Sensing (NCRS), Jos.
Nigeria – Sat 1	2005,2010	32 meters	National Space Research and Development Agency (NARSDA) Abuja.
Topo. Maps	1972	1 :50,000 Sheet 18-22	Federal Surveys Unit, Kaduna. FCDA, Abuja

For the data analysis, ArcGIS 9.2 was used to carry out on-screen digitizing, editing of the various layers. Colour composites were carried out to enhance major land uses before the map overlay operations to identify and detect the increase or decrease in landuse classes.

3. Background of the Study Area

Abuja, the capital city of Nigeria is located in the centre of the country, within the Federal Capital Territory (FCT). As a planned city, it officially became Nigeria's capital on 12 December 1991, replacing Lagos which is similar to Brazil building its capital Brasília. At the 2006 census, the city of Abuja had a population of 776,298, (NPC, 2007). See Figure 2 for the geographical location of the city within the country. Abuja and the FCT have experienced a huge population growth; it has been reported that some areas around Abuja have been growing at 20–30% per annum.

Kuje is one of the Area Council in the Federal Capital Territory (FCT), it lies between latitude $8^0 27'43''$ to $8^0 56'32''$ North and longitude $6^0 58'13''$ to $7^0 33'11''$ East. The landed area covers 1,800 square kilometers, which is about 22.5% of the FCT total land area. It is bounded by Gwagwalada Area Council to the West, eastward by Municipal Area Council, and Abaji Area Council to the South-West. The major ethnic groups dominating the area are the Bassa, the Gade, the Koro, the Ganagana and the Gwandara; all of which have profound attachment with the kwa speaking people. The major occupation of the original inhabitants of Kuje is subsistence farming and the main farm produce are guinea corn, yam, maize, millet and beans. The council area serves a dual function of absorbing excess population from the city centre of Abuja as well as supporting the FCT agriculturally. The area designated for the development of satellite town covers approximate 93.16 square kilometers, (Kuje Master Plan, 2004). Also, Pegi situated in council to accommodate squatter settlers from Jiwa Chiefdom, while Yangoji situated within Kwali Area Council will take care of squatter settlers from the Airport axis of Chika, Aleita, Piwoyi, Kuchingoro and Karomanjiji (Nnabugwu, 2012).

Figure 2: *Kuje -Abuja, Nigeria*

3.1. Data Presentation

One of the socio-economic impacts of Abuja on Kuje is the dramatic occupational mobility as discovered in the field survey. In 1975, the occupational distribution was of the people was predominantly 83% farming, 9% civil service and the organized private sector, 4% engaged business and trading, while 2% were engaged in other forms of occupation. But as at the year 2010, 16% of the surveyed residents are engaged in farming, 38% in the civil service and the organized private sector, 27% are engaged in various forms of businesses and trading, 13% are artisans, while 6% are engaged in other forms of occupation. There is a sharp drop in Farming between the year 1975 and 2010 as revealed in Figure 3.
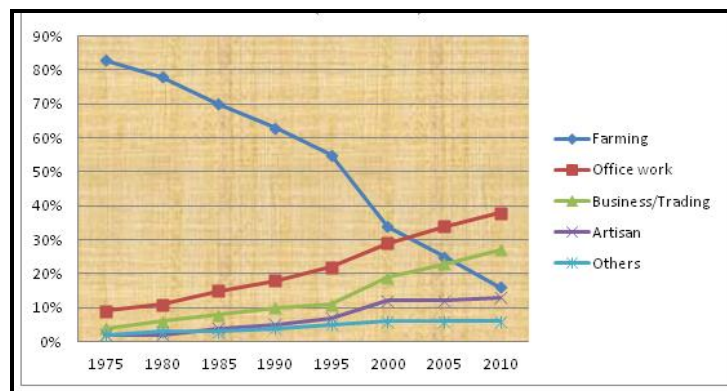

Figure 3: *Occupational Transformation in Kuje Area Council (1975 – 2010)*

An examination of the length of year's resident spent in the area reveals that about 70% (544) of the sampled population moved to Kuje area within the last ten (10) years, and the implication of this is the high loss of agricultural land to built up areas as reveals in Figure 4.
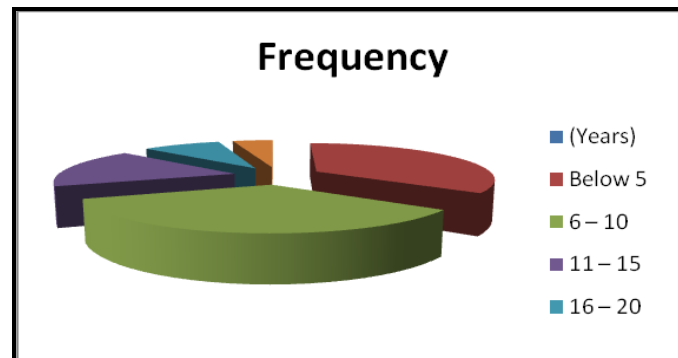

Figure 4: Length of Residency at Kuje Area Council

In the area of resident work location, 17% (136 respondents) have their work place or business location within the area council while 83% (647 respondents) work in the other part of the territory. Information on the level of farmer/construction agencies reveals that sizeable numbers of farmers are often displaced for construction activities. In fact, 95% (330) of the farmers interviewed have experienced one form of displacement or the other. See Plate 1 for such construction in the area.

Plate 1: Road Construction Connecting Kuje to Gwagwalada at Pasali Area

3.2. Image Analysis

The multitemporal images acquired were analysis at five years interval in the Table and according to subject areas as displayed in the Appendixes, the urban encroachment on arable land, fadama land and forest land were examine separately. The image enhancement of each of the years for proper interpretation is also displayed in Figures A to H in the Appendix.

3.2.1. Changes in Arable Land

The analysis of the Lansat imageries reveals a downward trend in the available arable land from the year 1975 to 2010 as indicated in the bar chart Figures 5 to 8. This is attributed to the continuous increase in developmental activities of migrants from all over the country.
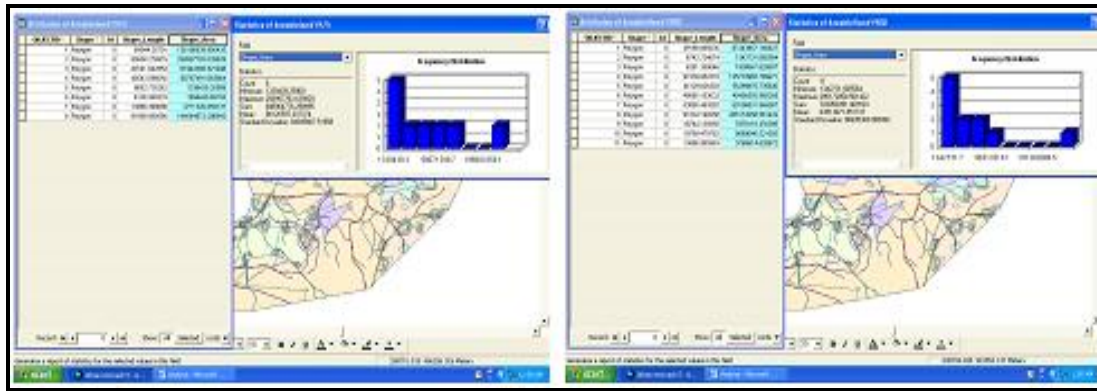
Figure 5: Statistics of Arable
Land in the year 1975

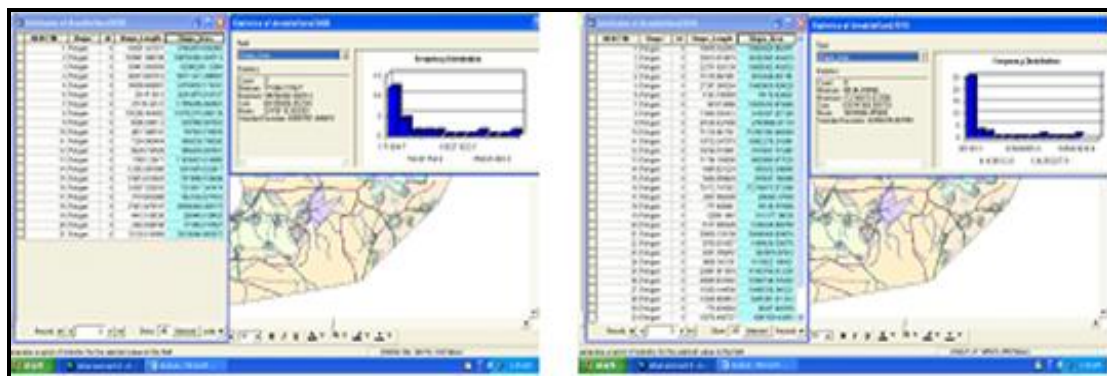**Figure 6:** Statistics of Arable
Land in the year 1980

Figure 5: Statistics of Arable
Land in the year 2000

Figure 6: Statistics of Arable
Land in the year 2010

The changes between the 2000 to 2010 (10 years) amount the loss of one hundred and seventy square kilometers of arable land about 29.2% of the total land, as indicated in Table 3 and Figure 7. This is very critical in view of the food security challenges in country where mechanized agriculture is still very low.

Table 3: Change in Arable Land in Km^2 per Year

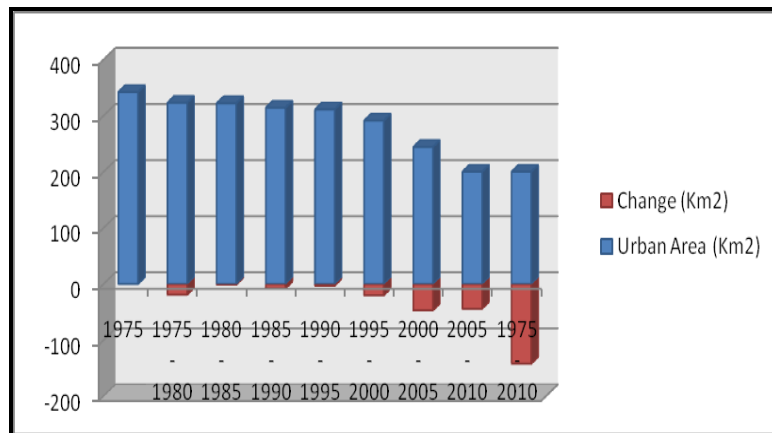| Period (Years)	Area(Km^2)	Change(Km^2)	Change% Area
1975	582		
1975 - 1980	576	-6	-1.03
1980 - 1985	566	-10	-1.74
1985 - 1990	551	-15	-2.7
1990 - 1995	547	-4	-0.73
1995 - 2000	533	-14	-2.6
2000 - 2005	480	-53	-9.94
2005 - 2010	412	-68	-14.2
Total		-170	-29.2

Source: Author's image Analysis

Figure 7: Change in Arable Land in Km² per Year in Kuje Area Council

3.2.2. Changes in Fadama Land

Fadama farming is a major agricultural area in Nigeria that is now attracting foreign aid to the federal government. In all the northern part of the country, there are various schemes Targ Fadama 1 to Fadama 5. The Fadama scheme is almost like the irrigation scheme in the country that is been used by the government as a way of reducing unemployment problem and at the same time responding to the food security challenges. The result of the image analysis as presented in Table 4 and Figure 8 reveals that there is negative change since 1975 till date. The huge change between the year 1995 and 2005 (10 years) may be attributed to the mass movement of major governmental and none governmental head offices together with their staffs to Abuja.

Table 4: Change in Fadama land in Km² per Year

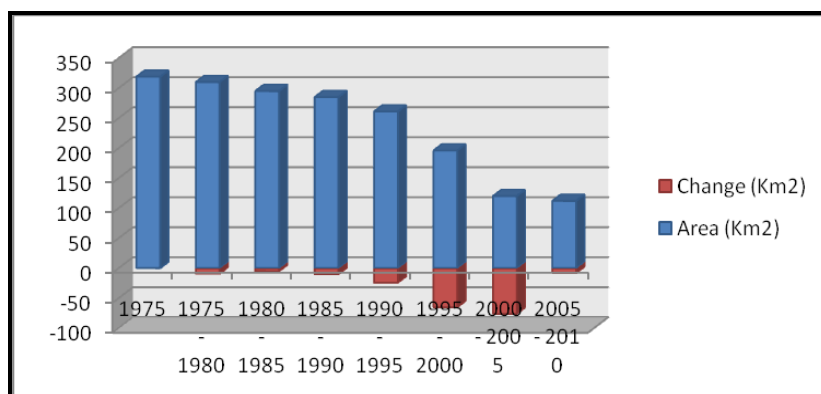| Period (Years)	Area (Km²)	Change (Km²)	Change % Area
1975	319		
1975 - 1980	310	-9	-2. 8
1980 - 1985	295	-5	-1.6
1985 - 1990	285	-10	-3.4
1990 - 1995	261	-24	-8.4
1995 - 2000	196	-65	-23
2000 - 2005	120	-76	-39
2005 - 2010	112	-8	-6.7

Figure 8: Change in Fadama land in Km² per Year in Kuje Area Council

4. Findings

Kuje Area Council of the Nigeria FCT is experiencing a lot of socio-economic and political changes that is impacting negatively on the ecological landscape. In the area of agricultural sector as assessed in this study, the following observations are noteworthy:

i.   Abuja's Urbanization is taking its toll on Kuje Area Council faster than envisaged by the Master Plan and even the administrators.

ii.   The urbanization growth rate of the area is increasing significantly from 12% annually between 1975 and 1980 to 13.4% annually between 2005 and 2010.

iii.   Developmental activities are encroaching into the agricultural lands at an alarming rate of 15.7 Km^2 annually. If of this growth rate continues, it implies that by the year 2030, an additional 282.6 square kilometers agricultural land (arable land, fadama land and forest) would have further been lost to urban encroachment.

iv.   A total of 509 Km^2 of agricultural land have been lost to urban encroachment within 35 years period under study. Out of this, 170 Km^2 is from arable land; 207 Km^2 from Fadama land; and 142 Km^2 from forest land cover.

v.   Road developments were also identified as a major agent of change in the area within the 35 year period. About 200 Km^2 of major roads were constructed between 1975 and 2010.

vi.   Lateral development is dominant in the area; in fact, single unit residential housing (bungalows) also known as the "Brazilian housing type" occupy a sizeable portion of the area in the new estates.

5. Conclusion

The invasive nature of urbanization in this area council may be seen as a mark of national development for now, but the continuous compromising of fertile agricultural lands to structural deployments may be a pathway to international slavery in the form of aid dependent or corking a huger gun that may trigger at any time. It must be borne in mind that the food produced at the suburb areas is playing a major complementary role to the food transported from other parts of the country to the Federal Capital Territory.

Recommendation

▪   There is an agent need to carry out the Master Plan Renewal to secure the agricultural lands, particularly the fadama lands.

▪   Vertical as a against dominant horizontal development should be encourage from now on to curtail the natural force of demand and supply that will edge out land for agriculture.

▪   Agricultural programmers that enhances mechanize agriculture, hybrid crops production, and urban agriculture should be vigorously pursued by the government.

▪   The theories and techniques of Remote Sensing and GIS should be built into the man power development programmers of the relevant environmental agencies in the territory. This will mean that the area council land administration should be incorporated into the Abuja

Geographical Information System (AGIS) to enhance the monitoring and control of developmental activities.

References

Adesina F.A., 2005: *Geoinformation and Natural Resources Exploitation in Africa; United Nations Economic and Social Council.* Paper Delivered in: Fourth Meeting of the Committee on Development Information, Addis Ababa on 23-28 April.

Bojle T.B., 2005: *Urbanization: An Environmental Force to Be Reckoned with, Population Reference Bureau.* www.prb.org/Articles2004.

Brockherhoff M.P. *An Urbanizing World.* Population Bulletin. 2000. 55 (3) 33.

Cariboni D., 2002: *Cities of the South on the Verge of Collapse.* Inter Press Service, SanJose, California, 4.

Cohen B. *Urban Growth in Developing Countries: A Review of Current Trends and a Caution Regarding Existing Forecasts.* World Dev. 2004. 32.

Elvidge C., Baugh K., Kihn E, & Davis R., 1997: *Mapping City Lights with Nighttime Data from the DMSP Operational Line Scan System.* Photogrammetric Engineering and Remote Sensing. Inter Press Service, San Jose. California, 8.

Ekpenyong R., 2006: *Analysis of the Implications of Urban Growth and Urbanization in Akwa Ibom State, Nigeria Using GIS Based Landuse/ Landcover Change Early Warning System.* In Cartography, GIS and Agricultural Development Journal. Abaama Publishing Co. Uyo.

El-Shakhs S. and Amirahmadi H., 1993: *Population Dynamics, Urbanization, and the Planning of Large Cities in the Arab World.* In: Amirahmadi H., and EL-Shakhs, S., Eds. Urban Development in Muslim World, New Brunswich, New Jessey, Centre for Urban Policy Research. 233-236.

FAO, 2003: State of the World's Forests 2003 Food and Agricultural Organization, Rome-Italy. In: Njomo D., Ed. Mapping Deforestation in Congo Basin Forest using Multi Temporal SPOT-VGT Imagery from 2000-2004.

Hardoy E., 2001: *Environmental Problems in an Urbanizing World.* Oxford University Press, UK.

Heimlich R.E. and Anderson W.D., 2001: *Development at the Urban Fringe and Beyond: Impacts on Agriculture and Rural Land.* Vol. 803. Economic Research Service, U.S. Department of Agriculture, Washington D.C., 80.

Ifatimehin O. and Musa S. *Application of Geoinformatic Technology in Evaluating Urban Agriculture and Urban Poverty in Lokoja.* Journal of Geography and Environment. 2008. 1; 21-23.

Ifetimehin O. and Ufuah E. *An Analysis of Urban Expansion and Loss of Vegetation Cover in Lokoja, Using GIS Technique.* Zaria Geogr. 2006. 17 (1) 31.

Elvidge T., Paul E., Levin, M., Prevalsky E., and Brown V. *Using Nighttime DMSP/OLS Images of City Lights to Estimate the Impacts of Urban Land Use on Soil Resources in the U.S.* Remote Sensing of Environment Journal. (1997b). 61; 105-112.

Kelarestaghi A., Ahmadi H., Jafari M., and Tahmoures M., 2006: *Landuse Change Detection and Spatial Distribution Using Digital and Satellite Data: A Case Study of Farim Drainage Basin, Northern Iran*. http://www.tropentag.de/2007/abstracts/full/330.pdf.

Kramer A., 1994: *A.19 DMSP (Defense Meteorological Satellite Program and A.19.1 DMSP Data Availability-Visible and Infrared Imagery*. In: Observation of the Earth and its Environment. Survey Missions and Sensors. Springer Verte, Berlin. 63.

Kuje Master Plan, 2004: A Publication of Federal Capital Territory Administration. Abuja.

Kwasi N.G., 2004: *Urbanization Process–Environmental and Health Effect in Africa.* Population Environment Research Network (PERN) Cybersermina, Urban Expansion: The Environmental and Health Dimension.
http://www.populationenvironmentresearch.org/papers/Nsiah-Gyaabah_contribution.pdf.

Lambin F., Geist H., and Lepers E., 2003: *Dynamics of Land Use and Land Cover Tropical Regions.* http://www.globalrestorationnetwork.org/uploads/files/LiteratureAttachments/93_dynamics-of-land-use-and-land-cover-change-in-tropical-regions.pdf.

National Population Commission. *Legal Notice on Publication of the Details of the Breakdown of the National and State Provisional Totals 2006 Census*. Federal Republic of Nigeria Official Gazette, 2007. 94 (24), Government Notice 2, May 15.

Njomo D., 2008: Mapping Deforestation in Congo Basin Forest Using Multi-Temporal SPOT VGT Imagery from 2000–2004. http://www.eproceedings.org/static/vol07_1/07_1_njomo1.pdf.

Nnabugwu F., 2012: *N150bn Needed for Competition: Abuja Ancestral Villages Bow to Urbanization.* In: Vanguard August 05, 2012.
http://www.vanguardngr.com/2012/08/n150bn-needed-for-competition-abuja-ancestral-villages-bow-to-urbanization/#sthash.mjNOihaH.dpuf.

Ralph G., 2008: *The American Farmland Trust.* Duxbury Press, California, 46.

Riebsame W.E, Meyer W.B., and Turner B.L. *Modeling Land-use and Cover as Part of Global Environmental Change.* Journal of Climate Change. 1994. 28 (45).

Sarma P.K., Lahkar B.P, Ghosh S., Rabha A., Das J.P., Nath N.K., Dey S., and Brahma N. *Land Use and Land Cover Change and Future Implication Analysis in Manas National Park, India Using Multi-Temporal Satellite Data*. Curr. Sci., 2008. 95 (2) 2: 23-227.

Skole D., and Tucker C.J. *Tropical Deforestation and Habitat Fragmentation in the Amazon: Satellite Data from 1978 to 1988*. Journal of Science. 1993. 190-192.

Turner L., and William B., 1994: *Changes in Land use and Land Cover: Global Perspective*. Cambridge University Press, U.S.A., 14-15.

Twumasi Y.A, Cole T.C, and Manu A., 2004: *Biodiversity Management Using Remotely Sensed Data and GIS Technologies: A Case of Digya National Park, Ghana.* 31st Int'l Symposium on Remote Sensing and Environment, Saint Petersburg, Russian Federation.

Ujoh F., kwabe I.D., and Ifatimehin O. *Understanding Urban Sprawl in the Federal Capital City, Abuja: Towards Sustainable Urbanization in Nigeria*. Journal of Geography and Regional Planning. 2010. 3 (5) 106-113.

United Nations Center for Human Settlements (UNCHS), 1996: *An Urbanizing World: World Global Report on Human Settlements.* Oxford University Press, New York.
United Nations, 2004: *World Urbanization Prospect the 2003* Revision. U.N., New York, USA.

United Nations, 2008: *World Urbanization Prospects 2007 Revision.* United Nations Department of Economic and Social Affairs Population Division, New York, USA.

Yang X., and Lo. C. *Modeling Urban Growth and Landscape Changes in the Atlanta Metropolitan Area.* International Journal of Geographical Information Science*.* 2008. 17 (5) 263-265.

Appendixes

Table A: Percentage Change Distribution of Landuse / Landcover in Kuje Area Council

S. N.	Landuse Land cover	1975 Area Km²	Area (%)	1980 Area Km²	Area (%)	1985 Area Km²	Area (%)	1990 Area Km²	Area (%)	1995 Area Km²	Area (%)	2000 Area Km²	Area (%)	2005 Area Km²	Area (%)	2010 Area Km²	Area (%)
1	Built -up	47	2.6	75	4.2	111	6.2	143	7.9	180	10	302	16.8	462	25.7	596	33.1
2	Road	131	7.3	159	8.8	184	10.2	221	12.3	266	14.8	276	15.3	310	17.1	331	18.4
3	Fadama	319	17.7	310	17.2	295	16.4	285	15.8	261	14.5	196	10.9	120	6.7	112	6.2
4	Arable land	582	32.3	576	32	566	31.4	551	30.6	547	30.4	533	29.6	480	26.7	412	22.9
5	Forest	342	19	323	17.9	322	17.9	314	17.4	311	17.3	291	16.2	244	13.6	200	11.1
6	Hill	228	12.7	218	12.2	201	11.2	198	11	180	10	164	9.1	152	8.4	125	6.9
7	Water body	151	8.4	139	7.7	121	6.7	88	5	55	3	38	2.1	32	1.8	24	1.3
8	Total	1800	100	1800	100	1800	100	1800	100	1800	100	1800	100	1800	100	1800	100

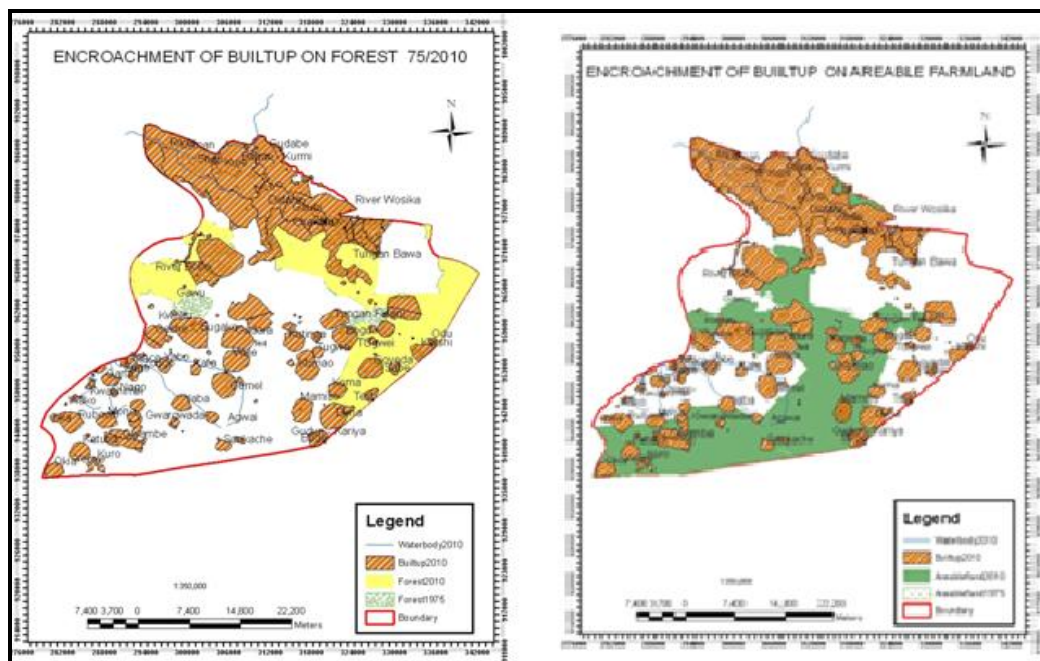**Source:** Derived from Landsat and NigeriaSat-1 Imageries for the various Years

Figure A: Encroachment of Built–up Areas On Forest Land between 1975 and 2010

Figure B: Encroachment of Built-up Areas on arable land between 1975 and 2010
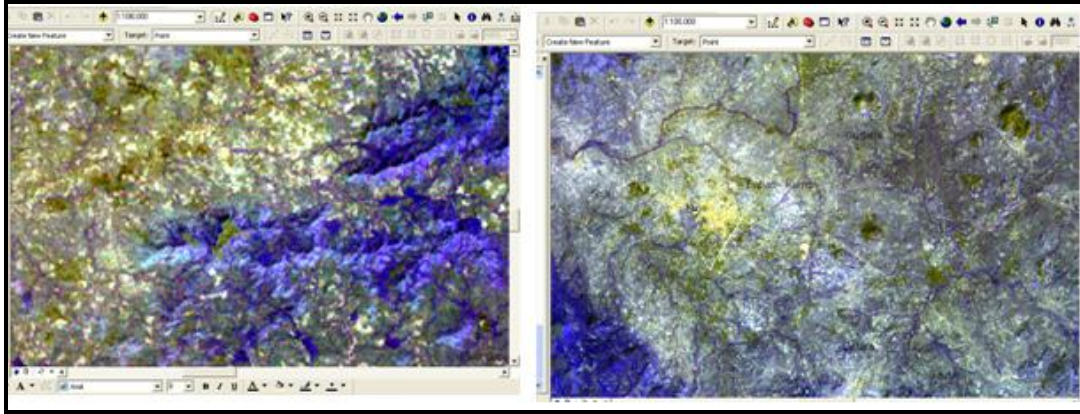
Figure E: *Composite Image of Abuja, 1980*   **Figure F:** *Composite Image of Abuja, 1990*
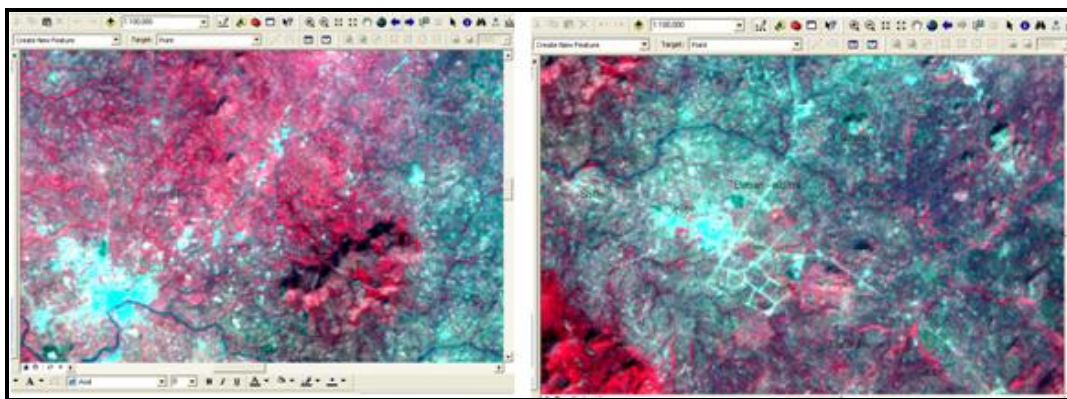

Figure G: *Composite Image of Abuja, 2000*   **Figure H:** *Composite image of Abuja 2010*

Cloud Publications

Research Article

Open Access

Urban Growth, Land Use Changes and Its Impact on Cityscape in Sonipat City Using Remote Sensing and GIS Techniques, Haryana, India

Sandeep Kumar and Randhir Singh Sangwan

Department of Geography, M.D. University, Rohtak, Haryana, India

Correspondence should be addressed to Sandeep Kumar, sndeepvats@gmail.com; randhirsangwan56@gmail.com

OPEN ACCESS

Abstract Urban growth of Sonipat city within the last 42 years is observed through MC map of different time which points out the dramatic change in the cityscape. The land use change is based on satellite imagery of LISS-III 2002 and 2011. Land use/land cover classification is based on supervised classification. Supervised classification was performed for the four major land use/land cover category; built-up area, agricultural land/vegetation, open/bare land and water bodies through Eradas 9.0. Arc GIS 9.3 software is used to prepare the thematic maps. Ground truth observations were also performed to check the accuracy from Google earth. Toposheets at a scale of 1:50000 have been used for geo-referencing the MC map of study area. Census data and MC map have been used to analyse the population growth and areal extension.

Keywords *Urban Growth; Land Use Changes; Areal Extension and GIS*

1. Introduction

Urban growth refers to the route of growing concentration of people inside a town or city which commence from a small dot and after that it spreads in dissimilar ways with varying intensity of growth from one urban place to another. (Paul and Dasgupta, 2013). The rapid urban growth through economic development has been an issue of concern to the planners in all over the world. (Singh, A.L., 2012). The rapid urbanization has changed the Indian scenario also and the landscape has felt the consequence of land conversion. Various causes of urban expansion for example population growth, economic development, migration and infrastructural innovations are resulting in transformation of villages into towns, towns into cities and cities into metro cities (Singh, et.al, 2008).

The rapid urbanization through industrial development is responsible for unsystematic and unplanned growth of cities and the pressure of urban population in the city has a direct (positive and negative) impact on its adjoining rural area. This type of urban growth creates the tribulations like unhealthy

slums, infected environment, industrial and commercial areas resulting in traffic bottle necks and such many other problems (Sangwan et.al. 2012). The analysis of spatial and temporal changes in land use/land cover is one of the effectual ways to understand the current environmental status of an area and its ongoing changes. Urbanization makes unpredictable and long lasting changes on the landscape (Singh and Kumar, 2012). In this regard, Sonipat city is no exception because of its prime location on N.H.1 and its easy accessibility and connectivity to both National Capital of Delhi and Union Territory of Chandigarh. The new economic environment of the city demands sustainable land management and spatial information of land use and their change over the time are important for planning and management. The association between urban growth and land use changes and their impacts on cityscape has been analyzed in the present study. So, satellite data of different time periods are useful to city planners to monitoring urban growth and development of a sustainable land use plan for the future.

2. Study Area

Sonipat city is the head quarter of Sonipat district which lies in the national capital region. As per 2011 census, the total population of the city is 277053 persons. Its closeness to NCT Delhi and easy fast accessibility to it through N.H.1 has led to urbanization of the city. According to city development plan, the Sonipat city which is a satellite town of the National Capital Region (NCR) has been divided in 31 wards by Municipal Corporation which has grown up as residential, industrial and commercial areas.
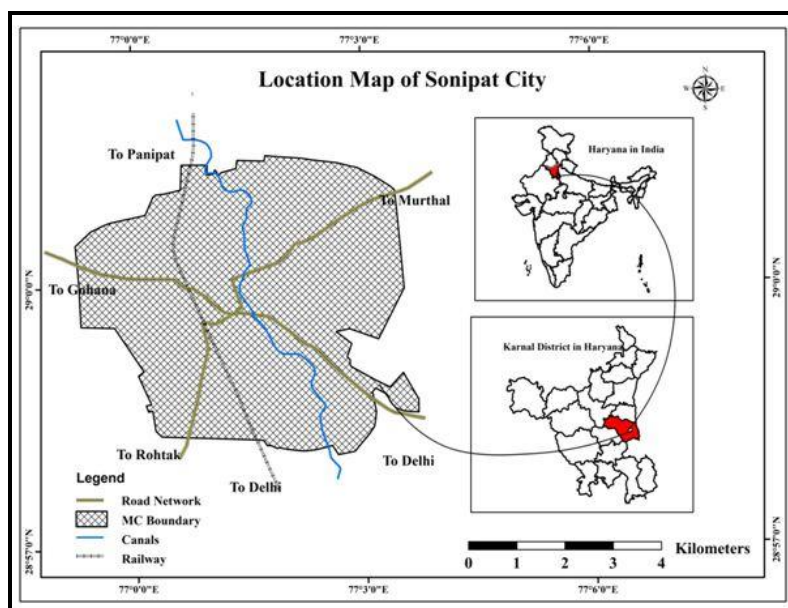

Figure 1: Location Map of Study Area

3. Objectives

- ➢ To identify the land use changes in Sonipat city;
- ➢ To examine the areal extension and direction of Sonipat city;
- ➢ To identify the relationship between population growth and areal extension.

4. Materials and Methods

Present paper is based on the remote sensing spatial as well as the non-spatial data available from the various sources for different periods. The sources are Statistical Abstract of Haryana, Town and Country Planning, District Gazetteer of Sonipat district and Town directory of Haryana. Satellite data

of the study area for 2002 and 2011 was obtained from HARSAC (Haryana Space Application Centre), Hisar. Topographic sheet No. H43Q16, H43R4, H43W13 and H43X1 at scale of 1:50,000 are used for the geo-referencing of M.C. map of study area in different time periods. Urban growth of the study area for 2002 and 2011 has been mapped with the help of satellite data. To measure the areal extension of city different time MC map has been used. The changes in land use pattern have also been assessed and mapped with the help of Arc GIS 9.3 and Erdas 9.0 software. Field verification was performed throughout the study area using GPS and obtained correct setting for each land use class incorporated in the categorization format. The study is based on supervised classification and visual interpretation of different time satellite imageries. The 2002 land use pattern could not be checked against the ground truth but, the available historical data for the study area were used to confirm the interpretation made (Singh and Kumar, 2012). However, LISS III supervised image of 2011 was directly checked against ground truth all the way through the study area. Urban expansion through economic development has direct impact of cityscape and changes in land use of study area. The paper focuses on interpreting city's land use change pattern and growth based on spatial and non-spatial data. LISS III 2002 and 2011 satellite data are used to identify different patterns of land use changes and growth of the study area. Analysis of Sonipat growth over a period of 10 years allows a good understanding of urban development.

5. Sonipat City: Land Use in 2002

In 2002 agriculture land/vegetation emerged as the dominant land use class. It covers an area of 1955.64 hectares i.e. 58.15 percent of the city area followed by built up area, open/bare land and water bodies i.e. 31.70 percent, 5.40 percent and 4.75 percent respectively. In 2002 built up area had increased because the new economic reform, after 1991 giving a way of urban development of Sonipat city with industrisation on the cost of agriculture/vegetation and open/bare land. As compared to peripheral area, central part of the city, which represents the establishment of the city, is highly dense and used for the residential, commercial, public and semi-public purpose.
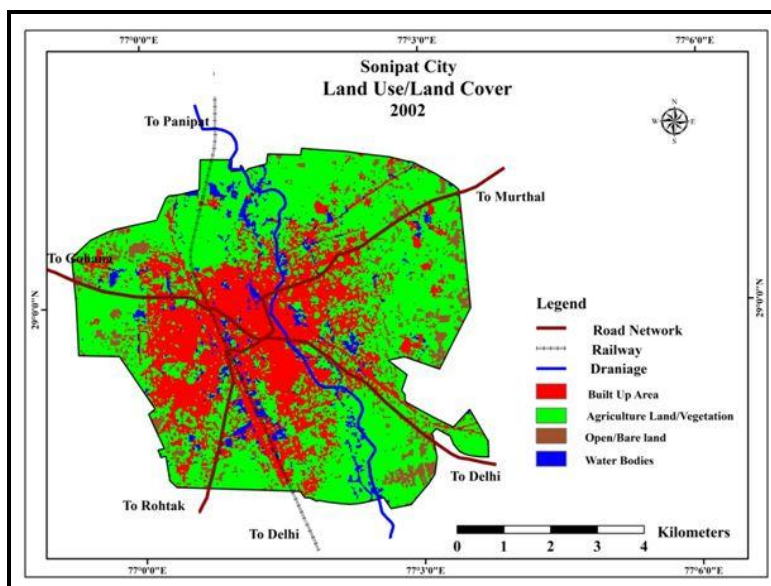

Figure 2: *Sonipat City: Land Use/Land Cover 2002*
Source: Based on LISS III Image (2002)

5.1. Sonipat City: Land Use in 2011

In 2011 the built up area has increased due to urbanization which has given a way to urban development of the city. It increased near about 30.62 percent whereas agricultural land/vegetation has been decreased 449.71 hectares i.e. 23.46 percent.
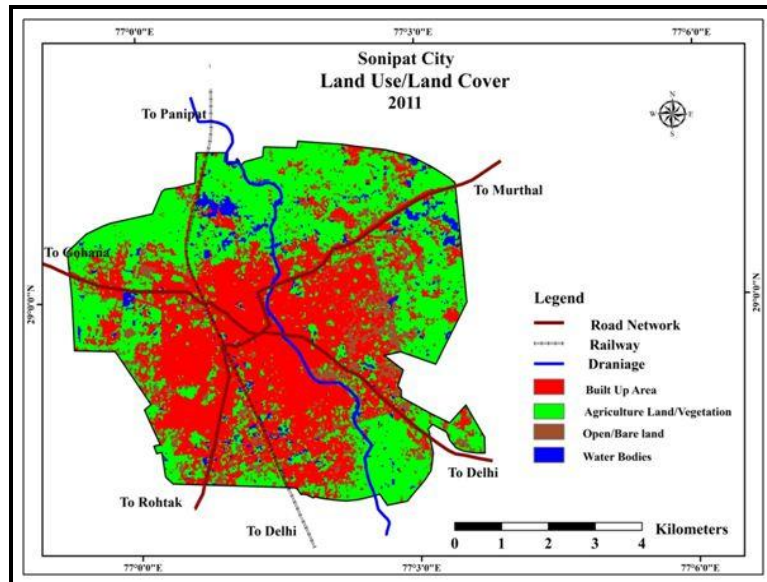

Figure 3: *Sonipat City: Land Use/Land Cover 2011*
Source: Based on LISS III Image (2011)

Open/bare land has been increased due to acquisition of land for residential and commercial purpose through Haryana Urban Development Authority and private builders, but there are no constructions, so it has been included in open land category. Water bodies have also been decreased 30.57 hectares i.e. 19.51 percent due to population pressure.

Table 1: *Change Detection Statistics: 2002-2011*

Land Use Categories	2002		2011		2002-2011	
	Area (Hect.)	Area (%)	Area (Hect.)	Area (%)	Change (Hect.)	Change (%)
Built up Area	1010.31	31.70	1371.46	41.40	320.45	30.62
Agriculture Land/Vegetation	1955.64	58.15	1465.23	44.51	-449.71	-23.43
Open/Bare Land	178.40	5.40	339.09	10.27	160.70	90.08
Water Bodies	156.72	4.75	126.14	3.82	-30.57	-19.51
Total	3301.06	100.0	3301.06	100.00		

Source: Based on LISS III (2002) LISS III (2011) Images
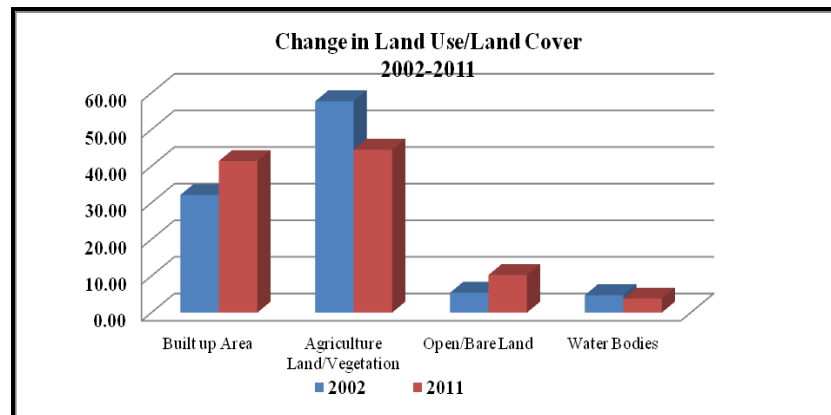
Figure 4: *Change in Land Use/Land Cover 2002-2011*
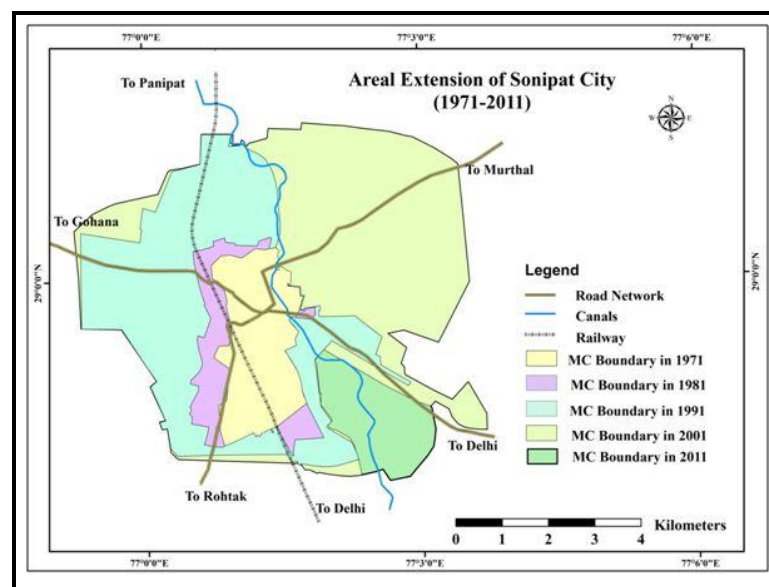**Source:** Based on Table 1

Figure 5: *Areal Extension of Sonipat City (1971-2011)*
Source: Municipal Office, Sonipat City

6. Analysis of Land Use/Land Cover 2002 and 2011

Change detection statistics calculated from the processed image of year 2002 and 2011 which covers a period of 10 years. Table 1 reveals that there is a remarkable change in built up area and agricultural land use categories. The built up area has increased from 31.70 percent in 2002 to 41.40 percent in 2011 whereas area under agriculture land/vegetation category decreased from 58.15 percent (in 2002) to 44.51 percent (in 2011).

After 1991 new economic reform liberalization, privatization and globalization policies of the Government of India and opening up of FDI in real estate sector have brought a big boom in the development of large scale private industries and townships and its location, and active role of Haryana Urban Development Authority (HUDA) in well-organized sectors of industrial/commercial/residential purposes. So built up area has rapidly increased. It is observed that the low concentration of population in the central part was also converting in higher concentration. The land use statistics analysis that built up and agricultural land/vegetation is matter of concern.

The natural growth and attraction of people from surrounding rural areas due to availability of better facilities have resulted in diminution of agricultural/ vegetation area and on this cost built up area has got increase.

The conversion of agricultural land/vegetation for residential and commercial purposes along with major roads and in south eastern part of the city outside the MC boundary is mainly because value of land is lowest as compared to central part.

6.1. Accuracy Assessment

Accuracy assessment basically three types that are over all accuracy, user accuracy and producer accuracy in four categories namely built up area, agricultural /vegetation, water bodies and open/bare land have been analyzed which is based on error matrix. The error matrix was used to assess the mapping accuracy. The overall accuracy only considers the correction of diagonal elements in the matrix. The overall accuracy calculated from 2002 and 2011 is 85.66 percent and 90.64 percent respectively which is acceptable for such change analysis (Table 2).

Table 2: Accuracy Assessment in 2002 and 2011

Land Use Categories	Producer's Accuracy in Percent		User Accuracy in Percent	
	2002	**2011**	**2002**	**2011**
Built up	95.35	93.08	93.68	97.45
Agricultural/Vegetation	73.22	84.74	93.03	91.3
Water Bodies	93.18	93.33	49.79	35.9
Open/bare	93.13	96.57	33.59	29.6
Overall Accuracy (2002)= 85.66% and **(2011)**= 90.64%				

Source: Based on Error Matrix on LISS III (2002) LISS III (2011) Images

6.2. Population Growth and Areal Extension

The population growth is a main factor for the areal extension and sprawl because administration of the city has extended the city boundary to manage the population pressure. Population pressure creates several problems like unhealthy slums, infected environment, less development of residential area, industrial and commercial areas resulting in traffic bottle necks and many other problems. There is significant positive relationship between population growth and areal extension. There is increase of 81529 people in the population from 1971 to 1991 whereas the area has increased 12.97 hectares during the same period. In 2001 the population has been recorded 225074 which have increased up to 278149 into 2011 (Table 3). There is not any significant increase in area within MC boundary. It has increased only 2.78 hectares from 2001 to 2011. The reason behind this little extension of the area is that National Highway 1 is far from the city at a distance of 6 km.

Table 3: Population Growth and Areal Extension 1971-2011

Census year	Population (Within MC)	Variation in Population	Growth Rate in Percentage	Area in Hectares (MC Boundary)
1971	62393	16511	-----	4.03
1981	109369	46973	75.29	6.02
1991	143922	34553	31.59	17.01
2001	225074	81152	56.39	30.24
2011	278149	53075	23.58	33.03

Source: Primary Census Abstract 1991, 2001 and 2011
     MC Office, Sonipat City, Haryana

7. Conclusion

Present study reveals the urban growth and its Impact on Cityscape in Sonipat city. Urban growth is a worldwide fact that comes with the land use change, population growth and economic development. Urbanization is a main cause for the Sonipat city where rate of urban expansion has occurred very fast in the recent time. The city landscape is likely to expand at a very rapid rate. After 1991 new economic reform liberalization, privatization and globalization policies of the government of India and opening up of FDI in real estate sector have brought a big boom in the development of large scale private industries and townships in study area. Present time development of industries, education institutions, tourism, hospitals, private residential builders and good road system has contributed the quick urban expansion and land use transformation in Sonipat city which influence sustainable use of land. The study also find out that productive agricultural land has been occupied by residential, commercial and industrial sectors which can be credited to the human interventions with the environment. The extent and pace of urban transformation has made an alarm about the city sustainability. As a result, the valuable urban planning and administration with a target of long term sustainability is required for the monitoring and management of the growing city.

Acknowledgment

References

Singh Nina and Kumar Jitendra. *Urban Growth and its Impact on Cityscape: A Geospatial Analysis of Rohtak City, India.* Journal of Geographic Information System. 2012. 4 (1) 12-19.

Singh, A.L., 2012: *Urban Sprawl: Causes, Consequences and Policies.* B.R. Publishing Corporation, Delhi. 17-18.

Singh, A.L., and Mansoor, A.S. *Effect of City Expansion on the Countryside: A Case Study.* Punjab Geographer. 2012. 4; 17-25.

Tejpal Kumar, Yogender, and Dr. Kumar Manoj. *Mapping and Monitoring of Land Transformation Due to Urban Sprawl in Rewari City,* International Journal of Remote Sensing and Geoscience. 2013, 2: (4) 1-6.

Sangwan, R.S. Kumar, Sandeep, and Maximal. *Impact of Urban Sprawl on City Environs: A GIS Based Study of Karnal City, Haryana.* India, Journal of Water and Land Use Management. 2012. 2 (2) 1-6.

Paul S., and Dasgupta A. *Spatio-Temporal Analysis to Quantify Urban Sprawl Using Geoinformatics.* International Journal of Advances in Remote Sensing and GIS. 2013. 1 (3) 264-278.

Research Article   **Open Access**

Mapping of Lineaments in Some Part of Betul District, Madhya Pradesh and Amravati District of Maharashtra, Central India Using Remote Sensing and GIS Techniques

B.S. Manjare

Department of Geology, RTM Nagpur University (MS), Maharashtra, India

Correspondence should be addressed to B.S. Manjare, yogesh_manjare1@rediffmail.com

Abstract Lineament analysis around Salbardi and adjoining area were carried out using a remotely sensed IRS-LISS-3 Satellite imagery for the analysis of the areas based on the frequency and density of lineaments on the lithology. The area comprising 252 lineaments in the rocks of Proterozoic, Deccan trap, and Upper Gondwana formation. The extracted lineaments were statistically analyzed to determine lengths and intersections of the lineaments to create rose diagram and lineament map. The lineament from the study area which is important part of the Son Narmada Tapti Lineament has numerous long and short fractures/lineation whose structural trends are mainly to the Son Narmada Tapti Lineament and gets the special significance to the given study area. The calculated lineaments from the given study area has been utilized for the correlation to the Salbardi fault and Son Narmada Tapti Lineament.

Keywords *Lineaments; Azimuths; Remote Sensing; Geographic Information System*

1. Introduction

The planned study area is one of the important elements of the Tapti-Purna lineament which is a major component of SONATA (Son-Narmada-Tapti Lineament) trending ENE-WSE direction. In the area the Salbardi fault is one of the important structural features present. The Salbardi fault is probably the eastern continuation of well known Gavilgrah/Elichpur fault (Rajurkar 1981).

Auden (1949) had guessed the through of this fault to be anywhere between 1800-1400 mts in Gawilgrah region and extends in the north east direction. It was variously described as Gawilgrah fault, Ellictipur fault and Salbardi fault in different stretches (Rajukar 1992, Saxena, 1994, Tiwari, 1985).

Lineaments seen on remote sensing data like satellite image/aerial photographs and geophysical data etc. are of great relevance to geoscientists as they reflect various structural feature of an area.

Mapping and analysis of lineaments help in understanding the structural and tectonic set-up of an area. Lineaments, which represent faults, fractures, shear zones, joints, litho-contacts, dykes etc. Can be mapped easily using remote sensing data. Mapping and analysis of lineament are only help in understanding the structural/tectonic aspect of an area but also in turn are useful in exploration of mineral, ground water, oil and in understanding the seismicity of a given area.

2. Study Area

The study area lies in the Survey of India top sheet no. 55 k/2, 55 k/3, 55 G/14, 55 G/15 and bounded by latitude and longitude 21^0 20' to 21^0 35' E and 77^0 45' to 78^0 10' N respectively. The present study area falls in to two states i.e. one part comes under the state of Maharashtra district Amravati and other falls under the state of Madhya Pradesh district Betul (Figure 1).
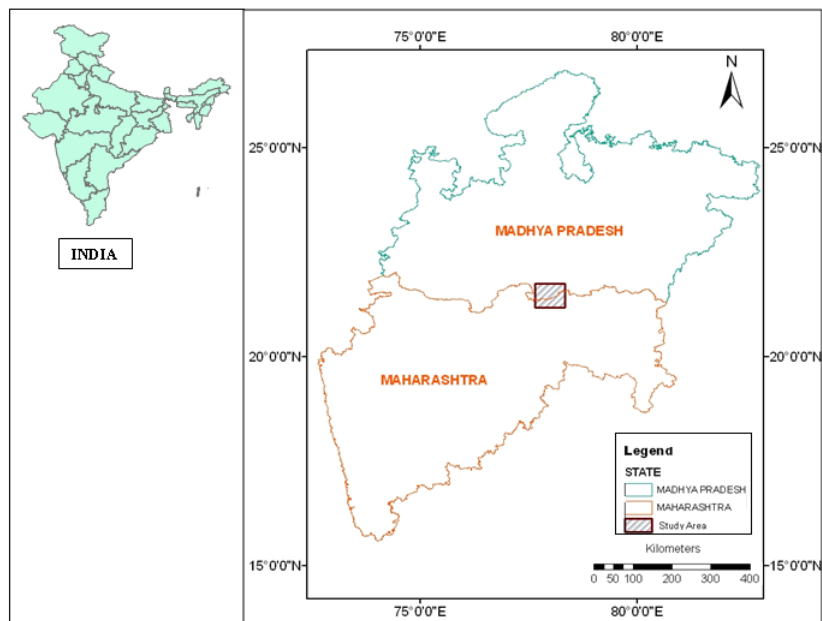

Figure 1: *Location Map of the Study Area*

3. Geology of the Study Area

Geologically though the area is occupied mainly by Deccan traps the rocks belonging to other ages also form and an important of the geological sequence. Stratigraphycally the area consist of litho units like granites, gneisses, quartzite, and felspathic gneisses and are followed by upper Gondwana and Lameta belonging to upper cretaceous period. This formation is unconformably overlained by Deccan trap and which is in turn is overlain by the alluvium of quaternary period.

4. Lineament

Lineaments/fractures are defined as mappable linear surface features, which differ distinctly from the patterns of adjacent features and presumably reflect subsurface phenomena (O'Leary et al. 1976). Satellite data along with aerial photographs are widely used to extract lineaments for different studies. Since satellite data are obtained from varying wavelength and frequencies with different intervals of the electromagnetic spectrum, they are considered to be an enhanced device to discriminate the lineaments and to produce healthier information than conventional studies. The purpose of this study is to analyze the spatial distribution of lineaments extracted from remotely sensed satellite data to

analysis length and orientation to the understanding of the faults and their association to the Son Narmada Tapti Lineaments and Salbardi fault.

5. Origin of Lineaments

Number of hypothesis have been put up by various scientists to explain the origin of lineaments, the prominent among them are Global Regmatic Shear pattern, wrench fault tectonics, Deep tectonic zones and Global Tectonics concept. Lineaments could be thought of as observable physical responses of a host of interrelated geodynamic phenomena such as lithospheric accretion and destruction, oceanization and cratonization, seismicity and taphrogenesis and mountain building, pluton emplacement and metallogeneis (Bhave et al., 1989).

6. Methodology for Lineament Analysis

Lineaments usually become visible as straight lines or "edges" on the satellite data images or on aerial photos which contributed to the tonal and textural differences within the earth surface. The lineaments vary from 2 kms to more than even 1000 kms in length with linear and curvilinear expressions. The study of these lineaments in relation to geology, structure, magmatism, mineralisation and deep geophysical responses etc. led to the classification of these lineaments into various groups and classes.

1) Stream and streams segment designates relatively short; straight channel reaches commonly connecting at sharp, angular junctions. Stream segments include the shortest lineaments recognized, as short as 2 kms long. Stream segments were delineated only if they were part of a distinctive sequence of linear channels.

2) Drainage line designates linear valley trends independent of the orientation or linearity of channel segments.

3) Scarp and fault line scrap designates a prominent topographic break evident because of changes in land cover or land use, changes in drainage pattern, variations in outcropping rock units, or the presence of shadows on the imagery.

4) In dividing lineaments between the high plains and rolling plains categories, the scarps of the caprock escarpment boundary feature are considered separately as a unique physiographic category.

5) Geologic contact designates linear contacts between surficial materials with different reflectivity.

6) Tonal anomaly designates as a linear feature.

    Based on the length of individual lineaments, such lineaments have been classified:

    (i)   Micro: <2km
    (ii) minor: 2-10 km
    (iii) medium: 10-100 km
    (iv) major: 100-500 km
    (v)   mega > 500 km. (K. Ganesh Raj, GSI, 2003)

6.1. Lineament Extraction

According to literature there are two common methods for the extraction of lineaments from satellite images:

1) Visual extraction: At which the user primarily starts by image processing method to make edge enhancements, using the directional and non directional filters such as the Laplacian, and Sobel, then the lineaments are digitized manually by the user.

2) Automatic (digital) extraction: different computer-aided methods for lineament extraction have been proposed. Mainly used in the lineament extraction methods are based on edge enhancement techniques. The most commonly used software for the automatic lineament extraction is the 'LINE' module of the PCI Geomatica or which can be calculated in the ERDAS.

By using these above different techniques 252 numbers of lineaments are extracted from IRS LIIS-4 and IRS LISS-3 images data. The resulted lineament map and their frequency distribution are shown in Figures 2 and 3, respectively. Manually extracted lineaments are evaluated in order to extract further information on the distribution and nature of the lineaments (Figure 2).
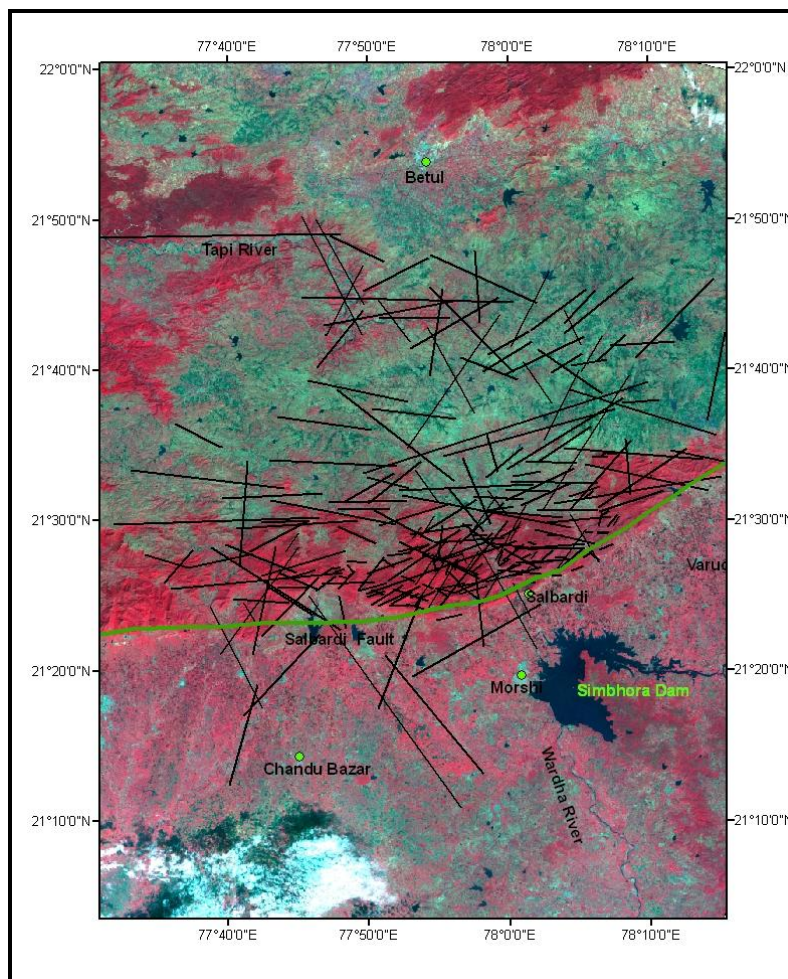

Figure 2: Representation of Lineaments on the IRS LISS-3 Satellite Image of Some Part of Betul (M.P) and Maharashtra

6.2. Lineament Length

In the study area, there are 252 lineaments of different length (as counted using Arc GIS 9.3 software). There are 68 lineaments of the micro type (< 2km) which is equal to about 26.98% (per number) and 125 lineament are minor type which is equal to 49.60% and covers the larger part of the study area while rest are of medium category and equal to 23.41% (Table 1) respectively. The resulting map reveals a range of lengths which are indicative of several geo-tectonic and geomorphic controls, mainly the power of the tectonic forces, rock hardness and consolidation, geomorphic setting of terrain where lineaments exist (Figure 3 & 4).

Table 1: Classification of Lineament in the Study Area

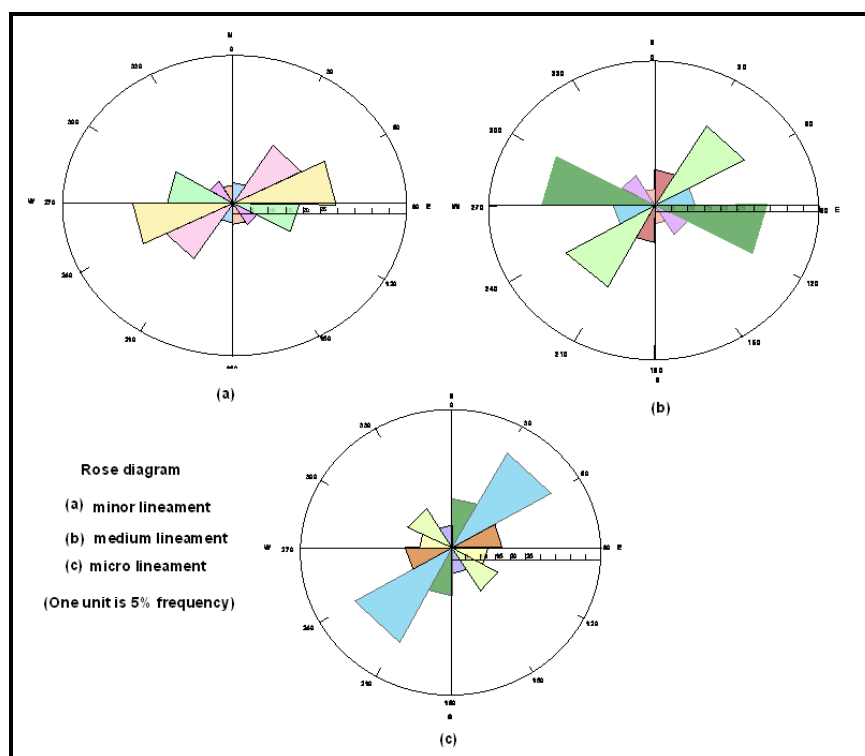| Sr. No.	Lineament Class	Numbers	%	Length(mts)
1	Micro lineament	68	26.98	101986.6
2	Minor lineament	125	49.60	728163.4
3	Medium lineament	59	23.41	973969.5
4	Major lineament	---	---	---
5	Mega lineament	---	---	---
	TOTAL	252	---	1804119.5

Figure 3: Rose Diagram of the Medium, Minor and Micro Lineament Orientation (One Unit is 5% Frequency)

6.3. Classification of Lineaments

In general there is no minimum length for lineaments, but significant crustal feature are typically measured in tens or hundreds of kms. (Kowalik and Gold, 1976) suggested a lengthwise classification of lineaments/linear feature. The classification is as follows (Table 1): (a) short/minor – 1.6 to 10 km (b) Intermediate – 10 to 100 km (c) long/major – 100 to 500 km (d) mega - > 500 km. However, no uniform classification system has been evolved yet (Figure 3 & 4).

The authors feel that keeping in mind the high resolution data/large scale of mapping (up to 1:5000) possible currently, lineaments can be classified based on their length as (i) micro: <2 km, (ii)minor: 2-10 km, (iii) medium: 10-100 km, (iv) major: 100-500 km, and (v) mega > 500 km.

7. Lineament Trends in the Area

The trends of the all lineaments of the study area given in Tables 1-4. Most of minor, major, micro lineaments trends are NE, ESE, SE, SSW in which minor lineaments gives the frequency % of 7.29,24.00,30.40,21.60,8.80,8.00 respectively while medium lineament gives the trends of 11.86,28.81,11.86,32.20,10.16,5.08 frequency % respectively and micro lineaments shows 16.17,35.29,14.70,10.29,16.17,7.35 frequency % respectively (Table 2, 3 and 4). It suggesting that the trends are N- S, NNE-SSW, ENE-WSW, SE-SW and E-W axis which is also the principal direction of the regional structures directions. In the study area the major lineament and mega lineament are absent.

Table 2: Micro Lineament Trends in Study Area

Sr. No.	Trends	Number of Fraction	%	Length (mts)
1	0^0-29^0	11	16.17	16905.69
2	30^0-59^0	24	35.29	35264.63
3	60^0-89^0	10	14.70	18713.93
4	90^0-119^0	07	10.29	10424.18
5	120^0-149^0	11	16.17	18405.75
6	150^0-179^0	05	7.35	7790.12
	TOTAL	68	----	101986.6

Table 3: Minor Lineament Trends in Study Area

Sr. No.	Trends	Number of Fraction	%	Length (mts)
1	0^0-29^0	09	7.20	52257.48
2	30^0-59^0	30	24.00	176925.00
3	60^0-89^0	38	30.4	198383.4
4	90^0-119^0	27	21.60	165325.8
5	120^0-149^0	11	8.80	66750.34
6	150^0-179^0	10	8.00	64723.45
	TOTAL	125	---	728163.4

Table 4: Medium Lineament Trends in Study Area

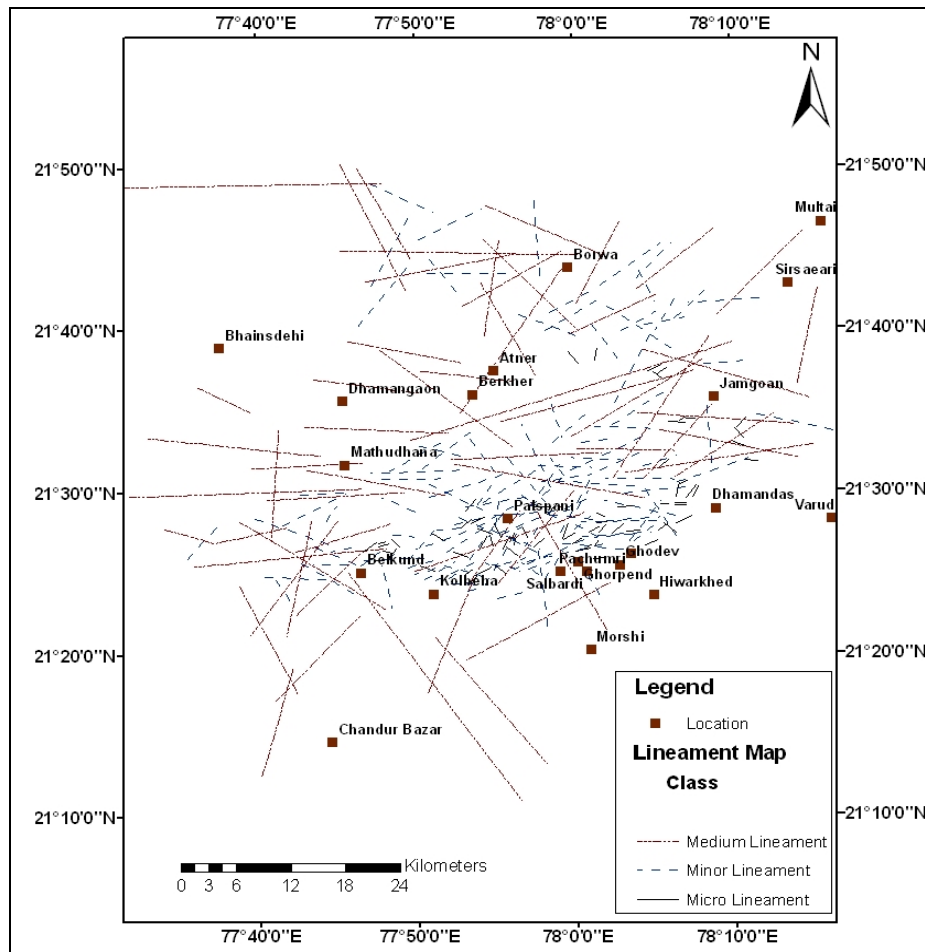| Sr. No.	Trends	Number of Fraction	%	Length (mts)
1	0^0-29^0	07	11.86	95253.3
2	30^0-59	17	28.81	228688.5
3	60^0-89^0	07	11.86	143692.01
4	90^0-119^0	19	32.20	353773.3
5	120^0-149^0	06	10.16	109649.31
6	150^0-179^0	03	5.08	42913.05
	TOTAL	59	----	973969.5

Figure 4: *Lineament Map of the Study Area*

8. Conclusion

Satellite data has provided evidence to lineament identification and mapping. This study demonstrates the satellite lineament interpretation of study area. The result gets from the study area of the analysed lineament/fracture indicated that the area has numerous long and short fractures whose structural trends are mainly in north- east to south west direction. The cross-cutting lineaments are relatively high areas around the central, north-eastern and south-western parts of the study area but low in the other part of the study area (Figures 2 & 3, 4). The lineament intersection density are shows the tectonic activity in the study area. We found that most of the major orientations in the field could be successfully detected from the satellite image. The results show that the remote sensing and GIS technique is competent of extracting lineament trends for the tectonic analysis. The totals of 252 lineaments were extracted from the satellite image with a total length of 1804119.5 mts (Table 1). In which medium Lineament covers 973969.5 mts. lengths, minor lineament gives total length of 728163.4 mts and the length of micro lineament is 101986.6 mts. In the central, northeastern and southwestern parts of the study area has a relatively high density value. According to Edet et al., 1998, the zones of relatively high lineament density are identified as zones of high degree of rock fracturing which are prerequisite for groundwater channel development in an area. The rose diagram (Figure 3) shows the directional frequency of the mapped lineaments over the area which has major trends in the north east and south west trends. The major trends of the lineament in the study area are in the direction of N- S, NNE-SSW, ENE-WSW, SE-SW and E-W axis which is also the principal direction of the regional structures directions (Figure 3). Apart part from the prominent trends the lineament from the study area correlated with the Salbardi fault (ENE-WSW) and interpretation of

hidden subsurface tectonic arrangement in form of linear features intersection and cross cutting geological structures that are diagnostics of deep seated fracture/ fault medium are interpretable on the lineament map and hence it suggested the area is good for ground water extraction.

Acknowledgement

References

Auden, J.B., *Geological Discussion of the Satpura Hypothesis*. Proc. Natl. Inst. Sci. India. 1949. 15; 315-340.

Bhave, K.N., Ganju, J.L., and Jokhan, Ram, 1989: *Origin, Nature and Geological Significance of Lineaments.* In: Qureshy, M.N., and Hinze, W.J (Ed.). Regional Geophysical Lineaments their Tectonic and Economic Sgnifivcance. Mem. Geol. Soc. India, Vol. 12; 35-42.

Kowalik, W.S., and Gold, D.P. *The Use of Landsat-1 Imagery in Mapping Lineaments in Pennsylvani*a. Proceeding First Int. Conf. on the New Basement Tectonics, Utah Geol. Assoc. 1976. 5; 236-249.

O'Leary, D.W., Freidman, J.D., and Pohn, H.A., *Lineaments, Linear, Lineation-Some Proposed New Standards for Old Terms.* Geological Society of America Bulletin. 1976. 87; 1463-1469.

Rajurkar, S.T., 1992: *Photographic Interpretation of Upper Wardha Project and Surrounding Area Wardha, Amravati and Betul Districts, Geol Suvy. India*. Golden Jubilee Symposium Volume, Department of Geology, Nagpur. 269-292.

Saxena, R.K., 1994: *Geothermal Investigation of Salbardi around Hot Spring Area*, Dist. Betul (M.P) and Amravati Maharashtra, Geol. Surv. Ind. F.S. 1981-82.

Tiwari, M.P. *Neotectonism in Tapti Purna Valleys and its Probable Correlation with Geothermal Activity*. In: Geothermal Energy of India. Geo. Surv. India, Spe. Pub. 1985. 45; 325-332.

Research Article   **Open Access**

Change Detection in Synthetic Aperture Radar Images Using Contourlet Based Fusion and Kernel K-Means Clustering

Venkateswaran K., Kasthuri N., Balakrishnan K., and Prakash K.

Department of Electronics and Communication Engineering, Kongu Engineering College, Erode, Tamil Nadu, India

Correspondence should be addressed to Venkateswaran K., vvenkates05@gmail.com

Abstract Change detection algorithms play a vital role in overseeing the transformations on the earth surface. Unsupervised change detection has an indispensable role in an immense range of applications like remote sensing, motion detection, environmental monitoring, medical diagnosis, damage assessment, agricultural surveys, surveillance etc. In this paper, a novel method for unsupervised change detection in multitemporal images based on image fusion and kernel K-means clustering is proposed. Here difference image is generated by performing image fusion on mean-ratio and log-ratio image and for fusion contourlet transform is used. On the difference image generated by collecting the information from mean-ratio and log-ratio image kernel K-means clustering is performed. In kernel K-means clustering, non-linear clustering is performed, as a result the false alarm rate is reduced and accuracy of the clustering process is enhanced. The aggregation of image fusion and kernel K-means clustering is seen to be more effective in detecting the changes than its preexistences.

Keywords *Change Detection; Difference Image; Image Fusion; Kernel-K Means Clustering; Synthetic Aperture Radar*

1. Introduction

Multitemporal remote sensing represents a powerful source of information for investigating the evolution of the Earth's surface, for instance, in environmental monitoring or disaster management. A relevant task is the identification of the changes that occurred in a given area between two observation dates. Change Detection is aimed at identifying the differences between images of same area acquired during different instance of times. The result is a binary change map that represents the changes that occurred between those two areas. When using an unsupervised approach, i.e., when no training data are available at either date, image differencing and image (log-) ratioing are often applied to address this task with optical and synthetic aperture radar (SAR) data, respectively. Manual or automatic thresholding can then be used to distinguish changed and unchanged areas in the difference and (log) ratio images. The process of change detection is of

widespread interest since it is having a wide variety of applications in diverse domains like remote sensing [3], motion detection [4], video surveillance [5], damage assessment [6], agricultural surveys [7], environmental monitoring [8], analysis of urban changes [9], and medical diagnosis [10].

A wide variety of change detection techniques have been introduced in the literature. Due to the massive growth of the geographic database, it is more practical to focus on the unsupervised approach than the supervised one. Currently, many unsupervised change detection techniques have been proposed. Some of these are image algebra, transformation of the multitemporal images, image classification, advanced models; Geographical Information System (GIS) approaches etc. With the advancement in the remote sensing technology, unsupervised change detection in remote sensing images is becoming vital.

In the literature, unsupervised change detection in multitemporal images is achieved in three main steps [11]: 1) pre-processing; 2) pixel by pixel comparison to get the difference image; 3) Analysis of the difference image. The objective of pre-processing step is to reduce the noise and hence increase the SNR. After pre-processing, difference image is generated by the pixel by pixel comparison of the multitemporal input images. In multitemporal optical images, the subtraction operator is used to generate the difference image. Also by taking the ratio operator, the multiplicative noise can be changed to additive noise. In the third step, the difference image is analyzed by using either thresholding techniques [12] clustering techniques. In Multitemporal SAR Images change detection is performed using a new statistical similarity measure [17] and bivariate gamma distributions [19]. Thus, the accuracy of the change detection algorithm in multispectral images depends on the virtue of the difference image and the efficiency of the classification technique. In this paper, in order to improve the quality of the difference image, image fusion based on countourlet transform is used for fusing two types of ratio images namely the mean-ratio image and the log-ratio image. Secondly the exactness of the classification technique is enhanced by using kernel k-means clustering, in which a linear algorithm is applied in a higher dimensional feature space to consider the non-linearities. Thus the rate of false alarm is reduced, resulting in a better change map than the existing methods.

2. Materials

The dataset is a portion (301x301 pixels) of two images taken by European Remote Sensing 2 satellite SAR sensor above the region in the vicinity of the city of Bern, Switzerland during April (Figure 1 A) and May (Figure 1 B), 1999 correspondingly. During this period the river Aare flooded wholly the cities of Thun and Bern, and hence the Aare valley was selected as the test site. In order to validate the accuracy of the proposed approach quantitatively, the results obtained has been compared with the ground truth for the Bern area. This ground truth was obtained through past information and photo analysis.

3. Methods

Let us consider the two co-registered intensity SAR images:

$$X_1 = \{X_1(i,j), 1 < i < H, 1 < j < W\} \, and \, X_2 = \{X_2(i,j), 1 < i < H, 1 < j < W\} \qquad (1)$$

Each image have a size $H \times W$, i.e., acquired over the same geographical area at two different times. Our objective is aiming at producing a difference image that represents the change information between the two times; then, a binary classification is applied to produce a binary image corresponding to the two classes: change and unchanged. The proposed unsupervised distribution-free change detection approach is made up of two main phases: 1) generate the difference image using the contourlet fusion based on the mean-ratio image and the log-ratio image; and 2) automatic analysis of the fused image by using an improved clustering algorithm.
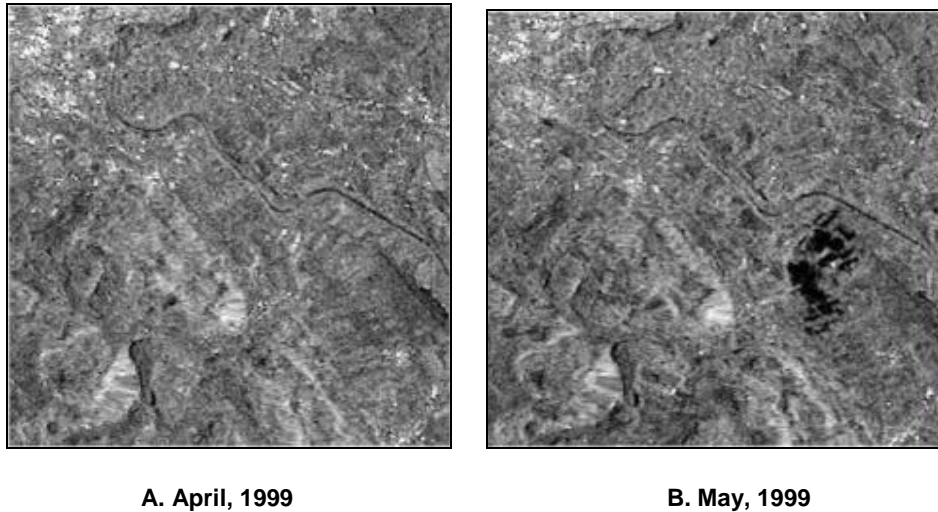
A. April, 1999   **B. May, 1999**

Figure 1: Multitemporal Images for the City of Bern

3.1. Mean Ratio and Log Ratio

As mentioned in the previous section, we assume that there is only one typology of changes between the two acquisitions. Hence, the normalized mean-ratio operator should be applied to generate the mean-ratio image. It can be defined as follows:

$$X_m(i, j) = 1 - \min\left(\frac{\mu_1(i, j)}{\mu_2(i, j)}, \frac{\mu_2(i, j)}{\mu_1(i, j)}\right) \qquad (2)$$

Where $\mu_1(i, j)$ and $\mu_2(i, j)$ represent the local mean values of the pixels involved in a neighbourhood of point (i, j) in X_1 and X_2, respectively. Equation (2) shows that the mean-ratio operator produces DI by using the local mean information of each pair of co-located pixels. In a similar way, the absolute valued log-ratio operator is applied in our letter to indicate the change areas. It can be defined as

$$X_l = \left|\log\left(\frac{X_2}{X_1}\right)\right| = \left|\log X_2 - \log X_1\right| \qquad (3)$$

Where log stands for natural logarithm. Both operators regard the increasing and decreasing radiometry as the same typology of changes. It makes the identification of changed areas independent of the order with which the images are considered in change indicator [8].

With the use of log-ratio operator, the multiplicative noise is changed to additive. The log-ratio operator enhances the low-intensity pixels and deteriorates the high intensity pixels; as a result the categorization of the pixels into the changed and the unchanged classes is made more symmetrical. Also the background of the log-ratio image is flat. But the drawback in using the log-ratio operator is that, the information about the changed areas gained from the log-ratio image is not in accordance with real change trends, since the log-operator deteriorates the high intensity pixels. Thus in the mean-ratio operator the difference image is produced by comparing the mean value of the co-located pixels in the multitemporal input images. The disadvantage of using the mean-ratio image is that, it does not take into account the changes that may occur without altering the local mean value and also the background of the mean-ratio image is rough.

Thus, both the mean ratio and log-ratio images are having merits and demerits. For this reason, image fusion technique is used in the proposed approach, so that the information from both the ratio images can be combined to get the finest difference image in which the changed pixels will be having high intensity values when compared to the unchanged pixels.

3.2. Image Fusion

Image fusion is the method in which information from two or more images are combined to get a fused image which is more worthy for the specified application. In the past for performing fusion, Intensity, Hue, Saturation (IHS) transform, Principle Component Analysis (PCA), statistical and arithmetic combination, [13], and the recently accepted multiscale fusion. One of the popularly used multiscale transform is the wavelet transform. In the proposed approach, the image fusion is done in the frequency domain and here contourlet transform is used when compared with other multiscale transforms, contourlet transform is more condensed, highly directional and provides unique information at each resolution. The contourlet transform focuses on representing point discontinuities and conserving the time and frequency details in image. Its simplicity and its ability to uphold image details with point discontinuities make the fusion scheme based on contourlet transform suitable for the change detection process [14]. The steps involved in the image fusion are described (Figure 2).
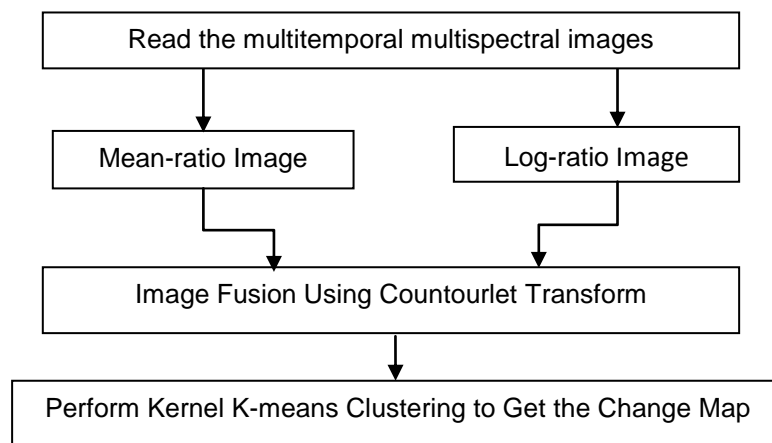

Figure 2: *Steps Involved in the Image Fusion*

Step 1: The contourlet transform for both the log-ratio and mean ratio image is taken. Here one level of decomposition is done on both the images.

Step 2: The fusion rule is applied on the approximate, diagonal, horizontal and vertical coefficients of both the images. For high frequency and low frequency band, separate fusion rule is proposed. The fusion rule is defined below:

$$F_{LL} = \frac{L_{LL} + M_{LL}}{2} \tag{4}$$

$$F_{\rho}(i,j) = \begin{cases} M_{\rho}(i,j), if, E^{M}(i,j) < E^{L}(i,j) \\ L_{\rho}(i,j), if, E^{M}(i,j) \geq E^{L}(i,j) \end{cases} \tag{5}$$

Where M_{LL}, F_{LL} and L_{LL} represent the approximate coefficients (low frequency band) of the log-ratio, mean-ratio and the fused image respectively. Then F_{ρ} represents the high frequency bands

(diagonal, horizontal and vertical coefficients). E^M and E^L represents the energy coefficients of the mean-ratio and log-ratio image.

Step 3: Perform inverse contourlet transform to get the fused image.

As mentioned above, here the low frequency and high frequency bands are fused individually. The low frequency bands accurately represents the changed regions from both the log and mean ratio image, average operation is done in the low frequency band. For the high frequency band the rule of minimum local energy of the contourlet coefficients is chosen. This is to combine the homogeneous regions of the high-frequency portion from the mean-ratio image and the log-ratio image.

3.3. Kernel K-Means Clustering

The purpose to process the difference image is to discriminate changed area from unchanged area. The difference image obtained by image fusion is sorted out into changed and unchanged area using kernel k-means clustering algorithm. In order to improve the accuracy of the binary change map, the data samples obtained by fusing the log-ratio and mean-ratio images are projected to a higher dimensional feature space, in which a linear algorithm can be applied to separate the changed and unchanged pixels.

Mapping to the feature space is done by using kernel functions. The kernel function compute the similarity between training samples S using pair-wise inner products between mapped samples, and thus, the so-called kernel matrix contains all the necessary information to perform classification by means of linear algorithms in the feature space. Kernel K-means clustering algorithm is applied on the data samples of the fused image in order to perform non-linear clustering.

The kernel techniques allows linear evaluation of data in higher dimensional feature space, which results in nonlinear clustering of data samples present in the input space [15]. The higher dimensional feature space is generated by a mapping function $\phi(.)$ applied on the image obtained by fusing the log-ratio and mean ratio image.

```
┌─────────────────────┐
│     Fused Image     │
└─────────────────────┘
           │
           ▼
┌─────────────────────┐
│   Feature mapping   │
│    using kernel     │
└─────────────────────┘
           │
           ▼
┌─────────────────────┐
│   Minimum angle     │
│   classification    │
└─────────────────────┘
           │
           ▼
┌─────────────────────┐
│ Generation of binary│
│     change map      │
└─────────────────────┘
```
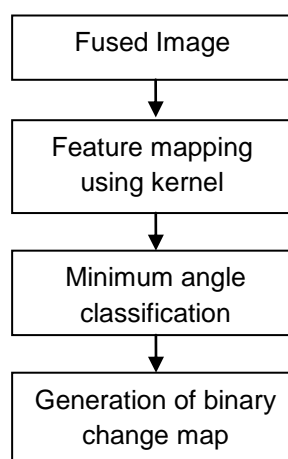
Figure 3: Flow Chart for the Generation of Change Map

The kernel technique is used instead of dot product; it returns the inner product of the fused image directly in higher dimensional feature space. The flow diagram given below depicts the steps involved in performing clustering on fused image (Figure 3).

The cost function used to perform kernel k-means clustering on fused data samples is given as,

$$\Theta^* = \arg\min\left\{\frac{\sum_p \frac{1}{|\Pi_p|} \sum_{i\in\Pi_p} \left(a^2\Phi(x)\right), \mu_p}{\sum_{p=q} a^2(\mu_p, \mu_q)}\right\} \tag{6}$$

The reduction of the angle between the samples and the centroid is represented as $a^2\phi(x)$.

The average samples allocated to the cluster p in the feature space is given by,

$$\mu_p = \frac{1}{|\Pi_p|} \sum_{j\in\Pi_p} \phi(x) \tag{7}$$

Where $\prod_p$ is the samples assigned to cluster p and $\left|\prod_p\right|$ is the total number of samples assigned to cluster p.

4. Results and Discussion

Here the efficacy of the proposed blending of the Contourlet transform based image fusion (Figure 4) and kernel K-means clustering (Figure 5) is established by comparing the accuracy of the binary change of the proposed method with the change map obtained from the log-ratio (Figure 4 & 5A) and mean–ratio images (Figure 4 & 5B). The fusion image of Contourlet transform (Figure 4C) and kernel K-means clustering (Figure 5C) are also shown in the figure. The testing is done to show the efficacy of the kernel K-means clustering. So, this clustering is performed on the three difference images and it is shown that the combination of fused image (Figure 5C) and kernel K-means clustering is capable of detecting the changes more efficiently.

4.1. Accuracy Assessment and Performance Evaluation

The quantitative analysis can be done using the ground truth reference and check rules. The general approach to obtain ground truth reference [18] is to perform field survey with the assistance of historical GIS data.

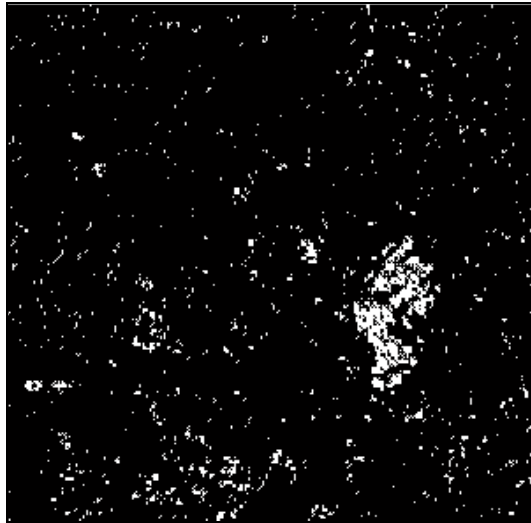*Table 1*: *Change Detection Results Obtained by Using Kernel K-Means Clustering on the Difference Images*

Difference Image	Accuracy
Mean-Ratio	89.999
Log-ratio	92.542
Fused Image	95.357
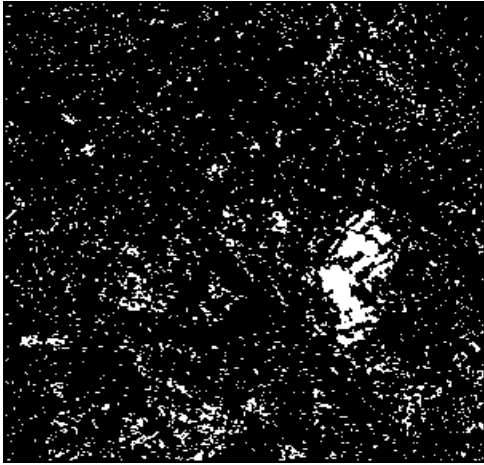
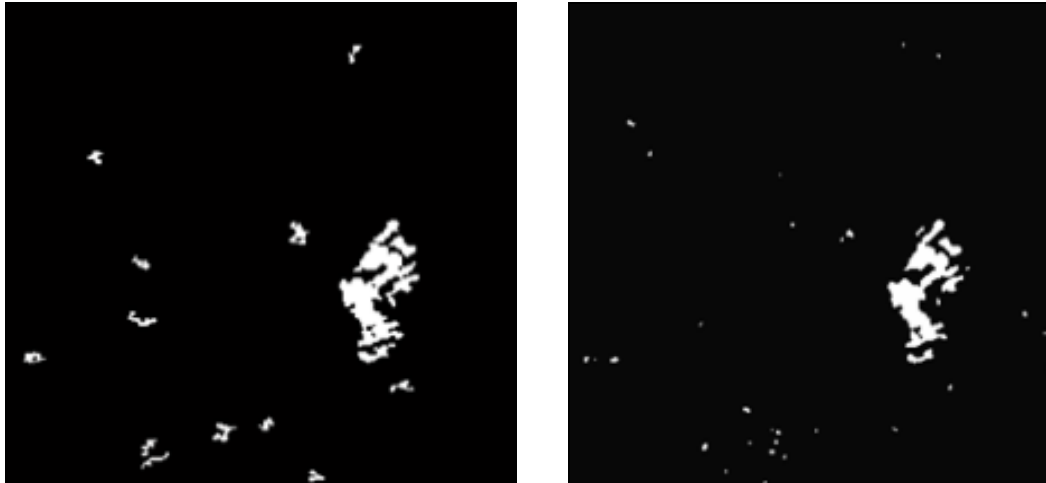**A. Log-Ratio Image**
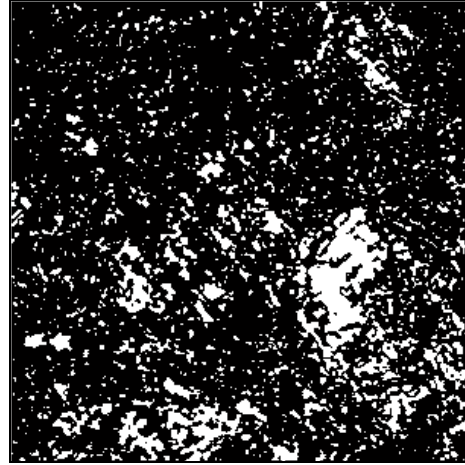
B. Mean-Ratio Image

C. Fused Image

Figure 4: Contourlet Transform Based Image Fusion

A. Log-Ratio Image

B. Mean-Ratio Image

C. Fused Image

Figure 5: *Change Detection Results Obtained by Using Kernel K-Means Clustering*

Since the input images are subjected to various noises during acquisition, it is necessary to evaluate the robustness of the change detection algorithm (Figure 6) to noise [16]. It can be done by plotting the values of PSNR and tau which can be determined as follows:

$$PSNR = 10\log_{10}\left(\frac{255}{\sum\limits_{i=1}^{M}\sum\limits_{j=1}^{N}\left(x(i,j)-\hat{x}(i,j)\right)^2}\right) \tag{8}$$

Where M and N are number of rows and number of columns of the input image, $x(i,j)$ is the input image in the absence of noise and $\hat{x}(i,j)$ is the noisy version of the input image.

$$\tau = 1 - \frac{\sum\limits_{i=1}^{M}\sum\limits_{j=1}^{N}\left|C_1(i,j) - C_2(i,j)\right|}{MN} \tag{9}$$

Where $C_1(i,j)$ the change map is generated from the input images in the absence of noise and $C_2(i,j)$ is change map generated by using the noisy version of the input images. The change detection results obtained by using kernel K-means clustering on the difference images are tabulated (Table 1).
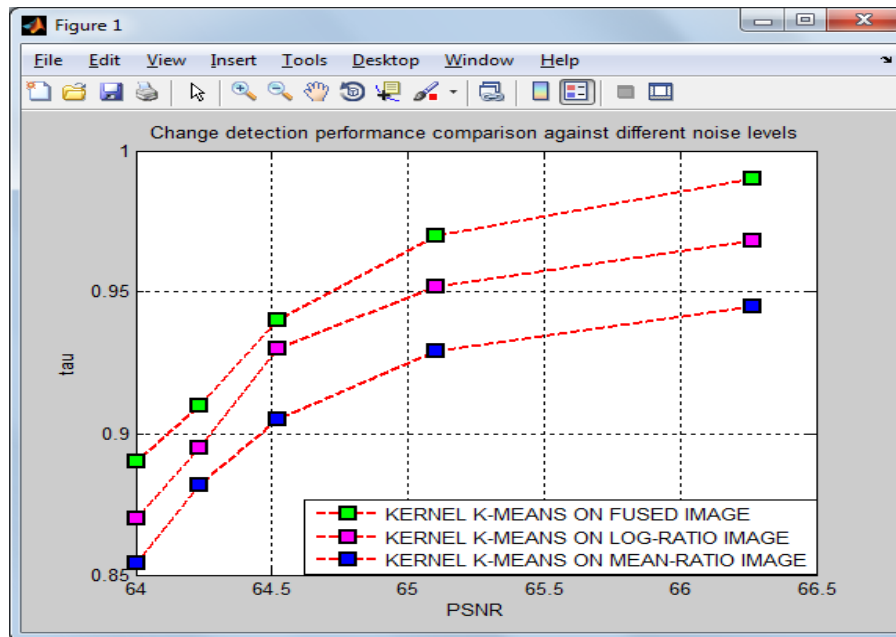

Figure 6: *Graph Showing the Robustness of Change Detection Algorithms*

5. Conclusion

An innovative method for unsupervised change detection in SAR images which is based on image fusion and kernel K- means clustering has been implemented in this paper. Here full advantage of the contourlet transform has been utilized to form the fusion rule and hence to get a difference image containing complementary information from the mean ratio and log ratio images. On the fused image kernel K-means clustering has been performed. Since kernel K-means clustering takes into consideration non-linearities. It is suited well for the clustering process in SAR images. Consequently this approach for change detection yields better results than its pre-existences.

References

[1] S.M., Metev, and V.P. Veiko., 1998: *Laser Assisted Micro Technology*. 2nd Ed. R.M. Osgood, Jr., Ed. Springer-Verlag, Berlin, Germany.

[2] L., Bruzzone, and D.F., Prieto. *Automatic Analysis of the Difference Image for Unsupervised Change Detection*. IEEE Trans. Geosci. Remote. Sens. 2000. 38 (3) 1171-1182.

[3] L., Bruzzone, and D.F., Prieto. *An Adaptive Semi Parametric and Context-Based Approach to Unsupervised Change Detection in Multitemporal Remote-Sensing Images*. IEEE Trans. Image Processing. 1996. 11 (4) 66-77.

[4] C., Dumontier, F., Luthon, and J.P., Charras. *Real-Time DSP Implementation for MRF-Based Video Motion Detection.* IEEE Trans. Image Process. 1999. 8 (10) 1341-1347.

[5] R., Collins, A., Lipton, and T., Kanade. *Introduction to Special Section on Video Surveillance.* IEEE Trans. Pattern Anal. Mach. Intell. 2000. 22 (8) 745-746.

[6] K., Grover, S., Quegan, and C. da Costa Freitas. *Quantitative Estimation of Tropical Forest Cover by SAR.* IEEE Trans. Geosci. Remote Sens. 1999. 37 (1) 479-490.

[7] L., Bruzzone, and S.B., Serpico. *An Iterative Technique for the Detection of Land-Cover Transitions in Multitemporal Remote- Sensing Images.* IEEE Trans. Geosci. Remote Sens. 1997. 35; 858-867.

[8] P.S., Chavez, Jr., and D.J., MacKinnon. *Automatic Detection of Vegetation Changes in the South Western United States Using Remotely Sensed Images.* Photogramm. Eng. Remote Sensing. 1994. 60 (5) 1285-1294.

[9] K.R., Merril, and L., Jiajun. *A Comparison of Four Algorithms for Change Detection in an Urban Environment.* Remote Sens. Environ. 1998. 63 (2) 95-100.

[10] T., Celik. *A Bayesian Approach to Unsupervised Multiscale Change Detection in Synthetic Aperture Radar Images.* Signal Process. 2010. 90 (5) 1471-1485.

[11] Y., Bazi, L., Bruzzone, and F., Melgani. *An Unsupervised Approach Based on the Generalized Gaussian Model to Automatic Change Detection Inmultitemporal SAR Images.* IEEE Trans. Geosci. Remote Sens. 2005. 43 (4) 874–887.

[12] M., Sezgin, and B., Sankur. *A Survey over Image Thresholding Techniques and Quantitative Performance Evaluation.* J. Electron. Image. 2004. 13 (1) 146-165.

[13] Vrabel, J. *Multispectral Imagery Band Sharpening Study.* Photogrammetric Engineering and Remote Sensing. 1969. 62; 1075-1083.

[14] M., Gong, Z., Zhou, and J. Ma. *Change Detection in SAR Images Based On Image Fusion and Improved Fuzzy Clustering.* IEEE Trans. Imag. Process. 2012. 21 (4) 2141-2151.

[15] Volpi, M., Tuia, D., Campo-Valls, G., and Kanevski. M. *Unsupervised Change Detection with kernels.* IEEE Trans. Geosci. Remote Sens. 2012. 9 (6) 1026-1030.

[16] G.H., Rosenfield, and A., Fitzpatrick-Lins. *A Coefficient of Agreement as a Measure of Thematic Classification Accuracy.* Photogramm. Eng. Remote Sens. 1986. 52 (2) 223-227.

[17] J., Inglada, and G., Mercier. *A New Statistical Similarity Measure for Change Detection in Multitemporal SAR Images and Its Extension to Multiscale Change Analysis.* IEEE Trans. Geosci. Remote Sens. 2007. 45 (5) 1432-1445.

[18] A., Singh. *Digital Change Detection Techniques Using Remotely Sensed Data.* Int. Journ. Remote Sens. 1989. 10 (6) 989-1003,

[19] F., Chatelain, J.Y. Tourneret, and J., Inglada. *Change Detection in Multisensory SAR Images Using Bivariate Gamma Distributions.* IEEE Trans. Image Process. 2008. 17 (3) 249-258.

Research Article   **Open Access**

Tracing the Changes in the Pattern of Urban Landscape of Dehradun over Last Two Decades using RS and GIS

Sadhana Jain[1], Sawitree Laphawan[2], and Pradeep K. Singh[3]

[1]Scientist, Urban and Regional Planning Department, Indian Institute of Remote Sensing, Dehradun,
 Uttarakhand, India
[2]Department of Public Works and Town & Country Planning, Ministry of Interior, Royal Thai Government,
 Thailand
[3]Department of Geography, ICSE School, Kanpur, Uttar Pradesh, India

Correspondence should be addressed to Sadhana Jain, sadhana@iirs.gov.in; jain_sadhana@yahoo.com

Abstract Impact of population explosion is clear on urban landscape of not only metropolitan cities but also on small and medium towns of India. Dehradun, the interim capital of Uttrakhand state, India also witnessed tremendous developments over last two decades. It alters the landscape pattern of the city. In this study, changes in the landscape pattern of Dehradun city and surroundings has been explored using Landsat TM image of 1986 and IRS-1C/1D LISS III image of 1998 and 2011. For this purpose, the calculation of the metrics i.e., percentage of landscape (PLAND), number of patch (NP), mean patch size (MPS) have been carried out with public domain software– *Fragstatsver 4.1*. The results of the study highlights the three fold increase in the built-up area with drastic decrease in river/ water body and open spaces during 1986-2011. The built-up growth was higher between 1986-1998 in comparison to 1998-2011. Also, availability of built-up area available per 1000 persons has increased from 8.5 ha in 1986 to 11.5 ha in 2011. It may be due to the people interest to invest in property as a safe means because of weak economic conditions.
Keywords *Land Use/Land Cover; Urban Landscape; Spatial Metric*

1. Introduction

Landscapes are geographic areas identified by interacting patches or ecosystems and human activities within them [1, 2]. Urban areas have highly fragmented and heterogeneous landscapes shaped by environmental processes and socio-economic drivers [3]. The urban centers are undergoing a constant landscape change due to the pressure of population. Changes in the urban landscape highlight the association of land use/ land cover structure and function. Composition of the urban landscape must be considered explicitly to facilitate the understanding of causes and mechanisms of these changes over the time. A delineation of the landscape into discrete patches serves as a basis for calculating metrics that describe landscape fragmentation, connectivity or

human influences [4, 5]. These simple quantitative indices can be used to objectively quantify the structure and pattern of an urban environment by computing them directly from thematic maps [6].

The combination of remote sensing and geographical information system provides opportunities in representing and understanding the changes in complex urban structure. Landscape metrics integrated with the conventional change detection techniques would help in monitoring land use changes [7, 8]. Adopted from landscape ecology, where they are termed landscape metrics [9, 10, 6], recent studies have employed spatial metrics in urban landscape. Analysis results of landscape indices between spatial patterns and processes can be used to inform planners or researchers about landscape functions, which sometimes are difficult or impossible to measure directly [11]. FRAGSTATS is a computer software program designed to compute a wide variety of landscape metrics for categorical map patterns [12].

Nesting on the foot hills of Himalaya, Dehradun city resides in eco-sensitive zone. It has undergone rapid economic development and urbanization over the past decades after becoming the interim capital of newly formed state Uttrakhand in the year 2000. The objectives of this study are twofold: first, quantifying spatial and temporal changes of landscape patterns in Dehradun and surroundings; secondly, anthropogenic influence on the availability of spaces. It may improve our understanding of the patterns of urbanization in the Dehradun and its vicinity as well as provide key information for decision making and management of natural resources. In this study, landscape pattern has been explored through PLAND, MPS and NP spatial metrics. These metrics provide a comprehensive view of landscape pattern including area, compactness/ size and number of patches.

2. Literature Review

The process of global urbanization is accelerating and has potentially large influences on landscape and ecosystem function in cities and surrounding areas [13, 14, 15, 16]. Landscape change associated with urbanization, particularly urban sprawl, has been significant during the last half century and is expected to continue through the next decades [17, 18]. The expansion of urban areas contributes significantly to regional and global environmental change [18, 19, 20, 21]. Quantitatively exploring the causes and effects of urban land-use and land-cover dynamics is important because spatial patterns can be used to assess environmental impacts of various urban planning, policy, and management schemes at landscape and regional levels [16].

Spatial metrics are quantitative measurements to describe spatial heterogeneity. The characterization of urban patterns through indices is not new, although different types of indices are created and used for different purposes [22, 23]. Hundreds of metrics are available on the basis of shape, complexity and interspersion etc. However, some authors have reported that very few of these metrics contain unique information and thus the calculation or reporting of all of them is redundant [9]. The most commonly used metrics for urban studies are class area [23, 24, 25], percentage of landscape [27, 24, 28]; edge density [27, 25, 29, 26], landscape shape index [30, 29], mean patch size [30, 25, 29, 28], number of patches [25, 26], and largest patch index [29, 31]. When applied to multi-scale or multi-temporal datasets, spatial metrics can be used to analyze and describe change in the degree of spatial heterogeneity [27].

3. Study Area

Study area, Dehradun city lies at latitude 30º19'N and longitude 78º20'E. It is one of the most picturesque valleys and one of the most important towns of Uttarakhand state of India. The most striking physical features of the valley is its natural physical features viz. the Himalayan range of mountains in the north, the Shiwalik mountain ranges on the south, river Ganga on the east and river Yamuna on the west. The city is located at an altitude of 696m above mean sea level.

Dehradun is the administrative centre and the interim capital of the newly formed state of Uttarakhand. Dehradun is situated at the Himalayan foot hills in the fertile Doon Valley. It is famous for agriculture products like Basmati rice as well as mango and litchi fruit trees. The valley is well known for its salubrious climate and natural beauty.

A cursory scan on the landscape of the Dehradun City shows that the physical growth of the city is governed by its topography. There has been growth and development of the city because of the establishment of many national institutes. Consequently the road network has been developed to match the growth in-spite of many constraints including terrain conditions. Presence of several places of interest in and around the city attracted tourists from rest of the country.

4. Data Used & Methodology

Data used for this study includes Landsat TM image of 17th April 1986 and IRS-1C/1D LISS III image of 28th October 1998 and 8th October 2011 to trace the changes in the urban landscape over the period of time.

Image-to-image registration has been performed to bring the entire image in the same geometry (projection- UTM and datum- WGS 84) with sub-pixel accuracy. After the registration, all three images were classified into five Land use/ Land Cover (LULC) categories including built-up, forest, green spaces, open spaces and river. The term *green spaces* in the city are used to mean the vegetation cover, which includes trees, shrubs, gardens etc. It excludes other hard paved *open spaces* including stadium, playground, vacant land, fallow/ barren land etc. The term *forest cover* intends to *protected forest* in the vicinity of the city. Vegetation has a different colour from other hard paved open spaces in the multi-spectral image and easier to extract using digital classification techniques.

In this study, supervised classification has been carried out along with the hybrid approach to improve the classification accuracy. Masking for manual editing has been performed on perennial/dry river and forest classes to segregate it from built-up and green spaces within the city respectively. These classified images were input for the further analysis in the *ArcGIS* and *Fragstat software*. The amount of green spaces have been quantified within the 7 buffer zone of 1 km from city center to find the pattern of changes in the green spaces due to influence of population. Also, landscape pattern has been explored through PLAND, MPS and NP spatial metrics.

5. Results and Discussion

5.1. Change in Land use/ Land cover

The pattern of urban growth in Dehradun is influence of the topography and socio-economic structure of people. Here, urban growth includes extension of residential, commercial services, industrial, transportation, communications activities resulting in the expansion of built-up area. Figure 1 shows the classified image of three time period for the study area. Table 1 shows the pattern of urban landscape and its changes during 1986-1998-2011. The built-up area in Dehradun and surroundings was 2837.60 ha, which was 12.83% of the study area in the year 1986. It increased to 4337.58 ha (19.61%) in 1998 and 8244.90 ha (37.27%) in 2011. In the last two decades, built-up area has increased more than three fold. Most of the developments have been taken place on open spaces, and it has shown maximum decrease (4367 ha) in last two decades i.e. 1986-2011. It is also supported by growth rate as built-up increased with a rate of 4.27%; open spaces decreased with a rate of -5.00%. The growth rate of built-up was higher during 1998-2011 in comparison to 1986-1998. Dehradun became the capital of newly formed state of Uttrakhand in the year 2000. This is a major reason for the high growth rate during 1998-2011 apart from the natural growth and rural-urban

migration. The extent of built-up has increased with the compactness in the city center. It is contributing significantly in the environmental condition deterioration as well as urban heat island.
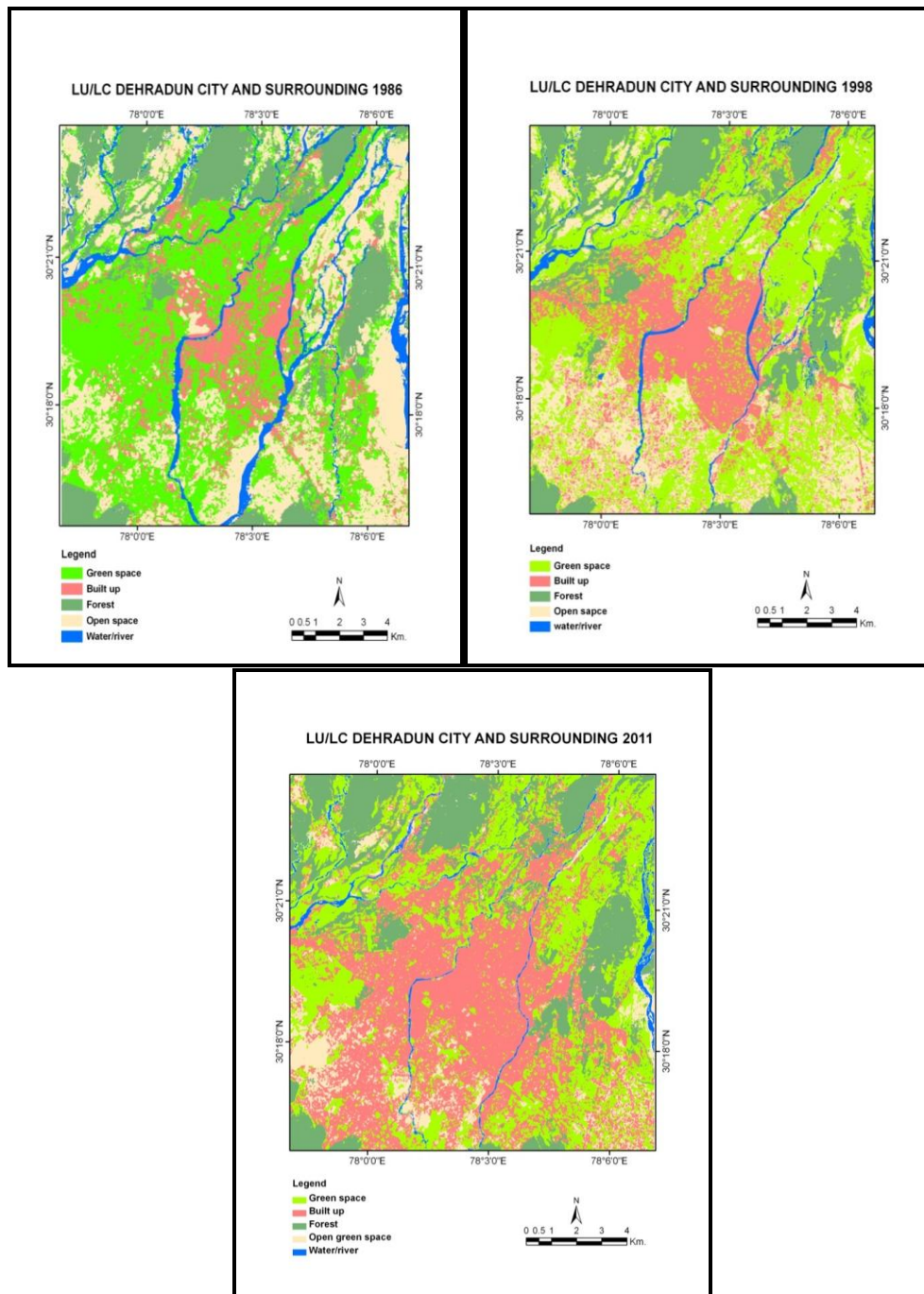

Figure 1: Classified Image of Dehradun and Its Environment for the Year 1986, 1998 and 2011

Figure 2 (a) compares the distribution of LULC categories in urban landscape during 1986, 1998 and 2011. The total area under green space in the year 1986, 1998 and 2011 was 8024.95 ha, 8491.98 ha, and 6883.97 ha respectively. Green space exhibits slight increase from 1986 to 1998 with the rate of 0.47%, whereas negative growth was observed during 1998 to 2011 with a rate of -1.61% (Figure 2 (b)). Overall, green spaces observed a decrease over last two decades. Area under forest cover increased slightly about 744.94 ha (3.37%) and 312 ha (1.41%) during 1986-1998 and 1998-2011 respectively.

Protected Forest towards north and south maintains the status of greenery in the vicinity of the Dehradun city.

Table 1: Statistics Showing the Pattern of Urban Landscape and Its Changes during 1986-1998-2011

Classification	Y1986		Y1998		Y2011		Y1986-1998		Y1998-2011		Y1986-2011	
/ Year	Area (ha.)	%	Area (ha.)	%	Area (ha.)	%	Changes	%	Change	%	Change	%
Built up	2837.6	12.83	4337.58	19.61	8244.9	37.27	1499.98	6.78	3907.32	17.66	5407.29	24.44
Forest	3578.93	16.18	4323.88	19.55	4635.89	20.96	744.94	3.37	312.01	1.41	1056.96	4.78
Green space	8024.95	36.28	8491.98	38.39	6883.97	31.12	467.03	2.11	-1608.01	-7.27	-1140.98	-5.16
Water/river	1558.62	7.05	925.13	4.18	602.68	2.72	-633.49	-2.86	-322.45	-1.46	-955.94	-4.32
Open space	6120.2	27.67	4041.74	18.27	1752.88	7.92	-2078.46	-9.4	-2288.86	-10.35	-4367.32	-19.74
Total	22120.31	100	22120.31	100	22120.31	100						
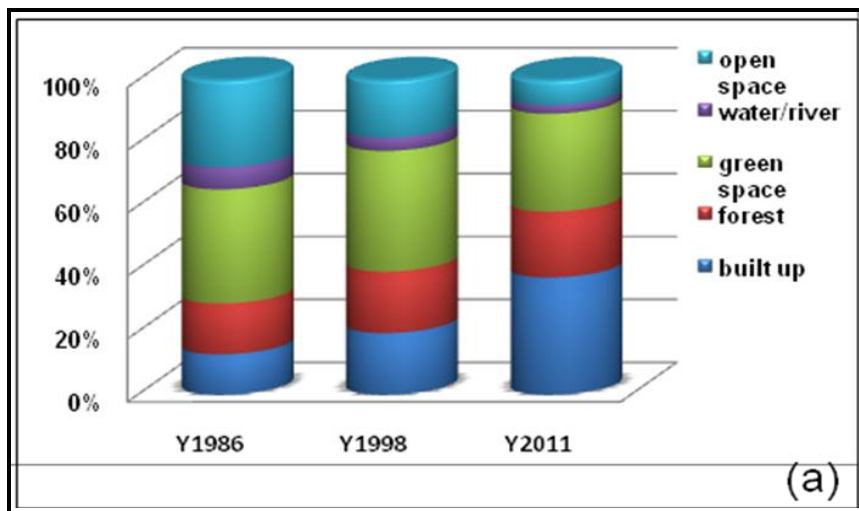
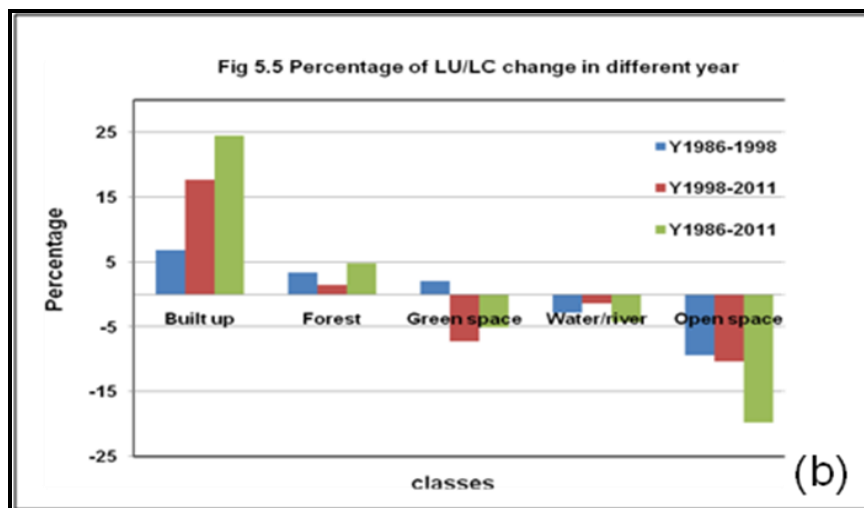*Figure 2 (a): Comparison of Land Use Pattern during 1986-1998-2011*

Figure 2 (b): Percentage of LU/LC Change in Different Year

The alarming changes have been observed in the river-bed during last two decades as the area under this category is reduced by 955.94 ha, which is about 4% of the study area. The major reason for this is encroachment on the river-bed. Most of the encroachment in the river bed is un-authorized developments with the low standard of living of the people due to a low level of income. It results in

the problems of destruction of natural landscape, inadequate open spaces, environmental degradation and lack of appropriate amenities. The rate of encroachments in river bed was higher during 1986-1998 in comparison to 1998-2011. It causes a decrease in the area under riverbeds with a rate of 2.86% during 1986-1998 and 1.46% during 1998-2011.

The major obstacle in improving the urban landscape is largely associated with the limitation of plan implementation due to lack of political will and effective administration. In developing countries, where the most rapid urban growth is occurring, urban policy structures are often weaker than those in the developed world because of a lack of expertise, holistic environmental assessments, and scientific support in the decision making process [16].

5.2. Green Spaces within Different Buffer Zones

Due to urban agglomeration, the view of the countryside from the town, a symbol of pre industrial dependence has disappeared and size of cities are increasing at faster rate. The proximity of green spaces has been studied through the seven buffer of 1 km around the city centre (clock tower) to check the quality of urban environment (Figure 3). The statistics derived from the same is given in Table 2 and Table 3. There is a drastic decrease in the percentage of green spaces within 1 km buffer zone, from 34.62% in 1986 to 7.78% in 1998 and 2.81% in 2011. Changes up-to 32% has been observed in the first four buffers during 1986-2011. It highlights compact development pattern up-to 4 km from city center.

Table 2: Concentration of Green Spaces within 7 Buffer Zones of 1 km from City Center

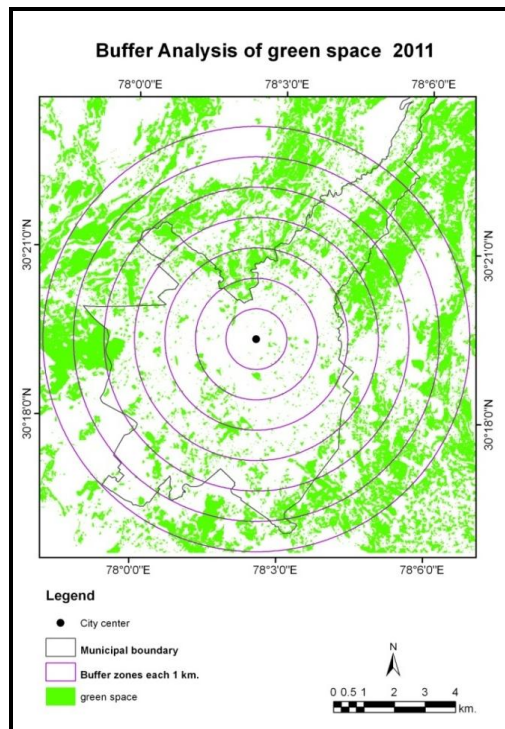|	1 km.		2 km.		3 km.		4 km.		5 km.		6 km.		7 km.	
	Area (ha)	%	Area (ha)	%	Area (ha)	%	Area (ha)	%	Area (ha)	%	Area (ha)	%	Area (ha)	%
Y1986	108.75	34.62	383.42	40.68	712.48	45.36	1113.77	50.65	1445.76	51.13	1361.61	39.4	1397.51	34.22
Y1998	24.44	7.78	164.33	17.44	443.62	28.24	851.88	38.74	1256.2	44.43	1542.46	44.64	1799.88	44.07
Y2011	8.89	2.81	84.23	8.94	264.25	16.82	447.07	20.33	910.85	32.22	1279.92	37.04	1594.46	39.04
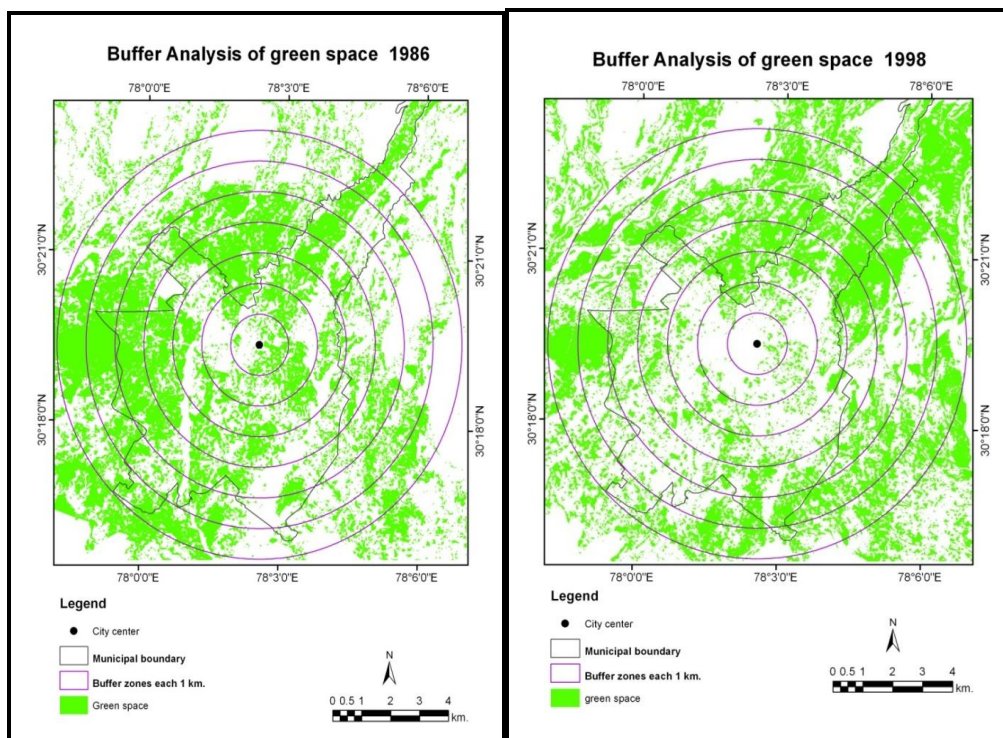
Figure 3: Distribution of Green Spaces within 7 Buffer Zones of 1 km from City Center for the Year 1986, 1998 and 2011

The area under the green spaces decreased in the buffer zones up to 5 km during the period 1986 to 1998 and 2011. But there is an increase in the amount of green spaces from 1361.61 ha to 1542.46 ha (buffer zone 5-6 km) and 1397.51 ha to 1799.88 ha (buffer zone 6-7 km) during the year 1986-1998. From 1998 to 2011, amount of green spaces decreased from 1542.46 ha to 1279.92 ha in the buffer zone 5-6 km and 1799.88 ha to 1594.46 ha in the buffer zone 6-7 km from city center. The percentage of green spaces increases with the distance from the city center. Concentration of green spaces, more or less, follows the pattern of municipal boundary. Most of the green spaces are concentrated just outside the municipal boundary.

Table 3: Changes in the Pattern of Green Spaces from City Center

Year	1km		2km		3km		4km		5km		6km		7km	
	Area (ha)	%	Area (ha)	%	Area (ha)	%	Area (ha)	%	Area (ha)	%	Area (ha)	%	Area (ha)	%
1986-1998	-84.31	-26.84	-219.09	-23.25	-268.86	-17.12	-261.89	-11.91	-189.57	-6.7	180.85	5.23	402.38	9.85
1998-2011	-15.55	-4.95	-80.1	-8.5	-179.36	-11.42	-404.81	-18.41	-345.35	-12.21	-262.54	-7.6	-205.42	-5.03
1986-2011	-99.86	-31.79	-299.19	-31.75	-448.22	-28.54	-666.7	-30.32	-534.91	-18.92	-81.69	-2.36	196.96	4.82

High changes in the city center exhibits the anthropogenic influence on the structure and availability of green spaces. It is due to the cutting of the roadside trees for road widening, construction activities to meet the demand of increasing population.

5.3. Population vs. Built Up and Green Spaces

As per the Census of India, population of Dehradun urban agglomeration was 293010 in 1981, 367411 in 1991, 560120 in 2001 and 714223 in 2011. This is used to calculate the population growth rate, and further for the projection of population for the year 1986 and 1998. Population of Dehradun city is projected to 332672 in 1986 and 530400 in 1998. While analyzing population growth, population grew at an average annual growth rate of 4.95 % during the period 1986-1998 and growth rate was relatively slow to 2.67 % in 1998-2011. Opposite of this, built up growth was less between 1986-1998 but very high between 1998-2011.

Table 4: Availability of Built-Up and Green Spaces per Thousand Persons

Year	Population	Built up Area (ha)	Density Persons/ ha	Built-up/1000 persons (ha)	Green Area	Density Persons/ha	Green Spaces/1000 Persons (ha)
1986	332672	2837.6	117	8.53	8024.95	41	24.12
1998	530400	4337.58	122	8.18	8491.98	62	16.01
2011	714223	8244.9	87	11.54	6883.97	104	9.64

Figure 4 depicts the relationship between population and built-up as well as green spaces. According to this, built-up area increased three fold from 2837 ha in 1986 to 8244.9 ha in 2011. Also, availability of land per 1000 persons increased from 8.53 ha (in 1986) to 11.54 ha (in 2011), as given in Table 4. Increase in land availability per thousand persons indicates towards the less concentration of population within the existing built-up area. This is also an indicator of new developmental activities in the city.
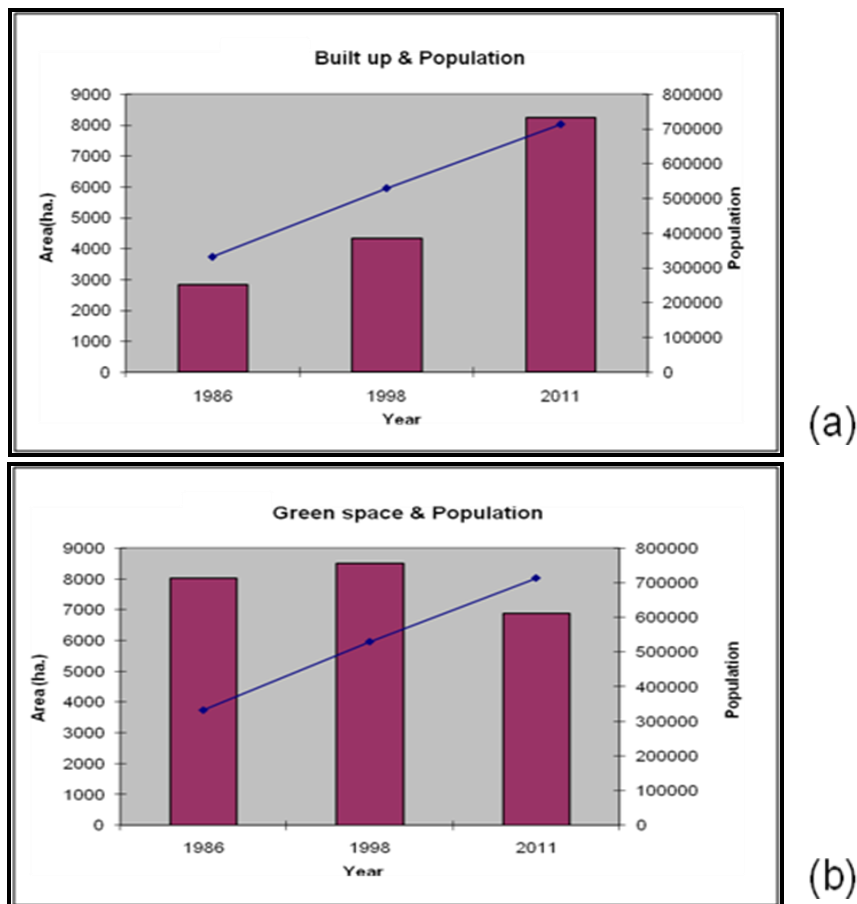

Figure 4: Comparison of Population Change with the (a) Built-Up (b) Green Spaces

This has a direct impact on the availability of the green spaces (Figure 2). The area under green spaces in 1986, 1998 and 2011 was 8024.95 ha, 8491.98 ha, and 6883.97 ha respectively. The amounts of green space available per 1000 persons were 24.12 ha in 1986, which get reduced to 16.01 ha in 1998 and further to 9.64 ha in 2011 respectively in the study area. Within the city, most of the green spaces are concentrated in the premises of government institutions.

5.4. Changes in the Pattern of Urban Landscape

Percentage of LU/LC change during 1986, 1998 and 2011 is given in Figure 2 (b). The pattern of urban landscape has also been explored through spatial metrics. The calculation of the metrics i.e., percentage of landscape (PLAND), number of patch (NP), mean patch size (MPS), has been carried out with public domain software– Fragstats version 4.1. Table 5 gives the value of landscape metrics derived for all five LULC categories. It reveals the pattern of urban landscape over the last two decades.

Table 5: Value of PLAND, NP and MPS Metrics for Different LULC Classes

	PLAND			NP			MPS		
	Y1986	Y1998	Y2011	Y1986	Y1998	Y2011	Y1986	Y1998	Y2011
Built up	13.32	19.57	36.93	2969	7468	2859	0.99	0.59	2.86
Forest	16.15	19.37	20.95	801	1850	1735	4.45	2.34	2.68
Green space	36.26	37.96	31.07	2458	4290	3145	3.25	1.98	2.19
Water/River	7.00	4.16	2.73	480	2510	731	3.22	0.37	0.83
Open Space	26.81	18.58	8.16	1645	4868	2993	3.59	0.85	0.60

The pattern of urban landscape depicts high degree of fragmentation in the year 1998. Whereas, compactness has been observed in the pattern of 1986 and 2011 built-up as well as green spaces. Decrease in the open spaces is also clear from PLAND and MPS value of the same. Though, PLAND of forest has increased from 1986 to 2011, the low MPS and high NP during the period indicates towards the fragmentation in the forest cover.

6. Conclusion

Remote sensing provides spatially consistent data sets that cover large areas with high spatial, spectral and temporal frequencies to detect, quantify and analyze temporal changes in urban landscape. Spatial metrics are useful for quantifying structure and pattern of urban landscape. It has been found that a combination of remote sensing and spatial metrics leads to an improved understanding and representation of urban dynamics and can help to develop alternative conceptions of urban spatial structure and change, thus supporting the modeling of change processes. The pattern of urban landscapes in Dehradun has been modified from the concentric zone pattern to a patchy urban form with multiple centers of specialized land uses. The development pattern of the city is governed by the topography as well as transportation network. Built-up area in Dehradun increased three fold during 1986-2011 with the increase in the availability of land per 1000 persons. This is due to the change in the status of Dehradun from institutional and tourist city (prior to 2001) to an administrative city (post 2001). This change has witnessed the conversion of fertile agriculture land into vacant open spaces and further its conversion into built-up area. Comparison of PLAND, NP and MPS metrics reveals the dispersed/fragmented development in 1998 with large NP and low MPS value. Built-up area has high value of PLAND and MPS in 2011, which indicates towards the urban agglomeration during last one decade. Thus, there is a need for landscape planning to minimize the impact of urbanization on environments well as to preserve fertile agriculture land.

Acknowledgment

References

[1] Turner, M.G., Gardner, R.H., and O'Neill, R.V. *Landscape Ecology in Theory and Practice*. 2001. Springer-Verlag, New York, USA.

[2] Paudel S., and Yuan F. *Assessing Landscape Changes and Dynamics Using Patch Analysis and GIS Modeling*. International Journal of Applied Earth Observation and Geoinformation. 2012. 16; 66-76.

[3] Buyantuyev A., and Wu J. *Urbanization Alters Spatiotemporal Patterns of Ecosystem Primary Production: A Case Study of the Phoenix Metropolitan Region*. USA Journal of Arid Environments 2009. 73; 512-520.

[4] Ivits E., Koch B., Blaschke T., Jochum M., and Adler P. *Landscape Structure Assessment with Image Grey Values and Object-Based Classificational Three Spatial Resolutions*. International Journal of Remote Sensing. 2005. 26; 2975-2993.

[5] Plexida S.G., Sfougaris A.I., Ispikoudis I.P., and Papanastasis V.P. *Selecting Landscape Metrics as Indicators of Spatial Heterogeneity-A Comparison among Greek Landsca*pes. International Journal of Applied Earth Observation and Geoinformation. 2014. 26; 26-35.

[6] Herold M., Goldstein N.C., and Clarke K.C. *The Spatio-Temporal form of Urban Growth: Measurement, Analysis and Modeling*. Remote Sensing of Environment. 2003. 86; 286-302.

[7] Rainis R. *Application of GIS and Landscape Metrics in Monitoring Urban Land Use Change*. In: Hashim, N.M., Rainis, R. (Eds.). Urban Ecosystem Studies in Malaysia: A Study of Change. 2003. 267-278.

[8] Ramachandra T.V., Bharath H. Aithal, and Durgappa D. Sanna. *Insights to Urban Dynamics through Landscape Spatial Pattern Analysis*. International Journal of Applied Earth Observation and Geoinformation, 2012. 18; 329-343.

[9] Gustafson E.J. *Quantifying Landscape Spatial Pattern: what is State of the Art*? Ecosystems. 1998. 1 (2) 143-156.

[10] O'Neill R.V., Krummel J.R., Gardner R.H., Sugihara G., Jackson B., Deangelis D.L., Milne B.T., Turner M.G., Zygmunt B., hristensen S.W., Dale V.H., and Graham R.L. *Indices of Landscape Pattern*. Landscape Ecology. 1988. 1; 153-162.

[11] Botequilha Leitáo, L. Miller, J. Ahern J., and McGarigal K., Measuring Landscapes- a Planner's Handbook. 2006. Island Press, Washington.

[12] Leitao A.B., and Ahern, J. *Applying Landscape Ecological Concepts and Metrics in Sustainable Landscape Planning*. Landscape and Urban Planning. 2002. 59 (2) 65-93.

[13] Riley S.P.D., Busteed G.T., Kats L.B., Vandergon T.L., Lee L.F.S., Dagit R.G., Kerby J.L., Fisher R.N., and Sauvajot R.M. *Effects of Urbanization on the Distribution and Abundance of Amphibians and Invasive Species in Southern California Streams*. Conservation Biology. 2005. 19 (6) 1894-1907.

[14] Xian G., Crane M., and Su J. *An Analysis of Urban Development and its Environmental Impact on the Tampa Bay Watershed*. Journal of Environmental Management. 2007. 85 (4) 965-976.

[15] Wu J. *Toward Landscape Ecology of Cities: Beyond Buildings, Trees, and Urban Forests, Ecology*. In: M.M. Carreiro, Y.C. Song, J. Wu (Eds.). Planning and Management of Urban Forests: International Perspectives, Springer. 2008. 10-28

[16] Li Y., Zhu X., Sun X., and Wang F. *Landscape Effects of Environmental Impact on Bay-Area Wetlands Under Rapid Urban Expansion and Development Policy: A Case Study of Lianyungang, China*. Landscape and Urban Planning. 2010. 94; 218-227.

[17] Alberti M., Booth D., Hill K., Coburn B., Avolio C., and Coe S. *The Impact of Urban Patterns on Aquatic Ecosystems: an Empirical Analysis in Puget Lowland Sub-Basins.* Landscape and Urban Planning. 2007. 80; 345-361.

[18] Su W., Gu C., Yang G., Shuang C., and Zhen F. *Measuring the Impact of Urban Sprawl on Natural Landscape Pattern of the Western Taihu Lake Watershed, China*. Landscape and Urban Planning. 2010. 95; 61-67.

[19] Mills G. *Cities as Agents of Global Change*. International Journal of Climate. 2007. 27; 1849-1857.

[20] Seto K.C., and Satterthwaite D. *Interactions between Urbanization and Global Environmental Change*. Current Opinion in Environmental Sustainability. 2010. 2; 127-128.

[21] Pandey B., Joshi P.K., and Seto Karen C. *Monitoring Urbanization Dynamics in India Using DMSP/OLS Night Time Lights and SPOT-VGT Data*. International Journal of Applied Earth Observation and Geoinformation. 2013. 23; 49-61.

[22] Clifton K., Ewing R., Knaap G., and Song Y. *Quantitative Analysis of Urban Form: A Multidisciplinary Review*. Journal of Urbanism: International Research on Placemaking and Urban Sustainability. 2008. 1; 17-45.

[23] Kaza Nikhil. *The Changing Landscape of the Continental United States*. Landscape and Urban Planning. 2013. 110; 74-86.

[24] Juan S., Hanping X., Chongyu L., and Kun X. *A Gradient Analysis Based on the Buffer Zones of Urban Landscape Pattern of the Constructed Area in Guigang City, Guangxi, China*. Acta EcologicaSinica. 2006. 26; 655-662.

[25] Seto K.C., and Fragkias M. *Quantifying Spatiotemporal Patterns of Urban Land-Use Change in Four Cities of China with Time Series Landscape Metrics*. Landscape Ecology. 2005. 20; 871-888.

[26] Taubenböck H., Wegmann M., Roth A., Mehl H., and Dech S. *Urbanization in India– Spatiotemporal Analysis Using Remote Sensing Data*. Computers, Environment and Urban Systems 2009. 33 (3) 179-188.

[27] Herold M., Couclelis H., and Clarke Keith C. *The Role of Spatial Metrics in the Analysis and Modeling of Urban Land Use Change*. Computers, Environment and Urban Systems. 2005. 29; 369-399.

[28] Corry R.C., and Nassauer J.I. *Limitation of Using Landscape Pattern Indices to evaluate the Ecological Consequences of Alternative Plans and Designs*. Landscape and Urban Planning. 2005. 72 (4) 265-280.

[29] Zhang L., Wu J., Zhen Y., and Shu J. *A GIS-Based Gradient Analysis of Urban Landscape Pattern of Shanghai Metropolitan Area, China*. Landscape and Urban Planning. 2004. 69; 1-16.

[30] Luck M., and Wu J. *A Gradient Analysis of Urban Landscape Pattern: A Case Study from the Phoenix Metropolitan Region, Arizona, USA*. Landscape Ecology. 2002. 17; 327-339.

[31] DiBari J.N. *Evaluation of Five Landscape-Level Metrics for Measuring the Effects of Urbanization on Landscape Structure: The Case of Tucson, Arizona, USA*. Landscape and Urban Planning. 2007. 79; 308-313.

Research Article   **Open Access**

Development of "Biomass-Infosys" Tool for Above Ground Biomass Estimation Using Geo-Informatics

Mintu Medhi[1] and R. Sivakumar[2]

[1]Department of Forestry, NERIST, North Eastern Regional Institute of Science and Technology, Nirjul, Papum Pare, Arunachal Pradesh, India
[2]Department of Civil Engineering, SRM University, SRM Nagar, Kattankulathur, Kancheepuram, Tamilnadu, India

Correspondence should be addressed to Mintu Medhi, medhimintu123@gmail.com; sivakumar.r@ktr.srmuniv.ac.in

Abstract The important processes interacting between biosphere and atmosphere like Carbon cycle, CO_2 storage capacity of an ecosystem etc. are much affected by the plant life and its biomass. But, while estimating the spatial extent of the biomass, the common method of ground estimation of biomass is found deficient. Traditionally biomass estimation involved harvesting of the trees which also contributes to the everlasting problem of forest depletion. In this context, the necessity for non-destructive method like satellite remote sensing data which can be obtained as frequently as required to provide information for determination of quantitative and qualitative changes in biomass in the accessible as well as inaccessible areas needs to be encouraged. The biomass estimation process from satellite data uses calculation of Tasseled Cap brightness index (BI), and wetness index (WI) method which involve long and tedious calculation. In this study an attempt has been taken to develop a tool "Biomass-Infosys" using C# (Microsoft Visual Studio 2008) in Arc Object programming which generalizes the Biomass estimation process from satellite remote sensing images. Using this tool Tasseled Cap brightness index (BI), and wetness index (WI) can be calculated with a single click and also Carbon content and Carbon dioxide content will be estimated. The tool has been tested with some example data and its efficiency has also been examined.

Keywords *Biomass; Brightness Index (BI); Wetness Index (WI); Land Sat TM; Arc Object*

1. Introduction

Broadly, biomass comprises of two categories, above-ground e.g. trees, shrubs, vines etc and below-ground like roots, the dead mass of litter associated with soil etc. Majority of the R & D activities related to biomass estimation consider above-ground biomass (AGB) only because of the complexity associated with data collection on below-ground life forms (Dengsheng, 2006). The name, AGB is mostly acquainted with biomass energy like fuel energy that can be extracted directly or indirectly

from bio- resources. The quantification of biomass is essential as principal inventory information to evaluate the productivity dynamics of vegetation (Esser, 1984). Conventional process of biomass estimation includes harvesting of vegetation which is a destructive method. But, with intensifying concern over forest conservation and protection the need for non-destructive method also arises (Kale *et al.*, 2002). Remotely sensed satellite data can be used effectively to estimate biomass in non-destructive way using image processing techniques. In this study, we used the formula given by Roy and Shirish (Roy and Shirish, 1996), which also require calculation of Wetness Index (WI) and Brightness Index (BI) following the formulae given by Crist. *et al* (Crist. *et al.*, 1986). This is manual method of image processing and is very tedious owing to the long and complex formulated calculations. The details formulae are mentioned in the methodology section below. But, without in dept knowledge in image processing, the steps of image processing are quite tough and time consuming.

The recent advancement in Geoinformtics technology plays a significant role in developing a customized solution for any kind of spatial and non spatial information or data. Arc Object desktop programming is a module in Arc GIS which enables to create and integrate a customized tool according to requirement of the user. In this study, we attempted to develop a tool named as "Biomass-Infosys" using the most recent programming language C# (Microsoft Visual Studio 2008) to calculate Biomass, Carbon content and Carbon Dioxide and eventually eliminate the tedious job of mathematical calculation of raster data. The "Biomass- Infosys" tool is based upon DLL (Dynamic Link Library) technology which is based on open structure technology. With open structured DLL technology it is possible to pass object from DLL to ArcMap. The developed DLL files are written using command line in a way to interact directly with ArcGIS (Nejatbakhsh, 2008) to work as customized tool. In this study we also attempted to verify the tool using example data. The example study area falls in Watershed codes BRML106 (Brahmaputra Lower 106).

The area contains parts of Kamrup district, Darrang district and East Khasi hills in Maghalaya. The extent of the study area is approximately 1500 sq km. The base map of the study area was prepared by digitizing all the features like boundary major river, road, railways and permanent features as shown in Figure 1. The watershed is drained by several rivers like Khunda Jan, Bar Nadi, Mora Nadi, Barpani Nadi, Bukat Nadi, Digaru river, Bardong Nadi, Brahmaputtra, SokhajaNadi, Kalhog river, Um Sen, Puthimari Nadi, Kurijani Nadi, Um Tashu, Um Tri, Um Bhanga, Um tru, Um pri etc.
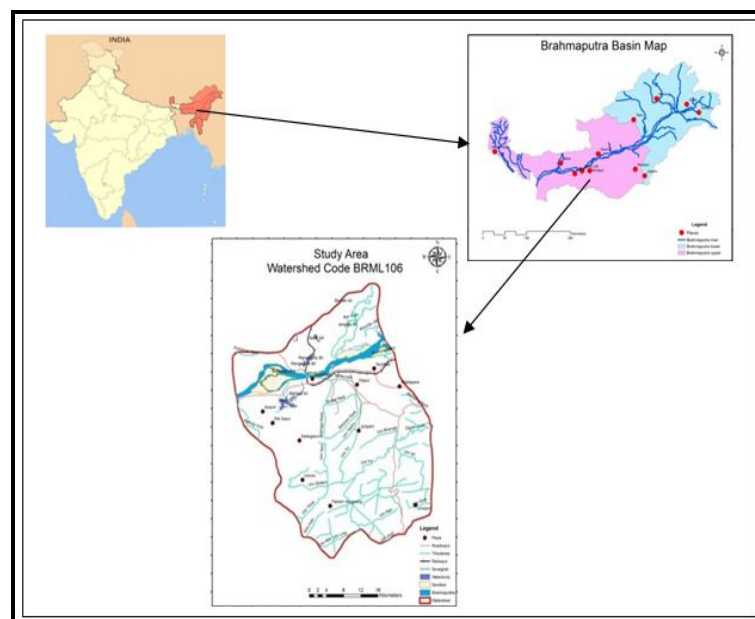

Figure 1: Base Map

2. Materials and Methods

2.1. Data Used

The top sheets, watershed atlas and published maps were the source for delineation of the watershed. LANDSAT TM Satellite image of 2010 was used.

2.2. Software

Arc GIS 9.3 was used for vectorization, thematic database generation and analysis. Microsoft Visual studio 2008 was used for Arc Object Desktop customization and development of "Biomass-Infosys". The codes were run on Arc GIS 9.3 platform for raster analysis.

2.3. Methodology

2.3.1. Formulae Used

The formula for calculating Wetness Index (WI) and Brightness Index (BI) includes:

$$BI = .2909 \times (TM1) + .2493(TM2) + .4806 \times (TM3) + .5568 \times (TM4) + 4438 \times (TM5) + .1706 \times (TM7) \qquad (1)$$

$$WI = .1446 \times (TM1) + .1761 \times (TM2) + .3222 \times (TM3) + .3393 \times (TM4) - .6210 \times (TM5) + .4186 \times (TM7) \qquad (2)$$

Where TM1, TM2, TM3, TM4, TM5, and TM7 are Blue band (Band1), Green band (Band2), Red band (Band3), NIR band (Band4), MIR band (Band5) and FIR band (Band7) respectively.

The expression for BI and WI was used from the published work by Crist. *et al.* (Crist. *et al.*, 1986).

Biomass was calculated using the following formula:

$$\text{Log}_{10}y = 3.7163 - .01078 \times BI + .007065 \times WI \qquad (3)$$

Where 'y' is biomass (kg) (Roy and Shirish, 1996).

Carbon content has been calculated using the following formula:

$$\text{Carbon content (C)} = \text{Biomass(y)} \times .5 \qquad (4)$$

Carbon Dioxide content has been calculated using the following formula:

$$\text{Carbon Dioxide equivalent (CO}_2) = \text{Carbon content (C)} \times 3.6667 \qquad (5)$$

Equation 5 and 6 are from Canada's model forest program (2000) (Canada's Model Forest Program, 2000).

2.3.2. Development of "Biomass-Infosys"

Biomass information system "Bio-Infosys" tool was developed from Arc Object programming(C#) which is shown in Figure 2.
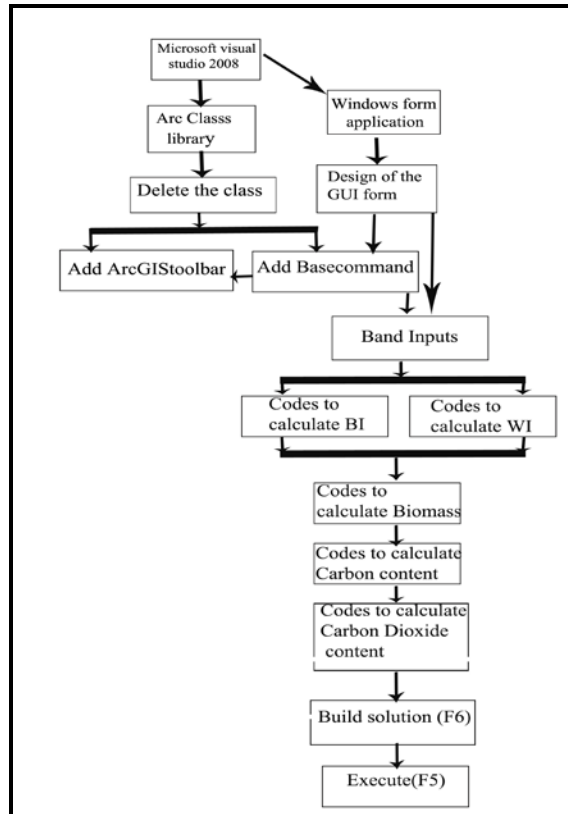
Figure 2: Flow Chart for "Biomass-Infosys" Tool Development

2.3.2.1. Connecting ArcGIS with Microsoft Visual Studio 2008

To customize ArcGIS 9.3 through Microsoft Visual Studio 2008 an extension of Arc GIS 9.3, Arc SDK.exe needs to be installed. It will enable to customize Arc GIS 9.3 under Microsoft Visual studio 2008.NET(C#) environment.
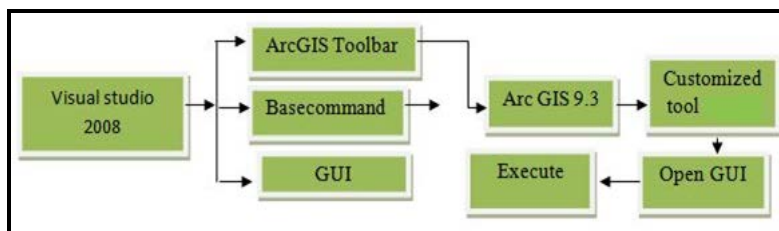

Figure 3: Flow Chart for "Biomass-Infosys" Customization

2.3.2.2. GUI & Base Command

GUI stands for Graphical User Interface is an interface that helps the user to understand the complex matter in a generalized form. The quality of the user interface (UI) has a great bearing on the utility of a GIS. Thus, the UI is one of the strong points of GIS. To increase the efficiency of GIS, the UI must provide a simple conceptual model of what is happening to the database (Collins *et al.,* 1983). The UI should not launch complex algorithms or data structure etc to the users. Instead, it should be effortless to understand, appear natural. In order to do that, UI should be programmed to appear as a user friendly arrangement for the users not as complex collection of algorithms (Driver and Liles, 1983).

The combination of graphical representations as well as non-programming users can be beneficial for both GIS software and application program designers. The algorithmic processing of the data can better be understood by the programmers interacting with the GUI representation of their data (Boecker *et al.*, 1986). Both the beginners and expert programmers can think about what a program executes as well as the procedure of execution through writing codes, testing and debugging. GUI representation of the algorithms applied to the data structures of great use. Data flow diagrams have been automated and animated using GUIs to demonstrate the internal execution of programs and are helpful for both designing tool and documentation mechanism. For this study purpose the GUI for "Biomass-Infosys" (Figure 4) is created with the option for the input of the required bands as well as the directory of the input bands are displayed in the text boxes nearby each band name. To execute the interface with ArcGIS toolbar appropriate codes are essential and that can be written in Arc GIS base command under over ridden class.

Tool "Biomass-Infosys" includes calculation of Brightness Index (BI) and Wetness Index (WI) and estimation of biomass which requires application of raster math. Finally Brightness Index, Wetness Index (WI) and Biomass are displayed in ArcGIS and are also saved in specified directory in .img format.

For "Biomass-Infosys" tool the references required are added through Arc class library. The basic reference required is ESRI.ArcGIS.GeoAnalyst, ESRIArcGIS.SpatialAnalyst, ESRI.ArcGIS.Carto, ESRI.ArcGIS.Geodatabase, ESRI.ArcGIS.Geo.Analyst, ESRI.ArcGIS.SpatialAnalyst, ESRI.ArcGIS. DataSourcesRaster, ESRI.ArcGIS.Carto, ESRI.ArcGIS.Geodatabase, ESRI.ArcGIS. DataSources Raster, ESRI.ArcGIS.ArcMapUI, System.Runtime.InteropServices, System.Windows.Forms.

As the next step ArcToolbar and Basecommand options are created. The Basecommand is called in the ArcToolbar option by calling the Program ID of Basecommand in ArcToolbar. The codes to execute "Biomass-Infosys" tool is written inside overriden class of Basecommand. The Arctoolbar is created to call the codes written to execute "Biomass-Infosys" tool through Basecommand. The "Biomass-Infosys" tool has been tested using example data as mentioned above.

4. Results and Discussion

    a. Creation and designing of GUI (Figure 4). The GUI is used to input the bands (Band 1 to Band 5). This is a user friendly interactive interface which will guide the users to select proper band and displays the directory of input bands and output indices.
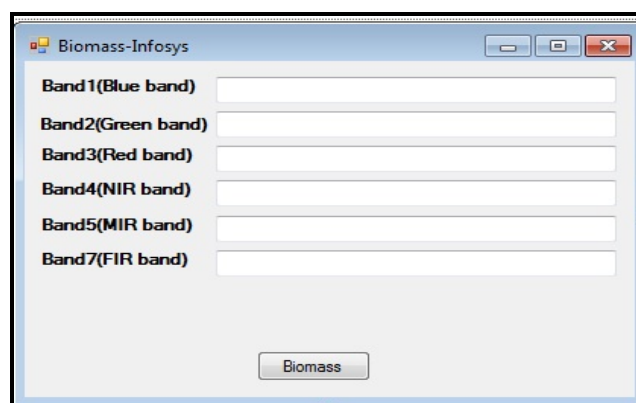

Figure 4: GUI Created for "Biomass-Infosys" Tool

    b. Writing code in Microsoft Visual Studio 2008 for display of the input bands, calculating, saving and displaying AVI, BI and SSI in ArcGIS and execution of ArcGIS using Microsoft Visual

Studio 2008 (Figure 5). On successful debugging, ArcMap.exe has been executed and ArcMap opens.
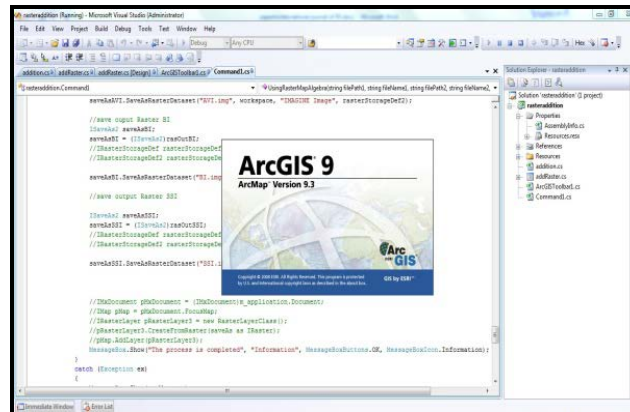

Figure 5: Execution of ArcGIS using Microsoft Visual Studio 2008

c. Adding the new tool "Biomass-Infosys" to ArcGIS 9.3 (Figure 6). The new tool "Biomass-Infosys" may not be directly visible. To display it in the ArcGIS toolbar, it needs to be enabled from View tab and then Toolbar option.
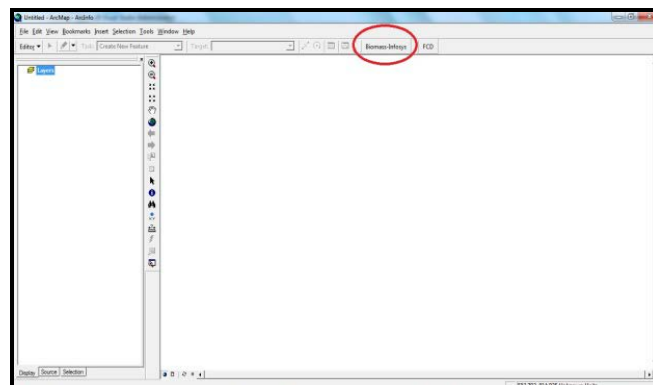

Figure 6: Adding the new Tool "Biomass-Infosys" to ArcGIS 9.3

d. Execution of GUI using ArcGIS (Figure 7). After displaying the "Biomass-Infosys" tool in toolbar, when it is clicked it executes and displays the GUI mentioned above.
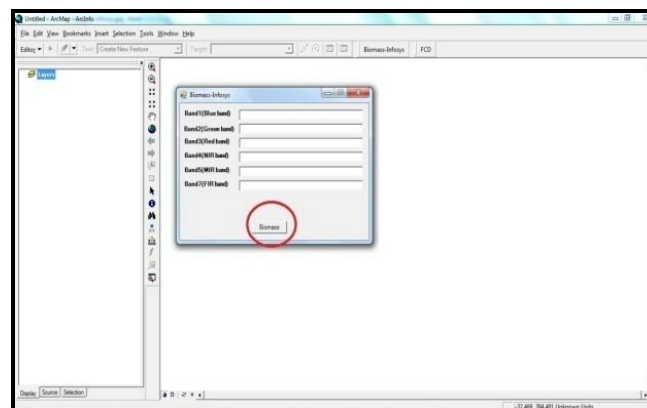
Figure 7: Execution of GUI "Biomass-Infosys" Using ArcGIS

e. Information box asking the user to input Band1 (Blue Band) (Figure 8). An information box will appear asking the user to give input for the Band 1.
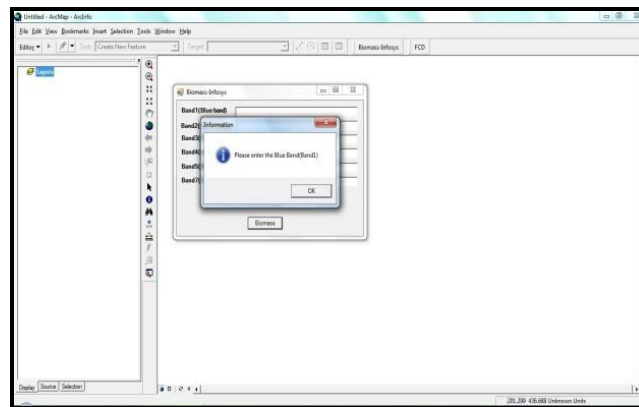
Figure 8: Information Box Asking User to Input Band1 (Blue Band)

f. Browsing window for Band1 (Blue Band) selection (Figure 9). On clicking the "ok" button browsing window will appear where the user can select required band and the directory of the input band appears in the textbox in the GUI adjacent to respective bands.
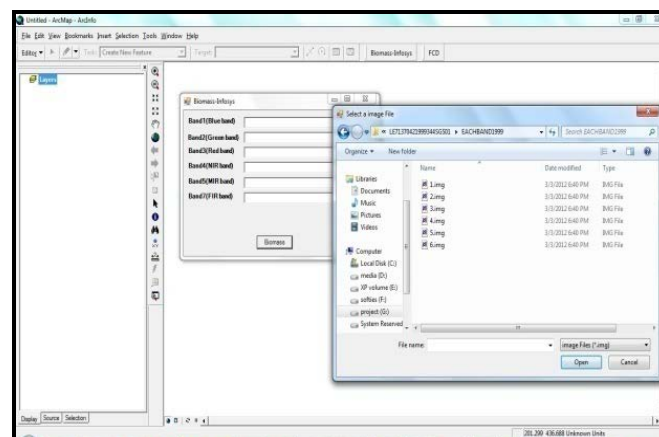

Figure 9: Browsing Window for Band1 (Blue Band) Selection

g. The directory of Band1 (Blue band) displayed in the text box.

h. The input for all the 6 bands are given as mentioned in step 7, 8 and 9.

i. When all the band inputs has been given, processing starts and WI, BI and biomass has been calculated and shown in TOC and displayed in ArcGIS (Figure 10).
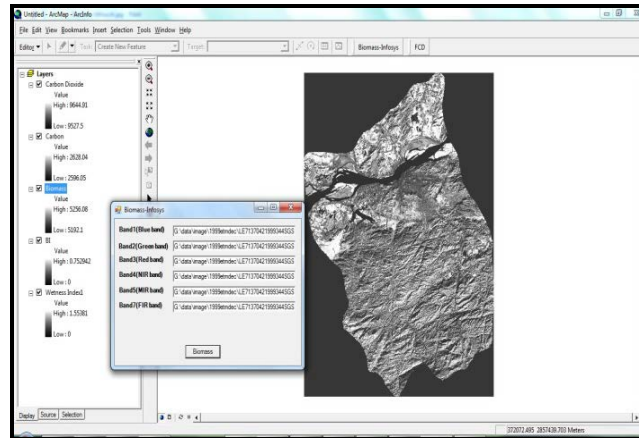
Figure 10: Displayed in ArcGIS

The developed tool "Biomass-Infosys" has been applied on example data which is a watershed boundary named as BRML106 (Brahmaputra Lower 106). The LANDSAT TM data for the year of 2010 has been collected from Earth Explorer (*earthexplorer.usgs.gov).* As a part of Pre-processing, each of the 7 bands has been subsetted using the boundary of the watershed (BRML 106). The subsetted 7 bands are processed using "Biomass-Infosys" tool.

WI and BI, Biomass, Carbon content and Carbon Dioxide have been calculated for the year of 2010 using "Biomass-Infosys" tool. The biomass estimation maps for the year of 2010 are shown in Figure 11.

The minimum and maximum quantity of Biomass observed for the year of 2010 is .33 t hac^{-1} and 271.44 t hac^{-1} respectively (Figure 11). It is estimated that in Guwahati region the amount of biomass is approximately 19 t hac^{-1} for the year of 2010.
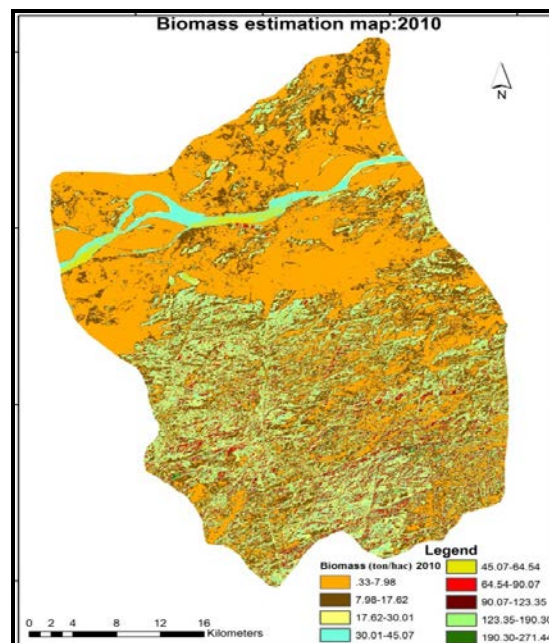

Figure 11: Biomass Estimation Map – 2010

It is estimated that in Guwahati region the amount of carbon content is approximately 8 t hac^{-1} for the year of 2010 (Figure 12). The carbon content of Pabam Nongrang region is observed as very low as it

is estimated at 24 t hac^{-1} for the year of 2010 and some patches towards south of Umdam is classified with moderate carbon content as the carbon content estimation is approximately 120 t hac^{-1}.
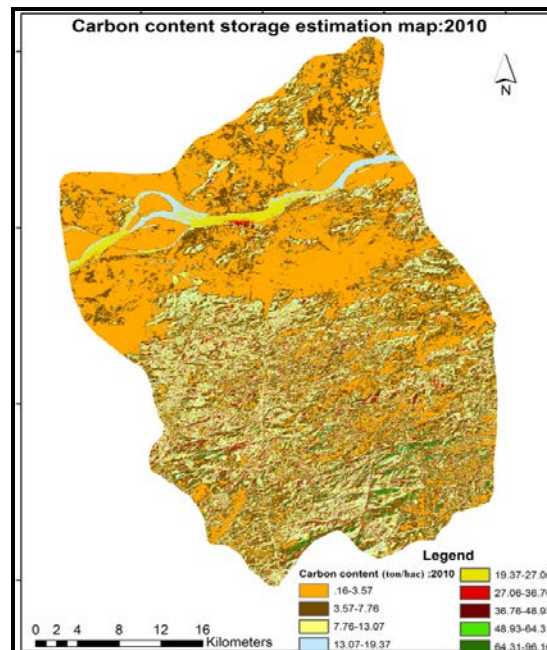

Figure 12: *Carbon Content Storage Estimation-2010*

Figure 13 shows the Carbon Dioxide storage estimation for the year of 2010.The minimum amount of Carbon Dioxide storage estimated as 0.60 t hac^{-1} and maximum amount of Carbon Dioxide storage as 498.09 t hac^{-1} for the year of 2010. It is observed that in Guwahati region the amount of Carbon Dioxide storage is approximately 32.7 t hac^{-1} for the year of 2010. The Carbon Dioxide storage of Pabam Nongrang region is observed as very low as it is estimated 40 t hac-1 for the year of 2010. The Carbon Dioxide storage is high towards the south of Umdam as the estimation is approximately 440.4 t hac^{-1}.
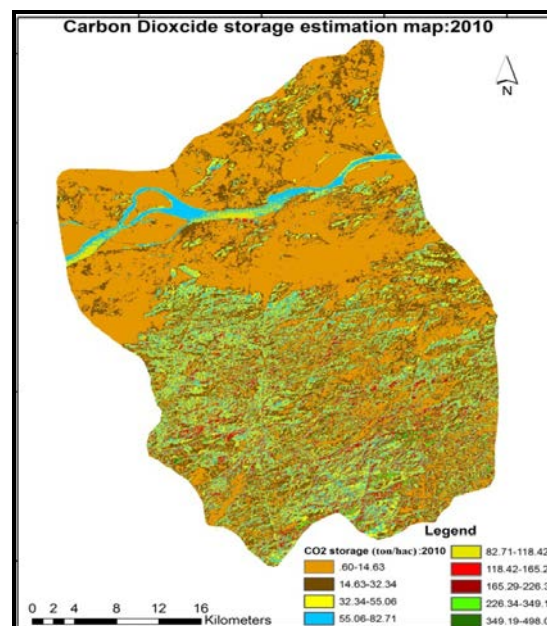

Figure 13: *Carbon Dioxide Storage Estimation- 2010*

5. Conclusion

From the biomass study the amount of stock of biomass is predicted. Comparatively area which is less disturbed is having high biomass. This study provides a tool named as "Biomass-Infosys" for eliminating the exhaustive manual procedure for biomass estimation. It is clearly understood that this tool can be effectively be used in biomass estimation with single click. The analysis part for calculation of Biomass, Carbon content and Carbon Dioxide was done effectively with "Biomass-Infosys" tool, whereas the reclassification and map layout part only was carried out with Arc GIS 9.3 predefined tools. A rough comparison was made between the time required to compute Biomass, Carbon content and Carbon Dioxide manually using models in ERDAS 9.2 and raster calculator in Arc GIS 9.3 and the time requirement to calculate the same using "Biomass-Infosys". The time required for ordinary process was approximately 4-5 hrs whereas the same is only 30 minutes to 1 hr only in case of "Biomass-Infosys". This gives an idea about the effectiveness of the tool. So, coding with Arc Object for generating customized tool for Arc GIS may be good solution for shortening the lengthy steps and same tool can be used repetitively to get output in the quickest possible way.

Limitation and Recommendation

Coding with Arc Object requires good bundle of knowledge on programming language which is not a primary objective of most of the Institutes offering GIS courses in India. As, a result the use of capabilities of Arc Object customization is still not popularized in India which needs to be addressed very soon.

References

Boecker H., Fisher G., and Nieper H., 1986: *The Enhancement of Understanding through Visual Representations.* Proceedings of the CHT86 Conference, Human Factors in Computing Systems, 44-50.

Boecker H., and Nieper H., 1985: *Making the Invisible Visible: Tools for Exploratory Programming,* Proceedings of the First Pan Pacific Computer Conference, the Australian Computer Society, Melbourne, Australia.

Canada's Model Forest Program, 2000: *Carbon Budget Accounting at the Forest Management Unit Level: An Overview of Issues and Methods.* Canadian Forest Service, Ottawa, 13.

Crist E.P., Laurin R., and Cicone R.C., 1986: *Vegetation and Soils Information Contained in Transformed Thematic Mapper Data.* In Proceedings of the 1986 International Geosciences and Remote Sensing Symposium, Zurich, 8-11 September (New York: Institute of Electrical and Electronics Engineers). 1986. 2; 1465-1470.

Collins S.H., Moon G.H., and Leham T.H. *Advances in Geographic Information Systems.* Steering Committee of the Canadian National Committee for the Sixth International Symposium on Automated Cartography. 1983. 1; 324-334.

Driver B., and Liles W., 1983: *A Communication Model for the Design of a Computer Assisted Cartographic System'.* Proceedings of the Fifth International Symposium of Cartography and Computing, American Congress on Surveying and Mapping, Falls Church, VA, 267-274.

Dengsheng L.U. *The Potential and Challenge of Remote Sensing Based Biomass Estimation.* International Journal of Remote Sensing. 2006. 27 (7) 1297-1328.

Esser G. The Significance of Biospheric Carbon Pools and Fluxes for the Atmospheric CO2: A Proposal Mode Structure in Progress in Biometeorology H Lieth, Swets and Zeithinger B V Lisse. 1984. 3; 253-294.

Kale M.P., Singh Sarnam, and Roy P.S. *Biomass and Productivity Estimation Using Aerospace Data and Geographic Information System.* International Society for Tropical Ecology, Tropical Ecology. 2002. 43 (1) 123-136.

Nejatbakhsh Nazereh, 2008: *Implementation of a Customized GIS-Based Tool for Tunnel Construction Sites Management (Tunnel Cs Tool)'.* The International Archives of the Photogrammetry, Remote Sensing and Spatial Information Sciences. Vol. XXXVII. Part B2. Beijing.

Roy P.S., and Shirish A. Ravan. *Biomass Estimation Using Satellite Remote Sensing Data- An Investigation on Possible Approaches for Natural Forest.* Journal of Bioscience. 1996. 21 (4) 535-561.

Research Article   **Open Access**

Integrated Land Use Planning of Aizawl District, Mizoram, India Using Geospatial Techniques

R.K. Lallianthanga and Hmingthanpuii

Mizoram Remote Sensing Application Centre, Science & Technology, Planning Department, Aizawl, Mizoram, India

Correspondence should be addressed to R.K. Lallianthanga, rklthanga@yahoo.com

Abstract This paper deals with the land use planning for improved land use system in Aizawl district, Mizoram wherein an integrated approach of land use planning had been derived using geospatial techniques. As geospatial planning has emerged as an effective and reliable platform to assist in this process of developmental planning even at the grassroots level, the present study incorporates remote sensing and GIS techniques to map land use, land cover, slope, and soil, and also to formulate viable land resource management plans for improved land use system which will be more sustainable and productive. Integration of the thematic layers in a GIS system helped in formulation of different suitable land use scenarios with economic and biophysical benefits. The study further reveals that the district has a very good potential for Agro-horticultural systems and Agri/horticultural plantations which could increase productivity of land use systems.

Keywords *Aizawl; Geospatial; GIS; Land Use Planning; Remote Sensing*

1. Introduction

Resources in the study area have constantly been under pressure to suffice the needs of increasing population. With a decadal growth of 24.07% in the population of the study area [1], the need for proper planning of land use and conservation of resources becomes a much concerned issue in the present scenario. Sustained utilization of available resources requires a scientifically approached land use planning process which incorporates integration of various data, analysis of these data, faster or precise information generation for participants in the land use planning approach. There is, thus, an urgent need for research and evolution of proper strategically plans and policies based on reliable and sound technologies to find new alternatives.

Several plans and policies have been formulated and implemented to eradicate shifting cultivation in the state by providing the practicing farmers alternative solutions and amenities. For example, Garden Colony, Jhum Control Project, Mizoram Intodelh Project (MIP) and New Land Use Policy (NLUP).

These policies had basic objectives for improving the rural economy and the socio-economic condition of rural population. A policy with a coherent approach for balancing productivity and conservation practices through constant monitoring and identification of problem areas [2] will go a long way in ensuring sustained utilization of natural resources. On a holistic view point, improved land use planning lies in recognizing the importance of various natural resources in sustaining the livelihood of the locals and considering its optimized utilization and strategic management according to its capability, as an essential input during the planning process.

Land resource inventory, prepared using topographical map and updated from the satellite imagery data on the same scale, is essentially qualitative as it reveals ground truth to the extent the scale of the map permits. Previous studies done to map the pattern of spatial distribution of various land use/land cover categories and area coverage in Serchhip rural development block highlighted the need for natural resource based planning for proper utilization and conservation of natural resources [3]. Similar studies based on satellite Remote Sensing techniques has also formulated strategic land and water resource development plans for Mat watershed, Aizawl district and has proven the effectiveness of IRS data for micro-level planning of rugged hilly terrain [4]. Geographic Information System (GIS), which has a strong capacity in data integration, analysis and visualization, has become an important tool to support land use planning approaches [5]. Advancement in this system has also helped in evolving improved techniques of geospatial planning. In the context of land use planning, geospatial techniques and models have been researched and developed for its effective use in sustainable development of land resources by integration of various GIS layers, which further demonstrates that geospatial techniques help in generation of a reliable spatial and non-spatial information database [6]. Geospatial modeling techniques used for locating various levels of biological richness has also been envisaged to be useful in land-use zonation and planning for sustainable use of natural resources [7].

Mapping of spatial patterns of land use, slope and other related natural landforms and features based on fine resolution Indian satellite data provides relevant, reliable and timely information as shown during the course of this study. Besides facilitating the creation of a comprehensive geo-database, spatial analysis in GIS has enabled the generation of an environmentally and economically sound land-water resource plan for implementation in the study area.

2. Materials and Method

2.1. Study Area

The study area - Aizawl district, is located in the northern part of Mizoram. It lies between 24°25'16.04" and 23°18'17.78"N latitudes and 92°37'03.27" and 93°11'45.69"E longitudes [7]. It is bounded by Champhai district and Manipur state in the east, in the west by Mamit district and Kolasib district, in the north by Assam state and in the south by Serchhip district (Figure 1). The geographical area of the study area is 3576 sq km, occupying 16.96% of land cover of Mizoram.
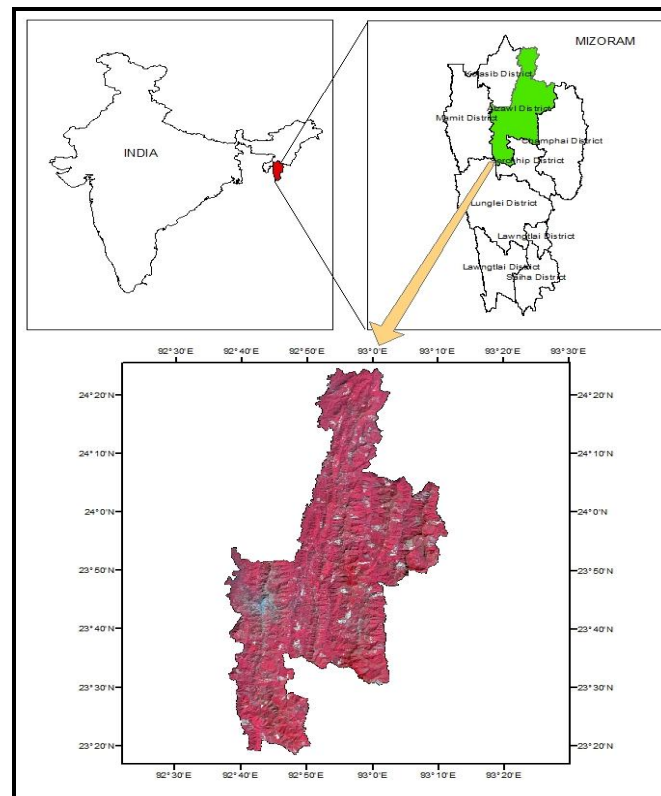
Figure 1: *Location Map of Study Area*

The study area experiences moderate humid tropical climate owing to its tropical location. It is observed that the average mean summer temperature is (April to June) 23.83°C and average mean winter temperature (November to February) is 19.05°C [8]. The area also receives heavy rainfall as it is under the direct influence of south-west monsoon. The average annual rainfall is 3155.3 mm [8].

According to the 2011 census, the total population of the study area is 404,054 [1]. Aizawl city, the capital of Mizoram is situated in the central part of Aizawl District. There are three notified towns namely Sairang, Darlawn and Saitual, and 98 villages. The forest cover type of Aizawl district is mainly tropical wet evergreen forest mixed with semi evergreen and tropical moist deciduous forests comprising mainly of bamboo. Aizawl district has good road networks. The whole length of the district is traversed by various road networks [7].

2.2. Data Used

IRS LISS III and Cartosat I (stereo pair ortho kit) satellite data were utilized to prepare base maps and to map the existing land use/ land cover of the study area. Ancillary data including past records/reports/maps collected from various sources like Department of Environment and Forest, Government of Mizoram, Department of Agriculture, Government of Mizoram and others were used for reference and collection of primary data. Survey of India Toposheets was also utilized for preparing and obtaining base maps and physiographic information.

2.3. Method

In the present study, a standard technique of remote sensing and geographic information system (GIS) was followed for mapping of the land use/ land cover features. Image processing and enhancements was carried out using Image Processing system (Erdas Imagine) and Geographic Information System (Arc Info) to increase the visual perceptibility of land use features.

Visual interpretation and on-screen digitization techniques were used for classifying and delineating the various land use/ land cover classes from the satellite data. The pattern of land use and extent of land cover was mapped focusing on the level at which features could be extracted at the given scale. Cartosat I data was utilized to derive and generate other ancillary information (eg. roads, drainage) and also effectively used for generation of slope maps. These maps and GIS layers are first prepared prior to generating land resources plans. They constitute important base layer information of existing natural resources which will later assist in preparation of proposed plans.

A geospatial plan for improved land use system was generated on the basis of various parameters of the present land use, slope percent and soil conditions in the study area. There are various criteria adopted for this purpose as given in Table 1 and the process of generating these proposed land use systems were done in a GIS environment. Most of the proposed land use systems require the integration and analysis of base layers like drainage, contour, soil, road, and slope layers, which become important pre-requisite data during the land use planning process.

Ground truthing forms the core activity of the study. Pre-field interpretations and plans prepared in map forms were, therefore, subjected to evaluation on-site. Various field information necessary for assessing and validating the accuracy of the maps prepared were collected during ground truth surveys. Participation of local village representatives in the plan preparation was also solicited during the field visits. Data from these surveys were then incorporated during the final stages of map corrections, accuracy assessment and plan preparation at operational village level.

Table 1: Guidelines for Generation of Proposed Land Use Systems

S. No.	Present Land Use	Slope	Soil	Proposed Land Use
1	Single cropped agricultural land, current jhum, abandoned jhum	0 – 25%	Fine Loamy Fluventic Dystrochrepts and Fine Loamy Fluvaquentic Dystrochrepts, very deep, good moisture.	Wet Rice Cultivation (WRC)/ Pisciculture
2	Single cropped agricultural land, current jhum, abandoned jhum	25 – 35%	Fine Loamy Fluventic Dystrochrepts and Fine Loamy Fluvaquentic Dystrochrepts, deep, good moisture.	Terrace cultivation
3	Current jhum, abandoned jhum	35 – 50%	Fine Loamy Typic Dystrochrepts. Loamy Skeletal Umbric Dystrochrepts and clayey, Typic Haplohumults, very deep, good moisture.	Agro-Horticulture
4	Existing plantation. Bamboo, current jhum & abandoned jhum adjacent to road communication.	25 – 50%	Fine Loamy Typic Dystrochrepts. Loamy Skeletal Typic Hapludults and clayey, Typic Haplohumults, very deep, good moisture.	Agri/Horti plantations
5	Scrub lands, hill top/crest	25 – 50%	Loamy Skeletal Typic Dystrochrepts, deep, moderate moisture	Silvi-pasture
6	Current jhum, abandoned jhum, open forest	More than 50%	Loamy Skeletal Typic Dystrochrepts and Loamy Skeletal Typic Hapludults, deep,	Afforestation

				moderate moisture
7	Forest (dense & open) and bamboo	-	-	To be conserved as forest and bamboo reserves

3. Results and Discussion

3.1. Land use/ Land cover

The major land use/ land cover classes in the study area were broadly classified into built-up land, agricultural land/horticultural land, forests (dense and open), bamboo forest, forest plantation, jhum land (current and abandoned jhum/shifting cultivation), scrubland and water body. The land use/ land cover statistics is given in Table 2 and corresponding map is shown in Figure 2.

Table 2: Land Use/ Land Cover Statistics of Aizawl District

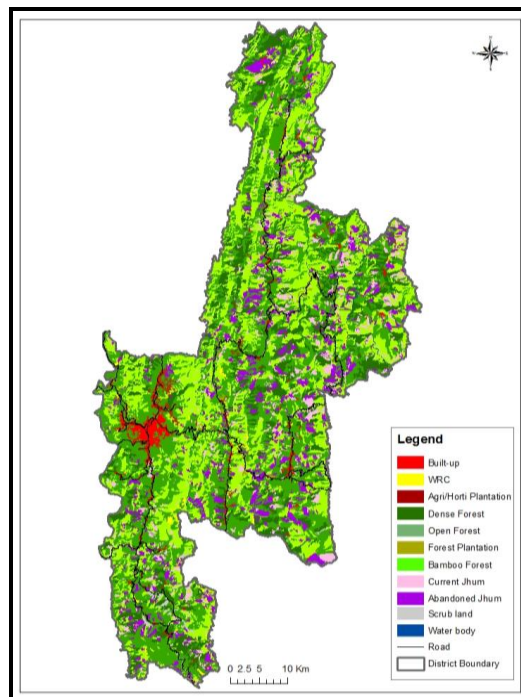| Land Use/ Land Cover Categories	Sq.km	%
Built-up	66.77	1.87
WRC	16.53	0.46
Agri/Horti Plantations	24.32	0.68
Dense Forest	482.18	13.48
Open Forest	1320.15	36.92
Forest Plantation	19.45	0.54
Bamboo	1134.45	31.72
Scrubland	12.77	0.36
Water Body	18.66	0.52
Current Jhum	177.55	4.96
Abandoned Jhum	303.16	8.48
Total	**3576.00**	**100.00**

Figure 2: Land use/ Land cover Map of Aizawl District

3.2. Soil

The soils found in the study area were mostly of red and yellow loamy. They were also acidic in nature due to heavy rainfall [7]. They contained high amount of organic carbon and were high in available nitrogen, low in phosphorus and potassium content. On the basis of rainfall and humidity, the soil moisture regime was classified as Udic. The soils found at order level were - Entisols, Inceptisols and Ultisols [10]. The classification of soil in the study area upto Family level was referred to as per previous project work done by MIRSAC.

3.3. Slope

The study area is uniquely characterized by several prominent hill ridges running parallel to each other, most of which roughly runs from north to south, except the southernmost hill ridges, where the hill ridges run in north-west to south-east direction. It may be roughly stated that the eastern part of the study area (Figure 3) is comparatively higher in elevation than the rest of the study area, while the northern part is uniformly characterized by lower elevation.
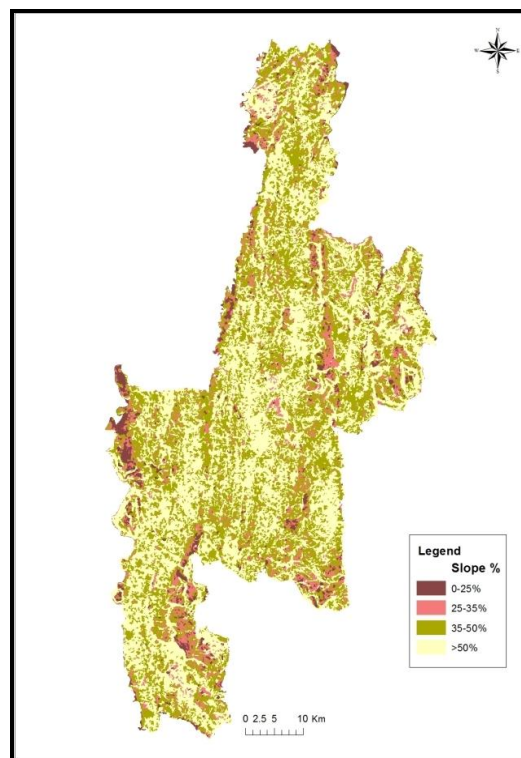

Figure 3: Slope Map of Aizawl District

3.4. Integrated Land Use Plan

The land use planning for development of land resources in the study area was prepared keeping in mind the objectives of making best use of available land for socio-economic improvement and to facilitate dependence of farmers on permanent farming system. Various sustainable land use practices (as discussed below) were modeled using the layers generated in GIS environment and considerations were also given to the socio-feasibility and implementation by incorporating data from ground surveys. The area statistics is given in Table 3 and the map showing areas for various proposed land development activities are shown in Figure 4.
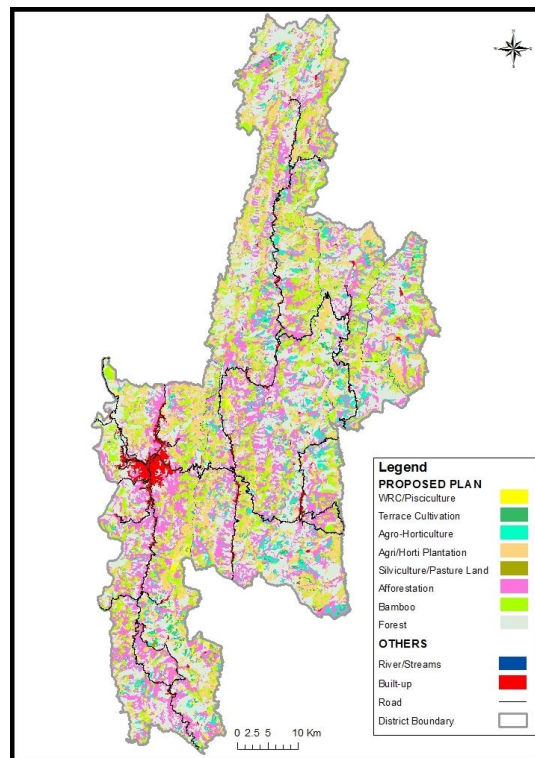
Figure 4: *Land Use Plan Map for Aizawl District*

3.4.1. Wet Rice Cultivation/ Pisciculture

The wet rice cultivation areas are usually located at the banks of rivers and streams. A small patch of the wet rice cultivation is found to scattered at the central and southern part of the district. From the studies and field verifications, it is found that most of the wet rice cultivation areas are found at the banks of R.Tuivawl, R.Tuirini and R.Tuivai, which eventually irrigates the paddy fields either directly or through its tributaries, and small patches are found near R.Tuirial, R.Chite, R.Changte, R.Lik, R.Lao and R.Mat. In addition to paddy cultivation, these areas can be further brought under cultivation of other crops along with practice of Pisciculture. Such a system refers to a form of farming called agro-aquaculture system. The main components of the system are composite fish culture with paddy or vegetables. Terrace farming is also possible in such category of sloping lands. The area proposed for this land use system is 29.65 sq.km, which is 0.83% of the total study area. *Oryza sativa* (rice) is recommended as the main crop during the kharif season. The Rabi crops recommended are legumes and vegetables.

3.4.2. Terrace Farming

Terrace farming occupies an important proposed form of farming in the study area, which not only ensures soil and water conservation but also suits the cropping needs of the farmers on sloping lands. Good irrigation facilities are the basic needs prior to lying out of a terrace farm. Paddy cultivation can be also carried out in the terraces. Other crops and vegetables can be cultivated in rotation. These areas are also suitable for double cropping. The analysis has shown that terrace farming can be carried out in several places within the study area. The proposed area for this form of farming occupies 41.82 sq. km or 1.17% of the total study area.

3.4.3. Agro-Horticultural System

In this farming system, both fruit bearing trees and field crops can be grown together in many variations. Perennial crops, seasonal crops and nitrogen fixing plants may be grown in an alternate manner. Crop rotation will be necessary in case of seasonal crops. The recommended crops for this system include Citron (*Citrus medica*), Valencia Orange (*Citrus sinensiis*), Banana (*Musa paradisiacal*), Orange (*Citrus reticulate*), Passion fruit (*Passiflora spp*), Pineapple (*Ananas comosus*), Red oil palm (*Elaies guinensis*), Jatropha (*Jatropha curcas)* etc. with vegetables and other root crops. The proposed area for this system is 182.24 sq.km which is 5.10% of the total study area.

3.4.4. Agricultural/Horticultural Plantation

The study area has several sites suitable for agriculture/horticulture plantations. However, the existing land use and slope factor determine the selection of suitable places for these plantations. Some plantations have to be confined to specific locations keeping in mind the socio-economic value of such plantations. Some of the species identified as suitable crops for plantation under this system includes Tea (*Camellia sinensis*), Coffee (C*offea spp*), Sugarcane (*Saccharus officinarum*), Broomgrass (*Thysanolaena maxima*), Ginger (*Zingiber officinale*), Turmeric (*Curcuma domestica*), etc. The area planned for taking up these plantations covers 597.55 sqkm or 16.71% of the total study area.

3.4.5. Silvi-Pastoral System

This proposed system refers to cultivation of fodder crops along with trees and occupies the largest portion for proposed land development in the study area. The inclusion of tree component in the system can also suggest an initiation towards conservation of forest resources. Besides providing fuel and fodder, the system helps in maintaining a good vegetative cover. Degraded forest areas in the study area have potential for cultivation of grasses and trees and such sites have been selected for this system. Species having fodder, firewood and fruit bearing values as well as adaptable to the sites may be selected. Generally, the tree species such as *Ficus hirta*, *Litsea semicarpifolia*, *Ficus spp., Mangifera indica, Leucaena leucocephala,* etc. are recommended for plantation and the grass species such as *Stylosanthes spp., Pennisetum pedicellatum, Thysonalaena maxima, Erianthus longisetosus,* etc. are recommended for cultivation in this system. Other agroforestry systems such as Horti-olericultural systems, Agri-silvicultural systems, Agri-horti-pastural systems, Horti-sericultural system, home gardens, etc. can also be practiced depending upon the terrain and the local needs. The area proposed for this system of land use is 11.07 sq.km which covers 0.31% of the total study area.

3.4.6. Afforestation

The pressure on land for food production has resulted in deforestation which continues to prevail due to practice of shifting cultivation. Therefore, there is need for taking up afforestation programmes in such affected sites. Various afforestation programmes in which commercial tree species are planted as Government or private plantations like Teak (*Tectona grandis)*, Michelia (*Michelia* champaca), Pine *(Pinus kesiya)* plantations have been taken up. The wastelands can also be reclaimed through reforestation programmes. The recommended species for this system are – *Michelia oblonga, Quercus serrata, Acacia auriculiformis, Albizzia odoratissima, Albizzia chinensis, Gmelina arborea,* etc and other native tree species found in the area may also be planted under such programmes. The area proposed for afforestation is 871.76 sq km of land or 24.38% of the total study area.

3.4.7. Forest

Forests of the study area comprise dense and open forests, as well as other reserve forests and forest plantations (Govt. owned and private). Most of the open forests are also successive secondary successions of fallow lands (7 years and above), once used for shifting cultivation, but have remained unused for a long period of time [11]. It is proposed that the existing forest cover and the supply/community reserves be preserved, and additional conservation techniques may be adopted to prevent encroachment and exploitation of forests for unsolicited commercial purposes. Declaration and demarcation of forest areas as Reserve Forests/Supply Reserve forests in areas where their conservation is needed can help in preservation of the adjoining natural forests. Voluntary organizations/NGOs may be encouraged and entrusted the task of further protection of these forests as well as extension of the forests in the form of parks, etc. The steps taken by the Government through Village councils, Village Forest Development Agency and various management schemes is noteworthy and can be made more effective for this purpose. The proposed area under tree forest is estimated to be 1197.33 sq km, constituting 33.48 % of the total study area.

3.4.8. Bamboo Forest

Bamboo forests are more confined to lower altitudes and are generally found between 80-1400 m MSL [12]. The study area also has bamboo growing stock within this altitudinal range. The genetic stock of these bamboos needs to be conserved and propagated to continue the existence of the bamboo forests. Projects under the state and central government can assist in ensuring the conservation and rehabilitation of stocks. Initiative taken up by the village communities in the form of bamboo reserves can be encourage by providing proper incentives. The present bamboo growing stock in the study area needs conservation as it is also affected by shifting cultivation. The bamboo flowering phenomenon in 2007 also had a drastic effect on the bamboo cover of the study area. To recoup the bamboo forest, besides the existing reserves, an estimated proposed area of 559.09 sq km or 15.63% of the total study area has been demarcated.

Table 3: Proposed Land Development Plan for the Aizawl District

S. No.	Proposed Land Development Plan	Sq.Km	%
1	WRC/Pisciculture	29.65	0.83
2	Terrace Cultivation	41.82	1.17
3	Agro-Horticultural system	182.24	5.10
4	Agri/Horti plantations	597.55	16.71
5	Silvi-pastoral system	11.07	0.31
6	Afforestation	871.76	24.38
7	Forest	1197.33	33.48
8	Bamboo forest	559.09	15.63
Non-Planned Area			
9	Water body	18.71	0.52
10	Built-up	66.77	1.87
	Total	**3576.00**	**100**

4. Conclusion

The study area, i.e., Aizawl district shows diverse forms of land uses with fragmented structures of natural land cover. A considerable percentage (4.96%) of land is still used for shifting cultivation, which forms the main farming system adopted for crop production. Land use planning in shifting cultivation areas is a challenging task, as it is deeply rooted in the cultural life of the farmers. Hence, an integrated planning approach which considers both socio-economic conditions and scientifically proven technologies of remote sensing and GIS is required. The present study has adopted such

approach in order to find an alternative to shifting cultivation and identifying appropriate land use systems that are practically feasible and acceptable by the farmers. Efforts under Government schemes to bring land under sustained utilization has shown progress, yet there is still potential for increased crop productivity under Agriculture/Horticulture plantation and Agricultural/Horticultural farming systems. These system of land use, as proposed in the present study, could not only increase land productivity but also focuses on conservation of natural resources and maintaining ecological balance in the study area.

References

[1] Directorate of Census Operations, 2011: *Census of India 2011: Provisional Population Totals Paper 2, Volume 1 of 2011, Mizoram Series 1.* Directorate of Census Operations, Mizoram.

[2] Lallianthanga R.K., 1999: *Satellite Remote Sensing for Sustainable Development of Mizoram in the 21st Century.* Proceedings of Symposium on Science & Technology for Mizoram in the 21st Century. Aizawl; 17-18 June, 155.

[3] Lallianthanga R.K., and Goswami D.C. *Land Use Satellite Mapping of Land Cover Patterns in Mizoram, India: A Case Study of Serchhip Rural Development Block, Aizawl District.* Indian Journal of Landscape System & Ecological studies. 1997. 20; 64-68.

[4] Trung N.H, Le Quang Tri, Mensvoort, MEF van, and Bregt A.K., 2006: *Application of GIS in Land-Use Planning, a Case Study in the Coastal Mekong Delta of Vietnam.* Proceedings International Symposium on Geoinformatics for Spatial Infrastructure Development in Earth and Allied Sciences, Ho Chi Minh, Vietnam; 1-11 November.

[5] Kushwaha S.P.S., Suchismita Mukhopadhyay, Hari Prasad V., and Suresh Kumar. *Sustainable Development Planning in Pathri Rao Sub-Watershed using Geospatial Techniques.* Current Science. 2010. 98; 1486.

[6] Chandrashekhar M.B., Sarnam Singh, and Roy P.S. *Geospatial Modeling Techniques for Rapid Assessment of Phytodiversity at Landscape Level in Western Himalayas, Himachal Pradesh.* Current Science. 2003. 84; 669.

[7] MIRSAC, 2007: *Natural Resources Mapping of Mizoram using Remote Sensing and GIS, Aizawl District (A Project Report).* Mizoram Remote Sensing Application Centre, Science Technology & Environment, Aizawl. 2007. 2; 37.

[8] MIRSAC, 2012: *Meteorological Data of Mizoram.* Mizoram Remote Sensing Application Centre, Science & Technology, Aizawl. 2012. 37; 39.

[9] Economics & Statistics, 2010: *Statistical Handbook, Mizoram.* Directorate of Economics & Statistics, Govt. of Mizoram. 2010. 152.

[10] USDA, 1988: *Soil Taxonomy. A Basic System of Soil Classification for Interpreting Soil Surveys.* US Department of Agriculture, Soil Conservation Service. Robert E. Krieger Publishing Company Inc, Krieger drive, Malabar, Florida 32950. 1988. 179, 227, 349.

[11] Lallianthanga R.K, Goswami D.C., and Sarma C.M. *Satellite Monitoring of Secondary Succession Subsequent to Shifting Cultivation: A Case Study of Kolasib District, Mizoram.* Journal of Ecology. Environment & Conservation. 1999. 5 (1) 32.

[12] Lallianthanga. R.K., and Sailo R.L. *Monitoring of Bamboo Flowering using Satellite Remote Sensing and GIS Techniques in Mizoram, India.* Science Vision. 2012. 12; 147.

Location Privacy in Location Based Services: Unsolved Problem and Challenge

Rajchandar Padmanaban

Institute for Geoinformatics, University of Muenster, Germany

Correspondence should be addressed to Rajchandar Padmanaban, Charaj7@gmail.com

Abstract Location Based Services (LBS) is one of the emerging technologies in the mobile, networking and information services. LBS, the branch of computer program-level services used in various fields and support, the application are broadly classified as Maps and Navigation, Information service, Tracking service, Games, Social networking, Vehicular navigation and Advertising. Location is mainly determined into two levels such as internally by a device or externally by systems and kind of networks with which the device interrelates. The advanced mobile networking and communication lend a hand to the civilization with various location based mobile application but while concerning about location privacy, there is most prominent question from the society, how about my location privacy? This article reviews a selected level of privacy in location based services that have been published in the different research journal. The review throws light on the threat and remedy on location privacy in the location based application and services that are represented.

Keywords *Location-Based Service; Location Privacy; Security, Threats; Computational System*

1. Introduction

By tradition, mobile networks utilized customer location for data transmission and voice broadcast but recent days the user location extensively employed for Location Based Services. Secrecy is the most considered factor for the people and is the most important feature the developers to keep in mind while developing the applications. Over the last few decades many research focus on the location privacy but still contradiction and challenges in conquer these risk. The techniques and methodology varied according to the application of location based service.

The major component of location privacy differentiates according to the information processing and temporal sequence. These activities are including, (1) collection of data; (2) retention or improper storage; (3) use of data; (4) revelation of location associated information. Some of the suggested techniques used in the last few decades to overcome the location privacy threats such as spatial k-anonymity, dummy location, cloaking/obfuscation, cryptographic, Trusted third party protocol (TTP),

simple and multiple pseudonym, semi distributed protocol, Private Information Retrieval protocol (PIR), collaborative protocol, and user centric and so on. This paper is structured in three sections. The first section focuses the review of literature in the branch of location privacy. The second section describes the location privacy threats, how they are affecting the individual. The third section illustrates the various techniques used in the location privacy in the last few years in the research community; what are all the frequent and contradiction among the techniques. The last section focus on the present and future thought about the location privacy in location based service.

2. Literature Review

In generally threats can be classified into two types they are communication privacy threats and location privacy threats [1]. MarcoGruteser and Dirk Grunwald ponder on sender anonymity on communication privacy threats. Anonymity in LBSs must be addressed at multiple levels in the network stack depending on what entities can be trusted [1]. In matching approach, Bugra Gedik and Ling Liu develop a spatio-temporal cloaking model, called Clique-Cloak algorithms, its aid to offer high quality location privacy k-anonymity model, development at avoiding position privacy threats before handoff the request to location based service provider [2].

In addition, Obfuscation model used in the pervasive computing environment. Obfuscation, framework, negotiation is employed to make sure that a location-based service supplier receives only the information which is need to provide a service [3].

Mohamed F. Mokbel *et al.,* developed a system called Casper; it encloses two mechanisms, including: Location anonymizer and privacy-aware query processor. The privacy-aware query processor is installed inside the LBS database server to facilities cloaked spatial area rather than the precise position of the mobile user's [4]. In related to that various set of Location based Quasi-identifiers as spatio-temporal patterns suggested by Claudio Bettini *et al*.

In research, mix zone model proposed by Alastair R. Beresford and Frank Stajano, the plan of the mix zone is to stop tracking of long-term mobile user's activities, but still permit the operation of many short-term location-aware applications [6]. The location privacy can be achieved by nearest neighbourhood analyses likewise space Twist technique developed by Man LingYiu *et al.,* rectifies these inadequacy for k nearest neighbour (kNN) queries. Starting with a position dissimilar from the user's actual location, nearest neighbours are retrieved incrementally until the query is answered correctly by the mobile terminal [7].

In the sequence of suggestion, dummies also used for avoiding threats in location privacy, this system personal user of a location-based service generates several false position data (dummies) sent to the service provider with the true position data of the user [8].

Diversely Location privacy based on a homomorphism developed by Solanas Agusti and Antoni Martínez-Ballesté, homomorphism as a tool for processing mobile network communication data with the assist of encryption and decryption function. Likely, Cryptographic is the prominent tool used in the communication data conversion for avoiding risk from location privacy. One of the application from cryptographic called blind signature it was proposed by Qi He, Carnegie Mellon University, which is used to produce a certified anonymous ID that restore the real ID of an authorized mobile communication device [10].

Lothar Fritsch and Tobias Scherner suggested a middleware system to control the flow of information and to guard the interest of every party. This system comprised of three components such as matcher, identity management system and process control. Privacy mechanism also based on

different service component, including: (1) LBS service component; (2) Localization component; and (3) communications component [13].

Protecting privacy in vehicular service is also one of the great deal while concerning location privacy, the Vpriv is the vehicular based location privacy application fashioned by Raulca ada papa *et al.,* this system the cryptographically produced random tags are used for the registration to avoid location stealing. In different way location privacy in vehicular network can protect through Path Confusion method. The path perturbation algorithm developed by Baik Hoh and Marco Gruteser at WINLAB, The key idea in this algorithm based on cross path in area where at least two or more users meet at same time and confuse the path of different users [15].

A Privacy-Preserving Location proof Updating System (APPLAUS) fashioned by Zhichao Zhu and Guohong Cao, the main key factor of this system capable of generating different Periodical pseudonyms are used by the mobile devices in order to protect the mobile users location privacy from each other, and from the un- trusted location proof mobile communication server [16].

3. Location Privacy Invading

Location information of mobile user's been collected and employ, knowingly or unknowingly; the geographic location of mobile user can easily expose in the location based service application. Knowing where is the customer, what he is doing: attending any meeting or event, spending time in the bar, visiting a doctor, taking public transport and so on. The location information assist to analyse the individual interest of consumer, which place mostly visited by consumer: information used for advertising and marketing. When Location data combined it reveal consumer regular habits and everyday work: how often in that particular place, what is the individual interest, whom and how he spends time. Location based service also make easy to collect information about customers / users such as name, age, sex, friends or relatives details and so on, individual information also steals by someone for their personal interest.

3.1. Location Privacy Threat in Geo-Tagging

Geo-tagging is also direct to threats in location privacy, modern device like iphone, smart phone, digital camera and video camera enclose geo-tagging option, while enabling geo-tagging option in the device its automatically tag the geolocation of the user in the picture, while uploading these pictures in the social network such as YouTube, Facebook, twitter, Google + and Flickr may leads to invading of personal interest and location with the scrutinize of metadata in the server / database.

4. Techniques Involved in the Location Privacy

Anonymity is the prominent model for providing trustable location based application to the society. This system carries connection between the mobile nodes and anonymity server, initially the encryption process carried out in the anonymity server, during the communication between mobile nodes and server, the position and other information will decrypts at anonymity server and its remove other information like address of the network and position data. In same way several algorithm proposed in the literature [1, 2] but recent research says that these techniques refers to spatio anonymization problem. As briefly the idea of the spatio anonymization problem is that user of the location based application can be identified through their position / location, and consequently user's privacy become endangered if a widespread request holds precise information about mobile user's location.

Existing approaches to the spatio anonymization problem [1, 17, 18] propose techniques that are secure also in the case in which the attacker obtains the precise location information of every mobile

user. Even though various research overcome the anonymity problem still we need the appropriate framework to model for privacy attack based on the multiple requests.

To protect the micro data in the server can accomplish by K Anonymity technique K anonymity mainly helps to preserve the truthfulness of the user's information. Multilevel databases used in the k anonymity techniques, the different level arrangement has facilitate to store the data at different security classification and also user's holding dissimilar security authorization but unfeasible to consider every possible attack. In other concern numerous holder share same data and repression reduce the quality of the data so feasible approach need to overcome the disadvantage of K anonymity.

In order to overcome the traceable problem in Location Based Services, a new type of anonyms technique proposed in the literature [8] is Dummies location. It sends the position of the user information including noise to the service provider. The noise consists of false location of the user's called dummies. Hidetoshi Kido *et al.*, proposed the dummy generation algorithm with two set of models are Moving in Neighborhood and Moving in a Limited Neighborhood accomplished in different external server but another approach proposed in the literature [20] focusing on the Circle-Based dummy generation and Grid-Based dummies generation algorithm requires lightweight server-side front-end to integrate the existing mobile network system.

Potentially, three set of limitation can observe in the spatial information while using assorted location privacy models they are imprecision, ambiguity and inaccuracy. Obfuscation [3] also degrading the superiority of information about an individual position in order to protect that mobile user's position.

Cryptography technique also used in the research group for avoiding position traceable, it's capable of sharing information with high security, data integrity in several database and intense authentication in mobile network. In privacy model cryptography served in both online and offline trusted third party. Trusted third party schema mostly based on spatial K- anonymity and cloaking/obfuscation for protecting the association between user identity and location. Hilbert based algorithm [24] and Icliqueclock [25] are the recent research focused on providing better model to overcome the various disadvantage faced in the location privacy frame work, the main difference between these two algorithm are Hilbert is based on the geographic related algorithm and icliquecloak related on the geometry based algorithm, icliquecloak clearly its adapted from the K anonymity and cloaking algorithm. The Table 1 shows the various models of location privacy system and its pros and cons proposed by literatures in last ten years.

Table 1: *Various Models / Framework of Location Privacy*

Models / Framework	Advantage	Disadvantage	Academic Literature
Simple Pseudonym	Identity privacy	Low accuracy Unlink ability	Hauser, Christian, and Matthias Kabatnik, 2001
K anonymity	Location Privacy	No identity privacy Unlink ability	Gruteser Marco & Dirk Grunwald, 2003 Gedik, Bugra, and Ling Liu,2005 Bettini, Claudio, X. Sean Wang, and Sushil Jajodia, 2005
Mixzone	Location and sampling accuracy	Operation Lack in multiple responder	Beresford, Alastair R., and Frank Stajano, 2004
Obfuscation	High server efficiency Location privacy	No identity privacy Unlink ability	Duckham, Matt, and Lars Kulik, 2005
False Position Data/ Dummies	Easy to integrate with existing mobile network	Operation Lack in multiple responder	Kido, Hidetoshi, Yutaka Yanagisawa, and Tetsuji Satoh, 2005
Location Anonymizer – Cloaking Algorithm	Accuracy, Flexibility	Unlink ability	Mokbel, Mohamed F., Chi-Yin Chow, and Walid G. Aref, 2006

K nearest Neighbor (kNN) Queries	No need of middleware Sever side granular search technique	Cost model	Yiu, Man Lung, et al.,2008
Trusted Third Party (TTP) - Pseudonymisation	Robust against the collusion of a Malicious user	Not centralized	Solanas, Agusti, and Antoni Martínez-Ballesté, 2008
Cryptographic	Automated	High cost	Popa, Raluca A., Hari Balakrishnan, and Andrew J. Blumberg,2009
Private Information Retrieval (PIR) Protocol	Location privacy	Low LBS server efficiency	Ghinita, Gabriel, 2009
ICliqueCloak	Many responders	Possibility of attack	Pan, Xiao, Jianliang Xu, and Xiaofeng Meng. 2012
Hilbert Based	Quick query processing time Location privacy	High cost	To, Quoc Cuong, Tran Khanh Dang, and Josef Küng, 2013

5. Conclusion

Current research focuses on the location user privacy and trouble-free frame work for interconnecting the mobile network and privacy model server. There are well-known model, k anonymity and cloaking algorithm used in various literatures but still we need efficient tool to handle the location privacy threats, topical framework focus on the geographic based algorithm instead of geometry based algorithm. As literally review shows system naturally need competent model to protect from unauthorized access as well as mobile user need the well-organized tool to secure their context information from illegal access. This paper surveyed various techniques used in the different approach based solutions for attaining privacy protection in the Location Based Service (LBS).

Location privacy research is still in fundamental level. Even though inventive model have been proposed to resolve the privacy problem in Location Based Service (LBS), there are many challenges faced by research group. Inventing a new structure of algorithm the various disadvantage of existing model should taken into consider. In one hand, interlinking of mobile network and secure framework still many challenges to be addressed, in another hand lack of technology in multiple responders' problem. Furthermore research also needed in location privacy, including: (1) Link ability problem; (2) Collusion of malicious user trouble; (3) Operation in multiple responder; (3) Identity privacy; (4) LBS server difficulty; and (5) Middleware network issue. We are look forward to many beneficial investigate on the difficulty in mounting location privacy system.

References

[1] Gruteser Marco and Dirk Grunwald. Anonymous Usage of Location-Based Services through Spatial and Temporal Cloaking. Proceedings of the 1st International Conference on Mobile Systems, Applications and Services. ACM, 2003.

[2] Gedik Bugra and Ling Liu. Location Privacy in Mobile Systems: A Personalized Anonymization Model. Distributed Computing Systems, 2005. ICDCS 2005. Proceedings of 25th IEEE International Conference on. IEEE, 2005.

[3] Duckham Matt and Lars Kulik. *A Formal Model of Obfuscation and Negotiation for Location Privacy. Pervasive Computing.* Springer Berlin Heidelberg. 2005. 152-170.

[4] Mokbel Mohamed F., Chi-Yin Chow, and Walid G. Aref. *The New Casper: Query Processing for Location Services without Compromising Privacy*. Proceedings of the 32nd International Conference on Very Large Data Bases. VLDB Endowment, 2006.

[5] Bettini Claudio, X. Sean Wang, and Sushil Jajodia. *Protecting Privacy against Location-Based Personal Identification.* Secure Data Management. Springer Berlin Heidelberg. 2005. 185-199.

[6] Beresford Alastair R. and Frank Stajano. *Mix Zones: User Privacy in Location-Aware Services.* Pervasive Computing and Communications Workshops, 2004. Proceedings of the Second IEEE Annual Conference on. IEEE, 2004.

[7] Yiu Man Lung, et al. Spacetwist: Managing the Trade-Offs Among Location Privacy, Query Performance, and Query Accuracy in Mobile Services. Data Engineering, 2008. ICDE 2008. IEEE 24th International Conference on. IEEE, 2008.

[8] Kido Hidetoshi, Yutaka Yanagisawa, and Tetsuji Satoh. *Protection of Location Privacy Using Dummies for Location-Based Services.* Data Engineering Workshops, 2005. 21st International Conference on. IEEE, 2005.

[9] Solanas, Agusti, and Antoni Martínez-Ballesté*. A TTP-Free Protocol for Location Privacy in Location-Based Services.* Computer Communications. 2008 31 (6) 1181-1191.

[10] He Qi, Dapeng Wu and Pradeep Khosla. *The Quest for Personal Control over Mobile Location Privacy.* Communications Magazine, IEEE. 2004. 42 (5) 130-136.

[11] Popa Raluca A., Hari Balakrishnan, and Andrew J. Blumberg. *VPriv: Protecting Privacy in Location-Based Vehicular Services.* USENIX Security Symposium. 2009.

[12] Fritsch Lothar and Tobias Scherner. *A Multilaterally Secure, Privacy-Friendly Location-Based Service for Disaster Management and Civil Protection.* Networking-ICN 2005. Springer Berlin Heidelberg, 2005. 1130-1137.

[13] Zhong Sheng et al. *Privacy-Preserving Location-Based Services for Mobile Users in Wireless Networks.* Yale Computer Science, Tech. Rep. YALEU/DCS/TR-1297 2004.

[14] Cheng Reynold et al. *Preserving User Location Privacy in Mobile Data Management Infrastructures.* Privacy Enhancing Technologies. Springer Berlin Heidelberg, 2006.

[15] Hoh Baik and Marco Gruteser. *Protecting Location Privacy through Path Confusion.* Security and Privacy for Emerging Areas in Communications Networks, 2005. SecureComm 2005. First International Conference on. IEEE, 2005.

[16] Zhu Zhichao and Guohong Cao. *Applaus: A Privacy-Preserving Location Proof Updating System for Location-Based Services.* INFOCOM, 2011 Proceedings IEEE. IEEE, 2011.

[17] Bettini Claudio, Sergio Mascetti and X. Sean Wang. *Privacy Protection through Anonymity in Location-Based Services.* Handbook of Database Security. Springer US. 2008. 509-530.

[18] Bettini Claudio, et al. *Anonymity in Location-Based Services: Towards a General Framework.* Mobile Data Management*,* 2007 International Conference on. IEEE, 2007.

[19] Sweeney Latanya. *K-Anonymity: A Model for Protecting Privacy.* International Journal of Uncertainty, Fuzziness and Knowledge-Based Systems. 2002. 10 (5) 557-570.

[20] Lu Hua, Christian S. Jensen, and Man Lung Yiu. *Pad: Privacy-Area Aware, Dummy-Based Location Privacy in Mobile Services*. Proceedings of the Seventh ACM International Workshop on Data Engineering for Wireless and Mobile Access. ACM, 2008.

[21] Magkos Emmanouil. *Cryptographic Approaches for Privacy Preservation in Location-Based Services: A Survey*. International Journal of Information Technologies and Systems Approach (IJITSA). 2011. 4 (2) 48-69.

[22] Hauser, Christian, and Matthias Kabatnik. 2001: *Towards Privacy Support in a Global Location Service.* Proc. of the IFIP Workshop on IP and ATM Traffic Management.

[23] Ghinita Gabriel. 2009: Private Queries and Trajectory Anonymization: a Dual Perspective on Location Privacy.

[24] To Quoc Cuong, Tran Khanh Dang, and Josef Küng. *A Hilbert–Based Framework for Preserving Privacy in Location–Based Services.* International Journal of Intelligent Information and Database Systems. 2013. 17 (2) 13-134.

[25] Pan Xiao, Jianliang Xu, and Xiaofeng Meng. *Protecting Location Privacy against Location-Dependent Attacks in Mobile Services.* Knowledge and Data Engineering, IEEE Transactions on. 2012. 24 (8) 1506-1519.

Case Study **Open Access**

Remote Sensing and GIS Application in Change Detection Study Using Multi Temporal Satellite

Patekar P.R. and Unhale P.L.

School of Earth Science, Solapur University, Solapur, Maharashtra, India

Correspondence should be addressed to Patekar P.R., punamrpatekar@gmail.com

Abstract Land use/Land cover leads with how people are using the land. Change detection study gives service to analyze temporal data and detect changes which have been taken place in study region. Mapping land use/land cover (LULC) and change detection on GIS platform is an area of interest that has been attracts increasing attention. This paper is an attempt to assess the changes in land use/land cover Basin of Bhima River in Solapur district over a 14 year period. The aim of this study is to detect land use changes between 1991 to 2005 using satellite images of Landsat TM (1991) and ETM+ (2005). Landsat TM (1991) and ETM+ (2005) images were classified by using supervised classification method. In this method maximum likelihood classification algorithm technique is used. In the present study major changes occurred in Agriculture, fallow land and settlement. Population growth increase presser on land resources. The result of present study help to the researcher, environmental developer for understanding to real time condition manage land use more effectively according to the provide needs. Geographical Information System & Remote sensing technique play very important role in land use land cover change detection study. It is a user-friendly and accurate technique for environmental managers.

Keywords *Land Use/Land Cover; Change Detection; GIS; Remote Sensing*

1. Introduction

Land use/land cover deals with physical characteristics of earth surface (Vegetation, Water) and feature created by human activities (settlement). Land use/Land cover leads with how people are using the land (S. Prabaharan, K. Srinivasa Raju, C. Lakshumanan, and M. Ramalingaz, 2010). Change detection study gives service to analyze temporal data and detect changes which have been taken place in study region. Mapping land use/land cover (LULC) and change detection on GIS platform is an area of interest that has been attracts increasing attention.

Mapping land use/land cover (LULC) and change detection on GIS platform is an area of interest that has been attracting increasing attention. This paper is an attempt to assess the changes in land use/land cover Basin of Bhima River in Solapur district over a 14 year period.

2. Aim and Objective

The aim of this study is to assess the changes in land use/land cover Basin of Bhima River in Solapur district over a 14 year period between 1991 to 2005 using satellite data of Landsat TM (1991) and ETM+ (2005).

3. Study Area

Basin of Bhima River in Solapur District of Maharashtra, India.

3.1. Drainage Pattern in Solapur District

The district is drained by numerous streams and rivers. River Bhima, Nira, Man, Sina and Bhogawati are some important rivers in the district. During the rains all these rivers flows full and strong with occasional floods. But after the rains, they rapidly dwindle and in the hot summer season and pools remains only in the deeper hollows, with an occasional flow in the parts between. These rivers play important role in supplying water for drinking, agriculture and industrial purposes. The entire district is drained by the Bhima River.

3.2. Bhima River

The river Bhima is Major River in the district and locally it is called 'Chandrabhaga' due to its present shape near holy place Pandharpur. The Bhima is main tributary of Krishna River; she rises at Bhimashankar in Sahyadri Mountain in the Pune district. First she flows towards east and then south-east direction in Pune districts and enters in Solapur district near Jinti village in the Karmala tahasil. & flows to south-east direction. Total length of her course in the district is 288 km. The Nira, Man and Sina are the main tributaries of Bhima. Hence the Bhima valley drains most of part of the district & then meets to Krishna in Karnataka state.
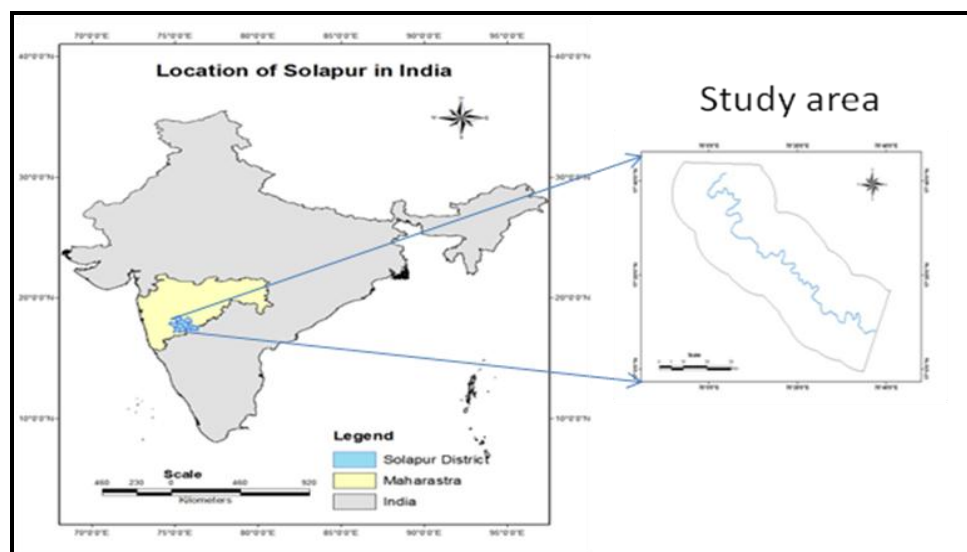
Map of Study Area

Figure 1: Map of Study Area

3.3. Digital Image Processing

The study depended on the use of computer-assisted interpretation of Landsat imageries in ERDAS Imagine. Field survey was performed over the study area using Global Positioning System (GPS). The field survey was conduct to obtain accurate location for training sites and signature generation. Those location points are also used for supervised classification of image and also for accuracy assessment. The Landsat 5 image of year 1991 shows situation which exist 14 year before and recent image of Landsat 7 shows real time situation. Landsat 5 image could not check out through ground truth but the Landsat 7 ETM+ image cross checked against ground truth. Detail of satellite D data is shown in Table 1.

3.4. Data Used

Table 1: Data Used

Sr. No.	Data Type	Scale	Source of Data
1	Landsat TM (1991)	30 m resolution	GLCF site
	ETM+(2005)		
2	GPS	GPS point	Garmin

3.5. Software Used for Present Work

Basically, following software's is used for this project viz;

  i.   Arc GIS 9.3 – It was used to compliment the display and processing the data.
  ii.   ERDAS IMAGINE 9.1- It was also used to processing the data.

4. Methodology
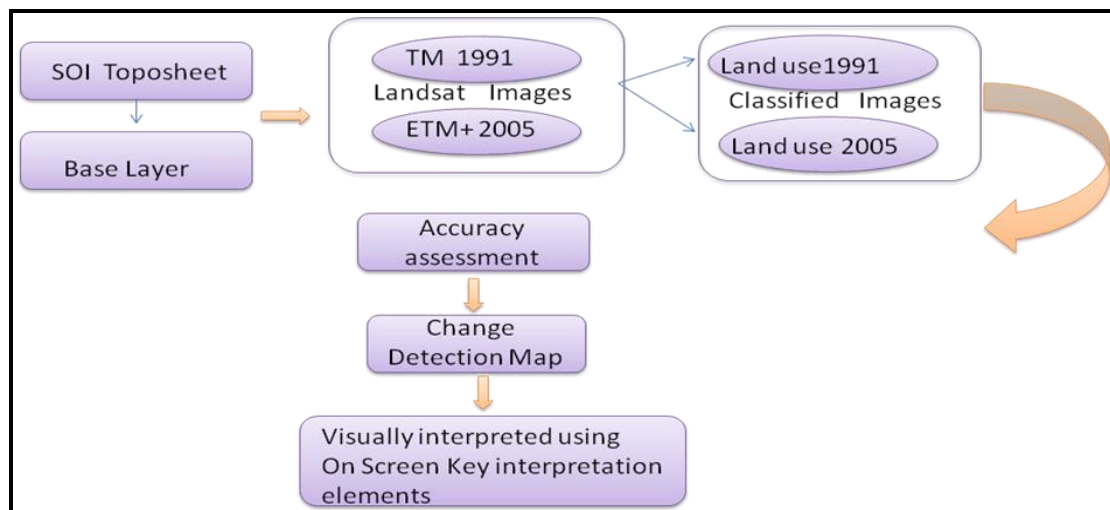
Figure 2: Methodology

5. Change Detection

Change detection is the study of change has been taken place in study region in the study period. In general the change detection study includes whether change or not change has occurred (R. Manonmani, G. Mary, and Divya Suganya, 2010).
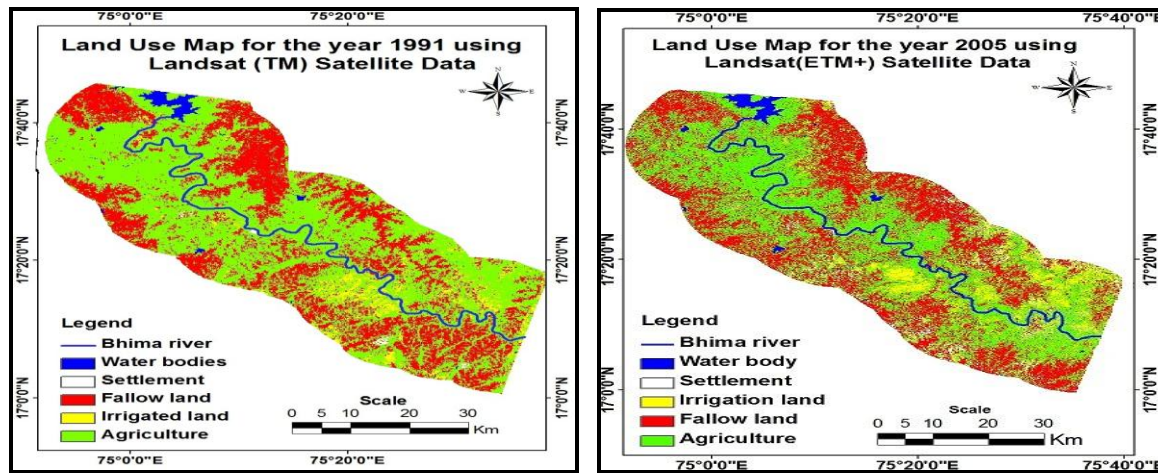
Figure 3: *Change Detection during 1991-2005*

6. Results

The land use categories such as built-up land, agriculture, water body, wasteland and others have been identified and mapped from the Landsat TM and ETM+ of 1991 and 2005. Table 2 shows the Land use/land cover changes and areas of each Land use type in km^2. About 38.44 % of the areas are occupied by agriculture land during 1991 and about 33.01 % areas are occupied by agriculture during 2005. People utilize the land for agricultural purposes. Under utilization, mismanagement could be observed in the field. As a result the yield is not optimum. This is due to shifting of agricultural land to built-up. Increase of about 1.26% of the settlement land during 2005 when compared to 1991. Fallow land is increased about 2.72 % in 2005. The increase in the area under built up lands may lead to a lot of environmental and ecological problems. Agriculture is main source of income in this region but from 1991 to 2005 this classes have been decreased due to new settlement and infrastructure developments. Here proper land use planning is needed. Land use/land cover changes are shown in Figure 3 and Figure 4.

Table 2: *Area under Different Land Use/Land Cover Categories during 1991-2005*

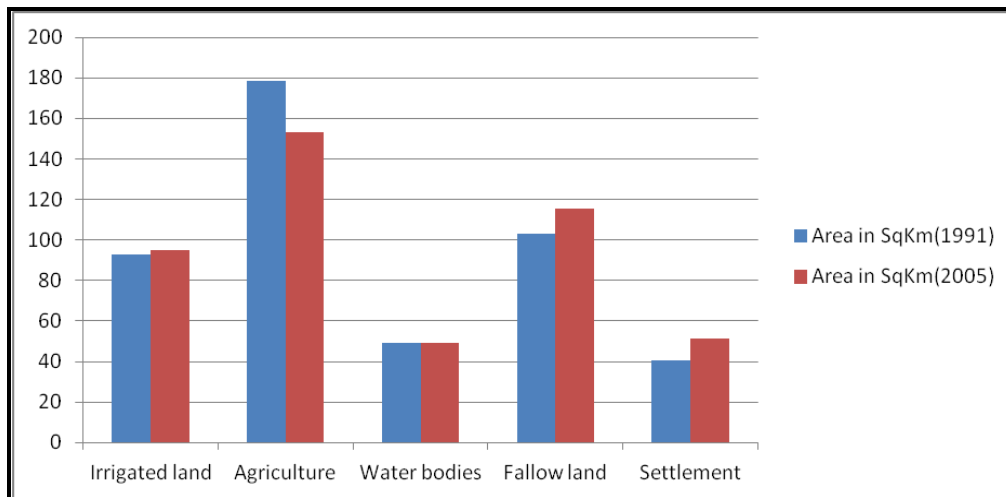| Land use / Land cover Types	1991(Km^2)	Area in (%)	2005 (Km^2)	Area in (%)	Difference
Irrigated land	93.05	20.03 %	95.1	20.47 %	+0.44
Agriculture	178.47	38.44 %	153.30	33.01 %	-5.43
Water bodies	49.09	10.58 %	49.09	10.58 %	0
Fallow land	102.95	22.16 %	115.54	25.89 %	+2.72
Settlement	40.81	8.79 %	51.34	10.05 %	+2.26
Total	464.37	100%	464.37	100%	

Figure 4: *Area under Different Land Use/Land Cover Categories during 1991-2005*

7. Conclusion

Remote Sensing and Geographical Information System is very effective for Land use/Land cover change detection study. Remote sensing data like Landsat TM & ETM+ provides accurate data for land use/land cover change detection and analysis. The overall accuracy of this study found 81 % in the process of accuracy assessment. The land use/land cover occurred changing day by day due to the forces of utilization of potential land, population growth during the study period of 14 years.

References

Mohamed Ait Belaid, 2003: *Urban-Rural Land Use Change Detection and Analysis Using GIS & RS Technologies.* 2nd FIG Regional Conference Marrakech, Morocco, December 2-5.

R. Manonmani, G. Mary, and Divya Suganya, 2010: *Remote Sensing and GIS Application in Change Detection Study in Urban Zone Using Multi Temporal Satellite.* International Journal of Geomatics and Geosciences. 2010. (1).

S. Prabaharan, K. Srinivasa Raju, C. Lakshumanan, and M. Ramalingaz, 2010: *Remote Sensing and GIS Applications on Change Detection Study in Coastal Zone Using Multi Temporal Satellite Data.* 2010. 1 (2) 159-166.

Cloud Publications

Research Article   **Open Access**

Simulation of Water Behavior Includes Inundation and Flow on its Streambed Based on GeoSpatial Processing Functions

Hooshang Eivazy

Department of GIS and Geomatic, Technology University of Arak, Daneshgah, Arak, Iran

Correspondence should be addressed to Hooshang Eivazy, h_eivazy@yahoo.com

Abstract Many organizations concentrate on water inundation [1] behavior because of its important role in different aspects of people day to day life. Prevalent software solutions to simulate have serious limitations and restrictions which make them difficult for all to be deployed. It makes the things even worse while some leave the process alone and do it with traditional manual methods. To come over the problem a new basic conceptual solution was proposed to use Geo-Spatial functions [2] in combination with traditional strength points; well form hydraulic equations and best proved conceptual algorithm to solve the hydraulic problems. The proposed solution expands a new concept to construct a computation environment [3] within GIS computation environment which simply matches the other Geo-Spatial problems. Nevertheless idea coincides some potential problems include conceptual fitness of real hydraulic environment with available geo-functions, arrangement of geo-functions in algorithm to solve the problem and tuning the geo-spatial functions proportional to problems. In this paper, mentioned points have been covered and results were proposed for a sample study area on a river part, named "Ghare-Chai" which is located in Markazi [4] province. The results' comparison with measured observations reconfirms the wonderful potential ability of Geo-Spatial functions to solve spatial problems [5].

Keywords *Geo-Spatial Functions; Pixel-Agent; Water Inundation; Water Simulation; Streambed*

1. Introduction

Simulation of water behaviors is important almost in any organization which faces the water management affairs. It is essentially e.g. for engineering water district department to determine, rivers' and floodways' streambed and more important their security risk buffers [6] to avoid settlement of any activities in it.

This idea mainly arises from previous disasters occurred in last decades in different countries (Global Flood Survey, 2013). According to such problems legal restraining decree were issued to avoid settlement and refuse any ownership petition. Since then, Water Engineering department is

responsible to determine streambed security risk buffer and continuous advertisement to report any infringes in those districts.

To determine river or floodway risk buffer, there are so many different instructions and scripts all are based on mathematical hydraulic equations. These equations start by Manning's roughness coefficient [7] and the ways to define it for a demanded district. These are followed by equations to determine water flow on stream bed. Finally different solutions are proposed to compute water inundation.

Of course water accumulation in upper watershed area has been neglected whereas it is not the main scope of this paper. This is the same for streambed extraction which has been covered in other issues. (Eivazy, 2013).

Regardless of its vast and great applications in several fields, simulation process itself has involved so many experts to get it practical in the context of commercial software. So many mathematical equations have been set to mimic the water behavior but all suffer from common point. In fact development of equations in the context of one practical algorithm is so difficult (Brownlee, 2011).

Nevertheless some pre-developed vector-based solutions are available in commercial market which all has common weak points (Merwade, 2012). Each solution contains just a part of final solution. In addition whereas algorithms have been regulated based on sequential simple vector computation, pre-defined standards should be followed by a user to get the software compute.

Estimation is the other common point in almost every traditional solution. Indeed a user hover the field himself and then decide about critical lines, points and districts. Designated spots then will be critical on computation approximation. In addition users have to determine basic structure of water body themselves. These structures are the back bone of whole process and are deployed sequentially in proceeding process.

On other side, there are plenty of spatial functions are available but are left intact whereas they are not obviously match to real world problems such as water inundation simulation process. According to previous experiences (Eivazy, 2013) which refuse the lateral assumption, geoprocessing functions have wonderful ability to fit real world problem requirements. The most important problem arises from two points; conceptual modeling fitness and specified real world functions.

Except for mentioned problems, their potentials could be easily deployed to automate the process, decreasing the time, decreasing dependencies on users' actions and human decisions, simplifying the whole process, better data interoperability with other Geo-data sources [8], better visualization and increasing the deployment of results in other applications. In addition conceptual deployment of Geo-Processing functions defines new computation environment which simply match the other Geo-Spatial problems. The left point is the genius to Geo-Spatial function arrangement and tuning [9]. Altogether these actions are efficient steps to construct and develop new full geo-computational environment as the best geo-simulator tool. I hope for!

2. Methodology

2.1. Prevalent Approach

Water behavior simulation has been important since humans decide to settle beside water bodies. While people gain directly from its benefits and base their life on it, water bodies have their own behaviors and sometimes may exceed their normal borders and would hurts its neighbors. However these disasters are not something unexpected. These occur under the direct effect of water bodies'

temporal behaviors. In fact ignoring these temporal phenomena is the main reason to such disasters (CollinsFosu, Eric K. Forkuo, and Mensa Y. Asare, 2012).

Tropical hurricanes and storm surges [10] are among the most important motivations which push the experts to use practical solutions. Using prediction numerical surge model would be the simplest solution. Among the prevalent model such one is used within the Army and Navy community is the Advanced CIRCulation Model. It is a well-known two-dimensional model that vertically integrates shallow water equations and is used to predict surge and of course storm surge heights (C.A. Blain, R.H. Preller, and A.P. Rivera, 2002). Then it would be easy to derive water inundation by exerting previous results to costal DEM model (C.A. Blain, T.C. Massey, J.D. Dykes, and P.G. Posey, 2007) Regardless of their importance and concentrations, (sidereal simulation model e.g. coastal erosion or bathymetric data acquisition) indeed the most important problem arises from their point of view (Neil G. Dickson, Kamran Karimi, and Firas Hamze, 2010).

In River flood simulation process there are excellent reviews of storm sewer modeling (Abbott, M. B., Bathurst, J.C., Cunge, J.A., O'Connell, P.E., and Rasmussen, J., 1986; Akan, 1993; Institute, 2000). All has concentrated on water behavior equations and the approaches to fit the model with observed parameters. Although their fitness or drift is important to water experts but none negotiates on the approach to implement solutions in a predicative, sequential or descriptive Programming Language [11] (Brownlee, 2011; Algorithm Implementation, 2010).

Indeed using numerical algorithms [12] lead to approximated results. Comparison of results with real observation demonstrates considerable amount of errors which can't be neglected.

Nevertheless some equations guide to such algorithms are practically so difficult to implement (Algorithm Implementation, 2010). Of course difficult and sophisticated algorithms' implementation, usually cause restrictions in module efficiency. Therefore there would be some software with limited abilities and stiff manual script that should be strongly followed by users. So it would be clear, any deviancies won't be stood by software and result in alarm messages.

Among the commercial software available in trading market, DHI MikeStrom is a good paradigm. It is an engineering professional software package for simulation of flows, water bodies, sediment transport in estuaries, irrigation system and other water bodies. Most of all, it is able to simulate the tidal stormy water bodies and of course water inundation (Mike11, 2011).

While users work with software, first of all should create different mandatory script files according to a rigid format. Script files include structural data e.g. river boundaries, axels, cross sections, and equation parameters. In this software, the most important part of data should be provided manually or under direct stewardship of users. Figure 1 displays the tools are used to digitize and edit stream network.

Figure 1: Editing Toolbar of Mike11 which is used to Manipulate Stream Network

In such software it has tried to deploy best hydraulic equations but fitness process is done due to users' test and tries activities.
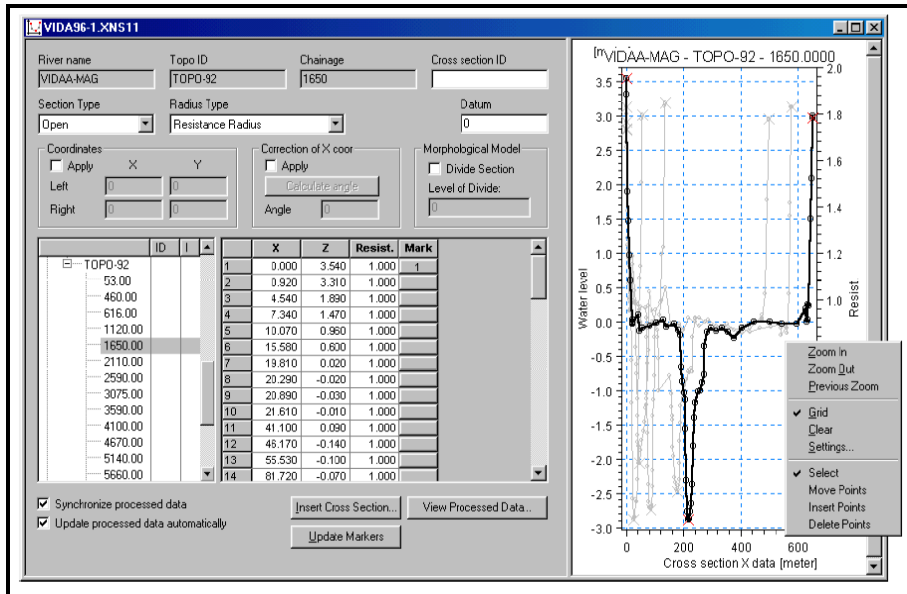
Figure 2: *Mike 11 Cross Section Editor*

Figure 2 demonstrates Mike GUI [13] which has been specified for user editing process. Nevertheless, temporal behavior simulation of water bodies via time series is considerable due to its realistic graphical report.
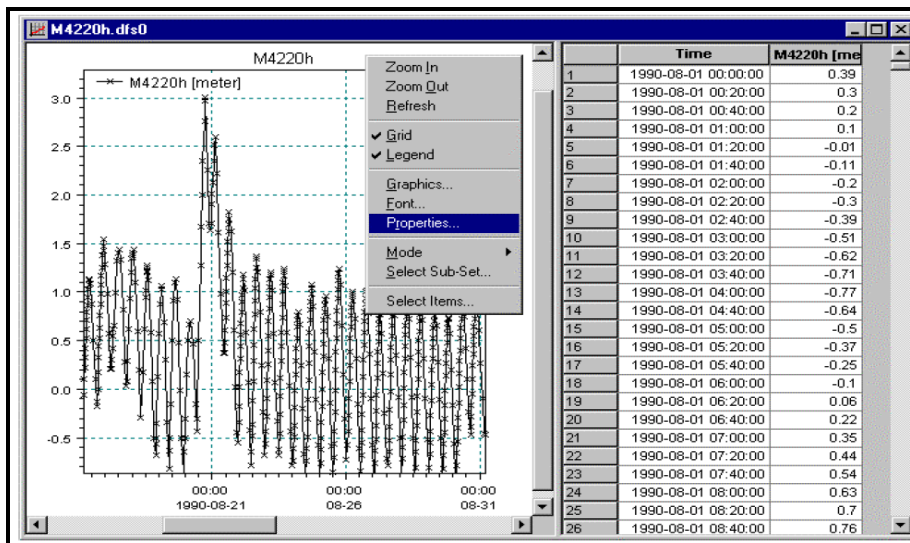

Figure 3: *Time Series Editor Toolbar*

Figure 3 depicts the tool that handles storm temporal data. Regardless of error volume, bulky data entering and editing can be interpreted as a weak point and make the deployment of software difficult to the users. In addition, to predict water inundation volume, a complete data cycle has to be done, many parameters should be regulated and many editors should be edited. So this process is too time consuming. But the main weak point arises from vector processing method and algorithms' implementation approaches.

Another good example could be seen in HecRAS. As Mike, HecRAS uses the Saint Venant hydraulic equations. Therefore it is expected that altitude be exactly taken in to account. In the other words, the mentioned equation is so sensitive to DEM deposition and tries to compute accurate results based on

stream cross sections. Nevertheless most of users usually use estimated morphologic parameters to decrease the time and expenses (Firas S.M. SALEH, Agnès DUCHARNE, and Ludovic OUDIN, 2010).

HecRAS is free software which has been developed by US Army Corps of Engineers Hydrologic Engineering Center. It is well known software among water engineer experts mainly because it is free and although because of its abilities. Some users use it alone specially those who do not care about data storage issues. But GIS experts usually use it along with other free module is called GeoRAS.

GeoRAS is although a free pre-developed module has been designed by US Army Corps. The module is added to ArcMap and ArcCatalog environment to form a new hydraulic graphical user interface in general ArcGIS interface.

Starting GeoRAS procedure requires setting input raster data (usually DEM or TIN) according to instruction. Then bulky manual process is begun by the user to create vector data requirements which takes considerable amount of time. Figure 4 displays the input vector data should be set before simulation.
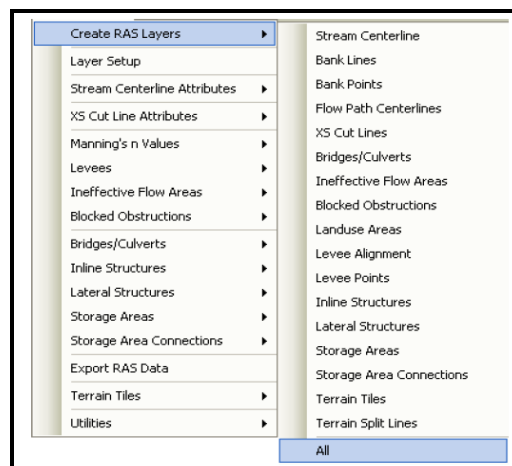
Figure 4: Vector Data Initialization Dialog Box of Geo-RAS

This creates complete hydraulic conceptual model in ArcGIS geodatabase which is essential to water body simulator engine of HecRAS software. Then user has to start digitization of important water body structure depends on his or her water knowledge. Of course digitization should follow instructions too.
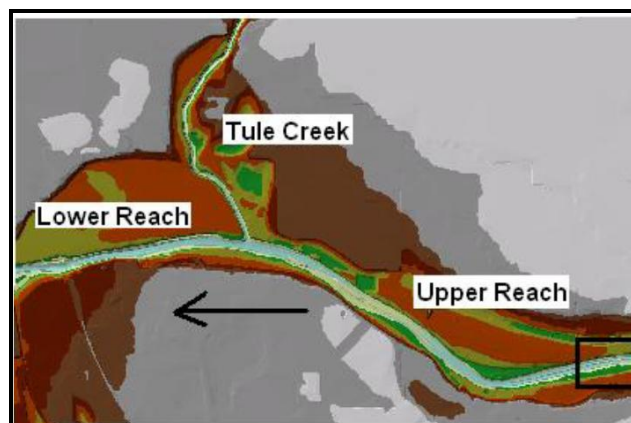

Figure 5: Digitization Direction of Water Bodies in Arcmap Environment

For example Figure 5 notes that digitizing should be directional from upstream to downstream. Otherwise you will receive perplex results than can't be interpreted by you. Worst of all, in digitizing process all topological rules should obey by user himself. This makes the process even more confusing and tiresome.

Then mandatory descriptions and parameters of body structure should be introduced by user one by one. After all, data should be exported to HecRAS to compute cross sections and earning the final results. Of course this procedure is user-based and needs user direct advertisement. Finally vector results will be ready to be imported back to geodatabase environment and should be regulated by user to be prepared for presentation (Merwade, 2012).

2.2. Purification of Final Scopes According to Experiences

Therefore, it can be claimed that empirical hydraulic equations, have two major weak points. They neglect morphological details of streambed which deflect the simulation. Although it is tried to fit them to real nature of water bodies using derivation techniques and additional parameters, but they still remain weak are not coincidence with real field observations. In addition these equations are mostly numeric and are not conceptually suitable to be fitted with commercial programming languages. In other words, it is so difficult to envision such equations in the context of software.

But commercial pre-developed software such as Mike and HecRAS use better equations. They are not merely empirical instead they are strongly under the effect of geometrical aspect of water bodies. This makes them more accurate than previous ones. In addition they use specific types of equations which are easier to be implemented in a prevalent predicative programming language.

Nevertheless, there are some problems too. As it was mentioned in part 2.1, hydraulic commercial simulation software is not fully automated. They are strongly dependent on user actions and knowledge. In addition the module process became more difficult to users because they have to exactly follow stiff manual instruction.

Mentioned reasons were good motivations to design and implement new solution to minimize the previous problems.

3. Designing and Implementing

3.1. Planning for Primary Project Requirements and Project Conduction

Whereas phenomena such as rivers have continuous nature are expected to be modeled in raster [14] space. It is obvious stream model conversion to vector, subsequently decrease demanded accuracy. Therefore implementing a GIS functional solution based on grid space, has the high potential of keeping accuracy because it doesn't change the primary nature of altitude data. (Eivazy, 2013).

The most important data required for GIS solution is DEM. In contrary with traditional approaches which focus on hydraulic descriptions, GIS methods have strong correlation with geometry. According to previous experiences, using contours could be evaluated as a suitable tool to create DEM (Eivazy, 2008). Regardless of GIS based studies that prove the advantages of contour deployment, efficient hydrological software offer the same solution. Figure 6 demonstrates the contour data role in water bodies' simulation according to water expert research (CollinsFosu, Eric K. Forkuo, and Mensa Y. Asare, 2012).
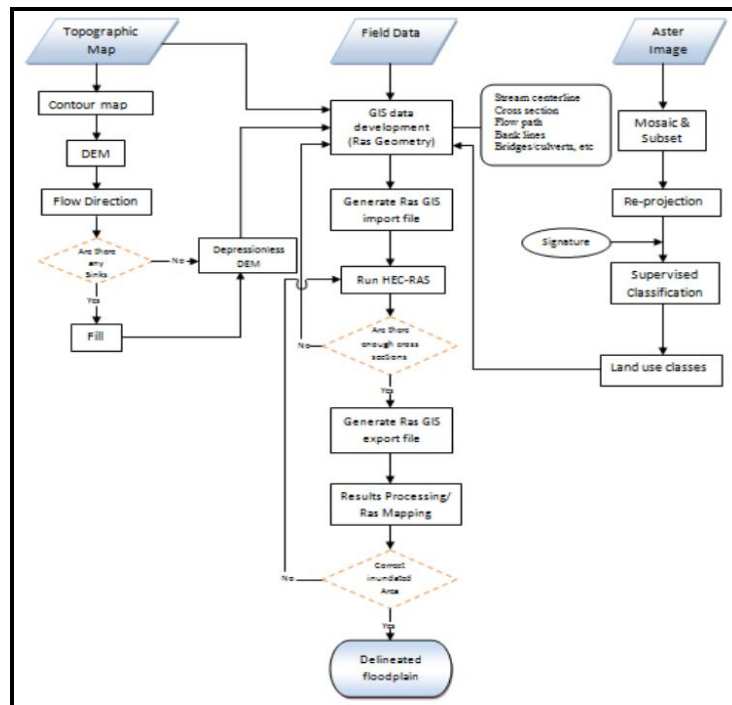
Figure 6: *Stream Simulation Algorithm According to Hecras Requirements*

Therefore a data preparation process [15] was exerted on contour sheet based data, and then TIN was created on each data sheets. Data sheet size TINs, were converted to raster data and finally all data were combined together using mosaic function [16]. Figure 7 display the Markazi province DEM extent.
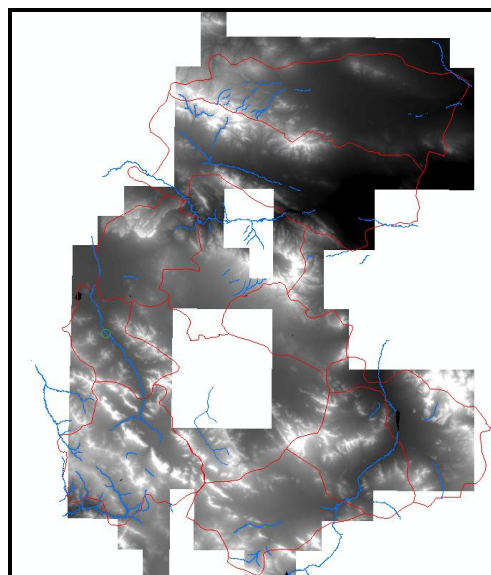

Figure 7: *Markazi Province DEM as Output of Mosaic Function*

For the scope of this project, part of DEM which underlies a river named "Ghare chai" was selected and clipped with other spatial function. This part of river was selected because there was some water level measurement and flow meters instruments installed which would help us to give real observation values. Such values would be compared against the simulated parameters and thus could be suitable verifying approach to test the proposed solution.

Next figure displays a river part with its streambed DEM which has been extracted from province DEM. As it mentioned it is simply done due to deployment of a spatial function "Clipping".
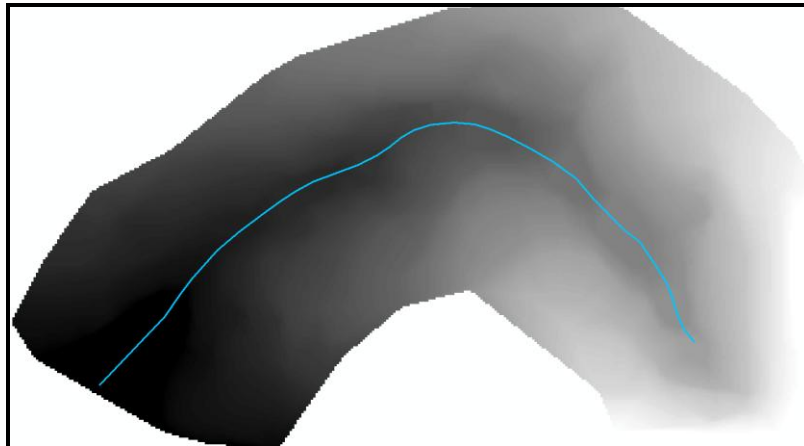
Figure 8: *Part of Streambed and its Axel that was selected*

3.2. Defining Raster Spatial Function as the Solution Main Key

According to previous empirical experience, it was decided to use another spatial function as the main platform. This function which is classified in propagation group is so called 'cost distance'.

From the cell perspective, the objective of the cost functions is to determine the least costly path to reach a source for each cell location in the Analysis window. The least accumulative cost path to a source, the source that allows for the least-cost path, and the least-cost path itself must be determined for each cell.

Cost distance functions apply distance in cost units, not in geographic units. This point is the key point of proposed solution. All cost functions require a source dataset and a cost raster. If the source dataset is a raster, it may contain single or multiple zones. These zones may or may not be connected. The original values assigned to the source locations (raster or feature) are retained. There is no inherent limit to the number of sources in the input raster or feature source data. Here in the study, source is equal to streambed axel. It is painted with blue in Figure 8.

If the source dataset is a feature dataset as in this study, it will be converted internally to a raster at the resolution determined by the environment; if the resolution is not explicitly set there, it will be the same as the input cost raster. If the source data is a raster, the cell size of that raster will be used.

The cost raster, the most important part of solution, can be a single raster and is generally the result of the composite of multiple rasters. Here it is created as the output of some hydraulic equation which will be discussed late. The units assigned to the cost raster here is the some kind of hydraulic energy volume. It is strongly defined relative to the cost assigned to other cells.

The cost values assigned to each cell are per-unit distance measures for the cell. That is, if the cell size is expressed in meters, the cost assigned to the cell is the cost necessary to travel one meter within the cell. If the resolution is 50 meters, the total cost to travel either horizontally or vertically through the cell would be the cost assigned to the cell times the resolution (total cost = cost * 50). To travel diagonally through the cell, the total cost would be 1.414214 times the cost of the cell times the cell resolution [total diagonal cost = 1.414214 (cost * 50)].

To determine the cost for a path to pass through cells to reach a source, the cost surface functions are based on the node/link cell representation used in the graph theory [15]. In the node/link cell representation, each center of a cell is considered a node and each node is connected by multiple links. Every link has impedance associated with it. The impedance is derived from the costs associated with the cells at each end of the link (from the cost surface) and the direction of movement through the cells. If the movement is from a cell to one of the four directly connected neighbors, the cost to move across these links to the neighboring node is one times cell 1 plus cell 2, divided by two.

$$a1 = (cost1 + cost2)/2$$

Where cost1 is the cost of cell 1, cost2 is the cost of cell 2, and a1 is the cost to move from cell 1 to cell 2.
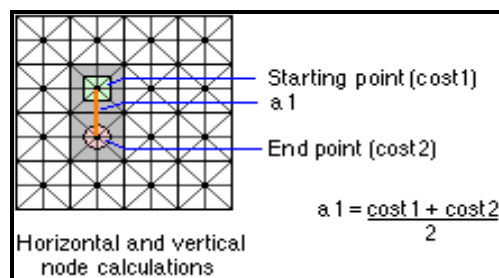
Figure 9: Cost Computation without Any Midpoint

The accumulative cost to move from cell 1 to cell 3 is determined by the following formula:
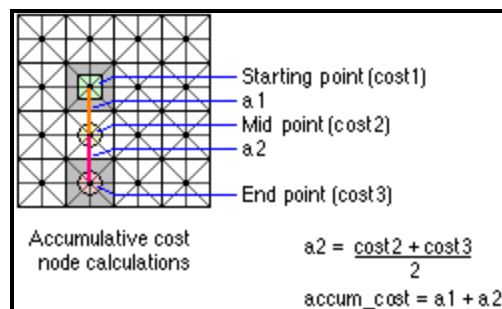

Figure 10: Cost Computation Includes Midpoint

Where cost2 is the cost of cell 2, cost3 is the cost of cell 3, and a2 is the accumulative cost.

If the movement is diagonal, the cost to travel over the link is 1.414214 or the square root (sqrt) of 2 (accounting for the difference in the orthogonal link or the longer distance to travel), times the cost of cell 1 plus the cost of cell 2 divided by two.

$$a1 = 1.414214(cost1 + cost2)/2$$

When determining the accumulative cost for diagonal movement from cell 1 to cell 3, the following formula must be used:

$$a2 = a1 + 1.414214(cost2 + cost3)/2$$

A cost path consists of sequentially connected links that provide the route for each cell location to reach a source cell. A cost path distance (or cost distance) from any cell to a source cell is the

accumulative cost of all links along the path for the cell to reach the source cells. There are many possible paths to reach each source cell, and there are many paths to reach the many source cells. There is one least-cost path. The least-cost path distance from a cell to a source cell is the smallest (or least) cost distance among all cost path distances from the cell to the source cells.

Since the cost distance is based on an iterative allocation, the lowest accumulative cost for each cell to a source is guaranteed. The accumulative values are based on the cost unit specified on the cost surface.

The output back-link raster identifies, for each cell, which cell to move or flow into on its way back to the source that will be least costly to reach. The values range from 0 through 8. The source cells are assigned 0 since they have reached the goal (the source). If the least costly path is to pass from the existing cell location to the lower right diagonal cell, the existing cell will be assigned 2; if traveling directly down or south, the existing cell would receive the value 3, and so forth. The back link is used to reconstruct the least-cost path from every cell of a raster.
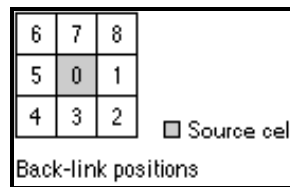

Figure 11: *Directional Surrounding Values for Each Given Pixel*

The cost allocation identifies, for each cell, which source would be the least costly to reach. The values on the output raster would contain the same values assigned to the cells in the input source raster or the values associated with each source location derived from the {in_value_raster}.

The cost distance raster tells how much it would cost each cell to return to a source via the least-cost path; the cost allocation raster defines, for each cell, the least costly source to reach; and the cost back link identifies how to return to the source. The cost distance and cost back link rasters must be created before initiating the Cost Path function. As long as the source and the cost rasters do not change, Cost Path can be run as many times as necessary with as many different destinations or combination of destinations (ESRI, 2011).

3.3. Extracting Proper Cause Hydraulic Equations

The next step is to fuse distance function with hydraulic behavior simulators. As long, experts in water engineering field have had great interests to numerical equation simulators. Among these experts, (Abbott, 1998) gives suitable paradigm in context of derivative equations to simulate behavior.

It is possible to neglect the momentum effects because that is small in comparing with gravitational and frictional parameters of flow.

The most important parameters we are looking for is average depth. This equation would be as below:

$$\frac{\partial d}{\partial t} + \frac{\partial[(1-\beta)ud]}{\partial x} + \frac{\partial[(1-\beta)vd]}{\partial y} = q_s(x,y,t) - q_i(x,y,t) \quad (1)$$

$$-\frac{\partial h}{\partial x} = S_{fx} + \frac{\lfloor q_s(x,y,t)\rfloor u}{gd} \quad (2)$$

$$-\frac{\partial h}{\partial y} = S_{fy} + \frac{\lfloor q_s(x,y,t)\rfloor v}{gd} \quad (3)$$

In above equations, d is water depth, $\beta = \sqrt{\frac{A_b}{A}}$ is a detaining ratio which convey the linear ratio of building area to all area related to river cross section, u and v are velocity components related to water flow; x, y are two main directions one is parallel to river path and the other means y is perpendicular to primary axis, and h=d+z is the water surface height. Mentioned equations try to simulate temporal behavior of water flow using derivative mathematical approaches. In Raster Environment it is simply done due to derivation definition. It means

$$f'(x) = \frac{f(x+\Delta x)-f(x)}{\Delta x} \quad (4)$$

Take equation (4) while the denominator is tended to zero. In raster environment, it would be the sensitivity of spatial function due to small changes in function inputs. Therefore it is simple to execute above functions using two raster dataset. Two other components are

$$S_{fx} = \frac{n^2 u \sqrt{u^2+v^2}}{d^{\frac{4}{3}}} \quad (5)$$

$$S_{fy} = \frac{n^2 v \sqrt{u^2+v^2}}{d^{\frac{4}{3}}} \quad (6)$$

These are the friction slopes along the x and y directions which are mainly supported by terrain slopes. In other words functions (5) and (6) are used to determine raster datasets pixels. These raster datasets will be used instead of normal slope map. $q_s(x,y,t)$ and $q_i(x,y,t)$ are the rate of water entering and leaving ground surface per unit area, which are expressed as below:

$$q_s(x,y,t) = I(x,y,t) + \sum_k Q_s(x_k,y_k,t)\delta(x-x_k,y-y_k) \quad (7)$$

$$q_i(x,y,t) = \sum_k Q_i(x_k,y_k,t)\delta(x-x_k,y-y_k) \quad (8)$$

Which I(x, y, t) is the rainfall excess intensity, $Q_s(x_k,y_k,t)$ the outflow discharge from surcharged river, $Q_i(x_k,y_k,t)$ the inlet discharges and inlet system, where the outflow discharges and inlet drainages which occur in river canal systems are considered as point sources and sinks in 2D overland flow, and δ is the Dirac delta function. In Equation (7) and (8), it is assumed that the influx direction of rainfall effluent is normal to the overland surface and the inlet drainage leaves with practically the overland flow velocity components u and v (Abbott, 1998). The unknown parameters include d, u and v in Equations (1) to (3) are solved by an alternating direction explicit scheme. The derivation of finite difference equations was depicted in the authors' earlier studies (Hsu, M.H., Chen, S.H., and Chang, T.J., 2000) which have been specified for manmade canals and urban water discharging systems.

Although such solutions was introduced among the best solution (Ming-Hsi Hsu, Shiuan-Hung Chen, and Tsang-Jung Chan, 2002) which meet the requirements of manmade and natural streambed, regardless of its strength points (slope, temporal behavior) it doesn't care the altitude. In other words, it has focused on hydraulic behavior instead. Such solution was taken first and was examined via the real control points on streambed. Results depict a great amount of errors which can't be neglected.

Other equation was examined due to its fusion in pixel agent solution [17] was USACE's UNET (Barkau, 1985) model which is simple enough to be deployed in pixel solution. It was expected that this model present better results whereas complexity of previous deployed model caused undesired deflection.

$$\frac{\partial Q}{\partial x} + \frac{\partial A}{\partial t} - q_1 = 0 \qquad (9)$$

Where:

Q = Discharge (L^3/T)

A = Cross Sectional Area (L^2)

x = the distance along the longitudinal axes of the channel or floodplain (L)

t = Time (T)

q_l = Lateral inflow per unit length ((L^3/T)/L)

$$S_f = S_0 - \frac{\partial y}{\partial x} - \frac{V}{g}\frac{\partial V}{\partial x} - \frac{\partial V}{g\partial t} \qquad (10)$$
$$\quad\ \ \text{a}\quad\ \ \text{b}\quad\ \ \text{c}\quad\ \ \text{d}\quad\ \ \text{e}$$

Where:

S_o = Bottom slope

S_f = Friction slope

V = Velocity (L/T)

y = Flow depth (L)

g = Acceleration due to gravity (L/T^2)

Term a, is the friction slope and reflects the resistance to flow. Term b is the bed slope and reflects the body force from gravity. Term c is the pressure term and reflects the change in depth in the longitudinal direction. Term d is the convective acceleration and reflects both spatial variation of the flow ($\partial Q/\partial x$) and longitudinal change in the cross-section area ($\partial A/\partial x$). Term e is the local acceleration and reflects unsteady flow. Terms b and c combine to give the water-surface slope.

To simplify the problem it is assumed: (1) a horizontal water surface at each cross section normal to the direction of flow, (2) the exchange of momentum between the channel and the floodplain was negligible; (3) the discharge was distributed according to conveyance, i.e.

$$Q_c = \varphi Q \qquad (11)$$

Where

$$\varphi = \frac{K_c}{K_c + K_f} \qquad (12)$$

$$K = \frac{1}{n} A R^{\frac{2}{3}} \qquad (13)$$

$$Q = KS^{\frac{1}{2}} \qquad (14)$$

Where:

φ = Discharge distribution factor (dimensionless)

Q_c = Flow in channel (L^3/T)

Q = Total flow (L^3/T)

K_c = conveyance in the channel (a measure of the carrying capacity of a channel)

K_f = conveyance in the floodplain

n = Manning's roughness coefficient (dimensionless)

A = Flow area (L^2)

R = Hydraulic radius (L)

3.4. Fusing Hydraulic Equation with Spatial Function

Therefore according to equations (9-14), first flow is computed along the longitudinal stream axes for each given stream segment. Axes segment length should be equal to pixel size. This part should be done due to approximately bulky vector processing function. The main reason is that all geometrical and a spatial description of streambed should be attached to stream section.

Then, longitudinal stream axes segment is changed to raster based on its flow attribute. It is done by feature to raster spatial function. Up to this point, source dataset which is necessary for cost distance function is ready. Then resistance or cost raster dataset, as the other mandatory input of cost distance function, should be prepared.

This would be designed for both, symmetric river cross section and asymmetric ones. Of course, symmetric ones are easier to implement but not accurate whereas most streambeds are not symmetric.

$$A = \int_a^b f(x)dx \qquad (15)$$

Where,

"a" is the central point on axis.

"b" is the point far from the axis in direction which is perpendicular to stream flow. In other words, "b" is the costal point or river, which is marked by water inundation.

A is flow area

F(x) is the surface function

In equation (15), "b" is unknown and should be solved. To solve it an alternative equation (16) is deployed:

$$A = \sum_{i=1}^{n} d_i P \qquad (16)$$

Where,

"d" is depth related to each pixel is computed from subtracting DEM elevation from lowest point in each cross section of streambed

P is the pixel size

This mimics the geometrical description of streambed cross section. Sigma process or integrator process is done by cost distance function and d_i is simulated due to cost raster dataset or resistance layer.

To create resistance raster layer, another spatial function was developed whereas there was no suitable spatial function which full fit desired requirements.

Developed spatial function, calculate reciprocal geometric description of pixels in both sides of longitudinal axes of streambed. To do it, a combination of spatial join, near point, proximity, point in polygon, spatial selection was deployed. Picture below demonstrate the developed spatial algorithm and solution.
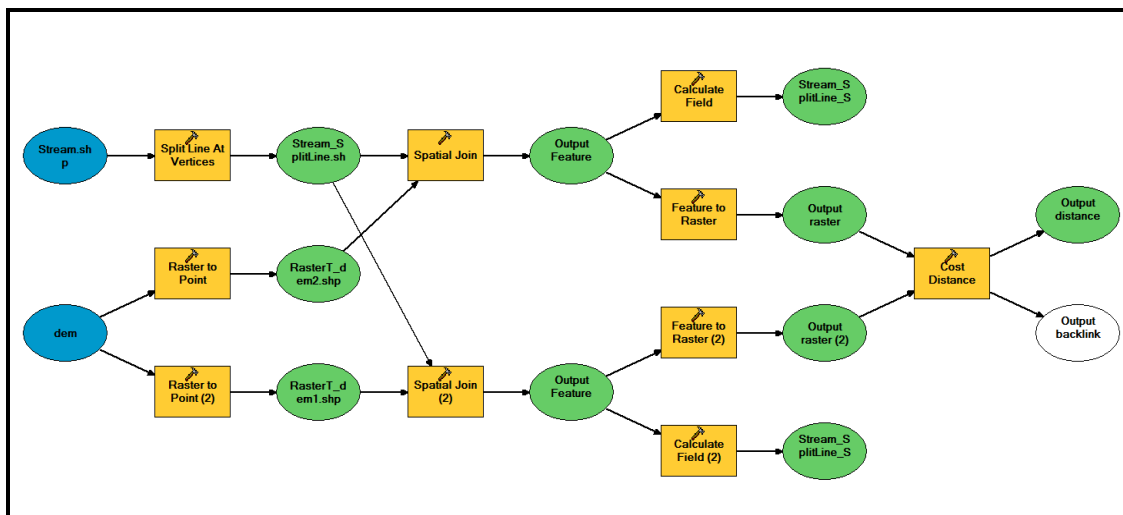
Figure 12: Design Solution in Model Environment

As it is clear in Figure 12, DEM is used in two split but parallel process. In upper line, it is converted to raster [Raster to point] and then a spatial joining process [Spatial Join] is begun to calculate the resistance layer which is important and feed the cost distance function [Cost Distance]. To do it, output of split function [Split Line at Vertices] is taken as entrance of spatial function Join [Spatial Join]. As it is clear its output is processed by a field Calculator function [Calculate Field] is shown in upper right of the Figure 12. This calculation exerts geometrical aspect of streambed and its reciprocal interactions. Then this output is used as entrance for conversion function [Feature to Raster].

In lower part of model, DEM is used for another calculation. First it is converted to raster [Raster to Point (2)] and then altitude point data is joined to stream axes which comes from split line function [Stream_Split_Line]. The spatial join is done due to spatial join function [Spatial Join (2)]. The output is processed to mimic the hydraulic behavior of stream length according to manning's equations and its proper parameters such as slope, hydraulic radius and other ones. This is done by calculator function [Calculate Field (2)]. Its output create resource raster layer which is another important input of cost distance function. Finally cost function [Cost Distance] takes two raster layers and gives the main output [Output Distance] as the water inundation level. Process is simply done using a given value for input flow water.

4. Results; Presentation and Discussion

Figure 13 shows the result for a given value of 5.7 (water flow) using symmetric streambed equations.
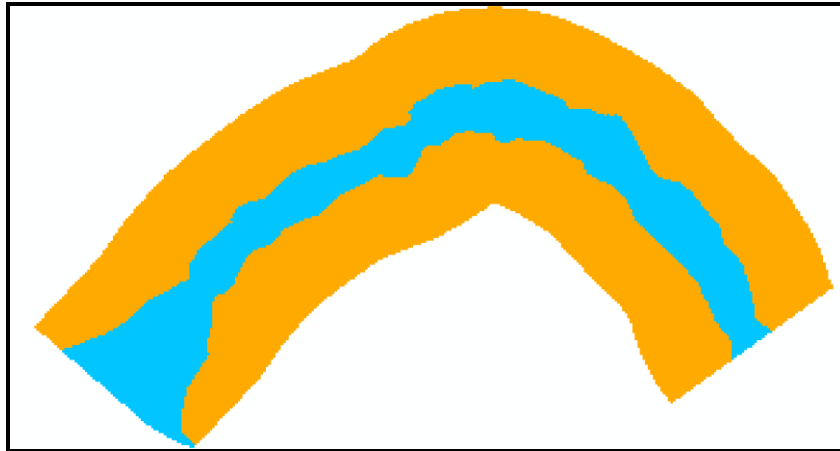

Figure 13: Water Inundation Based on Symmetric Streambed Equations

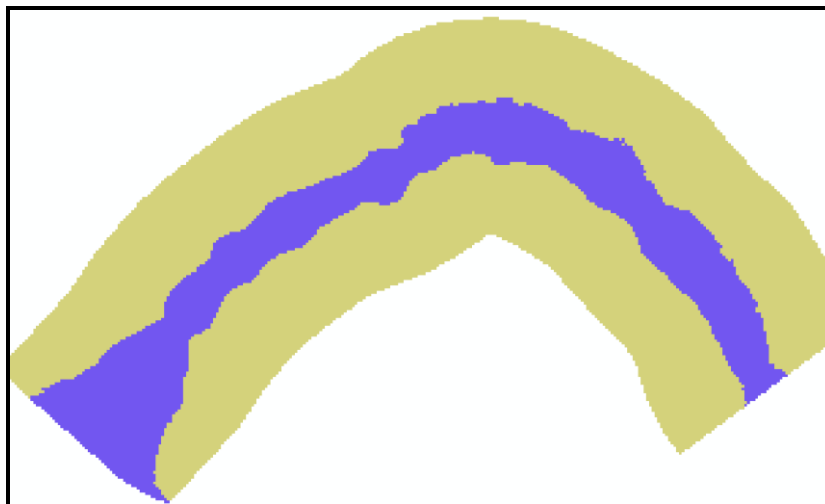Figure 14 demonstrates result for the same value using asymmetric streambed equations.

Figure 14: Water Inundation Based On Asymmetric Streambed Equations

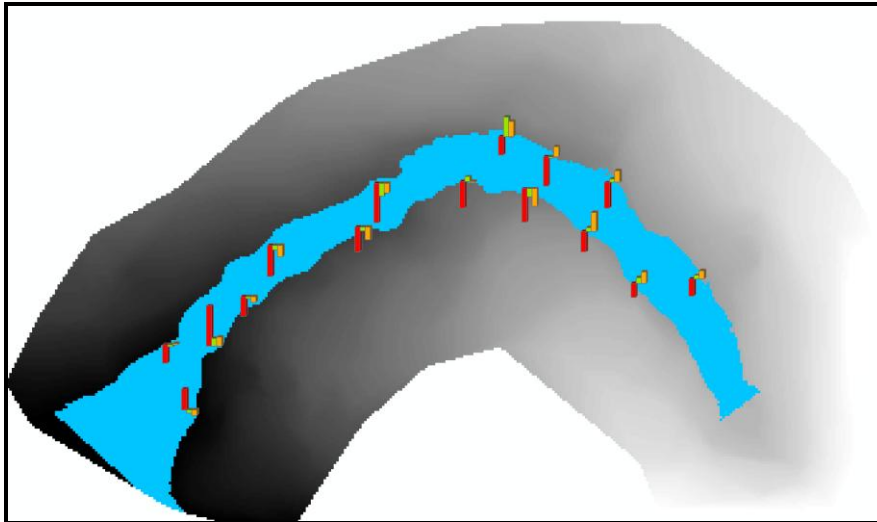To check the result, real depth was measured in 15 different locations of study area at the time of flow measurement.

Figure 15: Displays the Check Points.

Figure 15 Comparison among errors arise from three examined methods, red bars belongs to numeric method, orange one belongs to pixel spatial solution with symmetric streambed and green one represents error of spatial pixel agent solution with asymmetric streambed equation.

Figure 15 demonstrates errors of three examined methods. To compute the errors, real measured depth values have been subtracted from simulated values in three methods. Thus negative errors define that simulated values are much more than real ones.

As it is clear, numeric values depict a great amount of errors which generally have exaggerated depth. Figure 16 compare different method results against the observed values.
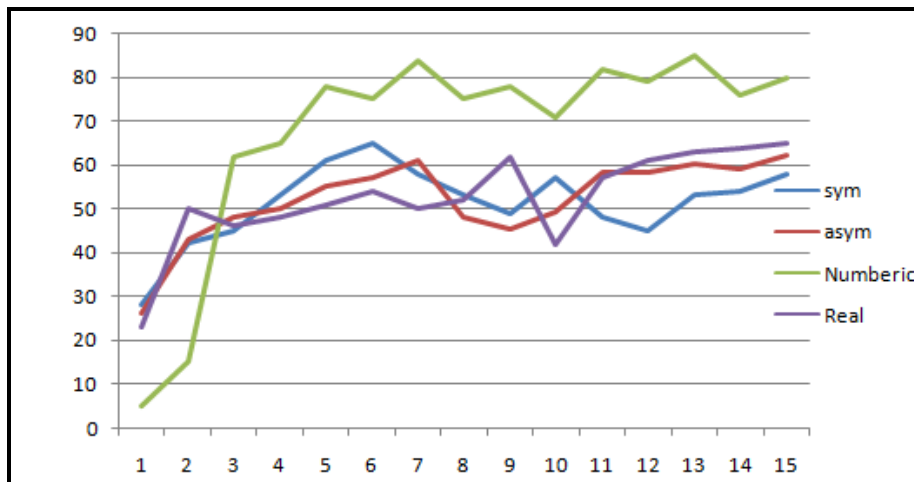
Figure 16: Displays That Prevalent Numeric Method

Figure 16 comparisons among values, blue represent spatial agent pixel solution based on symmetric streambed assumption, red belongs the spatial agent pixel solution based on asymmetric streambed, and green displays valued related to prevalent numeric equation method.

Graph 16 displays that prevalent numeric method is to some extent far from real observed values except for one point (that would be by chance). Otherwise proposed spatial pixel agent solutions are

relatively better in comparison. Table 1 shows the calculated total measured errors on 15 check points.

Table 1: Comparing Standard Deviation Related to each Method

STD_e_s	STD_e_as	STD_e_num
9.844989	6.620315	18.052305

According to Table 1, proposed spatial pixel agent solution based on asymmetric streambed equation, gives the best result with accuracy equal to 6.62 centimeters. The significant point is where this method released maximum amount of error. As it is clear in Figure 16, this point is located on stream bend. This might be under the effect of neglecting river momentum and its inundation effect.

5. Conclusion

Water engineers have done lots of efforts to optimize stream simulation but most concentrate on mathematical equations. Although optimized math equations had improved reality and fitness of model on real environment but according to experience there is always a significant shift, bios and errors in results which are interpreted as manning's coefficient problem or some other similar things. Therefore empirical surveying observation is necessary to calibrate the models. In addition, traditional methods include bulky and of course difficult manual process which prohibit the others to use them.

In this research the main idea was to deploy powerful and geo-accurate spatial functions which all are predesigned in GIS software and computation environment. Whereas GIS is general simulator, logically it has not expert tools to be proper enough to simulate the stream inundation behavior. Therefore hydraulic equations were considered and one is selected which was most efficient and easy to be developed using geo-spatial functions.

Fusion of hydraulic equations was done due to specification of geo-spatial functions and of course a specific new spatial function was developed to complete the solution. A plan was designed to arrange geo-functions together to form a new module. This module uses small pixels or agents with almost simple behavior to simulate water inundation. There were two candidates for geometric module equations. Both were developed and along with traditional approach were examined in a streambed part.

Three groups of simulated values were compared against real observed values which indicated the significant amount of fitness in simulated values by developed geo-spatial pixel-agent module. Regardless of improvement of fitness, this module eases the process considerably along with decreasing the time. In the other words, now it is perfectly easy for anyone to use the module with the least requirements.

In addition, combination of geo-spatial functions to solve the mentioned problems depicts the high potential of GIS geo-spatial function to solve any other spatial problems too. Nevertheless, there are some weak points coherent with proposed method which requires more attention. Upcoming water on bends e.g. is among the issues should be covered by more efforts to complete pixel-agent behavior via the better deployment of hydraulic equations. This had not done because implementation of hydraulic equations was not enough simple while one should do it via pre-designed and limited geo-spatial functions. This problem would be solved due to develop new geo-spatial functions which can do more than before.

References

Abbott M.B. *Computational Hydraulics.* 2nd Ed. Ashgate Publishing Company, Vermont., 1998.

Abbott M.B., Bathurst J.C., Cunge J.A., O'Connell P.E., and Rasmussen J. An *Introduction to the European Hydrological System.* Journal of Hydrology. 1986. 77-87.

Akan A.O. *Urban Stormwater Hydrology.* Technomic Publishing Co. 1993.

Wikibooks, 2010: *Algorithm Implementation.*

Barkau R.L. *A Mathematical Model of Unsteady Flow Through a Dendritic Network.* Ft. Collins, Co. 1985.

Brownlee Jason. *Clever Algorithms.* Nature-Inspired Programming Recipes, Lulu Enterprises. 2011.

C.A. Blain, R.H. Preller, and A.P. Rivera. *Tidal Prediction Using the Advanced Circulation Model (ADCIRC) and a Relocatable PC-based System.* Oceanography. 2002. 15 (1) 77-87.

C.A. Blain, T.C. Massey, J.D. Dykes, and P.G. Posey. *Advanced Surge and Inundation Modeling.* Featured Research. 2007. 89-97.

CollinsFosu, Eric K. Forkuo, Mensa Y. Asare. *River Inundation and Hazard Mapping – a Case Study of Susan River - Kumasi.* Proceedings of Global Geospatial Conference. Quebec, Canada, 2012.

Eivazy, Hooshang. *Automation of Streambed Extraction Due to Optimized Hydraulic Mathematical Functions and Exertion of it to Spatial Geo Processor Functions.* European Journal of Research and Science. 2013.

Geomatic 88. NCC, 2008. Considering Spatial Data Structure for Hydrology and their Construction and Preparation Process.

ESRI. *ArcGIS Desktop Help 9.3,* 2011. http://www.esri.com, 2011.

Firas S.M. SALEH, Agnès DUCHARNE, and Ludovic OUDIN. *Hydraulic Modeling of Flow, Water Levels and Inundations: Serein River Case Study.* Programme PIREN-Seine. 2010.

Pacific Disaster Center. *Global Flood Survey.* http://www.pdc.org/weather/index.php /category/ global-flood-survey/, 2013.

Hsu M.H., Chen S.H., and Chang T.J. *Inundation Simulation for Urban Drainage Basin.* Journal of Hydrology. 2000. 24; 21-37.

Institute, Danish Hydraulic. *User's Manual.* Horsholm, Denmark: Danish Hydraulic Institute, 2000.

Merwade, Venkatesh. *Tutorial on using HEC-GeoRAS with ArcGIS 10 and HEC-RAS Modeling.* School of Civil Engineering, Purdue University, 2012.

Mike11*, A Modeling System for Rivers and Channels.* DHI Water and Environment Incorporation, DHI, 2011.

Ming-Hsi Hsu, Shiuan-Hung Chen, and Tsang-Jung Chan. *Dynamic Inundation Simulation of Storm Water.* Journal of the Chinese Institute of Engineers. 2002. 171-177.

Neil G. Dickson, Kamran Karimi, and Firas Hamze. *Importance of Explicit Vectorization for CPU and GPU Software Performance.* Computer Science, 2010.

Appendix

[1] Whenever water flows in its streambed, it touches its streambed and come up to reach specific point according to streambed cross-section and water flow.

[2] Pre-developed functions such as software module which has been specified to solve or done spatial problem or process. These functions are able to be combined with each other in specific environment (such as ArcGIS Model environment) to do more sophisticated spatial processes.

[3] That is a high level environment same as what offered by different PL but very specific. It contains its operations, procedures and functions but not general. These all have been specified for special scope.

[4] It is a political division in Iran which clearly corresponds to State in USA in some reasons.

[5] Some things such as mathematical problems but difference mainly arise from their geometry dependencies. They are more complex in comparing with math problems whereas there so many aspects should be kept in mind along with its sophisticated geometrical specifications.

[6] It is a buffer which surround the stream main axes and is critical and dangerous because any settlement it this area would result in losses of lives on flood time.

[7] It is a coefficient which defines streambed friction against water flow.

[8] There are some great and powerful Geodatabase which are governed by organizations and are responsible for suitable and standard spatial data sources. For an instance National Cartography Center of Iran, established a great Geodatabase which includes all countries spatial data within.

[9] Each spatial function or procedure has many settings parameter which considerably define the way that function behaves. Fining and regulation of these parameters is called tuning.

[10] Upcoming waves from water bodies such as river or sea.

[11] In such PLs, commands, procedures or functions should be read and then executed one after one in a regular sequence.

[12] Algorithms which just concern about numerical cause model equations. They even behave the geometry as the least importance factor e.g. cross section geometry is replaced by an area volume.

[13] It is abbreviation form of Graphical User Interface.

[14] It is a data model which is proper enough to model continuous natural phenomena. Model is comprised from Small Square that is arranged in regular grid and each has its own specific value.

[15] In this main process, different sub-processes should be done includes, data molding, rasterization, interpolation, cleaning, structuring etc.

[16] It is a spatial function which combines different raster datasets with common spatial coordination system.

[17] Pixel agent is assumed as a small simple object poses the least complicated behaviors and properties. Upcoming solution will be based on combination of such agents. Of course combination of simple agents is able to demonstrate sophisticated behaviors.

Spatio-Temporal Dynamics of Almora Town Area, India

J.S. Rawat[1], Manish Kumar[1], and Ravindra Nath Pathak[2]

[1]Centre of Excellence for NRDMS in Uttarakhand, Department of Geography, Kumaun University, SSJ Campus, Almora, Uttarakhand, India
[2]Haryana Space Applications Centre (HARSAC), CCS Haryana Agriculture University Campus, Hisar, Haryana, India

Correspondence should be addressed to J.S. Rawat, jsrawat1955@gmail.com

Abstract The present study illustrates an integrated approach of remote sensing and GIS (Geographical Information System), i.e., Geospatial techniques for measuring physical growth of Almora town of district Almora in the Kumaun region of Central Himalaya. Landsat satellite imageries of three different time periods, i.e., Landsat TM of 1990, Landsat TM 1999 and Landsat TM of 2010 were acquired and quantify the changes in the Almora town from 1990 to 2010 over a period of 20 years. Supervised Classification methodology has been employed using Maximum Likelihood Technique in ERDAS 9.3. The images of the study area were categorized into three different classes, viz., built-up area, vegetation and others. The results indicate that during the last two decades (i.e., 1990-2010), built-up area of the Almora town area has been increased about 80.73% (i.e. 2.04 km^2) while areas under vegetation and other land categories have decreased about 43.42% (i.e. 1.32 km^2) and 37.31% (i.e. 0.72 km^2), respectively. The results of the paper on digital change detection techniques shall be helpful in proper land use planning for a sustainable and uniform urban growth of the Almora town area.

Keyword *Land Use/Cover; Spatio-Temporal; Multi-Temporal Satellite Imagery; Remote Sensing*

1. Introduction

Land is becoming a scarce resource due to immense urban development and demographic pressure. Hence, information on land use/cover and possibilities for their optimal use is essential for the selection, planning and implementation of land use schemes to meet the increasing demands for basic human needs and welfare. This information also assists in monitoring the dynamics of land use resulting out of changing demands of increasing population. The Land use/cover pattern of a region is an outcome of natural and socio-economic factors and their utilization by man in time and space. Information on land use/cover is important to support urban management and planning, sustainable management of natural resources and socio-economic development (Kontes et al., 2000). Land cover is a fundamental parameter describing the Earth's surface. This parameter is a considerable variable

that impacts on and links many parts of the human and physical environments (Foody, 2002). On the other hand, land use refers to man's activities which are directly related to the land (Clawson and Stewart, 1965). Land use involves the management and modification of natural environment or wilderness into built environment such as fields, pastures, and settlements. Land use/cover change has become a central component in current strategies in managing natural resources and monitoring environmental changes. Land use/cover dynamics are widespread, accelerating and significant process driven by human action but also producing changes that impact humans (Agarwal *et al.*, 2002). Land use/cover change, as one of the main driving forces of environmental change, is central to the sustainable development debate. Land use/cover changes have impacts on a wide range of environment and landscape. The change in land cover occurs even in the absence of human activities through natural processes where as land use change is the manipulation of land cover by human being for multiple purposes-foods, fuel wood, timber, fodder, leaf, litter, medicine, raw materials and recreation. Many socio-economic and environmental factors are involved for the change in Land use/cover. Land use/cover change has been reviewed from different perspectives in order to identify the drivers of land use/cover change, their process and consequences. The advent of high spatial resolution satellite imagery and more advanced image processing and GIS technologies, has resulted in a switch to more routine and consistent monitoring and modeling of land use/cover patterns. Using remote sensing techniques to develop land use classification mapping is a useful and detailed way to improve the selection of areas designed to agricultural, urban and/or industrial areas of a region (Selçuk, 2003). Remote-sensing has been widely used in updating land use/cover maps and land use/cover mapping has become one of the most important applications of remote sensing (Lo, 2004). The mapping of land use/cover can be performed in a cost-effective manner using Earth observation remote-sensing technologies in conjunction with geographical information systems (Weng, 2002) and GI Science (Wilson, 2008).

The present study demonstrates the application of multi-temporal satellite imageries in defining land use/cover dynamics of a Himalayan town, viz. Almora located in the Uttarakhand State in the Central Himalayan region of Kumaun Himalaya.

2. Study Area

The study area, viz., Almora town (Figure 1) in Uttarakhand, India extends between 29°05'16"N to 29°17'28"N latitudes and 79°24'07"E to 79°37'05"E longitudes and encompasses an area of 7.27 km². The average height of the town stands at 1,651 meters above mean sea level. Almora town enjoys the cool temperate climatic conditions.
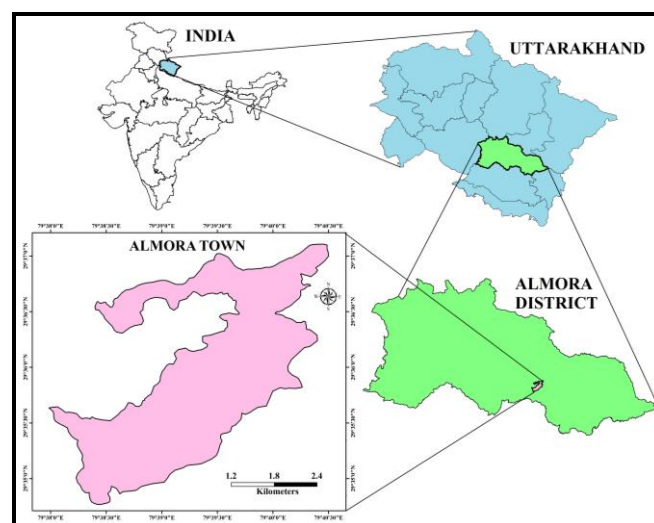

Figure 1: *Location Map of the Study Area*

3. Methodology

3.1. Land Use/Cover Detection and Analysis

To work out the land use/cover classification, Landsat TM at a resolution of 30 m of 1990, 1999 and 2010 using bands 2 (green), 3 (red) and 4 (near-infrared) were used. The satellite data covering study area were obtained from Global Land Cover Facility (GLCF) site. These data sets were imported in ERDAS Imagine version 9.3 (Leica Geosystems, Atlanta, U.S.A.), satellite image processing software to create a False Colour Composite (FCC). The layer stack option in image interpreter tool box was used to generate FCCs for the study areas. The sub-setting of satellite images were performed for extracting study area from both images by taking geo-referenced out line boundary of Almora town map as AOI (Area of Interest). The FCC images of the study area were then digitally processed for land use/cover identification and mapping. Image classification procedure is used to classify multispectral pixels into different land cover classes. The Maximum Likelihood Algorithm of Supervised Classification was used for pixel clustering. Three land use/cover types are identified in the study area viz., (i) vegetation (ii) built-up land (iii) others.

3.2. Land Use/Cover Change Detection and Analysis

For performing land use/cover change detection, a post-classification detection method was employed. A change matrix (Weng, 2001) was produced with the help of ERDAS Imagine software. Quantitative areal data of the overall land use/cover changes as well as gains and losses in each category were determined between 1990 and 2010 and then compiled.

3.3. Land Use/Cover Status

Figure 2 depicts spatial distributional pattern of land use/cover of the Almora town area for the year 1990, Figure 3 for the year 1999 and Figure 4 for the year 2010. These data reveal that in 1990, about 31.63% (2.30 km^2) area of Almora town was under built-up land, 41.82% (3.04 km^2) under vegetation and 26.55% (1.93 km^2) under others land categories. During 1999 the area under these land categories was found 40.85% (2.97 km^2) area of Almora town was under built-up land, 38.97% (2.82 km^2) under vegetation and 20.36% (1.48 km^2) under others land categories. During 2010 the area under these land categories was found 59.68% (4.34 km^2) area of Almora town was under built-up land, 23.66% (1.72 km^2) under vegetation and 16.66% (1.21 km^2) under others land categories.

Table 1: Distribution of Land Use/Cover during 1990, 1999 and 2010

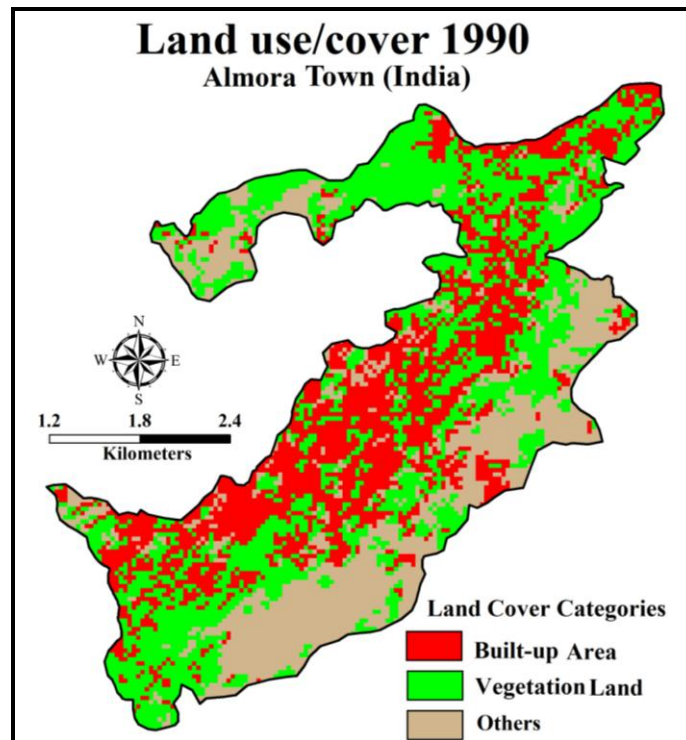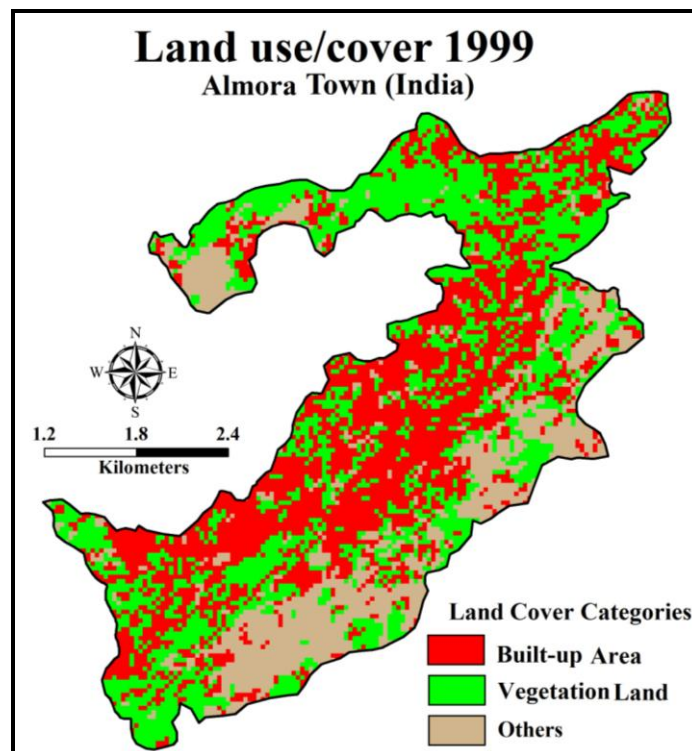| Land use/cover	1990		1999		2010	
	Km^2	%	Km^2	%	Km^2	%
Vegetation	3.04	41.82	2.82	38.79	1.72	23.66
Built up Area	2.30	31.63	2.97	40.85	4.34	59.68
Others	1.93	26.55	1.48	20.36	1.21	16.66
Total	7.27	100	7.27	100	7.27	100

Figure 2: Land Use/Cover Map of 1990 of the Almora Town, District Almora (Based on Landsat Thematic Mapper Satellite Imagery)

Figure 3: Land Use/Cover Map of 1999 of the Almora Town, District Almora (Based on Landsat Thematic Mapper Satellite Imagery)
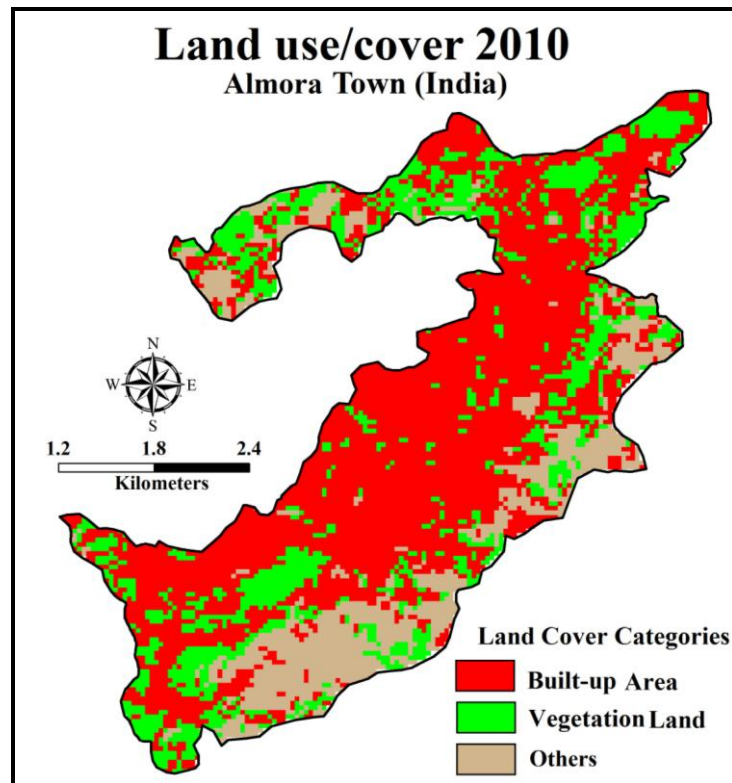
Figure 4: *Land Use/Cover Map of 2010 of the Almora Town, District Almora (Based on Landsat Thematic Mapper Satellite Imagery)*

3.4. Land Use/Cover Change

The data registered in Table 2 & 3 and Figure 5 & 6 depict that both positive and negative changes occurred in the land use/cover pattern in the Almora town area. During the last two decades the built-up area has increased from 2.30 km^2 in 1990 to 2.97 km^2 in 1999 and 4.34 km^2 in 2010 which accounts for 80.73% of the total sprawl area. The vegetation cover has been decreased from 3.04 km^2 in 1990 to 2.82 km^2 in 1999 and 1.72 km^2 in 2010. This decreased in vegetation accounts for 43.42% of the total town area. The land under other categories has been decreased from 1.93 km^2 in 1990 to 1.48 km^2 in 1999 and 1.21 km^2 in 2010. This decreased in other land category accounts for 37.31 % of the total town area.

The study reveals that in between 1990 to 1999 and 1999 to 2010 Almora town is increasing at the rate of 0.07 km^2/year and 0.12 km^2/year, respectively which was 0.10 km^2/year increased during the two decades (i.e., 1990-2010) (Table 3).

Table 2: *Area and Amount of Change in Different Land Use/Cover Categories in the Almora Town Area during 1990 to 2010*

Land use/cover Categories	1990-1999		1999-2010		1990–2010	
	km^2	%	km^2	%	km^2	%
Vegetation	-0.22	-7.24	-1.10	-39.00	-1.32	-43.42
Built Up Area	0.67	30.56	1.37	47.24	2.04	80.73
Others	-0.45	-23.32	-0.27	-18.24	-0.72	-37.31

Table 3: *Area and Amount of Change in Different Land Use/Cover Categories in the Almora Town Area during 1990 to 2010*

Land use/cover category	1990-1999	1999-2010	1990-2010
	Km²/year	Km²/year	Km²/year
Vegetation	-0.02	-0.1	-0.06
Built up Area	0.07	0.12	0.10
Others	-0.05	-0.02	-0.03
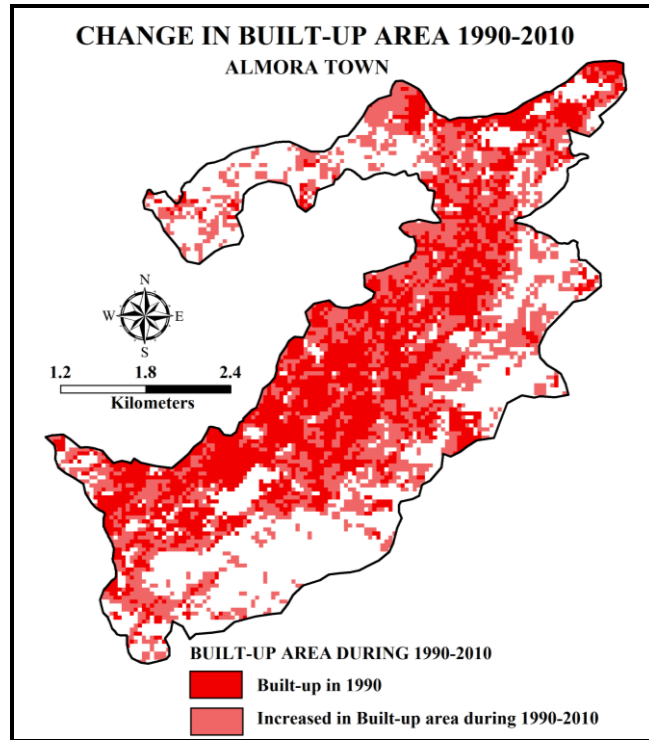
Figure 5: *Change in Built-Up Area during 1990-2010 of the Almora Town, District Almora (Based on Landsat Thematic Mapper Satellite Imagery)*
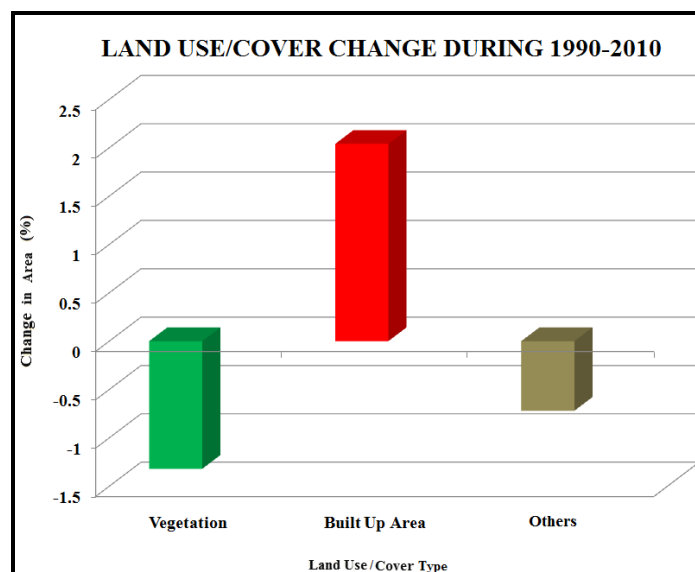
Figure 6: *Diagrammatic Illustration of Land Use/Cover Change during the Last Two Decades (1990-2010) in the Haldwani Town Area*

3.5. Land Use/Cover Change Matrix

To understand land encroachment in different land use/cover categories, change detection matrix (Table 4) was prepared which reveals that during the last two decades (1990–2010)

i)   About 49% of vegetation covered has been converted into built-up land and about 08.11% into others land category;

ii) About 25.76% of land into others category has been converted into vegetation cover and 24.39% into built-up land.

Table 4: Land Use/Cover Change Matrix Showing Land Encroachment (in %) in Almora Town Area during 1990–2010

	Land Use/Cover Categories	Year 1990		
		Vegetation	Built-up Area	Others
Year 2010	Vegetation	42.89	0.00	25.76
	Built-up Area	49.00	100.00	24.39
	Others	08.11	0.00	49.85
	Class Total	100.00	100.00	100.00
	Class Change	57.11	0.00	50.15

4. Conclusion

The study conducted in one of the towns of the Uttarakhand state located in the Central Himalaya, India, viz., Almora advocates that multi-temporal satellite imagery are very useful to detect the changes in land use quickly and accurately. The study reveals that the major land use in the Almora town area is built-up area. During the last two decades the area under built-up land has been increased 80.73% (2.04 km^2) due to construction of new buildings on agricultural and vegetation land while the area under vegetation and others land category have decrease by 43.42% (i.e. 1.32 km^2) and 37.31% (i.e. 0.72 km^2), respectively. The approach adopted in this study clearly demonstrated the potential of GIS and remote sensing techniques in measuring change pattern of land use/cover in town area which is otherwise not possible to attempt through conventional mapping. Change detection is made possible by these technologies in less time, at low cost and with better accuracy.

Acknowledgement

References

Agarwal C., Green G.M., Grove J.M., Evans T.P., and Schweik C.M., 2002: *A Review and Assessment of Land-Use Change Models: Dynamics of Space, Time, and Human Choice.* Technical Report, Pennsylvania, U.S.A. 61.

Clawson and Stewart L., 1965: *Land Use Information: A Critical Survey of U.S. Statistics Including Possibilities for Greater Uniformity: Baltimore, Md.* The Johns Hopkins Press for Resources for the Future, Inc. 402.

Foody P.M. *Status of Land Covers Classification Accuracy Assessment.* Remote Sensing of Environment. 2002. 80; 185-201.

Kontes C.C., Raptis V., Launer M., and Oberstadler R. *The Potential of Kernel Classification Techniques for Land Use Mapping in Urban Areas using 5m-Spatial Resolution IRS-1C Imagery.* International Journal of Remote Sensing. 2000. 21; 3145-3151.

Lo C.P. and Choi J. *A Hybrid Approach to Urban Land Use/Cover Mapping using Landsat 7 Enhanced Thematic Mapper Plus (ETM+) Images.* International Journal of Remote Sensing. 2004. 25; 2687-2700.

Selçuk R., Nişanci R., Uzun B., Yalçin A., Inan H., and Yomralioğlu T., 2003. *Monitoring Land–Use Changes by GIS and Remote Sensing Techniques: Case Study of Trabzon.* Proceedings 2nd FIG Regional Conference, Morocco.

Weng Q. *A Remote Sensing–GIS Evaluation of Urban Expansion and Its Impact on Surface Temperature in the Zhujiang Delta, China.* International Journal of Remote Sensing. 2001. 22; 1999-2014.

Weng Q. *Land Use Change Analysis in the Zhujiang Delta of China is using Satellite Remote Sensing, GIS, and Stochastic Modeling.* Journal of Environmental Management. 2002. 64; 273-284.

Wilson J.P. and Fortheringham A.S., 2008: *The Handbook of Geographic Information Science.* Blackwell Publishing, USA.

Research Article   **Open Access**

Hyperspectral Remote Sensing Approach for Lithological Discrimination by ASTER Data – A Case Study of Thenkalmalai and Odhimalai Hills, Tamilnadu, India

Kuldeep Singh, K. Rajaprian, M. Vinothkumar and R.S. Kumar

Department of Earth Sciences, Annamalai University, Annamalai Nagar, Tamilnadu, India

Correspondence should be addressed to Kuldeep Singh, kdsinghgeo@gmail.com

Abstract Hyperspectral studies are the recent advanced studies in the field of remote sensing. In present study it is focused on lithological mapping of rocks found in and around Thenkalmalai and Odhimalai along Moyer–Bhavani shear zone near Sirumugai. Hyperspectral sensor is also known as image spectrometer (spectroradiometer) which collects image of a scene in tens to hundreds of contiguous narrow spectral bands nearly simultaneously. The spectral features are acquired images which are significant in the identification of minerals, vegetation condition and more; moreover every material is having their own unique spectral signature. It is a quantitative measurement of the properties of an object at one or more wavelengths and this spectral signature of the rocks depends upon the physical and chemical properties. In the present study the Advance Spaceborne Thermal Emission and Reflectance Radiometer (ASTER) data were used for the lithological classification of the study area.
Keywords *Moyar-Bhavani Shear Zone, Mineral Mapping, Hyperspectral, Remote Sensing, Anorthosite, Gabbro*

1. Introduction

The term Hyperspectral Remote Sensing – 'Hyper' refers to 'too many' and "Spectral" refers to the large number of measured wavelength bands. They provide ample spectral information to identify and distinguish spectrally unique materials. Hyperspectral imagery provides the potential for more accurate and detailed information, extraction than any other type of conventional remote sensing data. Imaging spectroscopy (Goetz et al., 1985) in Hyperspectral imaging is concerned with the measurement, analysis, and interpretation of spectra acquired from a given scene (or specific object) at a short, medium or long distance by an airborne or satellite sensor. The concept of imaging spectroscopy originated in 1980 by NASA's Jet Propulsion Laboratory began a revolution in remote sensing by developing new instruments such as the Airborne Imaging Spectrometer (AIS), which is known as AVIRIS, for Airborne Visible Infra-Red Imaging Spectrometer (Green et al., 1998). In India,

the study on hyperspectral remote sensing data applications are comprehensive especially; the mineral application studied on various parts of the country. Modern study was conducted by (Rajendran et al., 2008) and has attempted the hyperspectral tools for discrimination of different minerals of Nainarmalai region of part of Namakkal District of Tamilnadu using the TM sensor images on board the satellite LANDSAT 5. He has also pointed out the Minimum Noise Fraction (MNF), Pixel Purity Index (PPI) functions applied for the different lithology such as quartzite, pyroxene granulite and hornblende biotite gneiss which is discriminated well and shows a strong correlation with landscape. (Sanjeevi S., 2008) has targeting limestone and bauxite deposits in southern India by spectral unmixing of hyperspectral image data. In the present study JPL spectral library signatures were used as spectral signatures of different type of rocks and minerals. Subsequently the Advance Spaceborne Thermal Emission and Reflectance Radiometer (ASTER) data were used for the lithological classification of the study area. Location map of the study area is shown in Figure 1.
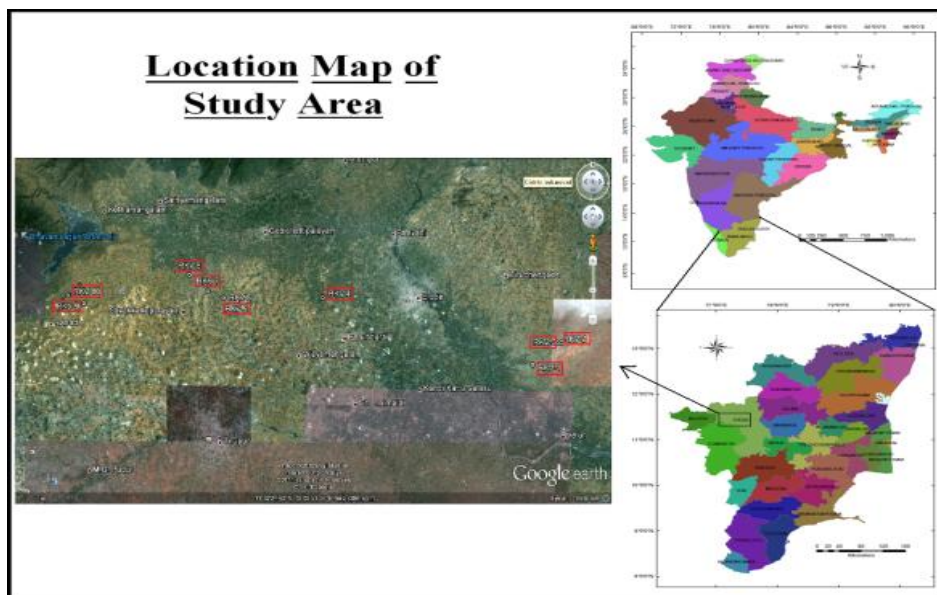

Figure 1: Location Map of the Study Area

The shear zones transecting the South Indian shield was first recognized by (Drury et al., 1980) on the basis of LANDSAT imagery. Moyar, Bhavani and Palghat shear zones separate the South Indian Dharwar Craton (SIDC) from the Nilgiri and Madurai high-grade supracrustal provinces. A Sm–Nd garnet age of 2355±18 Ma obtained from a granulite remnant in the MSZ records early Palaeoproterozoic high-grade metamorphism (Birgit Meißner et al., 2002). Satyamangalam Group is suite of highly contorted fissile migmatite gneisses (Bhavani gneisses). The supracrustal rocks include a shallow water facies association of metapelites and quartzites, ferruginous quartzites, calc–silicate rocks and marbles, mafic and ultramafic amphibolites and granulites. These are associated with large and small lenses of dismembered, granulite facies layered anorthosite–gabbro–pyroxenite–chromitite bodies, such as the classic Sittampundi and Bhavani complexes. The Bhavani complex is dominated by the presence of layers of ultramafic rocks chiefly composed of Leucogabbro, Anorthosite with Chromite layers, Pyroxinites and Peridotite. These rock bodies trend in E-W direction showing parallel to the trend of main shear of Bhavani–Moyar Shear Zone (Gopalakrishnan K., 1995). In the present study, Thenkalmalai of Sirumugai region was considered for the Region of interest (ROI), which was selected from the ASTER data. This is selected as a subset from the available data shown in Figure 2 and 3.
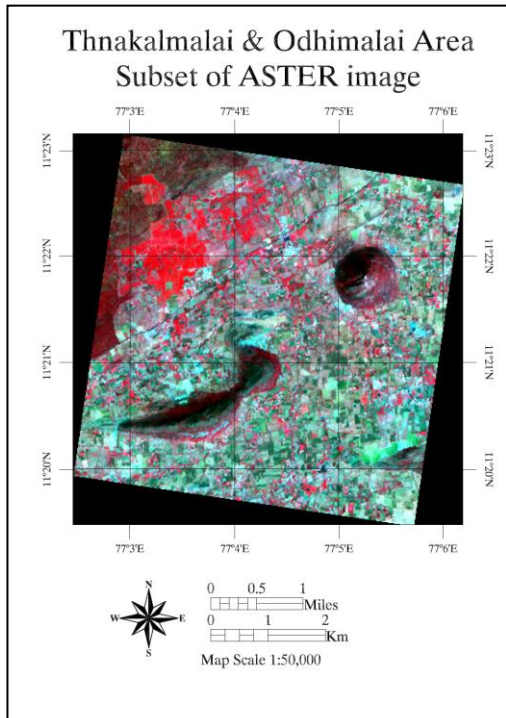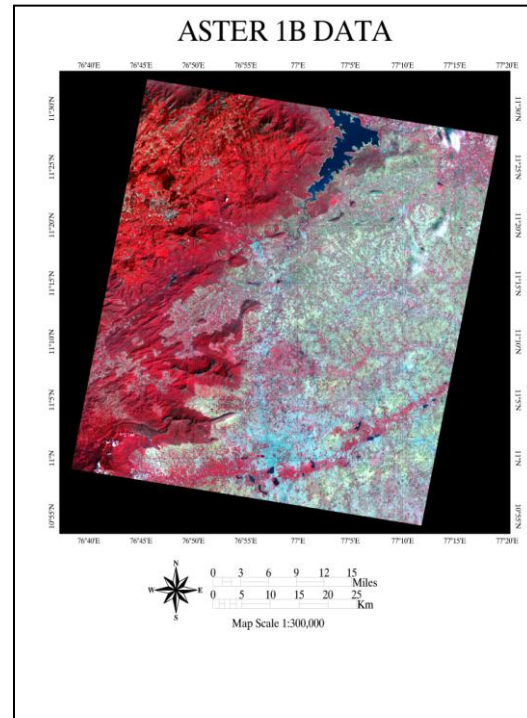
Figure 2: Subset of ASTER Image

Figure 3: ASTER 1B Data for the Sirumugai and Adjoining

2. Methodology

We are used following data and instrument for the study:

1. ASTER 1B Data
2. ASTER Spectral Library (JPL)
3. Geological Map of Tamilnadu

The methodology adopted for the study was illustrated in the Figure 4.
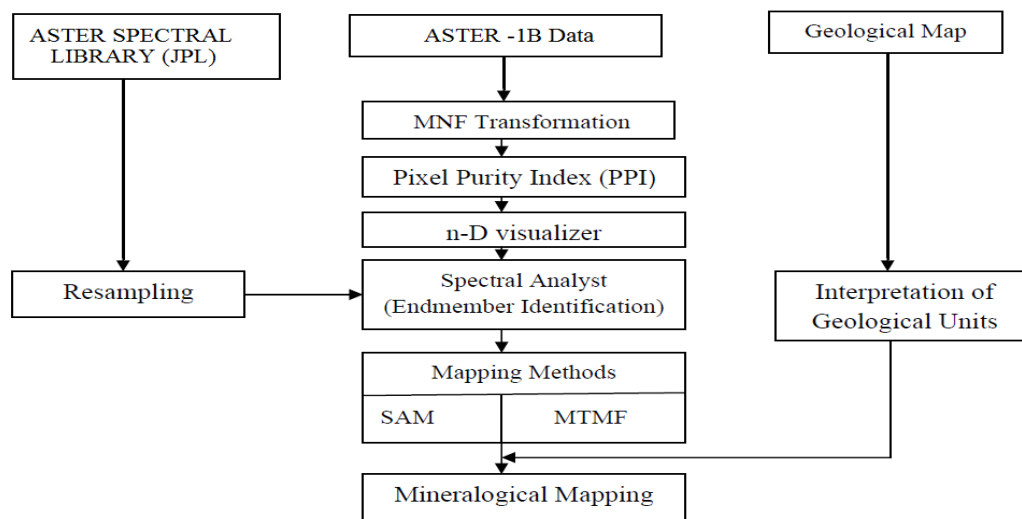

Figure 4: Methodology

ASTER scene of the study area was acquired on 23rd December 2011. ASTER covers a wide spectral region with 14 bands from the visible to the thermal infrared with high spatial, spectral and radiometric resolution. An additional backward-looking near-infrared band provides stereo coverage. It obtains image in the 3 channels in VNIR (0.52-0.86 µm) and an additional backward telescope for stereo; 6 channels in SWIR (1.6-2.43 µm) and 5 channels in TIR region (8.1-11µm), useful for the mapping variations in the silica content of the rock (Moghtaderi et al, 2007). The VNIR band has 15 m resolution and SWIR and TIR bands have 30m and 90 m resolution respectively. The Aster 1B data is geometrically and radiometrically corrected.

3. Results and Discussion

Silicates are the most common mineral groups in crustal rocks, which show characteristic spectral bands in the TIR region due to the presence of SiO_4 tetrahedron. Si-O stretching phenomenon in silicates dominates 8-12 µm regions. General trends of the spectra of common silicate minerals are outlined as follows.

  a. In the region 7-9 maximum peaks are occurred and its location migrates systematically with the composition. From the band 7 to 9 it varies from felsic to ultramafic respectively.
  b. In the region 8.5-12 µm an intense silicate band occurs, centered on 10 µm, its exact position is sensitive to the silicate structure and shifts from nearly 9 µm to 11.5 µm.
  c. In the 12-15 µm region absorption bands of silicates and aluminium silicate structure of tectosilicate type.

To identify and map quartz, carbonate and mafic minerals, band ratioing techniques were developed based on the shapes of laboratory reference spectra and applied to the TIR region in ASTER Level 1 radiance at sensor products. In this study we used different indices such as quartz index, mafic index and carbonate index. The emissivity spectra of different rocks are given in Figure 5.
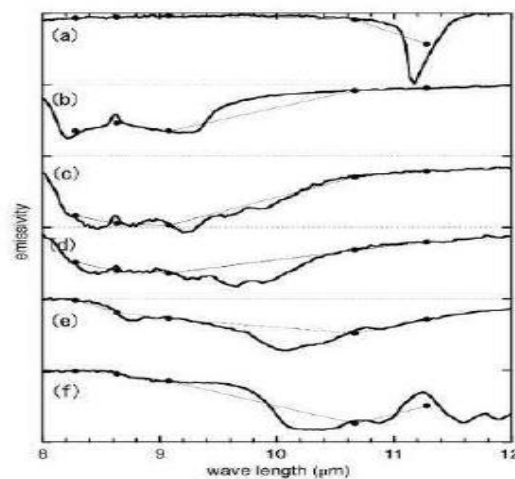

Figure 5: Emissivity Spectra of (a) Carbonate Rock (b) Quartzose Rocks (c) Granite (d) Diorite (e) Gabbro (f) Peridotite with Spectra Convolved to ASTER TIR Band Passes. (After Ninomiya et al., 2005)

3.1. Minimum Noise Fraction (MNF)

MNF rotation transform is using to determine the inherent dimensionality of image data, to segregate noise in the data, and to reduce the computational requirements for subsequent processing (Boardman and Kruse, 1994).

The MNF transform is composed of two consecutive principal component (PC) transforms (Green et al., 1988). The first PC transform focuses on whitening noise by decorrelating and rescaling the noise in the data, producing data in which the noise has unit variance and no band-to-band correlations. The transformed noise-whitened data are then subjected to a second standard PC transform, giving rise to final outputs that are not correlated and are arranged in terms of decreasing information content (Research Systems, Inc., 2002).

In a common practice, MNF components with eigenvalues less than 1 are usually excluded from the data as noise in order to improve the subsequent spectral processing results, since eigen images with near-unity eigenvalues are normally noise-dominated (Jensen, 2005). Consequently, all the 9 bands of the ASTER data were retained for subsequent data processing. The MNF transform applied to the ASTER data achieved a reasonable separation of coherent signal from complementary noise, therefore the MNF transformed eigen images were employed and coupled with pixel purity index and n-dimensional visualization techniques to facilitate the extraction of the end members.

3.2. Pixel Purity Index (PPI)

Pixel Purity Index (PPI) means to determine automatically the relative purity of the pixels from the higher order MNF eigen images using the convex geometry argument (Boardman, 1993; Boardman et al., 1995). By repeatedly projecting n-dimensional scatter plots of the MNF images onto a random unit vector, a PPI image is formed in which the digital number (DN) of each pixel corresponds to the total number of times that the pixel was judged as ''extreme'' (i.e., falling onto the ends of the unit vector) in all projections. Typically, the brighter the pixel in the PPI image the higher the relative purity because it was more frequently recorded as being a spectrally extreme pixel. To reduce the number of pixels to be analyzed for end member determination and to facilitate the separation of purer materials from mixed, a 10,000-projection of the scatter plot and a threshold factor of 2.5 are applied to the PPI image to select the most pure PPI pixels.

3.3. n-D Visualization

To further refine the selection of the most spectrally pure end members from the derived two dimensional PPI image and more importantly, to label them with specific endmembers types (i.e., to assign these end members to specific mineral types), it is essential to re-examine visually the selected pixels in the n-dimensional feature space and to assign them manually to appropriate types (Boardman and Kruse, 1994). The selected classes were exported to Region of Interest (ROI) and used as input for further spectral processing.

3.4. Spectral Angle Mapper (SAM)

Spectral angle mapper (SAM) is a procedure that determines the similarity between a pixel and each of the reference spectra based on the calculation of the "spectral angle" between them (Boardman and Kruse, 1994). This method treats both (the questioned and known) spectra as vectors and calculates the spectral angle between them (Figure 6). It works on images with apparent reflectance and determines the similarity between two spectra by calculating the "spectral angle" between them, treating them as vectors in a space with dimensionality equal to the number of bands. A smaller angle means a closer match between the two spectra and the pixel is identified as the fixed class. SAM determines the similarity of an unknown spectrum t to a reference spectrum r, by applying the following equation.

$$\alpha = \cos^{-1}\left(\frac{\vec{t} \bullet \vec{r}}{\|\vec{t}\| \bullet \|\vec{r}\|} \right) \qquad (1)$$

Equation (1) shows the relationship of known and unknown spectrum.

Also, this can be written as:

$$\alpha = \cos^{-1}\left(\frac{\sum\limits_{i=1}^{nb} t_i r_i}{\left(\sum\limits_{i=1}^{nb} t_i^2\right)^{1/2} \left(\sum\limits_{i=1}^{nb} r_i^2\right)^{1/2}} \right) \qquad (2)$$

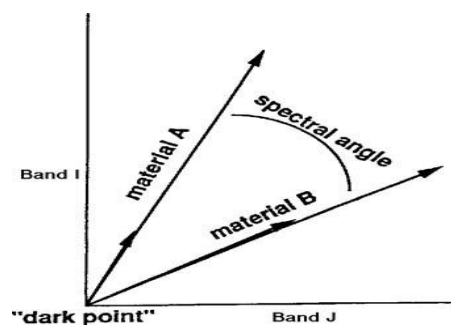Equation (2) is the elaboration of equation (1)

Figure 6: Diagram Shown Spectral Relation Between Two Materials

3.5. Mixture-Tuned Matched Filtering (MTMF)

Matched Filtering removes the requirement of knowing all of the endmembers by maximizing the response of a known end member and suppressing the response of the composite unknown background, thus matching the known signature (Chen and Reed, 1987; Harsanyi and Chang, 1994). It provides a rapid means of detecting specific minerals based on matches to specific library or image endmembers spectra. This technique produces images similar to the unmixing, but with significantly less computation and without the requirement to know all the endmembers. Mixture-Tuned Matched Filtering (MTMF) is a hybrid method based on the combination of well-known signal processing methodologies and linear mixture theory (Boardman, 1998). This method combines the strength of Matched Filter method (no requirement to know all the endmembers) with physical constraints imposed by mixing theory (the signature at any given pixel is a linear combination of the individual components contained in that pixel). MTMF uses linear spectral mixing theory to constrain the result to feasible mixtures and to reduce false alarm rates (Boardman, 1998).

In the present study a simple unsupervised classification of the subset was carried out in the software ENVI and the result is shown in Figure 7. Unsupervised classification is used here to cluster pixels in a dataset based on statistics only, without any user-defined training classes. The available unsupervised classification techniques are K-Means and ISODATA. In this classification, K-Means unsupervised classification was employed to calculate initial class means which is evenly distributed in the data space, then iteratively clusters the pixels into the nearest class using a minimum-distance technique. Each iteration recalculates class means and reclassifies pixels with respect to the new means. All pixels are classified to the nearest class unless a standard deviation or distance threshold is specified, in which case some pixels may be unclassified if they do not meet the selected criteria. This process continues until the number of pixel each class changes by less than selected pixel

change threshold or the maximum number of iterations is reached. The Geological map prepared with the field checkups is also shown in Figure 8.
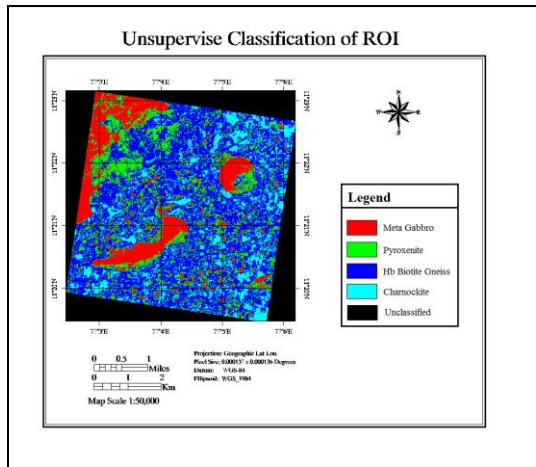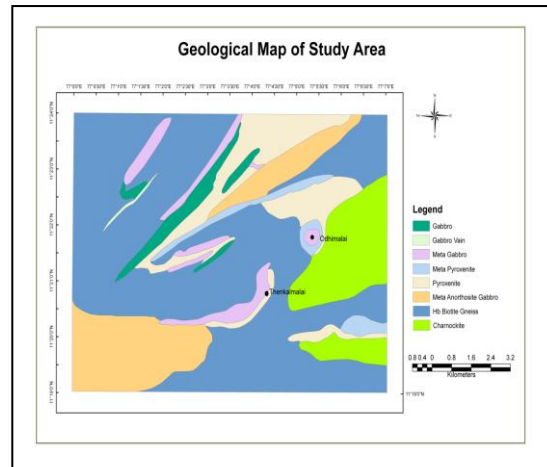

Figure 7: *Unsupervised Classification of Subset*

Figure 8: *Geological Map of Study Area*

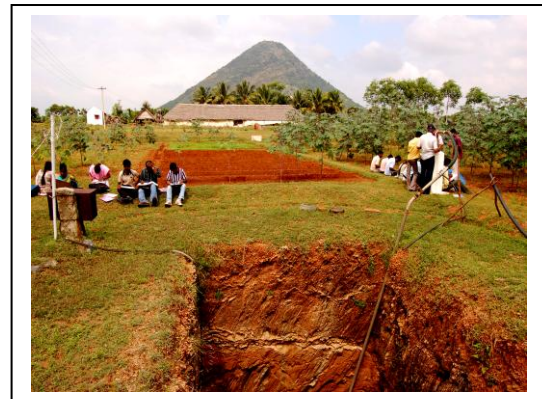**Figure 9:** *Panoramic view of Odhimalai*

Figure 10: *Plain Terrain of Gneissic* Charnockite with Odhimalai in the background

Figure 11: *Close up view of the Gabbro With Coarse Grained Development of Garnet*

Figure 12: *Close up view of Pyroxenite from the Thenkalmalai*

4. Conclusion

In the present study using ASTER data, Thenkalmalai area was classified lithologically which were later conforming to field checkup. The particular region of interest was dominantly composed of ultramafic rocks sequences. The lithology was identified as a linear body trending E-W direction parallel to the major shear zone. The different lithological units can be differentiated which ranges in dimension more than 5 meters. Thus, the region of interest exhibits gabbro, pyroxinite, peridotite as linear lensoidal bodies interbanded with one another.

References

Boardman J.W., et al., 1994: *Automatic Spectral Analysis: A Geological Example Using AVIRIS Data, North Grapevine Mountain, Nevada.* In: 10th Thematic Conference on Geologic Remote Sensing, Ann Arbor, MI, USA, 407–418.

Boardman J.W., et al., 1995: *Mapping Target Signatures via Partial Unmixing of AVIRIS Data.* In: Summaries, Fifth JPL Airborne Earth Science Workshop, Pasadena, CA, 23–26.

Boardman J.W., 1998: *Leveraging the High Dimensionality of AVIRIS Data for Improved Sub-Pixel Target Unmixing And Rejection Of False Positives: Mixture Tuned Matched Filtering.* In: Summaries of the Seventh Annual JPL Airborne Geoscience Workshop, Pasadena, CA, 55.

Chen J.Y., et al. *A Detection Algorithm for Optical Targets in Clutter.* IEEE Trans. on Aerosp. Electron. Syst. 1998. AES-23 (1) 46-59.

Drury S.A., et al. *Precambrian Tectonics and Crustal Evolution in South India.* J. Geol. 1984. 92; 3–20.

ENVI Tutorials, 2002. Research Systems, Inc., Boulder, 640.

Gopalakrishnan K., 1995: An overview of Southern Granulite Terrain, India—constraints in reconstruction of Precambrian assembly of Gondwanaland. Gondwana Nine. Vol. 2. Oxford and IBH Publishers, New Delhi, India, 1003–1026.

Goetz A.F.H., et al. *Imaging Spectrometry for Earth Remote Sensin*g. Science. 1985. 228, 1147-1153.

Green R.O. *Imaging Spectroscopy and the Airborne Visible / Infrared Imaging Spectrometer (AVIRIS).* Remote Sensing of Environment. 1998. 65; 227-248.

Harsanyi J.C., et al. *Hyperspectral Image Classification and Dimensionality Reduction: An Orthogonal Subspace Projection Approach.* IEEE Transactions on Geoscience and Remote Sensing. 1994. 32; 779-785.

Jensen J.R., 2005: *Introductory Digital Image Processing.* Person Prentice Hall, Upper Saddle River, New Jersey, 52.

Meißner Birgit et al. *Geochronological Evolution of the Moyar, Bhavani and Palghat Shear Zones of Southern India: Implications for East Gondwana Correlations.* Precambrian Research. 2002. 114; 149–175.

Moghtaderi A., et al. *The Application Of Advanced Space-borne Thermal Emission and Reflection (ASTER) Radiometer Data In the Detection of Alteration in the Chadormalu Paleocrater, Bafq Region, Central Iran*. Journal of Asian Earth sciences. 2007. 30; 238-252.

Ninomiya Y., et al. *Detecting Lithology with Advanced Space Borne Thermal Emission and Reflection Radiometer (ASTER) Multispectral Thermal Infrared "radiance-at-sensor" Data*. Remote Sensing of Environment. 2005. 99; 127-139.

Rajendran, 2008: Discrimination of Selected Features from Multispectral Landsat TM Data. Using Hyperspectral Tools, Edited Volume Hyper spectral Remote Sensing and Spectral Signature Applications, 161-168.

Sanjeevi S. 2008: Targeting Limestone and Bauxite Deposits in Southern India by Spectral Unmixing of Hyperspectral Image Data. The International Archives of the Photogrammetry, Remote Sensing and Spatial Information Sciences. Vol. XXXVII. Part B8. Beijing.